PHASE EQUILIBRIA IN MAFIC SCHIST

AND THE POLYMETAMORPHIC HISTORY OF VERMONT

Thesis by

Jo Laird

In Partial Fulfillment of the Requirements

for the Degree of

Doctor of Philosophy

California Institute of Technology

Pasadena, California

1977

(Submitted May 27, 1977)

Vermont has some fine state symbols - the sugar maple is the state
tree and the Morgan horse the state animal.

The trouble was that Vermont did not have a state rock. A lady
member of the Vermont House of Representatives proposed a bill
which would give that honor to a rock called green schist. Now
green schist is plentiful in Vermont. It can frequently be seen
along roadcuts on the new interstate throughways, where it takes
on a lovely soft green color when wet. The only drawback to
adopting green schist as the state stone was that its name must
always be pronounced, to avoid misunderstanding, with great care
and clarity.

The wags in the House were soon on their feet. One member observed
that it was a good choice because there was so much of it in
Vermont. Another favored the suggestion because it was so easily
picked up along the roadside. A third questioned the choice because
Vermont would then have to be known as the Green Schist State. After
more of the same, the matter was referred back to committee for
further study. If memory serves, we have never heard about the
matter again.

                              from "The Old-Timer Talks Back"

                                    by Allen R. Foley
                                       Prof. Emeritus, American
                                               History
                                       Dartmouth College

ACKNOWLEDGMENTS

ABSTRACT

Phase relationships in metamorphosed mafic rocks from Vermont and adjacent Quebec are presented and used to develop an understanding of the petrogenesis of this common rock type and to reconstruct the Paleozoic history of the region. Samples have been collected from Cambrian to Devonian mafic and pelitic schists. The metamorphic grade defined by the phase assemblages in the pelitic layers ranges from biotite to sillimanite. Electron microprobe analyses of the minerals in the mafic rocks are correlated with the physical conditions of metamorphism, and overgrowth relationships in amphibole grains record relative time. From these data and field and isotopic studies, mineral growth periods are characterized by metamorphic grade and facies series and assigned to two Ordovician and two Devonian events. The continuous and discontinuous reactions which describe the mineral chemistry and abundance variations in basaltic compositions are inferred from graphical and least-squares analyses.

In mafic rocks the common assemblage observed is amphibole-chlorite-epidote-plagioclase-quartz-carbonate-K mica-Ti phase-Fe^{3+} oxide. Medium-pressure progressive metamorphism of this assemblage causes the following continuous changes. 1) Ca-amphibole is enriched in the tschermakite and edenite end members. 2) Biotite and chlorite become richer in Al. 3) The discontinuous change from albite to oligoclase is followed by a continuous increase in the anorthite content of plagioclase. 4) Calcite becomes more ankeritic. Hornblende occurs with albite in the

low garnet zone and oligoclase in the medium to high garnet zone. Accompanying these compositional variations are the growth of amphibole, the consumption of chlorite, epidote, and plagioclase, and the liberation of H_2O. In contrast, during the medium- to low-pressure metamorphism of mafic rocks, plagioclase grows and the transition from actinolite to hornblende is not complete in rocks where the albite to oligoclase jump has already occurred. Epidote disappears at a lower grade than for medium-pressure metamorphism.

Higher pressure metamorphism results in an increase of the glaucophane/riebeckite substitution in the amphibole and of the phengite substitution in the K-rich white mica. Ultimately, the transition from medium-pressure to high-pressure metamorphism yields the observed assemblage Ca-rich amphibole - glaucophane which results from the cross-over reaction:

actinolite + chlorite + albite → glaucophane + epidote.
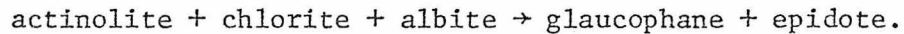
The cross-over reaction:

hornblende+chlorite+epidote+plagioclase$_1$+quartz = cummingtonite+plagioclase$_2$, where the product plagioclase$_2$ is more abundant and anorthitic than the reactant plagioclase$_1$, occurs in Ca-poor mafic rocks in the medium- to low-pressure garnet zone. In medium-pressure Fe-rich basaltic rocks, the assemblage actinolite-chlorite-stilpnomelane occurs in the biotite-albite zone. It is replaced by hornblende-chlorite in the garnet-albite zone and by hornblende-chlorite-garnet in the garnet-oligoclase zone.

The Silurian and Devonian mafic rocks in northeastern Vermont record medium- to low-pressure and low-pressure mineral growth which is assigned to two events during the Devonian Acadian orogeny. It is proposed that the lower pressure event was the later. These two events are expressed by medium-pressure and medium- to low-pressure mineral growth in the Cambrian and Ordovician rocks to the west.

Two periods of Ordovician metamorphism are recorded in the Lower Paleozoic units and are assigned to the Taconic orogeny. High-pressure, medium- to high-pressure, and medium-pressure metamorphism are observed. The higher than "normal" Barrovian facies series metamorphism is confined to northern Vermont and southern Quebec. Locally, glaucophane-bearing rocks and omphacite assemblages record high-pressure facies series metamorphism.

TABLE OF CONTENTS

Tables

Plates

Figure Captions

Figures

CHAPTER I

INTRODUCTION

A. Purpose of study and historical background

The purpose of this investigation is to understand the mineral equilibria in rocks of mafic composition so that their phase relationships can be used to characterize the physical conditions realized in metamorphic terranes.

The work of Eskola (1920, 1939) resulted in a general understanding of the petrogenesis of mafic rocks. He used the characteristic mineral assemblages in metamorphosed basalts to categorize metamorphic facies. Each pressure-temperature field, or facies, was named after a common rock type in which the diagnostic phases are present. He recognized the effects of both temperature and pressure. Greenschist facies rocks form at low temperature and shallow depths, and amphibolite facies rocks indicate higher temperature metamorphism. Contact metamorphic rocks are grouped in the hornfels facies. Eclogite facies rocks form at high pressures.

Miyashiro (1961) divided regional metamorphic rocks into five temperature sequences differing in the pressure to temperature relations. Each sequence, or facies series, was named after the diagnositc minerals in either pelitic or mafic rocks. Low-pressure rocks belong to the andalusite-sillimanite series, medium-pressure rocks to the kyanite-sillimanite series, and high-pressure rocks to the jadeite-glaucophane series. Two other facies series are included: low-pressure and high-

pressure intermediate. He divided each facies series by metamorphic grade and listed the mineralogical variations in pelitic and mafic rocks.

Most of the previous studies on the progressive metamorphism of mafic rocks are summarized by Miyashiro (1973). Recently, Graham (1974) and Cooper (1972) presented electron microprobe data on mafic rock minerals from the Dalradian series of Scotland and the Haast Schist group of New Zealand, respectively. Harte and Graham (1975) proposed a graphical representation to describe the petrogenesis of these rocks. As yet, however, mafic rocks have not been shown to be as useful in defining the physical conditions of metamorphism as pelitic.

This situation has resulted primarily because the mineral assemblage changes with smaller increments of pressure and temperature in the more aluminous rocks. Therefore, the phase equilibria in pelitic schist can be determined simply by the recognition of the key minerals in the field or in thin section. If it can be shown that the partitioning of elements among the coexisting phases in mafic schist is more sensitive to variations in metamorphic grade than their gross mineralogy, they can be used as independent control on the physical conditions of metamorphism.

B. Method of approach

Until recently a detailed study of the phase equilibria in amphibolitic schist was impracticable because of the arduous task of mineral separation and wet chemical analysis. Such an investigation is now feasible because the development of the automated electron microprobe offers the capability of obtaining rapid, complete chemical analyses of

a small volume of an individual mineral grain. This tool has been used to determine the composition of all the phases in mafic rocks from the regional metamorphic terrane of the northern Appalachian Mountains. The results are described in this dissertation.

Most of the samples studied are from Vermont; some are from adjacent regions of Quebec. This area was selected because the geology is mapped and the metamorphic isograds delineated on the basis of pelitic rock assemblages. The Vermont state map by Doll, Cady, Thompson, and Billings (1961) summarizes these data. Biotite to sillimanite grade pelitic schist is intercalated with mafic schist and provides control on the metamorphic grade.

Sixteen weeks during the summers of 1971, 1973, and 1975 were spent collecting samples from Vermont and southern Quebec. The field procedure was to locate and sample in detail outcrops from different metamorphic grades which have interlayers of mafic and pelitic schists. To expand the range of bulk rock compositions sampled and the metamorphic grades represented, adjacent outcrops with mafic and aluminous chemistry were also located and sampled. From the 1100 samples of mafic and pelitic schists, 900 thin sections were petrographically examined, and 3700 complete electron microprobe analyses of the minerals in 60 rocks were obtained. The sample locations for these 60 rocks are shown on figure 1. More detailed locations plus rock descriptions and estimated modes are given in the appendix.

Six prefixes are used to identify samples: LA, A-BM, 71VJL, 73VJL, 75VJL, and 73QJL. LA400 numbers were collected with Arden Albee

in 1971; he provided the LA500 samples. Alfred Chidester collected the A-BM samples. VJL and QJL rocks are from Vermont and Quebec, respectively. The number preceding the letter prefix refers to the year in which I collected them. The LA and A-BM prefixes are retained throughout this dissertation. For simplicity, the prefixes for the other sample numbers are shortened to V and Q in the text and on figure 1.

C. Geologic setting

A generalized geologic map of Vermont and adjacent Quebec is shown in figure 1. The references for this figure are the Vermont state map complied by Doll and others (1961) and the regional tectonic map from Cady (1969). The primary structural features are delineated; metamorphic units are divided by protolith age; and plutonic rocks are grouped as on the state map. The location of each sample analyzed with the electron microprobe is shown. Figure 2 is an index map indicating the quadrangles from which rocks were studied and several place names used in this thesis.

The Precambrian basement delimited on figure 1 has been dated by Faul, Stern, Thomas, and Elmore (1963) at about 1 billion years. Unconformably overlying the basement are Cambrian and Ordovician units. A major unconformity separates the Ordovician from the Silurian and Devonian rocks, which are combined on figure 1. These rocks have been regionally metamorphosed, and both sedimentary and volcanic protoliths are represented.

In northeastern Vermont Silurian and Devonian rocks are intruded by the New Hampshire plutonic series dated by Faul and others (1963) and Naylor (1971) as Devonian. Several ultramafic bodies intrude the

Cambrian and Ordovician units. Three areas where ultramafic rocks crop out are large enough to be shown on figure 1. Two are in southern Vermont. A large ultramafic complex and several small ultramafic bodies are shown in north-central Vermont. The former is at Belvidere Mountain and is considered to be late Ordovician by Cady, Albee, and Chidester (1963).

Cady (1969) presented a regional synthesis of the tectonics of the northern Appalachian Mountains. Anderson (1977) and Rosenfeld (1968) focused on the structural history of northern and southeastern Vermont, respectively. Several thrust faults striking generally north-south are recognized on the west side of Vermont. These faults separate relatively unmetamorphosed rocks on the west from the metamorphic rocks to the east. The Green and Sutton Mountains anticlinorium is nearly continuous from south to north through Vermont and into Quebec.

Two major orogenic events are recognized in this section of the northern Appalachian Mountains. They have been distinguished by age and facies series. Cady (1969, table 2) presented a compilation of the published radiometric ages. Recently, Lanphere and Albee (1974) and Lanphere (written communications, 1975 and 1976) have provided further data. The Silurian and Devonian rocks in eastern Vermont were metamorphosed during the Acadian orogeny. Woodland (1965) and Albee (1968) characterized this Devonian event as low-pressure.

Harper (1968) first proposed that the middle Ordovician Taconic disturbance identified in southwestern Vermont and adjacent New York was responsible for metamorphic mineral growth in the Cambrian and Ordovician

units. Albee (1968), Lanphere and Albee (1974), and Lanphere (written communication, 1976) also interpreted Ordovician ages as dating Ordovician metamorphism. Albee (1968) proposed that the Taconic event in northern Vermont was medium-pressure in character. Zen (1974) reported prehnite- and pumpellyite-bearing rocks from southeastern Pennsylvania, eastern New York, Quebec, and western Newfoundland. He suggested that these high-pressure, low-temperature assemblages are relicts of the Ordovician Taconic orogeny.

Most workers accept the thesis that Devonian mineral growth is recorded by the Cambrian and Ordovician units in Vermont. Harper (1968) proposed that the Devonian ages he obtained are postmetamorphic cooling ages, but Dennis (1968) demonstrated that these must define a post-Silurian metamorphic event. Albee (1968) and Lanphere and Albee (1974) suggested that two periods of metamorphic mineral growth have affected some of the Cambrian and Ordovician rocks. They correlated the first with the Taconic orogeny and the second with the Acadian orogeny.

D. Outline of study

This thesis is divided into three sections. The analytical techniques used to acquire the chemical data (chapter II) and the results of previous studies (chapter III) make up the first part. The second section presents the mineralogy and phase chemistry data (chapter IV). The last part is devoted to the discussion of the data. The polymeta-morphic histroy of Vermont as interpreted from the chemical, petro-graphic, and radiometric evidence is presented in chapter V. The phase equilibria in amphibolitic schist are considered in chapter VI.

In the course of this study, several complex but very exciting results were obtained. Mineral grains are commonly zoned optically and chemically. This inhomogeneity is interpreted in many samples to reflect multiple periods of mineral growth and is used to help decipher the polymetamorphic history of the host rocks.

The culmination of this study is chapter VI. All the data are combined to characterize the progressive metamorphism of amphibolitic schist. The changes in the partition of elements among the coexising phases which result from variations in metamorphic grade and facies series are graphically presented. The continuous and discontinuous reactions which effect the observed mineral composition variations are modeled.

Because the figures for this thesis are so voluminous, they are bound separately from the text. The figures are grouped for each chapter and begin with the number 1. Each figure is labeled with a prefix to indicate the chapter. In the text this prefix is dropped except when the figure is from a different chapter from the one being presented. Tables are at the end of each chapter. The appendix follows the text, and the plates precede the figures.

CHAPTER II

ANALYTICAL TECHNIQUES AND TREATMENT OF DATA

A. Data acquisition

Complete chemical analyses of all the silicate, carbonate, and oxide phases in 60 samples from Vermont and adjacent Quebec were obtained with a Materials Analysis Corporation model 5-SA3 electron microprobe controlled by a Digital Equipment Corporation 12K PDP-8/L computer. The wavelength dispersive spectrometer system (WDA) was primarily used. Laird and Albee have listings of these data, and it is anticipated that they will be available on IBM 3740 compatible "floppy" disks. Additional analyses were acquired with an energy dispersive, lithium-drifted silicon detector and Tracor-Northern NS-880 multichannel analyzer system (EDA).

The computer program which controls the counting time and the order and number of elements analyzed for the WDA system went through major revision and rapid evolution during this investigation. Initially, for all silicates and carbonates 30 second counts were collected from each of the 12 elements Na, Mg, Al, Si, K, Ca, Ti, Cr, Mn, Fe, F, and Cl, taken three at a time. For oxide phases Na, K, F, and Cl were not analyzed. 60 second counts were accumulated for Mg, Al, Si, and Ti; while Ca, Cr, Mn, and Fe were analyzed for 30 seconds.

A major revision of the analytical procedure was allowed by the procurement of a Tennecomp Systems TP-1371 MiniDek magnetic cartridge tape deck. The program no longer had to be input on paper tape; longer programs could be used; and appropriate parts could be called in during

an analysis. The UNIVERSAL program was created to treat all phases separately. Based on intial 15 second counts, the time required for 1 percent relative standard deviation was calculated for each element and analysis. The total counting time adopted was the maximum (not greater than 120 seconds) needed for each three-element set. Zn and Ce were added to the list of elements analyzed, and only the elements pertinent to each phase were analyzed.

The computer language was then modified so that doubly subscripted variables could be used. This revision produced a faster system, and the number of possible elements to be analyzed was increased. The resulting ULTIMATE program has been described by Chodos, Albee, Gancarz, and Laird (1973). ULTIMATE is similar to UNIVERSAL in the separate treatment of minerals and the calculation of counting times.

The 12 element silicate program was used for samples V12G-H, V14H-J, and V15A. V94A, 97B, 100B, 106D, 107A, 108, 113B, 114B, 119C, 127A, 124B, 118D, E, O, P, and 126H were run with the UNIVERSAL program. ULTIMATE was used for the other rocks.

The standards used for the electron microprobe analyses are listed in table 1. Each day and as necessary within a run the standards were rerun. Peak position was determined by scanning across the spectrometer position for the previous day, and 30 second counts were obtained on each peak. For the standard and sample runs, 15 second counts above and below the peak were subtracted as background. For each amphibole, chlorite, mica, and pyroxene analysis, peak searches were made on Mg, Al, and Si. Al and Si peak searches were made for each feldspar and epidote analysis,

and the Ti peak was re-established for ilmenite analyses.

All three computer programs are written such that the operator only chooses the spot to be analyzed, focuses, and specifies the mineral type. The program directs the data collection and converts the counts to weight percent oxide using the Bence-Albee (1968) and Albee-Ray (1970) techniques. Three iterations are performed, and F and Cl equivalents are subtracted. CO_2 is determined for carbonates assuming the stoichiometric amounts that go with each element.

Except for F and Cl, only X-ray intensities of positively charged ions are measured; therefore, electron microprobe analytical techniques preclude the differentiation of FeO from Fe_2O_3 and the direct determination of H_2O. To take into consideration that many analyzed minerals are hydrous and/or rich in Fe_2O_3, total iron is treated as FeO, excess oxygen is calculated as the deficiency in the total from 100 percent, and two more iterations are performed. On line the data are converted to catatom percent and normalized to the formula appropriate for the mineral analyzed. End member percentages and/or appropriate ratios are calculated and printed out before the operator starts the next analysis.

The normal operating conditions for the WDA analyses were 15 kV accelerating voltage and 0.05 μA sample current on brass. The only exception was for the plagioclase analyses in V107A and V124B for which the sample current was 0.01 μA. Spot size was dictated by the stability (which was intially checked by monitoring element counting rates) and size of the analyzed domain. 20 micron spots for plagioclase, carbonate, and mica analyses were standard; for the other phases 15-20 μm spots were

generally used. In zoned amphibole and epidote grains, spots as small as 10 μm were used. 1 μm was common for garnet and Fe, Ti oxides. For the EDA analyses 100 second counts were accumulatd on 1 μm spots at a 15 kV accelerating voltage and a 0.005 μA sample current on brass.

B. Errors

To monitor the accuracy of the electron microprobe data, three internal standards were analyzed before and during each day's run. The reproducibility obtained in our laboratory for WDA analyses of the McGetchin garnet and the Leilenkopf sanidine known unknowns is reported by Champion, Albee, and Chodos (1975) to be between 1.5 and 3 times the counting statistics error. The third internal standard is a hornblende analyzed by Engel and Engel (1962, sample AE 338). During the time WDA data were acquired (June, 1972 to September, 1975) several grains in standard mounts 170-6 and 1A were analyzed a total of 202 times.

Table 2 compiles the data for the Engel hornblende known unknown. The relative error for all major components but Al_2O_3 is $\leq$ 2% or about twice the counting statistics error. The Al_2O_3 reproducibility for Leilenkopf sanidine (which was run just before the Engel hornblende at the start of each day) is 1% as indicated by Champion and others (1975). Therefore, the 4% error for Al_2O_3 may indicate that Engel hornblende is inhomogeneous. The reproducibility for each of the analyzed components MgO, FeO, and SiO_2 is between 1.4 and 2.1 times the counting statistics error. The variation in Al_2O_3 content could be absorbed by MgO + FeO and SiO_2. The reproducibility for minor oxides is at worst 8%.

For the actual samples one major source of error in the WDA data is that the analyzed sample volume may include more than one compositional domain. Intermediate compositions must be cautiously treated. Some of this error is eliminated in the EDA analyses because smaller spot sizes can be used. However, the accuracy of the EDA analyses is less than that for the WDA data, especially in Na_2O and SiO_2. The mean and standard deviation of nine EDA analyses on the hornblende internal standard are listed in table 2.

C. Mineral normalization and nomenclature

All the electron microprobe data have been converted to weight percent oxides using the techniques of Bence and Albee (1968) and Albee and Ray (1970). Since many of the phases analyzed are hydrous and/or rich in Fe_2O_3 and since electron microprobe analytical techniques do not allow direct determination of FeO, Fe_2O_3, and H_2O, cation rather than anion distribution assumptions are used in reducing the weight percent data to atoms. This method precludes the treatment of the O $\leftrightarrows$ (OH,F,Cl) substitution.

To determine the formula for each analysis, the atomic fractions are multiplied by a normalization factor appropriate for the particular mineral type. From the formula proportions, Fe^{3+}/Fe^{2+} estimates and end member assignments are made. These calculations and the nomenclature for each mineral type are presented below.

Amphibole

The generalized structural formula of amphibole is

$$A_{0-1}^{VIII-XII} \quad X_2^{VI-VIII} \quad Y_5^{VI} \quad Z_8^{IV} \quad O_{22} \quad (OH,O,F,Cl)_2.$$
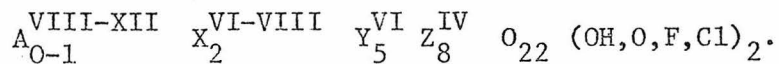
Na and K are in the A-site; Ca, Na, Mg, Fe^{2+}, and Mn are in the X-, or
M4, site. The smaller M1+M2+M3 Y-sites can be occupied by Al, Fe^{3+},
Cr, Ti, Mg, Fe^{2+}, and Mn. Si and Al fill the 4-fold, or Z-site. Be-
cause so many cation substitutions are possible in each of these
positions and the A-site is variably filled, no single, universally
correct cation distribution assignment can be made to normalize an
amphibole analysis to formula proportions.

Every analysis has been normalized in three ways, and charge
balance and site population considerations are used to choose the best
formula proportion set. The three methods are:

1) Total cations − (Na+K) normalized to 15. Na and K are assumed
to be present only in the A-site.

2) Total cations−K normalized to 15. Assume all the Na is in the
M4 site and K is in the A-site.

3) Normalize total cations − (Ca+Na+K) to 13. Fe^{2+}, Mg, and Mn
are not allowed in the M4 site.

For each formula proportion set the following are calculated:

Fe^{3+} = 46 − the total positive charge assuming all iron is ferrous

$Fe^{2+} = Fe_{Total} - Fe^{3+}$

$Al^{IV} = 8 - Si$

$Al^{VI} = Al_{Total} - Al^{IV}$.

Normalization method 1 forces all the sodium into the A-site, and the
second scheme allows only Na^{M4}. For method 3

$Na^{M4} = 7 - (Ca+Fe_{Total}+Mg+Mn+Al^{VI}+Ti+Cr)$

$Na^{A} = Na_{Total} - Na^{M4}$.

Two substitutions in an ideal actinolite, $Ca_2(Fe^{2+},Mg,Mn)_5Si_8O_{22}$ $(OH,F,Cl)_2$, cause a charge deficiency: $Na^{M4} \overset{\rightarrow}{\leftarrow} Ca$ and $Al^{IV} \overset{\rightarrow}{\leftarrow} Si$. To maintain charge balance these substitutions must be coupled to the following substitutions which create a charge excess: $(Na,K)^A \overset{\rightarrow}{\leftarrow}$ Vacancy and $(Al^{VI},Fe^{3+},Ti,Cr) \overset{\rightarrow}{\leftarrow} (Fe^{2+},Mg,Mn)$. As pointed out by Papike, Cameron, and Baldwin (1974), an estimate of the site population assignment accuracy can be attained by checking the charge balance. The charge deficiency and excess were calculated for each formula proportion set, and the one that gives the best agreement is considered to be the most accurate representation for the amphibole analysis.

If more than one group of formula proportions satisfies the charge balance condition, site population arguments are used to pick the best set. Typically, both normalization 2 and 3 will have a balanced charge, but method 2 will imply that Ca+Na > 2. In this case normalization 3 is better. For low Na analyses a balanced charge sometimes results from both normalizations 1 and 3. Without an accurate Fe^{2+}/Fe^{3+} determination, it is better to consider both sets of values. This problem does not exist for most of the amphibole analyses reported herein. Those analyses for which both normalizations 1 and 3 are reasonable are discussed in chapter IV.

The formulas for the amphibole end members pertinent to this study are listed in table 3 and illustrated on figure 1. These amphiboles can be described by four coupled substitutions in an ideal actinolite:

1) $((Na,K)^A,Al^{IV}) \overset{\rightarrow}{\leftarrow} (o,Si)$ or edenite substitution

2) $(Na^{M4},AF) \overset{\rightarrow}{\leftarrow} (Ca,FM)$ or glaucophane/riebeckite substitution

3) $(AF, Al^{IV}) \rightleftarrows (FM, Si)$ or tschermakite substitution

4) $FM^{M4} \rightleftarrows Ca$ or cummingtonite substitution

where o designates a vacancy in the A-site, AF is $Al^{VI} + Fe^{3+}$, and

$FM = Fe^{2+}+Mg+Mn$. The line from actionolite to tschermakite on figure 1a

separates calcic from soda-calcic and sodic amphiboles. Hornblende

plots on or below this line. Those analyses that show the glaucophane/

riebeckite coupled substitution fall above the line. On figure 1b calcic

amphiboles lie along the Ca/Na^A edge; soda-calcic and sodic amphiboles

have Na^{M4} and fall off the actinolite/hornblende edge. Coupled substi-

tutions 1-3 are combined on the graph in figure 1c. This is a useful

plot because it is independent of data normalization.

Biotite

Biotite is a trioctahedral mica and has the formula

$$X^{XII} \ Y_3^{VI} \ Z_4^{IV} \ O_{10} \ (OH, O, F, Cl)_2.$$
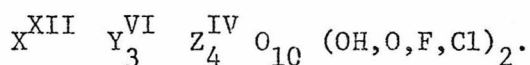
K, Na, and Ca are in the X-site. The Y-site is occupied by Mg, Fe^{2+}, Mn,

Zn, Al, Fe^{3+}, and Ti. Si and Al fill the Z-site. All biotite analyses

are normalized to the total octahedral and tetrahedral cations. The

formula proportion of $Al^{IV} = 4-Si$, and $Al^{VI} = Al_{Total} - Al^{IV}$. Relative

to an ideal biotite, $K(Fe^{2+}, Mg, Mn)_3(Si_3Al^{IV})O_{10}(OH)_2$, the total

$(Al^{VI}+Fe^{3+}+2Ti)$ causes a charge excess, and if $Al^{IV} > 1$ a tetrahedral

charge deficiency results. To maintain charge balance, these substitutions

must offset each other. Equating them allows Fe^{3+} to be estimated:

$Fe^{3+} = (Al^{IV}-1-Al^{VI}-2Ti)$. Divalent iron is then easily calculated:

$Fe^{2+} = Fe_{Total} - Fe^{3+}$.

Carbonate

The three pertinent carbonate end members and their formulas are:

calcite $CaCO_3$,

dolomite $CaMg(CO_3)_2$,

and   ankerite $Ca(Mg,Fe^{2+},Mn)(CO_3)_2$.

In this thesis the term dolomite is used for all calcium-ferromagnesian carbonates with $Mg/(Mg+Fe^{2+}+Mn) \geq 0.75$.

Chlorite

Chlorites have the formula $Y_6^{VI} Z_4^{IV} O_{10}(OH,O,F,Cl)_8$. Possible substitutions in the Y-sites include Mg, Fe^{2+}, Mn, Zn, Al, Fe^{3+}, Ti, and Cr. Si and Al fill the Z-site. These cations are normalized to 10 to convert the electron microprobe analyses to formula proportions. Assuming stoichiometry, $Al^{IV} = 4-Si$ and $Al^{VI} = Al_{Total} - Al^{IV}$. Charge balance requires that the $(Al^{VI},Fe^{3+},Cr,Ti) \rightleftarrows (Fe^{2+},Mn,Mg)$ substitution is coupled to $Al^{IV} \rightleftarrows Si$. Fe^{3+} can then be calculated by the equation

$$Fe^{3+} = Al^{IV} - Al^{VI} - Cr - 2Ti.$$

Divalent iron is then equated to total iron minus Fe^{3+}.

Epidote group

The elements Si, Al, Ti, Mg, Fe, Mn, Ca, Ce, and F were analyzed in epidote group minerals. According to the formula $X_2^{VIII} Y_3^{VI} Z_3^{IV} O_{12}$ (OH,F), each electron microprobe analysis was normalized to 8 cations. Si and Al fill the 4-fold site; Al, Fe^{3+}, Ti, and Mn^{3+} are in the Y position; and Ca, Mg, Fe^{2+}, and Mn^{2+} occupy the X-site. The two pertinent end members are epidote, $Ca_2(Fe^{3+}Al_2^{VI})Si_3O_{12}(OH)$, and clinozoisite, $Ca_2Al_3^{VI}Si_3O_{12}(OH)$. In allanite Ce^{3+} substitutes for Ca and is balanced

by Fe^{2+}, Mg, and Mn^{2+} in the Y-site. Ce was analyzed in all epidote group minerals; nonnegligible amounts are present only in allanite. For Ce-poor analyses stoichiometry implies that $Fe^{3+} = 3-Al^{VI}-Ti$ if all Mn is divalent. $Al^{VI} = Al_{Total} - (3-Si)$, and $Fe^{2+} = Fe_{total}-Fe^{3+}$.

Feldspar

The analyzed elements in feldspar, Si, Al, Ti, Mg, Fe, Ca, Ba, Na, and K, are normalized to 5 cations. The three end members albite ($NaAl^{IV}Si_3O_8$), anorthite ($CaAl_2^{IV}Si_2O_8$), and orthoclase ($KAl^{IV}Si_3O_8$) have been determined for every analysis. Celsian, $BaAl_2^{IV}Si_2O_8$, has also been calculated for potassic analyses.

Garnet

Garnet group minerals have the formula $X_3^{VIII} Y_2^{VI} Z_3^{IV} O_{12}$. Eight end members are generally used to describe a garnet analysis:

Pyrope	$Mg_3Al_2Si_3O_{12}$
Almandine	$Fe_3^{2+}Al_2Si_3O_{12}$
Spessartine	$Mn_3Al_2Si_3O_{12}$
Grossular	$Ca_3Al_2Si_3O_{12}$
Andradite	$Ca_3(Fe^{3+},Ti)_2Si_3O_{12}$
Uvarovite	$Ca_3Cr_2Si_3O_{12}$

Assuming stoichiometry, the formula proportion of $Fe^{3+} = (2-Al^{VI}-Ti-Cr)$, and $Al^{VI} = Al_{Total}-(3-Si)$. $Fe^{2+} = Fe_{Total}-Fe^{3+}$.

Pyroxene

Pyroxene analyses are normalized to 4 cations in accordance with their structural formula $X^{VI-VIII}Y^{VI} Z_2^{IV} O_6$. The cations Mg, Fe^{2+}, Mn, Ca, and Na occupy the X (M2) site. Mg, Fe^{2+}, and Mn can also substitute

into the Y (M1)site as can Al, Fe^{3+}, Cr, and Ti. Si and Al fill the 4-fold position. For each analysis the formula proportion of Fe^{3+} is equated to 12 minus the total cation charge assuming all ferrous iron. Fe^{2+} is then equal to the total Fe minus Fe^{3+}.

Nine end members are calculated for each analysis according to the following method:

$$NaFe^{3+}Si_2O_6 \qquad = \quad Fe^{3+}$$

$$NaCrSi_2O_6 \qquad = \quad Cr$$

$$NaAl^{VI}Si_2O_6 \qquad = \quad Na-Fe^{3+}-Cr$$

$$Mg_2Si_2O_6 \qquad = \quad Mg/2$$

$$Fe^{2+}_2Si_2O_6 \qquad = \quad Fe^{2+}/2$$

$$Mn_2Si_2O_6 \qquad = \quad Mn/2$$

$$CaTiAl^{IV}_2O_6 \qquad = \quad Ti$$

$$CaAl^{VI}(Al^{IV}Si)O_6 \qquad = \quad 1/2(Al-Na+Cr+Fe^{3+}-2Ti)$$

$$Ca_2Si_2O_6 \qquad = \quad 1/4(2Ca-Al+Na-Fe^{3+}-Cr)$$
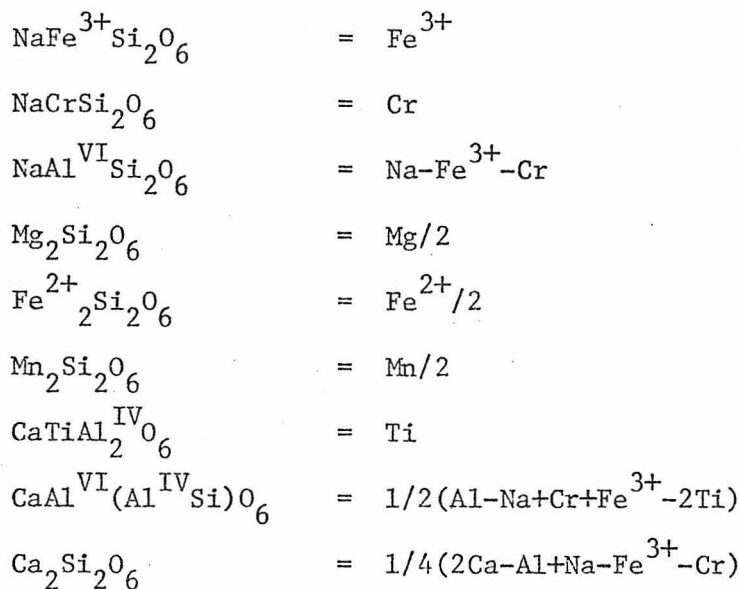
All the analyzed pyroxenes for this study are omphacite; they are primarily a combination of jadeite ($NaAlSi_2O_6$), acmite ($NaFe^{3+}Si_2O_6$), and diopside ($Ca(Mg,Fe^{2+},Mn)Si_2O_6$).

Stilpnomelane

The structural formula of stilpnomelane proposed by Eggleton (1972) is $(Ca,Na,K)_4 (Fe,Mg,Mn,Al,Ti)^{VI}_{48} (Si,Al)^{IV}_{72} (O,OH)_{216} \cdot n H_2O$. To convert each electron microprobe analysis to formula proportions, the octahedral and tetrahedral cations are normalized to 120. For the calculations in chapter VI, all iron is assumed to have been divalent at the time of metamorphism. Following the procedure outlined by Eggleton

(1972), (OH) is equated to (Fe+Mg+Mn-Ti) plus the charge excess resulting when $(2Ca+2Ba+Na+K) > Al^{IV}$. H is calculated from the charge deficiency if $(2Ca+2Ba+Na+K) < Al^{IV}$.

Sphene

Sphene analyses are normalized to 3 cations. The principal elements which occupy the cation positions in the formula $X^{VII}Y^{VI}Z^{IV}O_4(O,OH,F)$ are

X: Ca, Mn, Rare earth elements

Y: Ti, Al, Fe, Mg

Z: Si, Al

Ce was the only rare earth element analyzed; it is negligible for all analyses. All iron is considered trivalent for the calculations presented in chapter VI.

White Mica

All the electron microprobe analyses of white mica are normalized to the six octahedral and tetrahedral cations in the dioctahedral mica structural formula, $X^{XII} Y_2^{VI} Z_4^{IV} O_{10} (OH,O,F,Cl)_2$, where X = K, Na, Ca; Y = Al, Fe^{3+}, Ti, Mg, Fe^{2+}, Mn, Zn; and Z = Si, Al. Three end members, muscovite $(KAl_2^{VI}(Si_3Al^{IV})O_{10}(OH)_2)$, paragonite $(NaAl_2^{VI}(Si_3Al^{IV})O_{10}(OH)_2)$, and margarite $(CaAl_2^{VI}(Si_2Al_2^{IV})O_{10}(OH)_2)$ are recognized. The phengite substitution, $((Mg, Fe^{2+}, Mn, Zn), Si) \rightleftharpoons ((Al^{VI}, Fe^{3+}, Ti), Al^{IV})$, is commonly observed in K-rich white mica.

From stoichiometry $Al^{IV} = 4-Si$, and then $Al^{VI} = Al_{Total} - Al^{IV}$. Preserving charge balance by the phengite substitution implies that

$$Mg + Fe^{2+} + Mn + Zn - Ti = Si \text{ in excess of } 3.$$

Since $Fe^{3+} = Fe_{Total} - Fe^{2+}$,

$$Fe^{3+} = Fe_{Total} + Mg + Mn + Zn - Ti - (Si - 3).$$

Fe^{3+}/Fe^{2+} was estimated from these relationships.

Fe, Ti oxides

Si, Al, Cr, Ti, Mg, Fe, Zn, and Mn were analyzed in all oxide phases. The rhombohedral minerals are normalized to two cations, and magnetite is normalized to three cations. The sequences for the end member calculations adopted are shown below:

Rhombohedral Group

$$MgTiO_3 = Mg$$

$$MnTiO_3 = Mn$$

$$ZnTiO_3 = Zn$$

Ilmenite $\quad Fe^{2+}TiO_3 = Ti - (Mg + Mn + Zn)$

Hematite $\quad Fe^{3+}_2O_3 = 1/2(Fe_{Total} - Ti + Mg + Mn + Zn)$

Spinel Group

Spinel $\qquad FMO \cdot Al_2O_3 = Al/2$

Chromite $\qquad FMO \cdot Cr_2O_3 = Cr/2$

Ulvöspinel $\quad 2FMO \cdot TiO_2 = Ti$

Magnetite $\quad FMO \cdot Fe^{3+}_2O_3 = Fe_{Total}+Mg+Mn+Zn-\left(\dfrac{Al+Cr}{2}\right)-2Ti$
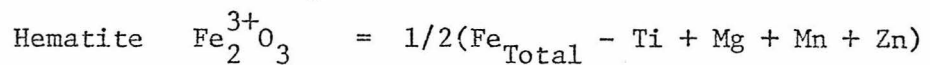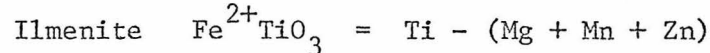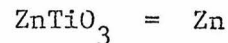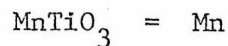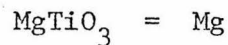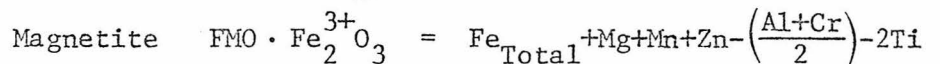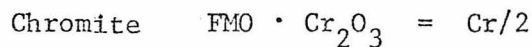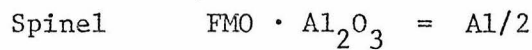
No Si end member is calculated. It was determined early in this study that most of the Si analyzed was on the surface of the oxide phases and was introduced during sample preparation. Cleaning each polished thin section ultrasonically for 30 seconds reduced the average analyzed Si from 0.3 to 0.1 weight percent oxide.

Table 1

STANDARDS

Element	Identification	
Na	Amelia albite	P-103
Mg	Synthetic oxide	P-85
Al*	Synthetic oxide	P-472
	Kyanite	P-236
Si	Brazil quartz	P-213
K	Asbestos microcline	P-102
Ca	Wollastonite	P-237
Ti	Synthetic oxide	P-530
Cr	Synthetic oxide	P-585
Mn	Nuevo garnet	P-130
Fe	Synthetic fayalite	P-514 and 669
Ba	Benitoite	P-372A
Zn	Synthetic oxide	P-471
F, Cl	Durango fluor-apatite	P-536
Ce	Glass	P-649

* Synthetic Al_2O_3 was used for the analyses run with the 12 element silicate and UNIVERSAL programs. Kyanite was the Al_2O_3 standard for ULTIMATE analyses.

Table 2

ANALYSES OF P328 HORNBLENDE

Oxide	Wet Chemical[+] Wt. Pct.	WDA[*] Mean ± 1σ S.D.	% Error	S.D./C.S.	EDA[†] Mean ± 1σ S.D.	% Error
NaO_2	1.33	1.39±0.04	3	1.3	1.77±0.25	14
MgO	8.65	8.81±0.19	2	2.1	8.73±0.17	2
Al_2O_3	13.09	12.80±0.47	4	3.9	12.16±0.33	3
SiO_2	42.18	41.52±0.49	1	2.0	43.25±0.32	1
K_2O	0.96	0.99±0.08	8	1.6	1.03±0.08	8
CaO	11.37	11.26±0.23	2	1.3	11.56±0.07	1
TiO_2	1.30	1.18±0.08	7	0.9	1.30±0.09	7
Cr_2O_3	0.03	0.03±0.03	100	0.1	0.06±0.07	117
MnO	0.32	0.33±0.02	6	0.7	0.41±0.10	24
FeO_T	18.68	18.60±0.27	1	1.4	18.66±0.37	2
F	0.11	0.08±0.07	87	0.1	N.D.	
Cl	0.03	0.03±0.01	33	0.1	0.04±0.02	50

+ From Engel and Engel (1962) Sample AE338

* Average of 202 wavelength dispersive electron microprobe analyses

† Average of 9 energy dispersive electron microprobe analyses

S. D.   1 σ standard deviation

C. S.   Maximum error due to counting statistics

N. D.   Not determined

FeO_T Total iron as FeO

Wt. Pct.   Weight Percent

Table 3

AMPHIBOLE END MEMBERS

Calcic Amphiboles

Actinolite	$Ca_2FM_5Si_8O_{22}(OH)_2$
Edenite	$Na^A Ca_2 FM_5 (Si_7 Al^{IV}) O_{22}(OH)_2$
Pargasite	$Na^A Ca_2 (FM_4 Al^{VI}) (Si_6 Al_2^{IV}) O_{22}(OH)_2$
Hastingsite	$Na^A Ca_2 (FM_4 Fe^{3+}) (Si_6 Al_2^{IV}) O_{22}(OH)_2$
Tschermakite	$Ca_2 (FM_3 AF_2) (Si_6 Al_2^{IV}) O_{22}(OH)_2$

Soda-Calcic Amphiboles

Winchite	$(CaNa^{M4}) (FM_4 AF) Si_8 O_{22}(OH)_2$
Barroisite	$(CaNa^{M4}) (FM_3 AF_2) (Si_7 Al^{IV}) O_{22}(OH)_2$
Kataphorite	$Na^A (CaNa^{M4}) (FM_4 AF) (Si_7 Al^{IV}) O_{22}(OH)_2$

Sodic Amphiboles

Glaucophane	$Na_2^{M4} (FM_3 Al_2^{VI}) Si_8 O_{22}(OH)_2$
Riebeckite	$Na_2^{M4} (FM_3 Fe_2^{3+}) Si_8 O_{22}(OH)_2$

FM Amphibole

Cummingtonite	$FM_7 Si_8 O_{22}(OH)_2$

$FM = Fe^{2+} + Mg + Mn$

$AF = Al^{VI} + Fe^{3+}$
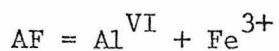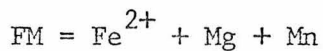
CHAPTER III

PREVIOUS INVESTIGATIONS

A. Introduction

Previous investigations of phase chemistry in metamorphosed mafic rocks are summarized in this chapter. Where possible, the mineral compositional variations observed in rocks with the common mafic assemblage, amphibole-chlorite-epidote-plagioclase, are discussed as a function of the metamorphic grade determined from intercalated pelitic schist. Amphibole, plagioclase, and white mica have been shown to be sensitive to the physical conditions of metamorphism, and these phases are discussed first.

B. Amphibole

Variations in amphibole composition as a function of metamorphic grade in mafic rocks have been extensively documented, especially the change from light-colored actinolite to darker hornblende. The literature investigations concerning this actinolite-hornblende transition are discussed, and then the analytical data are reexamined emphasizing the pressure dependence of amphibole chemistry in mafic composition rocks.

Metamorphic grade dependence

Phillips (1930) discussed the progressive metamorphism of the Green Bed group (metamorphosed sedimentary rocks of basaltic composition) from the Dalradian of Scotland. Hornblende is typical of the garnet and higher grade rocks; lower grade amphibole is optically distinct from

hornblende. His description of middle chlorite zone amphibole as being fibrous and lighter colored than hornblende is suggestive of actinolite.

In his classic study of the Dalradian epidiorites (metamorphosed diabase sills) in the Scottish Highlands, Wiseman (1934) documented the composition changes which occur in calcic amphibole with progressive metamorphism. Relative to lower grades, garnet zone amphibole is richer in Al, Na, and K; it is poorer in Si and Ca. FeO/MgO is greater in garnet zone amphibole grains than in lower grade ones. Within the garnet zone hornblende coexisting with garnet has a greater FeO/MgO value than hornblende in rocks devoid of garnet.

Recently, Graham (1974) reexamined the Dalradian epidiorites and established that both the Al^{VI} and Al^{IV} contents of Ca-rich amphibole increase with metamorphic grade. He also emphasized the dependence of amphibole Mg/(Mg+Fe) on that of the bulk rock. Cooper and Lovering (1970) recognized the actinolite to hornblende transition in metamorphosed mafic rocks from the Haast River group in New Zealand. With increasing metamorphic grade, Al^{IV}, Al^{VI}, Ti, and Na increase; Si and Mg decrease.

In the Sanbagawa terrane of Japan, Ernst, Seki, Onuki, and Gilbert (1970) showed that actinolite is the stable calcic amphibole in low grade metamorphic rocks, while hornblende is stable in high grades. Shido (1958) also observed the actinolite to hornblende transition with advancing metamorphic grade in the mafic rocks from the Abukuma Plateau of Japan. She analyzed several hornblende grains from the high grade rocks and concluded that the alkali and titanium contents increase with metamorphic grade while $Fe^{3+}/(Fe^{2+}+Fe^{3+})$ decreases. She found no systematic relationship between the Al^{IV} content of hornblende and metamorphic grade.

The published data on world-wide occurrences of rocks within the chemical volume defined by basaltic compositions indicate that amphibole chemistry is quite sensitive to the temperature of metamorphism. With increasing metamorphic grade calcic amphibole changes from actinolite to hornblende. In the next section it is demonstrated that amphibole composition in mafic rocks is also facies series dependent.

Pressure dependence

Amphibole analyses from mafic rocks from Scotland, New Zealand, Japan, and Norway are shown on four variation diagrams in figures 1-4. The last three diagrams correspond to figures 1a-c from chapter II. Included are the literature data discussed in the previous section; amphibole analyses from other areas are added for completeness. Some of the analyses are wet chemical; others were obtained with an electron microprobe. All are normalized and the best formula proportion set chosen as outlined in chapter II. For wet chemical analyses, FeO and Fe_2O_3 have been determined and are used in the data normalization. Fe^{3+}/Fe^{2+} is estimated for the electron microprobe analyses by the method discussed in chapter II.

As determined from the mafic rock assemblages, the Sanbagawa, Franciscan, and Norway terranes belong to the high-pressure facies series defined by Miyashiro (1961). Intercalated pelitic schist indicates that the mafic rocks from the Abukuma Plateau are low-pressure. The Haast River group and Dalradian rocks are characterized by medium-pressure, kyanite-sillimanite facies series metamorphism. Envelopes enclose the amphibole analyses from each facies series type on figures

1-4, and for the high-pressure terranes Ca-rich amphibole is distinguished from sodic amphibole.

Raase (1974) presented a diagram similar to figure 1. He showed that hornblende formed under high-pressure conditions tends to be enriched in Al^{VI}, and drew a line between the two groups of analyses. This line is delineated on figure 1. Also shown is the proposed Ca-amphibole maximum possible Al^{VI} content from Leake (1965). He suggested that calcic amphibole from rocks metamorphosed at high pressure would have compositions close to this line.

Since the analyses plotted on figure 1 include many that Raase (1974) discussed, it is not surprising that the preponderance of amphibole from the high-pressure mafic rocks have high Al^{VI} values compared to calcic amphibole from lower pressure basaltic composition rocks. The data from the low-pressure Abukuma Plateau plot the closest to the abscissa in figure 1 and have the least Al^{VI}. The medium-pressure Haast River group plots at the top of the Abukuma field but below the line of Raase (1974) The Dalradian envelope straddles this hypothetical high-pressure/low-pressure line. As suggested by Graham (1974), the Dalradian in southwestern Scotland may be characterized by medium- to high-pressure intermediate facies series metamorphism because the Al^{VI} content of the amphibole is between those of high- and medium-pressure terranes.

The $(Fe^{3+}, Mg) \rightleftharpoons (Al^{VI}, Fe^{2+})$ coupled substitution in amphibole is a function of P_{O_2} and can take place independently of metamorphic grade and facies series. Therefore, it is important to consider the riebeckite and ferri-tschermakite as well as the glaucophane and alumino-

tschermakite substitutions. Accordingly, all the amphibole analyses from the high-pressure mafic rocks taken from the literature are plotted on the (Al^{VI} + Fe^{3+} + Ti) versus Al^{IV} diagram in figure 2. The Ca- and Na-rich amphibole analyses from the high-pressure Sanbagawa, Franciscan, and Norway terranes plot above the actinolite to tschermakite (1:1) line. The low-pressure Abukuma terrane data define a field which falls the farthest below this line. The medium-pressure Haast River group calcic amphibole analyses and some of the Dalradian data are between the 1:1 line and the Abukuma data. Straddling the actinolite to tschermakite line are the Dalradian amphibole analyses from southwestern Scotland epidiorites. Figure 2 is similar to figure 1 in that Ca-rich amphibole from high-pressure basaltic composition rocks plot high, low-pressure mafic rocks define a field that is closest to the abscissa, and the medium- and high-pressure intermediate facies series amphibole data envelopes lie between the high- and low-pressure extremes.

As discussed in chapter II, amphibole analyses that lie above the 1:1 line on figure 2 must have glaucophane/riebeckite substitution. This relationship is demonstrated by figure 3. The Ca- and Na-rich amphiboles from the high-pressure Sanbagawa, Franciscan, and Norway terranes show significant Na^{M4} contents. The low-pressure Abukuma Plateau and medium-pressure Haast River group calcic amphibole analyses plot on or near the Ca - Na^{A} side of the diagram in figure 3 and therefore show mostly edenite substitution. In between these data sets are the Ca-rich amphibole analyses from the medium- to high-pressure Dalradian mafic rocks.

Together, the two diagrams in figures 2 and 3 show the coupled substitutions necessary to describe Ca and Na amphiboles. The tschermakite substitution is shown on figure 2, and it is an indicator of metamorphic temperature. As was discussed in the last section, with increasing grade calcic amphibole in mafic rocks changes from actinolite to hornblende. Superimposed on the temperature variation is the pressure, or facies series dependence. Amphibole analyses from basaltic composition rocks separate into groups which are consistent on figures 2 and 3. The glaucophane/riebeckite substitution is significant in amphibole from high-pressure terranes. These analyses plot high on figure 2 and away from the Ca-Na^A side of the quadrilateral shown in figure 3. Low-pressure calcic amphibole shows edenite and tschermakite substitutions. They plot close to the abscissa in figure 2 and show little Na^{M4} on figure 3. Intermediate to these two "end members" on figure 2 are the medium and medium- to high-pressure calcic amphibole analyses. The medium-pressure analyses lie closer to the low-pressure data envelope on figure 2 and show negligible Na^{M4} on figure 3. The intermediate high-pressure Ca-rich amphibole has more Na^{M4} than the low- and medium-pressure analyses but less than those from the high-pressure terranes.

The variation diagrams in figures 1-3 are to some extent dependent upon the normalization of the analyses. In figure 4 the literature data on amphibole from basaltic composition rocks are plotted on a Na/(Ca+Na) versus Al/(Si+Al) diagram. These ratios are independent of normalization. On this plot the analyses also separate by facies series. The high-pressure Sanbagawa, Franciscan, and Norway terranes have Ca- and Na-rich amphiboles which lie primarily on or above the 1:1 line. The medium-

pressure Haast River group and Dalradian mafic rocks are composed of calcic amphibole that lies below this line, and most of the low-pressure Abukuma Plateau hornblende analyses plot below it. Straddling the 1:1 line on figure 4 are the high-pressure intermediate facies series Ca-amphibole analyses from the southwestern Dalradian epidiorites.

Conclusion

Basaltic composition rocks throughout the world have been previously studied. The actinolite to hornblende transition with increasing metamorphic grade has been recognized and a correlation between amphibole composition and metamorphic facies series has been demonstrated. These relationships are consistent between areas because the mineral assemblage is predominantly the same: amphibole- chlorite- epidote-plagioclase. The constant mineral assemblage allows one to compare the composition of a single phase with the physical conditions of metamorphism. Keeping this requirement in mind, the amphibole composition data from mafic rocks in Vermont and adjacent Quebec have been plotted on the figure 1-4 variation diagrams and will be discussed in the following chapters.

C. Plagioclase

It has long been recognized that plagioclase becomes more anorthitic with progressive metamorphism. Ramberg (1952, p. 50-57) discussed some of the reactions responsible for this change in plagioclase composition. Of particular interest to the study of mafic rocks are equilibria involving the breakdown of epidote and the incorporation of Ca into the plagioclase. Ramberg (1952) presented a schematic diagram showing the temperature dependence of the plagioclase-epidote equilibrium.

Brown (1962) summarized the existing data on the pressure and temperature dependence of plagioclase composition and suggested that it is correlated with metamorphic facies series and bulk rock composition as well as metamorphic grade. For rocks of the same bulk chemistry and equivalent metamorphic grade, plagioclase is more anorthitic in the lower pressure facies series rocks. Miyashiro (1973, p. 250) calibrated this relationship for mafic rocks. The plagioclase in high- and medium-pressure terranes is albite when actinolite changes to hornblende. It is An_{20-30} in low-pressure regional terranes and labradorite in low-pressure contact areas.

Plagioclase is a potentially useful geothermometer. Miscibility between albite and oligoclase, the peristerite gap, is observed at metamorphic temperatures. Crawford (1966) and many other workers have proposed that a solvus is present between albite and oligoclase, but Smith (1974) preferred a binary loop. When the subsolidus phase relationships in the plagioclase feldspar system are better understood, albite-oligoclase pairs may offer control on metamorphic temperatures.

For this investigation the plagioclase composition in mafic rocks will be correlated with the metamorphic grade defined by the intercalated pelitic rocks. The order in which the albite-oligoclase and actinolite-hornblende transitions occur with increasing metamorphic grade will be noted.

D. White mica

White mica composition has been shown to be a geothermometer and a geobarometer. The muscovite-paragonite solvus delineated by Eugster,

Albee, Bence, Thompson, and Waldbaum (1972) can be used to estimate metamorphic temperatures. As proposed by Velde (1965, 1967), the phengite substitution in muscovite increases with pressure. If either temperature or pressure is known, the Si content of muscovite gives the other intensive parameter.

Velde (1967) and Boulter and Råheim (1974) argued that the phengite component is independent of bulk rock composition. However, in their recent review paper, Guidotti and Sassi (1976) underscored the importance of bulk rock composition on white mica chemistry and advocated comparing data within the same rock types and/or assemblage. They also discussed the interrelation of pressure and temperature on white mica composition.

Therefore, white mica analyses must be cautiously used as indicators of the physical conditions of metamorphism. For the mafic rocks from Vermont and Quebec, white mica composition will be compared in rocks with the same assemblage: amphibole-chlorite-epidote-plagioclase. Control on the bulk rock composition and assemblage allows the temperatures and pressures of metamorphism as determined from the muscovite-paragonite solvus and the phengite substitution to be compared.

E. Carbonate

Carbonate is described in mafic rocks from Scotland (Phillips, 1930 and Wiseman, 1934), New Zealand (Cooper, 1972), and Japan (Iwasaki, 1963; Banno, 1964; Shido, 1958; and Miyashiro, 1958). None of these workers has discussed its compositional variation as a function of metamorphic grade. However, carbonate composition has been shown to be sensitive to the physical conditions of metamorphism and is a potential geothermometer in the rocks studied.

Experimental work of Goldsmith and Newton (1969) delimited the
calcite-dolomite solvus. They discussed the effects of pressure on the
solubility of $MgCO_3$ in $CaCO_3$ and proposed that if a metamorphic terrane
can be categorized by high-, medium-, or low-pressure, the calcite-
dolomite equilibrium can be used as a geothermometer. Rosenberg (1967)
experimentally determined the phase relationships in the three component
system $CaCO_3$ - $MgCO_3$ - $FeCO_3$, and Barron (1974) used these data to esti-
mate metamorphic temperatures from rocks with coexisting $CaCO_3$ and
$Ca(Mg,Fe)(CO_3)_2$.

The carbonate composition in rocks with the common mafic assemblage
(amphibole-chlorite-epidote-plagioclase) can thus be used to estimate
metamorphic temperature. Calcite in equilibrium with a dolomite/ankerite
phase will give the temperature at which the two carbonates equilibrated.
The maximum substitution of $(Mg, Fe)CO_3$ in $CaCO_3$ indicates the minimum
temperature attained during metamorphism.

F. Epidote

The correlation between epidote composition and metamorphic grade
is ambiguous. Miyashiro and Seki (1958) proposed that with progressive
metamorphism the stability field of epidote enlarges toward greater and
lesser Fe^{3+} contents and is skewed toward more aluminous compositions.
This conclusion is based on theoretical considerations and $2V_x$ data from
mafic rocks from the Sanbagawa terrane, Japan. Their data on pelitic
and psammitic rocks are different from that for the mafic rocks, indi-
cating that epidote composition is dependent upon bulk rock chemistry.

Ernst and others (1970) analyzed epidote from mafic, felsic, and pelitic schists from the Sanbagawa terrane and found that $Al/(Al+Fe^{3+})$ increases with metamorphic grade. A detailed study of epidote composition in a prograde metamorphic sequence in Austria by Raith (1976) also indicates that epidote becomes more aluminous with metamorphic grade.

However, Shido (1958) and Cooper (1972) found no well-defined relationship between epidote composition and metamorphic grade in mafic rocks from the Abukuma Plateau of Japan and the Haast River group of New Zealand, respectively. Cooper (1972) proposed, and it has been confirmed by Holdaway (1972) that epidote composition is primarily a function of bulk composition and f_{O_2}. Immiscibility within the epidote-clinozoisite stability field may also be a complicating factor to understanding the geological significance of epidote composition. Raith (1976) summarized the published data on immiscibility within the epidote series and presented good evidence for a gap below 550°C.

These workers and Phillips (1930) and Wiseman (1934) reported zoned epidote grains, either more aluminous or ferric toward the rim, in metamorphosed mafic rocks. If good control can be obtained on the various factors that affect epidote composition, such zoned grains can be used as chronicles of metamorphic history. Clearly, though, epidote composition cannot be simply used as an indicator of metamorphic grade.

G. Biotite and chlorite

Biotite is commonly present in metamorphosed mafic rocks, but not many data are available on its chemical variation. Phillips (1930) stated that biotite from the Dalradian Green Bed group changes from a

green to a red-brown color as metamorphic grade increases from the chlorite to the garnet zone. Low grade biotite was found to be rich in ferric iron, and he assumed the color change with advancing grade is due to increased $FeO/(FeO+Fe_2O_3)$. Contradictorily, Wiseman (1934) found both green and brown biotite in Dalradian epidiorite from the chlorite and biotite zones. Cooper (1972) observed no well-defined relationship between metamorphic grade and biotite composition in mafic rocks from New Zealand. He did see a correlation between biotite and bulk rock compositions.

In biotite from rocks of compositions other than mafic, the color change from green to brown with advancing metamorphic grade has been commonly observed. Miyashiro (1958) ascribed this color change to increasing Ti content. Engel and Engel (1960) proposed that TiO_2/FeO increased. Crystal chemical investigations by Robbins and Strens (1972) confirmed the hypothesis that TiO_2 is responsible for the brown color in biotite. Fe^{2+} and Fe^{3+} are present in both green and brown biotite. The Ti content of biotite may therefore be sensitive to metamorphic grade.

As yet, no detailed studies have examined the relationship between chlorite composition in mafic rocks and metamorphic grade. Albee (1962) showed that chlorite chemistry is quite dependent upon bulk rock composition, especially Fe/(Mg+Fe). However, in rocks of the same composition, the Al^{VI}, Al^{IV}, and Ti contents of chlorite are potentially sensitive to pressure and temperature; and they will be examined in the mafic rocks from Vermont and southern Quebec.

H. Conclusion

Basaltic composition rocks have a constant mineral assemblage throughout much of pressure-temperature space. This constant paragenesis allows the chemistry of individual minerals to be studied as a function of metamorphic grade. Data from the literature show that in mafic rocks amphibole and plagioclase compositions are sensitive to metamorphic grade and facies series. White mica composition has also been used as a geothermometer and a geobarometer. As long as white mica chemistry is compared in rocks with the same assemblage, it can be used to estimate the physical conditions of metamorphism.

Coexisting Ca- and (Fe, Mg)-rich carbonate in rocks with the common mineral assemblage may also be used as a geothermometer. Investigations have not delineated the phase relationships of epidote, biotite, or chlorite well enough for these common mafic rock minerals to be as useful in determining the physical conditions of metamorphism.

CHAPTER IV

GEOLOGY, MINERALOGY, AND PHASE CHEMISTRY

OF INVESTIGATED AREAS

A. Introduction

In this chapter the petrographic and electron microprobe data for nine investigated areas are presented. Each of five formations comprise a study area in northern Vermont and southern Quebec: the Pinnacle, Underhill, Hazens Notch, Pinney Hollow, and Stowe Formations. Northeastern Vermont is considered a single study area. Southeastern Vermont is divided into three study areas by geography: the Saxtons River, Woodstock, and Wilmington quadrangles. For each area the data presentation is prefaced by an outline of the geologic setting. Mineral assemblages and phase chemistry are then discussed.

Figure I-2 provides the names of the topographic quadrangles from which samples were studied. The locations of those rocks that have been chosen for detailed investigation of phase composition are in figure I-1. The exact sample localities are given in the appendix along with rock descriptions and estimated modes. Complete chemical analyses of all the phases in these 60 samples were obtained with the electron microprobe, and the data can be obtained from Laird or Albee. These analyses are shown on several variation diagrams in this chapter. Where possible, particular attention is given to changes in mineral composition as a function of the metamorphic grade defined by interlayered pelitic rocks.

B. Pinnacle Formation

Geologic setting

The first area includes rocks from the Lower Cambrian Pinnacle Formation and is the only one with samples from Quebec. This formation crops out to the west of the Green-Sutton Mountains anticlinorium axis. Geologic maps for the area have been published by Christman (1959), Dennis (1964), Eakins (1964), and Osberg (1965).

The metamorphic grade in this area is low. It is in the biotite zone on the state map (Doll and others, 1961), and in Quebec Osberg (1965) mapped it as chlorite grade. Rickard (1965) measured a 420 ± 30 m.y. K/Ar age on muscovite from Pinnacle Formation graywacke near Sutton, Quebec. He proposed that this age dated the Taconic orogeny and recognized three phases of deformation. Cady (1969, p. 104) proposed that this age is a hybrid reflecting a Devonian overprint.

The Pinnacle Formation is composed primarily of metamorphosed graywacke and volcanic rocks. The Tibbit Hill Volcanic Member includes massive to schistose greenstone and amygdaloidal layers. Volcanic protoliths are indicated by pillow structures (identified by Dennis, 1964), vescicular layers, and porphyritic layers (noted in Christman, 1959). Many layers may be metamorphosed tuffs as is suggested by the presence of intercalated metasediments, and Dennis (1964) described cross-bedding in a greenstone outcrop. Basaltic, andesitic, and rhyolitic compositions are reported by Cady (1969), Pieratti (1976), and Osberg (1965).

Paragenesis

The mineral assemblage common to the Pinnacle Formation rocks not mapped as the Tibbit Hill Volcanic Member is chlorite-plagioclase-quartz-white mica-alkali feldspar-sphene. Carbonate, epidote, biotite, stilpnomelane, magnetite, and pyrite also occur. The typical assemblage in the Tibbit Hill Volcanic Member is amphibole-chlorite-epidote-plagioclase-quartz-carbonate-sphene-K mica (either biotite or white mica)-Fe^{3+} oxide (either hematite or magnetite)-chalcopyrite and/or pyrite. Stilpnomelane occurs in a few localities in the Mount Mansfield quadrangle. The more mafic rocks are green, while the felsic ones are gray.

Phase chemistry

Amphibole

The largest amphibole grains commonly have cores and rims with different pleochroic formulas. Plate 1a shows three grains with darker blue-green cores than rims; epidote grains are at the color discontinuities. Commonly the core/rim contact is optically sharp and the cores volumetrically larger than the rims. In most samples just two domains are observed, but more complexly zoned grains occur in Q3C. Colorless inner cores are surrounded by pale brown to dark blue-green pleochroic zones which in turn are overgrown by colorless to pale blue-green pleochroic rims.

The electron microprobe data are plotted in figure 1. Optically distinct domains are distinguished, and core to rim zoning arrows are delineated where they are known. Clearly, the color differences manifest major chemical variations. Dark cores in Q3C show more riebeckite

substitution than the light-colored rims, and the glaucophane substitution is greater in the LA426 cores than rims. The colorless, innermost cores of Q3C are more actinolitic than any of the other amphibole analyses in this sample. K, Ti, Al^{IV}, Fe^{3+}, and Na^{M4} are less and Si, Ca, and Mg are greater. The reversal in the zoning arrows delineated in figure 1 reflects the fact that the outermost rims have compositions intermediate to the two cores. Asbestiform amphibole has a composition similar to the outer edge of the dark, barroisite-rich cores.

Amphibole in LA434A and 435A is optically continuous with colorless to light blue-green pleochroism. The glaucophane/riebeckite coupled substitution primarily describes the chemical variation shown on figure 1. A coarse-grained epidote vein which cuts sample LA434A contains asbestiform amphibole mats which are less aluminous and have less Na/(Ca+Na) than the host rock amphibole; Na^A is greater.

Amphibole occurs as porphyroblasts in LA460B with dark green and colorless areas. The contacts between light and dark areas are sharp, but no overgrowth relationship is observed. The porphyroblasts are sheared and altered to chlorite, and the light-colored domains are adjacent to these sheared areas or at grain edges. They therefore probably represent later growth than the dark areas. As shown on figure 1, the light domains are depleted in K, Al^{VI}, Al^{IV}, Fe^{3+}, and Na but enriched in Ca, Fe^{2+}, and Si. They are more actinolitic than the dark domains.

Comparison of LA460B amphibole on figure 1 with that in the other Tibbit Hill Volcanic Member samples studied shows that the tschermakite substitution predominates and that the glaucophane/riebeckite substitution is much less in LA460B amphibole.

Mica

Biotite is a major phase in LA433C and a trace constitutent in
LA426. The electron microprobe analyses plotted in figure 2a show that
Al^{VI} exceeds the quantity (1-formula proportion Al^{IV}). This relationship
and the fact that all the analyses have total positive charges over 22
indicate that the normalization factor is too large and that some dioc-
tahedral substitution must exist. The brown-green biotite from LA433C
(which is a graywacke) is more Ti and Fe/(Fe+Mg) rich than the brown
biotite in the greenstone sample LA426.

Three K white mica analyses from LA433C show significant phengite
substitution as is indicated on figure 2b. These analyses are on acicular
grain bundles which define a rude foliation. The other analysis shown on
figure 2b is much less phengitic and is of a coarse grain in LA433C.
The fine-grained white mica is less paragonitic and has more Ti. The
estimated Fe^{3+} is also greater (0.24 - 0.28) than that in the coarse
white mica (0.01) as is indicated by the fact that (Fe_{Total}+Mg+Mn+Zn) is
much greater than Al^{IV}.

Chlorite

As is shown on figure 3 chlorite from the Pinnacle Formation shows
major chemical variations in Al and Mg/(Mg+Fe^{2+}). No correlation between
composition and grain orientation or mineralogical environment is recog-
nized to explain the Al variation in LA435A chlorite. In LA426 all the
chlorite grains analyzed appear to have formed before the slip cleavage;
the analysis with the lowest Al has a low total and may be erroneous.
Those LA460B chlorite grains which appear to be alteration products of

amphibole porphyroblasts are perhaps less aluminous than matrix chlorite. No difference between epidote vein and host chlorite in LA434A is observed. Ti, Al^{VI}, and Al^{IV} are similar for all analyses; and relative to the total iron, Fe^{3+} is small (0.3 formula proportion Fe^{3+} in LA434A vein chlorite is the maximum). $Fe^{3+}/(Mg+Fe)$ is no greater than 0.061; $Mg/(Mg+Fe^{2+})$ shows little intrasample variation, but the intersample variation is significant.

Stilpnomelane

Stilpnomelane occurs in both metagraywacke and metavolcanic layers in the Pinnacle Formation as acicular grains with pale yellow-brown to red-brown pleochroism. It is commonly associated with alkali feldspar in the graywacke. LA433C stilpnomelane was analyzed with the electron microprobe and has the average formula

$$(H_{7.3}K_{0.4}Na_{0.2}Ba_{0.1})(Fe_{31.4}Mg_{13.4}Mn_{1.3}Al^{VI}_{1.8})(Si_{63.9}Al^{IV}_{8.1})O_{170}(OH)_{46} \cdot$$
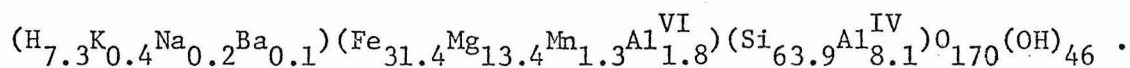
The chemical variation is small.

Epidote

All the electron microprobe analyses of epidote approach stoichiometry. Mn substitutes for Ca up to 0.06 formula proportion, Fe^{2+} is at most 0.05, and Ce is negligible. Ti substitution in the six-fold position is usually less than 0.01 formula proportion. Histograms in figure 4 show that LA460B epidote is much less ferric iron rich than that from the other samples, and the $Fe^{3+}/(Al^{VI}+Fe^{3+})$ variation observed within each sample is significant. A few epidote grains in LA426 and LA460B have optically distinct yellow cores and colorless rims, and the cores are richer in Fe^{3+}. Coarse grains in an epidote-rich vein in LA434A also

have bright yellow, iron-rich and light yellow, more aluminous domains; but no core/rim relationship is observed. Similar irregularly zoned epidote fills amygdules in Q3C.

Feldspar

As shown on figure 5, albite is observed in all the anlayzed samples from the Pinnacle Formation. In the mafic rocks (all samples but LA433C), the maximum anorthite and orthoclase components are 2.2 and 0.6%, respectively. Radiating bundles of plagioclase in amygdules and polysynthetically twinned matrix grains in LA435A are more anorthitic than the untwinned, more equant matrix and amygdule grains.

Detrital and metamorphic plagioclase in LA433C range from $An_{0.3}$ to $An_{5.8}$ as is shown on figure 5, and the maximum orthoclase component is 1.0%. Exsolution of the detrital alkali feldspar into patch and string perthite domains has occurred. The patches are albite with less than 0.5 molecular percent orthoclase. One analysis from within a more potassic, perthitic area is $Or_{34.6}$. Two other analyses, $Or_{16.0}$ and $Or_{18.5}$, appear to be a mixture of the two texturally different domains.

Carbonate, sphene, and Fe oxides

Calcite occurs in Q3C, LA426, LA460B, and in the coarse-grained epidote vein which cuts LA434A. Very little compositional variation is shown by the electron microprobe analyses in figure 6b. The largest ankerite component is about 6 molecular percent (in LA460B).

Sphene occurs in subhedral aggregates with an alteration film of leucoxene. Electron microprobe analyses show that these aggregates are indeed sphene, $Ca_{1.0}(Ti, Al, Fe)_{1.0}Si_{1.0}(O, OH, F)_{5.0}$. The primary

chemical variation is in the Ti-site. As is indicated in figure 6a, Al and (Fe+Mg) substitute for Ti up to 23.1% and 5.3%, respectively. These substitutions are balanced primarily by F, and the maximum formula proportion of F is 0.16 (in LA433C). The maximum OH needed to maintain charge balance is 0.13 formula proportion if all the iron is ferrous and 0.11 if the iron is ferric.

Magnetite in LA433C is $Fe^{2+}_{.99}(Zn,Mn)_{.01}Fe^{3+}_{1.99}Si_{.01}O_3$, and LA434A hematite is $Fe^{3+}_{1.93}Fe^{2+}_{.03}Ti_{.03}Si_{.01}O_3$.

C. Underhill Formation

Geologic setting

The Lower Cambrian Underhill Formation lies directly above, but may interfinger in part with, the Pinnacle Formation. Samples from this formation were collected west of the Green Mountain anticlinorium in the Camels Hump and Lincoln Mountain quadrangles (figures I-1 and 2). These quadrangles have been mapped by Christman and Secor (1961) and Cady, Albee, and Murphy (1962). Garnet, biotite, and perhaps chlorite grade pelitic rocks are interlayered with mafic rocks (the Greenstone Member) in this study area. In the low grades pelitic phyllite and metagraywacke occur; at higher grades pelitic schist predominates. Christman and Secor (1961) proposed that the mafic layers are metamorphosed lavas, but Cady and others (1962) implied that the protolith was epiclastic. No primary volcanic features have been observed, and the mafic layers are volumetrically very small compared to the intercalated metasedimentary rocks. The unequivocal assignment of the Underhill Greenstone to a lava flow protolith is unwarranted.

Harper (1968) obtained a 393 m.y. K/Ar age on muscovite from the
low grade Underhill Formation south of station LA430. He proposed
that this is a postmetamorphic cooling age subsequent to a recrystal-
lization event at least 439 m.y. ago. Dennis (1968) suggested that
Acadian overprinting of, rather than cooling after, the Taconic event
resulted in argon loss and the Devonian ages in this region. He demon-
strated that Harper's data must define a post-Silurian metamorphic
event about 345 m.y. ago. Marvin Lanphere (written communication, 1975)
measured K/Ar and $^{40}Ar/^{39}Ar$ total fusion ages on biotite and muscovite
from the kyanite-chloritoid zone 2 3/4 miles S-SE of V340. One age is
359 m.y.; the others are between 375 and 378 m.y.

Paragenesis

Petrographic examination of the samples collected from the Camels
Hump quadrangle shows that chlorite is the only diagnostic phase in the
pelitic layers. However, biotite, stilpnomelane, and chlorite are ob-
served with quartz and white mica in the metagraywacke layers. The
intercalated mafic rocks are thus probably biotite grade. The two
sampled localities in the Lincoln Mountain quadrangle are in the garnet
zone. Although Cady and others (1962) map the amphibolite layer west
of Appalachian Gap (V225) just below the garnet isograd, a new roadcut
has exposed biotite-chlorite-garnet pelitic schist at this locality.
Samples collected west of Lincoln Gap (V340) include chlorite-chloritoid-
garnet pelitic schist.

The mineral assemblage commonly observed in both biotite and garnet
grade mafic rocks is: amphibole-biotite-carbonate-chlorite-epidote-

plagioclase-quartz. Two mineralogical differences are observed. Stilpnomelane occurs in some rocks below the garnet isograd but is absent above it. Sphene is ubiquitous in the biotite zone; ilmenite is usually the Ti-rich phase in the garnet zone. Alkali feldspar is observed in some samples in both grades, and biotite-absent samples in the garnet zone contain white mica.

Although the mineralogy is similar, biotite and garnet grade mafic rocks look quite different. The low grade rocks are green and fine grained, while the higher grade rocks are gray and medium grained. Mineral composition is also distinct in the mafic rocks from the two metamorphic grades.

Phase chemistry

Amphibole

Indicted in figure 7 are the electron microprobe analyses of amphibole grains from two biotite grade Underhill Formation Greenstone samples. Actinolite occurs in LA504B, and actinolite to actinolitic hornblende is observed in LA430B. The glaucophane/riebeckite and tschermakite substitutions predominantly describe the observed chemical variations. Two amphibole analyses in LA430B show more edenite substitution and are anomalous.

Grain morphology obscures the significance of the chemical variation in LA504B amphibole. Zoning profiles could not be obtained on the asbestiform amphibole mats or the acicular grains in the epidote vein which cuts this sample, and the data are ambiguous for host rock grains. No correlation is observed between amphibole compositional variation

and mineral assemblage (see the appendix for the estimated modes of each layer in this rock). "Poikiloblasts" are formed by optically continuous, pale green to blue-green to green pleochroic clusters of elongated or prismatic grains. They tend to have K, Ti, Al^{IV}, Na^{M4}, and Fe^{3+} richer and Si, Ca, and Mg poorer interiors. Some coarse grains zone toward more actinolitic edges while others become more hornblendic. Finer grains tend to be enriched in actinolite. The growth direction is probably toward actinolite-rich compositions as is indicated on figure 7.

The observed compositional variations in LA430B amphibole are more readily explained. Porphyroblasts with pale brown to blue-green to green pleochroic cores and colorless to light blue-green pleochroic rims occur. Plate 1b shows the typical abrupt contact between the dark core and light rim (which is slightly darker toward the edge of the grain). Although core and rim extinguish simultaneously, the rim is composed of several prismatic grains which are oriented perpendicular to the core/rim boundary and which get darker away from the contact. Prismatic and acicular amphibole grains are present in the matrix, and some of the larger grains are optically zoned like the grains forming the porphyroblast rims. Colorless to pale blue-green pleochroic cores are overgrown by pale brown to blue to green pleochroic rims. Porphyroblast and matrix grain compositions are distinguished on figure 7 as are cores and rims. Porphyroblast cores zone toward actinolite, and matrix grains show the reverse trend from core to rim. Two of the matrix grain rim analyses have a significant edenite component.

Hornblende occurs in the garnet grade mafic samples, and the analyses are plotted in figure 8. Optically uniform, pale brown to green-blue to green pleochroic amphibole grains in V340B are continuously zoned toward more hornblende-rich compositions at their margins. A more complex zoning pattern is exhibited by V225B amphibole. The general trend is for rims to have more edenite and tschermakite solid solution, but the cores show a zoning reversal in Ti, Al^{VI}, $Na/(Ca+Na)$, and $Mg/(Mg+Fe)$.

The observed chemical variation in V225B amphibole is only partially manifested optically. All but the smallest grains have a somewhat lighter colored, narrow rim on a pale brown to green-blue to green pleochroic core. These rims have the edenite-rich compositions shown on figure 8. Several porphyroblasts have a lighter colored core interior to the dark one. These innermost cores are richer in Al^{VI}, Ti, $Mg/(Mg+Fe)$, and $Na/(Ca+Na)$ than the dark cores adjacent to them. No correlation between composition and grain orientation is observed. The larger porphyroblasts are elongate parallel to the foliation; whereas, many of the smaller porphyroblasts are not. Both have dark cores more actinolitic than the light rims. The only difference seems to be that the cores of the smaller porphyroblasts tend to have somewhat greater Al^{IV} contents.

The composition envelopes for amphibole from all four Underhill Greenstone samples are delineated in figure 9. As indicated by the intercalated pelitic rocks, LA430B and 504B are from the biotite zone, while V225B and 340B are from the garnet zone. With increasing

metamorphic grade, amphibole is enriched in K, Ti, Al^{VI}, Al^{IV}, Na/(Ca+Na), and Fe/(Mg+Fe). The actinolite to hornblende transition occurs between the biotite and garnet zones. The plagioclase in all four samples is albite, and the albite-oligoclase transition must occur at a higher grade.

Biotite

Biotite in LA504B has pale brown to olive-green pleochroism; it is pale to dark brown in the other samples. The electron microprobe data plotted in figure 10 show that Ti is lower in the green biotite than in the brown. Ti, Mn, and Al^{IV} appear to be a function of metamorphic grade, and the garnet zone biotite is richer in Ti and Al^{IV} but poorer in Mn than that in the biotite zone. Most analyses have Al^{VI} in excess of $(1-Al^{IV})$. The positive charge totals greater than 22, and dioctahedral substitution must be significant. Vein biotite in LA504B may have less Al^{VI} than that in the transition zone.

Chlorite

Chlorite is a major constituent of all the samples analyzed from the Underhill Greenstone. The electron microprobe analyses in figure 11 show that Ti, Al^{VI}, and Al^{IV} increase with metamorphic grade. All but one analysis have Al^{IV} in excess of Al^{VI} indicating octahedral Fe^{3+} substitution. The maximum formula proportion calculated for Fe^{3+} is 0.14, and Fe^{3+}/(Mg+Fe) is never greater than 3.0%.

Stilpnomelane

Acicular, brown stilpnomelane is observed in both biotite grade graywacke and mafic layers. It typically occurs in clusters with

individual grains distinguished only in reflected light. The chemical variation for stilpnomelane in LA504B is delineated in figure 12. A crude, negative correlation between Al and Mg/(Mg+Fe) is observed, and bulk composition appears to be correlated with the composition of stilp-nomelane. The epidote-absent amphibolite layer (see the appendix for the rock description) has the least Al^{VI}- and Al^{IV}-rich stilpnomelane. The alkali content is quite variable, but no obvious correlation exists with mineral assemblage. All but three analyses require H to compensate the charge deficiency caused by $Al^{IV} \rightleftarrows Si$. The analysis with no cal-culated Al^{VI} and the maximum Al^{IV} is on a tiny grain and may be erroneous. For the other analyses the maximum calculated formula proportion of H is 5.9, and OH ranges between 45.9 and 52.5.

Epidote

The clinozoisite content is quite variable within and among epidote grains, but as shown in figure 13 no relationship between epidote com-position and metamorphic grade is observed. Only in LA504B can the chemical variation be correlated with mineral growth. Within the host rock many epidote grains have colorless to yellow pleochroic cores which are richer in Fe^{3+} than the colorless rims. Coarse grains within the epidote vein exhibit multiple concentric zones with the yellowest ones the most Fe^{3+} rich. The zoning trend from the core to the contact between the outermost rim and first interior zone is toward more Fe^{3+} composition. The outermost rim is Al rich.

Very little variation in Ca, Mn, Ti, or Si is observed in the Un-derhill Greenstone epidote; analyses approach $Ca_2(Al^{VI}, Fe^{3+})_3Si_3O_{12}(OH)$.

Mn and Fe^{2+} replace Ca up to 0.03 formula proportion each, and Ce is negligible. The formula proportion of Ti is less than 0.02.

Feldspar

As shown in figure 14 the maximum anorthite component observed in the plagioclase is 1.2%, and mole percent orthoclase is less than 0.7. Plagioclase grains are generally about 50 µm across in the Underhill Greenstone, precluding detailed zoning profiles. The arrow delineating zoning toward more anorthitic compositions in V340B is for plagioclase poikiloblasts.

Orthoclase and albite-orthoclase perthite occur in LA504B. In the orthoclase celsian comprises up to 2.3 molecular percent (the end members Ab, An, Or, and Cs have been calculated for these analyses). The anorthoclase compositions plotted in figure 14 are of inclusions in amphibole "poikiloblasts" and may include albite and orthoclase domains.

Carbonate

The carbonate analyses plotted in figure 15 suggest that calcite becomes more ankeritic with metamorphic grade. Calcite from V340B shows the most ankerite solid solution, and dolomite also occurs in this sample. The dolomite has more Mg and Mn than the coexisting calcite, and brown alteration along grain boundaries distinguishes the dolomite optically.

Sphene

Sphene occurs in the biotite zone samples both as coarse, anhedral masses altered to leucoxene and as euhedral grains included in amphibole.

In LA504B the euhedral grains are slightly more aluminous. All the analyses have the stoichiometric Ca and Si contents; negligible Mn and Ce are detected. Figure 16a shows the minor Al and (Fe+Mg) replacement of Ti. The maximum amount of fluorine analyzed is 0.04 formula proportion. If all the iron is trivalent, the calculated OH is 0.10 formula proportion; it is 0.12 if the iron is divalent.

Sphene is conspicuously absent in the garnet grade mafic rocks. It is observed in V225B but only as inclusions in amphibole.

Fe, Ti oxides

Trace hematite in LA504B has the formula $Fe^{3+}_{1.93}Fe^{2+}_{.01}Ti_{.01}Al_{.02}Si_{.02}O_3$. Significant $(Mn+Mg)TiO_3$ occurs in ilmenite from the garnet grade samples as is indicated on figure 16b. Up to 3.6 molecular percent $MnTiO_3$ occurs in V225B ilmentite, and 1.4% is the maximum in V340B. $MgTiO_3$ in V340B ilmenite is as great as 1.0%, and a maximum of 0.5% is present in the V225B analyses. Zn is negligible. The zoning arrow delineated on figure 16b indicates that V340B ilmenite grain interiors appear to be richer in hematite than their exteriors and V225B ilmenite.

D. Hazens Notch Formation

Geologic setting

The Cambrian Hazens Notch Formation crops out in the northern half of Vermont and is the oldest unit confined to and east of the Green Mountain anticlinorium. Mafic and interlayered pelitic schists from the upper Missisquoi Valley region have been studied in detail. A reconnaissance investigation of this unit at the southern edge of the Lincoln Mountain quadrangle has also been effected. Geologic maps for

these subareas have been published by Cady, Albee, and Chidester (1963) and Cady and others (1962).

Much of the Hazens Notch Formation is considered to be within the biotite zone by Doll and others (1961). Cady and others (1963) delimited a hornblende isograd in the Missisquoi Valley region which separates greenschist from epidote-amphibolite facies rocks, and which is transformed into a garnet isograd on the state map (Doll and others, 1961). They suggested that in the vicinity of the Belvidere Mountain ultramafic body (figure I-2) retrogradation has masked an earlier, more widespread garnet grade metamorphism.

The upper Missisquoi Valley region is one of the few places in Vermont where large scale east-west structures are observed. Anderson (1977) considered them Ordovician. Cady and others (1963) suggested that they, along with the metamorphism, are Middle Devonian. Radiometric dating by Harper (1968) indicates Late Ordovician-Early Silurian recrystallization. He obtained a 439 m.y. K/Ar age on muscovite just southeast of Hazens Notch. Near Jay Peak and east of the Green Mountain anticlinorium axis, muscovite from the Hazens Notch Formation gave a 423 m.y. K/Ar age which he interpreted to represent the time of metamorphic recrystallization and to correlate with the Taconic distrubance in southwestern Vermont and adjacent New York. Renewed deformation and /or local recrystallization is the suggested cause for a 384 m.y. age Harper (1968) measured west of the Green Mountain anticlinorium axis in this area.

Important to the geologic setting in the upper Missisquoi Valley are the ultramafic rocks. They are considered Late Ordovician by Cady

and others (1963) and to have been emplaced considerably below their magmatic temperatures. These ultramafic rocks are part of a generally north-south trending belt from Massachusetts, through Vermont, and into Quebec. Chidester and Cady (1972) proposed that the ultramafic bodies were intruded through predominantly continental crust.

Chemical analyses reported by Cady (1969, table 4, analyses 2-9) indicate that the Hazens Notch Formation mafic rocks in the upper Missisquoi Valley have tholeiitic affinities. Cady and others (1963) asserted that the protolith is volcanic; Albee (1957) proposed that the parent of the Belvidere Mountain Amphibolite Member is water-laid volcanic detritus. As no primary volcanic features have been found and metasedimentary interlayers are common, an epiclastic origin seems plausible.

Paragenesis

As observed by Cady and others (1963), the Belvidere Mountain Amphibolite Member of the Hazens Notch Formation is finer grained and lighter green below the hornblende isograd than above it. However, the mineralogy is the same: amphibole-chlorite-epidote-plagioclase-sphene± biotite, carbonate, and quartz. Garnet is observed in the higher grade rocks only, and chlorite in garnet-bearing rocks seems to be an alteration product of garnet and perhaps amphibole. Magnetite and sphene commonly occur in the low grade rocks; rutile and ilmenite are more common above the hornblende isograd. Acicular to prismatic amphibole with colorless to light blue-green pleochroism occurs in low grade rocks, and a few of the largest grains have darker cores than rims. The higher grade

amphibole on top of Belvidere Mountain is coarse grained and optically zoned. Cores have the pleochroic scheme: pale brown to gray blue to brown green. Rims are colorless to light blue to gray blue. Biotite from rocks south of the hornblende isograd is brown green. Near the isograd on the east and within the higher grade zone, biotite is brown.

Figure 17 is taken from Cady and others (1963) and shows the geology and outcrops sampled in the vicinity of Tillotson Peak just north of Belvidere Mountain (figure I-2). As reported by Laird and Albee (1975), the paragenesis in the trilobite-shaped exposure is unique in the eastern United States. Sodic amphibole occurs throughout the exposure, and omphacite is observed in the southern half. The rest of the assemblage is more mundane and is similar to the Belvidere Mountain Amphibolite elsewhere. Epidote and sphene are omnipresent, and Ca-rich amphibole, carbonate, chlorite, plagioclase, garnet, magnetite, quartz, and white mica occur in many samples. Biotite is rare. Pelitic interlayers exhibit the diagnostic assemblages biotite-chlorite and chlorite-garnet.

Glaucophane is conspicuously absent from all but one sample of the Hazens Notch lower amphibolite unit (Cha on figure 17). No omphacite is observed in this unit, and the common rock type is amphibole-chlorite-epidote-plagioclase-garnet-quartz-sphene greenstone to greenschist.

With the exclusion of the glaucophane, omphacite, and garnet assemblages, the mafic layers in the Hazens Notch Formation which crop out in the Lincoln Mountain quadrangle are mineralogically identical to

those in the Missisquoi Valley vicinity. The rocks are green gray amphibole-chlorite-epidote-plagioclase-quartz-sphene schist. Biotite, carbonate, magnetite, and white mica are other observed phases. Intercalated pelitic schist is not diagnostic of metamorphic grade as only chlorite assemblages are observed.

None of the phases in the Lincoln Mountain quadrangle, Hazens Notch Formation samples has been analyzed with the electron microprobe. Doolan, Drake, and Crocker (1973) reported formulas for a calcic and a soda-calcic amphibole from the mafic layer southwest of Warren. They observed (10$\bar{1}$) exsolution lamellae, patchy intergrowths, and zonal structures. In the samples I collected from this area, mottled amphibole grains with dark and light domains plus areas altered to chlorite and biotite occur, but no exsolution lamellae are observed. Some amphibole porphyroblasts have green-blue to green pleochroic, euhedral cores and ligher rims, and sharp contacts separate cores from rims.

Most of the amphibole in the Hazens Notch Formation mafic layers in the Lincoln Mountain quadrangle is acicular to rectangular and has colorless to light green-blue pleochroism. Mafic layers near Kew Hill are close to the garnet isograd, and the amphibole here is darker and more gray blue than that in the amphibolite layers to the south (which are further from the garnet isograd).

The extraordinary phase assemblages observed in the Belvidere Mountain Amphibolite warrant detailed examination. Seven samples were chosen for electron microprobe investigation, and the analytical data are presented in the following section.

Phase chemistry

Amphibole

Of the analyzed samples from the Belvidere Mountain Amphibolite, two contain Ca- and Na-rich amphibole, four have sodic amphibole only, and one has just soda-calcic amphibole. This last sample is from Belvidere Mountain, and the rest are from the vicinity of Tillotson Peak. Diagrams showing the chemical variation in sodic amphibole from the rocks without Ca-rich amphibole are presented in figure 18. In all the analyses the A-site is nearly empty, and the majority have $Al^{VI}/(Al^{VI}+Fe^{3+}+Ti+Cr)$ > 0.7; they are true glaucophane.

Glaucophane in most of the samples from Tillotson Peak is not the intense blue color that is usually associated with this phase. The pleochroic formula is generally colorless to light blue to lavender. Some grains as is shown in plate 1c are optically zoned with darker interiors. Electron microprobe analyses indicate that the color intensity is correlated with the riebeckite substitution. As is shown in figure 18d, dark areas in V337B glaucophane are Fe^{3+} richer and Fe^{2+} poorer than the light domains, but $Mg/(Mg+Fe)$ is equivalent. Figure 18a indicates that the dark domains are depleted in Al^{VI}. No variation between the two domains is observed in K, Ti, Na^{A}, or Na^{M4} (figures 18a and c). The dashed envelopes in figures 18a-c delimit the other glaucophane analyses from Tillotson Peak; those from V337B have more Na^{M4} and $(Al^{VI}+Fe^{3+}+Ti+Cr)$ but tend to have less Al^{VI}.

No optical zoning is observed in glaucophane from the other samples, but V380C glaucophane is chemically zoned. Al^{VI}, Si, Na^{M4}, and Fe^{2+}

decrease while Al^{IV}, Ca, and Fe^{3+} increase toward grain edges. One porphyroblast shows a reversal in this trend at the edge as is indicated by the zoning arrows in figure 18. K, Ti, and Mg/(Mg+Fe) remain constant. A well-defined zoning pattern is not observed, but the data suggest that in V383B glaucophane Al^{VI}, Si, and Na^{M4} decrease toward grain edges and Al^{IV} and Ca increase.

Glaucophane inclusions in sheared garnet poikiloblasts in A-BM-99 are distinguished from the other glaucophane at Tillotson Peak only in a smaller Mg/(Mg+Fe) value. No glaucophane is observed outside of garnet in this sample.

In two of the analyzed samples from the Belvidere Mountain Amphibolite, V337A and A-BM-100, both Ca- and Na-rich amphibole occur, and the electron microprobe analyses are plotted in figure 19. Separate grains of colorless to pale blue-green to pale green pleochroic actionolite and of colorless to pale blue to lavender pleochroic glaucophane occur in V337A. The grains are optically continuous but show chemical zoning. As delineated by the arrows on figure 19 for the V337A actinolite grains, Al^{IV}, Ti, Al^{VI}, Na^{A}, Na^{M4}, and Fe^{3+} increase toward grain edges while Si, Ca, and Fe^{2+} decrease. With metamorphic grain growth the glaucophane/riebeckite and tschermakite substitutions increase. Glaucophane grain edges in V337A have more riebeckite solid solution than their interiors (figures 19b and f). Mg/(Mg+Fe) and Mg/(Mg+Fe^{2+}) are less in the glaucophane, but the formula proportions of K and Ti are equivalent (figure 19a).

Calcic, soda-calcic, and sodic amphiboles occur in A-BM-100, and complexly zoned grains are common. Often the zoning is concentric with

as many as three optically distinct domains. Plate 1d shows one such elegantly zoned grain. The innermost core (zone 1) displays pale yellow-brown to blue-green pleochroism; it is surrounded by a colorless to lavender pleochroic rim (zone 2), which has been overgrown by a final rim (zone 3) with faint yellow-brown to light green pleochroism. Amphibole grains with two optically distinct zones are more common, and the observed core to rim sequences are: 1 to 2, 1 to 3, and 2 to 3. A Becke line often demarcates the color discontinuity. Optically continuous grains of domains 2 and 3 are present, but unrimmed zone 1 grains are observed only as inclusions in garnet.

In figure 19 the electron microprobe analyses for each optically distinct domain are differentiated. Type 1 amphibole is soda-calcic, closest to the barroisite end member in composition. Type 2 is glaucophane, and type 3 ranges from actinolite to barroisitic actinolite. Wide compositional gaps separate the glaucophane from the actionolite and barroisite; however, a much smaller gap exists between the actinolite and the barroisite fields.

The compositional differences across these complexly zoned grains are examined in plates 2 and 3 and in figures 20-22. A line drawing for an amphibole grain with a dark barroisite core and a light actinolite rim is shown in plate 2. Elemental X-ray traces produced by moving the electron beam across the color discontinuity (electron beam scans) are also presented, and superimposed on the scan is an X-ray intensity plot measured across the middle of the field. Figure 20 illustrates the complete electron microprobe analyses obtained on 4 traverses across

the grain, and the analyzed point locations are indicated on plate 2. Three traverses are across the dark/light color boundary and show, along with the beam scans, that the decrease in color intensity between core and rim is marked by an abrupt change in chemical composition. The barroisite core is richer in FeO_{Total}, Al_2O_3, Na_2O, and TiO_2 but poorer in SiO_2, MgO, and CaO than the lighter actinolite rim. The analysis of point 14 is anomalous. Optically, it does not look like an overlap of the dark and light domains, but it does chemically.

A reversal in the zoning trend of the actinolite rim is indicated by the traverse from point 16 to 10 (plate 2). Between points 16 and 9, as is shown on figure 20, SiO_2, MgO, and CaO increase while FeO_{Total}, Al_2O_3, Na_2O, and TiO_2 decrease. The analysis at the edge of the grain (10) has more FeO_{Total}, Al_2O_3, Na_2O, and TiO_2 than the other analyses and less SiO_2, MgO, and CaO.

On plate 2, scan A a Na- and Al-rich lenticle is delimited at the contact of the actinolite rim with the barroisite core. This feature is glaucophane.

Another type of zoned amphibole grain observed in A-BM-100 is shown in plate 3. The core is barroisite; the rim is glaucophane. The beam scans for Ca and Na show a chemical discontinuity at the core/rim contact as do the complete chemical analyses obtained across this grain (figure 21). The glaucophane rim is richer in SiO_2, Al_2O_3, and Na_2O but has less FeO_{Total}, MgO, CaO, and TiO_2 than the barroisite core. It should be noted that the complete chemical analyses show no decrease

in Ca or Na toward the core interiors. The apparent decrease delineated by the beam scans is probably due to spectrometer defocusing.

Delineated on figure 22 are the tie lines between all the analyzed barroisite-actinolite, barroisite-glaucophane, and glaucophane-actinolite pairs. For the two grains illustrated in plates 2 and 3 and in figures 20 and 21, the analyzed point numbers are indicated. All but one pair (glaucophane-actinolite, grain C2) are in an overgrowth relationship; the composition on the core side of the boundary is indicated by a filled symbol, and the rim side is shown as an open symbol. The tie lines indicate that the position of the composition gap is not consistent within or between grains.

One problem with this hypothesis is that pairs may not accurately represent the boundary compositions. The spot size used was 10 microns, and the core/rim contact is not known in the third dimension. However, a correlation between pairs does exist. The most $(Al^{VI}+Fe^{3+}+Ti+Cr)$-rich barroisite cores are paired with the glaucophane with the most $(Al^{VI}+Fe^{3+}+Ti+Cr)$. A similar relationship appears to be defined by the Al^{IV} contents of the glaucophane- actinolite pairs. Such a consistent correlation supports the proposal that the inter-and intragranular composition gaps are variable.

All the amphibole analyses from A-BM-100 are plotted in figure 19, and the arrows delineate the compositional variation observed toward domain exteriors. Barroisite cores with actinolite rims become more actinolitic towards core/rim contacts. After a gap this zoning trend continues within the actinolite rims until a reversal occurs. The complete

zoning profile occurs in a few grains as is shown in figure 20. Several continuously zoned calcic amphibole grains without barroisite cores show an outward change in composition from actinolite to barroisite, and the edge compositions nearly fill the gaps between the barroisite cores and actinolite rims.

Barroisite cores with glaucophane rims are nearly homogeneous, but they may get more actinolitic toward the core/rim contact (figure 21). Glaucophane cores with actinolite rims zone toward Si, Al^{VI}, Na^{M4}, Fe^{3+} poorer but K, Ti, Al^{IV}, and Ca richer compositions (figures 19a, b, e, and f). In contradistinction, rims and optically continuous grains zone outward to Si, Al^{VI}, and Na^{M4} greater but K, Ti, Al^{IV}, and Ca poorer compositions.

All the amphibole in A-BM-100 exhibits extensive glaucophane/riebeckite substitution. The calcic to soda-calcic amphibole transition is primarily effected by the tschermakite substitution, but some edenite replacement also occurs.

No glaucophane is observed on Belvidere Mountain, but soda-calcic amphibole is. Poikiloblastic grains in V360B are discontinuously zoned with pale brown to gray-blue to brown-green pleochroic cores and colorless to light blue to gray-blue pleochroic rims. A Becke line often marks the color boundary, and cores are anhedral to subhedral. Smaller, matrix grains have the same pleochroic formula as the poikiloblastic grain rims. Along grain boundaries and sheared zones, a distinctly blue-green amphibole occurs. The electron microprobe analyses, which are plotted in figure 23, show that these optically distinct domains are also chemically distinct.

Relative to the lighter rims, the cores show more edenite substitution and have a smaller Mg/(Mg+Fe) value. The three analyses of the blue-green domains are less Al^{VI} rich and have smaller Na/(Ca+Na) and Mg/(Mg+Fe) values. The dashed envelopes in figure 23 delimit the barroisite core compositions from A-BM-100. Except for the Fe^{3+}/Fe^{2+} value, (and consequently the Al^{VI} content), rim amphibole at Belvidere Mountain is equivalent to the A-BM-100 barroisite. The cores are more edenite rich.

Omphacite

At Tillotson Peak omphacite is pleochroic from colorless to pale green, and as is illustrated in plate 1e commonly is surrounded by fine-grained, gray, alteration material which seems to be partly plagioclase. The electron microprobe analyses plotted in figure 24 identify the phase as omphacite. Diopside ranges from 35 to 56 molecular percent, jadeite from 29 to 45%, and acmite from 5 to 22%. The sum of Ti and Cr does not exceed 0.01 formula proportion. The size of the plotted triangles in figure 24b indicates the relative amount of $CaAl(AlSi)O_6$, and it is correlated with the acmite substitution.

V383B omphacite has a greater acmite component than that in A-BM-100, and a greater chemical variation is observed. The zoning arrows delineated on figure 24 show that toward grain margins the diopside component increases at the expense of both jadeite and acmite. Mg/(Mg+Fe) increases, but the estimated $Mg/(Mg+Fe^{2+})$ decreases.

Chlorite

Electron microprobe analyses on chlorite from Tillotson Peak show very little intrasample variation. Two intersample differences are apparent

in figure 25. Chlorite in V337B has more Al^{VI} and Al^{IV} than that in the other samples, and $Mg/(Mg+Fe^{2+})$ is less in A-BM-99 chlorite. Most analyses plot below the 1:1 line on the Al^{VI} versus Al^{IV} diagram, indicating the presence of Fe^{3+}, and the estimated Fe^{3+} is less than 0.2 formula proportion.

White mica

Elongated grains of phengite align parallel to the foliation in four of the analyzed samples from Tillotson Peak. Clusters of acicular paragonite also occur in V337B, and are also often at the edges of coarser phengite grains. Figure 26a shows that the paragonite in this sample has less Ti, (Fe+Mg+Mn+Zn), and Si than the K-rich white mica. It also has a minor amount of Ca (Ca/(K+Na+Ca) ranges from 0.004 to 0.011); whereas, few of the phengite analyses show detectable Ca. The dashed envelope encompasses the phengite analyses from the rocks without paragonite (these data are contained in figure 26b) and shows that K/(K+Na+Ca) and Si tend to be less in V337B phengite. All but one white mica analysis requires Fe^{3+} to maintain charge balance as is indicated on figure 26c. Compared to the phengite, paragonite has a smaller Mg/(Mg+Fe) value.

Epidote

Epidote is ubiquitous in the Belvidere Mountain Amphibolite and approaches stoichiometry. Mn substitutes for Ca an average of 0.02 formula proportion in V337B but is less than 0.01 in the other samples (which are carbonate and/or garnet-bearing). The calculated Fe^{2+} is generally less than 0.03 formula proportion, Ce is negligible, and Ti is about 0.05 formula proportion. The histograms of Fe^{3+} content in figure 27 show major intrasample variation which is correlated with grain growth.

Two populations are defined by A-BM-99 epidote. That in the matrix is more clinozoisite rich than the epidote grains included in garnet porphyroblasts. Many grains in A-BM-100 have subhedral cores which are overgrown by rims with lower birefringence, and the cores are more epidote rich. An additional rim occurs in some grains. It is more birefringent and Fe^{3+} rich than the middle zone but less ferric than the innermost core. All zones extinguish simultaneously and are colorless. Some grains without cores visible in crossed Nicols are zoned toward more aluminous compositions; some show the reverse trend.

More highly birefringent cores in V337A, 380C, and 383B are also more epidote rich than the corresponding rims. In the latter sample some of the cores are pleochroic from colorless to yellow ; whereas, the rims and other grains are colorless. One of these cores was analyzed, and it is the most ferric-rich analysis shown on figure 27. A reversal in the zoning arrow is delineated in figure 27 for V380C epidote. Near grain edges the Al-enrichment trend is replaced by an Fe^{3+} increase.

Subhedral cores visible in X-Nicols in V360B are less birefringent and epidote rich than corresponding rims. Three analyses have greater Fe^{3+} contents than most of the analyses from this sample and are from sheared areas. Epidote from V337B is more Fe^{3+} rich than most of the epidote analyses from the other samples. No optical discontinuity is observed, and the grains are pleochroic from colorless to yellow. They appear to be more aluminous at the edge.

Plagioclase

Plagioclase is often absent from the Belvidere Mountain Amphibolite. Where it is present, it is albite as is shown in figure 28. At

Tillotson Peak a maximum of 1.1 molecular percent anorthite and 0.3% orthoclase is observed in the plagioclase. At Belvidere Mountain (V360B) the anorthite content ranges from 1.7 to 2.7% and molecular percent orthoclase is 0.3 to 0.4. Only in V337B plagioclase is a zoning trend discerned; grain margins are enriched in albite.

Fine-grained, gray material which appears to have formed from glaucophane and omphacite (plate 1e) is ubiquitous in the Tillotson Peak samples. Wavelength scans show this material to be primarily Na, Al, and Si, and it may be albite.

Garnet

The electron microprobe analyses for Belvidere Mountain Amphibolite garnet are plotted in figure 29, and profiles across representative grains are delineated in figure 30. Garnet on top of Belvidere Mountain (sample V360B) is more Mg rich than that at Tillotson Peak, and grains show a decrease in Mn with an increase in Mg and Ca toward the rim. At the edge Ca decreases, causing a bend or kink in the zoning arrows delineated in figure 29.

Garnet at Tillotson Peak shows a decrease in spessartine toward grain margins with concomitant increase in almandine, grossular, and usually pyrope. The analyses for A-BM-99 garnet delimit two distinct compositional fields. Rims, low Mn matrix grains, and porphyroblasts have compositions similar to garnet from the other samples. Euhedral matrix grains with Mn-rich cores and inclusions within porphyroblastic amphibole pseudomorphs have grossular-poor compositions. A compositional discontinuity is observed between cores and rims in the matrix grains,

and this is optically manifested (plate 1f). A Becke line separates the cores from the rims in which concentric growth rings can be observed. The kink in the zoning arrow delineated in figure 29a for the WDA analyses is confirmed by EDA zoning profiles illustrated in figure 30b. The decrease in Ca with concomitant increase in Fe at the core/rim boundary may be due to depletion zoning.

Carbonate

Figure 31 shows that calcite occurs in the Belvidere Mountain Amphibolite at Tillotson Peak. In addition, dolomite is observed. V383B contains both carbonate phases, but it is not clear if they coexist. The dolomite is typically subhedral to euhedral with cleavage traces and grain edges marked by yellow-brown stains. Calcite is anhedral to subhedral and shows neither the yellow-brown alteration nor well-developed rhombohedral cleavage.

A-BM-99 calcite grains appear to zone outward to more ankeritic compositions. BaO is negligible in the calcite but occurs in the dolomite up to 0.24 weight percent.

Sphene and Fe, Ti oxides

At Tillotson Peak sphene is subhedral to euhedral; it occurs as rims on rutile and ilmenite cores at Belvidere Mountain. Little deviation from stoichiometry is observed in the electron microprobe analyses, and the formula proportions of Ca and Si are $1.00 \pm .03$. The maximum estimated formula proportion (OH) is 0.12 (all Fe^{2+}) or 0.10 (all Fe^{3+}). F is at most 0.07 formula proportion, and Ce is negligible. Figure 32 shows that the (Fe+Mg) substitution into the Ti position is no greater than 2

atom percent, and the Al replacement ranges from 3 to 7%.

Magnetite, $Fe^{3+}_{2.00}Fe^{2+}_{1.00}O_4$, is nearly ubiquitous at Tillotson

Peak and is a major phase in many rocks. It is absent from the samples

collected from the top of Belvidere Mountain. Ilmenite and rutile occur

in V360B and as inclusions in garnet porphyroblasts in A-BM-99. In the

former sample the two phases are intergrown. Ilmenite in A-BM-99 has

the formula $Fe^{2+}_{.94}Mn_{.03}Fe^{3+}_{.05}Ti_{.97}O_3$.

E. Pinney Hollow Formation

Geologic setting

Intercalated mafic and pelitic rocks occur throughout the Cambrian

Pinney Hollow Formation. In central Vermont samples were collected in

the Lincoln Mountain and Rochester quadrangles. Geologic maps covering

this area have been published by Cady and others (1962) and Osberg (1952),

and the localities from which samples have been studied with the electron

microprobe are annotated in figure I-1. Doll and others (1961) assigned

this area to the biotite zone, but the garnet isograd is a few miles west

as delineated by Cady and others (1962) and Osberg (1952). The metamorphic

age of the Pinney Hollow Formation in this area has not been radiometric-

ally established.

Published reports are noncommital as to the premetamorphic origin

of the Greenstone Member of the Pinney Hollow Formation. The mafic layers

are quite widespread, and in the Rochester quadrangle they are contin-

uous. Compositional layering from millimeter to outcrop scale parallels

the foliation indicating an epiclastic protolith. Pyroclastic layers

may exist near the Hancock Tunnel in the Rochester quadrangle where epidote

porphyroblasts are suggestive of amygdules. The concordant nature of the bedding and schistosity is best observed in two roadcuts in the vicinity of Granville Notch, Lincoln Mountain quadrangle (figure I-2). These roadcuts were sampled in detail; their station numbers are V12 and V14 (figure I-1). The exact locations and rock descriptions plus estimated modes are listed in the appendix.

Paragenesis

In general, the mafic composition rocks in the Pinney Hollow Formation are fine- to medium-grained amphibole-biotite-carbonate-chlorite-plagioclase-quartz-sphene greenstone or greenschist. White mica, magnetite, pyrite, and chalcopyrite often occur, and stilpnomelane is observed in Allbee Brook at Lower Granville in the Rochester quadrangle. Intercalated with the mafic rocks chosen for electron microprobe investigation is biotite-chlorite-plagioclase-quartz-white mica-carbonate schist, which is consistent with biotite grade metamorphism. Garnet-chlorite pelitic layers in Allbee Brook indicate that there has been some garnet grade recrystallization in this area.

Phase chemistry

Amphibole

Fine-grained, prismatic and acicular, colorless to pale blue-green pleochroic amphibole occurs in the greenstone exposed by roadcuts at Granville Notch (V12, 14, and 15). It is often intergrown with chlorite and, because the colors are similar, is most easily distinguished in crossed polarized light. Coarser grains are intergrown with chlorite in concordant quartz-calcite veins. A common feature of the coarser amphibole

grains in the host rock and in veins is that they exhibit optically distinct cores and rims. Plate 5a shows three typical host rock grains. The dark cores have pale brown to dark blue-green to dark brown-green pleochroism, and a Becke line often separates the cores from the rims. Euhedral to anhedral cores occur, and they may or may not extinguish simultaneously with corresponding rims. In the quartz-calcite veins amphibole cores are usually pale blue green and rims are colorless, but the color contrast is not as great as in the optically zoned host rock amphibole. Some grains have a blue-green to green rim exterior to the colorless zone, and a blue-green domain interior to the colorless zone is not always present.

These optical discontinuities manifest chemical discontinuities. Plate 4 shows several elemental X-ray images of electron beam scans across a host rock amphibole grain with a dark core and lighter rim. An anhedral chlorite grain marks the contact in one place. The beam scans indicate a chemical discontinuity at the core/rim contact.

The complete chemical analyses for this grain and the others from the Pinney Hollow Greenstone shown on figures 33-35 also demonstrate that the cores and rims are compositionally distinct. The host rock amphibole cores from the roadcut at station V14 are more barroisitic than corresponding rims and optically continuous grains (figures 34 and 35). Host rock amphibole from the other roadcuts in this area is optically continuous and similiar in composition to the rims and unrimmed grains at V14 (compare figure 33 with 34 and see figure 35).

Vein amphibole from the V14 roadcut is chemically similar to the rim and optically continuous amphibole in the host rock. However, optically

discontinuous grains show reversed zoning from those in the host. As indicated by the arrows in figures 34 and 35, vein amphibole becomes less rather than more actinolitic outward. Vein amphibole grains from V12 and 15 have optically distinct cores which show extensive winchite substitution (especially in V15A); rims are more actinolite rich (figures 33 and 35).

Biotite and chlorite

In general, biotite in the Pinney Hollow Greenstone has pale brown to brown-green pleochroism. V14J biotite is browner and figure 36 shows that it is more Ti and Fe/(Mg+Fe) rich. Since all the analyses have more Al^{VI} than is necessary to compensate for the $Al^{IV} \overset{\rightarrow}{\leftarrow} Si$ replacement, some dioctahedral substitution must exist.

Chlorite is omnipresent; the Al and $Mg/(Mg+Fe^{2+})$ contents appear sample dependent. As is shown in figure 37a, $Mg/(Mg+Fe^{2+})$ increases in the order V18A < 14J < 14I < 12G ~ 14H ~ 12H < 15A. Chlorite from V18A is more aluminous than that from the other samples, both in Al^{VI} and Al^{IV} as is shown in figure 37b. For all analyses Al^{VI} is less than Al^{IV}, and Fe^{3+} is necessary to preserve charge balance. The estimated formula proportion of Fe^{3+} is greatest in chlorite from V18A, between 0.09 and 0.22.

Epidote and plagioclase

Major chemical variation in $Fe^{3+}/(Fe^{3+}+Al^{VI})$ is observed within the Pinney Hollow Greenstone epidote. Grains with yellow cores and colorless rims are common; and as illustrated in figure 38, these cores are richer in ferric iron. One grain in V15A is an exception, it has a colorless, aluminous core and a yellow, epidote-rich rim. Ti substitution in the

octahedral site is a maximum of 0.08 formula proportion, and up to 0.06 and 0.02 formula proportion Fe^{2+} and Mn, respectively, substitute for Ca. Ce was not analyzed in the Granville Notch samples (V12, 14 and 15), but it is negligible in V18A.

Plagioclase in all the Pinney Hollow Greenstone samples is albite. It occurs as matrix and poikiloblastic grains. Twinning is rare, making it difficult to distinguish from quartz. As is indicated in figure 39, the maximum observed anorthite and orthoclase contents are 1.4 and 1.0 molecular percent, respectively.

Carbonate, sphene, and magnetite

Calcite is ubiquitous, and the electron microprobe analyses in figure 40 show that a maximum of 6 atom percent (Mg+Fe+Mn) occurs. Vein and host rock calcite at Granville Notch have equivalent compositions, and calcite in V18A is zoned toward compositions with less ankerite substitution.

Sphene occurs as subhedral to euhedral grains commonly included in chlorite. Rutile cores with sphene rims are also observed. In V18A sphene has the average formula

$$Ca_{1.02}(Ti_{.94}Al^{VI}_{.03}Fe_{.02})(Si_{.99}Al^{IV}_{.01})(O_{4.91}(OH)_{.07}F_{0.2}).$$
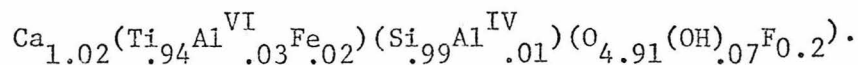
Magnetite, $Fe^{2+}_{1.00}Fe^{3+}_{1.99}Si_{.01}O_4$, occurs as subhedral to euhedral grains at Granville Notch and often forms stringers parallel to the layering.

F. Stowe Formation

Geologic setting

Doll and others (1961) assigned the Stowe Formation to the Upper

Cambrian/Lower Ordovician. This unit crops out east of the Green

Mountain anticlinorium axis, and in northern Vermont it is folded by

the Lowell-Worcester-Northfield Mountains anticlinorium. Pelitic phyl-

lite comprises much of the Stowe Formation; but a significant volume of

interlayered mafic schist forms the Greenstone/Amphibolite Member. Geo-

logic maps for this area have been made by Cady (1956), Albee (1957),

Cady and others (1962), and Cady and others (1963). In figure I-1 the

Stowe Formation is included in the Cambrian rocks and the localities from

which samples were collected for electron microprobe investigation are

annotated. The exact locations are given in the appendix. The rocks

studied are from three subareas shown in figures I-1 and 2: Eden Notch,

Elmore Mountain, and the Worcester Mountains.

Because intercalated mafic and pelitic rocks occur in the biotite,

garnet, and kyanite grades, samples from the Stowe Formation are important

to establishing the correlation between phase composition in mafic schist

and metamorphic grade. Eden Notch is below the hornblende isograd mapped

by Cady and others (1963); Doll and others (1961) considered it in the

biotite zone. Detailed mapping by Albee (1957) delineated a garnet and

a kyanite isograd at Elmore Mountain. Below the garnet isograd the diag-

nostic pelitic minerals are chlorite and chloritoid. (The absence of

biotite is probalby due to bulk rock composition.) The garnet and kyanite

grade assemblages have been extensively retrograded (Albee, 1957 and

1968). To the south Cady (1956) mapped a garnet isograd in the Worcester

Mountains.

Two Stowe Formation Greenstone samples from Eden Notch have been

chosen for detailed electron microprobe investigation. Both the Stowe

Amphibolite samples studied from Elmore Mountain are within the garnet zone; V50B is near the garnet isograd, and V44 is near the kyanite isograd. Five samples from the Worcester Mountains have been selected. V5B is just above the garnet isograd; the others are from the biotite zone.

Several published and two new radiometric age measurements have been made on Stowe Formation rocks from northern Vermont. Cady (1969) reported a 430 m.y. K/Ar age on muscovite from the Worcester Mountains which he interpreted as a hybrid of Cambrian and Devonian recrystallization. However, the age of the protolith is considered Late Cambrian/ Early Ordovician, making this explanation unlikely. Using the $^{40}Ar/^{39}Ar$ technique, Lanphere and Albee (1974) also obtained Ordovician ages on muscovite (439 ± 9 m.y.) and amphibole (457 ± 26 m.y.) from the Worcester Mountains. (The latter age is from the same location as V5.) These data and a 358 ± 4 m.y. age on fine-grained white mica pseudomorphic after kyanite led Lanphere and Albee (1974) to argue for two periods of metamorphic mineral growth. They correlated the first and higher grade event with the Ordovician Taconic orogeny and the second with Devonian, Acadian metamorphism.

Marvin Lanphere (written communication, 1976) measured Ordovician $^{40}Ar/^{39}Ar$ total fusion ages on amphibole from Elmore Mountain sample V50B. In this rock amphibole grains are discontinuously zoned; the cores are hornblende and the rims actinolite. The more iron-rich cores were magnetically separated from the rims and yielded a 437 ± 7 m.y. age. The actinolite rims gave 440 ± 9 m.y.

The low grade mafic rocks are typically light green, fine grained, and massive to schistose; while the higher grade rocks are much darker green to gray, coarser grained, and schistose. Epiclastic, pyroclastic, and volcanic flow layers may all be present in the Stowe Greenstone/ Amphibolite. The mafic and pelitic layers are concordant; good examples are exposed by roadcuts along Interstate 89. Laminations in the mafic rocks parallel the layering and foliation. These relationships suggest a parent of water-laid mafic volcanic material. A volcanic flow proto-lith is indicated by spherical clusters of epidote grains that may be amygdules. Cady (1956) also observed structures which could be pillow lavas.

Paragenesis

The typical low grade Stowe Greenstone has the assemblage amphibole-biotite-carbonate-chlorite-epidote-plagioclase-quartz-sphene. Magnetite, sulfides, and white mica also occur. Stilpnomelane-amphibole-biotite-chlorite-epidote-plagioclase-sphene±alkali feldspar rocks crop out 1.75 miles east of North Hill in the Montpelier quadrangle. Some of these rocks are graywacke and are similar to those in which stilpnomelane occurs in the Pinnacle and Underhill Formations; others contain amphibole porphyroblasts with relict brown cores.

The pelitic rocks intercalated with the low grade samples chosen for detailed investigation are chlorite-plagioclase-quartz-white mica schists; biotite is rare. Pelitic layers exposed along Route 100B in the southwestern Montpelier quadrangle contain garnet as remnants in plagioclase porphyroblasts, suggesting a period of earlier, higher grade

metamorphism. No pelitic samples were studied from the garnet zone areas. As discussed by Albee (1957), the kyanite and garnet grade assemblages at Elmore Mountain have been retrograded to sericite, chloritoid, and chlorite.

In hand specimen the distinction between low and high grade mafic rocks is pronounced. Whereas low grade samples are fine grained and green, higher grade rocks are coarser grained and darker green to gray. The mineral assemblage is similar however; amphibole-biotite-chlorite-epidote-plagioclase-quartz rocks are typical. Carbonate and white mica frequently occur, but biotite and white mica usually do not coexist. Three mineralogical differences are noted. Stilpnomelane is unique to the biotite zone; garnet appears only in the garnet and kyanite zones; and sphene is common in the biotite zone, while rutile is more often the Ti-rich phase in the higher grades. Magnetite and sulfides are observed in both low and high grade rocks.

Phase chemistry

Amphibole

In the biotite zone acicular and prismatic amphibole commonly occurs in chlorite clusters, and coarser grains are often characterized by color discontinuities. At Eden Notch these cores have colorless to blue-green to green pleochroism and are darker than the colorless to pale blue-green pleochroic rims; cores and rims may or may not be in optical continuity. Amphibole occurs in the host rocks and in concordant quartz-calcite veins along Interstate 89 in the Worcester Mountains. The host rock amphibole has colorless to pale blue-green pleochroism; vein amphibole is coarser

grained, and many grains have colorless to pale gray-blue pleochroic cores and colorless rims. A few grains display a third zone which has overgrown the colorless one and which is greener than the innermost zone. Domain boundaries appear sharp.

Figure 41 shows the chemical variation for host rock and vein amphibole in the biotite grade Stowe Greenstone. In the two samples from Eden Notch (V28A and 30A), the optically distinct amphibole cores have a greater glaucophane/riebeckite component than the rims and unrimmed grains. V3C is a greenstone in contact with a quartz-calcite vein, and a chlorite-rich border zone separates the host from the vein. Border zone grains have barroisite richer cores than rims like the amphibole at Eden Notch. V11A amphibole is similar in composition to these cores but is richer in Al^{VI}, Al^{IV}, and Na^{A}. Amphibole porphyroblasts in this sample are partially replaced along edges and cleavage traces by chlorite $\pm$ biotite. As indicated by the arrows in figure 41, these prophyroblasts show slight actinolite substitution and $Fe^{3+}/(Mg+Fe)$ enrichment outward. Like the rims and unrimmed grains at Eden Notch and in V3C, V6B amphibole has a minor glaucophane/riebeckite component; it is actinolite.

At Elmore Mountain pale brown to blue-green to brown-green pleochroic amphibole constitutes as much as 75% of a sample. Interstitial to and overgrowing these dark domains is a lighter blue to green amphibole. Rim development is minor in the high grade samples; it is more extensive in the lower grades as is shown in plate 5b. Fractures perpendicular to the foliation cut amphibole grains and are filled by the lighter colored amphibole. The electron microprobe analyses for two

garnet grade samples are plotted in figure 42. Three chemically distinct
fields are defined and are related by a complex zoning pattern. The
dark, interior domains zone outward to more tschermakite and edenite-
rich compositions. Light-colored domains are actinolite and zone toward
more actinolitic edges. Generally, a wide composition gap separates core
edge from rim compositions. However, some grains in V44 have domains
intermediate in composition and color intensity between the core and rim.

A garnet grade amphibolitic schist has also been analyzed from the
Worcester Mountains, and the amphibole data are shown in figure 43. No
optical zoning occurs, but as the arrows indicate grains show more
tschermakite substitution outward. For comparison, envelopes delimit
the other Stowe Formation amphibole analyses. V5B amphibole differs from
the dark, garnet zone hornblende at Elmore Mountain in that it is K, Ti,
and Ca poorer but Al^{VI} and Na^{M4} richer; it is more barroisitic.

The most sodic biotite grade amphibole (core compositions at Eden
Notch and V11A amphibole) have Na^{M4}/(Ca+Na) values like the barroisitic
hornblende in V5B, but Na^{A}/(Ca+Na) is much less. Actinolite (rims and
unrimmed grains at Eden Notch and in V3C and V6B) are similar in compo-
sition to the rim and interstitial grains at Elmore Mountain. The
tschermakite and edenite substitutions in the garnet grade amphibole (V5B
and cores at Elmore Mountain) exceed those in the biotite grade and
indicate that with increasing grade, as determined by the intercalated
pelitic rocks, amphibole changes from actinolite to hornblende. As will
be discussed in a following section, the plagioclase in all these rocks
is albite. Therefore, the albite-oligoclase transition must occur at a
higher grade than the actinolite to hornblende change.

Mica

Low grade biotite is primarily brown green; it is brown in the garnet grade Stowe Formation mafic rocks. Brown grains do occur along fractures and as an alteration product with or without chlorite in both grades. Figure 44 shows that brown and green biotite in V11A and V30A appear to have equivalent chemistry. Ti content does not distinguish the two differently colored grain types. A correlation between metamorphic grade and Al content is indicated. Biotite from the garnet zone mafic rocks (V5B and 44) is richer in Al^{VI} than that from the biotite zone. Since the calculated Al^{VI} for all analyses is greater than is necessary to balance the $Al^{IV} \rightleftarrows Si$ substitution, the normalization factor appears to be too large, and some dioctahedral substitution probably exists.

Plotted in figure 45a are the electron microprobe analyses of white mica from the Stowe Greenstone/Amphibolite. Muscovite occurs in the garnet grade (V5B); biotite zone white mica is more phengitic (V3C and 6B). Both K- and Na-rich white mica occur in the pelitic sample V3H (figure 45b). Paragonite is finer grained and is oriented along the slip cleavage, but both schistoisity and slip cleavage K-rich white mica occur. Intergrowths of both white micas ± chlorite are observed. Figure 45b shows that the paragonite has less Ti, (Fe+Mg+Mn+Zn), and Si than the K-mica, and those K-mica grains which are aligned with the slip cleavage are more phengitic. They approach the phengite composition in the mafic layers at this outcrop (V3C) which is delimited by the dashed envelope.

In figures 45a and b all analyses have (Fe+Mg+Mn+Zn) > (Si-3) suggesting the presence of ferric iron, and figure 45c shows the ratio of

the estimated $Fe^{3+}/(Mg+Fe)$. $Mg/(Mg+Fe)$ is greater in the K-rich white mica than the paragonite, and this ratio increases in the order V3C < V5B < V6B for the potassium white mica in the mafic rocks. Porphyroblastic phengite in this last sample is zoned outward to greater Fe^{3+}/Fe^{2+} values; concomitantly, Si decreases (figure 45c and a).

Chlorite

Chlorite is a major phase in the biotite grade mafic rocks. It is only minor in the garnet zone and is interstitial to and along fractures within amphibole or forms from the alteration of garnet. In figure 46 the chlorite analyses appear to correlate with metamorphic grade and bulk rock composition. Chlorite in the Stowe Amphibolite/Greenstone is Al^{VI} and Al^{IV} richer in the garnet zone than in the biotite zone, but biotite grade chlorite in the pelitic sample (V3H) is more aluminous than that in any of the mafic layers. Furthermore, most of the pelitic schist chlorite analyses do not require Fe^{3+} to balance Al^{IV}, but the majority of the chlorite analyses from the mafic rocks have nonzero Fe^{3+} estimates. Fe^{3+} is calculated to be small, though, and $(Mg/(Mg+Fe)-Mg/(Mg+Fe^{2+}))$ is less than 3%.

Intrasample chlorite variation is not appreciable in most samples. Vein border zone and host rock chlorite in V3C are chemically variable, but no interlayer difference is observed. Chlorite forming from the alteration of amphibole in V11A is poorer in Al^{IV} than matrix chlorite, and that from garnet alteration in V5B is less Mg rich than the corresponding matrix chlorite.

Epidote

Epidote from the Stowe Greenstone/Amphibolite is stoichiometric $Ca_{2.0}(Al^{VI},Fe^{3+})_{3.0}Si_{3.0}O_{12}(OH)$. Figure 47 shows the $Fe^{3+} \rightleftarrows Al^{VI}$ substitution, and no correlation between Fe^{3+} content and metamorphic grade (determined by the interlayered pelitic rocks) is obvious. Significant intrasample variation is observed. Grain edges in the biotite zone samples V11A and 6B are clinozoisite richer than the interiors, but the opposite relationship is observed for epidote in V50B. In V6B and 50B epidote, subhedral cores can be distinguished from rims by differential birefringence. Cores are turbid in the latter sample, while rims are "clean". However, the only difference in composition observed is the previously noted $Fe^{3+} \rightleftarrows Al^{VI}$ substitution.

Plagioclase

In the biotite zone plagioclase occurs as small grains and coarser poikiloblasts. Epidote and amphibole inclusions define straight trails parallel to the foliation in V6B; they are not oriented in the other samples. The electron microprobe data contained in figure 48 show that the two grain types are not distinguished by composition. All biotite zone plagioclase is albite with less than 1.7 molecular percent $CaAl_2Si_2O_8$ and 0.5 percent $KAlSi_3O_8$. Coarse, zoned grains are observed. V28A and 6B albite has less anorthite solid solution at grain margins, and V30A and 3H plagioclase grains zone toward more anorthitic edges.

Garnet grade albite is more anorthitic, but the orthoclase content is equivalent to biotite zone albite. It is interstitial to and present within fractures in amphibole, and grain size precludes a detailed

composition profile with the 20 μm spot size necessary for the WDA analyses. Accordingly, EDA traverses (which allow a 1 μm spot to be used) have been made across two plagioclase grains in V5B that show differential core/rim extinction. These profiles are delineated in figure 49; they show continuous zoning from $An_{7.0}$ cores to $An_{0.5}$ rims.

Garnet

Small, euhedral, pink garnet grains in the matrix and within plagioclase porphyroblasts occur in the biotite zone pelitic sample V3H. Figure 50 shows that the spessartine component is significant, ranging from 47 molecular percent in the core to 28 percent at the rim. In the garnet grade mafic sample V5B, garnet prophyroblasts are much less Mn rich. Correspondingly, Fe^{2+} and Mg are significantly greater. A Mn depletion coupled with Fe^{2+} and Mg enrichment from core to rim is observed for both sets of garnet analyses; but the grossular component decreases toward grain exteriors in V5B while it increases slightly in V3H.

Carbonate

Contained in figure 51 are the carbonate analyses from the Stowe Formation. Less than 3 atom percent (Fe+Mg+Mn) occurs in the calcite. Compared to 1% or less Mn in the calcite from this area, V3H ankerite has 13 to 14 atom percent Mn. The maximum atom percent Ba is 0.3 and is in ankerite. In thin section ankerite is distinguished by rhombohedral morphology and strong differential refractivity. Grains are colorless and untwinned. Calcite is anhedral to subhedral and shows less change in relief.

Sphene and Fe, Ti oxides

In the biotite grade mafic rocks sphene forms euhedral grains and stringers; it often rims rutile in the higher grade rocks. The average formula is $Ca_{1.01}(Ti_{.93}Al_{.05}Fe_{.02})Si_{.99}(O_{4.90}(OH)_{.08}F_{.02})$, and the variation in the content of the Ti position is shown in figure 52.

Magnetite, $Fe^{2+}_{1.00}Fe^{3+}_{2.00}O_4$, occurs in the biotite zone mafic layer at Eden Notch. Hematite, in the pelitic sample from the Worcester Mountains (V3H), has partially exsolved to ilmentite, and the lamellae are commonly segregated in grain interiors. The analyses range between $Fe^{3+}_{1.77}Fe^{2+}_{.11}Ti_{.11}O_3$ and $Fe^{3+}_{1.49}Fe^{2+}_{.25}Ti_{.25}O_3$.

G. Northeastern Vermont

Geologic setting

In Vermont a major unconformity separates Cambrian and Ordovician units to the west from Silurian and Devonian ones to the east. The former comprise the Green Mountain anticlinorium; whereas, the younger rocks are in the Connecticut Valley-Gaspé synclinorium. By volume, the Lower Devonian Waits River and Gile Mountain Formations dominate the metamorphic sequence in eastern Vermont. Calcereous rocks constitute much of these units and are more abundant than in the Green Mountain anticlinorium.

Of interest is the Standing Pond Volcanic Member in the Waits River Formation at its contact with the Gile Mountain Formation. In northeastern Vermont this unit is intercalated with pelitic schist of biotite to sillimanite grade and has been sampled in the Burke and St. Johnsbury quadrangles. Geologic maps by Woodland (1965) and Hall (1959) are

available for this area; figures I-1 and I-2 show the sample localities studied in detail and the quadrangle locations.

Massive to schistose and fine- to coarse-grained amphibolitic rocks make up the Standing Pond Volcanic Member. Some layers are predominantly amphibole, while others are more felsic. The layering parallels the schistosity. Amphibole fasicles which weather out characterize the felsic layers. Hall (1959) recognized pillow structures, and Woodland (1965) proposed that flows are incorporated into this unit. They also suggested that tuffaceous and intrusive progenitors are represented.

Several periods of metamorphic mineral growth have been recognized. Woodland (1965) identified two prograde events; the first was accompanied by deformation and was characterized by biotite, garnet, and perhaps (as suggested by Anderson, 1977, p. v) higher grade recrystallization. The second was a regional thermal event and has been associated with the emplacement of the New Hampshire plutonic series (figure I-1) which in this area has a Rb/Sr age between 354 and 380 m.y. (Naylor, 1971). Postdeformational porphyroblastic mineral growth occurred during this event; and biotite, garnet, staurolite, andalusite, kyanite, and sillimanite grade recrystallization is observed. Woodland (1965) also recognized a third event which caused the retrogradation of mineral assemblages formed during the first two periods of metamorphism.

Paragenesis

The common mineral assemblage in the Standing Pond Volcanic Member is calcic amphibole-plagioclase-biotite-chlorite-carbonate-quartz-ilmenite. Epidote is conspicuously absent in all but the sillimanite

zone. In garnet and staurolite-andalusite grade outcrops near St. Johnsbury Center, cummingtonite occurs with calcic amphibole, biotite, carbonate, chlorite, plagioclase, and quartz. This is the first reported occurrence of cummingtonite in Vermont west of the Ammonoosuc fault. The rocks in which this multiple amphibole assemblage is found are medium- to coarse grained and massive, and the calcic amphibole is green and por- phyroblastic. In some samples acicular, colorless to light brown cum- mingtonite is visible with a hand lens.

Phase chemistry

Three Standing Pond Volcanic Member samples have been chosen from the biotite, garnet, and sillimanite zones for detailed electron micro- probe investigation. The exact sample locations plus rock descriptions and estimated modes are listed in the appendix. The chemical data are presented below.

Amphibole

Biotite grade calcic amphibole is colorless to pale green brown and occurs as acicular and prismatic grains. The latter can have pale cores which, as is shown by the electron microprobe analyses contained in figures 53-55, are more actinolitic than the darker rims. Optically con- tinuous colorless grains parallel to and across the foliation are not chemically distinct. Although the most tschermakite- and edenite-rich analyses are on cross foliation grains, other postdeformation amphibole has the same composition as that defining the foliation.

Calcic amphibole in the higher grade rocks forms poikiloblasts and has brown-green to blue-green pleochroism. Cores are often browner

than rims. Figure 56 shows that in V36A these cores are richer in Ti than the rims but are not otherwise compositionally distinguished. In the sillimanite zone sample studied (V53), the cores are richer in K, Ti, Al^{IV}, and Fe^{2+}/Fe^{3+} (figures 55 and 57).

Colorless to pale brown cummingtonite occurs as sprays of acicular grains as is shown in plate 5c; it is often associated with calcic amphibole. A wide compositional gap separates the analyses on adjacent hornblende and cummingtonite domains in V36A as delineated by the tie lines on figures 55-56. Besides the expected Al^{VI}, Al^{IV}, and Ca difference, the hornblende is also richer in K, Ti, and Fe^{3+}. $Mg/(Mg+Fe^{2+})$ is equivalent to greater in the calcic amphibole, while $Mg/(Mg+Fe)$ is slightly less. The intermediate composition analyses are enigmatic. They are from pale blue domains within cummingtonite and at hornblende/ cummingtonite contacts and may be a mixture of the two phases.

The analyses plotted on figures 54, 55, and 57 for V53 are for amphibole normalization 3 (total cations - (Ca+Na+K) = 13). However, normalization 1 (total cations - (Na+K) = 15) is also permissible from charge balance considerations. The major difference between these two formula proportion sets is in the Fe^{3+} estimate which is greater for method 3. The short-dashed envelope on figure 55 delimits the method 1 formula proportion set; Fe^{3+}/Fe^{2+} is less than for the plotted analyses normalized by method 3. By assumption, no Na^{M4} is allowed for set 1, but figure 54 shows that little Na^{M4} is calculated for set 3. K and Ti are equivalent; Al^{VI} is slightly greater and Al^{IV} slightly less for the first normalization. (On the Al^{VI} versus Al^{IV} diagram in figure 57, compare the short-dashed envelope to the plotted points.)

As defined by the pelitic interlayers, V38A is in the biotite zone and V36A is garnet grade. On the diagrams in figures 54 and 57 these two samples define linear trends and show that with increasing metamorphic grade the tschermakite and edenite substitutions increase. The sillimanite zone sample (V53) falls off the linear compositional trend of the other two samples. It shows much less glaucophane/riebeckite substitution. This relationship is true for both normalization sets 1 and 3 and on the normalization independent diagram (Na/(Ca+Na) versus Al/(Si+Al)).

Chlorite and biotite

Figure 58 suggests that Al^{VI} and Ti increase in chlorite between the biotite and garnet zones. They also appear to increase with metamorphic grade in the biotite which is brown in the Standing Pond Volcanic Member. The normalization of the biotite analyses to total cations - (Na+K+Ca) = 7 forces most of the analyses to have a total positive charge greater than the stoichiometric 22 primarily because the calculated Al^{VI} is greater than $(1-Al^{IV})$. The normalization factor thus appears to be too large, and some dioctahedral substitution probably exists.

Feldspar

Plagioclase is a major phase in the mafic rocks from northeastern Vermont and occurs as anhedral to subhedral grains. Few are twinned but undulose and concentric extinction are common. The electron microprobe data indicate that these grains are zoned toward more anorthitic edges. Figure 59a shows that the anorthite content is positively correlated with metamorphic grade. In the biotite zone (V38A) the plagioclase is An_{22-25}; garnet zone plagioclase (V36A) ranges from An_{22} to An_{37}. Most

of the plagioclase in the sillimanite zone sample (V53) is An_{84-90} and is twinned and inclusion filled. One grain which is interstitial to amphibole and has no inclusions is more sodic, An_{38-39}.

All the plagioclase in the Standing Pond Volcanic Member samples studied has more anorthite solid solution than An_{20}, and the amphibole is actinolitic hornblende to hornblende. Therefore, the albite-oligoclase transition must have occurred at about the same grade as or at a lower grade than the actinolite-hornblende transition.

Alkali feldspar with microcline twinning occurs in V53 with bytownite. As shown in figure 59b, between 8 and 20 molecular percent albite solid solution is measured in the alkali feldspar. The maximum orthoclase content of the plagioclase from all the studied samples in this area is 0.6 percent.

Calcite, epidote, sphene, and ilmenite

Calcite, epidote, and sphene occur only in the sillimanite zone sample studied (V53). Calcite is homogeneous $(Ca_{.98} Fe_{.01} Mg_{.01})CO_3$, and euhedral, colorless epidote grains have the average formula $(Ca_{1.99}Mn_{.01})$ $(Al^{VI}_{2.56}Fe^{3+}_{.44})Si_{3.00}O_{12}(OH)$. Sphene occurs as matrix grains, as inclusions in amphibole, and as rims on ilmenite. Electron microprobe analyses reduce to the average formula $Ca_{1.01}(Ti_{.94}Al^{VI}_{.03}Fe_{.02})(Si_{.98}Al^{IV}_{.02})(O_{4.90}$ $(OH)_{.08}F_{.02})$.

Ilmenite is altered to rutile in V38A. Stringers which pass through the other phases in V36A are $(Fe^{2+}_{.96}Mn_{.02}Mg_{.01})Ti_{.98}Fe^{3+}_{.02}Si_{.01}O_3$. Sphene ubiquitously rims ilmenite in the sillimanite zone sample (V53), even when it is included in amphibole. The ilmenite is $(Fe^{2+}_{.94}Mn_{.04}Mg_{.01})$

$(Ti_{.99}Fe^{3+}_{.01})O_3$ and has a greater $MnTiO_3$ component but less Fe_2O_3 than ilmenite in the garnet zone sample (V36A).

H. Saxtons River quadrangle

Geologic setting

The Saxtons River quadrangle in southeastern Vermont (figure I-2) is an excellent sample area for this investigation because mafic rocks are intercalated with biotite, garnet, and staurolite-kyanite grade pelitic schist. The quadrangle was mapped by Rosenfeld (1954); Rosenfeld (1968) emphasized the tectonic and metamorphic history. Southeastern Vermont is dominated by the Chester, Athens, Lake Rayponda, and Sadawga Pond domes (figure I-1). These domes are Precambrian basement mantled by metamorphosed Cambrian, Ordovician, Silurian, and Devonian rocks.

Rosenfeld (1968) proposed from rotated garnet studies that the Chester and Athens domes were domed upward (event II) after a period of intense folding (event I). He suggested that no significant hiatus separated the two events and that I was Acadian (Devonian) and II Appalachian (Permian?). In Cambrian rocks Rosenfeld (1968) observed an earlier period of garnet rotation and metamorphism which he tentatively assigned to the Taconic (Ordovician) orogeny.

Much of southeastern Vermont is shown in the garnet zone by Doll and others (1961). The metamorphic intensity increases to staurolite-kyanite grade near the Athens and Chester domes. To the west Doll and others (1961) delimited a sliver of biotite grade rocks. The Cambrian Pinney Hollow Formation in the eastern part of the Saxtons River quadrangle crosses the garnet (Rosenfeld, oral communication, 1971)

and oligoclase (Rosenfeld, 1954) isograds from north to south. The Chester Amphibolite Member crops out nearly continuously in this area, and a detailed traverse was made to collect mafic and pelitic interlayers across these isograds. The pelitic rocks were used to verify the metamorphic grade of the mafic layers.

To ascertain the mineral assemblage and phase chemistry in higher grade mafic schist, three other localities west of Athens dome were studied in the Saxtons River quadrangle: Townshend Dam, Acton Hill, and Hinkley Brook (figure I-2). At a roadcut above the Townshend Flood Control Dam, pelitic and mafic layers of the Moretown Member of the Missisquoi Formation crop out just below the staurolite isograd. Rosenfeld (1972, stop 3) described this location and observed garnets rotated during his event I and a relict oligoclase isograd encapsulated in the garnets. The Missisquoi Formation is Middle Ordovician and lies just below the major unconformity that separates Cambrian and Ordovician rocks from Silurian and Devonian.

At Acton Hill Rosenfeld (1972, stop 6 and oral communication, 1971) has reported Pinney Hollow Formation staurolite-kyanite pelitic schist interlayered with amphibolite. Rosenfeld (1968) observed two periods of garnet rotation here and correlated the first with the Taconic orogeny and the second (his event I) with the Acadian orogeny. Rosenfeld (oral communications, 1971 and 1976) reported interlayered staurolite-kyanite pelitic schist and amphibolitic schist from the Middle Cambrian Ottauquechee Formation at Hinkley Brook.

For the data presentation in the next sections, the Saxtons River quadrangle is divided into four subareas: Chester Amphibolite Member of the Pinney Hollow Formation, Townshend Dam, Acton Hill, and Hinkley Brook. The locations of each analyzed sample is shown in figure I-1, and the exact locations are tabulated in the appendix along with the rock descriptions and estimated modes.

Chester Amphibolite Member of the Pinney Hollow Formation

Paragenesis

Rosenfeld (1954) observed that with increasing metamorphic grade southward in the Saxtons River quadrangle, the Chester Amphibolite changes from greenstone and greenschist to dark green-gray amphibolitic schist. The mineral assemblage amphibole-biotite-carbonate-chlorite-epidote-plagioclase-quartz commonly occurs in both rock types; but accompanying the change in physical appearance, chlorite and epidote become less abundant while the amount of amphibole increases. Below the oligoclase isograd sphene and magnetite are observed. Hematite, ilmenite, and rutile are more common above this isograd. Sulfides occur in both low and higher grade rocks. In the mafic rocks garnet occurs only above the oligoclase isograd, but this phase is present in both garnet-albite and garnet-oligoclase pelitic rocks.

Amphibole

Although optically continuous, light to dark green pleochroic amphibole grains predominate in the Chester Amphibolite, the coarsest grains characteristically have light and dark green domains. Usually, the

light areas are in grain cores, and light green amphibole without a dark rim is not observed. Grains with euhedral light cores (plate 5d) occur as do more mottled grains (plate 5e). A line drawing and Al X-ray scan of the composite grain in plate 5d are shown in plate 6. Four optically distinct zones are observed. An inner, anhedral, Al-rich, dark green core (zone 1) is surrounded by a lighter green, Al-poor, euhedral rim (zone 2). A narrow, colorless domain (zone 3) separates this pale green zone from a dark green, Al-rich outermost rim (zone 4). Other amphibole grains of intermediate color intensity and with moderate Al content are included between zones 2 and 4, and between domains 3 and 4.

To determine the composition of each color domain, four EDA traverses have been made using a 1 micron spot; the location of these traverses are indicated on plate 6, and the chemical analysis profiles are delineated in figure 60. Compared to the light areas, the dark ones have more Al_2O_3, TiO_2, FeO_{Total}, Na_2O, and K_2O. They have less SiO_2, MgO, and CaO. The chemical variation within each zone is small compared to that between zones, and the abrupt slope changes shown by the profiles demonstrate that the optical discontinuities manifest chemical discontinuities. All oxide profiles go through slope reversals on both sides of the colorless zone (figures 60a, b, d). Similar profiles are observed between the dark, innermost core (zone 1) and the light core (domain 2) on figure 60d. These relationships and the narrowness of the colorless zone (about 10 microns) suggests that depletion zoning has occurred during the growth of zone 2 on zone 1 and of domain 4 on domain 2.

In figure 61 the WDA amphibole analyses from this sample (V127A) are plotted. The EDA analyses are included only on the atomic ratio graph because they are not accurate enough for good formula proportion estimates. All the analyses on light cores are actinolite; the dark cores, rims, and optically continuous grains are hornblende. Although the WDA analyses delimit a wide compositional gap between actinolite and hornblende, the EDA analyses fill in much of this gap.

Five other samples from the Chester Amphibolite with amphibole grains displaying optically distinct cores and rims have been studied in detail, and the electron microprobe analyses are plotted in figures 62-66. In all these samples the cores have the most actinolite-rich compositions. They have less K, Ti, Al^{VI}, Al^{IV}, Fe^{3+}, and Na^A but more Si and greater values of $Mg/(Mg+Fe)$ and $Ca/(Ca+Na)$. The tschermakite substitution primarily relates the cores to the rim and optically continuous grain compositions. To a lesser extent, the edenite and glaucophane/riebeckite substitutions have also occurred. A compositional gap is always observed between the two different colored domains, but a comparison of figures 61-66 shows that the position of the gap is not consistent.

Continuous zoning in the hornblende rim of one V124B composite amphibole grain is described by the inflections in the arrows delineated in figure 66. Near the edge of the rim, Na^{M4} and Fe^{3+} begin to decrease while Na^A and Fe^{2+} increase. The edenite substitution increases while the riebeckite substitution decreases. This chemical variation cannot be observed optically.

No composite amphibole grains are observed in the other five samples chosen for electron microprobe analysis. The grains have pale brown to blue-green to dark green pleochroism like the optically continuous grains and rims in the other samples. The analyses plotted in figures 67 and 68 show this amphibole to be hornblende. V94A and 114B (figure 67) amphibole is chemically equivalent to the hornblende rims and optically continuous grains in the other samples. V113B, 106D, and 119C amphibole (figure 68) is richer in Al^{IV} and Fe/(Mg+Fe). Garnet occurs in these last three samples but is absent from the others.

Hornblende ± actinolite cores are observed on both sides of the oligoclase and garnet isograds. Amphibole grain margin compositions in oligoclase grade samples are richer in K, Ti, Al^{VI}, and Al^{IV} than the amphibole in the lower grade rocks. The tschermakite and edenite substitutions increase with progressive metamorphism from the garnet-albite to garnet-oligoclase zones, but biotite grade amphibole (V94A) is not distinct from garnet-albite grade hornblende.

Mica

Biotite from the Chester Amphibolite is brown, and its composition is dependent upon metamorphic grade and bulk rock composition. Figure 69 shows that Al^{VI} is less if albite is present rather than oligoclase, but the biotite in V94A (biotite-albite zone) has the same Al content as that in the garnet- albite zone (V97B). Garnet-bearing rocks have the most Al^{VI}- and Ti-rich biotite. All analyses have more $Al^{VI} \rightleftarrows$ (Fe, Mg, Mn, Zn) substitution than $Al^{IV} \rightleftarrows$ Si, suggesting trioctahedral vacancies.

White mica is absent in most of the samples collected. It is a major phase in V106D where its average formula is

$$(K_{0.8}Na_{0.1})(Al^{VI}_{1.6}Fe^{3+}_{0.2}Mg_{0.2})(Si_{3.1}Al^{IV}_{0.9})O_{10}(OH)_2.$$
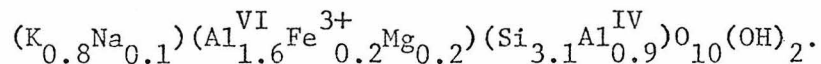
Chlorite

Chlorite composition can also be correlated with bulk rock chemistry and perhaps metamorphic grade. Figure 70 shows that garnet-bearing rocks tend to have more aluminous chlorite than other Chester Amphibolite samples with oligoclase. If albite rather than oligoclase occurs, less Al- and perhaps Ti-rich chlorite is observed. (No difference between biotite-albite zone and garnet-albite zone chlorite is detected.) Minor Fe^{3+} is estimated in those analyses which plot below the 45° line on the Al^{VI} versus Al^{IV} graph, but $Mg/(Mg+Fe)$ deviates from $Mg/(Mg+Fe^{2+})$ no more than 2%.

Epidote

Epidote from the Chester Amphibolite is stoichiometric. The $Fe^{3+}/(Fe^{3+}+Al^{VI})$ value varies significantly within and between samples; however, figure 71 shows no relationship between the ferric iron content and metamorphic grade or composition of the host rock. Some of the largest epidote grains in V97B, 100B, 114B, and 124B have subhedral, yellow cores and colorless rims; and the zoning arrows delineated in figure 71 show that these cores are richer in Fe^{3+}. This relationship is reversed for V107A epidote where the cores are lighter and less Fe^{3+} rich than the rims.

Subhedral, orange allanite is rimmed by epidote in V113B, and between 7.8 and 9.6 weight percent Ce_2O_3 is observed in the allanite. No other rare earth elements were analyzed, but low totals suggest that

others are present. CaO ranges from 12 to 14 percent; whereas, epidote
typically has 22 to 23 weight percent CaO. The rare earth elements are
probably substituting for Ca.

Plagioclase

Plagioclase composition is the best indicator of metamorphic grade
in the western part of the Saxtons River quadrangle. The Chester Am-
phibolite crosses the oligoclase isograd mapped by Rosenfeld (1954)
between stations V97 and 100 (figure I-1). The electron microprobe
analyses show that oligoclase is absent below the isograd and that the
plagioclase is albite. Oligoclase is observed in all samples above the
isograd; some also contain albite.

Figure 72 shows the plagioclase compositions in the rocks collected
below the oligoclase isograd. The maximum anorthite and orthoclase con-
tents are 1.2 and 0.4 molecular percent, respectively. In the biotite
zone sample (V94A) plagioclase grains are zoned outward to more anorthite-
rich compositions, but are not different in composition from the garnet-
albite grade plagioclase. The plagioclase analyses from the oligoclase
zone samples are ordered from top to bottom in figure 73 by the decreasing
southward distance from the isograd. (V100B was collected 2.7 miles
south of where the oligoclase isograd delineated by Rosenfeld (1954)
crosses the Chester Amphibolite, and V124B is from 8.7 miles to the south.)
No well-defined correlation between plagioclase composition and spatial
relationship to this isograd is observed.

Nonuniform extinction occurs in many plagioclase grains from above
the oligoclase isograd. The electron microprobe analyses indicate that

this is a manifestation of chemical zoning. Where single grain compositional variation has been determined, grain margins are more anorthitic than interiors. The maximum anorthite content is 25.9 molecular percent. The orthoclase component is insignificant in all analyses, 0.6 percent at most.

Discrete grains of albite and oligoclase occur in V107A and V124B. In the former sample both phases are subhedral and average 50 μm across. Albite occurs as porphyroblasts and smaller grains in V124B; the oligoclase is small and often at the edges of albite porphyroblasts. When the two phases are in contact, the boundary is often sharp, but a differently extinguishing domain sometimes separates the albite from the oligoclase. These domains also occur at albite/hornblende contacts. To determine the nature of the albite-oligoclase contacts, most of the analyses were obtained at $0.01\,\mu$A with a $10\,\mu$m spot, and Ca X-ray images (beam scans) were used to locate each domain.

Plates 7 and 8 illustrate these electron beam scans for one area in each sample. Annotated on the line drawings are the anorthite contents of some of the analyzed points. A diffuse optical and chemical zone separates albite from oligoclase in the area covered by scan 1, plate 7. Compositions in this area range from $An_{2.4}$ to $An_{10.0}$. The albite side of this domain is $An_{0.6}$, while the oligoclase is $An_{16.4-18.7}$. The contacts between albite and oligoclase in the area covered by scan 2 are more sharply defined. The albite averages $An_{2.3}$ and the oligoclase $An_{17.7}$. Plate 8 shows two albite grains separated by an oligoclase grain. On one side a sharp contact separates $An_{0.6}$ from An_{18}. On the other side

an An_{6-7} zone is present between the oligoclase and the albite which has less than 1 molecular percent anorthite.

All the plagioclase data from these two samples are contained in figure 73. The optically diffuse domains are distinguished, and they range between An_2 and An_{13}. Most of the oligoclase is between $An_{16.5}$ and $An_{20.5}$, and optically distinct albite is generally less than $An_{2.5}$. In V124B most of the albite is An_1 or less, and the average oligoclase is An_{18}. An_2 and An_{18} are the average albite and oligoclase compositions in V107A.

Garnet

In the Chester Amphibolite garnet is restricted to above the oligoclase isograd. Porphyroblastic and smaller grains occur. As is shown in figure 74, the spessartine component decreases from core to rim with concomitant increase in almandine. Grossular also tends to decrease, while pyrope is greater in V119C and V106D rims but less in V113B garnet rims.

Carbonate

The carbonate electron microprobe analyses for this subarea are illustrated in figure 75. Separate grains of calcite and dolomite occur in V100B where the dolomite is identified by red-brown stained cleavage traces and in places is altered to calcite. This calcite is less ankerite rich than the separate calcite grains. Dolomite is the only carbonate in V108, and calcite occurs in the other four samples. Two calcite populations are observed in V94A and 114B with "clean" grains richer in the ankerite component than the grains which appear to be

altered. The opposite relationship is defined by V97B calcite; brown, altered grains are the more ankeritic. Dolomite is not observed below the oligoclase isograd. No well-defined relationship between calcite composition and metamorphic grade is observed.

Sphene and Fe, Ti oxides

Subhedral to euhedral sphene usually occurs in the Chester Amphibolite below the oligoclase isograd and is often included in chlorite. In V127A stringers of fine-grained sphene are aligned along the foliation. The electron microprobe analyses show that sphene is stoichiometric $Ca_{1.0}(Ti, Al, Fe, Mg)_{1.0}Si_{1.0}(O,(OH)_{.04-.13}F_{0-.03})_5$. The Al, Fe, and Mg substitutions for Ti are small as is shown in figure 76a.

Anhedral porphyroblasts of magnetite, $Fe^{3+}_{2.00}Fe^{2+}_{1.00}O_4$, occur in biotite, garnet-albite, and garnet-oligoclase samples but are more common below the oligoclase isograd. Elongated grains of ilmenite in V114B 106D, 107A, and 113B have exsolved hematite blebs, and the analyses are shown in figure 76b. Separate grains of ilmenite with hematite lamellae and of hematite with ilmenite lamellae occur in V97B, 119C, and 124B. The comparison of these ilmenite analyses (figure 76c) with those in samples without hematite (figure 76b) shows that ilmenite occurring with hematite tends to have more Fe_2O_3 solid solution than ilmenite in hematite-absent samples. $(Mn, Mg, Zn)TiO_3$ does not correlate with the presence or absence of hematite; but for hematite-ilmenite pairs, $MnTiO_3$ is greater in the ilmenite. Figure 76c suggests that hematite occurring with ilmenite is richer in $FeTiO_3$ in the garnet-oligoclase zone than in the garnet-albite zone.

Townshend Dam

Paragenesis

Light gray pelitic-rich and dark gray to green mafic-rich layers crop out at the roadcut above the Townshend Flood Control Dam in the Saxtons River quadrangle. Four samples from this subarea have been studied in detail. V118D is from one of the light gray layers which are biotite-chlorite-garnet-plagioclase-quartz-white mica±amphibole±epidote schist. V118E is from a garnet amphibolite boudin within a pelitic layer; and V118O and P are from the mafic, amphibole-chlorite-epidote-plagioclase-quartz±biotite±carbonate layers.

Phase chemistry

Amphibole from the pelitic and mafic layers is optically homogeneous hornblende with pale brown to blue-green to green pleochroism. As can be seen in figure 77, the hornblende from the garnet-bearing assemblages (V118D and E) is richer in Al^{VI}, Al^{IV}, and $Fe/(Mg+Fe)$ than that in the garnet-absent samples (V118O and P). Figures 78a and 79 show that biotite (which is brown) and chlorite are also more aluminous and Fe rich in the garnet-bearing samples.

Epidote composition does not appear to be correlated with bulk rock chemistry. All the analyses have between 1.9 and 2.1 formula proportion of Ca, and Si is between 2.95 and 3.04. Figure 78b illustrates the epidote substitution and the clinozoisite enrichment between yellow cores in V118O and lighter rims. A subhedral, red-brown allanite core in epidote from V118D has been analyzed. Ce_2O_3 is 18.8 weight percent, and other rare earth elements are probably present because the analysis

totals low. CaO is 8.2 weight percent compared to the normal 22 to 23 percent for epidote, indicating that the rare earth elements are substituting for Ca.

Figure 80 shows the plagioclase analyses. The anorthite solid solution ranges between 16 and 33 molecular percent, and grains with nonuniform extinction zone toward more anorthitic margins. The orthoclase component is small, less than 0.5 molecular percent. The garnet-bearing sample V118E has the most anorthitic plagioclase, but V118D plagioclase is not distinct from that found in the garnet-absent samples.

Almandine-rich garnet occurs as skeletal porphyroblasts in V118D and E; euhedral grains are also abundant in the latter sample. The electron microprobe analyses are plotted in figure 81b and show little chemical variation within grains or between samples. Skeletal garnet in V118D zones toward somewhat less grossular-rich and more almandine- and pyrope-rich grain exteriors; Mn slightly decreases from core to rim. However, euhedral grains in V118E are richer in spessartine but poorer in almandine at grain edges. The relative Ca and Mg contents do not change.

The other phases that occur at Townshend Dam are muscovite, calcite, magnetite, rutile, hematite, and ilmenite. Muscovite in V118D is acicular and defines the foliation. No appreciable chemical variation is observed, and the average formula is

$$(K_{.74}Na_{.09})(Al^{VI}_{1.69}Fe^{3+}_{.16}Ti_{.02}Mg_{.12})(Si_{3.08}Al^{IV}_{.92})O_{10}(OH)_2.$$
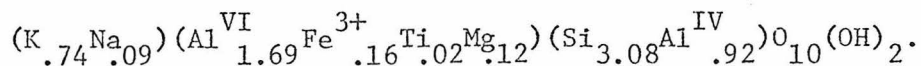
Calcite in V118O has between 6.4 and 9.0 atom percent (Fe+Mg+Mn) as is shown in figure 81a. Magnetite in V118D is euhedral and stoichiometric.

Ilmenite in V118D, E, and O occurs as elongated grains with hematite lamellae, and in the first sample hematite grains with ilmenite lamellae are also present. Rutile is associated with ilmenite in V118O. Figure 82 shows that relative to hematite, ilmenite is richer in $(Mn+Mg+Zn)TiO_3$.

Acton Hill

Paragenesis

Rosenfeld (1972, stop 6) reported garnet-staurolite-paragonite-muscovite schist with chloritoid and staurolite grains included within the garnet at Acton Hill. Biotite-garnet and biotite-chlorite-garnet-staurolite pelitic assemblages also occur. In the near vicinity Rosenfeld (1972) observed garnet-kyanite-staurolite-paragonite schist. Inter-layered with the pelitic rocks are mafic layers with the assemblage amphibole-biotite-chlorite-epidote-plagioclase-quartz±carbonate, garnet, and white mica. The amphibole-bearing rocks are schistose to gneissic and mafic rich to more silicic. The phases in three samples were analyzed with the electron microprobe, and the data are reported below.

Phase chemistry

Amphibole is poikiloblastic and is pleochroic from pale brown to blue green to green. It is optically homogeneous, and the analyses plotted in figure 83 show it to be hornblende. Only minor intra- or intersample variation is observed, and no consistent zoning pattern can be related to grain growth. Biotite and chlorite also have relatively constant compositions in the three studied samples as is shown in figures 84b and 85, respectively. Garnet is absent from V153C; but amphibole, biotite, and chlorite in this sample do not differ in composition from these

phases in the garnet-bearing rocks. Neither is there any difference between the hornblende, biotite, or chlorite in the silicic versus the mafic layer in V152.

Small, subhedral, and colorless epidote occurs as a minor phase. Figure 84a shows a wide variation in the determined Fe^{3+} contents, but no correlation between epidote composition and that of the bulk rock is observed. Mn substitutes for Ca less than 0.04 formula proportion, and Fe^{2+} is at most 0.05; Ce is negligible. Si is the stoichiometric value, 3.0.

Plagioclase often shows differential extinction, either concentric or irregular. A sharp discontinuity sometimes occurs at domain boundaries, and some grains are twinned. As delineated by the arrows in figure 86, grain margins are richer in anorthite than the interiors. The orthoclase component is small for all analyses, less than 0.5 molecular percent.

Garnet in V152 is euhedral; subhedral porphyroblasts occur in V154B. The average formula is $(Fe_{1.9}Ca_{0.5}Mn_{0.3})Al_{2.0}Si_{3.0}O_{12}$, and the analyses are illustrated in figure 87. Acicular and coarse-grained muscovite has the average formula

$$(K_{.71}Na_{.16})(Al^{VI}_{1.70}Fe^{3+}_{.14}Ti_{.02}Mg_{.12}Fe^{2+}_{.02})(Si_{3.11}Al^{IV}_{.89})O_{10}(OH)_2$$

in V152 and

$$(K_{.77}Na_{.15})(Al^{VI}_{1.69}Fe^{3+}_{.10}Ti_{.03}Mg_{.12}Fe^{2+}_{.06})(Si_{3.15}Al^{IV}_{.85})O_{10}(OH)_2$$
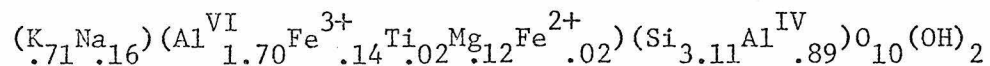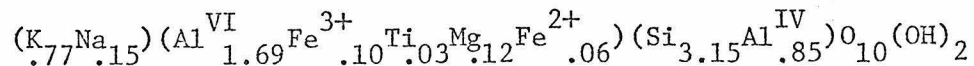
in V153C.

Ilmenite with hematite lamellae ranges between 84 and 91 molecular percent $FeTiO_3$ as is indicated in figure 88. Hematite with ilmenite lamellae

also occur in V154B. The hematite has 30 to 37 molecular percent $FeTiO_3$ and is poorer in $(Mn, Mg, Zn)TiO_3$ than the ilmenite with which it occurs.

Hinkley Brook

Paragenesis

At the Hinkley Brook subarea biotite-chlorite-garnet-staurolite-plagioclase-quartz-white mica schist and amphibole-biotite-chlorite-epidote-plagioclase-quartz±garnet±white mica schist crop out. One sample with pelitic and mafic layers (V126H) was chosen for electron microprobe investigation.

Phase chemistry

In both the mafic and the more pelitic layers of V126H, amphibole is poikilitic and anhedral to subhedral. It has pale brown to blue-green pleochroism and is optically homogeneous. The electron microprobe data contained in figure 89 indicate that the amphibole is hornblende. The scatter delimited by the data points cannot be related to compositional variation of the different layers or to grain growth.

Figure 90 suggests that biotite and chlorite in the pelitic layer are slightly richer in Fe/(Mg+Fe) than these phases in the mafic layer. The biotite is brown in both layers. Separate grains of muscovite and paragonite occur in V126H. In addition to the difference in alkali content, figure 91 shows that the paragonite has less Si, (Fe+Mg+Mn+Zn), and Ti but more Ca than the muscovite. Mg/(Mg+Fe) is greater in the muscovite.

Plagioclase is often twinned and zoned toward more anorthitic rims at Hinkley Brook. The range in composition, as is shown in figure 92a, is from $An_{15.5}$ to $An_{32.1}$. The most anorthite-rich analyses are from the pelitic layer. The orthoclase content is small, less than 0.4 molecular percent. Garnet occurs only in the pelitic layer. It is euhedral and has the average formula $(Fe_{1.9}Ca_{0.5}Mg_{0.3}Mn_{0.3})Al_{2.0}Si_{3.0}O_{12}$. The chemical variation is illustrated in figure 93; and cores are richer in Mn and Ca but poorer in Mg and Fe than the rims.

$Hem_{70}Ilm_{30}$ and $Ilm_{86}Hem_{12}$ with 2 molecular percent $MnTiO_3$ are the compositions of the hematite-ilmenite pairs in V126H (figure 92b). Separate grains of hematite with ilmenite lamellae and of ilmenite with hematite lamellae occur. Composite grains such as the one illustrated in plate 5f are also observed. To obtain analyses on each domain including the lamellae, spot sizes up to 20 microns were used.

Comparison of subareas

Composition envelopes for amphibole from each of the four studied subareas in the Saxtons River quadrangle (1. Chester Amphibolite, 2. Townshend Dam, 3. Acton Hill, and 4. Hinkley Brook) are delimited in figure 94. In subareas 1 and 2 amphibole coexisting with garnet has a different composition from amphibole in garnet-absent rocks, and the two types are differentiated in figure 94. At subareas 3 and 4 amphibole composition is not dependent upon the presence or absence of garnet.

Excluding the garnet-present samples from subareas 1 and 2, a good correlation between amphibole chemistry and metamorphic grade is observed. Actinolite-rich cores with hornblende rims commonly occur

in the garnet-albite and garnet-oligoclase zone in subarea 1. They are absent from the high garnet and staurolite-kyanite zone rocks (subareas 2-4), suggesting that actinolite cores are not preserved past medium to high garnet grade metamorphism. Between the garnet-albite and staurolite-kyanite zone, hornblende is enriched in Al^{IV}, Al^{VI}, $Na/(Ca+Na)$, and $Fe/(Mg+Fe)$; Si decreases, and K and Ti are nearly equivalent. This change is in the same direction but is much smaller than the change from actinolite. Since hornblende occurs with both albite and oligoclase, the actinolite-hornblende transition must occur at a lower grade than the change from albite to oligoclase. Garnet-oligoclase zone hornblende occurring with garnet in the Chester Amphibolite and at Townshend Dam is more Al^{IV} and $Fe/(Mg+Fe)$ rich than hornblende from the staurolite-kyanite zone.

The aluminum content of biotite and chlorite also increases with metamorphic grade as is shown in figure 95. In garnet-present rocks from the garnet zone, biotite and chlorite are more aluminous and iron rich than they are in garnet-absent rocks of the same metamorphic grade. Biotite and chlorite from staurolite-kyanite grade rocks have the same Al content as those in the lower grade, garnet-bearing samples.

No consistent relationship between epidote composition and metamorphic grade is observed, but plagioclase chemistry is highly correlated with grade. Below the oligoclase isograd the maximum molecular percent anorthite is 1.2. In the garnet-oligoclase zone separate grains of albite ($An_{0.5-3.0}$) and oligoclase (An_{16-26}) are observed. Intermediate compositions occur at the edges of albite and are optically diffuse.

Plagioclase from the highest garnet and staurolite-kyanite grade mafic rocks has the greatest anorthite content, An_{14} to An_{33}.

Compositional variation within garnet grains is greater for garnet grade rocks from the Chester Amphibolite than for those from higher grade samples. Garnet cores in the lower grade rocks are richer in Mn and Ca; rim compositions from all samples are equivalent. Carbonate is present only in the garnet grade rocks (subareas 1 and 2); it does not coexist with garnet. The maximum ankerite component in calcite from the garnet zone in the Chester Amphibolite is equivalent to that observed in the high garnet zone at Townshend Dam. However, less ankeritic calcite also occurs in the Chester Amphibolite; and calcite may get more ankeritic with metamorphic grade.

Figures 76c, 82, 88, and 92b show that for all subareas, $ilmenite_{85}$ is paired with hematite. Although ambiguity results because some analyses may be composites of hematite and ilmenite domains, hematite appears to be enriched in the ilmenite component with progressive metamorphism. Using the analyses on the largest grains, $hematite_{83}$ is paired with the ilmenite in the garnet-albite zone; $hematite_{77}$ occurs in the garnet-oligoclase zone, and $hematite_{68}$ is observed in the staurolite-kyanite zone.

I. Woodstock quadrangle

Geologic setting

The Woodstock quadrangle (figure I-2) has been mapped by Chang, Ern, and Thompson (1965). South of the town of Bridgewater in Curtis Hollow, they described (p. 34) a stream bed where mafic and silicic

volcanic layers of the Barnard Volcanic Member of the Missisquoi Formation crop out. Several samples have been collected from this area, and three have been chosen for electron microprobe investigation. Their descriptions and estimated modes are given in the appendix; and the station number (V80) is shown on the Vermont state map in figure I-1.

The Missisquoi Formation is Middle Ordovician and lies just below the major unconformity that separates Ordovician from Silurian rocks. Chang and others (1965) mapped this area in the garnet zone and adopted the proposals of Rosenfeld (1968) for the metamorphic history of southeastern Vermont. The Barnard Volcanic Member is predominately biotite gneiss, hornblende gneiss, and amphibolite; and a volcanic origin is suggested by epidote+white mica±chlorite, quartz, and plagioclase clusters which appear to be amygdules. Chang and others (1965) noted relicts of altered plagioclase and quartz phenocrysts, and from modes they calculated a quartz basalt composition for the amphibolite and a dacite to rhyodacite composition for the more silicic-rich gneiss.

The collected samples have the mineral assemblage amphibole-chlorite-epidote-plagioclase-quartz±biotite, garnet, and white mica. The phase chemistry is discussed below.

Phase chemistry

Amphibole has pale brown to blue-green to dark green pleochroism. It is prismatic and defines the foliation in V80B and the crinkled foliation in V80C. V80D amphibole is coarser, poikilitic, and not lineated. Twinned grains are common, but individual grain twin members are not distinguished by composition. Little inter- or intrasample

variation is shown by the analyses in figure 96, and only in V80D can the compositional scatter be related to grain growth. In this sample some amphibole grains have lighter colored rims which have less K, Al^{IV}, Na^{M4}, and Fe^{3+}/Fe^{2+} but more Si and Na^{A} than grain interiors.

In V80C biotite is brown and has the formula

$$(K_{.81}Na_{.02}Ca_{.02})(Mg_{1.31}Fe_{1.22}Mn_{.01}Al^{VI}_{.34}Ti_{.12})(Si_{2.78}Al^{IV}_{1.22})O_{10}(OH_{1.96}F_{.04}).$$
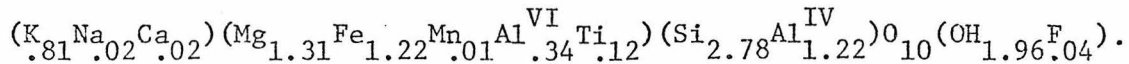
Two types of chlorite occur in this sample. Brown-green anomalous bi-refringent grains (type 1) are in chlorite-rich layers and amygdules. Brown to purple birefringent chlorite (type 2) is associated with amphibole and white mica, perhaps as an alteration product. Figure 97 shows that an analysis of a brown-purple birefringent grain has less Al^{IV} and $Mg/(Mg+Fe^{2+})$ but more Ti than the type 1 grains, and the chlorite analyses from the other samples are like the brown-green birefringent grains. The estimated formula proportion Fe^{3+} ranges from 0 to 0.19. The white mica analyzed in V80B is muscovite,

$$(K_{.78}Na_{.18})(Al^{VI}_{1.77}Fe^{3+}_{.15}Ti_{.01}Mg_{.06}Fe^{2+}_{.01})(Si_{3.06}Al^{IV}_{.94})O_{10}(OH)_2.$$
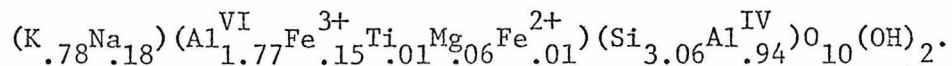
Paragonite, $(Na_{.74}K_{.07}Ca_{.03})(Al^{VI}_{1.91}Fe^{3+}_{.06}Mg_{.01}Fe^{2+}_{.01})(Si_{2.99}Al^{IV}_{1.01})O_{10}(OH)_2$, occurs in V80C. The paragonite has less phengite substitution than the muscovite; it is richer in Ca and has a greater Fe/(Mg+Fe) value.

Epidote is a major phase only in V80B where it occurs in fine-grained aggregates and as coarser grains; the latter have the average formula

$$(Ca_{1.95}Fe^{2+}_{.02}Mn_{.01})(Al^{VI}_{2.13}Fe^{3+}_{.86}Ti_{.01})Si_{3.02}O_{12}(OH).$$
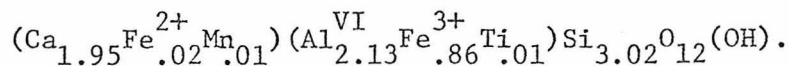
V80D epidote has the composition:

$$(Ca_{1.94}Fe^{2+}_{.04}Mn_{.02})(Al^{VI}_{2.22}Fe^{3+}_{.77}Ti_{.01})Si_{3.00}O_{12}(OH).$$
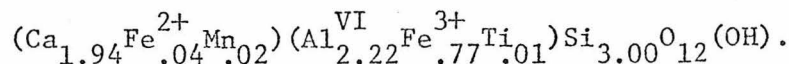
As shown in figure 98a, V80C epidote analyses vary significantly in ferric iron content. In the chlorite-poor layer, yellow grains are Fe^{3+} rich, colorless grains have less Fe^{3+}, and pale yellow grains have compositions intermediate to the other two grain types. No optically zoned grains are observed.

The electron microprobe analyses of plagioclase are contained in figure 98b. Subhedral and fine-grained plagioclase in V80B has an average of 16 molecular percent anorthite. V80C plagioclase ranges from $An_{16.1}$ to $An_{31.4}$. The most anorthitic grains analyzed are from the chlorite-rich layer and amygdules, and grains zone toward more anorthitic rims. Plagioclase in V80D is twinned and does not extinguish uniformly. The analyses range from $An_{15.4}$ to $An_{22.9}$, with grain exteriors more anorthitic than interiors.

Garnet at Curtis Hollow is nearly homogeneous as indicated by figure 99b. Edges are slightly less Mn and Ca rich and have more Fe and Mg than grain interiors. V80C garnet is almandine richer but pyrope poorer than that in V80D. Euhedral magnetite in V80B and C is

$$Fe^{2+}_{1.00}Fe^{3+}_{1.99}Si_{.01}O_4.$$
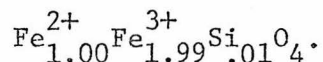
Hematite is elongated and often contains ilmenite exsolution lamellae. The analyses are plotted in figure 99a.

J. Wilmington quadrangle

Geologic setting

In figure I-1 four Precambrian gneiss domes are delimited in southeastern Vermont. The two farthest south are the Lake Rayponda and Sadawga Pond domes in the Wilmington quadrangle. The Cambrian and

Ordovician rocks which mantle these domes are high garnet grade (Skehan, 1961). Skehan and Hepburn (1972) asserted that they were regionally metamorphosed during the Acadian orogeny and Harper (1968) and Faul and others (1963) measured 318 to 348 m.y. K/Ar ages in this area.

The minerals in two samples from the Wilmington quadrangle have been analyzed with the electron microprobe. Both are from the Chester Amphibolite Member of the Pinney Hollow Formation and are interlayered with biotite-chlorite-plagioclase-garnet-quartz-white mica±epidote schist. The exact locations of these samples and their descriptions are in the appendix; the phase chemistry data follow.

<u>Phase chemistry</u>

<u>Amphibole</u>

The largest grains in V146A commonly have lighter cores than rims. The contact between the optical domains is diffuse rather than sharp, and the pleochroic formula for the rims is the same as for optically continuous grains (which comprise most of the amphibole): pale brown to blue green to green. The cores are more actinolitic than the rims, and electron microprobe traverses across several grains suggest the zoning delineated in figure 100. Following an increase in Al^{IV}, Al^{VI}, Na/(Ca+Na), and Fe^{3+}/(Mg+Fe) toward the rims, there is a reversal in these parameters caused by a decrease in the glaucophane/riebeckite substitution. K and Ti continue to increase.

Acicular and elongated prismatic amphibole grains with pale brown to blue-green to dark green pleochroism define the foliation in V158A.

The grain size is a few tens of microns making multiple analyses per grain difficult. Two of the largest grains are zoned as indicated in figure 100. Grain margins are richer in K, Ti, Al^{VI}, and Al^{IV} but poorer in Si. Compared to V146A amphibole, that from V158A has greater values of $Na^A/(Ca+Na)$ and $Fe/(Mg+Fe)$.

Carbonate

Separate grains of dolomite, $(Ca_{1.02}Mg_{.77}Fe_{.18}Mn_{.02})(CO_3)_2$, and calcite, $(Ca_{.92}Mg_{.05}Fe_{.02}Mn_{.01})CO_3$, are observed in V146A. The dolomite has higher relief than the calcite and is present as poikiloblastic and ground mass grains; calcite occurs only as ground mass grains. Fine- and coarse-grained calcite is associated with chlorite layers in V158A, and the former is more ankeritic. Evident from figure 101a is that V158A calcite has less ankerite substitution than calcite in V146A.

Biotite and chlorite

Brown bioite from the Chester Amphibolite in the Wilmington quadrangle has the average formula

$$(K_{.88}Na_{.02}Ca_{.01})(Fe,Mg,Mn,Zn)_{2.61}Al^{VI}_{0.29}Ti_{.10}(Si_{2.83}Al^{IV}_{1.17})O_{10}(OH_{1.99}F_{.01}).$$
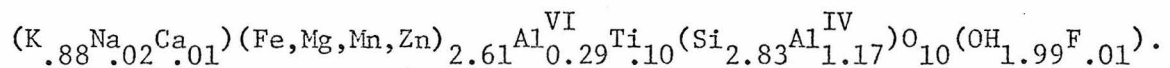
As is shown in figure 101b, V146A biotite is more Al^{VI} and $Mg/(Mg+Fe)$ rich than that from V158A. All the analyses have more Al^{VI} than is needed to balance the $Al^{IV} \rightleftarrows Si$ substitution. Chlorite from V146A is also the more magnesian, but all the analyses reduce to the formula

$$(Fe^{2+},Mg,Mn,Zn)_{4.7}Al^{VI}_{1.2}Fe^{3+}_{0.1}(Si_{2.7}Al^{IV}_{1.3})O_{10}(OH)_8.$$
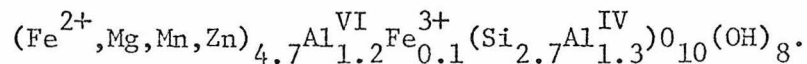
Epidote

Epidote from both the studied samples is generally between 10 and 50 microns across, is anhedral to subhedral, and has pale yellow

pleochroism. A few of the largest grains have darker yellow cores which, as is illustrated in figure 102a, are more ferric iron rich. The $Fe^{3+} \rightleftarrows Al^{VI}$ substitution is the only variable that shows significant inter- or intrasample change. Mn and Fe^{2+} substitute for Ca up to .03 formula proportion each, and Ce is negligible.

Plagioclase

Anhedral to subhedral plagioclase in V146A ranges in composition from $An_{12.6}$ to $An_{21.2}$, and the maximum orthoclase content shown in figure 102c is 0.4 molecular percent. In some grains a sharp contact separates differently extinguishing cores from rims; but generally, the contact is diffuse. Grain margins are more anorthitic than interiors.

Albite and oligoclase occur in V158A, and electron beam scans indicate that each is a distinct phase. As illustrated in figure 102c, the albite ranges from $An_{0.3}$ to An_{20}, while the oligoclase has 16 to 18 molecular percent anorthite. Both phases appear to be enriched in anorthite toward grain margins and to have equivalent potassium contents ($Or_{0.4}$ is the maximum). The $An_{3.7}$ and $An_{4.5}$ analyses may include both albite and oligoclase domains, as an electron beam scan of this area reveals only Ca-absent and Ca-present plagioclase.

Fe, Ti oxides

Magnetite, $Fe^{2+}_{1.00}Fe^{3+}_{2.00}O_4$, and hematite are observed in V158A. The hematite occurs as elongated grains with aligned ilmenite lamellae. The electron microprobe analyses show a significant scatter (Hem_{61-78}) suggesting that varying amounts of each phase were analyzed. (A 15 to

20 μm spot was used for the analyses to average the hematite host and ilmenite lamellae.) One analysis on an ilmenite lamella is Ilm_{86} as is shown in figure 102b; it has a greater $(Mn,Mg,Zn)TiO_3$ content than the hematite analyses.

CHAPTER V

POLYMETAMORPHIC HISTORY OF VERMONT AND ADJACENT QUEBEC

A. Introduction

In this chapter the physical conditions of metamorphism in each investigated area are characterized from the mineral chemistry and overgrowth relationships in mafic rocks and the interlayered pelitic rock assemblages. Field and isotopic studies are used to assign ages to these mineral growth events, and a polymetamorphic history of Vermont and adjacent Quebec is proposed.

Pressure and temperature

Phase chemistry from world-wide occurrences of mafic rocks was summarized in chapter III. It was shown that in mafic rocks amphibole and plagioclase compositions correlate with metamorphic grade and facies series. With increasing grade actinolite changes to hornblende and plagioclase becomes more anorthitic. High-pressure metamorphism favors the glaucophane-riebeckite substitution in amphibole. It displaces the incorporation of anorthite in plagioclase toward higher temperature. White mica and carbonate are also indicators of the physical conditions of metamorphism. Muscovite-paragonite and calcite-dolomite/ankerite pairs are usable geothermometers. The phengite substitution in K white mica is pressure sensitive.

The paragenesis and mineral composition data from mafic rocks from Vermont and adjacent Quebec were presented in chapter IV. Most of these rocks contain the assemblage amphibole-chlorite-epidote-plagioclase-quartz. A carbonate, K-mica phase, a Ti phase, and an Fe^{3+} oxide are

also commonly present. Since the mineral assemblage is constant, the compositions of individual phases can be compared between rocks and used to characterize the temperature and pressure environments.

The temperature dependence of Ca-amphibole was documented for the Underhill and Stowe Formations, in northeastern Vermont, and in the Saxtons River quadrangle. The data agree with those from the world-wide occurrences. With increasing metamorphic grade as defined by the intercalated pelitic rocks, amphibole is enriched in the tschermakite component and changes from actinolite to hornblende. In the Saxtons River quadrangle and in northeastern Vermont, plagioclase becomes more anorthitic with metamorphic grade.

The phase assemblages and compositions also argue for high-, medium-, and low-pressure facies series metamorphism. The high pressure assemblage glaucophane-omphacite-garnet-phengite is observed in the Hazens Notch Formation at Tillotson Peak. Significant glaucophane/riebeckite substitution occurs in Ca-rich amphibole from other Cambrian and Ordovician mafic rocks in northern Vermont and southern Quebec. Staurolite-andalusite-sillimanite pelitic assemblages and edenite-rich Ca amphibole+anorthite-rich plagioclase mafic assemblages in the Silurian and Devonian units in northeastern Vermont indicate regional low-pressure metamorphism. In the Cambrian and Ordovician units, chloritoid-staurolite-kyanite pelitic schist and hornblende-albite mafic schist suggest medium-pressure metamorphism.

Time

Field, petrologic, and isotopic studies indicate that the northern Appalachian Mountains had a polymetamorphic history. Woodland (1965)

and Anderson (1977) recognized two major periods of metamorphic mineral growth in the Devonian rocks in northeastern Vermont. They assigned both events to the Devonian Acadian orogeny and correlated the second with the emplacement of the New Hampshire plutonic series. Rosenfeld (1968, 1972) identified two periods of mineral growth in the Silurian and Devonian units in southeastern Vermont. In addition, he observed an earlier period of mineral growth which he tentatively assigned to the Ordovician Taconic orogeny. In the Cambrian and Ordovician units in northern Vermont and southern Quebec, radiometric data indicate widespread Devonian metamorphism (Cady, 1969). Rickard (1965), Albee (1968), Harper (1968), and Lanphere and Albee (1974) have proposed that Ordovician metamorphism is also recorded by these rocks.

The petrographic and chemical evidence presented in chapter IV also argue for multiple periods of metamorphic mineral growth. Overgrowth relationships are common, and optically and chemically discontinuous amphibole grains are ubiquitous. Another explanation for these zoned grains must be considered as several workers (see for example Shido, 1958; Klein, 1968; Cooper and Lovering, 1970; Brady, 1974; and Misch and Rice, 1975) have proposed that a miscibility gap exists between actinolite and hornblende. However, neither the actinolite-hornblende nor the actinolite-barroisite pairs observed appear to be due to immiscible intergrowth. The discontinuously zoned grains tend to be the largest amphibole in a thin section. Unrimmed grains have compositions similar to the rims. No separate grains with the chemistry of the core are observed. Cores may be anhedral or euhedral and may or may not be

in optical continuity with the rims. In some cases the rims appear to be a cluster of several small grains. Other minerals such as chlorite or epidote are observed at core/rim boundaries.

The actinolite-hornblende pairs from the same grade and facies series have different compositions and cannot be ordered by increasing grade to give any consistent miscibility gaps. Similarly, the actinolite-barroisite pair compositions show no consistent relationship to metamorphic grade. Zoning trend reversals such as were documented in chapter IV for the Pinnacle Formation, Hazens Notch Formation, Stowe Formation, and Saxtons River quadrangle also argue against the discontinuously zoned Ca-rich amphibole grains being immiscible intergrowths.

The mineral growth events indicated by overgrowth relationships in the amphiboles can be correlated with the radiometric age assignments. Each generation can be petrologically characterized from the phase chemistry of the mafic rocks and the paragenesis in the interlayered pelitic schist. Combining these data yields the polymetamorphic history of Vermont and adjacent Quebec proposed here.

B. Petrologic characterization and chronology of mineral growth events

A summary of the mineral growth events recognized in the mafic rocks is presented in table 1. The events are petrologically characterized, and the proposed age assignments are given. The tabulated Ordovician ages have been radiometrically determined by Marvin Lanphere. Lanphere and Albee (1974) reported a 457 ± 26 m.y. $^{40}Ar/^{39}Ar$ total fusion age on barroisitic hornblende from the Worcester Mountains (Stowe

Formation, station V5). Hornblende cores and actinolite rims were mag-
netically separated from sample V50B from the Stowe Formation, Elmore
Mountain subarea, and given to Marvin Lanphere. He measured a $^{40}Ar/^{39}Ar$
total fusion age of 437 ± 7 m.y. on the hornblende cores and 440 ± 9 m.y.
on the actinolite rims. Lanphere and Albee (1974) argued against the ap-
parent Ordovician ages being simply anomalously old because of excess
radiogenic argon. Their consistency argument is strengthened by the
Ordovician ages at Elmore Mountain. It would be exceedingly fortuitous
for the muscovite (for which Lanphere and Albee (1974) also obtained an
Ordovician age) and amphibole in the Worcester Mountains and the actino-
lite and hornblende at Elmore Mountain to have incorporated the correct
amount of argon relative to their potassium contents to yield the same
age.

The mineral growth in these two dated samples has been assigned to
O2 in table 1. Metamorphic events which can be petrologically correlated
with the known O2 events are also assigned to O2. Growth periods prior
to O2 are referred to as O1; no absolute age assignment can be made
for O1.

In the Silurian to Devonian mafic rocks, a medium- to low-pressure
and a low-pressure mineral growth generation is observed. These events
may be correlated with the two periods of Devonian mineral growth observed
by Woodland (1965) and Anderson (1977) and are tabulated as D1 and D2.
Naylor (1971) reported a minimum emplacement age of 380 m.y. for the New
Hampshire plutonic series. Ages from 350 to 380 m.y. indicating Devonian
mineral growth in Cambrian and Ordovician units are reported by Harper

(1968), Lanphere and Albee (1974), and Marvin Lanphere (ongoing research). Anderson (1977) reported two periods of Devonian mineral growth in pre-Silurian rocks. In table 1 two periods of Devonian growth are also indicated for Cambrian and Ordovician rocks. D1 and D2 have been tentatively assigned 380 and 350 m.y. ages, respectively.

The metamorphic grade indicated for each sample in table 1 is determined from the interlayered pelitic rocks. For events recognized in relict amphibole cores only, the grade is listed as medium or low.

The facies series assignments in table 1 are based on the amphibole composition associated with each growth period. On figures 1-4 envelopes delimit three groups of Ca-rich amphibole analyses from the mafic rocks studied. These are the same diagrams used to examine the pressure dependency of the world-wide occurrences of amphibole in mafic rocks (see chapter III). Groups I and II are from the Cambrian and Ordovician units. The first encompasses the calcic and soda-calcic amphibole from the high-pressure terrane at Tillotson Peak (from the Hazens Notch Formation study area). Also included are analyses that have chemical affinities with these high-pressure amphiboles. The other pre-Silurian study areas have amphibole which plots within envelope II. Group III encloses the compositional variation observed in calcic amphibole from northeastern Vermont.

Comparison of figures 1-4 in chapter III with figures 1-4 of this chapter shows that calcic amphibole from mafic rocks from Vermont and southern Quebec have the same compositional distribution as the world-wide occurrences. The envelopes for amphibole from high-pressure terranes lie predominately above the high-pressure line of Raase (1974)

(figure III-1) and the 1:1 lines on figures III-2 and III-4. They show significant Na^{M4} substitution (figure III-3). Similarly, Group I amphibole plots high on figures 1, 2, and 4 and is rich in Na^{M4} (figure 3).

The envelopes for low-pressure Abukuma and the medium-pressure Haast River amphibole analyses plot below Raase's line (figure III-1) and the 1:1 lines on figures III-2 and III-4. They lie close to the Ca-Na^A side of the graph in figure III-3. Group III amphibole has this compositional range. Group II analyses straddle the Raase (1974) line and the 1:1 lines on figures 1, 2, and 4. They plot between Groups I and III on these graphs and on figure 3. This position is delimited by calcic amphibole from the Dalradian in southwestern Scotland (figures III-1 to 4).

On the basis of this correlation, the amphibole from mafic rocks from Vermont and southern Quebec are characterized by facies series in table 1. The glaucophane-forming generations are classified as high-pressure. Barroisite, barroisitic hornblende, and barroisitic actinolite are considered medium- to high-pressure. Analyses which straddle the 1:1 lines on the diagrams in figure 2 and 4 and which show glaucophane/riebeckite and edenite substitution on the figure 3 quadrilateral are classified as medium-pressure. Those analyses which lie below the 1:1 lines and lie close to the Na^A-Ca side of the quadrilateral are put into medium- to low-pressure or low-pressure facies series; the latter group shows the least glaucophane/riebeckite substitution.

All the medium- to low-pressure amphibole generations are assigned Devonian ages and correlated with the relatively low-pressure metamorphism

observed in northeastern Vermont. Since no high- or medium- to high-pressure amphibole is observed in Silurian and Devonian rocks, all the amphibole generations formed under the relatively high-pressure conditions are shown as Ordovician on table 1. Ordovician and Devonian ages from the mafic and intercalated pelitic rocks indicate that both Ordovician and Devonian medium-pressure metamorphism has occurred.

Each study area is now considered in the sequence in which it was discussed in chapter IV. All the phase chemistry, petrographic, field, and isotopic data are combined. Since all four facies series specific diagrams in figure 1-4 show the same relationship among the three amphibole groups, only the normalization independent diagram (figure 4) is used to show the amphibole compositional variation, and envelopes enclose the analyses which are plotted in chapter IV.

Pinnacle Formation

Figure 5 shows the data envelopes for amphibole from the Tibbit Hill Volcanic Member of the Pinnacle Formation. Samples Q3C and LA426, 434A, and 435A contain amphibole with significant glaucophane/riebeckite substitution which lies in the medium- to high-pressure facies series group. Relatively high-pressure metamorphism is also suggested by phengite (Si = 3.47) in LA433C. In contradistinction, LA460B amphibole straddles the 1:1 line on figure 5 indicating medium-pressure growth.

The combined zoning arrow for the medium- to high-pressure analyses is delineated on figure 5. In general, cores are more barroisitic than rims. Q3C shows a more complicated history and is responsible for the indicated zoning reversal. Actinolite cores are interior to barroisitic

actinolite domains, which are overgrown by actinolite. On table 1
these inner cores are called 01. Since they are actinolite, they indicate medium-pressure, low grade metamorphism. The barroisitic actinolite
cores for all the Pinnacle Formation samples are grouped as 02; they indicate low grade, medium- to high-pressure metamorphism. Actinolite rims
and separate grains are medium-pressure. They are probably biotite grade
because the interlayered pelitic rocks belong to this metamorphic zone.
It is likely that these rims formed during Devonian metamorphism because
Harper (1968) reported Devonian K/Ar ages on muscovite in this area.
There is no petrological evidence which allows these rims to be assigned
to D1 versus D2.

Sample LA460B amphibole is anomalous, and it is not included in
table 1. Two periods of medium-pressure mineral growth are observed.
The light, actinolite domains appear to postdate dark, more hornblende
rich areas and be due to lower grade metamorphism.

Underhill Formation

As shown in figure 6 amphibole from the Underhill Formation mafic
rocks records medium-pressure metamorphism. In all four samples the
plagioclase is albite. Since the amphibole ranges from actinolite to
hornblende, the albite-oligoclase transition must occur at a higher grade
than the change from actinolite to hornblende. This relationship also
indicates medium-pressure metamorphism.

The interlayered pelitic rocks suggest that two samples are from
the biotite zone and two are from the garnet zone. Most of the amphibole
in the biotite grade sample LA430B shows more tschermakite substitition and

is higher grade than the amphibole in the other biotite grade sample (LA504B). The two garnet zone samples show more tschermakite substitution than either of the lower grade ones. Calcite and dolomite coexist in V340B. The geothermometer of Barron (1974) gives a value of 475°C.

A complicated metamorphic history is indicated by the zoning arrows in figure 6. LA504B may show retrograde growth. More tschermakite substitution is observed in the actinolitic hornblende porphyroblast cores in LA430B than in the actinolite rims, also indicating retrogradation. However, a final actinolitic hornblende to hornblende rim on some of the matrix and prophyroblast rim grains in this sample indicates later prograde growth which may have been lower pressure. Prograde amphibole growth has occurred in the garnet grade samples V340B and 225B. Amphibole cores in V225B indicate a period of mineral growth prior to the rims, and rims may be slightly lower pressure.

Devonian mineral growth in this area is suggested by K/Ar mica ages reported by Harper (1968) and Lanphere (written communication, 1975). On muscovite and biotite provided by Arden Albee, Lanphere measured 380 and 359 m.y. conventional K/Ar and $^{40}Ar/^{39}Ar$ ages at Mount Grant in the Lincoln Mountain quadrangle near V340. Although the two ages are not statistically different they could correspond to multiple periods of Devonian metamorphism. The amphibole cores in LA430B and V225B are tentatively assigned to D1, and D2 growth for the rims is possible. D2 may have been lower pressure than D1. There is no basis for assigning LA504B or V340B amphibole to either D1 or D2.

Hazens Notch Formation

Two subareas have been studied from the Hazens Notch Formation, Tillotson Peak and Belvidere Mountain. The polymetamorphic history of Tillotson Peak is characterized first.

Tillotson Peak

Glaucophane and omphacite assemblages at Tillotson Peak are unique in Vermont and the east coast of the United States. They show that this area has been metamorphosed at high pressure. The eclogite assemblage garnet-omphacite in A-BM-100 plots within the high-pressure metamorphic field on the K_D diagram shown by Miyashiro (1973, p. 318). Fe^{2+}/Mg garnet ranges between 6.8 and 10.5, while this ratio for omphacite is 0.28 to 0.34.

To estimate the phsycial conditions which caused this extraordinary paragenesis, several pertinent stability curves are plotted in figure 7. The stippled area indicates the probable range of pressure and temperature responsible for the peak metamorphic mineral growth at Tillotson Peak. The lower temperature limit is based on the K white mica-paragonite equilibrium in V337B. The phengite has K/(K+Na+Ca) = .925 and gives a temperature of 350°C on the solvus delineated by Eugster and others (1972). Considerable scatter is shown by the paragonite analyses (the muscovite component ranges from 4.5 to 29 mole %).

Andalusite is not observed in pre-Silurian rocks in Vermont, but kyanite is. This relationship restricts the pressures attained to greater than the andalusite-kyanite breakdown. The aluminum silicate phase diagrams of Richardson, Gilbert, and Bell (1969) and Holdaway (1971) are

indicated on figure 7. Kyanite is reported by Albee (1968) about 10 miles east of Tillotson Peak, and Cady and others (1963) observed chloritoid about 5 miles southeast of this subarea. Therefore, the breakdown of chloritoid + Al_2SiO_5 to staurolite + quartz taken from Richardson (1968) is used for the 550°C upper temperature limit.

The maximum amount of Si in the K white mica is 3.45. Interpolating from the curves of Velde (1967) gives the lower pressure limit shown on figure 7. Velde's curve for Si = 3.4 is also reproduced on this diagram. Extrapolating Kushiro's (1969) curve for the formation of omphacite (Jd_{40}) to the region of interest provides an indication of the pressure-temperature regime at Tillotson Peak. It is close to the calcite-aragonite transition experimentally determined by Johannes and Puhan (1971). Aragonite is not observed, but calcite and dolomite are. This line is therefore used as the upper limit to the pressures attained.

The garnet-omphacite equilibrium in A-BM-100 provides a check on the estimated P-T regime for the peak of metamorphism at Tillotson Peak. Råheim and Green (1974) presented the relationship

$$T \ (°K) \ = \ \frac{3686 + 28.35 * P(Kb)}{\ln K_D + 2.33} \qquad K_D \ = \ \frac{(Fe^{2+}/Mg) \ garnet}{(Fe^{2+}/Mg) \ clinopyroxene} \ \ .$$

Both the omphacite and garnet in this sample are zoned, and it is not known what compositions were in equilibrium, but a reasonable pressure of 8.3 kb at 425°C is calculated for the average garnet rim and the average omphacite.

On figure 8 envelopes surround the observed amphibole compositions at Tillotson Peak. Also indicated are the combined zoning arrows.

Barroisite cores show retrograde growth. A sharp optical and chemical break separates these cores from barroisitic actinolite rims. Rims and separate grains continue retrograde growth until prograde metamorphism is indicated by a reversal in the zoning pattern. In table 1 the barroisite cores are shown as Ordovician event 1 and the actinolitic rims as O2. The occurrences of glaucophane are as follows: glaucophane cores with barroisitic actinolite rims, barroisite cores with glaucophane rims, and optically continuous glaucophane grains. These morphological relationships indicate that barroisite and glaucophane could have been stable at one time; glaucophane and barroisitic actinolite could have coexisted at a later time. A high-pressure O1 event and a high-pressure O2 event are listed in table 1. Since barroisite has more tschermakite substitution than barroisitic actinolite, the first event was higher grade than the second. However, prograde growth observed in the calcic amphibole nearly reaches the grade represented by the initial generation as is indicated by the zoning arrow in figure 8.

Belvidere Mountain

Two periods of medium- to high-pressure facies series metamorphism are recorded at Belvidere Mountain, two miles south of Tillotson Peak. Barroisite cores and rims are delimited by the envelopes for this subarea in figure 8. The cores have been assigned to O1 and the rims to O2. The absence of glaucophane indicates lower pressure metamorphism than at Tillotson Peak because with increased pressure barroisite + quartz breaks down to glaucophane + actinolite + epidote.

Pinney Hollow Formation (Granville Notch)

As indicated by the amphibole analyses for which envelopes are shown in figure 9, barroisite cores in the host rocks and winchite-rich actinolite cores in the veins record a medium- to high-pressure event at Granville Notch. Since the vein amphibole cores show less tschermakite substitution than the host amphibole cores, lower temperature mineral growth is recorded by the veins. In table 1 these medium- to high-pressure growth events are assigned to the second period of Ordovician metamorphism.

Overprinting this event is a later, low grade, medium-pressure event responsible for the actinolite rims and separate grains. Presumably, the biotite grade metamorphism observed in the interlayered pelitic rocks records this last event. Whole rock K/Ar ages reported by Harper (1968) indicate late Devonian mineral growth in this area, and the medium-pressure, biotite grade mineral generation is tentatively assigned to D2 in table 1.

Stowe Formation

The amphibole data envelopes for the three Stowe Formation subareas studied are shown in figure 10. The biotite zone samples at Eden Notch (28A and 30A) and sample V3C from the Worcester Mountains have discontinuously zoned amphibole grains with more barroisitic cores than rims. These cores and the barroisitic actinolite in the biotite zone sample V11A from the Worcester Mountains suggest low grade, medium- to high-pressure facies series metamorphism. Barroisitic hornblende from the garnet zone sample V5B (Worcester Mountains) also indicates relatively high-pressure metamorphism.

The actinolite rims on these medium- to high-pressure cores and the actinolite in the biotite zone sample V6B from the Worcester Mountains appear to have formed under more medium-pressure conditions. Samples V44 and V50B from Elmore Mountain also contain medium-pressure amphibole. Two growth events are recorded. Actinolitic hornblende and hornblende cores are zoned toward more tschermakite substitution and therefore higher grade. The actinolite rims indicate low grade metamorphism. That the second generation was lower grade than the first is also indicated by the pelitic rocks as was proposed by Albee (1957). From the spatial relationship of V44 and 50B to the isograds delineated by Albee (1957), the peak of metamorphism in the former should have been higher. Indeed, V44 amphibole cores are richer in tschermakite than those in V50B.

The barroisitic hornblende from station V5 has been dated by Lanphere and Albee (1974) at 457 ± 26 m.y., and O2 mineral growth is indicated for V5B on table 1. The medium- to high-pressure cores in the biotite zone samples can be petrologically correlated with the barroisitic hornblende and are also assigned to O2 metamorphism. Radiometric evidence indicates that Devonian mineral growth has occurred in this area. Marvin Lanphere (written communication, 1975) measured a 348 ± 5.1 m.y. $^{40}Ar/^{39}Ar$ age on a muscovite vein northeast of Eden Notch. Lanphere and Albee (1974) reported a 358 ± 4 m.y. $^{40}Ar/^{39}Ar$ plateau age on muscovite from the Worcester Mountains. The actinolite rims and optically continuous grains at Eden Notch and in the Worcester Mountains are therefore tentatively listed as D2 in table 1.

As previously discussed Marvin Lanphere (written communication, 1976) reported Ordovician $^{40}Ar/^{39}Ar$ ages on hornblende cores and

actinolite rims from Elmore Mountain (sample 50B). These data suggest that the prograde growth here was arrested and followed by low grade metamorphism with no hiatus of geologic time. Alternatively, the hornblende could have formed earlier and the record of its age could have been erased by total outgassing during the time the actinolite rim formed. However, this seems less likely becuase the rim is actinolite, indicating low grade metamorphism. Moreover, in the Worcester Mountains Lanphere and Albee (1974) reported that the earlier event was preserved in the barroisitic hornblende during the later, low grade event.

Northeastern Vermont

Three samples from the Silurian and Devonian rocks in northeastern Vermont were studied in detail. The calcic amphibole compositions measured are contained by envelopes on figure 11. All analyses fall below the 1:1 line and indicate relatively low metamorphic pressures. As shown on figure I-1 sample V53 was collected next to one of the New Hampshire series plutons. Woodland (1965) showed this locality within the andalusite-sillimanite zone, supporting the conclusion that low-pressure metamorphism has occurred here. The biotite and garnet zone amphibole analyses suggest somewhat higher pressure metamorphism. Oligoclase coexists with actinolitic hornblende in the biotite zone sample (V38A), and Miyashiro (1973, p. 250) assigned this paragenesis in mafic rocks to low-pressure regional metamorphism. On table 1 V38A is listed as medium- to low-pressure facies series. V36A hornblende appears to have also formed at medium- to low-pressure conditions but at a higher grade than V38A. The interlayered pelitic rocks also indicate that V36A is higher grade, and the plagioclase in this sample is more anorthitic.

Since V53 was collected adjacent to a pluton, it is assigned to the last Devonian event, D2. V38A and 36A indicate somewhat higher metamorphic pressures than V53 and they were collected farther from the New Hampshire series plutons, they are tentatively assigned to the earlier Devonian event (D1) on table 1.

Two periods of mineral growth are observed in the biotite zone sample; but they appear to belong to the same facies series, and it is not clear if they are separated in time. Some amphibole grains have more actinolitic cores than rims, and cross foliation amphibole tends to be more tschermakitic than the amphibole parallel to the foliation. As is shown in figure 11, there is considerable overlap in the data, making it chemically difficult to distinguish the two morphologically different amphiboles.

Late low grade metamorphism appears to be recorded by V53. Most of the plagioclase in this sample is bytownite, but one analyzed grain which is intergranular to hornblende porphyroblasts is andesine. The chemical zoning in amphibole from this sample also suggests retrograde growth toward grain margins.

Saxtons River quadrangle

On figure 12 amphibole analyses from the Saxtons River quadrangle are grouped by metamorphic grade, which is established from the pelitic layers. Although sample V94A appears to be in the high biotite zone (Rosenfeld, oral communication, 1971), it is grouped with the garnet zone amphibole coexisting with albite because it is chemically indistinguishable. Since it was shown in chapter IV that garnet-oligoclase grade

amphibole coexisting with garnet is more tschermakitic than that in garnet-absent assemblages, only amphibole from the common mafic rock assemblage amphibole-chlorite-epidote-plagioclase-quartz is included in the envelopes in figure 12.

All these amphibole analyses straddle the 1:1 line and appear to record medium-pressure metamorphism. The plagioclase compositions also support this conclusion. Hornblende occurs in both albite- and oligoclase-bearing rocks, indicating that the actinolite-hornblende transition occurs at lower grades than the albite-oligoclase transition. The small extent of phengite substitution in K-rich white mica (Si averages 3.1) provides further evidence for medium-pressure mineral growth.

Multiple periods of mineral growth are indicated by the zoned amphibole grains present in the garnet grade samples. In general, as is shown on figure 12, the optically distinct cores are more actinolitic than the rims indicating lower grade growth. Evidence for a medium grade event prior to the low grade mineral growth that formed the actinolite cores is found in V127A. Hornblende cores occur interior to the actinolite in a few grains. In the one grain analyzed, the hornblende core is similar in composition to the hornblende rims and optically continuous grains in the sample. It is anhedral indicating that it has been partially consumed during the growth of the euhedral actinolite core.

Rosenfeld (1968, 1972) assigned the mineral growth at Townshend Dam and Acton Hill to his Devonian event I. Amphibole growth in these two subareas of the Saxtons River quadrangle are assigned to D1 in table 1. As his second event is not extensively developed on the west side of

Athens dome, the hornblende rims and optically continuous grains from
the Chester Amphibolite subarea are also assigned to D1. The actinolite
cores are correlated with the Ordovician (?) event recognized by Rosenfeld
(1968) and listed as O2 in table 1. The earlier event suggested by horn-
blende interior to the actinolite cores is tentatively assigned to O1.

Evidence for a late change to somewhat lower pressure conditions
is observed in V124B hornblende. Near grain edges the edenite substi-
tution increases while the glaucophane/riebeckite substitution decreases.
This zoning pattern is shown by the curve in the solid arrow on figure 12.
There is no optical evidence of this compositional variation. This change
in facies series may be correlated with the doming of Athens and Chester
domes. Rosenfeld (1968) tentatively assigned this event (II) to the
Appalachian orogeny (Permian?). However, he suggested that little time
separated the doming from his earlier event I. The lack of any optical
or chemical discontinuity in the amphibole also argues against a long
hiatus, and the apparent decrease in dP/dT toward grain edges may be
due to a change in metamorphic conditions at the end of the Acadian
orogeny. In table 1 this mineral growth is assigned to D2.

No discontinuously zoned amphibole grains occur in the high garnet
grade rocks at Townshend Dam or the staurolite-kyanite grade rocks at
Hinkley Brook and Acton Hill. Since overgrowth relationships are common
in the lower grade rocks, high garnet zone metamorphism appears to have
been sufficient to eradicate the earlier, low grade event. Coexisting
muscovite and paragonite ($K/(K+Na+Ca)$ = 0.78 and 0.13, respectively) at
Hinkley Brook can be used to estimate the temperature in the staurolite-

kyanite zone. The muscovite limb gives 570°C and the paragonite 640°C on the solvus of Eugster and others (1972).

Woodstock quadrangle

Amphibole from the Woodstock quadrangle study area shows little chemical variation. Presence or absence of garnet in the assemblage does not affect the amphibole composition on the diagram in figure 13. The envelope containing the amphibole analyses from this area is compared to amphibole analyses from the Saxtons River quadrangle. It overlaps the high garnet and staurolite-kyanite zone analyses, and relatively high grade, medium-pressure metamorphism is thus indicated. Chang and others (1965) mapped this area as garnet grade, and it is therefore listed in table 1 as high garnet grade.

The white mica and plagioclase compositions are consistent with this metamorphic grade assignment. The phengite component (Si = 3.06) of the K white mica is small and argues against "abnormally" high pressures. Muscovite in V80B gives 530°C on the solvus of Eugster and others (1972); paragonite in V80C gives 600°C. The plagioclase shows prograde growth with a maximum anorthite content (An_{31}) like that in the high garnet zone and staurolite-kyanite zone Saxtons River quadrangle mafic rocks.

In accordance with the medium- pressure metamorphism in pre-Silurian rocks to the south, mineral growth in this area is assigned to D1.

Wilmington quadrangle

Mineral growth in the two samples analyzed from the Wilmington quadrangle appears to be medium-pressure and to reach the garnet-oligo-clase zone. The amphibole analyses envelope delimited in figure 14 for

this area overlaps that for the Saxtons River quadrangle, garnet--oligo-clase zone rocks. Hornblende occurs with albite and oligoclase in V158A and with oligoclase in V146A, indicating that the actinolite-hornblende transition has occurred at a lower grade and that the facies series is medium-pressure. A moderate temperature of about 450°C is estimated for the calcite-dolomite pair in V146A using the solvus delineated by Barron (1974).

Both plagioclase and amphibole record prograde growth. The zoning arrow for amphibole shown on figure 14 was documented in chapter IV for sample V146A. This pattern is similar to the zoning observed in the Saxtons River quadrangle sample, V124B. Edge compositions have more edenite substitution than grain interiors. This relationship suggests that a later, lower pressure period of mineral growth overprinted the medium-pressure growth generation. In table 1 this lower pressure event is assigned to D2, and the medium-pressure growth is listed as D1.

C. Summary and suggestions for further work

The compositions of amphibole, plagioclase, white mica, and car-bonate characterize the physical conditions of metamorphism in the investigated areas. Overgrowth relationships in the amphiboles indicate relative time. Correlating the mineral growth events in the mafic rocks with field and isotopic studies yields the tentative age assignments shown in table 1. Two periods of high-, medium- to high-, and medium-pressure mineral growth are observed in the Cambrian and Ordovician rocks from Vermont and southern Quebec and have been assigned to the Ordovician. Overprinting of medium- and medium- to low-pressure

metamorphism on the earlier growth generations has been assigned a Devonian age. In the Silurian to Devonian rocks from northeastern Vermont, all mineral growth appears to have been relatively low-pressure. Medium- to low-pressure and low-pressure growth generations are recognized.

The high-pressure metamorphism is confined to the vicinity of Tillotson Peak in the Hazens Notch Formation. Medium- to high-pressure metamorphism is observed on Belvidere Mountain to the south and in the Worcester Mountains. Barroisite-rich and winchite-rich cores in the Pinnacle Formation, from the Stowe Formation (Eden Notch and Worcester Mountains subareas), and from the Pinney Hollow Formation (Granville Notch subarea) appear to be remnants of relatively high-pressure mineral growth. Only medium-pressure metamorphism is observed at Elmore Mountain (Stowe Formation study area) and in the Underhill Formation, indicating the possible eastern and western extents of the medium- to high-pressure event. The farthest to the south it has been observed is in the Pinney Hollow Formation at Granville Notch.

It is clear that the polymetamorphic history of Vermont is much more complicated than that indicated by Doll and others (1961) on the state map. The complex zoning relationships observed in amphibole are best explained by disequilibrium and multiple periods of metamorphic growth. A reconnaissance study of amphibole compositions in the rocks collected but not chosen for electron microprobe analysis will aid in the delineation of a new facies series and isograd map for Vermont. It will show more accurately the extent of the high- and medium- to high-pressure events and aid in the understanding of the Paleozoic history of the northern Appalachian Mountains.

In the thin sections from the Silurian and Devonian rocks collected from southeastern Vermont, amphibole grains with distinct cores and rims are observed. It will be important to try to correlate the physical conditions indicated by the compositions of these amphibole domains with the two tectonic events identified by Rosenfeld (1968) in the Silurian and Devonian units. Has moderately low-pressure metamorphism occurred in these rocks as it appears to have in the Silurian to Devonian rocks in northeastern Vermont?

The age assignments in table 1 are necessarily tentative except for the two sample localities from which isotopic ages have been obtained. They are based on consistency arguments using field and isotopic evidence from rocks in the immediate vicinity. To place more accurate ages on the mineral growth events observed, amphibole was separated from the following key areas: 1) Pinnacle Formation (LA426), 2) Underhill Formation (V225), 3) Hazens Notch Formation at Tillotson Peak (V337A) and at 4) Belvidere Mountain (V360), 5) Pinney Hollow Formation (V14), and 6) the Chester Amphibolite from the Saxtons River quadrangle (V107). The separates have been given to Marvin Lanphere for $^{40}Ar/^{39}Ar$ dating. Distinct amphibole cores and rims occur in all but sample area 3. Incremental heating experiments on these zoned grains may allow the growth periods to be dated.

Implicit in this discussion of amphibole growth generations is that all grains cannot grow if the rock remains a closed system. Where rim development is extensive, the cores make up a small volume compared to the rims and optically continuous grains. Most of the early generation

appears to have been consumed, and only a few of the largest grains remain. Amphibole grains preserved during retrograde growth often appear resorbed; lower grade cores are sometimes euhedral. The elements necessary to make the rims must come primarily from core compositions breaking down in other parts of the rock and from breakdown of the other phases. It will be shown in the next chapter that prograde amphibole grain growth is effected by the consumption of the other phases in the rock, primarily chlorite, epidote, and plagioclase.

Table 1   MINERAL GROWTH EVENTS, VERMONT AND ADJACENT QUEBEC

EVENT	ISOTOPIC AGE	FACIES SERIES	GRADE	STUDY AREA	SAMPLE	AMPHIBOLE COMPOSITION AND GRAIN MORPHOLOGY	OTHER DIAGNOSTIC PHASES
01		High-P	Medium	Hazens Notch Fm (Tillotson Peak)	A-BM-100	Barroisite & glaucophane cores	Albite, omphacite phengite
		Medium/High-P	Medium	Hazens Notch Fm (Belvidere Mtn)	V360B	Barroisitic hornblende cores	
			Medium	Saxtons River quad (Chester Amphibolite)	V127A	Hornblende cores	
		Medium-P	Low	Pinnacle Fm	Q3C	Actinolite cores	
	457 ±26 m.y. (a)	High-P	Garnet	Hazens Notch Fm (Tillotson Peak)	A-BM-100; V337A&B, 380C,383B	Glaucophane & barroisitic actinolite rims & separate grains	Albite, omphacite phengite
			Garnet	Hazens Notch Fm (Belvidere Mtn)	V360B	Barroisite rims & separate grains	Albite
				Stowe Fm (Worcester Mtns)	V5B	Barroisitic hornblende, optically continuous	Albite
		Medium/High-P	Medium	Pinney Hollow Fm (Granville Notch)	V14H-J	Barroisite cores in host	
			Biotite	Stowe Fm (Worcester Mtns)	V11A	Barroisitic actinolite, optically continuous	Albite
02			Low	Pinnacle Fm	Q3C;LA426, 434A,435A	Barroisitic actinolite cores	
			Low	Pinney Hollow Fm (Granville Notch)	V12G-H,15A	Winchite-rich actinolite cores in veins	
				Stowe Fm (Eden Notch & Worcester Mt)	V28A,30A,3C	Barroisitic actinolite cores	
	437 ± 7 m.y.(b)	Medium-P	Garnet	Stowe Fm (Elmore Mtn)	V44,50B	Hornblende cores	Albite
	440 ± 9 m.y.(b)		Low	Stowe Fm (Elmore Mtn) Saxtons River quad (Chester Amphibolite)	V44,50B V97B,100B, 107A,108, 124B,127A	Actinolite rims Actinolite cores	
		Staurolite -Kyanite		Saxtons River quad (Hinkley Brook & Acton Hill)	V126H,152, 153C,154B	Hornblende, optically continuous	Oligoclase/andesine
			High	Saxtons River quad (Townshend Dam) Woodstock quad (Curtis Hollow)	V118D,E,O,P V80B-D	Hornblende, optically continuous	Oligoclase/andesine
D1	380(c-e)		Garnet	Saxtons River quad (Chester Amphibolite)	V100B,106D, 108,113B, 114B,119C V146A	Hornblende rims & separate grains	Oligoclase
		Medium-P	Garnet	Wilmington quad Saxtons River quad (Chester Amphibolite)	V107A,124B '158A	Hornblende rims & separate grains	Albite & Oligoclase
			Medium	Wilmington quad Saxtons River quad (Chester Amphibolite)	V97B,127A	Hornblende rims & separate grains	Albite
			High	Underhill Fm	V225B	Hornblende cores	
			Biotite	Saxtons River quad (Chester Amphibolite)	V94A	Hornblende, optically continuous	Albite
			Low	Underhill Fm	LA430B	Actinolitic hornblende porphyroblast cores	Oligoclase/andesine
		Medium/Low-P	Garnet	Northeastern Vermont	V36A	Hornblende & cummingtonite separate grains	Oligoclase/andesine
			Biotite	Northeastern Vermont	V38A	Actinolitic hornblende, X & || foliation	Oligoclase
			Garnet	Underhill Fm	V225B	Hornblende grain exteriors	Albite
		Medium-P		Underhill Fm	LA430B	Actinolite to hornblende matrix grains & rims on porphyroblasts	Albite
	350		Biotite	Pinney Hollow Fm (Granville Notch)	V12G-H, 14H-J,15A	Actinolite rims & separate grains. Host & vein	Albite
D2	(a,d,e)			Stowe Fm (Eden Notch & Worcester Mtn)	V28A,30A, 3C,6B	Actinolite rims & separate grains	Albite
		Medium/Low-P	Garnet	Wilmington quad	V146A	Hornblende grain exteriors	Oligoclase
		Low-P		Saxtons River quad (Chester Amphibolite)	V124B	Hornblende grain exteriors	Albite & Oligoclase
			Andalusite -sillimanite	Northeastern Vermont	V53	Hornblende	Bytownite
D1 or D2		Medium-P	Garnet	Underhill Fm	V340B	Hornblende, optically continuous	Albite
			Biotite	Pinnacle Fm	Q3C;LA426, 434A,435A	Actinolite rims & separate grains	Albite
				Underhill Fm	LA504B	Actinolite, optically continuous	Albite

(a) Lanphere & Albee (1974)
(b) Marvin Lanphere (written communication, 1976)
(c) Harper (1968)
(d) Marvin Lanphere (written communication, 1975)
(e) Naylor (1971)

CHAPTER VI

PHASE EQUILIBRIA IN AMPHIBOLITIC SCHIST

A. Introduction

The minerals amphibole, chlorite, epidote, plagioclase, and quartz plus a carbonate, a K mica, a Ti-rich phase, and an Fe^{3+} oxide comprise many of the mafic rocks studied from Vermont and southern Quebec. Although this phase assemblage does not change with the pressure and temperature of metamorphism, the mineral compositions and abundances do. In chapter IV phase chemistry was examined as a function of metamorphic grade in the Underhill Formation, the Stowe Formation, northeastern Vermont, and the Saxtons River quadrangle. Within the constant mineral assemblage, the following variations with increasing metamorphic grade are observed: The formula proportions of Na, K, Al^{VI}, Ti, and Al^{IV} increase in calcic amphibole, while (Fe+Mg+Mn) and Si decrease. Al^{VI} and Al^{IV} increase in biotite and chlorite. Plagioclase is enriched in the anorthite component and calcite in the ankerite component. The carbonate in the biotite grade mafic rocks is calcite. Both calcite and dolomite are in the higher grade samples. Biotite and K white mica are present in low and higher grade mafic rocks, but usually not in the same sample. The Ti-rich phase in low grade mafic rocks is typically sphene, and magnetite is frequently present. Ilmenite, rutile, and hematite are commonly part of the higher grade assemblage.

In a closed system chemical variation within any one phase must be balanced by compositional changes in other phases and/or by a perturbation of the proportions of each mineral. Two approaches are used to

understand how the polyhedron defined by the common mafic rock phase assemblage is deformed in multidimensional space in response to changes in the physical conditions of metamorphism. First, several simplifying assumptions are made to allow the data to be graphically represented. Using the assignments from chapter V, the electron microprobe analyses are grouped by metamorphic facies series and grade. Mineral composition is then examined as a function of temperature and pressure. The effect of bulk rock chemistry on phase composition and mineral assemblage is discussed.

Since the reactions which describe the metamorphic transformation of the polyhedron delimited by amphibole, chlorite, epidote, plagioclase, quartz, carbonate, K mica, Ti phase, and Fe^{3+} oxide are continuous, it is not practicable to generate a petrogenetic grid for mafic rocks by writing all the possible reactions among the observed compositions. An alternative is to find a composition interior to this multiphase volume and determine the amount of each mineral necessary to make this hypothetical rock.

Using this device, the phase compositions in several samples are modeled by least squares in the last section of this chapter. Each phase and component is treated, and the metamorphic reactions which relate these rocks are inferred. It is demonstrated that basaltic bulk rock compositions can be used to model the mineral compositions observed from each facies series and metamorphic grade. In addition to the common assemblage, FeO-rich rocks can contain either stilpnomelane or garnet. The reactions involved in the progressive metamorphism of these "abnormal" rocks are also examined.

B. Graphical representation

Theory

Nine mineral types are present in the "normal" mafic rock: amphibole; chlorite; epidote; plagioclase; quartz; calcite or dolomite; biotite or K white mica; sphene, ilmenite, or rutile; and magnetite or hematite. In addition, stilpnomelane, garnet, paragonite, and pyroxene are observed in some samples. To describe these phases twelve oxides must be considered. These are SiO_2, Al_2O_3, Fe_2O_3, TiO_2, MgO, FeO, MnO, CaO, Na_2O, K_2O, H_2O, and CO_2. Such a complicated system can be treated graphically by making thermodynamically "legal" assumptions (see Greenwood, 1975) to reduce the number of components.

Since quartz is a pure phase and only one Ti-rich and one K-rich phase are usually present, SiO_2, TiO_2, and K_2O can be excluded from the graphical representation. Assuming H_2O and CO_2 are boundary value components (i.e., their chemical potentials are externally fixed) and combining Al_2O_3 + Fe_2O_3(AF_2O_3) and FeO+MgO+MnO(FMO) allows the remaining phases to be described in a tetrahedron. Figure 1a shows the positions of the pertinent minerals in this tetrahedron; mole percent oxide is plotted. Illustrated by figure 1b are three faces of this tetrahedron onto which the phase compositions are projected from the fourth component.

Because plagioclase and epidote are nearly omnipresent, they can be used as projection points to simplify the system further. Plagioclase is predominantly < An_{30} in the samples studied, and much is albite. For simplicity, the other phases can be projected from albite onto the

base of the tetrahedron in figure 1a. Projecting from epidote (which is a point because Al_2O_3 and Fe_2O_3 are combined) to the AF_2O_3 - FMO edge and then separating MgO from FMO results in the diagram in figure 1c. This projection can be used to illustrate the MgO/(FeO+MgO+MnO) partition among the ferromagnesian minerals.

Medium-pressure facies series

The electron microprobe data from rocks that show medium-pressure metamorphism during the last period of mineral growth are shown on these three graphs in figures 2-4. Tie lines are drawn between averaged phase compositions, and the analyses of cores from discontinuously zoned amphibole grains and from garnet are excluded. The biotite-albite, garnet-albite, garnet-oligoclase, and staurolite-kyanite-oligoclase grades are represented. (Each grade is defined by the index mineral or minerals in the interlayered pelitic schist and the plagioclase in the amphibolitic schist.)

Between the biotite-albite and garnet-albite zones, amphibole is enriched in AF_2O_3 and Na_2O but depleted in FMO; it changes from actinolite to hornblende. Chlorite in amphibole-bearing rocks also becomes more aluminous. Calcite with more ankerite substitution is observed in the higher grade rocks, and dolomite is present. Dolomite is absent from the biotite-albite zone mafic rocks studied. The plagioclase in both grades is albite. In the biotite-albite zone, stilpnomelane is observed in FeO-rich bulk compositions. The assemblage actinolite-stilpnomelane-chlorite is replaced by hornblende-chlorite in the garnet-albite zone. Biotite-albite grade rocks with bulk compositions more

aluminous than the albite-epidote-chlorite plane on figure 2a are devoid of actinolite or stilpnomelane. The chlorite in these rocks is enriched in Al and has a composition similar to garnet-albite zone chlorite.

The AF_2O_3 content of the amphibole continues to increase with progressive metamorphism, but the compositional change is not as large as for the actinolite-hornblende transition. No variation in the calcite or chlorite compositions can be correlated with increasing metamorphic grade. The major change in the plagioclase-epidote-amphibole-chlorite volume shown on figure 2 between the garnet-albite and garnet-oligoclase zones is caused by the albite-oligoclase transition. In medium-pressure rocks this transition is at a higher grade than the change of amphibole from actinolite to hornblende.

In the mafic rocks chosen for electron microprobe investigation, garnet is first observed in the garnet-oligoclase zone. Figure 4 shows that it is present in FeO-rich compositions. As discussed in chapter IV, the Saxtons River quadrangle samples indicate that hornblende and chlorite are more aluminous in garnet-bearing rocks than in rocks without garnet from the same metamorphic grade. This relationship is illustrated on figures 2c, 3c, and 4c. Also visible on figures 2c and 3c is that plagioclase tends to be more anorthitic in the garnet-present samples.

Comparison of the data for the garnet-albite and garnet-oligoclase zones on figures 4b and c shows that hornblende-chlorite-garnet replaces hornblende-chlorite with progressive metamorphism. This three-phase assemblage persists into the staurolite-kyanite -oligoclase zone (figures 2d, 3d, and 4d), and the hornblende-chlorite breakdown continues

to more MgO-rich bulk rock compositions. AF_2O_3 continues to increase in the amphibole with increasing grade. In the staurolite-kyanite-oligoclase zone, figure 4d shows that amphibole and chlorite from garnet-bearing assemblages are distinguished from those that coexist with garnet only by $MgO/(FeO+MgO+MnO)$.

Figure 4a indicates that MgO/FMO is distinctly greater in actinolite than coexisting chlorite in the biotite-albite zone. Higher grade hornblende and chlorite have about the same MgO to FMO ratios (figures 4b-d). Cooper (1972) and Harte and Graham (1975) also observed that the Mg/Fe partition between Ca-amphibole and chlorite changes with increasing metamorphic grade. However, they proposed that the partition flips and that hornblende is appreciably more iron rich than coexisting chlorite. Cooper (1972) and Harte and Graham (1975) treated total iron as FeO. Significant Fe_2O_3 appears to be present in the hornblende from Vermont (making $MgO/FMO > MgO/(FMO+Fe_2O_3)$), and it is reasonable to expect Fe_2O_3 in hornblende from the Haast River Schist group and the Dalradian mafic rocks they studied. The apparent change in MgO/FMO partition between amphibole and chlorite with increasing metamorphic grade is probably not as large as these workers suggested.

Medium- to low-pressure facies series

Three medium- to low-pressure facies series samples from northeastern Vermont were chosen for electron microprobe investigation. One sample is interlayered with biotite grade pelitic rocks; one is from the garnet zone; and the third is within the sillimanite zone. The electron microprobe data for the coexisting phases are plotted in figures 5-7.

Even though the plagioclase is quite anorthitic and epidote is absent from two of the samples, the mafic mineral compositions are projected from albite and epidote onto the graph in figure 7 so that they can be compared with the medium- and high-pressure data. (The albite-epidote projection approximates a phase diagram for medium- and high-pressure mafic rocks.)

Between the biotite-oligoclase and garnet-oligoclase/andesine zones, amphibole is enriched in AF_2O_3 and Na_2O but depleted in FMO. It changes from actinolitic hornblende to hornblende. More anorthite component is present in the higher grade plagioclase; chlorite does not change composition appreciably. Figures 2 and 3 show that in medium-pressure rocks albite coexists with actinolite in the biotite zone and hornblende in the garnet zone. However, in the medium- to low-pressure biotite zone, oligoclase coexists with actinolitic hornblende. The albite-oligoclase transition is retarded with respect to the actinolite-hornblende transition in medium-pressure rocks; the opposite relationship is true for the lower pressure facies series.

The most anorthite-rich plagioclase in the investigated samples is from the sillimanite grade sample V53. This grade is also the highest reached by any of the studied rocks, indicating that plagioclase in mafic rocks continues to be enriched in anorthite with progressive meta-morphism to the sillimanite zone. Figure 5 shows that the plagioclase-epidote-amphibole-chlorite volume for sillimanite grade rocks is very small and that this typical mafic rock assemblage is restricted to a nar-rower range of bulk rock composition in the high grade than in the lower grade rocks.

Epidote is commonly absent from the medium- to low-pressure Devonian mafic rocks. In the biotite and garnet zones, bulk rock compositions more sodic than the oligoclase-actinolite/hornblende-chlorite plane delineated on figure 5 will be cut off from epidote. The composition of much of the Standing Pond Volcanic Member of the Waits River Formation, then, is probably outside of the oligoclase-epidote-actinolite/hornblende-chlorite tetrahedron. However, as is shown in figure 2, compositions above the oligoclase-calcic amphibole-chlorite plane but below the albite-calcic amphibole-chlorite plane will contain epidote in the biotite-albite and garnet-albite zones. A greater part of the $Na_2O-AF_2O_3-CaO-FMO$ tetrahedron is available to epidote-bearing assemblages of the biotite-albite and garnet-albite zones than the biotite-oligoclase and garnet-oligoclase/andesine zones. Even if the medium-pressure rocks have the same composition as the epidote-absent, medium- to low-pressure samples, epidote could be present in the medium-pressure rocks. This relationship may explain why epidote is more common in the Cambrian and Ordovician mafic layers.

Cummingtonite is present in the garnet-oligoclase/andesine sample studied. As shown on figure 7, cummingtonite and coexisting hornblende have about the same MgO/FMO ratio. Visible on figure 5b is that the assemblage cummingtonite-plagioclase-epidote is unstable at the physical conditions represented by the V36A mineral assemblage. The presence of hornblende and cummingtonite divides the plagioclase-epidote-amphibole-chlorite tetrahedron into three 4-phase volumes: oligoclase/andesine-hornblende-cummingtonite-chlorite, oligoclase/andesine-epidote-hornblende-chlorite, and hornblende-chlorite-cummingtonite-epidote.

High-pressure facies series

High-pressure metamorphism also causes the plagioclase-epidote-amphibole-chlorite volume to divide into several 4-phase fields. The mineral chemistry data from the high-pressure metamorphic terrane at Tillotson Peak are plotted in figures 8 and 9. In contradistinction to medium- and lower pressure rocks, plagioclase is not omnipresent. As can be seen in figure 8a, the glaucophane-epidote-chlorite plane divides the volume into two tetrahedra. Albite forms an apex of one and actinolite an apex of the other; albite and actinolite can only coexist in rock compositions within the glaucophane-epidote-chlorite plane. Reflecting this relationship is that glaucophane and chlorite are more aluminous in the albite-bearing assemblages.

A comparison of figure 3 and 8 and of figures 4 and 9 shows the following relationships between medium- and high-pressure mineral compositions: The garnet in medium-pressure rocks is depleted in Ca but richer in Mg/FM compared to the high-pressure rocks at Tillotson Peak. Chlorite has the same composition in the biotite-albite zone as that in the albite-absent rocks. The more aluminous garnet zone chlorite is equivalent to high-pressure chlorite in albite-present rocks. Actinolite is somewhat enriched in CaO but depleted in Na_2O in the medium-pressure mafic rocks. Some albite has more anorthite solid solution than the albite observed at Tillotson Peak.

Omphacite and glaucophane are present in the samples from Tillotson Peak; these diagnostic high-pressure phases are absent from the lower pressure samples. Calcite, dolomite, and paragonite assemblages are

observed and epidote is ubiquitous at Tillotson Peak and in medium-pressure mafic rocks.

Summary

The progressive metamorphism of mafic rocks at "normal" geothermal gradients effects a continuous change in mineral composition, primarily in calcic amphibole and plagioclase, which is manifested on figure 2 by a deformation of the plagioclase-epidote-amphibole-chlorite tetrahedron. This four-phase field decreases in volume with metamorphic grade. At high and low pressures continuous changes are also observed, but this tetrahedron is divided into several four-phase volumes because two amphiboles coexist.

In the next section the continuous and discontinuous reactions which describe these perturbations of the mafic rock mineral assemblage polyhedron in pressure-temperature space are modeled.

C. Inferred reactions modeled by least squares
Theory

The amount of each mineral in rocks with bulk compositions interior to the volume defined by the common mafic rock assemblage, amphibole-chlorite-epidote-plagioclase-quartz-carbonate-K mica-Ti phase-Fe^{3+} oxide, is dependent upon the composition of that phase. Mafic rocks with this paragenesis have been studied from several metamorphic grades and facies series, and each phase has been analyzed with the electron microprobe. By comparing the amount of each mineral in rocks of the same compositions, the reactions which relate these rocks can be inferred.

The composition of a rock is equal to the sum over all phases of the amount of each mineral times its composition. A rock can therefore be described by a series of mass balance equations of the form $c_i = \sum_{j=1}^{k} A_j x_{ij}$, where c_i is the weight percent of the ith oxide in the bulk rock C, x_{ij} is the weight percent of this oxide in the jth phase, A_j is the amount of the jth phase, and k is the number of phases in the rock. The x_{ij} values are known for the minerals in the studied samples. If C is assumed the A_j values can be calculated. By modeling rocks to the same C, the calculated coefficients (A_j) for each phase which is common to the modeled rocks can be compared.

For the samples studied the number of components is greater than or equal to the number of coexisting phases ($i \geq k$), so a least-squares analysis can be used to model the rocks. Reid, Gancarz, and Albee (1973) presented the theory for the constrained least-squares solution to such a set of linear equations, and their computer program was used for the models discussed in this chapter.

The computer program written by Reid and others (1973) allows errors only on the c_i values. However, for this problem C is considered constant so that the A_j values can be compared among samples. Errors are associated with the mineral compositions (the known x_{ij} values), and they must be considered. To approximate the uncertainties in x_{ij}, weighting factors for each mass balance equation can be used as the errors on c_i. These weighting factors must be constant for each sample modeled to a particular C so that the calculated coefficients can be compared. The weighting factors adopted for every model are 2% of the

SiO_2 content, 5% of Al_2O_3, MgO, and CaO, 7.5% of FeO and Na_2O, 10% of TiO_2, 15% of Fe_2O_3, and 50% of MnO and K_2O. Initially, weighting factor sets for several low and high grade samples were determined by calculating the sum of the estimated mode of each phase times its total error due to inhomogeneity and counting statistics. The constrained least-squares coefficients and their 1σ errors changed with the weighting factors, but the relative amounts of each phase in the samples did not.

A possible major source of error in this analysis is that since mineral zoning is ubiquitous, the coexisting compositions can only be inferred. The analyses of cores in discontinuously zoned grains can reasonably be excluded as can high Mn garnet grain interior data, but the rest of the analyses for each phase must be averaged. Another source of error is that Fe^{3+}/Fe^{2+} is unknown. The values used are estimated from cation distribution as outlined in chapter II.

Reid and others (1973) emphasized the importance of including constraints in the least-squares solution. The calculated coefficients for all the models discussed are constrained to 1, and the total mass of the system is conserved to ±5%. Additional constraints were sometimes required to disallow large negative coefficients. Constraining the minor phases which were initially calculated to have large negative abundances to 5 ± 4% eliminated these physically impossible results.

Discussion of the least-squares solutions

Several samples within the amphibole-chlorite-epidote-plagioclase-other phases composition volume have been modeled by least squares. Rocks from different metamorphic grades and facies series are modeled to

the same bulk rock composition. Comparison of the calculated amounts of each phase coupled with the known compositional variations of the minerals allows the reactions which effect the perturbation of the common mafic rock assemblage polyhedron to be inferred.

The least-squares analysis treats all the phases and includes most of the elements analyzed. H_2O and CO_2 are excluded from the mass balance solutions and are calculted from the determined coefficients assuming the minerals are stoichiometric. F and Cl are considered zero because the electron microprobe analyses show only trace amounts. The minor constituents Cr, Ba, and Zn are also neglected.

Six models are presented. The bulk rock compositions used are listed along with their CIPW norms in table 1, and they are plotted on the unfolded $Na_2O-AF_2O_3-CaO-FMO$ tetrahedron in figure 2a. (It should be noted that because Fe_2O_3 is included with Al_2O_3 this is not a regular ACFM projection.) These are typical basaltic compositions. Bulk rock A is the average of analyses 1-20 from Cady (1969, table 4). These analyses are of mafic rocks from units studied for this dissertation. The other compositions are modified analyses from Cady (1969, table 4) or van de Kamp (1970, table 3).

Initially, medium-, high-, and medium- to low-pressure mafic rocks from several metamorphic grades were modeled to the average of analyses 1-20 from Cady (1969, table 4), and many give good least-squares solutions. The calculated composition of some samples agree poorly with the modeled bulk compositions; MgO and FeO values are especially bad fits. To obtain better solutions for the rocks that do not fit model composition A,

published analyses were found which plot on the unfolded $Na_2O-AF_2O_3-CaO-$
FMO tetrahedron and the albite-epidote projection within the volume of
these rocks. These analyses were used as the basis for model compo-
sitions B-F. They were then modified by trial and error until all the
samples fit the modeled bulk rock composition.

The purpose of this analysis is not to determine the actual compo-
sition of each sample but to discern whether the amount of each common
phase increases or decreases when the mineral compositions of one rock
are transformed by metamorphism to those of another rock. The bulk rock
composition is only necessary because the formulation of the problem does
not allow the amounts of each phase to be calculated for more than one
rock at a time. It is sufficient to find an analysis interior to the
compositional space contained by the mineral assemblages of all the rocks
modeled to a particular bulk rock. Then the calculated phase abundances
can be compared between rocks and the reaction relationships inferred.

Model Composition A

Four medium-pressure mafic rocks from the biotite-albite, garnet-
albite, and garnet-oligoclase grades give good least-squares fits to
model bulk rock A. (Although Rosenfeld (oral communication, 1971) sug-
gested that station V94 is in the biotite zone, V94A is considered gar-
net-albite grade because the amphibole is not compositionally distinct
from amphibole in the rocks he proposed were in the garnet-albite zone.)
Table 2 lists the compositions and the calculated amounts (A) with
their 1σ errors for each phase. The continuous reaction which relates
these rocks can be inferred by examining the variations in mineral
chemistry and amounts. In figures 3 and 4 tie lines join the averaged

analyses used for the least-squares solutions. (The data on these figures are plotted as mole percent.) Figure 10 illustrates the calculated coefficients. For each phase the four rocks are plotted from left to right with increasing metamorphic grade.

From figure 10 it can be seen that the amounts of amphibole, quartz, and carbonate increase while chlorite, epidote, and probably plagioclase decrease during the medium-pressure progressive metamorphism of mafic rocks. This reaction is continuous through the actinolite to hornblende transition from the biotite-albite to the garnet-albite zone and the change from albite to oligoclase within the garnet zone. Figures 2 and 3 aid in visualizing this reaction. As the amphibole is enriched in Na_2O and AF_2O_3 with progressive metamorphism, it gets closer to the bulk rock composition. Therefore, the amount of amphibole increases at the expense of the other phases which define the assemblage polyhedron.

Between the biotite-albite and garnet-albite zone, sphene is replace by ilmenite as the Ti phase. To compensate for the increase in the K and Ti contents of amphibole compounded by the greater amount of this mineral, the biotite and Ti-phase coefficients multiplied by their K_2O and TiO_2 contents, respectively, decrease. Magnetite has small negative coefficients in V14J and V94A; it is absent from the other two rocks. Therefore, the Fe_2O_3 content of each sample can be balanced among the silicate phases. The weight percent of H_2O in the modeled rocks is calculated from the coefficients and ideal amounts in each phase, and the values are listed in table 2. H_2O does decrease between successively higher grade modeled rocks.

Also tabulated are the calculated CO_2 values which, since the amount of carbonate increases, are greater for higher grade rocks. However, a_{CO_2} is not the major driving force for the continuous reaction which causes the observed mineral compositional variations. Samples V108 and V1180 are both from the garnet-oligoclase zone. Dolomite is present in the former; calcite is in the latter. The calculated amount of carbonate is equivalent in the two samples, indicating that CO_2 is not significantly involved in the reaction. As shown in table 2B, V108 plagioclase is more calcic than that in V1180. Amphibole and chlorite have similar compositions. The reaction relationship between these two rocks is chlorite+epidote+plagioclase$_1$ = hornblende+plagioclase$_2$ +H$_2$O, where plagioclase$_2$ is more anorthitic than plagioclase$_1$. This same reaction relates V94A with both V1180 and V108. It is independent of the carbonate phase present.

Model composition B

As shown in table 1, the model B bulk rock contains more FeO and less CaO than model A. It does plot in the near vicinity of model A on figure 3a. Table 3 lists the data used for five rocks with least-squares solutions in good agreement with bulk rock B. V380C is from the high-pressure terrane at Tillotson Peak and V11A is from the medium- to high-pressure biotite-albite zone. The other three samples record medium-pressure metamorphism. LA426 is from the biotite-albite zone; V340B and V113B are from the garnet-albite and garnet-oligoclase zones, respectively. On figures 3, 4, 8, 9, and 11, tie lines join the averaged mineral compositions for each sample.

The calculated mineral abundances in each rock modeled to bulk rock B are listed in table 3 and illustrated in figure 12. Comparison of the phase compositions and their calculated coefficients for LA426, V340B, and V113B with those for the other medium-pressure rocks which were modeled to composition A (table 2 and figure 10) shows that the same continuous reaction is implied by both data sets. The actinolite to hornblende transition between the biotite-albite and garnet-albite zones is accompanied by the growth of amphibole and quartz and the consumption of chlorite, epidote, and plagioclase. Carbonate appears to increase and become more ankeritic. Biotite is more aluminous in the higher grade rocks and may be less abundant. Ilmenite has already replaced sphene in the garnet-albite zone sample V340B; however, sphene is the Ti phase in V94A. This reaction continues up grade. Plagioclase becomes more anorthitic and changes from albite to oligoclase. The amphibole continues to be enriched in Al_2O_3, Fe_2O_3, TiO_2, and Na_2O; and more Al_2O_3 is also present in the higher grade chlorite and biotite. H_2O decreases with grade; CO_2 appears to increase, but the calculated coefficients for carbonate are small and do not appear to depend on whether calcite and/or dolomite are present.

Importantly, the variations in phase abundances indicated by these least-squares models are corroborated by the petrographic observations. As was noted in chapter IV for the discussion of the Saxtons River quadrangle area, the estimated chlorite and epidote abundances decrease with progressive metamorphism while amphibole increases.

Based on the amphibole composition, it was argued in chapter V that V11A has been metamorphosed at medium to high pressures. In

figure 11 the amphibole in this rock is compared with actinolite from the medium-pressure biotite-albite zone samples and with the glaucophane from Tillotson Peak. Also included are amphibole core compositions from those samples which appear to preserve low grade, moderately high-pressure mineral growth. The plotted amphibole analyses lie between the actinolite and glaucophane composition envelopes, reemphasizing the conclusion that they record metamorphic growth intermediate to medium and high pressure.

To examine the reactions from actionolite- to winchite-rich actinolite- to glaucophone-bearing assemblages, the mineral compositions in LA426, V11A, and V380C have been modeled to bulk rock B. The data and calculated coefficients are listed in tables 3A and B. Figures 3,4,8,9, and 11 illustrate the compositions of the averaged phases, and figure 12 shows the relative abundances of each phase. V11A amphibole is richer in Al_2O_3, Fe_2O_3, and Na_2O but depleted in FMO and CaO compared to LA426 amphibole. Chlorite and epidote are more aluminous in V11A. The calculated amounts of each phase in the two samples are the same within the error of the least-squares solution, but the data suggest that the amounts of amphibole, epidote, and plagioclase decrease from LA426 to V11A and that chlorite, quartz, and carbonate increase in abundance.

The glaucophane-bearing sample V380C is devoid of plagioclase but contains garnet. The mineral assemblage in this rock is therefore very different from that in LA426 and V11A. Yet, tables 3A and B show that the observed mineral compositions in all three rocks can be modeled to the same bulk rock composition. A comparison of figures 2 and 8a reveals

that the model B rock must lie within the epidote-glaucophane-chlorite
plane. From figure 12 and table 3 it can be seen that the inferred
reaction between V11A and V380C is

albite+chlorite+actinolite+epidote = glaucophane+garnet+H_2O.
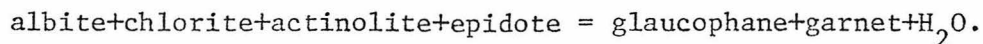
The amount of amphibole increases during this reaction. Sphene and
the carbonate and the K-mica phases do not enter the reaction.

Interestingly, figure 12 shows that only a trace amount of gar-
net is calculated for V113B when it is fit to bulk rock B but that 17
weight percent garnet is present in the least-squares solution of V380C
to this modeled composition. V380C garnet is richer in Ca but depleted
in Mg compared to that in the medium-pressure sample as is shown in
tables 3A and C.

Model composition C

By modifying the model B bulk rock composition to make it more
ferrous, the phase compositions in the medium- to low-pressure garnet-
oligoclase sample V36A can be fit by least squares. This bulk rock C
composition is listed in table 1; it plots in the same place on the
unfolded $Na_2O-AF_2O_3-CaO-FMO$ tetrahedron as B. To infer the reaction
relationship between the medium-pressure, garnet-oligoclase grade
sample V113B and V36A, the mineral compositions in each rock have been
modeled to rock C. The volumes delimited by the two mineral assemblages
are illustrated in figures 3c, 4c, 6b, and 7. The averaged analyses used
for the least-squares solutions are listed in table 4 along with the cal-
culated coefficients. Figure 13 shows the relative amounts of each
phase.

V113B and V36A are distinct in that epidote and garnet are present only in the former, and V36A contains cummingtonite. Figure 13 shows that within the error of the least-squares analysis, the amounts of hornblende, chlorite, biotite, and ilmenite are indistinguishable in the two samples. V113B hornblende, biotite, and chlorite are somewhat more aluminous than these phases in V36A; and ilmentite has more hematite solid solution. Plagioclase is more anorthitic in V36A.

Since the least-squares solution indicates that little epidote of the V113B composition is present in bulk rock C, the oligoclase-hornblende-chlorite plane in figure 2c must nearly contain the model C composition. However, the presence of cummingtonite in the modeled and real V36A implies that bulk rock C is above this plane.

Model composition D

Analysis number 20 from Cady (1969, table 4) is modeled composition D. It falls within the albite-epidote-glaucophane-chlorite polyhedron as is illustrated in figure 8b. The medium-pressure, biotite-albite zone sample V6B has the appropriate Mg/FM to give a good least-squares fit to bulk rock D as does V337B from Tillotson Peak. The mineral compositions in these two samples have been modeled to this bulk rock in order to infer the reaction that transforms the albite-epidote-actinolite-chlorite volume shown in figure 2a to the figure 8a topology. The data used for the least-squares solutions and the calculated coefficients are in table 5.

From the determined phase abundances, which are plotted in figure 14, and the known mineral chemistry, the reaction which relates V6B and

V337B can be inferred. It is albite + actinolite + chlorite = glauco-phane + epidote. Quartz, K white mica, sphene, and H_2O do not enter into the reaction. The total amount of amphibole increases. From table 5 it can be seen that the only phase in the common mineral assemblage that changes composition appreciably is amphibole; actinolite is observed in the medium-pressure sample and glaucophane in the high-pressure sample.

Model composition E

As is discussed in the second section of this chapter and shown on figure 4, stilpnomelane and garnet occur in FeO-rich, medium-pres-sure mafic rocks. The assemblage actinolite-chlorite-stilpnomelane which is present in biotite-albite grade samples is replaced by horn-blende-chlorite in the garnet-albite zone and hornblende-chlorite-gar-net in higher grade rocks. Bulk rock composition E was used to model representative samples with each of these assemblages. Table 1 lists the composition of modeled rock E. It is similar to B but much more FeO rich.

In table 6 the mineral composition data and calculated amounts are listed for the four samples fit to bulk rock E. One is from the biotite-albite zone, another is from the garnet-albite zone, and two samples are from the garnet-oligoclase zone. Figure 15 illustrates the calculated coefficients and 1σ errors. Between the biotite-albite and garnet-albite zones (the first two samples plotted for each mineral type), the following discontinuous reaction occurs:

$$\text{actinolite} + \text{biotite}_1 + \text{calcite}_1 + \text{chlorite}_1$$
$$+ \text{epidote} + \text{albite} + \text{stilpnomelane} + \text{sphene} =$$
$$\text{hornblende} + \text{biotite}_2 + \text{calcite}_2 + \text{chlorite}_2 + \text{quartz} + \text{ilmenite} + H_2O.$$
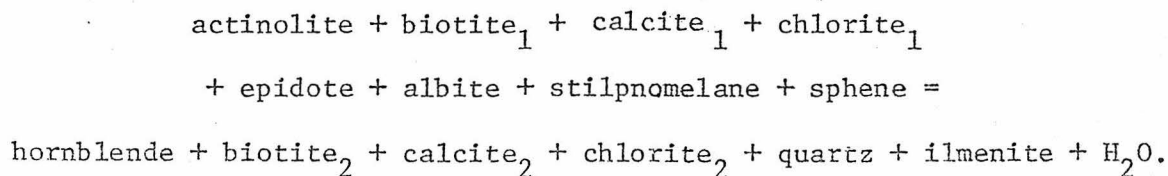
Biotite$_2$ and chlorite$_2$ are more aluminous than biotite$_1$ and chlorite$_1$, respectively. Calcite in the higher grade assemblage has more ankerite substitution. The amount of amphibole increases during this reaction; chlorite may decrease. The calcite and biotite coefficients are equivalent and small.

The reaction

hornblende$_1$ + biotite$_1$ + calcite$_1$ + chlorite$_1$ + epidote + albite =

hornblende$_2$ + biotite$_2$ + calcite$_2$ + chlorite$_2$ + oligoclase + garnet + H$_2$O

describes the transformation between the garnet-albite and garnet-oligoclase zones. The higher grade hornblende, biotite, and chlorite are the more aluminous. Calcite$_2$ is more ankeritic than calcite$_1$. The amounts of amphibole and perhaps calcite increase up grade, while the chlorite abundance decreases. The plagioclase, quartz, biotite, and ilmentite coefficients are equivalent.

These reactions show that the loss of stilpnomelane and incoming of garnet in FeO-rich mafic rocks are superimposed upon the continuous reaction which describes the progressive metamorphism of medium-pressure mafic rocks. As amphibole is enriched in Na$_2$O and AF$_2$O$_3$, biotite and chlorite in Al$_2$O$_3$, calcite in ankerite, and plagioclase in anorthite, the amount of amphibole increases at the expense of chlorite, epidote, and plagioclase.

Model composition F

To infer the reaction which relates medium-pressure, biotite-albite grade rocks with medium- to low-pressure biotite-oligoclase grade rocks, LA435A and V38A were modeled to bulk composition F. As shown by

table 1, this is a very MgO-rich bulk rock, and figures 4a and 7 indicate that these two samples are also very rich in MgO. On the Na_2O-AF_2O_3-CaO-FMO unfolded tetrahedron, rock F plots close to the other bulk compositions (see figure 3a). Listed in table 7 are the averaged mineral compositions; they are joined by tie lines on figures 3a and 6a. The abundances of each phase calculated in the least-squares solutions are also tabulated, and they are shown in figure 16.

These data indicate that with the major compositional jump from albite to oligoclase and the change from actinolite to actinolitic hornblende accompanied by the increase in Al_2O_3 content of the chlorite, the amounts of amphibole and plagioclase increase at the expense of epidote, chlorite, and probably quartz. This reaction has the same form as that which occurs during the progressive metamorphism of medium-pressure mafic rocks except that the amount of plagioclase appears to increase rather than decrease. In low-pressure rocks albite goes to oligoclase before the actinolite to hornblende transition. Therefore, the plagioclase composition moves closer to the bulk rock composition before the major increase in the hornblende content of the amphibole which drives it so close to the bulk rock. This relationship can be visualized by comparing figures 3a and 6a.

Also seen is that model F appears within the plagioclase-epidote-amphibole-chlorite volume in the biotite-albite zone. It is outside of this volume and contained by plagioclase, amphibole, and chlorite in the biotite-oligoclase zone.

Conclusions

The least-squares analysis described in this section demonstrates that the mineral assemblages and compositions observed can be fit to typical basaltic bulk rocks. Phase assemblages from medium-, high-, and medium- to low-pressure terranes can be fit by least squares to the same bulk rock compositions. Inferred from the least-squares solutions and the known mineral chemistry are the continuous reactions which describe the deformation of the composition polyhedron for the common mafic rock assemblage, amphibole-chlorite-epidote-plagioclase-quartz-carbonte- K mica-Ti phase-Fe^{3+} oxide, in pressure and temperature space. The phases predominately involved in the reactions are amphibole, chlorite, epidote, and plagioclase. Therefore, the delineation of this phase volume in the Na_2O-AF_2O_3-CaO-FMO tetrahedron is a close approximation to a phase diagram for mafic rocks.

Within the medium-pressure facies series, the progressive metamorphism of mafic rocks effects the increase in Na_2O and Al_2O_3 contents of the amphibole, and biotite and chlorite become more aluminous. Calcite is enriched in ankerite and plagioclase in anorthite. Sphene is replaced by ilmenite as the Ti phase. The actinolite to hornblende transition is between the biotite and garnet zones and precedes the change from albite to oligoclase which occurs in the garnet zone. During this continuous reaction amphibole grows and chlorite, epidote, and plagioclase are consumed. The amounts of the other phases do not change appreciably. The reaction causes dehydration, but CO_2 may be consumed or liberated. Calculated coefficients for the carbonate phase are small and appear to

be independent of whether calcite or dolomite is present. Discontinuous reactions which are responsible for the loss of stilpnomelane and the incoming of garnet in FeO-rich mafic rocks have the same form as the continuous reaction.

High-pressure metamorphism brings glaucophane into the rocks studied by the cross-over reaction

actinolite + chlorite + albite = glaucophane + epidote.
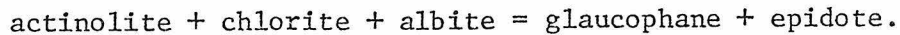
Another cross-over reaction occurs in medium- to low-pressure rocks:

hornblende + chlorite + epidote + plagioclase$_1$ + quartz =

cummingtonite + plagioclase$_2$.
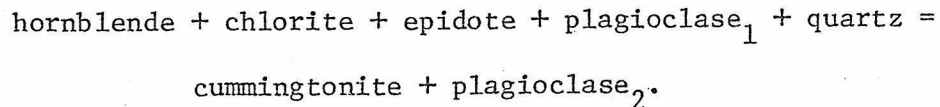
Plagioclase$_2$ is more abundant and anorthitic than plagioclase$_1$.

In medium- to low-pressure terranes the albite to oligoclase transition occurs at a lower grade than the change from actinolite to hornblende. The reaction from the biotite-albite to the biotite-oligoclase zone is

actinolite+albite+epidote+chlorite = actinolitic hornblende+
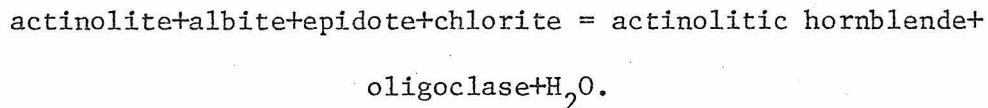
oligoclase+H$_2$O.

The amounts of amphibole and plagioclase increase. Epidote is absent in medium- to low-pressure mafic rocks with bulk rock compositions more sodic than the oligoclase-calcic amphibole-chlorite plane, but it is present in medium-pressure, biotite-albite and garnet-albite rocks of the same composition.

The least-squares approach has proved to be useful in quantifying the continuous and discontinuous reactions which occur in mafic schist and has eliminated the simplifying assumptions necessary for a graphical

representation of the observed assemblages. The actual application of the computer program written by Reid and others (1973) to this problem has been more time-consuming than necessary because only one sample could be considered at a time and because it was necessary to modify the modeled bulk rock composition by trial and error until a good fit was obtained. Rewriting the computer program to simultaneously compare the phase compositions (including the errors on each phase) in several rocks and to readily provide equations in formula units as well as weight units would be an important continuation of this research.

Because the medium-pressure samples analyzed include those of a broad range of $Mg/(Mg+Fe)$ and metamorphic grade, it has been possible to examine the progressive metamorphism of medium-pressure mafic schist in considerable detail. It will be important to locate basaltic composition samples from the other facies series so that their progressive metamorphism can be analyzed in the same manner.

Table 1

COMPOSITIONS FOR BULK ROCK MODELS (Weight Percent)

	A	B	C	D	E	F
SiO_2	47.7	46.63	46.63	50.9	46.0	51.2
Al_2O_3	15.1	16.25	15.87	16.5	16.5	15.0
Fe_2O_3	4.3	4.3	4.3	3.6	4.5	3.0
TiO_2	1.1	1.14	1.14	1.1	1.0	1.0
MgO	7.8	7.31	6.80	6.9	5.0	10.6
FeO	7.1	10.55	11.44	7.1	12.0	4.5
MnO	0.20	0.20	0.20	0.2	0.5	0.24
CaO	10.5	7.66	7.66	7.1	8.5	6.5
Na_2O	2.4	2.41	2.41	3.1	2.0	3.1
K_2O	0.25	0.25	0.25	0.2	0.5	0.1
Total	96.5	96.70	96.70	96.7	96.5	95.2

CIPW Norm

	A	B	C	D	E	F
Quartz	0	0	0	3.82	0.42	2.27
Orthoclase	1.53	1.53	1.53	1.22	3.06	0.62
Albite	21.05	21.08	21.08	27.12	17.53	27.53
Anorthite	30.79	33.91	32.84	31.57	35.83	28.06
Wollastonite	0	0	0	0	0	0
Diopside	18.70	4.42	5.33	3.93	6.59	4.59
Hypersthene	18.83	27.40	28.20	24.78	27.83	30.36
Olivine	0.46	2.96	2.32	0	0	0
Magnetite	6.47	6.45	6.45	5.40	6.76	4.57
Hematite	0	0	0	0	0	0
Ilmenite	2.17	2.24	2.24	2.16	1.97	1.99

A Average of analyses 1-20 from Cady (1969, table 4).
B Analysis #30 from van de Kamp (1970, table 3) with Fe_2O_3 increased and K_2O decreased to those for A. Al_2O_3 reduced to keep the total constant.
C Modified from B by making Mg/FM=0.51 but keeping Σ FM constant.
D Analysis #20 from Cady (1969, table 4) with K_2O increased.
E Hypothetical
F Modified analysis #1 from Cady (1969, table 4). TiO_2 and K_2O are less; MgO is greater and FeO less so that Mg/FM=0.8; and SiO_2 is increased to keep the total constant.

Table 2A   MODEL A COMPOSITIONS (Weight Percent)

71VJL14J (Biotite-Albite Zone)

	Model	Calculated	Amphibole	Biotite	Carbonate	Chlorite	Epidote	Plagioclase	Ti Phase	Magnetite	Quartz
SiO_2	47.7 ± 1.0	48.08	52.24	37.82	(0)	25.98	38.15	68.93	30.53	0.25	(100)
Al_2O_3	15.1 ± 0.8	15.25	2.71	15.58	(0)	19.86	25.02	19.69	0.80	0	(0)
Fe_2O_3	4.3 ± 0.6	4.29	4.86	(0)	(0)	0.85	11.32	(0)	2.99	67.19	(0)
TiO_2	1.1 ± 0.1	1.10	0.03	1.45	(0)	0.03	0.11	0	37.94	0.01	(0)
MgO	7.8 ± 0.4	7.70	13.77	11.98	0.30	16.97	0.03	0.02	0.02	0.01	(0)
FeO	7.1 ± 0.5	7.42	11.05	20.36	0.73	23.22	0.27	0.09	(0)	30.26	(0)
MnO	0.20±0.10	0.31	0.42	0.20	0.73	0.36	0.33	0.07	0.05	0.01	(0)
CaO	10.5 ± 0.5	10.65	10.71	0.11	51.38	0.16	23.15	0.11	27.91	0.05	(0)
Na_2O	2.4 ± 0.2	2.42	1.09	0.04	(0)	0.03	0.02	11.32	(0)	(0)	(0)
K_2O	0.25±0.13	0.25	0.12	9.33	(0)	0	0	0.06	(0)	(0)	(0)
Total	96.5 ± 4.8	97.47	97.00	96.87	53.14	87.46	98.40	100.29	100.24	97.78	100
H_2O*		3.09	2.07	3.92		11.53	1.90				
CO_2*		-0.79			43.88						
A_2			36.0±5.4	2.0±1.1	-1.8±2.3	14.8±3.4	29.9±3.1	17.9±1.5	2.7±0.2	-1.6±0.8	0.2±2.8
σ		0.6									

71VJL94A (Garnet-Albite Zone)

	Model	Calculated	Amphibole	Biotite	Carbonate	Chlorite	Epidote	Plagioclase	Ti Phase	Magnetite	Quartz
SiO_2	47.7	47.56	45.48	37.25	(0)	26.15	38.28	69.37	30.36	0.03	(100)
Al_2O_3	15.1	15.01	12.21	16.05	(0)	21.35	23.37	19.87	1.30	0	(0)
Fe_2O_3	4.3	4.32	7.68	(0)	(0)	0.95	13.62	(0)	1.05	69.39	(0)
TiO_2	1.1	1.10	0.35	1.55	(0)	0.05	0.06	0	37.70	0.04	(0)
MgO	7.8	7.84	11.00	13.48	0.73	19.31	0.03	0	0.03	0	(0)
FeO	7.1	6.96	9.52	16.91	0.95	20.01	0.64	0.14	(0)	31.32	(0)
MnO	0.20	0.18	0.20	0.11	0.62	0.22	0.22	(0)	0.03	0.01	(0)
CaO	10.5	10.44	10.84	0.08	53.42	(0)	22.43	0.13	28.64	0.01	(0)
Na_2O	2.4	2.39	2.00	0.05	(0)	(0)	(0)	9.34	(0)	(0)	(0)
K_2O	0.25	0.25	0.32	8.45	(0)	(0)	(0)	0.04	(0)	(0)	(0)
Total	96.5	96.05	99.60	93.93	55.72	88.04	98.65	98.89	99.11	100.79	100
H_2O*		2.89	2.05	4.01		11.76	1.88				
CO_2*		1.59			43.95						
A_2			44.3±3.4	1.2±0.4	3.6±0.8	14.3±1.6	13.3±1.0	16.1±0.9	2.4±0.1	-1.5±0.4	6.2±0.8
σ		0.07									

( ) Assumed
* Calculated assuming mineral stoichiometry
The carbonate is calcite, and the Ti phase is sphene.
Quartz is assumed to be present in 71VJL14J.

A_2 Amount (Weight %) calculated by least squares
σ^2 Measure of the fit as discussed by Reid and others (1973)

Table 2B   MODEL A COMPOSITIONS (Weight Percent)

71VJL1180 (Garnet-Oligoclase Zone)

	Model	Calculated	Amphibole	Biotite	Carbonate	Chlorite	Epidote	Plagioclase	Ti Phase	Magnetite	Quartz
SiO_2	47.7	47.22	43.24		(0)	26.43	38.34	64.37	0.90		(100)
Al_2O_3	15.1	14.89	14.08		(0)	22.30	26.35	22.42	0		(0)
Fe_2O_3	4.3	4.39	6.95		(0)	0	9.85	(0)	3.04		(0)
TiO_2	1.1	1.07	0.44		(0)	0.09	0.13	0	50.21		(0)
MgO	7.8	7.28	9.98		1.58	20.80	0.07	0.01	0.27		(0)
FeO	7.1	7.65	9.89		1.70	17.65	0.33	0.17	42.49		(0)
MnO	0.20	0.25	0.29		0.82	0.18	0.18	(0)	2.03		(0)
CaO	10.5	10.24	10.81	ABSENT	50.81	(0)	23.42	3.72	(0)	ABSENT	(0)
Na_2O	2.4	2.37	2.07		(0)	(0)	(0)	8.90	(0)		(0)
K_2O	0.25	0.20	0.37		(0)	(0)	(0)	0.05	(0)		(0)
Total	96.5	95.56	98.12		54.91	87.45	98.67	99.64	98.94		100
H_2O*		2.41	2.04			11.92	1.91				
CO_2*		1.98			44.00						
A			50.9±8.0		4.5±1.9	10.2±3.9	8.1±3.1	14.8±2.4	1.6±0.2		9.9±1.9
σ^2		0.8									

71VJL1108 (Garnet-Oligoclase Zone)

	Model	Calculated	Amphibole	Biotite	Carbonate	Chlorite	Epidote	Plagioclase	Ti Phase	Magnetite	Quartz
SiO_2	47.7	47.80	43.94		(0)	26.41	37.97	63.28	(0)		(100)
Al_2O_3	15.1	15.16	15.01		(0)	22.93	25.80	23.47	(0)		(0)
Fe_2O_3	4.3	4.51	6.17		(0)	0.21	10.77	(0)	(0)		(0)
TiO_2	1.1	1.10	0.36		(0)	0.08	0.06	0	(100)		(0)
MgO	7.8	8.21	10.94		13.94	21.76	0.04	0.02	(0)		(0)
FeO	7.1	6.33	8.57		7.73	16.34	0.59	0.27	(0)		(0)
MnO	0.20	0.19	0.22		0.91	0.11	0.16	(0)	(0)		(0)
CaO	10.5	10.49	11.27	ABSENT	29.72	(0)	23.16	4.34	(0)	ABSENT	(0)
Na_2O	2.4	2.41	1.81		(0)	(0)	(0)	8.87	(0)		(0)
K_2O	0.25	0.20	0.31		(0)	(0)	(0)	0.05	(0)		(0)
Total	96.5	96.41	98.60		52.30	87.84	98.55	100.30	100		100
H_2O*		1.82	2.07			12.00	1.90				
CO_2*		2.15			45.61						
A			62.0±10.8		4.7±2.9	3.5±4.2	6.4±3.1	14.5±2.6	0.9±0.1		8.0±2.3
σ^2		0.7									

( ) Assumed
* Calculated assuming mineral stoichiometry

A: Amount (Weight %) calculated by least squares
σ^2 Measure of the fit as discussed by Reid and others (1973)

Ilmenite is observed in 71VJL1180 and rutile is in 71VJL1108.
Dolomite is the carbonate in 71VJL1108.
Calcite is present in 71VJL1180.

Table 3A   MODEL B COMPOSITIONS (Weight Percent)

75VJL380C (High-Pressure)

	Model	Calculated	Amphibole	Calcite	Dolomite	Chlorite	Epidote	Plagioclase	Garnet	K Mica	Ti Phase	Quartz
SiO_2	46.63±0.93	46.97	57.28		(0)	26.36	38.03		38.16	49.84	30.70	(100)
Al_2O_3	16.25±0.81	16.49	10.80		(0)	19.75	26.68		21.17	26.99	1.39	(0)
Fe_2O_3	4.3 ±0.65	3.11	2.47		(0)	1.67	9.01		0.73	2.37	0.45	(0)
TiO_2	1.14±0.11	1.13	0.02		(0)	0.02	0.12		0.08	0.23	38.56	(0)
MgO	7.31±0.37	7.51	10.59		15.06	20.82	0.04		1.48	3.33	0.01	(0)
FeO	10.55±0.79	10.40	8.45	ABSENT	8.39	17.36	0.09	ABSENT	26.96	0.71	(0)	(0)
MnO	0.20±0.10	0.23	0.05		0.25	0.14	0.05		1.05	0.01	0.03	(0)
CaO	7.66±0.38	7.90	1.30		28.54	0.02	23.57		11.67	0	28.99	(0)
Na_2O	2.41±0.18	2.43	6.63		(0)	(0)	(0)		(0)	0.34	(0)	(0)
K_2O	0.25±0.13	0.27	0.01		(0)	(0)	(0)		(0)	10.40	(0)	(0)
Total	96.70±4.84	96.44	97.60		52.24	86.14	97.59		101.30	94.22	100.13	100
H_2O*		3.14	2.18			11.85	1.92			4.50		
CO_2*		0.12			45.79							
A_2			36.5±2.9		0.3±2.0	15.6±2.7	19.4±3.0		16.8±3.3	2.5±1.3	2.8±0.3	6.0±2.0
σ^2		1.2										

71VJL11A (Medium- to High-Pressure, Biotite-Albite Zone)

	Model	Calculated	Amphibole	Calcite	Dolomite	Chlorite	Epidote	Plagioclase	Garnet	K Mica	Ti Phase	Quartz
SiO_2	46.63	46.15	52.51	(0)		25.90	37.35	68.81		35.36	30.79	(100)
Al_2O_3	16.25	15.87	4.73	(0)		19.73	22.09	19.90		14.63	1.07	(0)
Fe_2O_3	4.3	4.38	5.55	(0)		1.07	14.99	(0)		(0)	0.48	(0)
TiO_2	1.14	1.14	0.07	(0)		0.04	0.08	0.01		1.07	38.36	(0)
MgO	7.31	7.33	13.11	0.22		16.40	0.07	0.02		11.29	0.08	(0)
FeO	10.55	9.74	10.48	0.51	ABSENT	24.16	0.14	0.16	ABSENT	20.75	0.04	(0)
MnO	0.20	0.13	0.23	0.34		0.24	0.09	(0)		0.10	0.04	(0)
CaO	7.66	7.51	9.75	53.07		(0)	22.87	0.17		0.22	28.96	(0)
Na_2O	2.41	2.39	1.99	(0)		(0)	(0)	11.42		0.03	(0)	(0)
K_2O	0.25	0.25	0.14	(0)		(0)	(0)	0.07		8.43	(0)	(0)
Total	96.70	94.90	98.56	54.14		87.54	97.68	100.56		91.88	99.78	100
H_2O*		4.47	2.08			11.50	1.87			3.93		
CO_2*		0.30		43.93								
A_2			13.5±4.4	0.7±1.5		32.0±3.1	21.8±2.4	18.6±1.3		2.6±1.2	2.8±0.2	8.1±1.9
σ^2		0.6										

( ) Assumed
* Calculated assuming mineral stoichiometry

A_2 Amount (Weight %) calculated by least squares
σ^2 Measure of the fit as discussed by Reid and others (1973)

The K mica in 75VJL380C is phengite; biotite is present in 71VJL11A.
The Ti phase is sphene.
Additional constraint: 75VJL380C, dolomite = 5±4%.

Table 3B MODEL B COMPOSITIONS (Weight Percent)

LA426 (Medium-Pressure, Biotite-Albite Zone)

	Model	Calculated	Amphibole	Calcite	Dolomite	Chlorite	Epidote	Plagioclase	Garnet	K Mica	Ti Phase	Quartz
SiO_2	46.63	46.07	54.33	(0)		25.73	37.45	68.89		37.36	30.84	(100)
Al_2O_3	16.25	15.42	1.31	(0)		18.95	21.01	19.33		14.65	1.92	(0)
Fe_2O_3	4.3	4.30	1.87	(0)		0.85	15.69	(0)		(0)	1.17	(0)
TiO_2	1.14	1.13	0.03	(0)		0.02	0.09	0.05		1.11	35.97	(0)
MgO	7.31	7.15	14.75	0.16		15.14	0.02	0.02		10.89	0.02	(0)
FeO	10.55	10.34	12.51	0.42	ABSENT	25.56	0.12	0.28	ABSENT	20.97	(0)	(0)
MnO	0.20	0.22	0.36	0.55		0.38	0.20	(0)		0.25	0.04	(0)
CaO	7.66	7.56	11.86	52.25		(0)	22.16	0.10		0.16	28.02	(0)
Na_2O	2.41	2.42	0.52	(0)		(0)	(0)	11.33		0.16	(0)	(0)
K_2O	0.25	0.25	0.07	(0)		(0)	(0)	0.08		9.08	(0)	(0)
Total	96.70	94.87	97.61	53.38		86.63	96.74	100.08		94.63	97.98	100
H_2O*		4.36	2.08			11.41	1.86			3.89		
CO_2*		-0.27		43.90								
A_2			15.0±4.6	-0.6±1.8		30.8±3.7	23.7±2.7	20.7±1.4		2.4±1.3	3.0±0.3	5.1±2.5
σ^2		0.8										

73VJL340B (Medium-Pressure, Garnet-Albite Zone)

	Model	Calculated	Amphibole	Calcite	Dolomite	Chlorite	Epidote	Plagioclase	Garnet	K Mica	Ti Phase	Quartz
SiO_2	46.63	46.39	45.06	(0)	(0)	25.42	38.12	68.96		36.85	0.11	(100)
Al_2O_3	16.25	15.96	12.40	(0)	(0)	21.50	24.39	19.54		16.34	0	(0)
Fe_2O_3	4.3	4.15	6.89	(0)	(0)	0.98	12.15	(0)		(0)	5.57	(0)
TiO_2	1.14	1.15	0.33	(0)	(0)	0.08	0.07	0.01		1.70	49.64	(0)
MgO	7.31	7.40	9.66	1.57	16.23	17.64	0.04	0.02		12.13	0.22	(0)
FeO	10.55	9.90	11.43	2.55	5.30	21.97	0.05	0.07	ABSENT	18.66	43.77	(0)
MnO	0.20	0.06	0.10	0.33	0.46	0.03	0.05	(0)		0.05	0.48	(0)
CaO	7.66	7.65	10.64	53.32	28.91	0.04	23.34	0.10		0.05	(0)	(0)
Na_2O	2.41	2.41	1.73	(0)	(0)	0	(0)	11.79		0.16	(0)	(0)
K_2O	0.25	0.25	0.38	(0)	(0)	(0)	(0)	0.04		8.85	(0)	(0)
Total	96.70	95.31	98.62	57.77	50.90	87.66	98.21	100.53		94.79	99.79	100
H_2O*		3.80	2.04			11.64	1.93			3.96		
CO_2*		0.97		41.66	46.73							
A_2			28.2±11.2	1.7±2.3	0.6±3.1	24.7±5.0	15.3±3.7	16.3±2.0		1.5±1.5	2.0±0.2	9.8±2.6
σ^2		1.0										

( ) Assumed
* Calculated assuming mineral stoichiometry

A_2 Amount (Weight %) calculated by least squares
σ Measure of the fit as discussed by Reid and others (1973)

The K mica is biotite
The Ti phase in LA426 is sphene; it is ilmenite in 73VJL340B.
Additional constraints: LA426, calcite = 5±4%; 73VJL340B, dolomite and calcite = 5±4%.

Table 3C   MODEL B COMPOSITIONS (Weight Percent)

71VJL113B (Medium-Pressure, Garnet-Oligoclase Zone)

	Model	Calculated	Amphibole	Calcite	Dolomite	Chlorite	Epidote	Plagioclase	Garnet	K Mica	Ti Phase	Quartz
SiO_2	46.63	46.66	41.50			25.56	37.52	62.89	38.01	36.54	0.28	(100)
Al_2O_3	16.25	16.37	16.21			22.39	24.65	23.54	21.56	17.61	0.03	(0)
Fe_2O_3	4.3	4.67	7.08			0.54	12.02	(0)	0.26	(0)	2.25	(0)
TiO_2	1.14	1.14	0.38			0.13	0.07	0.01	0.06	1.70	50.50	(0)
MgO	7.31	7.27	7.98			18.15	0.09	0.01	2.39	11.48	0.05	(0)
FeO	10.55	10.62	11.43	ABSENT	ABSENT	21.48	0.32	0.10	27.21	18.39	42.93	(0)
MnO	0.20	0.26	0.29			0.19	0.61	(0)	5.31	0.14	2.34	(0)
CaO	7.66	7.56	10.72			(0)	22.50	4.48	6.58	0	(0)	(0)
Na_2O	2.41	2.41	1.98			(0)	(0)	8.99	(0)	0.13	(0)	(0)
K_2O	0.25	0.25	0.37			(0)	(0)	0.07	(0)	8.57	(0)	(0)
Total	96.70	97.21	97.94			88.44	97.78	100.09	101.38	94.56	98.38	100
H_2O*		2.77	2.03			11.69	1.90			3.97		
CO_2*		0										
A			62.0±6.8			12.7±2.9	1.4±3.0	13.1±1.6	0.1±1.1	0.1±1.1	1.7±0.2	8.8±1.1
σ^2		0.5										

A Amount (Weight %) calculated by least squares
σ^2 Measure of the fit as discussed by Reid and others (1973)

( ) Assumed
* Calculated assuming mineral stoichiometry

The K mica is biotite, and the Ti phase is ilmenite.
Additional constraint: 71VJL113B, garnet = 5±4%.

Table 4   MODEL C COMPOSITIONS (Weight Percent)

71VJL113B (Medium-Pressure, Garnet-Oligoclase Zone)

	Model	Calculated	Hornblende	Cummingtonite	Biotite	Chlorite	Epidote	Plagioclase	Garnet	Ilmenite	Quartz
SiO_2	46.63±0.93	47.03	41.50		36.54	25.56	37.52	62.89	38.01	0.28	(100)
Al_2O_3	15.87±0.79	16.16	16.21		17.61	22.39	24.65	23.54	21.56	0.03	(0)
Fe_2O_3	4.3±0.65	4.74	7.08		(0)	0.54	12.02	(0)	0.26	2.25	(0)
TiO_2	1.14±0.11	1.16	0.38		1.70	0.13	0.07	0.01	0.06	50.50	(0)
MgO	6.80±0.34	7.10	7.98	ABSENT	11.48	18.15	0.09	0.01	2.39	0.05	(0)
FeO	11.44±0.86	10.59	11.43		18.39	21.48	0.32	0.10	27.21	42.93	(0)
MnO	0.20±0.10	0.28	0.29		0.14	0.19	0.61	(0)	5.31	2.34	(0)
CaO	7.66±0.38	7.66	10.72		0	(0)	22.50	4.48	6.58	(0)	(0)
Na_2O	2.41±0.18	2.43	1.98		0.13	(0)	(0)	8.99	(0)	(0)	(0)
K_2O	0.25±0.13	0.27	0.37		8.57	(0)	(0)	0.07	(0)	(0)	(0)
Total	96.70±4.84	97.42	97.94		94.56	88.44	97.78	100.09	101.38	98.38	100
H_2O^*		2.57	2.03		3.97	11.69	1.90				
A_2			64.3±9.0		0.3±1.4	10.6±3.8	0.7±4.0	12.9±2.1	0.5±1.6	1.8±0.2	9.0±1.5
σ		0.8									

71VJL36A (Medium- to High-Pressure, Garnet-Oligoclase/Andesine Zone)

	Model	Calculated	Hornblende	Cummingtonite	Biotite	Chlorite	Epidote	Plagioclase	Garnet	Ilmenite	Quartz
SiO_2	46.63±0.93	46.85	42.24	52.50	35.21	25.34		61.33		0.28	(100)
Al_2O_3	15.87±0.79	16.16	16.07	1.37	16.45	20.87		24.37		0.02	(0)
Fe_2O_3	4.3±0.65	4.28	6.73	0.95	(0)	0.60		(0)		1.22	(0)
TiO_2	1.14±0.11	1.14	0.37	0.06	1.80	0.09		0.04		51.51	(0)
MgO	6.80±0.34	6.75	7.47	14.79	11.22	15.88	ABSENT	0.02	ABSENT	0.24	(0)
FeO	11.44±0.86	11.93	12.55	26.39	20.00	24.26		0.19		45.01	(0)
MnO	0.20±0.10	0.19	0.24	0.65	0.06	0.09		(0)		0.85	(0)
CaO	7.66±0.38	7.70	10.80	1.21	0.21	(0)		6.07		(0)	(0)
Na_2O	2.41±0.18	2.40	1.79	0.12	0.14	(0)		8.10		(0)	(0)
K_2O	0.25±0.13	0.25	0.26	0.09	7.69	(0)		0.03		(0)	(0)
Total	96.70	97.67	98.52	98.13	92.78	87.13		100.15		99.13	100
H_2O^*		2.52	2.03	2.01	4.17	11.55					
A_2			62.1±1.4	2.6±1.7	1.1±0.6	10.1±1.6		15.8±0.9		1.7±0.1	6.6±0.9
σ		0.1									

( ) Assumed
* Calculated from mineral stoichiometry

A_2 Amount (Weight %) calculated by least squares
σ^2 Measure of the fit as discussed by Reid and others (1973)

Table 5   MODEL D COMPOSITIONS (Weight Percent)

71VJL6B (Medium-Pressure, Biotite-Albite Zone)

	Model	Calculated	Amphibole	Chlorite	Epidote	Plagioclase	K White Mica	Na White Mica	Sphene	Magnetite	Quartz
SiO_2	50.9±1.0	50.70	53.16	25.84	38.40	68.64	48.92		30.84		(100)
Al_2O_3	16.5±0.8	16.72	2.78	19.62	27.69	19.46	27.49		1.02		(0)
Fe_2O_3	3.6±0.5	2.01	1.71	0.89	7.34	(0)	2.43		0.46		(0)
TiO_2	1.1±0.1	1.09	0.04	0.04	0.16	0.01	0.18		38.03		(0)
MgO	6.9±0.4	6.83	15.27	17.83	0.03	0	3.06	ABSENT	0.11	ABSENT	(0)
FeO	7.1±0.5	7.01	9.90	21.29	0.05	0.12	0.42		0.04		(0)
MnO	0.2±0.1	0.15	0.29	0.27	0.16	(0)	0.02		(0)		(0)
CaO	7.1±0.4	7.27	11.84	0.14	23.74	0.10	0.01		29.01		(0)
Na_2O	3.1±0.2	3.05	0.64	0	0.01	11.38	0.34		(0)		(0)
K_2O	0.2±0.1	0.20	0.10	0.02	(0)	0.07	10.25		(0)		(0)
Total	96.7±4.8	95.04	95.73	85.94	97.58	99.78	93.12		99.51		100
H_2O*		3.82	2.09	11.63	1.93		4.51				
A_2			13.5±5.5	26.5±3.8	20.3±2.8	26.0±2.5	1.6±1.4		2.7±0.4		9.4±3.0
σ	96.7	2.2									

73VJL337B (High-Pressure)

	Model	Calculated	Amphibole	Chlorite	Epidote	Plagioclase	K White Mica	Na White Mica	Sphene	Magnetite	Quartz
SiO_2	50.9	50.63	57.49	25.50	37.82	68.74	49.72	46.77	30.42	0.17	(100)
Al_2O_3	16.5	16.44	9.85	20.96	24.13	19.65	26.79	37.25	1.61	0.02	(0)
Fe_2O_3	3.6	3.54	4.52	0.93	12.55	(0)	2.40	1.14	0.56	68.86	(0)
TiO_2	1.1	1.10	0.02	0.04	0.07	0.03	0.30	0.06	37.84	0.01	(0)
MgO	6.9	6.79	9.13	17.91	0.02	0.01	2.79	0.40	0.01	0	(0)
FeO	7.1	7.02	9.90	20.89	0.25	0.22	1.57	0.26	(0)	31.01	(0)
MnO	0.2	0.21	0.12	0.35	0.36	(0)	0.03	0.02	0.11	0.01	(0)
CaO	7.1	7.02	0.45	0.04	22.99	0.08	0.02	0.09	28.67	(0)	(0)
Na_2O	3.1	3.10	7.24	0.01	(0)	11.89	0.44	6.12	(0)	(0)	(0)
K_2O	0.2	0.19	0.02	(0)	(0)	0.04	10.14	1.53	(0)	(0)	(0)
Total	96.7	96.05	98.74	86.63	98.19	100.66	94.20	93.64	99.22	100.08	100
H_2O*		3.85	2.16	11.67	1.89		4.50				
A_2			33.2±1.7	20.7±0.9	26.3±0.5	4.0±1.1	1.3±0.3	3.5±0.8	2.8±0.1	-2.2±0.3	10.4±0.6
σ		0.09									

( ) Assumed

* Calculated from mineral stoichiometry

A_2 Amount (Weight %) calculated by least squares

σ^2 Measure of the fit as discussed by Reid and others (1973)

Additional constraints for 73VJL337B: Paragonite and plagioclase = 5±4%

Table 6A   MODEL E COMPOSITIONS (Weight Percent)

LA504B (Biotite-Albite Zone)

	Model	Calculated	Amphibole	Biotite	Calcite	Chlorite	Epidote	Plagioclase	K Feldspar	Garnet	Stilpnomelane	Ti Phase	Quartz
SiO_2	46.0±0.9	45.54	53.64	36.61	(0)	25.66	37.77	69.24	64.18		48.12	30.66	(100)
Al_2O_3	16.5±0.8	15.87	1.68	14.49	(0)	19.27	21.85	19.41	17.92		5.66	0.94	(0)
Fe_2O_3	4.5±0.7	4.86	2.31	(0)	(0)	0.81	15.30	(0)	(0)		(0)	0.84	(0)
TiO_2	1.0±0.1	1.00	0.05	1.09	(0)	0.03	0.09	0.02	0.02		0.03	38.33	(0)
MgO	5.0±0.3	4.99	13.75	9.99	0.16	14.65	0.03	0	0.03		7.13	0	(0)
FeO	12.0±0.9	11.31	13.77	22.76	0.42	26.32	0.06	0.07	0.11	ABSENT	28.06	(0)	(0)
MnO	0.5±0.3	0.34	0.37	0.25	0.54	0.41	0.18	(0)	(0)		1.09	0.02	(0)
CaO	8.5±0.4	8.32	11.70	0.05	53.66	0.05	22.93	0.07	0		0.63	28.64	(0)
Na_2O	2.0±0.2	2.01	0.54	0.04	(0)	0.01	(0)	10.66	0.15		0.07	(0)	(0)
K_2O	0.5±0.3	0.64	0.10	8.76	(0)	(0)	(0)	0.07	15.94		1.87	(0)	(0)
Total	96.5±4.8	94.89	97.91	94.04	54.78	87.21	98.21	99.54	98.35		92.66	99.48	100
H_2O*		4.10	2.06	3.88		11.37	1.87				5.47		
CO_2*		0.26			43.90								
A			2.5±6.6	2.7±3.7	0.6±3.0	22.0±7.7	30.1±4.2	18.5±1.8	0.6±2.3		16.2±6.9	2.4±0.3	4.5±5.1
σ^2		1.0											

73VJL225B (Garnet-Albite Zone)

	Model	Calculated	Amphibole	Biotite	Calcite	Chlorite	Epidote	Plagioclase	K Feldspar	Garnet	Stilpnomelane	Ti Phase	Quartz
SiO_2	46.0	45.97	42.77	35.35	(0)	24.75	38.05	68.84				0.11	(100)
Al_2O_3	16.5	16.43	13.81	15.01	(0)	20.10	24.13	19.24				0	(0)
Fe_2O_3	4.5	4.57	5.82	(0)	(0)	0.95	11.18	(0)				2.81	(0)
TiO_2	1.0	1.00	0.35	1.85	(0)	0.06	0.06	0.03				51.46	(0)
MgO	5.0	5.00	6.65	9.56	0.39	13.06	0.02	0.03				0.06	(0)
FeO	12.0	12.00	15.54	23.55	1.14	28.24	0.05	0.34	ABSENT	ABSENT	ABSENT	44.70	(0)
MnO	0.5	0.15	0.24	0.10	0.45	0.16	0.06	(0)				1.43	(0)
CaO	8.5	8.49	10.38	0	52.65	0.07	23.20	0.17				(0)	(0)
Na_2O	2.0	2.00	1.99	0.01	(0)	0.02	(0)	11.32				(0)	(0)
K_2O	0.5	0.50	0.58	9.26	(0)	(0)	(0)	0.04				(0)	(0)
Total	96.5	96.10	98.13	94.69	54.63	87.41	96.75	100.01				100.57	100
H_2O*		3.37	2.04	3.85		11.26	1.90						
CO_2*		0			43.88								
A			32.6±9.1	3.3±2.0	0±1.6	19.2±4.5	21.9±2.3	11.9±1.7				1.5±0.1	9.6±1.6
σ^2		0.4											

( ) Assumed
* Calculated from mineral stoichiometry

A Amount (Weight %) calculated by least squares
σ^2 Measure of the fit as discussed by Reid and others (1973)

The Ti phase for LA504B is sphene; ilmenite is observed in 73VJL225B.
Additional constraints for LA504B: Biotite and K Feldspar = 5±4%.

Table 6B   MODEL E COMPOSITIONS (Weight Percent)

71VJL113B (Garnet-Oligoclase Zone)

	Model	Calculated	Amphibole	Biotite	Calcite	Chlorite	Epidote	Plagioclase	K Feldspar	Garnet	Stilpnomelane	Ti Phase	Quartz
SiO_2	46.0	46.66	41.50	36.54		25.56	37.52	62.89		38.01		0.28	(100)
Al_2O_3	16.5	17.05	16.21	17.61		22.39	24.65	23.54		21.56		0.03	(0)
Fe_2O_3	4.5	4.63	7.08	(0)		0.54	12.02	(0)		0.26		2.25	(0)
TiO_2	1.0	1.02	0.38	1.70		0.13	0.07	0.01		0.06		50.50	(0)
MgO	5.0	5.25	7.98	11.48		18.?5	0.09	0.01		2.39		0.05	(0)
FeO	12.0	11.65	11.43	18.39	ABSENT	21.48	0.32	0.10	ABSENT	27.21	ABSENT	42.93	(0)
MnO	0.5	1.01	0.29	0.14		0.19	0.61	(0)		5.31		2.34	(0)
CaO	8.5	8.66	10.72	0		(0)	22.50	4.48		6.58		(0)	(0)
Na_2O	2.0	2.02	1.98	0.13		(0)	(0)	8.99		(0)		(0)	(0)
K_2O	0.5	0.60	0.37	8.57		(0)	(0)	0.07		(0)		(0)	(0)
Total	96.5	98.57	97.94	94.56		88.44	97.78	100.09		101.38		98.38	100
H_2O*		1.52	2.03	3.97		11.69	1.90						
A_2			51.7±11.8	4.7±4.0		1.3±5.8	7.4±5.4	11.0±2.9		14.5±3.7		1.4±0.3	7.9±2.1
σ		1.3											

71VJL118E (Garnet-Oligoclase Zone)

	Model	Calculated	Amphibole	Biotite	Calcite	Chlorite	Epidote	Plagioclase	K Feldspar	Garnet	Stilpnomelane	Ti Phase	Quartz
SiO_2	46.0	46.55	41.59	36.61	(0)	24.89	38.46	60.82		37.97		0.33	(100)
Al_2O_3	16.5	16.90	17.17	17.84	(0)	22.75	26.64	24.69		21.04		0.03	(0)
Fe_2O_3	4.5	4.24	7.26	(0)	(0)	0.54	9.16	(0)		0.79		9.84	(0)
TiO_2	1.0	1.02	0.41	1.71	(0)	0.07	0.12	0		0.06		46.81	(0)
MgO	5.0	5.24	7.59	11.03	1.58	16.77	0.08	0.01		2.83		0.12	(0)
FeO	12.0	11.71	11.21	18.76	1.70	22.75	0.39	0.09	ABSENT	26.93	ABSENT	40.87	(0)
MnO	0.5	0.94	0.38	0.11	0.82	0.20	0.26	(0)		4.79		0.99	(0)
CaO	8.5	8.70	10.49	0	50.81	(0)	23.11	6.50		6.43		(0)	(0)
Na_2O	2.0	2.02	1.92	0.17	(0)	(0)	(0)	7.77		(0)		(0)	(0)
K_2O	0.5	0.56	0.49	8.96	(0)	(0)	(0)	0.05		(0)		(0)	(0)
Total	96.5	97.87	98.51	95.19	54.91	87.97	98.22	99.93		100.84		98.99	100
H_2O*		1.54	2.03	3.94		11.61	1.91						
CO_2*		0.91			44.00								
A_2			52.2±13.7	3.3±3.9	2.1±2.3	2.8±6.6	1.7±5.2	12.9±3.9		14.5±4.1		1.6±0.3	8.9±2.6
σ		1.4											

( ) Assumed
* Calculated from mineral stoichiometry

A_2 Amount (Weight %) calculated by least squares
σ^2 Measure of the fit as discussed by Reid and others (1973)

The Ti phase is ilmenite. The calcite analyses used for 71VJL118E is the average from 71VJL180.

Table 7   MODEL F COMPOSITIONS (Weight Percent)

LA435A (Biotite–Albite Zone)

	Model	Calculated	Amphibole	Chlorite	Epidote	Plagioclase	Sphene	Rutile	Hematite	Quartz
SiO_2	51.2 ± 1.0	51.26	56.20	27.65	37.27	68.57	30.47		0.20	(100)
Al_2O_3	15.0 ± 0.8	14.82	0.92	19.34	22.07	19.51	1.27		0	(0)
Fe_2O_3	3.0 ± 0.5	3.01	3.99	1.63	14.75	(0)	1.32		93.05	(0)
TiO_2	1.0 ± 0.1	1.00	0.09	0.04	0.08	0.04	38.25		2.22	(0)
MgO	10.6 ± 0.5	10.46	19.20	24.37	0.12	0.02	0.48		0	(0)
FeO	4.5 ± 0.3	4.65	5.04	12.79	0.10	0.11	(0)	ABSENT	1.97	(0)
MnO	0.24±0.12	0.28	0.40	0.53	0.31	(0)	0		0.02	(0)
CaO	6.5 ± 0.3	6.53	11.41	0.07	22.67	0.14	27.30		(0)	(0)
Na_2O	3.1 ± 0.2	3.13	0.96	0.02	(0)	11.18	(0)		(0)	(0)
K_2O	0.1 ± 0.05	0.02	0.04	(0)	(0)	0.04	(0)		(0)	(0)
Total	95.2 ± 4.8	95.15	98.25	86.44	97.37	99.61	99.09		97.46	100
H_2O*		4.25	2.12	12.11	1.87					
A_2			16.9±2.9	29.5±1.9	17.0±1.6	26.5±1.4	2.5±0.2		-0.7±0.5	8.3±1.6
σ^2		0.6								

71VJL38A (Biotite–Oligoclase Zone)

	Model	Calculated	Amphibole	Chlorite	Epidote	Plagioclase	Sphene	Rutile	Hematite	Quartz
SiO_2	51.2	52.77	51.57	26.74		63.30		0.32		(100)
Al_2O_3	15.0	14.97	6.69	21.32		23.81		0.02		(0)
Fe_2O_3	3.0	1.90	4.27	1.00		(0)		0.45		(0)
TiO_2	1.0	1.02	0.20	0.06		0.03		99.24		(0)
MgO	10.6	11.76	17.53	23.83		0.03		0.10		(0)
FeO	4.5	4.58	4.72	13.11	ABSENT	0.21	ABSENT	(0)	ABSENT	(0)
MnO	0.24	0.05	0.10	0.05		(0)		0.04		(0)
CaO	6.5	6.55	12.42	(0)		4.86		(0)		(0)
Na_2O	3.1	3.35	0.85	(0)		8.96		(0)		(0)
K_2O	0.1	0.05	0.09	(0)		0.06		(0)		(0)
Total	95.2	97.02	98.44	86.11		101.26		100.17		100
H_2O*		3.29	2.13	12.15						
A_2			39.6±3.7	20.2±3.0		33.7±3.0		0.9±0.2		5.7±2.6
σ^2		2.6								

( )   Assumed
A   Amount (Weight %) calculated by least squares
A_2 Calculated from mineral stoichiometry
σ^2 Measure of the fit as discussed by Reid and others (1973)
The hematite analysis used for LA435A is from LA434A.

REFERENCES

Albee, A. L. (1957) Bedrock geology of the Hyde Park quadrangle, Vermont. U. S. Geological Surv. Quadrangle Map GQ-102.

Albee, A. L. (1962) Relationships between the mineral association, chemical composition and physical properties of the chlorite series. Amer. Mineral. 47, 851-870.

Albee, A. L. (1968) Metamorphic zones in northern Vermont. In E-an Zen, W. S. White, J. B. Hadley, and J. B. Thompson, Jr., Eds., Studies of Appalachian Geology: Northern and Maritime. Wiley Interscience, New York. pp. 329-341.

Albee, A. L., and L. Ray (1970) Correction factors for electron probe microanalysis of silicates, oxides, carbonates, phosphates, and sulfates. Analytical Chemistry 42, 1408-1414.

Anderson, J. R. (1977) The Polymetamorphic Sequence in the Paleozoic Rocks of Northern Vermont: A New Approach Using Metamorphic Veins as Petrologic and Structural Markers. Ph.D. Thesis, California Institute of Technology, Pasadena, California.

Banno, S. (1964) Petrologic studies on Sanbagawa crystalline schists in the Bessi-Ino district, central Sikoku, Japan. Tokyo Univ. Fac. Sci. J. Sec. II 15, 203-319.

Barron, B. J. (1974) The use of coexisting calcite-ankerite solid solutions as a geothermometer. Contrib. Mineral. Petrology 47, 77-80.

Bence, A. E., and A. L. Albee (1968) Empirical correction factors for the electron microanalysis of silicates and oxides. J. Geol. 76, 382-403.

Binns, R. A. (1967) Barroisite-bearing eclogite from Naustdal, Sogn og Fjordane, Norway. J. Petrology 8, 349-371.

Boulter, C. A., and A. Råheim (1974) Variation in Si^{4+}- content of phengites through a three stage deformation sequence. Contrib. Mineral. Petrology 48, 57-71.

Brady, J. B. (1974) Coexisting actinolite and hornblende from west-central New Hampshire. Am. Mineral. 59, 529-535.

Brown, W. L. (1962) Peristerite unmixing in the plagioclases and metamorphic facies series. Norsk Geol. Tidsskr. 42 (Feldspar Volume), 354-382.

Cady, W. M. (1956) Bedrock geology of the Montpelier quadrangle, Vermont. U. S. Geological Surv. Quadrangle Map GQ-79.

Cady, W. M. (1969) Regional Tectonic Synthesis of Northwestern New England and Adjacent Quebec. Geological Soc. Amer. Mem. 120, 181 pp.

Cady, W. M., A. L. Albee, and J. F. Murphy (1962) Bedrock geology of the Lincoln Mountain quadrangle, Vermont. U. S. Geological Surv. Quadrangle Map GQ-164.

Cady, W. M., A. L. Albee, and A. H. Chidester (1963) Bedrock geology and asbestos deposits of the upper Missisquoi Valley and vicinity, Vermont. U. S. Geological Surv. Bull. 1122-B, 78 pp.

Champion, D. E., A. L. Albee, and A. A. Chodos (1975) Reproducibility and operator bias in a computer-controlled system for quantitative electron microprobe analysis. Proc., Tenth Annual Microbeam Analysis Soc. Conf., 55A-55F.

Chang, P. H., E. H. Ern, Jr., and J. B. Thompson, Jr. (1965) Bedrock geology of the Woodstock quadrangle, Vermont. Vermont Geological Surv. Bull. 29, 65 pp.

Chidester, A. H., and W. M. Cady (1972) Origin and emplacement of Alpine-type ultramafic rocks. Nature 240, 27-31.

Chodos, A. A., A. L. Albee, A. J. Gancarz, and J. Laird (1973) Optimization of computer-controlled quantitative analysis of minerals. Proc., Eighth National Conf. Electron Probe Analysis, 45A-45C.

Christman, R. A. (1959) Geology of the Mount Mansfield quadrangle, Vermont. Vermont Gological Surv. Bull. 12, 75 pp.

Christman, R. A., and D. T. Secor, Jr. (1961) Geology of the Camels Hump quadrangle, Vermont. Vermont Geological Surv. Bull. 15, 70 pp.

Cooper, A. F. (1972) Progressive metamorphism of metabasic rocks from the Haast Schist group of southern New Zealand. J. Petrology 13, 457-492.

Cooper, A. F., and J. F. Lovering (1970) Greenschist amphiboles from Haast River, New Zealand. Contrib. Mineral. Petrology 27, 11-24.

Crawford, M. L. (1966) Composition of plagioclase and assorted minerals in some schists from Vermont, U. S. A., and South Westland, New Zealand, with inferences about the peristerite solvus. Contrib. Mineral. Petrology 13, 269-294.

Dennis, J. G. (1964) The geology of the Enosburg area, Vermont. Vermont Geological Surv. Bull. 23, 56 pp.

Dennis, J. G. (1968) Isotopic ages from the Appalachians and their tectonic significance: Discussion. Can. J. Earth Sciences 5, 959-961.

Doll, C. G., W. M. Cady, J. B. Thompson, Jr., and M. P. Billings (1961) Centennial geologic map of Vermont. Vermont Geological Surv.

Doolan, B. L., J. C. Drake, and D. Crocker (1973) Actinolite and subcalcic hornblende from a greenstone of the Hazen's Notch Formation, Lincoln Mountain quadrangle, Warren, Vermont. [abstr.] Geological Soc. Amer. Abstr. Programs 5, 157.

Eakins, P. R. (1964) Sutton map-area, Quebec. Geological Surv. of Canada Pap. 63-34, 3 pp.

Eggleton, R. A. (1972) The crystal structure of stilpnomelane. Part II. The full cell. Mineralogical Magazine 38, 693-711.

Engel, A. E. J., and C. G. Engel (1960) Progressive metamorphism and granitization of the major paragneiss, northwest Adirondack Mountains, New York, Part II - mineralogy. Geological Soc. Amer. Bull. 71, 1-58.

Engel, A. E. J., and C. G. Engel (1962) Hornblendes formed during progressive metamorphism of amphibolites, northwest Adirondack Mountains, New York. Geological Soc. Amer. Bull. 73, 1499-1514.

Ernst, W. G., Y. Seki, H. Onuki, and M. C. Gilbert (1970) Comparative Study of Low-Grade Metamorphism in the California Coast Ranges and the Outer Metamorphic Belt of Japan. Geological Soc. Amer. Mem. 124, 276 pp.

Eskola, P. (1920) The mineral facies of rocks. Norsk Geol. Tidsskr. 6, 143-194.

Eskola, P. (1939) Die metamorphen Gestein. In T. F. W. Barth, C. W. Correns, and P. Eskola, Die Entstehung der Gesteine. Springer, Berlin. pp. 263-407.

Eugster, H. P., A. L. Albee, A. E. Bence, J. B. Thompson, Jr., and D. R. Waldbaum (1972) The two-phase region and excess mixing properties of paragonite-muscovite crystalline solutions. J. Petrology 13, 147-179.

Faul, H., T. W. Stern, H. H. Thomas, and P. L. D. Elmore (1963) Ages of intrusion and metamorphism in the northern Appalachians. Amer. J. Sci. 261, 1-19.

Goldsmith, J. R., and R. C. Newton (1969) P-T-X relations in the system CaCO$_3$-MgCO$_3$ at high temperatures and pressures. Amer. J. Sci. 267-A (Schairer Volume), 160-190.

Graham, C. M. (1974) Metabasite amphiboles of the Scottish Dalradian. Contrib. Mineral. Petrology 47, 165-185.

Greenwood, H. J. (1975) Thermodynamically valid projections of extensive phase relationships. Amer. Mineral. 60, 1-8.

Guidotti, C. V., and F. P. Sassi (1976) Muscovite as a petrogenetic indicator mineral in pelitic schists. N. Jahrbuch Mineralogie Abhandlungen 127, 97-142.

Hall, L. M. (1959) The geology of the St. Johnsbury quadrangle, Vermont and New Hampshire. Vermont Geological Surv. Bull. 13, 105 pp.

Harper, C. T. (1968) Isotopic ages from the Appalachians and their tectonic significance. Can. J. Earth Sciences 5, 49-59.

Harte, B., and C. M. Graham (1975) The graphical analysis of greenschist to amphibolite facies mineral assemblages in metabasites. J. Petrology 16, 347-370.

Holdaway, M. J. (1971) Stability of andalusite and the aluminum silicate phase diagram. Amer. J. Sci. 271, 97-131.

Holdaway, M. J. (1972) Thermal stability of Al-Fe epidote as a function of f_{O_2} and Fe content. Contrib. Mineral. Petrology 37, 307-340.

Iwasaki, M. (1963) Metamorphic rocks of the Kôtu-Bizan area, eastern Sikoku. Tokyo Univ. Fac. Sci. J. Sec. II 15, 1-90.

Johannes, W., and D. Puhan (1971) The calcite-aragonite transition, reinvestigated. Contrib. Mineral. Petrology 31, 28-38.

Klein, C., Jr. (1968) Two-amphibole assemblages in the system actinolite-hornblende-glaucophane. Amer. Mineral. 54, 212-237.

Kushiro, I. (1969) Clinopyroxene solid solutions formed by reactions between diopside and plagioclase at high pressures. Mineral. Soc. Amer. Spec. Pap. 2, 179-191.

Laird, J., and A. L. Albee (1975) Polymetamorphism and the first occurrence of glaucophane and omphacite in northern Vermont. [abstr.] Geological Soc. Amer. Abstr. Programs 7, 1159.

Lanphere, M. A., and A. L. Albee (1974) $^{40}Ar/^{39}Ar$ age measurements in the Worcester Mountains: evidence of Ordovician and Devonian metamorphic events in northern Vermont. Amer. J. Sci. 274, 545-555.

Leake, B. E. (1965) The relationship between tetrahedral aluminum and the maximum possible octahedral aluminum in natural calciferous and subcalciferous amphiboles. Amer. Mineral. 50, 843-851.

Misch, P., and J. M. Rice (1975) Miscibility of tremolite and hornblende in progressive Skagit metamorphic suite, North Cascades, Washington. J. Petrology 16, 1-21.

Miyashiro, A. (1958) Regional metamorphism of the Gosaisyo-Takanuki district in the central Abukuma Plateau. Tokyo Univ. Fac. Sci. J. Sec. II 11, 219-272.

Miyashiro, A. (1961) Evolution of metamorphic belts. J. Petrology 2, 277-311.

Miyashiro, A. (1973) Metamorphism and Metamorphic Belts. John Wiley and Sons, Inc., New York. 492 pp.

Miyashiro, A., and Y. Seki (1958) Enlargement of the composition field of epidote and piemontite with rising temperature. Amer. J. Sci. 256, 423-430.

Naylor, R. S. (1971) Acadian orogeny: an abrupt and brief event. Science 172, 558-560.

Osberg, P. H. (1952) The Green Mountain anticlinorium in the vicinity of Rochester and East Middlebury, Vermont. Vermont Geological Surv. Bull. 5, 127 pp.

Osberg, P. H. (1965) Structural geology of the Knowlton-Richmond area, Quebec. Geological Soc. Amer. Bull. 76, 223-250.

Papike, J. J., K. L. Cameron, and K. Baldwin (1974) Amphiboles and pyroxenes: characterization of other than quadrilateral components and estimates of ferric iron from microprobe data. [abstr.] Geological Soc. Amer. Abstr. Programs 6, 1053-1054.

Phillips, F. C. (1930) Some mineralogical and chemical changes induced by progressive metamorphism in the Green Bed group of the Scottish Dalradian. Mineralogical Magazine 22, 239-256.

Pieratti, D. D. (1976) The origin and tectonic significance of the Tibbet Hill metavolcanics, northwestern Vermont. [abstr.] Geological Soc. Amer. Abstr. Programs 8, 246.

Raase, P. (1974) Al and Ti contents of hornblende, indicators of pressure and temperature of regional metamorphism. Contrib. Mineral. Petrology 45, 231-236.

Råheim, A., and D. H. Green (1974) Experimental determination of the temperature and pressure dependence of the Fe-Mg partition coefficient for coexisting garnet and clinopyroxene. Contrib. Mineral. Petrology 48, 179-203.

Raith, M. (1976) The Al-Fe (III) epidote miscibility gap in a metamorphic profile through the Penninic Series of the Tauern Window, Austria. Contrib. Mineral. Petrology 57, 99-117.

Ramberg, H. (1952) The Origin of Metamorphic and Metasomatic Rocks. U. Chicago Press, Chicago. 317 pp.

Reid, M. J., A. J. Gancarz, and A. L. Albee (1973) Constrained least-squares analysis of petrologic problems with an application to lunar sample 12040. Earth Planet. Sci. Letters 17, 433-445.

Richardson, S. W. (1968) Staurolite stability in a part of the system Fe-Al-Si-O-H. J. Petrology 9, 467-488.

Richardson, S. W., M. C. Gilbert, and P. M. Bell (1969) Experimental determination of kyanite-andalusite and andalusite-sillimanite equilibria; the aluminum silicate triple point. Amer. J. Sci. 267, 259-272.

Rickard, M. J. (1965) Taconic orogeny in the western Appalachians: experimental application of micro-textural studies to isotopic dating. Geological Soc. Amer. Bull. 76, 523-536.

Robbins, D. W., and R. G. J. Strens (1972) Charge-transfer in ferromagnesian silicates: the polarized electronic spectra of trioctahedral micas. Mineralogical Magazine 38, 551-563.

Rosenberg, P. E. (1967) Subsolidus relations in the system $CaCO_3$-$MgCO_3$-$FeCO_3$ between 350° and 550°C. Amer. Mineral. 52, 787-796.

Rosenfeld, J. L. (1954) Geology of the Southern Part of the Chester Dome, Vermont. Ph.D. Thesis, Harvard University, Cambridge, Massachusetts.

Rosenfeld, J. L. (1968) Garnet rotations due to the major Paleozoic deformations in southeast Vermont. In E-an Zen, W. S. White, J. B. Hadley, and J. B. Thompson, Jr., Eds., Studies of Appalachian Geology: Northern and Maritime. Wiley Interscience, New York. pp. 185-202.

Rosenfeld, J. L. (1972) Rotated garnets and tectonism in southeast Vermont. 64th Annual Meeting New England Intercollegiate Geological Conf., Field Trip 7, 167-178.

Shido, F. (1958) Plutonic and metamorphic rocks of the Nakoso and Iritono districts in the central Abukuma Plateau. Tokyo Univ. Fac. Sci. J. Sec. II 11, 131-217.

Shido, F., and A. Miyashiro (1959) Hornblendes of basic metamorphic rocks. Tokyo Univ. Fac. Sci. J. Sec. II 12, 85-102.

Skehan, J. W. (1961) The Green Mountain anticlinorium in the vicnity of Wilmington and Woodford, Vermont. Vermont Geological Surv. Bull. 17, 159 pp.

Skehan, J. W., and J. C. Hepburn (1972) Stratigraphy of the east flank of the Green Mountain anticlinorium, southern Vermont. 64th Annual Meeting New England Intercollegiate Geological Conf., Field Trip B-1, 3-26.

Smith, J. V. (1974) Feldspar Minerals I. Crystal Structure and Physical Properties. Springer-Verlag, Heidelberg. 627 pp.

van de Kamp, P. C. (1970) The Green Beds of the Scottish Dalradian series: geochemistry, origin, and metamorphism of mafic sediments. J. Geol. 78, 281-303.

Velde, B. (1965) Phengite micas: synthesis, stability, and natural occurrence. Amer. J. Sci. 263, 886-913.

Velde, B. (1967) Si^{4+} content of natural phengites. Contrib. Mineral. Petrology 14, 250-258.

Wiseman, J. D. H. (1934) The central and south-west Highland epidiorites: a study in progressive metamorphism. Quart. J. Geological Soc. London 90, 354-417.

Woodland, B. G. (1965) The geology of the Burke quadrangle, Vermont. Vermont Geological Surv. Bull. 28, 151 pp.

Zen, E-an (1974) Prehnite- and pumpellyite-bearing mineral assemblages, west side of the Appalachian metamorphic belt, Pennsylvania to Newfoundland. J. Petrology 15, 197-242.

APPENDIX

SAMPLE LOCATION AND DESCRIPTION

For this dissertation the phases in 59 samples from Vermont and one from Quebec were analyzed with the electron microprobe. The sample location and description of each rock are given in this appendix. Rocks are grouped by study area; the order is the same as that in chapter IV: Pinnacle Formation, Underhill Formation, Hazens Notch Formation, Pinney Hollow Formation, Stowe Formation, northeastern Vermont, Saxtons River quadrangle, Woodstock quadrangle, and Wilmington quadrangle. Following the rock descriptions for each area are tabulated modes estimated from thin section. The abbreviations used in these tables are:

Ca-Am	Calcic Amphibole
Na-Am	Sodic Amphibole
SC-Am	Soda-Calcic Amphibole
FM-Am	Monoclinic, Iron-Magnesium-Manganese Amphibole
Bio	Biotite
Ank	Ankerite
Dol	Dolomite
Cc	Calcite
Chl	Chlorite
Epi	Epidote
K-Fld	Alkali Feldspar
Plag	Plagioclase Feldspar
Gar	Garnet

Omph	Omphacite
Qtz	Quartz
Sphn	Sphene
Stilp	Stilpnomelane
Mus	K-White Mica
Par	Na-White Mica
Hem	Hematite
Ilm	Ilmenite
Mgt	Magnetite
Rut	Rutile
All	Allanite
Ap	Apatite
Graph	Graphite
Tour	Tourmaline
Zir	Zircon
Bor	Bornite
Mil	Millerite
Cpy	Chalcopyrite
Py	Pyrite
Po	Pyrrhotite
Alt	Alteration product
Incl	Inclusion
Tr	Trace

Pinnacle Formation

LA433C

Incipiently foliated, medium- to fine-grained graywacke from a glaciated outcrop 0.3 mile S 10° W of Lapland School, Enosburg Falls quadrangle, Vermont. Amygdaloidal greenstone and greenschist crop out 50 and 150 feet to the west.

Tibbit Hill Volcanic Member:

73QJL3C

Fine-grained, gray, amygdaloidal phyllite exposed in a roadcut 1.4 miles S35° E of Abbott Corners, Sutton quadrangle, Quebec. Metavolcanic layers with and without amygdules crop out. The amygdules are elongated parallel to the layering and often coalesce.

LA426

Fine-grained greenstone with a well-developed slip cleavage. Roadside outcrop 0.9 mile N 15° E of Fletcher, Mount Mansfield quadrangle, Vermont.

LA434A

Fine-grained greenstone cut by epidote-rich veins up to 0.5 inch thick. Cross-fiber amphibole is present in some veins. Roadcut of interlayered amygdaloidal and massive greenstone 0.5 mile S 5° E of Berkshire, Enosburg Falls quadrangle, Vermont.

LA435A

Fine-grained greenschist with a 1 inch thick metavolcanic interlayer which is massive, gray, and amygdaloidal. Amygdules are elongated and aligned parallel to the layering and to the foliation of the greenschist.

Several closely spaced, glaciated outcrops of greenschist and amygdaloidal greenstone 1.1 miles N 60° E of Berkshire, Enosburg Falls quadrangle, Vermont.

LA460B

Medium-grained greenstone with amphibole porphyroblasts. Glaciated outcrop 1.1 miles S 80° W of North Cambridge, Mount Mansfield quadrangle, Vermont.

Estimated Modes; Pinnacle Formation

	Ca-Am	Bio	Cc	Chl	Epi	K-Fld	Plag	Qtz	Sphn	Stilp	Mus	Hem	Mgt	Other
LA433C		7		2	3	5	15	25	2	3	35		3	Ap, Rut, Zir, Py
73QJL3C	5		5	5	35		25	tr	15			10		
LA426	25	tr	5	20	10		35	tr	5					Cpy, Py
LA434A														
Host	20			5	10		50		10			5		
Vein	10		15	5	35		35		tr			tr		
LA435A	3			3	20		45	4	15			10		Ap
LA460B	65		2	15	5		10	tr	3					Cpy

Underhill Formation

Greenstone Member:

LA430B

Medium-grained, layered, and folded greenschist. Epidote porphyro-blasts are abundant in one layer. Several outcrops of greenschist in meadow 1.3 miles N 70° E of Huntington, Camels Hump quadrangle, Vermont.

LA504B

Fine-grained greenstone with a 3.5 cm thick interlayer of coarse-grained, green-gray, massive amphibolite. In contact with coarse-grained amphibolite and parallel to the layering is a centimeter-wide epidote vein with asbestiform amphibole; epidote is present within the coarse-grained layer up to 1 cm from the vein. Blasted block from a railroad cut across U. S. Highway 2 from the Richmond, Vermont cemetery, Camels Hump quadrangle.

73VJL225B

Salt- and-pepper, gray-green, medium-grained amphibolitic schist from Beaver Meadow Brook 0.5 mile S 80° E of Gore School, Lincoln Mountain quadrangle, Vermont. The sample is from a 10 foot wide layer in biotite-chlorite pelitic schist, and the compositional layering is parallel to the foliation. Biotite-chlorite-garnet-quartz-white mica schist is exposed in the roadcut above the brook.

73VJL340B

Medium-grained, gray-green, amphibolitic gneiss from a lichen-covered outcrop in the woods 1.1 miles S 75° W from Lincoln Gap, Lincoln Mountain quadrangle, Vermont. Garnet-chlorite-chloritoid pelitic schist crops out to the west.

Estimated Modes; Underhill Formation

	Ca-Am	Bio	Dol	Cc	Chl	Epi	K-Fld	Plag	Qtz	Sphn	Stilp	Hem	Ilm	Other
Biotite Zone:														
LA430B	40	1		5	10	30		5	5	4				Ap
LA504B														
Epi Vein	5	2		10	5	70			5		3			
Transition	20	1		3	6	10	5	40	5	5	5			Py
Amphibolite	25			<1		tr	5	55		10	5	tr		Ap, Py
Garnet Zone:														
73VJL225B	30	<1		10	5	5		20	20	<1			10	Cpy, Py
73VJL340B	25	15	5	15	5	5		25	3				2	Ap, Py

Hazens Notch Formation

Belvidere Mountain Amphibolite Member:

73VJL360B

Medium-grained, massive, dark green-gray amphibolite with sub-hedral to enhedral porphyroblasts of garnet and amphibole. Outcrop at the summit of Belvidere Mountain, Jay Peak quadrangle, Vermont.

73VJL337A

Medium- to fine-grained, green-gray, garnetiferous schist. The foliation is contorted with the slip cleavage producing a lineation on the foliation surface. Long Trail at 3000 foot elevation on the SE side of Tillotson Peak, Jay Peak quadrangle.

73VJL337B

Fine-grained, greenish gray schist. Isoclinal folds with axes parallel to the mineral elongation are apparent in thin section, and epidote layers visible in the outcrop are isoclinally folded. Ledge-forming outcrop 60 feet off the top of Tillotson Peak to the south. Jay Peak quadrangle.

75VJL380C

Gray, medium- to fine-grained garnetiferous schist. A lineation on the foliation surface is caused by a well-developed slip cleavage, and within the foliation are quartz veins up to 2 mm wide. Ridge-forming out-crop 100 feet north of Frank Post Trail, 0.5 mile S 65° E of Tillotson Camp, Jay Peak quadrangle.

75VJL383B

Gray, medium- to fine-grained schist with apple-green omphacite. Moss-covered, ridge-forming outcrop between Long Trail and Tillotson

Pond, 0.1 mile N 50° W of Tillotson Camp, Jay Peak quadrangle.

A-BM-99

Medium-grained, gray, broadly folded schist with sheared, sub-hedral garnet porphyroblasts. Amphibolite outcrop between the 1960 and 2025 foot elevations, Tillotson Creek, Jay Peak quadrangle.

A-BM-100

Medium- to fine-grained, gray amphibolitic schist with garnet and amphibole porphyroblasts. Same outcrop as A-BM-99.

Estimated Modes; Hazens Notch Formation

	Ca & SC-Am	Na-Am	Dol	Cc	Chl	Epi	Plag	Gar	Omph	Qtz	Sphn	Mus	Par	Mgt	Ilm	Rut	Other
73VJL360B	45				Alt	20	<1	24		10	tr				<1	1	Ap, Py
73VJL337A	9	6		20	15	30		10		8	2			<1			Cpy, Py, Po, Mil
73VJL337B		15			9	45	5			tr	1	4	6	15			Ap
75VJL380C		20	10		4	25		10		20	1	10					Ap, Cpy, Py
75VJL383B		30	<1	tr		58			7	5	tr			<1			Ap, Cpy
A-BM-99		Incl		10	10	tr	10	25		20	4	20		1	Incl	Incl	Ap, Cpy, Py
A-BM-100	18	7		<1	3	30	2	20	<1		2	15		3			Ap, Cpy, Py

Pinney Hollow Formation

Greenstone Member:

71VJL12

1.8 miles N 20° W of Granville Notch on Route 100, Lincoln Mountain quadrangle, Vermont, is a roadcut in which a 120 foot thick greenstone layer in contact with plagioclase-quartz-white mica-carbonate-epidote-sphene schist is exposed. The layering and foliation are concordant. Within the greenstone 40 feet from the east end of the outcrop on the north side of the road is a 1 inch thick zone of quartz-carbonate veins. Coarse chlorite and blue-green amphibole segregations are present within these veins. Two samples from here were investigated with the electron microprobe:

G) Fine-grained greenstone cut by quartz veins. Coarse-grained amphibole and chlorite are present at vein borders.

H) Fine-grained greenstone in contact with a quartz-carbonate-amphibole vein.

71VJL14

Roadcut along Route 100, 0.5 mile S 20° W of Granville Notch, Lincoln Mountain quadrangle. 3 mafic and 4 pelitic layers from 10 to 50 feet thick are exposed and appear to be repeated by isoclinal folding. The layering is parallel to the foliation. The phases in three samples were analyzed with the electron microprobe.

H) Medium-grained, laminated greenstone from the middle mafic-rich layer. Plagioclase + carbonate, epidote, and chlorite + amphibole are segregated into $\leq$ 1 mm thick layers.

I) Medium-grained greenstone with plagioclase-carbonate-quartz layers up to 3 mm wide. Middle mafic-rich layer.

J) Fine-grained greenstone with concordant, 0.8 inch thick blue-green amphibole + carbonate + quartz vein. Mafic layer furthest to the west.

71VJL15A

Fine-grained greenstone in contact with a quartz-carbonate vein. A coarse-grained, blue-green amphibole layer is at the contact. Cliff-forming outcrop 170 feet west along Route 100 from station 71VJL14.

71VJL18A

Medium-grained greenschist with plagioclase-quartz-carbonate segregations stretched parallel to the foliation. Outcrop in the Middlebury River 0.9 mile S 80° W of Hancock, Rochester quadrangle, Vermont.

Estimated Modes; Pinney Hollow Formation

	Ca-Am	Bio	Cc	Chl	Epi	Plag	Qtz	Sphn	Mus	Mgt	Rut	Other
71VJL12G												
Host	5	3	3	20	35	25	5	1		3	Incl	
Vein	10	5	5	20	<1	5	50	<1		5		
71VJL12H												
Host	5	1	15	10	50	10	5	1		3		
Vein	20	<1	20	5	<1	<1	55		tr	<1		Ap
71VJL14H	10	tr	5	15	30	35		<1				Py
71VJL14I	13	tr	10	15	15	40	5	2			Incl	Py
71VJL14J												
Host	30	tr	3	<1	10	50		2		5		Py
Vein	60		35	tr	tr		5	<1	tr	tr		Ap
71VJL15A												
Host	10	3	5	15	20	30	5	2		10	Incl	
Vein	15		10				75					
71VJL18A			10	25	<1	40	20	5				Ap, Cpy

Stowe Formation

Greenstone and Amphibolite Member:

71VJL28A

Fine-grained greenstone with dark chlorite-rich and lighter plagio-
clase + calcite-rich layers. Roadcut at Eden Notch, southeast side of
Route 100, Hardwick quadrangle, Vermont.

71VJL30A

Fine-grained greenstone from outcrop 0.5 mile S 35° W of Eden
Notch. East side of Route 100, Hardwick quadrangle.

71VJL3

There are 3 roadcuts through a 660 foot thick layer of greenstone
on the northeast side of Interstate 89 1.5 to 1.7 miles southeast of the
Waterbury exit, Montpelier quadrangle, Vermont. 280 feet northwest of
the greenstone, pelitic schist crops out. Two samples were investigated:

C) Fine- to medium-grained greenstone with a concordant, medium-
grained, quartz-amphibole-calcite vein. A chlorite-rich
border zone is present at the vein/host contact. Greenstone
roadcut furthest to the southeast.

H) Medium-grained, gray pelitic schist with a well-developed slip
cleavage. Roadcut 280 feet northwest of the greenstone layer.

71VJL6B

Medium- to fine-grained, grayish greenschist with abundant plagio-
clase poikiloblasts. Inclusion trails in plagioclase are straight and
parallel to the foliation. Outcrop forming Loomis Hill, Montpelier
quadrangle.

71VJL11A

Medium- to fine-grained greenstone with mm-size amphibole porphyro-
blasts. Aligned solution pits on the weathered surface demarcate calcite
layers. Outcrop in field 0.7 mile S 5° E of Waterbury Center, Montpelier
quadrangle.

71VJL5B

Medium-grained, layered, dark gray amphibolitic schist. The cm-
scale layering is pseudoparallel to the foliation and is defined by grain
size. Coarser layers have abundant garnet porphyroblasts and have minor
plagioclase and quartz. Quarry east of road 1.4 miles N 15° E of
Loomis Hill School, Montpelier quadrangle.

71VJL44

Dense, medium-grained, dark gray-green amphibolite. Ledge-forming
outcrop at the end of the road which leads to an abandoned house 0.7 mile
S 45° E of the Elmore Mountain Lookout Tower. Hyde Park quadrangle, Ver-
mont.

71VJL50B

Medium-grained, dark gray-green amphibolitic schist. Outcrop on
north side of the trail across the southern end of Elmore Mountain.
0.3 mile S 75° E of Delano School, Hyde Park quadrangle.

Estimated Modes; Stowe Formation

	Ca-Am	Bio	Ank	Cc	Chl	Epi	Plag	Gar	Qtz	Sphn	Mus	Par	Hem	Mgt	Rut	Other
Biotite Zone:																
71VJL28A	8			15	20	25	20			2				10		
71VJL30A		10		1	30	30	20		5	1				2		
71VJL3C																
Host	1	2		5	20	60	10		<1	<1	<1					Cpy, Py
Vein	15	1		15	30	3	5		30	1						
71VJL3H			5		15		5	tr	50		15	5	5			Ap, Tour
71VJL6B	20				15	40	15		5	1	4					Py
71VJL11A	30	1		20	20	5	20			4						Cpy, Py, Po
Garnet Zone:																
71VJL5B	65	tr		<1	<1	<1	15	2	15	<1	1				1	Cpy, Py, Po
71VJL44	85	tr		<1	<1	10	1		1	1					<1	As, Ni, Co-rich Py; Cpy
71VJL50B	65					30	<1		5	<1						

Northeastern Vermont

Standing Pond Volcanic Member, Waits River Formation:

71VJL38A

Fine-grained, gray, layered amphibolitic schist. Mafic, graphitic, and isoclinally folded silicic layers parallel the foliation. Amphibole fascicles are nicely displayed on the foliation surface. Outcrop on top of the hill 1.1 miles S 30° E of Burke Hollow, Burke quadrangle, Vermont.

71VJL36A

Brownish gray, medium-grained, massive amphibolite. In hand specimen the amphibole observed is dark green and porphyroblastic. Outcrop in field 0.4 mile S 85° W of St. Johnsbury Center, St. Johnsbury quadrangle, Vermont.

71VJL53

Gray, medium-grained amphibolitic schist. Boulder in woods 100 yards to the northwest along strike of the amphibolite outcrop in the drainage 2.5 miles N 5° W of East Newark School, Burke quadrangle.

Estimated Modes; Northeastern Vermont

	Ca-Am	FM-Am	Bio	Cc	Chl	Epi	K-Fld	Plag	Qtz	Sphn	Ilm	Rut	Other
Biotite Zone:													
71VJL38A													
Mafic	40				20			35	5		<1	Alt	Tour, Graph
Silicic	20		<1		3			25	50			<1	Graph
Garnet Zone:													
71VJL36A	35	10	5		5			30	5		10		Ap
Sillimanite Zone:													
71VJL53	30		15	1		5	25	14	8	2	Incl		Ap, Tour, Cpy

Saxtons River Quadrangle

Chester Amphibolite Member of the Pinney Hollow Formation:

71VJL94A

Fine-grained, green phyllite with yellow-green, felsic-rich layers $\leq$ 1 mm thick parallel to the foliation. 0.8 mile N 85° E of North Windham. The nearest pelitic layer contains the index minerals chlorite and biotite.

71VJL127A

Medium-grained, light gray schist with porphyroblastic amphibole. Outcrop exposed by road builders in woods 0.9 mile S 55° E of North Windham. Chlorite ± garnet assemblages are present in the nearest pelitic layer.

71VJL97B

Fine-grained, green, mafic phyllite from an outcrop on the north side of Timber Ridge Lodge, 0.6 mile S 70° W of Lawrence Four Corners. The sample is from 10 feet of the exposed contact of this mafic layer with a chlorite-biotite-garnet pelitic schist.

71VJL100B

Green, fine-grained phyllite with orange carbonate porphyroblasts that weather out, leaving rectangular solution pits. Outcrop at the southeast corner of the road intersection 0.4 mile S 20° E of Burbees Pond.

71VJL113B

Gray, medium-grained garnet amphibolitic schist. A 1 cm thick, more mafic-rich layer is parallel to the foliation. Outcrop of dark green

amphibolite and more felsic amphibolitic schist. 1.1 miles N 35° W of South Windham.

71VJL108

Dark green, fine-grained phyllite with acicular amphibole lineated on the foliation surface. Orange carbonate porphyroblasts weather out; chlorite also forms porphyroblasts. Ledge outcrop 0.6 mile N 60° W of South Windham.

71VJL107A

Medium-grained, green-gray amphibolitic schist. Ridge-forming outcrop 0.5 mile N 60° W of South Windham.

71VJL106D

Gray, medium- to coarse-grained schist with mafic and pelitic layers ≤ 0.5 cm thick parallel to the foliation. Amphibole fascicles are present on the foliation surface. Outcrop in front lawn of a cabin 0.2 mile N 20° E of the South Windham Cemetery.

71VJL114B

Dark gray, medium-grained amphibolitic schist. Outcrop in clearing 1.0 mile S 20° E of South Windham.

71VJL119C

Dark gray, medium-grained, garnet amphibolitic schist with ≤ 1 mm thick felsic-rich layers parallel to the foliation. Ledge outcrop on the hillside above the West Townshend Cemetery. The contact between mafic and chlorite-biotite-garnet pelitic schists is exposed.

71VJL124B

Dark gray, medium-grained amphibolitic schist. Outcrop on the southeast side of the contact of this mafic layer with chlorite-biotite-

garnet pelitic schist.   East of the road 1.2 miles S 30° E of East
Jamaica.

Moretown Member of the Missisquoi Formation:

71VJL118

Mafic-rich and biotite-chlorite-garnet-quartz-white mica schists
are exposed in the roadcut above the Townshend Flood Control Dam 1.2
miles N 75° W of Townshend.   Mineral analyses were obtained from four
samples:

D)   Medium-grained pelitic schist with garnet porphyroblasts and
     biotite-chlorite-amphibole fascicles up to 3 inches long.
     Pelitic layer at the north end of the roadcut.

E)   Dark gray, medium- to coarse-grained garnet amphibolite boudin
     within the pelitic layer at the north end of the roadcut.

O)   Dark green, medium-grained amphibolitic schist with pyrite
     cubes up to 0.5 cm across.   Mafic layer at the south end of
     the roadcut.

P)   Dark green, medium-grained, isoclinally folded amphibolite
     with chlorite and amphibole porphyroblasts.   Southernmost
     mafic layer.

Pinney Hollow Formation:

Three samples along the power line 0.7 mile S 70° E of Acton Hill
were studied with the electron microprobe:

71VJL152

Gray, medium-grained garnet amphibolitic schist with silicic-rich
layers and lenticles up to 1 cm wide parallel to the foliation.

71VJL153C

    Dark gray, medium-grained, amphibolitic schist.

71VJL154B

    Gray, medium-grained, garnet amphibolitic schist. Felsic-rich layers up to 0.5 cm thick delineate symmetrical folds.

Ottauquechee Formation:

71VJL126H

    Medium-grained schist with cm-scale, dark gray amphibolitic and light gray pelitic layers parallel to the foliation. Outcrop on the hillside above Hinkley Brook 0.9 mile N 65° W of Grafton.

Estimated Modes; Saxtons River Quadrangle

Sample	Ca-Am	Bio	Dol	Cc	Chl	Epi	Plag	Gar	Qtz	Sphn	Mus	Par	Hem	Ilm	Mgt	Rut	Other
Biotite Zone:																	
71VJL94A	15	5		2	2	25	20		10	2					1		Cpy
Garnet–Albite Zone:																	
71VJL127A	40				8	20	20		10	2				⎱1			
71VJL97B	10	2		15	10	35	15		10	<1				⎰<1		2	Cpy
Garnet–Oligoclase Zone:																	
71VJL100B	45	1		⎰5	1	15	15		15					⎱1		3	Ap, Cpy
71VJL113B	15	15			1	10	30	10	15					4			All, Cpy
71VJL108	55		3		5	15	5		15							2	Ap
71VJL107A	35	1				25	5		30					4		tr	Cpy
71VJL106D	10	10			10	5	10	3	30		20			1	1		Ap, Tour, Zir
71VJL114B	50			5	3	20	5		15					⎱2		<1	Cpy
71VJL119C	55	tr			5	5	15	3	15					⎰2		<1	Ap
71VJL124B	40	tr		5	5	15	15		10					⎰10			Ap, Cpy
High Garnet Zone:																	
71VJL118D	4	15			4	2	15	2	50		5			⎱3	tr		Ap, All, Tour, Cpy, Py
71VJL118E	55	5		2	5	10	5	5	10			tr		3			Ap, Cpy, Py
71VJL1180	55			<1	2	20	10		10					2		1	Cpy, Py
71VJL118P	70	2			5	1	10		10							2	Ap, Py
Staurolite–Kyanite Zone:																	
71VJL152																	
Silicic	5	20			5	1	45	5	15		1			3		tr	Ap
Mafic	60	<1			3	5	15	2	5					10		<1	Ap
71VJL153C	50	10			5	1	20		10		1			⎱3		<1	Ap
71VJL154B	60	tr			1	<1	10	5	20					⎰4			Ap, Cpy, Py
71VJL126H																	
Pelitic	5	10			10	tr	30	10	20		⎱10			⎱5		tr	Ap, Tour, Zir
Mafic	40	5			5	tr	25		15			⎰5		⎰5			Ap, Zir

Woodstock Quadrangle

Barnard Volcanic Member, Missisquoi Formation:

71VJL80

Interlayered dark amphibolite and lighter colored gneiss crop out in the brook 0.1 mile N 10° E of Curtis Hollow School. The phases from three samples were analyzed:

B) Medium-grained, gray amphibolitic schist. Felsic-rich layers $\leq$ 0.1 mm thick parallel the foliation, and amphibole needles are lineated on the foliation surface. Epidote + white mica ± chlorite, quartz, and plagioclase "spots" may be amygdules.

C) Medium-grained, gray, crinkled garnet amphibolite. Chlorite-rich and poor layers parallel the foliation. Within the chlorite-poor layers are white mica + quartz + plagioclase ± epidote and chlorite segregations which could be amygdules.

D) Coarse-grained, dark-green amphibolite with garnet porphyro-blasts. The amphibole is lineated.

Estimated Modes; Woodstock Quadrangle

	Ca-Am	Bio	Chl	Epi	Plag	Gar	Qtz	Mus	Par	Hem	Mgt	Other
71VJL80B	35	tr	5	10	15		30	1		1	3	Ap, Py
71VJL80C												
Chl rich	30	2	10	<1	25		25		3	2	3	Cpy, Py
Chl poor	45		<1	<1	25	1	25		2	2	<1	
71VJL80D	60		15	<1	25	<1	<1			<1		

Wilmington Quadrangle

Chester Amphibolite Member of the Pinney Hollow Formation:

71VJL146A

Medium-grained, dark gray-green schist. Felsic layers ≤ 1 mm thick and mafic layers are parallel to the foliation and are crinkled. Outcrop of interfolded mafic and chlorite-biotite-garnet pelitic schist, east side of Route 9, 0.5 mile S 80° W of Adams School.

71VJL158A

Symmetrically folded, medium- to fine-grained, dark green amphibolitic schist. Outcrop north of road 1.1 miles S 35° E of Dover.

Estimated Modes; Wilmington Quadrangle

	Ca-Am	Bio	Dol	Cc	Chl	Epi	Plag	Qtz	Hem	Mgt	Rut	Other
71VJL146A	60	3	5	< 1	1	10	15	5			1	Ap, Cpy, Bor
71VJL158A	60	2		1	5	2	20	5	4	1	< 1	Ap, Tour

PLATES

1   Photomicrographs

a)   In the center of the field outlined in white are three discon-
tinuously zoned amphibole grains. The dark cores have more
glaucophane/riebeckite substitution than the lighter rims (best
seen toward the bottom of the picture). Tiny epidote grains
demarcate the core/rim boundaries. Plane polarized light.
LA426; Tibbit Hill Volcanic Member of the Pinnacle Formation.

b)   Dark actinolitic hornblende porphyroblast overgrown toward the
top of the picture by a light actinolite rim which becomes
darker and more hornblende rich toward the edge. The rim is
composed of small prismatic grains elongated perpendicular to
the core/rim boundary. Plane polarized light. LA430B; Green-
stone Member of the Underhill Formation.

c)   Zoned glaucophane lath and prismatic grains in an epidote matrix.
Dark cores are richer in riebeckite than the rims. Plane
polarized light. 75VJL383A; Belvidere Mountain Amphibolite
Member of the Hazens Notch Formation. Tillotson Peak subarea.

d)   Zoned amphibole grain in a matrix of barroisite actinolite and
epidote. Dark core is barroisite, light middle zone is glauco-
phane, and outermost rim is barroisitic actinolite. The rim
is lighter than the innermost core. Partially crossed polarized
light. A-BM-100; Belvidere Mountain Amphibolite Member of the
Hazens Notch Formation. Tillotson Peak subarea.

PLATES

1   e) Two large, anhedral, pale omphacite grains in the middle of the field are surrounded by a dark, fine-grained mass of plagioclase. Above the omphacite in the lower right quadrant is a zoned prismatic amphibole grain with a light glaucophane core and a dark barroisitic actinolite rim (particularly well-developed at the upper end of the grain.) Plane polarized light. Same sample as photomicrograph d.

       f) Zoned garnet. A Becke line separates the core from the rim, and growth rings are visible in the rim. Plane polarized light. A-BM-99; Belvidere Mountain Amphibolite Member of the Hazens Notch Formation. Tillotson Peak subarea.

2   Line drawing and elemental X-ray images (electron beam scans) of a zoned amphibole grain with a barroisite core and actinolite rim. Points analyzed with the electron microprobe are indicated. X-ray intensity profiles are taken across the center of each beam scan area. A-BM-100; Belvidere Mountain Amphibolite Member of the Hazens Notch Formation. Tillotson Peak subarea.

3   Line drawing and elemental X-ray images (electron beam scans) of a zoned amphibole grain with a barroisite core and glaucophane rim. Points analyzed with the electron microprobe are indicated. X-ray intensity profiles are taken across the center of each beam scan area. Same sample as plate 2.

PLATES

4   Line drawing and elemental X-ray images (electron beam scans) of

a zoned amphibole grain. Between the barroisite core (dark stipple)

and actinolite rim (light stipple) is an anhedral chlorite grain.

On either side of the zoned grain are actinolite grains (diagonal

lines). Points analyzed with the electron microprobe are annotated.

71VJL14J; Pinney Hollow Formation at Granville Notch.

5   Photomicrographs

a)   In the center of the field are three discontinuously zoned

amphibole grains made visible by dark cores overgrown by

lighter rims. The largest grain has an anhedral core, and the

two small grains have euhedral cores. Plane polarized light.

71VJL14J; Pinney Hollow Formation at Granville Notch.

b)   Anhedral zoned amphibole grains in matrix of epidote. Dark

cores are hornblende and light rims are actinolite. Plane

polarized light. 71VJL50B; Stowe Formation (Elmore Mountain

subarea).

c)   Radiating acicular grains of cummingtonite. Plane polarized

light. 71VJL36A; Standing Pond Volcanic Member of the Waits

River Formation; Northeastern Vermont.

d)   A zoned amphibole grain is in the center of the field. (See

plate 6 for a line drawing of this grain.) The dark, anhedral,

innermost core of hornblende is overgrown by a lighter, euhe-

dral, actinolite zone. The dark, outermost rim is hornblende.

Between the light euhedral zone and the dark, outermost rim

PLATES

5   is a narrow, colorless zone of actinolite (best seen on the right side of the grain). Plane polarized light. 71VJL127A; Chester Amphibolite Member of the Pinney Hollow Formation, Saxtons River quadrangle.

e) Zoned amphibole porphyroblast in a matrix of epidote and prismatic hornblende. The light, interior areas of the porphyroblast are actinolite; the darker, exterior areas are hornblende. Tiny, colorless inclusions are quartz grains. Plane polarized light. 71VJL107A; Chester Amphibolite Member of the Pinney Hollow Formation; Saxtons River quadrangle.

f) Hematite-ilmenite intergrowth. Darker, anhedral areas are ilmenite with exsolved hematite lamellae (light). Lighter domains are hematite with exsolved ilmenite lamellae (dark). Reflected light. 71VJL126H; Saxtons River quadrangle; Hinkley Brook subarea.

6   Line drawing and Al X-ray image (electron beam scan) of the zoned amphibole grain shown in plate 5d. The anhedral, innermost core (white) is hornblende and is overgrown by a euhedral (light stipple), actinolite zone. The outermost rim (dark stipple) is hornblende. The narrow (black) zone is actinolite. Other amphibole grains (slanted lines) are included within and adjacent to this grain. Arrows delineate EDA traverses.

PLATES

7   Line drawing and Ca X-ray images (electron beam scans) of albite
and oligoclase grains. The numbers on the line drawing are the
molecular percent anorthite of the analyzed point (indicated by the
decimal point). 71VJL107A; Chester Amphibolite Member of the
Pinney Hollow Formation; Saxtons River quadrangle.

8   Line drawing and X-ray images (electron beam scans) of albite and
oligoclase grains. The numbers on the line drawing are the molecular
percent anorthite of the analyzed point (indicated by the decimal
point). 71VJL124B; Chester Amphibolite Member of the Pinney Hol-
low Formation; Saxtons River quadrangle.

a ⊢——— 0.2 mm ———⊣

b ⊢——— 1.1mm ———⊣

c ⊢——— 1.1mm ———⊣

d ⊢——— 0.5mm ———⊣

e ⊢——— 1.1mm ———⊣
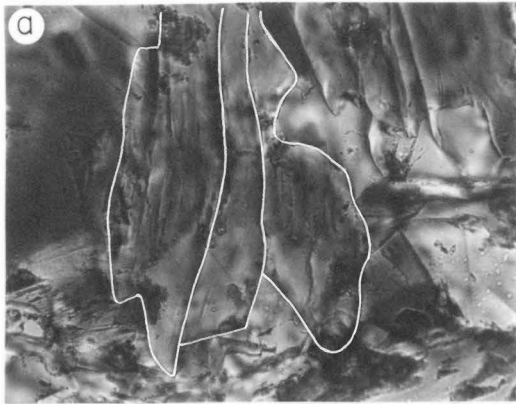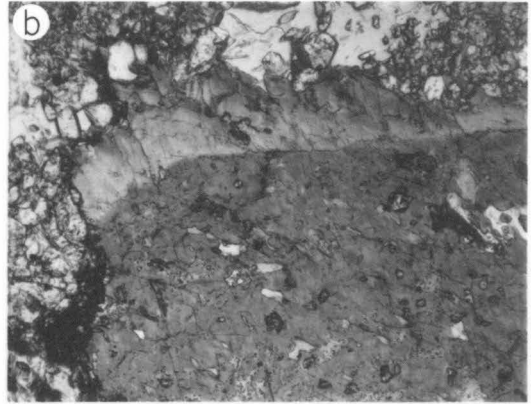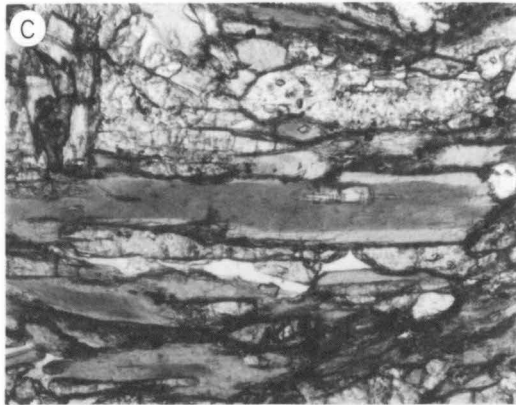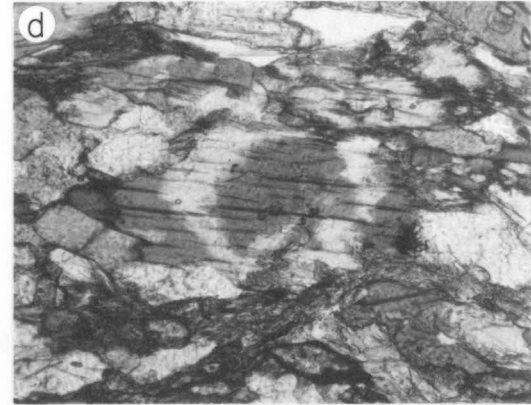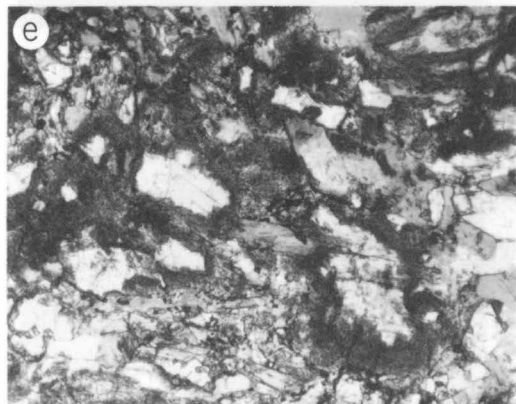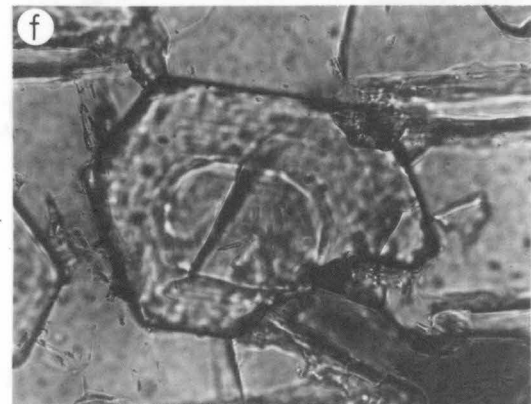
f ⊢——— 0.2 mm ———⊣

Plate 1

AMPHIBOLE GRAIN I, A-BM-IOO AREA A
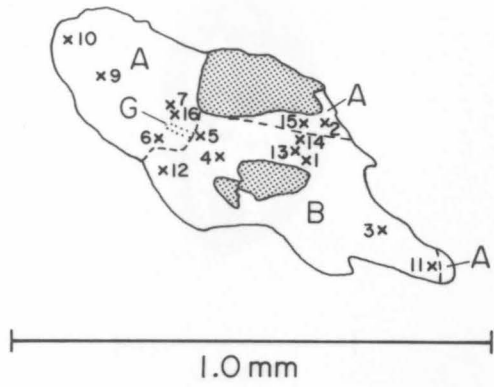
SCAN A: 12-6

SCAN B: 13-14-15

A ACTINOLITE
B BARROISITE
G GLAUCOPHANE
▒ EPIDOTE

1.0 mm

Al

Na
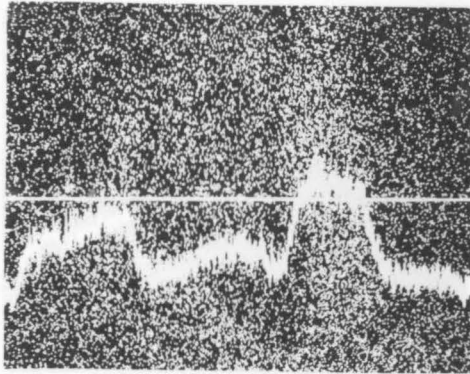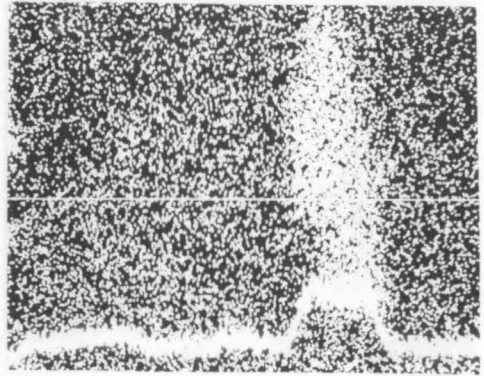
SCAN A
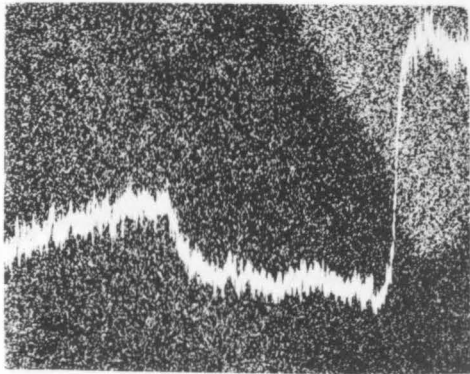
130 μm
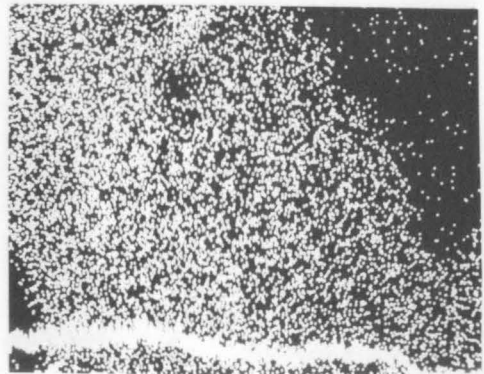
SCAN B

Plate 2

AMPHIBOLE GRAIN 1, A-BM-100 AREA C
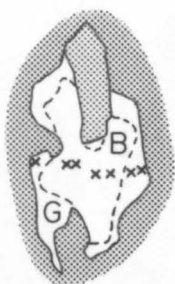
0.5 mm

× (l to r) 11, 8, 4, 7, 3, 2, 1

SCAN A: 7 - 3 - 2 - 1

SCAN B: 11 - 8 - 4

B   BARROISITE
G   GLAUCOPHANE
▨   EPIDOTE

Ca

Na
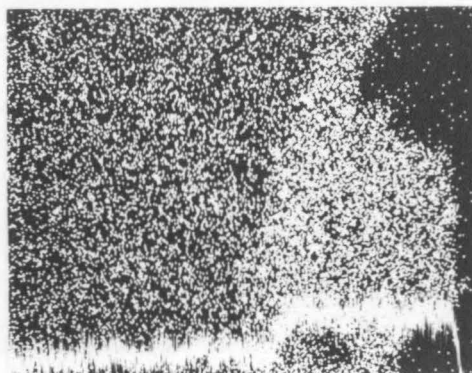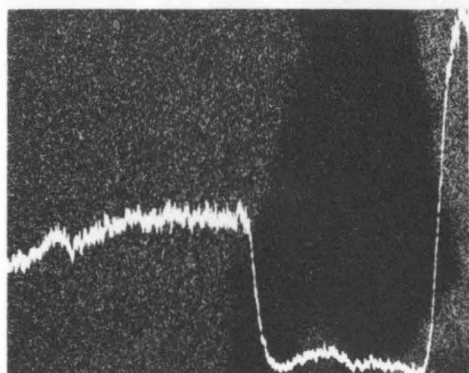
SCAN A

130 μm
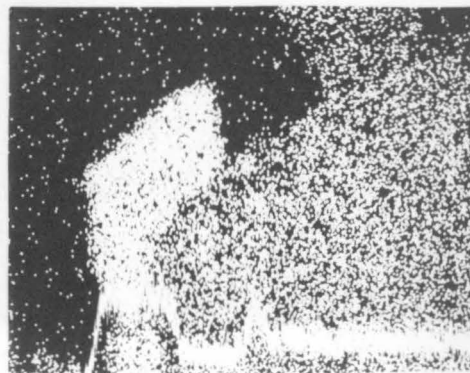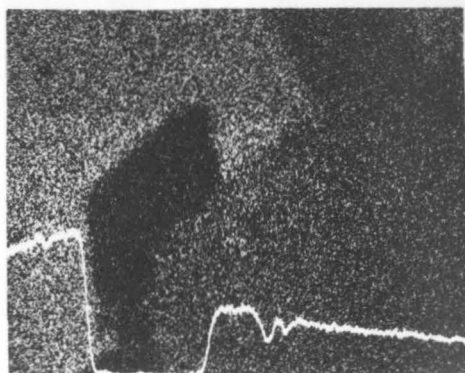
SCAN B

Plate 3

7IVJLI4J   Area C   Amphibole
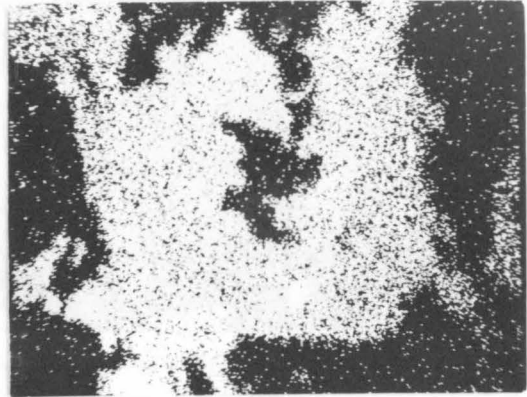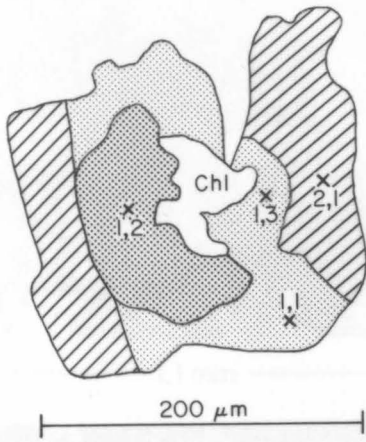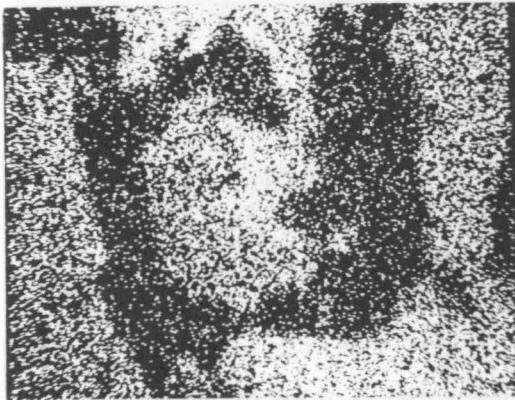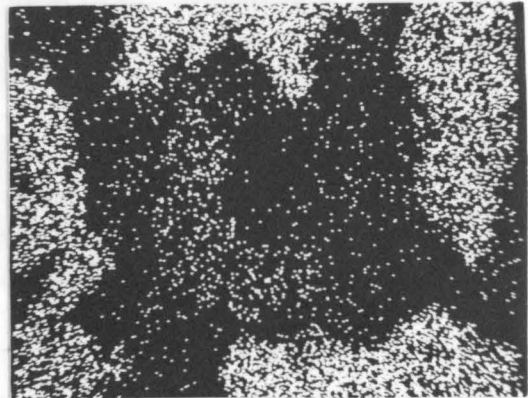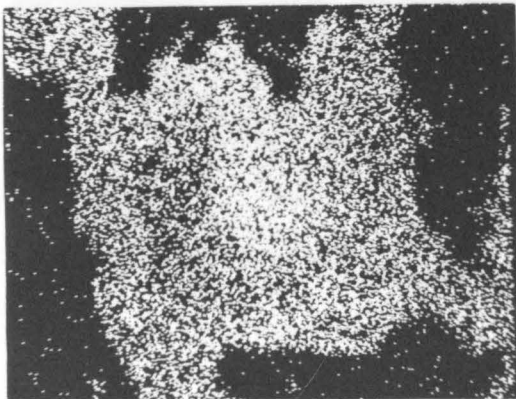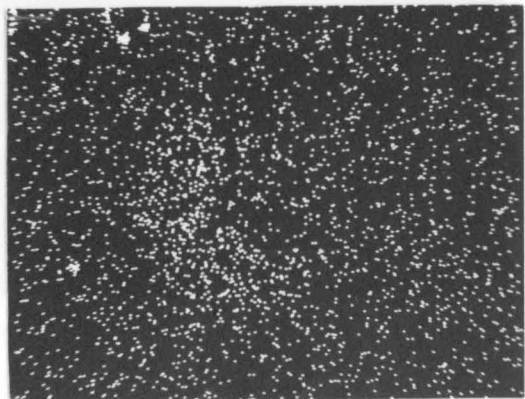
Plate 4

a

├──────── 1.1 mm ────────┤

d

├──────── 0.5 mm ────────┤

b

├──────── 1.1 mm ────────┤

e

├──────── 1.1 mm ────────┤

c

├──────── 1.1 mm ────────┤

f

├──────── 0.2 mm ────────┤

Plate 5

7IVJLI27A   AREA B   AMPHIBOLE GRAIN I

CHL

1:1

2

3
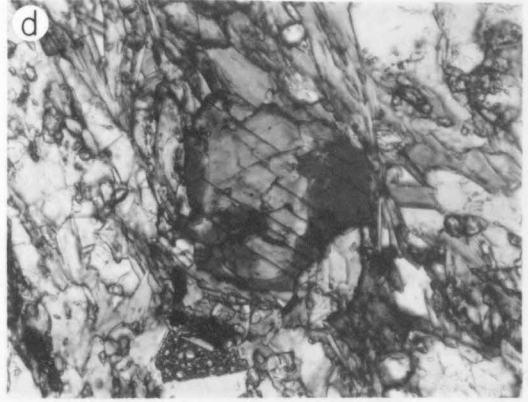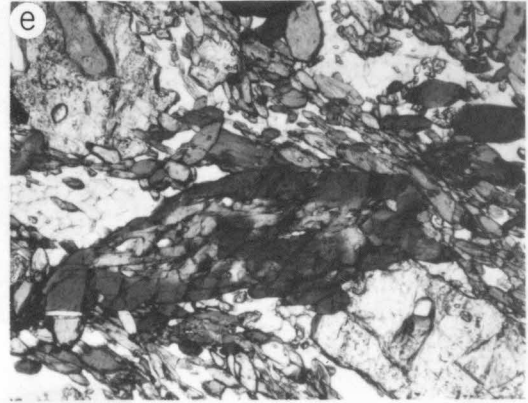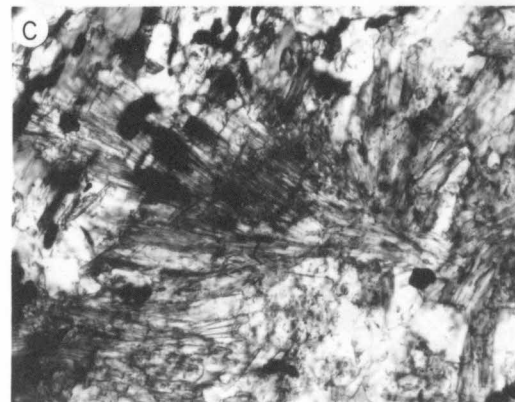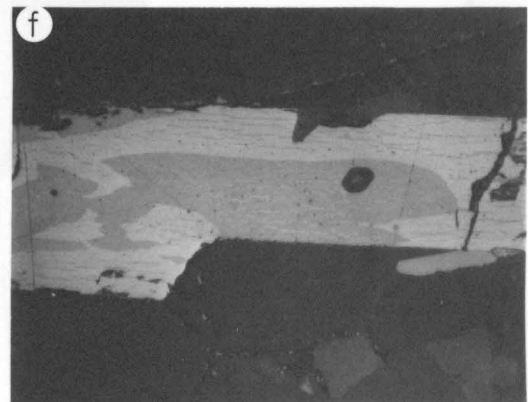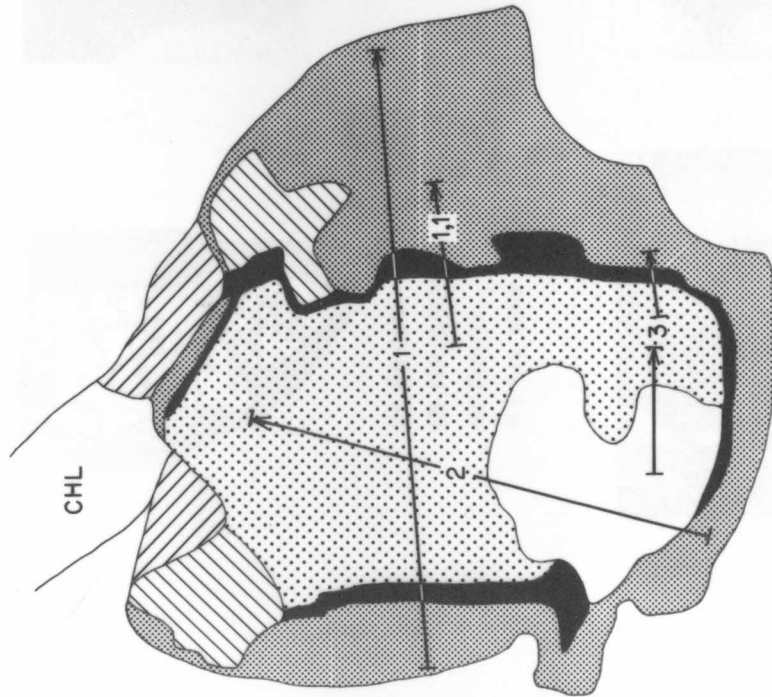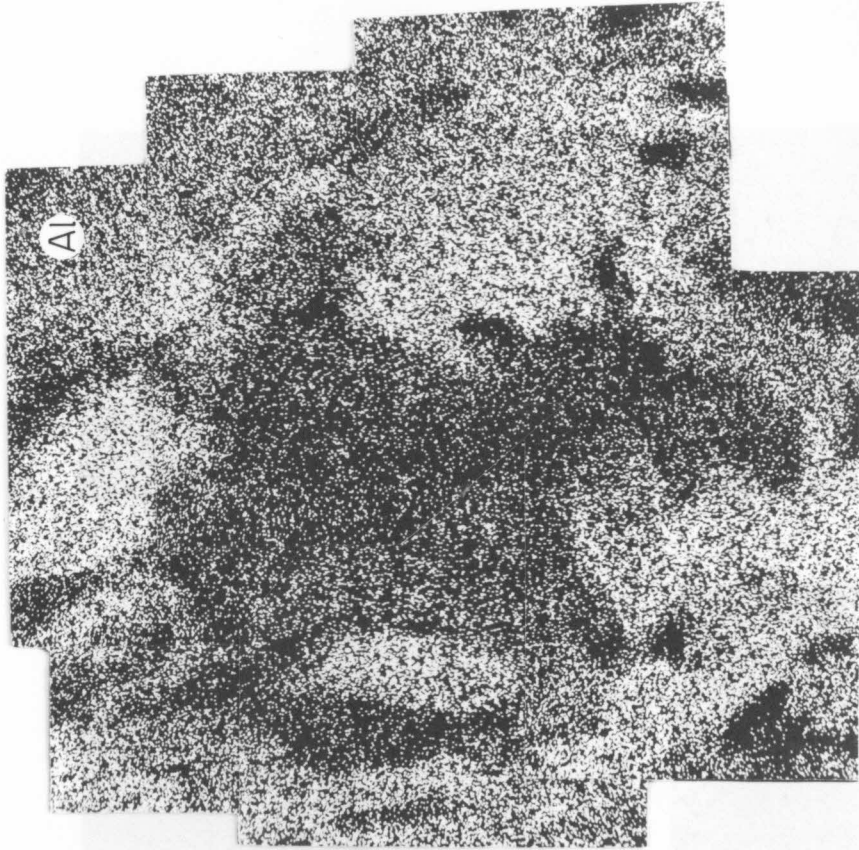
100 μm

Plate 6

71VJLI07A, AREA A
PLAGIOCLASE

SCAN 1: Ca

1000 ×

500 ×

SCAN 2: Ca

700 ×

300 ×

0.25 mm
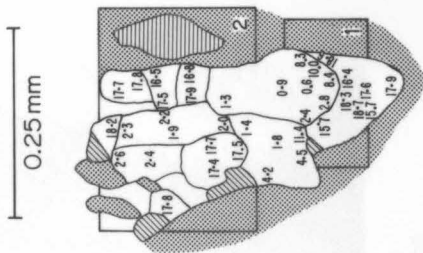
Epidote
Hornblende
Quartz
#'s are Mole %An

Plate 7
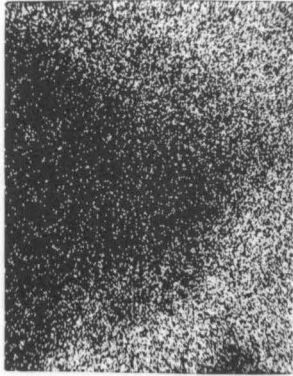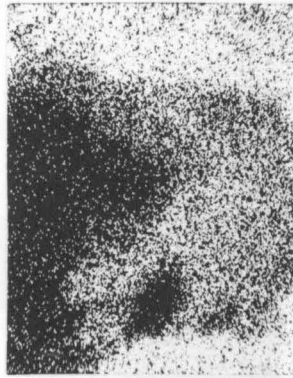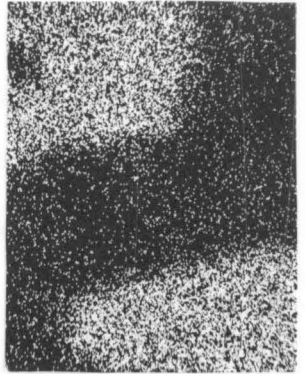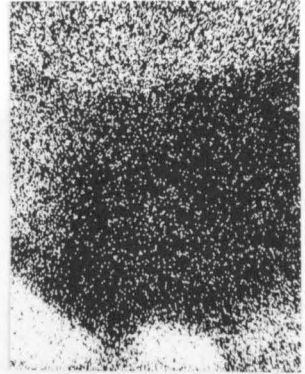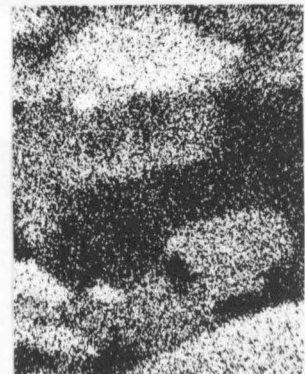
7IVJLI24B, AREA F
PLAGIOCLASE
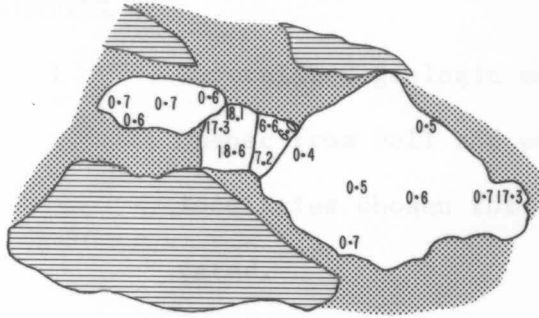
Epidote

Hornblende

#'s are Mole % An

0.5 mm

Ca   Na

200 ×

500 ×

Plate 8
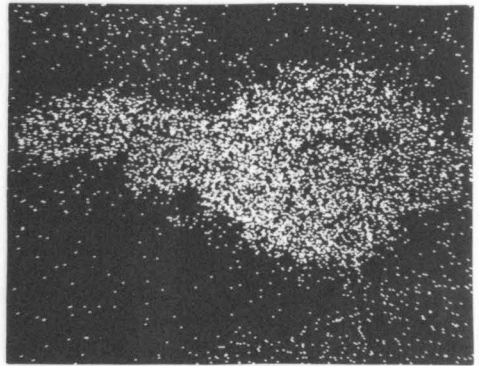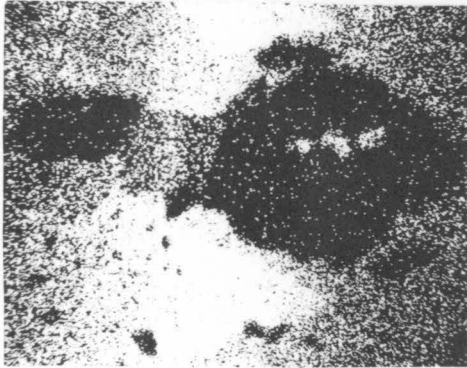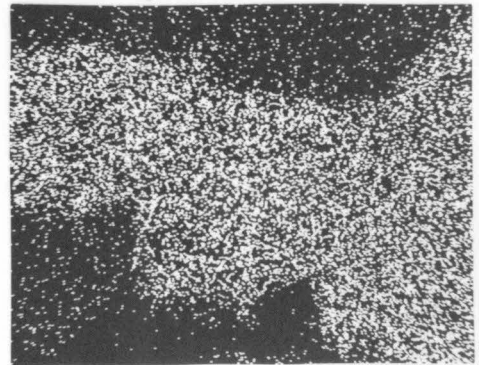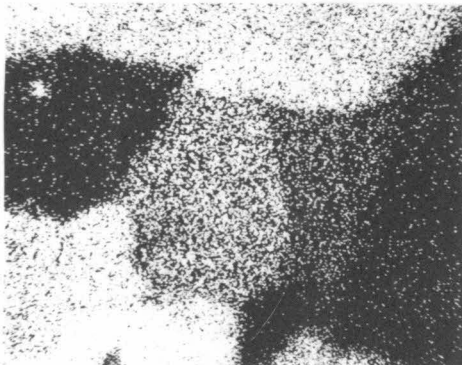
FIGURE CAPTIONS

CHAPTER I

1   Generalized geologic map of the state of Vermont and adjacent
     Quebec from Doll and others (1961) and Cady (1969). Sample
     localities chosen for electron microprobe analyses are anno-
     tated.

2   Index map of the topographic quadrangles from which samples
     were collected. Geologic maps referred to in the text
     for these quadrangles have been made by the workers listed.
     Places discussed in the text are indicated.

FIGURE CAPTIONS

CHAPTER II

1   Variation diagrams for end member Na and Ca amphiboles

a) $(Al^{VI} + Fe^{3+} + Cr + Ti)$ versus Al^{IV}. The monoclinic
    FM amphibole cummingtonite is also shown.

b) Na^A versus Ca versus Na^{M4}

c) 100 Na/(Ca + Na) versus Al/(Si + Al). The monoclinic
    FM amphibole cummingtonite is also shown.

FIGURE CAPTIONS

CHAPTER III

1   Al^{VI} versus Al^{IV} variation diagram for Ca- and Na-rich amphibole analyses from world-wide occurrences of mafic schist. The upper straight line is the proposed maximum possible Al^{VI} content in calcic amphibole from Leake (1965). The lower line is from Raase (1974). He proposed that this line separates hornblende from high-pressure and low-pressure terranes. (The latter plot below the line.) Filled and semi-filled symbols indicate electron microprobe data; open symbols refer to wet chemical analyses.

Calcic amphibole:

△ Abukuma Plateau, Japan (Shido, 1958; Shido and Miyashiro, 1959)

▼ Haast River group, New Zealand (Cooper and Lovering, 1970)

◇ Wiseman (1934)
                                } Dalradian, Scotland
◇ Shido and Miyashiro (1959)

◈ Graham (1974)   Dalradian in southwestern Scotland

⬡ Metamorphic eclogite, Norway (Binns, 1967)

⊖ Iwasaki (1963)
                                } Sanbagawa terrane, Japan
◓ Ernst and others (1970)

⊟ Goat Mountain, California. Franciscan terrane
    }
�merst and others (1970)

CHAPTER III

1   Sodic amphibole:

        ◐ Iwasaki (1963)
                               } Sanbagawa terrane, Japan
        ◕ Ernst and others (1970)

        ◪ Franciscan terrane at Goat Mountain, California
         }
        ◪ Ernst and others (1970)

2   ($Al^{VI} + Fe^{3+} + Ti$) versus Al^{IV} variation diagram for Ca-
and Na-rich amphibole analyses from world-wide occurrences
of mafic schist. Same symbols as for figure 1.

3   Na^A versus Ca versus Na^{M4} triangular diagram for Ca- and
Na-rich amphibole analyses from world-wide occurrences of
mafic schist. Same symbols as for figure 1.

4   100 Na/(Ca + Na) versus 100 Al/(Si + Al) variation diagram
for Ca- and Na-rich amphibole analyses from world-wide occur-
rences of mafic schist. Same symbols as for figure 1.

FIGURE CAPTIONS

CHAPTER IV

Pinnacle Formation

1   Amphibole analyses

       73QJL3C: △   Innermost core

                    ◉   Outer core

                    ○   Rim

                    +   Asbestiform

       LA426:   ◐   Core

                    ○   Rim and unrimmed

       LA434A: ○   Host

                    +   Vein

       LA435A: ○   Matrix

                    +   Amygdule

       LA460B: ◉   Dark

                    ○   Light

a)   Variation diagrams of Al^{VI}, Ti, and K versus Al^{IV}.

b)   Variation diagrams of 100 Na/(Ca + Na) versus 100 Al/ (Si + Al) and of $(Al^{VI} + Fe^{3+} + Ti + Cr)$ versus Al^{IV}.

c)   Triangular diagrams of Fe^{3+} versus Mg versus Fe^{2+} and of Na^{A} versus Ca versus Na^{M4}.

2   Mica analyses

a)   Variation diagrams for biotite. Al versus 100 Mg/(Mg + Fe), Mn versus Ti, and Al^{VI} versus Al^{IV}.

CHAPTER IV

Pinnacle Formation

2 b) Variation diagrams for white mica. Ti, $(Fe+Mg+Mn+Zn)$, and $K/(K + Na + Ca)$ versus Si. ○ Fine-grained.

◇ Coarse-grained.

3 Variation diagrams for chlorite analyses. Al versus 100 $Mg/(Mg + Fe^{2+})$, Ti versus Al^{IV}, and Al^{VI} versus Al^{IV}.

LA434A: ▣ & ○ Host

Χ Vein

LA460B: + Prograde

◇ & ○ Alteration of amphibole

4 Histograms of Fe^{3+} content for epidote analyses. Cores are indicated by filled boxes; vein compositions are denoted by Χ

5 Feldspar ternary diagrams

LA433C: ○ Alkali Feldspar

△ Plagioclase

LA435A: ○ Equant grains

+ Radiating bundles in amygdules and polysynthetically twinned grains in matrix

LA434A: ○ Host

+ Vein

6 a) Triangular diagram of Al versus (Fe + Mg) versus Ti for sphene analyses.

b) Triangular diagrams of Ca versus Mg versus Fe for carbonate analyses.

CHAPTER IV

Underhill Formation

7 Amphibole analyses from the biotite zone

  LA504B: o Epidote-absent layer

       △ Transition zone

       + Vein

  LA430B: o Matrix

       △ Porphyroblast

    Filled = core

a) Variation diagrams of Al^{VI}, Ti, and K versus Al^{IV}.

b) Variation diagrams of 100 Na/(Ca + Na) versus 100 Al/ (Si + Al) and of $(Al^{VI} + Fe^{3+} + Ti + Cr)$ versus Al^{IV}.

c) Triangular diagrams of Na^{A} versus Ca versus Na^{M4} and of Fe^{3+} versus Mg versus Fe^{2+}.

8 Amphibole analyses from the garnet zone

  73VJL225B: ▲ Innermost core

         ● Core

         o Rim and acicular grains

a) Variation diagrams of Al^{VI}, Ti, and K versus Al^{IV}.

b) Variation diagrams of 100 Na/(Ca + Na) versus 100 Al/ (Si + Al) and of $(Al^{VI} + Fe^{3+} + Ti + Cr)$ versus Al^{IV}.

c) Triangular diagrams of Fe^{3+} versus Mg versus Fe^{2+} and of Na^{A} versus Ca versus Na^{M4}.

9 Envelopes delimiting the biotite and garnet zone amphibole analyses.

CHAPTER IV

Underhill Formation

9   a)   Variation diagrams of Al^{VI}, Ti, and K versus Al^{IV}.

            b)   Variation diagrams of 100 Na/(Ca + Na) versus 100 Al/ (Si + Al) and of $(Al^{VI} + Fe^{3+} + Ti + Cr)$ versus Al^{IV}.

            c)   Triangular diagrams of Na^A versus Ca versus Na^{M4} and of Fe^{3+} versus Mg versus Fe^{2+}.

10   Variation diagrams for biotite analyses. Al versus 100 Mg/ (Mg + Fe), Mn versus Ti, and Al^{VI} versus Al^{IV}.

11   Variation diagrams for chlorite analyses. Al versus 100 Mg/ $(Mg + Fe^{2+})$, Ti versus Al^{IV}, and Al^{VI} versus Al^{IV}

           LA504B: ▨   Transition zone

                       +   Vein

12   Variation diagrams for stilpnomelane analyses. Al versus 100 Mg/(Mg + Fe), (K + Na + 2(Ca + Ba)) versus Al^{IV}, and Al^{VI} versus Al^{IV}

          o   Epidote-absent layer

          △   Transition zone

          X   Vein

13   Histograms of Fe^{3+} content for epidote analyses. Filled boxes indicate inclusions in plagioclase for 73VJL340B and cores for LA504B.

14   Feldspar ternary diagrams .

CHAPTER IV

Underhill Formation

Hazens Notch Formation

CHAPTER IV

Hazens Notch Formation

19   a) Variation diagrams of Ti and K versus Al^{IV}.

        b) Variation diagrams of Al^{VI} versus Al^{IV}.

        c) Variation diagrams of $(Al^{VI} + Fe^{3+} + Ti + Cr)$ versus Al^{IV}.

        d) Variation diagrams of $100\ Na/(Ca + Na)$ versus $100\ Al/(Si + Al)$.

        e) Triangular diagrams of Na^{A} versus Ca versus Na^{M4}.

        f) Triangular diagrams of Fe^{3+} versus Mg versus Fe^{2+}.

20   Zoning profiles in amphibole grain 1, A-BM-100 area A. Analyzed point positions are shown in plate 2. FeO_{T} is total iron as FeO.

21   Zoning profiles in amphibole grain 1, A-BM-100 area C. Analyzed point positions are shown in plate 3. FeO_{T} is total iron as FeO.

22      $(Al^{VI}+Fe^{3+}+Ti+Cr)$ versus Al^{IV} variation diagrams for barroisite-glaucophane, glaucophane-actinolite, and barroisite--actinolite pairs in A-BM-100.

23   Amphibole analyses from 73VJL360B

        ●   cores

        ○   rims and unrimmed

        X   blue-green, alteration product

        Dashed envelopes delimit soda-calcic amphibole analyses from A-BM-100.

CHAPTER IV

Hazens Notch Formation

23 a) Variation diagrams of Ti, K, and Al^{VI} versus Al^{IV}.

b) Variation diagrams of 100 Na/(Ca + Na) versus 100 Al/ (Si + Al) and of $(Al^{VI} + Fe^{3+} + Ti + Cr)$ versus Al^{IV}.

c) Triangular diagrams of Na^A versus Ca versus Na^{M4} and of Fe^{3+} versus Mg versus Fe^{2+}.

24 Triangular diagrams for omphacite analyses

a) Fe^{3+} versus Mg versus Fe^{2+}.

b) $NaAlSi_2O_6$ versus $(Ca, Fe, Mg, Mn)_2Si_2O_6$ versus $NaFe^{3+}Si_2O_6$.

25 Variation diagrams for chlorite analyses

a) Al versus 100 Mg/(Mg + Fe^{2+}) .

b) Ti and Al^{VI} versus Al^{IV}.

26 Variation diagrams for white mica analyses

a) Ti, (Fe + Mg + Mn + Zn), and K/(K + Na + Ca) versus Si for 73VJL337B. Dashed envelopes delimit the analyses from 75VJL380C, A-BM-99, and A-BM-100.

b) Ti, (Fe + Mg + Mn + Zn) and K/(K + Na + Ca) versus Si for 75VJL380C, A-BM-99, and A-BM-100.

c) Fe^{3+} versus Mg versus Fe^{2+}. Filled = paragonite.

27 Histograms of Fe^{3+} content for epidote analyses. Filled = core in X-Nicols, X = inclusion in garnet, and + = inclusion in soda-calcic amphibole.

CHAPTER IV

Hazens Notch Formation

CHAPTER IV

Pinney Hollow Formation

33   Variation diagrams for amphibole analyses from 71VJL12G, 12H, and 15A. ○ Host, △ vein, + vein border zone. Filled symbols are cores.

    a) $(Al^{VI} + Fe^{3+} + Ti + Cr)$, Al^{VI}, Ti, and K versus Al^{IV}.

    b) $100\ Na/(Ca + Na)$ versus $100\ Al/(Si + Al)$.

34   Variation diagrams for amphibole anlayses from 71VJL14H-J. Numbers refer to analyzed points shown in plate 4.

    a) Al^{VI}, Ti, and K versus Al^{IV}.

    b) $(Al^{VI} + Fe^{3+} + Ti + Cr)$ versus Al^{IV}.

    c) $100\ Na/(Ca + Na)$ versus $100\ Al/(Si + Al)$.

35   Triangular diagrams of Na^{A} versus Ca versus Na^{M4} and of Fe^{3+} versus Mg versus Fe^{2+}, ○ , □ , ◇ , host; △ vein; + vein border zone. Filled symbols are cores.

36   Variation diagrams for biotite analyses. Al versus $100\ Mg/(Mg + Fe)$, Mn versus Ti, and Al^{VI} versus Al^{IV}.

    71VJL12G: ○ Host, ● vein, + vein border zone

    71VJL12H: △

    71VJL14H: ◇

37   Variation diagrams for chlorite analyses. ● host, ○ vein, X vein border zone, + inclusion in 71VJL14J area C amphibole grain 1 between barroisite core and actinolite rim (see plate 4).

CHAPTER IV

Pinney Hollow Formation

37   a)   Al versus 100 $Mg/(Mg + Fe^{2+})$.

            b)   Ti and Al^{VI} versus Al^{IV}.

38   Histograms of Fe^{3+} content for epidote analyses. Boxes indicate host rock analyses, and filled boxes are cores. + indicates a vein border zone analysis.

39   Feldspar ternary diagrams.

40   Triangular diagrams of Ca versus Mg versus Fe for carbonate analyses. Filled triangles are vein analyses.

Stowe Formation

41   Amphibole analyses from the biotite zone. Filled symbols are cores.

         71VJL3C: o   Host

                   △ & zoning arrows   Vein Border Zone

                   ◇   Vein

         71VJL11A: o   Matrix

                   X & zoning arrows   Porphyroblast

         a)   Variation diagrams of Al^{VI}, Ti, and K versus Al^{IV}.

         b)   Variation diagrams of 100 Na/(Ca + Na) versus 100 Al/ (Si + Al) and of $(Al^{VI} + Fe^{3+} + Ti + Cr)$ versus Al^{IV}.

         c)   Triangular diagrams of Na^{A} versus Ca versus Na^{M4} and of Fe^{3+} versus Mg versus Fe^{2+}.

CHAPTER IV

Stowe Formation

42   Amphibole analyses from Elmore Mountain, garnet zone. Filled symbols are cores; χ denotes fracture fillings.

    a) Variation diagrams of Al^{VI}, Ti, and K versus Al^{IV}.

    b) Variation diagrams of 100 Na/(Ca + Na) versus 100 Al/ (Si + Al) and of $(Al^{VI} + Fe^{3+} + Ti + Cr)$ versus Al^{IV}.

    c) Triangular diagrams of Na^A versus Ca versus Na^{M4} and of Fe^{3+} versus Mg versus Fe^{2+}.

43   Amphibole analyses from Worcester Mountains, garnet zone. Dotted envelopes delimit amphibole analyses from the biotite zone (71VJL3C, 6B, 11A, 28A, and 30A). Dashed and solid envelopes indicate the analyses from the garnet zone at Elmore Mountain.

    a) Variation diagrams of Al^{VI}, Ti, and K versus Al^{IV}.

    b) Variation diagrams of 100 Na/(Ca + Na) versus 100 Al/ (Si + Al) and of $(Al^{VI} + Fe^{3+} + Ti + Cr)$ versus Al^{IV}.

    c) Triangular diagrams of Na^A versus Ca versus Na^{M4} and of Fe^{3+} versus Mg versus Fe^{2+}.

44   Variation diagrams of Al versus 100 Mg/(Mg + Fe), Mn versus Ti, and Al^{VI} versus Al^{IV} for biotite analyses. Filled symbols are for brown grains; open symbols indicate green grains.

CHAPTER IV

Stowe Formation

45   White mica analyses

    a) Variation diagrams of Ti, (Fe + Mg + Mn + Zn), and

       K/(K + Na + Ca) versus Si for 71VJL3C, 5B, and 6B.

    b) Variation diagrams of Ti, (Fe + Mg + Mn + Zn), and

       K/(K + Na + Ca) versus Si for 71VJL3H. $\triangle$ paragonite,

       o K-rich. Filled symbols indicate grains within the

       slip cleavage. Dashed envelopes indicate analyses from

       71VJL3C.

    c) Triangular diagrams of Fe^{3+} versus Mg versus Fe^{2+}. For

       71VJL3H filled symbols denote grains within the slip

       cleavage.

46   Variation diagrams of Al versus 100 $Mg/(Mg + Fe^{2+})$, Ti versus

    Al^{IV}, and Al^{VI} versus Al^{IV} for chlorite analyses. Filled =

    alteration product.

    71VJL3C: o & $\triangledown$ Host

           $\triangle$ Vein Border Zone

    Dashed envelope in Al^{VI} versus Al^{IV} diagram for 71VJL3H

    delimits analyses for 71VJL3C, 6B, 11A, 28A, and 30A. Solid

    envelope indicates 71VJL5B and 44 analyses.

47   Histograms of Fe^{3+} content for epidote analyses. Filled

    boxes are core compositions. χ = vein border zone

48   Feldspar ternary diagrams for WDA analyses. χ porphyroblast,

    o matrix grain, $\triangle$ vein border zone.

CHAPTER IV

Stowe Formation

49 100 An/(Ab + An + Or) profiles for EDA analyses

    of 71VJL5B plagioclase, area E grain 1 and area J grain 1.

    QUARTZ refers to a quartz inclusion in area J grain 1.

50 Triangular diagrams for garnet analyses. Ca versus Mn versus

    Fe^{2+}, Mn versus Mg versus Fe^{2+}, and Ca versus Mg versus Fe^{2+}.

    Solid line and filled circle = grain interior; dashed line and

    open circle = grain edge; dotted line and plus = inclusion in

    plagioclase.

51 Ca versus Mg versus Fe triangular diagrams for carbonate

    analyses.

52 Al versus (Fe + Mg) versus Ti triangular diagrams for sphene

    analyses. $\triangle$ vein border zone.

Northeastern Vermont

53 Variation diagrams for amphibole analyses from 71VJL38A.

    Al^{VI}, Ti, K, and $(Al^{VI} + Fe^{3+} + Ti + Cr)$ versus Al^{IV} and

    100 Na/(Ca + Na) versus 100 Al/(Si + Al).

     $\circ$ & zoning arrow Parallel to the foliation. Filled = core

     X Across the foliation

54 $(Na^{A} + K)$ versus Ca versus Na^{M4} triangular diagrams for calcic

    amphibole analyses. Filled symbols indicate cores. X = cross

    foliation. 71VJL38A zoning arrow is for grains parallel to

    the foliation ($\circ$).

CHAPTER IV

Northeastern Vermont

55 Fe^{3+} versus Mg versus Fe^{2+} triangular diagrams for amphibole

analyses. Filled symbols indicate cores.

 71VJL38A: ○ & zoning arrow Parallel to the foliation

      X Across the foliation

 71VJL36A: ○ Hornblende

      △ Cummingtonite

      X Light blue domains. May be a mixture of

       hornblende and cummingtonite.

Tie line connects fields for hornblende (delimited by solid

envelope) and cummingtonite (dashed envelope) analyses from

adjacent grains.

 71VJL53: Points plotted are for analyses normalized to

total cations - (Ca + Na + K) = 13. The short-dashed enve-

lope delimits where the analyses would plot if they were

normalized to total cations - (Na + K) = 15.

56 Variation diagrams for amphibole analyses from 71VJL36A. Al^{VI},

Ti, K, and $(Al^{VI} + Fe^{3+} + Ti + Cr)$ versus Al^{IV} and 100 Na/

(Ca + Na) versus 100 Al/(Si + Al).

 ○ Green, calcic amphibole. Filled = brownish core

 △ Colorless, monoclinic (Fe + Mg + Mn) amphibole

 X Light blue domains. May be a mixture of hornblende and

  cummingtonite.

Tie lines connect fields for hornblende (solid envelope) and

cummingtonite (dashed envelope) analyses from adjacent grains.

CHAPTER IV

Northeastern Vermont

Saxtons River Quadrangle

Chester Amphibolite Subarea

CHAPTER IV

Saxtons River Quadrangle

Chester Amphibolite Subarea

61-68   Variation diagrams for amphibole analyses. Na^A versus Ca versus Na^{M4}; Fe^{3+} versus Mg versus Fe^{2+}; Al^{VI}, Ti, K, and (Al^{VI} + Fe^{3+} + Ti + Cr) versus Al^{IV}; and 100 Na/(Ca + Na) versus 100 Al/(Si + Al). Filled symbols = cores.

61   71VJL127A

	WDA	EDA
Dark core		▲ & dashed envelope
Light core	✿ & solid envelope	◈
Colorless zone		+
Dark rim	○ & solid envelope	X

62   71VJL97B

63   71VJL100B

64   71VJL107A

65   71VJL108

66   71VJL124B

67   71VJL94A and 71VJL114B

68   71VJL113B, 106D, and 119C.

69   Variation diagrams for biotite analyses. Al versus 100 Mg/ (Mg + Fe), Mn versus Ti, and Al^{VI} versus Al^{IV}.

70   Variation diagrams for chlorite analyses. Ti versus Al^{IV}, Al^{VI} versus Al^{IV}, and Al versus 100 Mg/(Mg + Fe^{2+}).

CHAPTER IV

Saxtons River Quadrangle

<u>Chester Amphibolite Subarea</u>

CHAPTER IV

Saxtons River Quadrangle

<u>Townshend Dam Subarea</u>

77   Variation diagrams for amphibole analyses

     a)   100 Na/(Ca + Na) versus 100 Al/(Si + Al) and (Al^{VI} + Fe^{3+} + Ti + Cr), Al^{VI}, Ti, and K versus Al^{IV}.

     b) Fe^{3+} versus Mg versus Fe^{2+}. Garnet is present in V118D and E (dashed envelopes). Na^{A} versus Na^{M4} versus Ca.

78   a)   Variation diagrams of Al versus 100 Mg/(Mg + Fe), Mn versus Ti, and Al^{VI} versus Al^{IV} for biotite analyses.

     b)   Histograms of Fe^{3+} content for epidote analyses. Filled boxes indicate cores.

79   Variation diagrams for chlorite analyses. Al versus 100 Mg/ (Mg + Fe^{2+}), Ti versus Al^{IV}, and Al^{VI} versus Al^{IV}.

80   Feldspar ternary diagrams.

81   a)   Triangular diagram of Ca versus Mg versus Fe for carbonate analyses.

     b)   Triangular diagrams of Ca versus Mn versus Fe^{2+} for garnet analyses. Dashed = grain edge.

82   Triangular diagrams of $MnTiO_3$ versus Fe_2O_3 versus $FeTiO_3$ for ilmenite and hematite analyses.

CHAPTER IV

Saxtons River Quadrangle

<u>Acton Hill Subarea</u>

83 Variation diagrams for amphibole analyses.

   71VJL152: o Mafic layer

       $\triangle$ Silicic layer

  a) 100 Na/(Ca + Na) versus 100 Al/(Si + Al) and $(Al^{VI} + Fe^{3+}$ $+ Ti + Cr)$, Al^{VI}, Ti, and K versus Al^{IV}.

  b) Na^{A} versus Ca versus Na^{M4} and Fe^{3+} versus Mg versus Fe^{2+}.

84 a) Histograms of Fe^{3+} content for epidote analyses. χ = silicic layer in 71VJL152.

  b) Variation diagrams of Al versus 100 Mg/(Mg + Fe), Mn versus Ti, and Al^{VI} versus Al^{IV} for biotite analyses.

85 Variation diagrams of Al versus 100 Mg/(Mg + Fe^{2+}), Ti versus Al^{IV}, and Al^{VI} versus Al^{IV} for chlorite analyses.

  • = silicic layer in 71VJL152.

86 Feldspar ternary diagrams. $\triangle$ = silicic layer in 71VJL152.

87 Triangular diagrams of Ca versus Mn versus Fe^{2+} for garnet analyses. Dashed = grain edge.

88 Triangular diagrams for $MnTiO_3$ versus Fe_2O_3 versus $FeTiO_3$ for ilmenite and hematite analyses.

CHAPTER IV

Saxtons River Quadrangle

<u>Hinkley Brook Subarea</u>

89   Variation diagrams for amphibole analyses from 71VJL126H.

Al^{VI}, Ti, K, and $(Al^{VI} + Fe^{3+} + Ti + Cr)$ versus Al^{IV};

100 Na/(Ca + Na) versus 100 Al/(Si + Al); Na^A versus Ca

versus Na^{M4}; and Fe^{3+} versus Mg versus Fe^{2+}. $\triangle$ = pelitic layer.

90   Al versus 100 Mg/(Mg + Fe^{2+}), Ti versus Al^{IV}, and Al^{VI} versus

Al^{IV} variation diagrams for chlorite analyses from 71VJL126H.

Al versus 100 Mg/(Mg + Fe), Mn versus Ti, and Al^{VI} versus Al^{IV}

variation diagrams for biotite analyses from 71VJL126H.

$\triangle$ = pelitic layer.

91   Variation diagrams for white mica anlayses from 71VJL126H.

Ti, (Fe + Mg + Mn + Zn), and K/(K + Na + Ca) versus Si; Fe^{3+}

versus Mg versus Fe^{2+}; and Ca versus K versus Na.

$\triangle$ paragonite, $\bigcirc$ K-rich. Filled = pelitic layer.

92   71VJL126H. $\triangle$ pelitic layer

a) Feldspar ternary diagram.

b) Triangular diagram of $MnTiO_3$ versus Fe_2O_3 versus $FeTiO_3$

for ilmenite and hematite.

93   Triangular diagram of Ca versus Mn versus Fe^{2+} for garnet

analyses. Dashed = grain edge.

CHAPTER IV

Saxtons River Quadrangle

<u>Comparison of Subareas</u>

CA: Chester Amphibolite

    --------   Below the oligoclase isograd

    —— ——   Garnet-absent rocks above the oligoclase isograd.

    ————————   Garnet-present rocks above the oligoclase isograd.

TD: Townshend Dam

    ——— . ———   Garnet-absent rocks

    ————————   Garnet-present rocks

AH: --------   Acton Hill

HB: ········   Hinkley Brook

94   Variation diagrams for amphibole analyses. Fe^{3+} versus Mg versus Fe^{2+}; K, Ti, and Al^{VI} versus Al^{IV}; and 100 Na/(Ca + Na) versus 100 Al/(Si + Al).

95   Al versus 100 Mg/(Mg + Fe) variation diagram for biotite

    Al versus 100 Mg/(Mg + Fe^{2+}) variation diagram for chlorite.

Woodstock Quadrangle

96   Variation diagrams for amphibole analyses.

    71VJL80C: △ Chlorite-rich layer

                o Chlorite-poor layer

                X Amygdule

CHAPER IV

Woodstock Quadrangle

96   a)   100 Na/(Ca + Na) versus 100 Al/(Si + Al); $(Al^{VI} + Fe^{3+} + Ti + Cr)$, Al^{VI}, Ti, and K versus Al^{IV}.

         b) Na^A versus Ca versus Na^{M4} and Fe^{3+} versus Mg versus Fe^{2+}.

97   Al versus 100 Mg/(Mg + Fe^{2+}), Ti versus Al^{IV}, and Al^{VI} versus Al^{IV} variation diagrams for chlorite analyses.

      71VJL80C: $\triangle$ Chlorite-rich layer

               o   Chlorite-poor layer

               +   Alteration (?)

98   a)   Histograms of Fe^{3+} content for epidote analyses

          71VJL80C: Filled box   =   yellow grain

                  Open box   =   colorless grain

                      +   =   pale yellow grain in amygdule

         b)   Feldspar ternary diagrams

          71VJL80C: $\triangle$ Chlorite-rich layer

                   o   Chlorite-poor layer

                   +   Amygdule

99   a) $MnTiO_3$ versus Fe_2O_3 versus $FeTiO_3$ triangular diagram for 71VJL80C hematite analyses.

         b)   Ca versus Mn versus Fe^{2+} triangular diagram for garnet analyses. Dashed = grain edge.

CHAPTER IV

Wilmington Quadrangle

100   Variation diagrams for amphibole analyses. Filled = light core.

a) 100 Na/(Ca + Na) versus 100 Al/(Si + Al); $(Al^{VI} + Fe^{3+} + Ti + Cr)$, Al^{VI}, Ti, and K versus Al^{IV}.

b) Na^A versus Ca versus Na^{M4} and Fe^{3+} versus Mg versus Fe^{2+}.

101   a) Ca versus Mg versus Fe triangular diagram for carbonate analyses.

b) Variation diagrams for biotite analyses. Al versus 100 Mg/(Mg + Fe), Mn versus Ti, and Al^{VI} versus Al^{IV}.

c) Variation diagrams for chlorite analyses. Al versus 100 Mg/(Mg + Fe^{2+}), Ti versus Al^{IV}, and Al^{VI} versus Al^{IV}.

102   a) Histograms of Fe^{3+} content for epidote analyses. Filled boxes indicate cores.

b) $MnTiO_3$ versus Fe_2O_3 versus $FeTiO_3$ triangular diagram for hematite analyses. Negligible $(Mg + Zn)TiO_3$. Ilmenite analysis is on a lamella.

c) Feldspar ternary diagram. X may be composite of albite and oligoclase domains.

FIGURE CAPTIONS

CHAPTER V

1   Al^{VI} versus Al^{IV} diagram with envelopes delimiting the calcic
     and soda-calcic amphibole analyses from Vermont and adjacent
     Quebec. The investigated areas are divided into three groups:

     I   Pinnacle Formation, Hazens Notch Formation, Pinney Hollow
          Formation, and Stowe Formation (Eden Notch and Worcester
          Mountains subareas).

     II   Underhill Formation, Stowe Formation (Elmore Mountain sub-
          area), Saxtons River quadrangle, Woodstock quadrangle,
          and Wilmington quadrangle.

     III Northeastern Vermont.

2    $(Al^{VI} + Fe^{3+} + Cr + Ti)$ versus Al^{IV} diagram with envelopes de-
     limiting the calcic and soda-calcic amphibole analyses from
     Vermont and adjacent Quebec. The investigated areas are
     divided into the same three groups as for figure 1.

3   Na^A versus Ca versus Na^{M4} diagram with envelopes delimiting the
     calcic and soda-calcic amphibole analyses from Vermont and
     adjacent Quebec. The investigated areas are divided into the
     same three groups as for figure 1.

4   100 Na/(Ca + Na) versus 100 Al/(Si + Al) diagram. Envelopes
     encompass the calcic and soda-calcic amphibole analyses from
     Vermont and adjacent Quebec. The three groups of investigated
     areas are the same as for figure 1.

CHAPTER V

5   100 Na/(Ca + Na) versus 100 Al/(Si + Al) diagram for amphibole analyses from the Pinnacle Formation. Growth generations indicated by envelopes are assigned to Ordovician (O2 and O1) and Devonian (either D1 or D2) events. The combined zoning arrow for 73QJL3C and LA426, 434A, and 435A is indicated.

6   100 Na/(Ca + Na) versus 100 Al/(Si + Al) diagram for amphibole analyses from the Underhill Formation. Growth generation shown by envelopes are assigned to two Devonian events.

7   Range of pressure and temperature conditions (stippled area) at which the glaucophane- and omphacite-bearing assemblages observed at Tillotson Peak (subarea of the Hazens Notch Formation) formed. The andalusite-kyanite-sillimanite phase diagrams of Holdaway (1971) and Richardson, Gilbert, and Bell (1969) are delineated. The $Al_2 SiO_5$ + chloritoid = staurolite + quartz breakdown is from Richardson (1968). The stability curve for phengite (Si = 3.4) is from Velde (1967). The calcite to aragonite transition is from Johannes and Puhan (1971). The albite = omphacite (jadeite$_{40}$) + quartz breakdown is extrapolated from Kushiro (1969).

8   100 Na/(Ca + Na) versus 100 Al/(Si + Al) diagram for amphibole analyses from the Hazens Notch Formation. Envelopes encompass the data for each growth generation which have been assigned to two Ordovician events.

CHAPTER V

9   100 Na/(Ca + Na) versus 100 Al/(Si + Al) diagram for amphibole

        analyses from the Pinney Hollow Formation (Granville Notch sub-

        area). An Ordovician (O2) and a Devonian (D2) event is recog-

        nized.

10   Stowe Formation amphibole analyses on 100 Na/(Ca + Na) versus

        100 Al/(Si + Al) diagram. Ordovician (O2) and Devonian (D2)

        growth events are observed.

11   Amphibole analyses from northeastern Vermont on 100 Na/(Ca + Na)

        versus 100 Al/(Si + Al) diagram. Devonian D1 and D2 events are

        assigned to the analysis groups.

12   100 Na/(Ca + Na) versus 100 Al/(Si + Al) diagram for amphibole

        analyses from the Saxtons River quadrangle. Two Ordovician

        and two Devonian periods of mineral growth are observed.

13   100 Na/(Ca + Na) versus 100 Al/(Si + Al) diagram for amphibole

        analyses from the Woodstock quadrangle to which Devonian D1

        growth is assigned. For comparison envelopes for amphibole

        analyses from the Saxtons River quadrangle are delineated.

14   100 Na/(Ca + Na) versus 100 Al/(Si + Al) diagram for amphibole

        analyses from the Wilmington quadrangle. D1 and D2 Devonian

        mineral growth is observed. For comparison the Chester Amphib-

        olite (subarea of the Saxtons River quadrangle) amphibole

        analyses are delimited.

FIGURE CAPTIONS

CHAPTER VI

1   Phase relationships in the system $SiO_2 - Al_2O_3 - Fe_2O_3 - TiO_2$

        $- MgO - FeO - MnO - CaO - Na_2O - K_2O - H_2O - CO_2$.

        Abbreviations: AF_2O_3 $Al_2O_3 + Fe_2O_3$
                         FMO $FeO + MgO + MnO$

                         AB   Albite
                         ACT   Actinolite
                         AN   Anorthite
                         ANK   Ankerite
                         CC   Calcite
                         CHL   Chlorite
                         CUM   Cummingtonite
                         EPI   Epidote
                         GL   Glaucophane
                         GR   Grossular
                         HAST   Hastingsite
                         HBL   Hornblende
                         OMPH   Omphacite
                         PAR   Paragonite
                         PARG   Pargasite
                         PyAlSp   Pyrope + Almandine + Spessartine
                         STILP   Stilpnomelane
                         TSCH   Tschermakite

        a) $Na_2O - AF_2O_3 - CaO - FMO$ tetrahedron (molecular percent).

        b) Molecular percent triangular diagrams for Na_2O versus AF_2O_3
           versus CaO, AF_2O_3 versus CaO versus FMO, and Na_2O versus
           AF_2O_3 versus FMO.

        c) Albite + epidote projection onto $AF_2O_3 - FMO$ (molecular
           percent).

2       $Na_2O - AF_2O_3 - CaO - FMO$ tetrahedra for medium-pressure facies
        series mafic rock assemblages. Data fields encompass the

CHAPTER VI

2   analyses from the samples investigated. Abbreviations are the

same as in figure 1; plus

        DOL   Dolomite
        GAR   Garnet
        OLIG   Oligoclase

a) Biotite-ablite zone

    73QJL3C; LA426, 433C, 434A, 435A, 460B, and 504B;

    71VJL3C, 6B, 12G-H, 14H-J, 15A, 18A, 28A, 30A, 44, and 50B.

    Amphbiole cores are excluded and 71VJL44 plagioclase is not

    included.

b) Garnet - albite zone

    71VJL94A, 97B, 127A; 73VJL225B and 340B.

    Actinolite cores in 71VJL97B and 127A are excluded.

c) Garnet - oligoclase zone

    71VJL100B, 108, 114B, 1180 and P, 146A. Actinolite cores

    are excluded. These garnet-absent assemblages have less

    aluminous hornblende and chlorite and less anorthite-rich

    plagioclase than the garnet-present assemblages in

    71VJL80B-D, 106D, 113B, 119C, 118D and E. Garnet cores

    are excluded.

d) Staurolite - kyanite - oligoclase zone

    71VJL126H, 152, 153C, and 154B. Garnet cores are

    excluded.

CHAPTER VI

3   Na_2O versus AF_2O_3 versus CaO, AF_2O_3 versus CaO versus FMO,
     and Na_2O versus AF_2O_3 versus FMO triangular diagrams for
     medium-pressure facies series mafic rock assemblages.
     The plotted analyses are the same as listed for figure 2.
     Points A-F indicate bulk rock compositions and tie lines
     join averaged analyses used in the least-squares models.
     Abbreviations are the same as in figures 1 and 2.

     a)   Biotite-albite zone.

     b)   Garnet-albite zone.
           Tie lines are for 71VJL94A, 73VJL225B, and 73VJL340B.

     c)   Garnet-oligoclase zone.
           Samples 71VJL113B and 118E contain garnet.

     d)   Staurolite-kyanite-oligoclase zone.

4   Albite-epidote projections for medium-pressure facies series
     assemblages from mafic schist. The plotted points are the same
     as listed for figure 2, and tie lines join averaged analyses.
     Abbreviations are the same as those for figure 1.

     a)   Biotite-ablite zone.

     b)   Garnet-albite zone.

     c)   Garnet-oligoclase zone.

     d)   Staurolite-kyanite-oligoclase zone.

CHAPTER VI

5   Na_2O - AF_2O_3 - CaO - FMO tetrahedra for medium- to low-pressure

facies series assemblages from mafic schist. Data fields con-

tain the analyses from the studied samples, and most of the

abbreviations used are listed in figure 1.

AND	Andesine
BYT	Bytownite
OLIG	Oligoclase
SILL	Sillimanite

a) Biotite-oligoclase zone. Epidote is absent from the

     sample studied (71VJL38A) but is included for completeness.

b) Garnet-oligoclase/andesine zone. Epidote is absent from

     the investigated sample (71VJL36A) but is included for

     completeness.

c) Sillimanite-bytownite zone. Andalusite also occurs in the

     interlayered pelitic rocks. For completeness dashed lines

     to chlorite are shown even though this phase is absent from

     the studied sample (71VJL53).

6   Na_2O versus AF_2O_3 versus CaO, AF_2O_3 versus CaO versus FMO, and

Na_2O versus AF_2O_3 versus FMO triangular diagrams for phases

observed in mafic schist from medium- to low-pressure facies

series. The plotted analyses are the same as listed for

figure 5.

a) Biotite-oligoclase zone.

b) Garnet-oligoclase/andesine zone.

CHAPTER VI

6   c) Sillimanite-bytownite zone. Andalusite also occurs in the intercalated pelitic rocks.

7   Albite-epidote projection for medium- to low-pressure assemblages in mafic rocks. Tie lines join the averaged analyses used in least-squares models F (biotite-oligoclase zone, 71VJL38A) and C (garnet-oligoclase/andesine zone, 71VJL36A). Andalusite also occurs in the sillimanite-bytownite grade pelitic schist interlayered with 71VJL53.

8   Electron microprobe analyses for the phases in the high-pressure facies series mafic schist from Tillotson Peak (subarea of the Hazens Notch Formation). Data fields contain the analyses from the samples: 73VJL337A, 73VJL337B (includes albite), 75VJL380C, and 75VJL383B. Garnet core analyses are excluded. Abbreviations are explained in the captions for figures 1 and 2.

a) $Na_2O - AF_2O_3 - CaO - FMO$ tetrahedron.

b) Na_2O versus AF_2O_3 versus CaO, AF_2O_3 versus CaO versus FMO, and Na_2O versus AF_2O_3 versus FMO triangular diagrams. Bulk rock compositions B and D modeled by least squares are shown.

9   Albite-epidote projection for the high-pressure mafic rocks at Tillotson Peak (subarea of the Hazens Notch Formation). The analyses plotted are the same as in figure 8.

CHAPTER VI

10 Calculated phase abundances (coefficients) ±1σ errors for medium-pressure facies series mafic samples modeled to bulk rock composition A. Abbreviations are explained in the appendix.

11 Na_2O versus AF_2O_3 versus CaO, AF_2O_3 versus CaO versus FMO, and Na_2O versus AF_2O_3 versus FMO triangular diagrams for medium- to high-pressure, biotite-albite zone mafic rock phase assemblages. Tie lines join averaged compositions modeled to bulk rock composition B.

  ○ 71VJL11A

  ● Amphibole cores from 73QJL3C; LA426; 71VJL3C, 12G-H, 15A, 28A and 30A.

The dashed envelope delimits the actinolite analyses shown in figure 3a, and the dotted envelope contains the glaucophane analyses shown in figure 8b. Abbreviations are explained in the caption for figure 1.

12 Calculated phase abundances (coefficients) ±1σ errors for mafic schist samples modeled to bulk rock composition B. LA426, 73VJL340B, and 71VJL113B are medium-pressure facies series rocks. 71VJL11A is from the medium- to high-pressure facies series biotite-albite zone, and 75VJL380C is from the high-pressure garnet-albite zone. Abbreviations are explained in the appendix or in the caption for figure 1.

CHAPTER VI

13   Calculated phase abundances (coefficients) $\pm 1\sigma$ errors for
        mafic schist samples modeled to bulk rock composition C.
        71VJL113B is from the medium-pressure garnet-oligoclase zone,
        and 71VJL36A is from the medium- to low-pressure garnet-
        oligoclase/andesine zone.

14   Calculated phase abundances (coefficients) $\pm 1\sigma$ errors for the
        mafic rocks modeled to bulk rock composition D. 71VJL6B is
        from the medium-pressure biotite-albite zone, and 73VJL337B is
        from the high-pressure garnet-albite zone. Abbreviations are
        explained in the caption for figure 1.

15   Calculated phase abundances (coefficients) $\pm 1\sigma$ errors for the
        medium-pressure facies series mafic rocks modeled to bulk rock
        composition E. Abbreviations are explained in the appendix.

16   Calculated phase abundances (coefficients) $\pm 1\sigma$ errors for the
        mafic rocks modeled to bulk rock composition F. Abbreviations
        are explained in the appendix.

Figure I-1

Quebec, Canada
1 Richmond ⎱ Osberg (1965)
2 Orford ⎰
3 Sutton   Eakins (1964)

Vermont, USA
4 Enosburg Falls   Dennis (1964)
5 Jay Peak ⎱ Cady, Albee, & Chidester (1963)
6 Irasburg ⎰
7 Mount Mansfield   Christman (1959)
8 Hyde Park   Albee (1957)
9 Hardwick   Cady, Albee, & Chidester (1963)
10 Burke   Woodland (1965)
11 Camels Hump   Christman & Secor (1961)
12 Montpelier   Cady (1956)
13 St. Johnsbury   Hall (1959)
14 Lincoln Mountain   Cady, Albee, & Murphy (1962)
15 Rochester   Osberg (1952)
16 Woodstock   Chang, Ern, & Thompson (1965)
17 Saxtons River   Rosenfeld (1954)
18 Wilmington   Skehan (1961)

Figure I-2

Figure II-1b

Na, Ca AMPHIBOLE
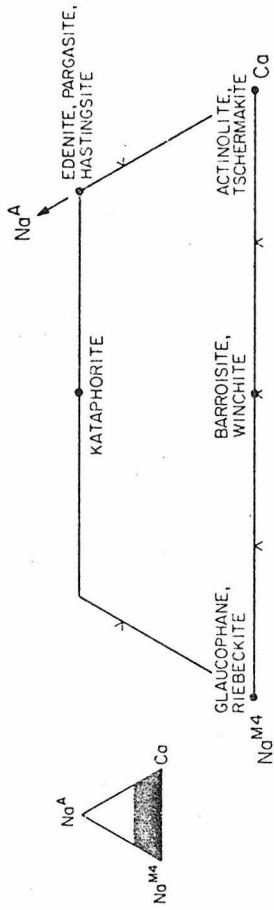
Figure II-1c
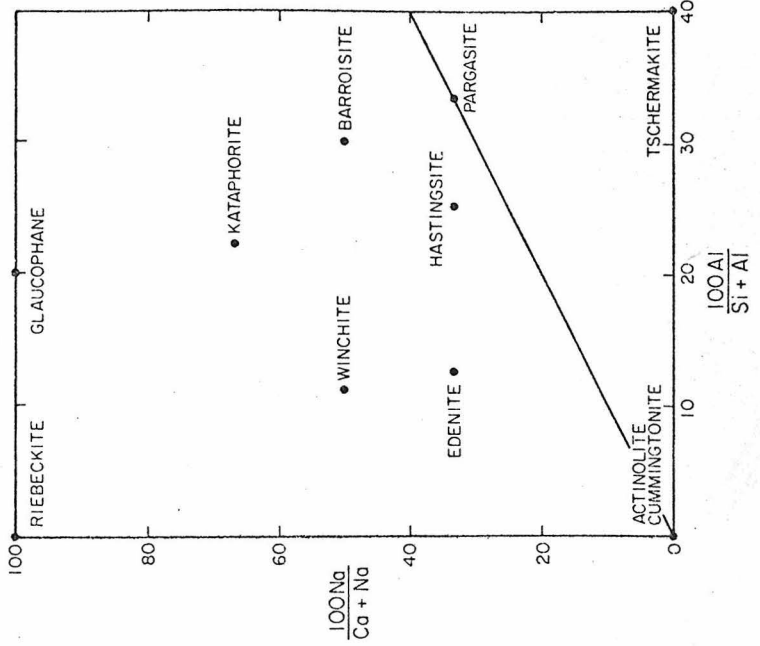
Figure II-1a
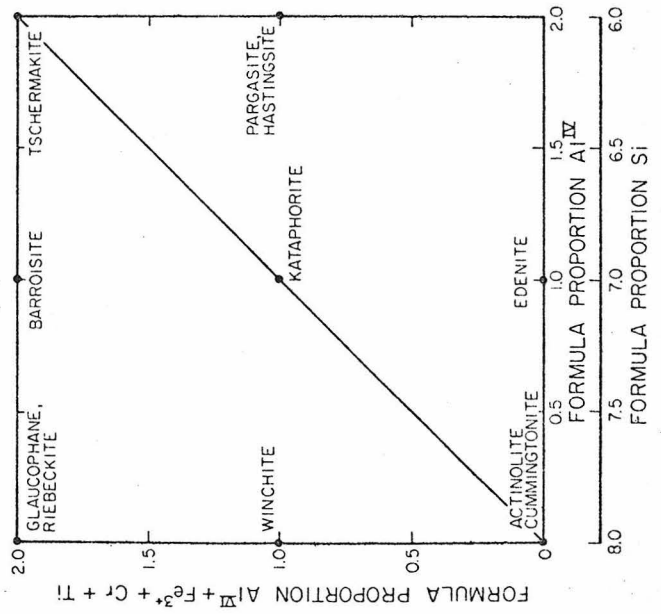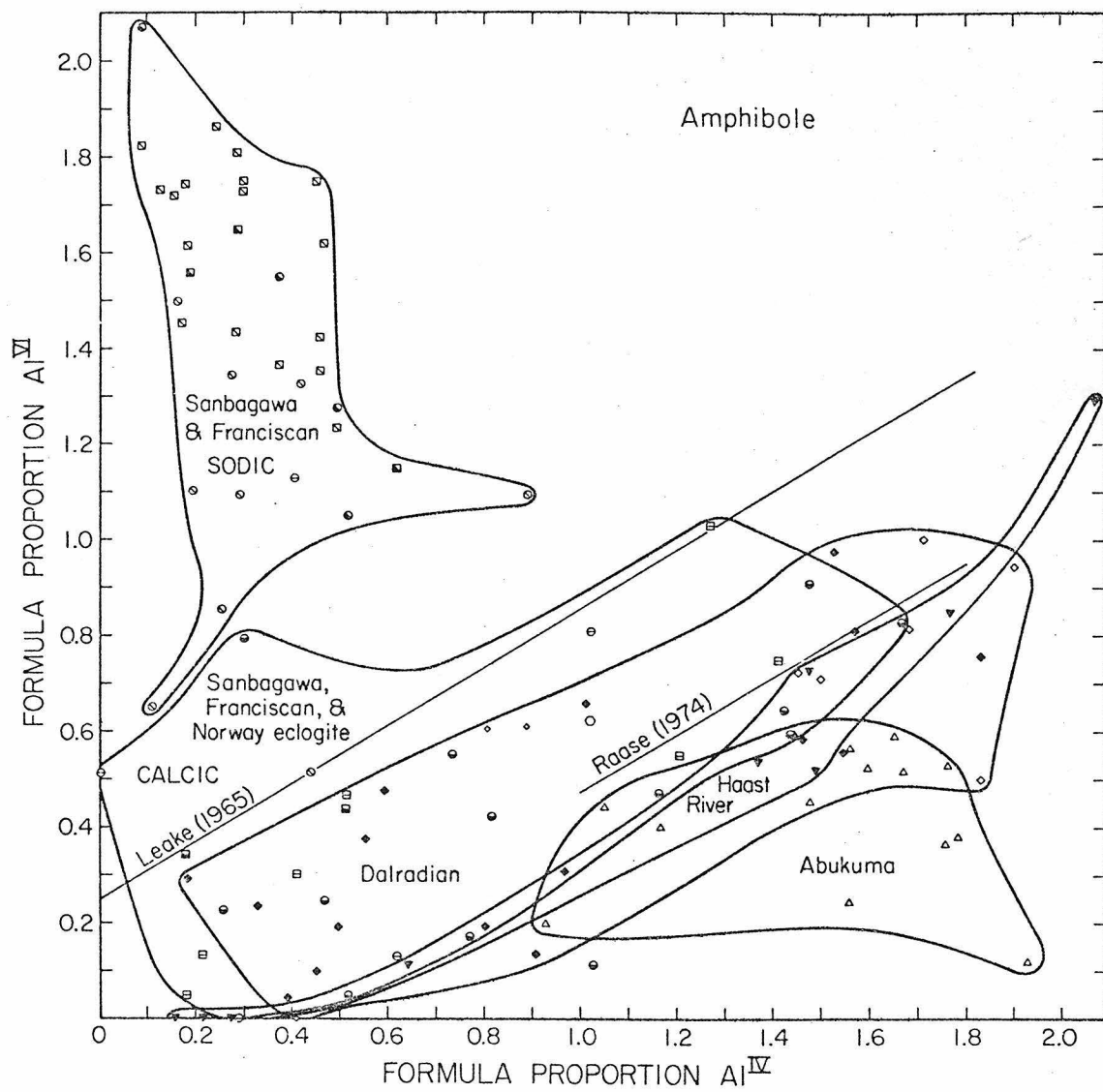
Figure III-1

Figure III-2

Figure III-3

AMPHIBOLE ANALYSES

HAAST RIVER

ABUKUMA

DALRADIAN

SANBAGAWA, FRANCISCAN, & NORWAY ECLOGITE

SANBAGAWA & FRANCISCAN

Figure III-4

AMPHIBOLE
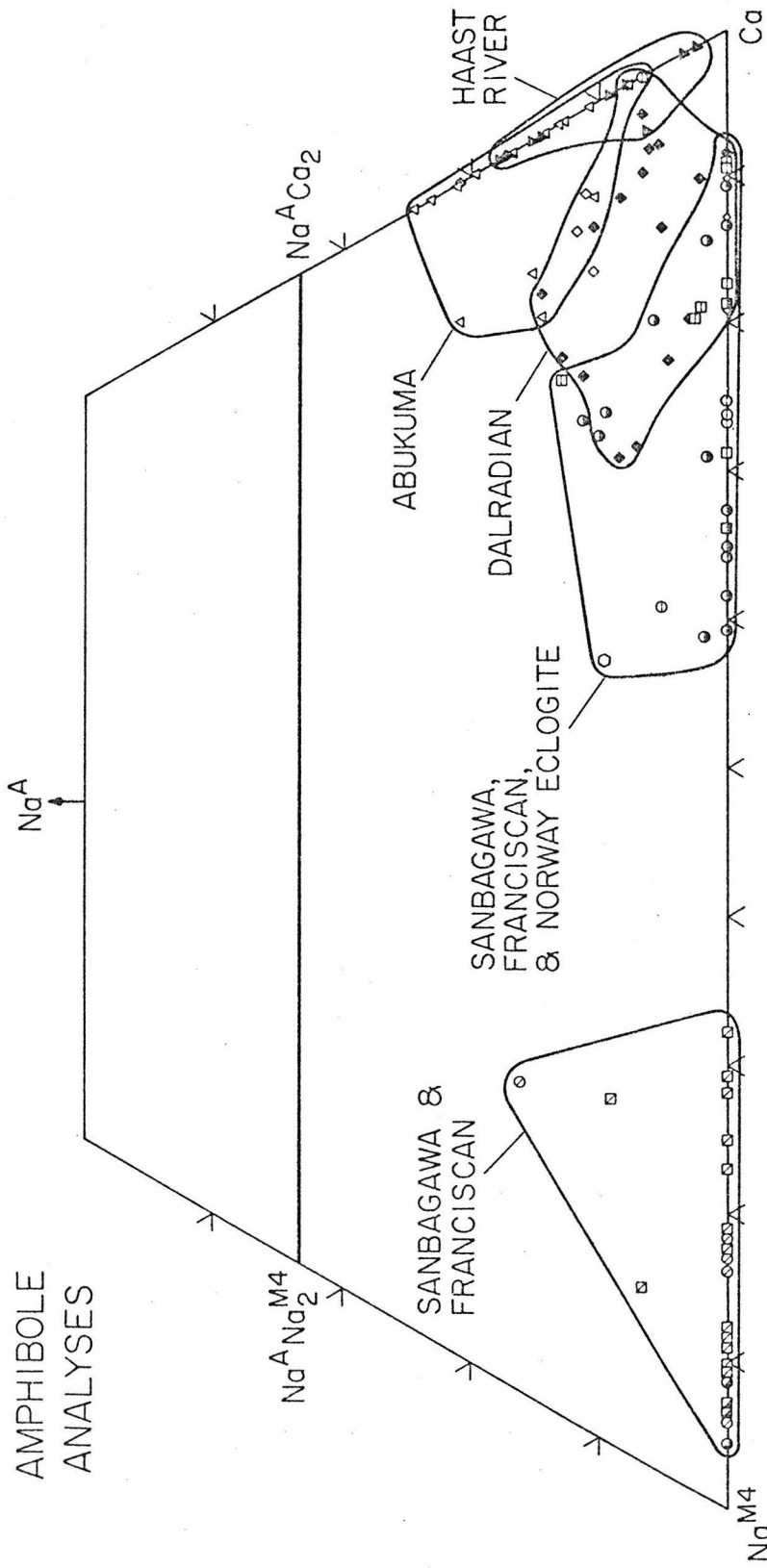
FORMULA PROPORTION Al^{IV}
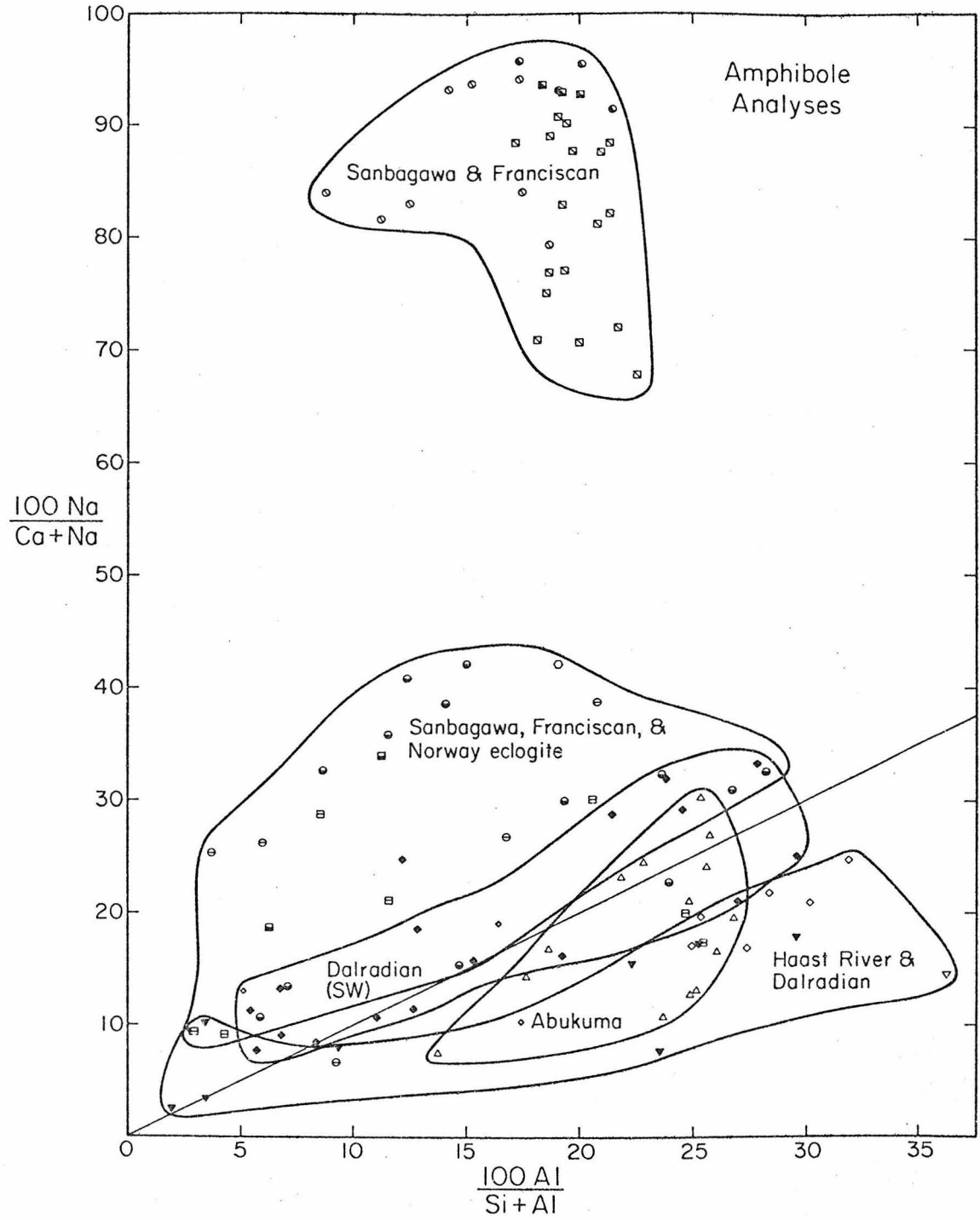
Figure IV-1a
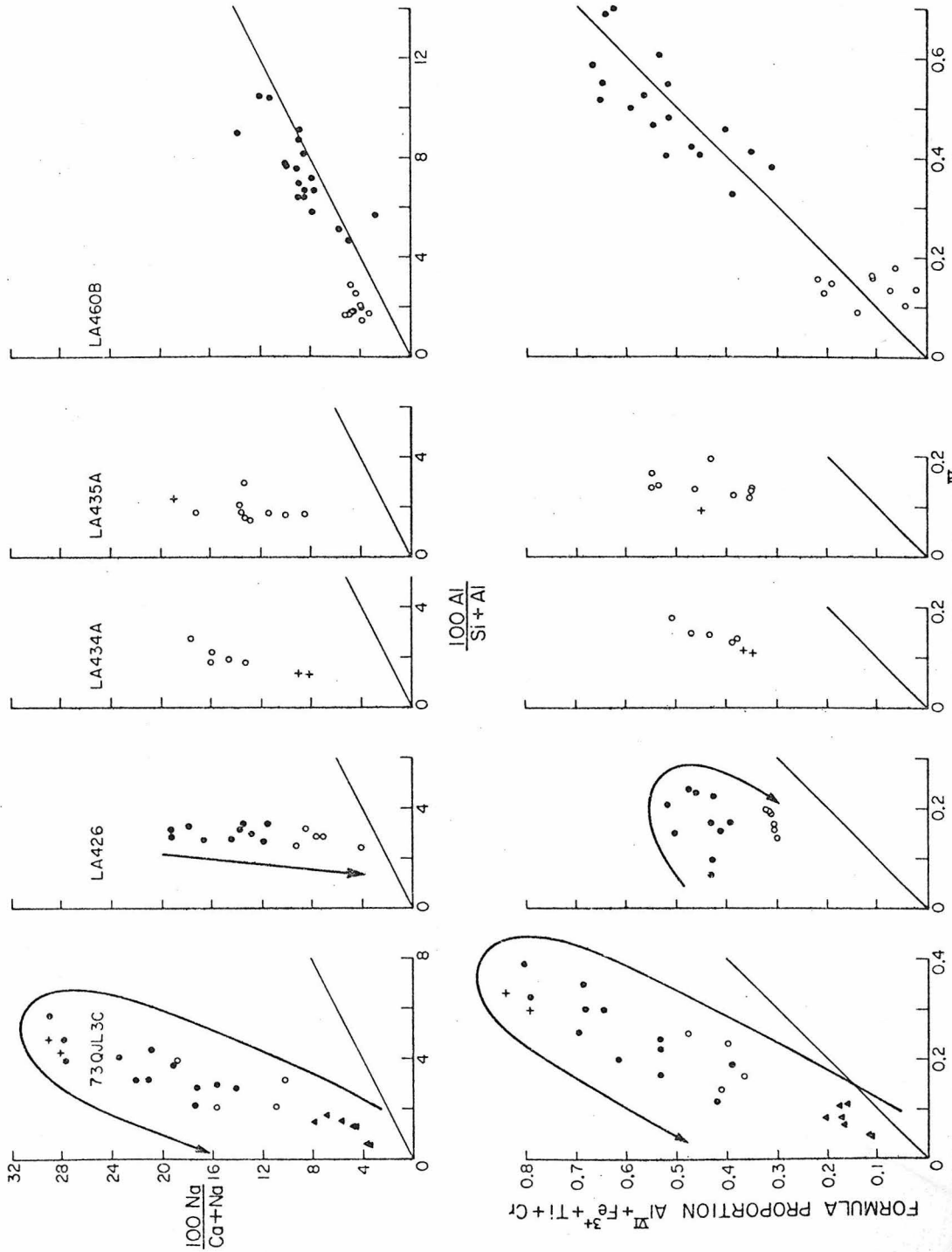
AMPHIBOLE

Figure IV-1b

AMPHIBOLE
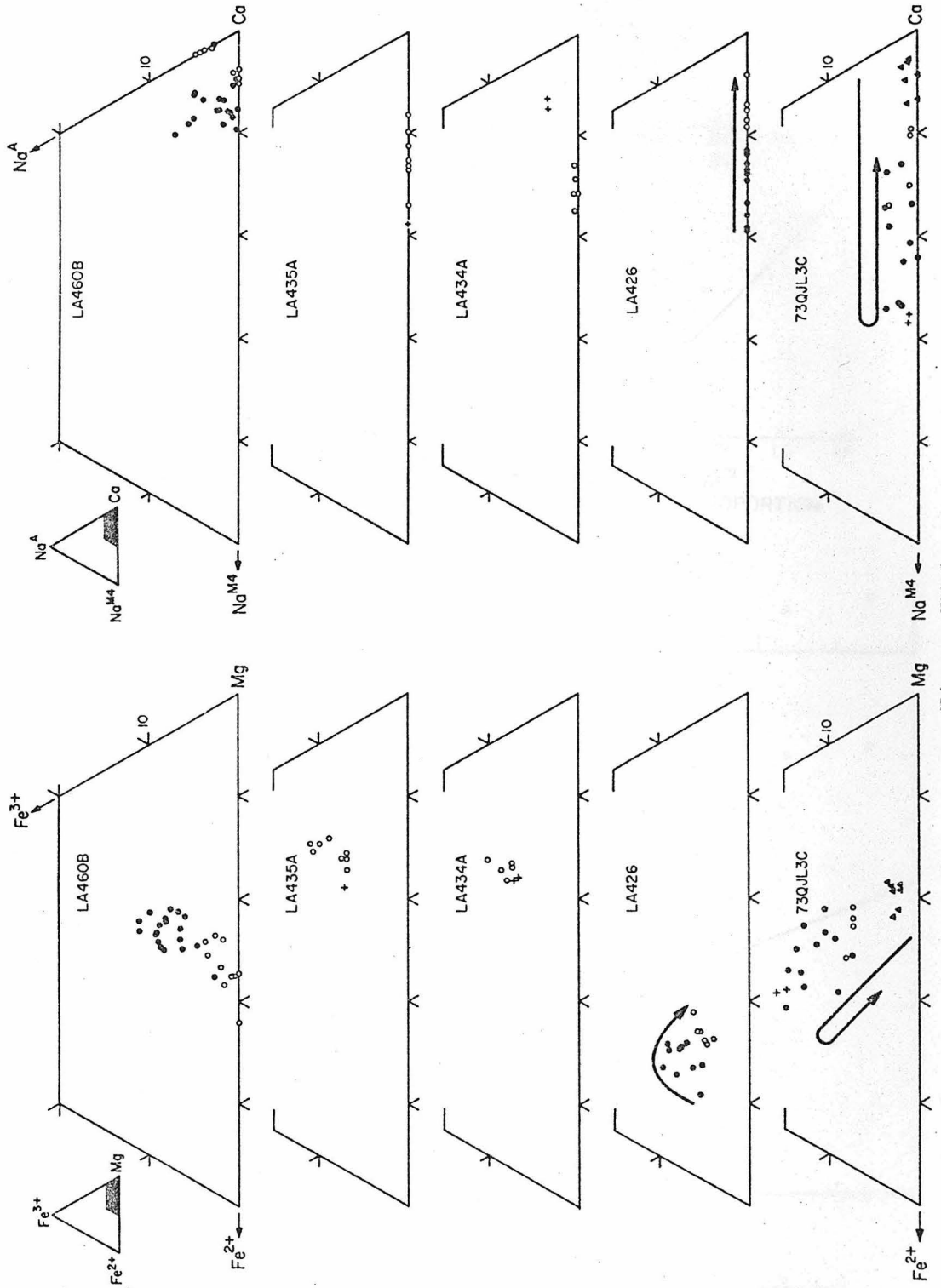
Figure IV-1c

Figure IV-2a   BIOTITE
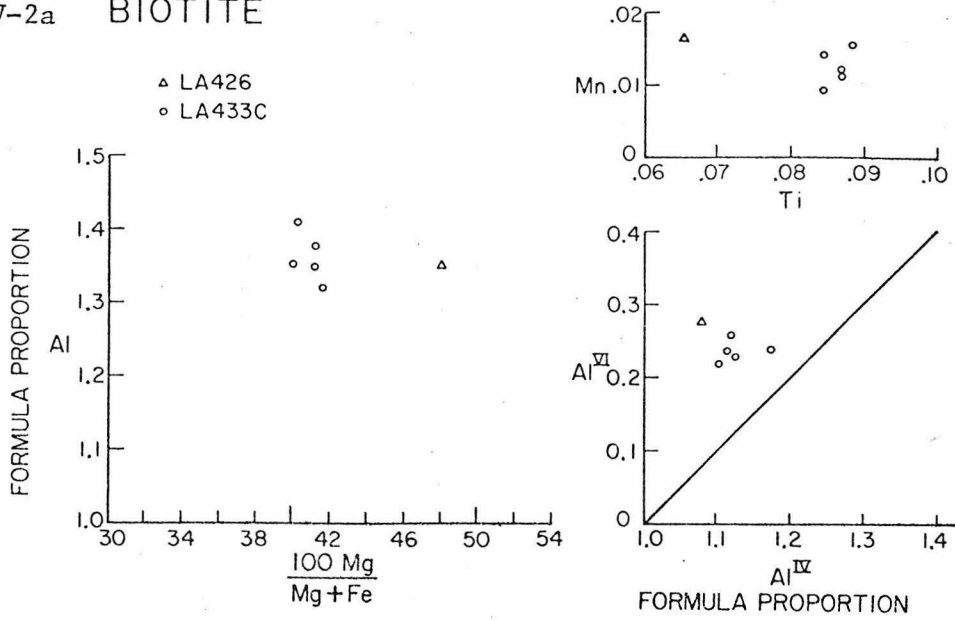
△ LA426
○ LA433C

Figure IV-2b   WHITE MICA LA433C

Figure IV-3

EPIDOTE

LA460B

LA435A

LA434A

LA433C

LA426

73QJL3C

NUMBER

FORMULA PROPORTION Fe^{3+}
Figure IV-4
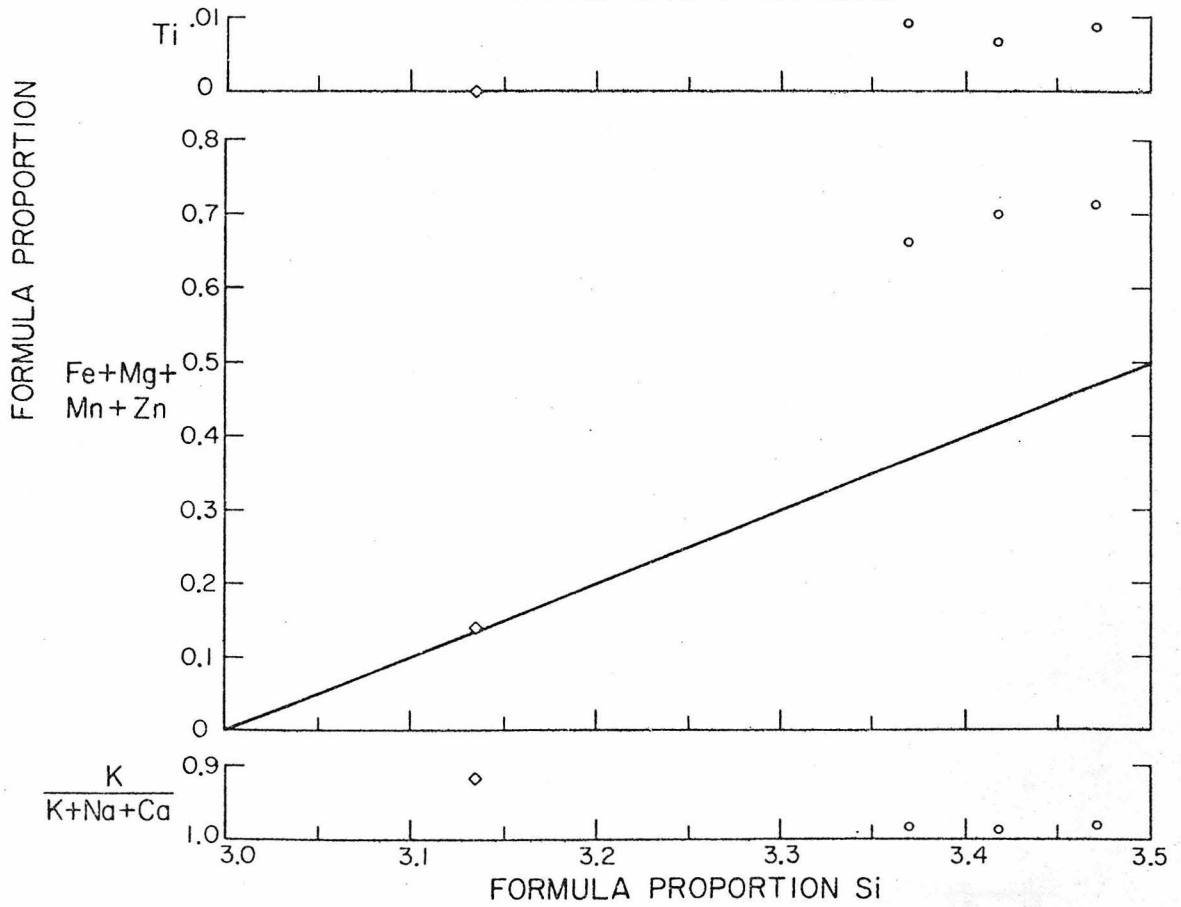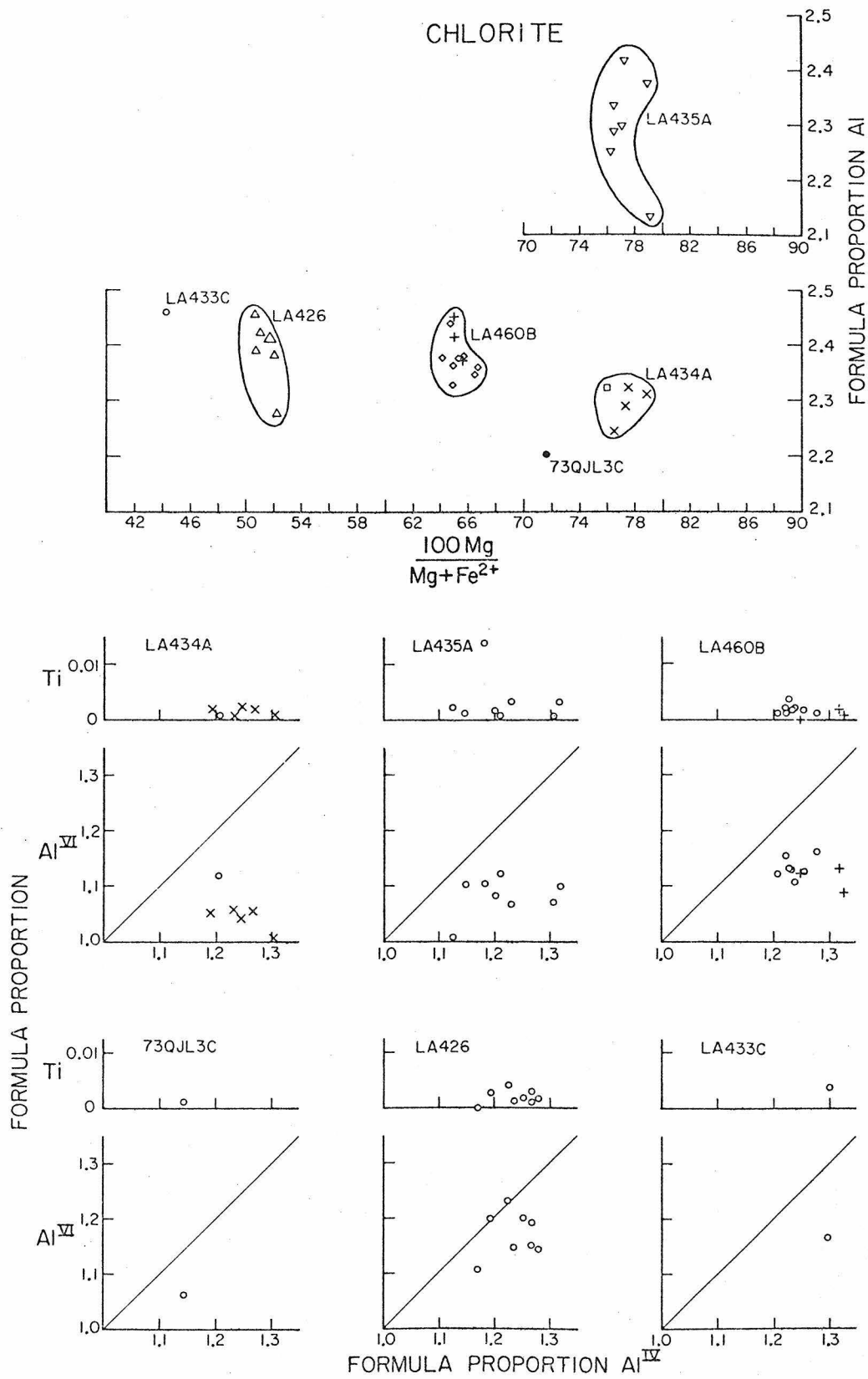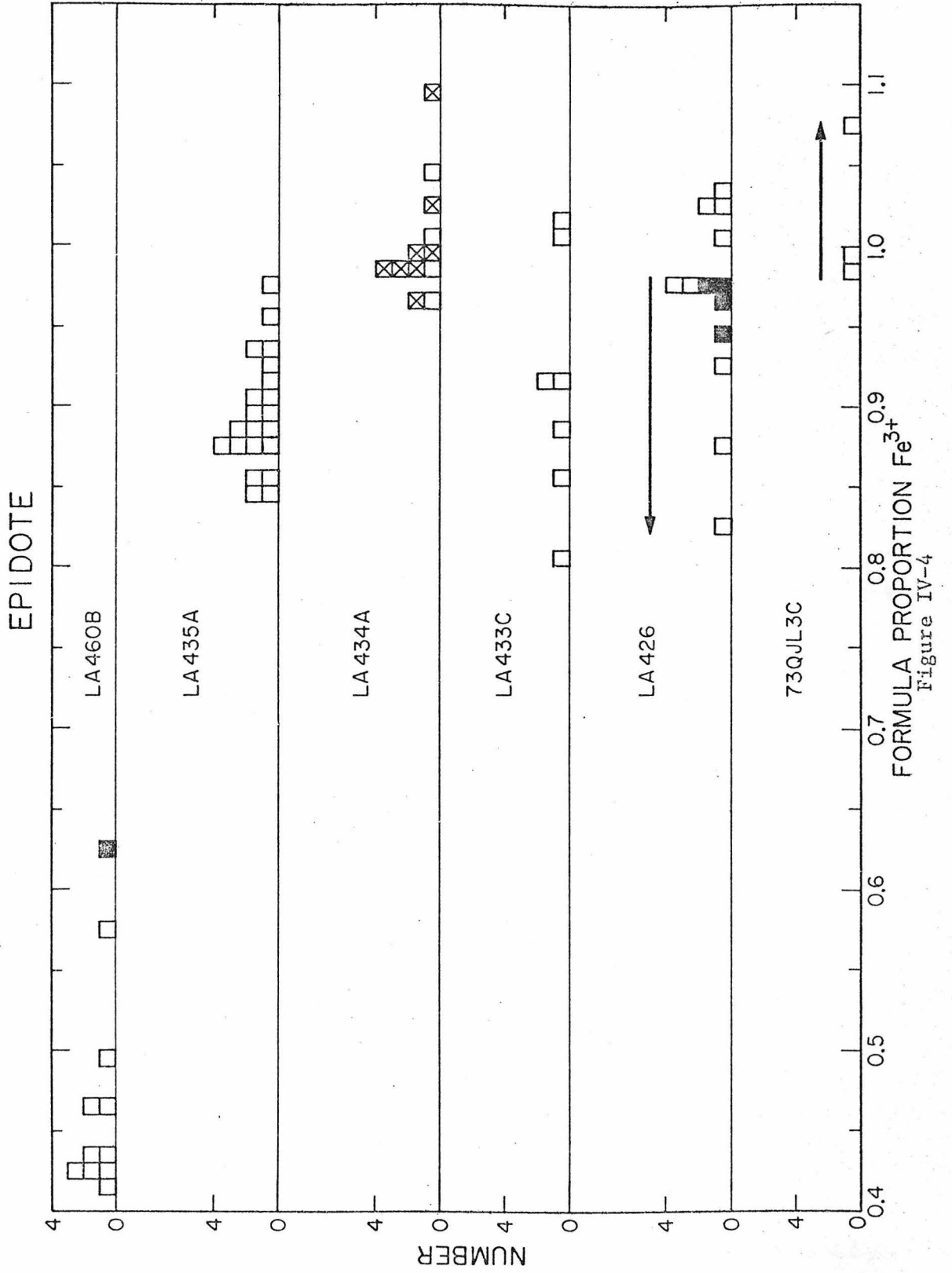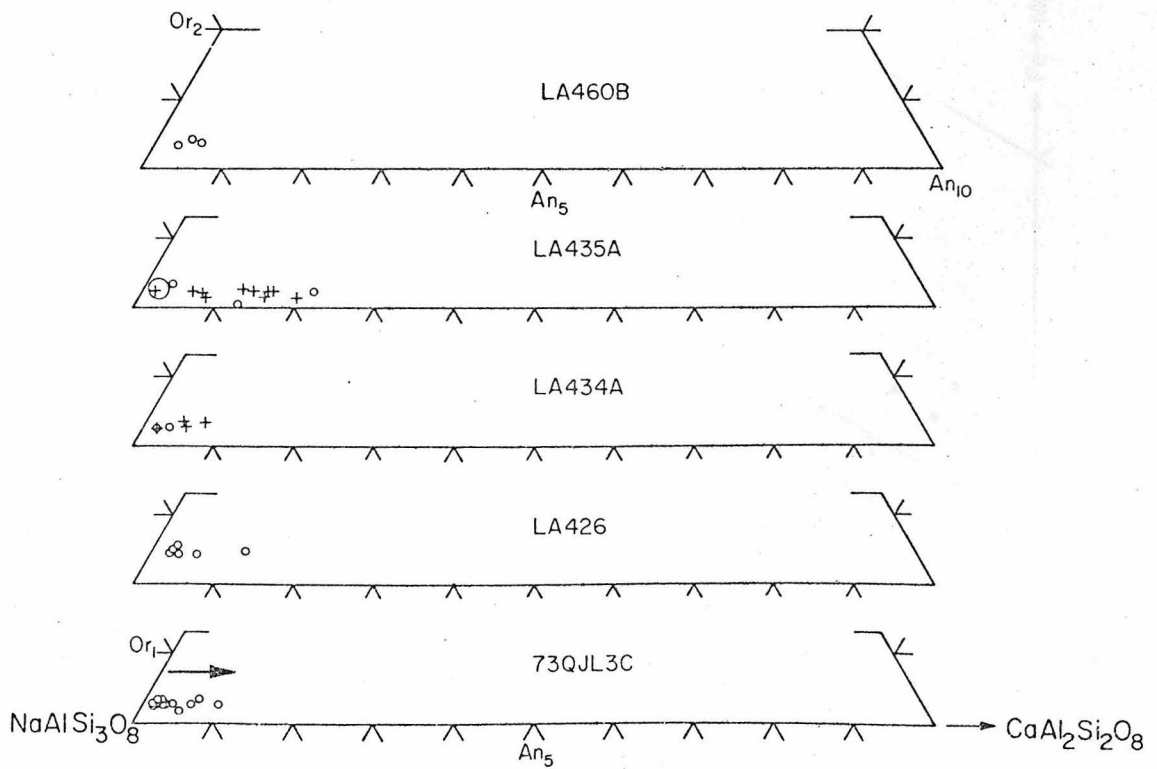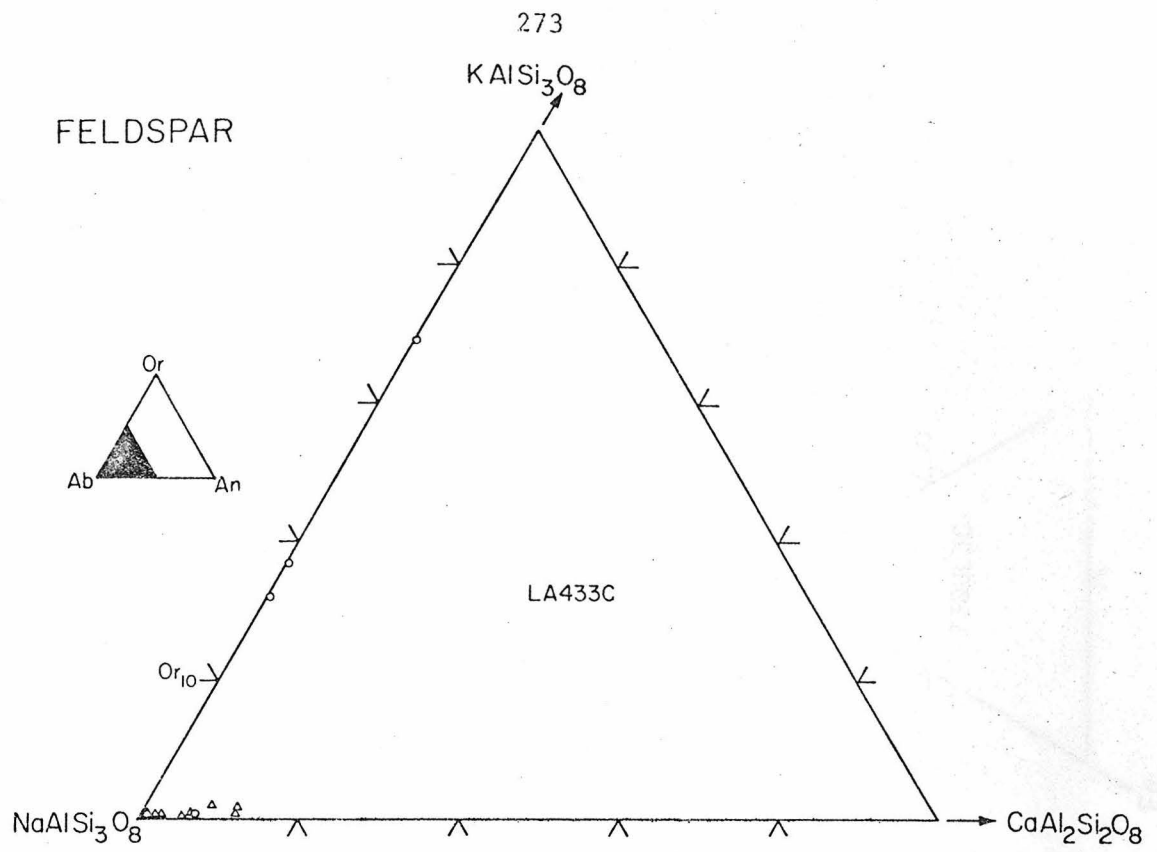
Figure IV-5

Figure IV-6b
CARBONATE

LA460B

LA434A

LA426

73QJL3C

△ 1% Mn
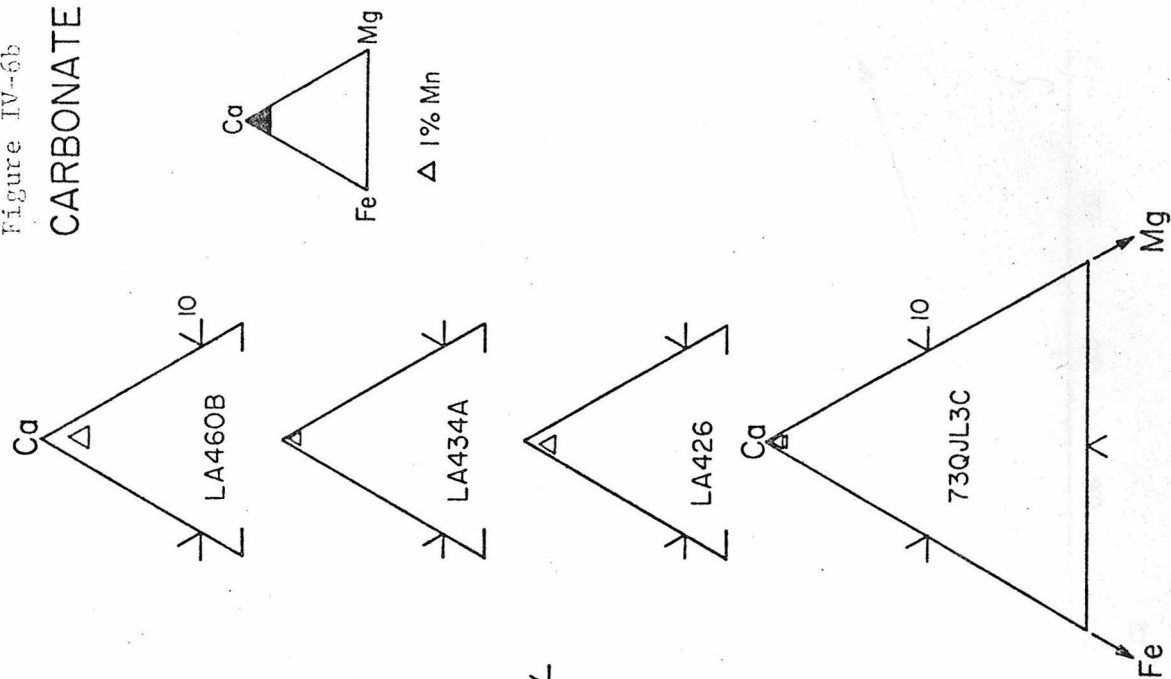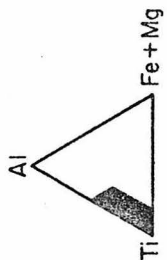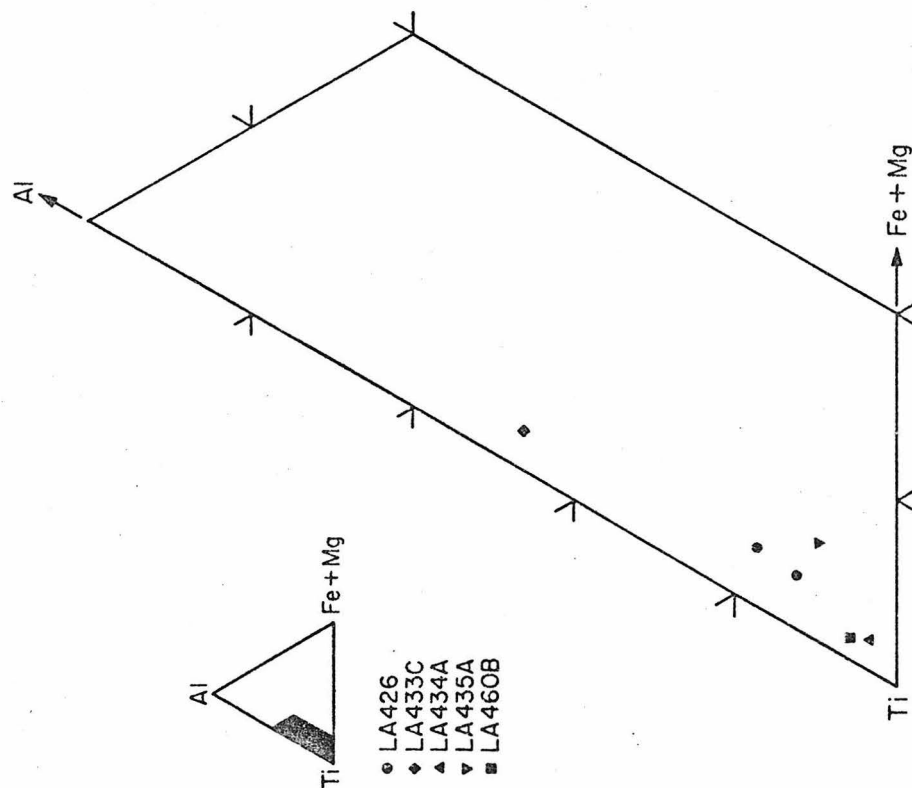
Figure IV-6a
SPHENE

LA426
LA433C
LA434A
LA435A
LA460B

Figure IV-7a

Figure IV-7b

AMPHIBOLE

LA430B

LA504B

LA430B

LA504B

Fe³⁺

Mg

Fe²⁺

Mg

Mg

Mg

Na^A

Ca

Na^A

Na^M4

Ca

Na^M4

Na^M4

Fe²⁺
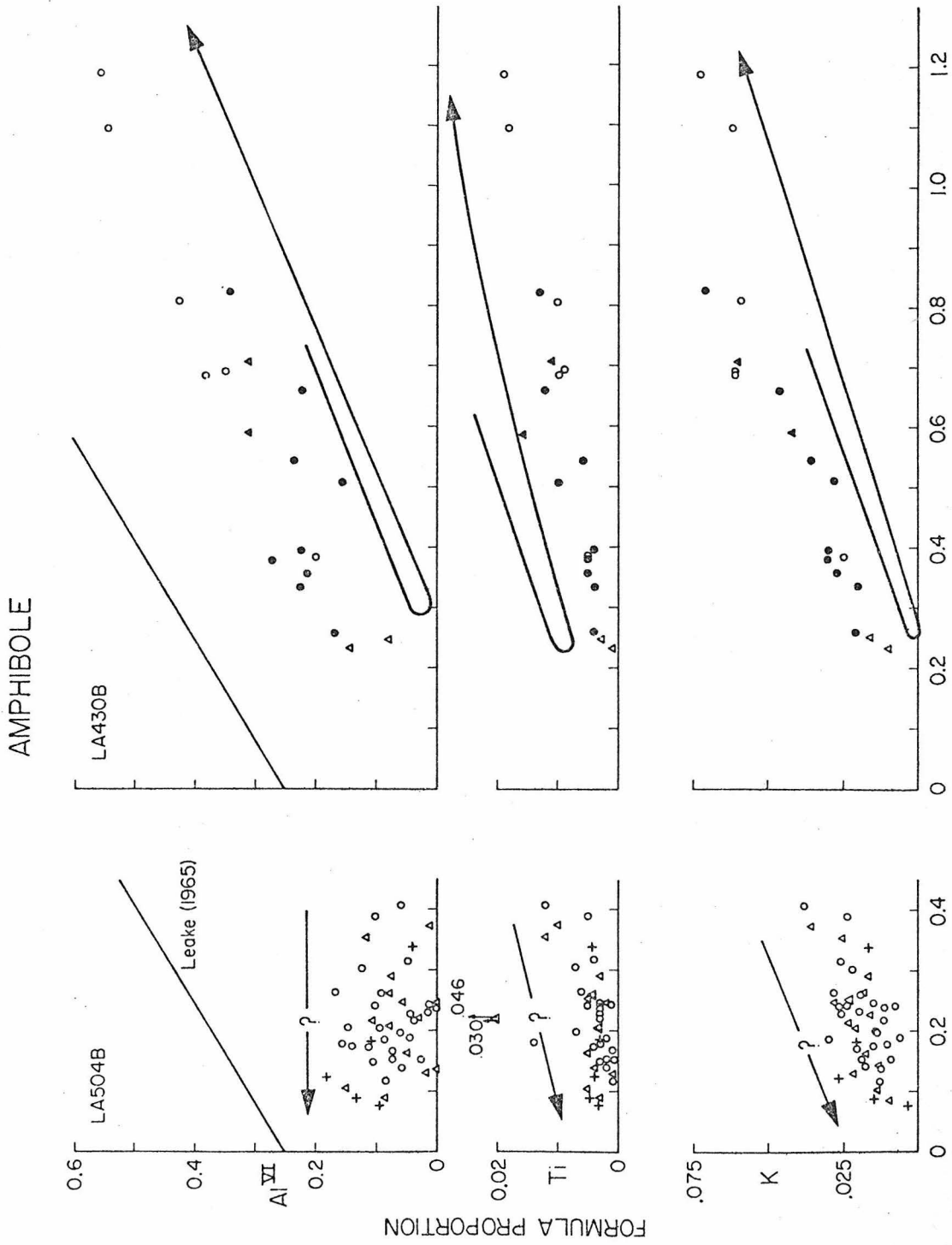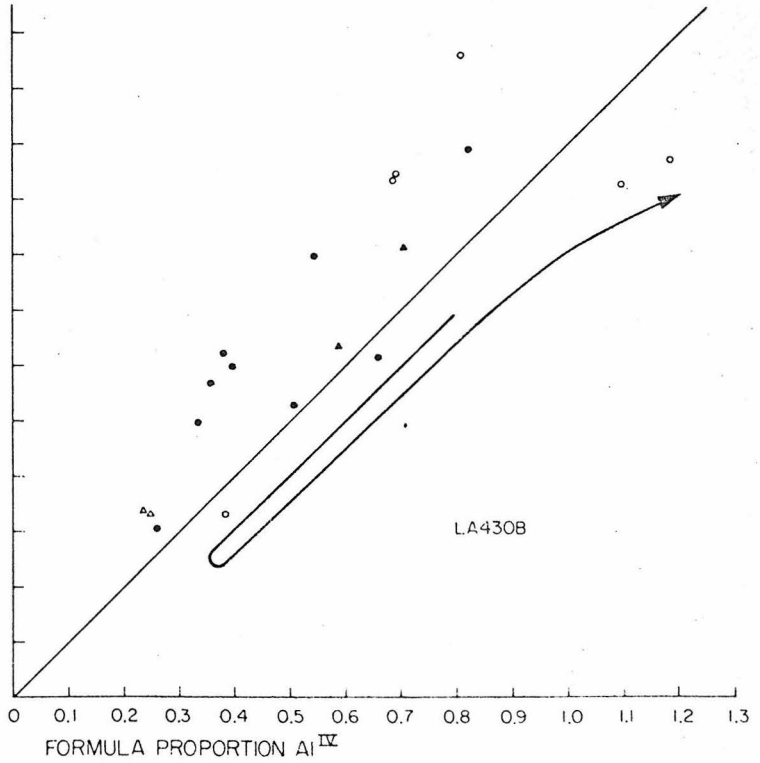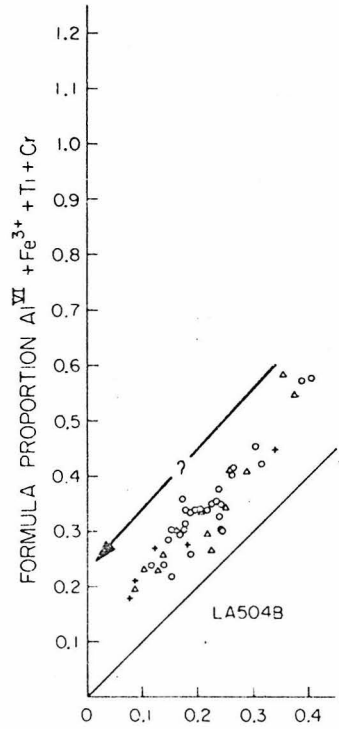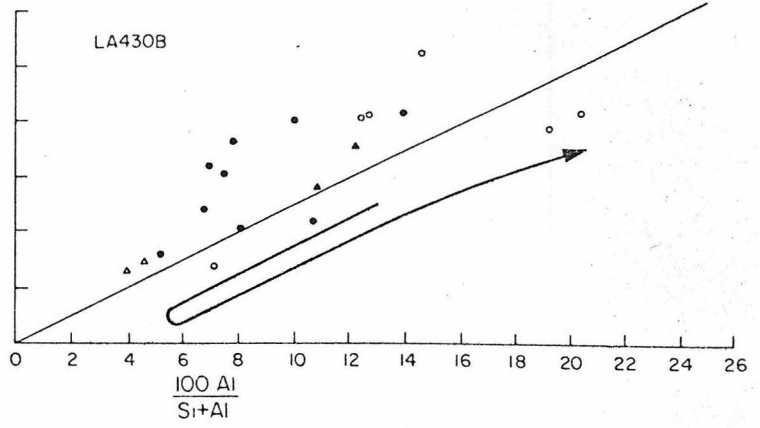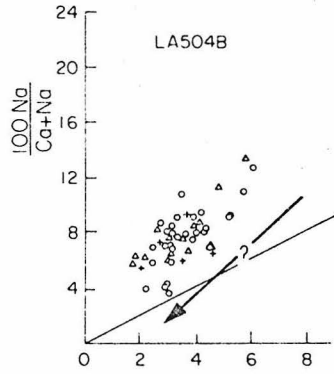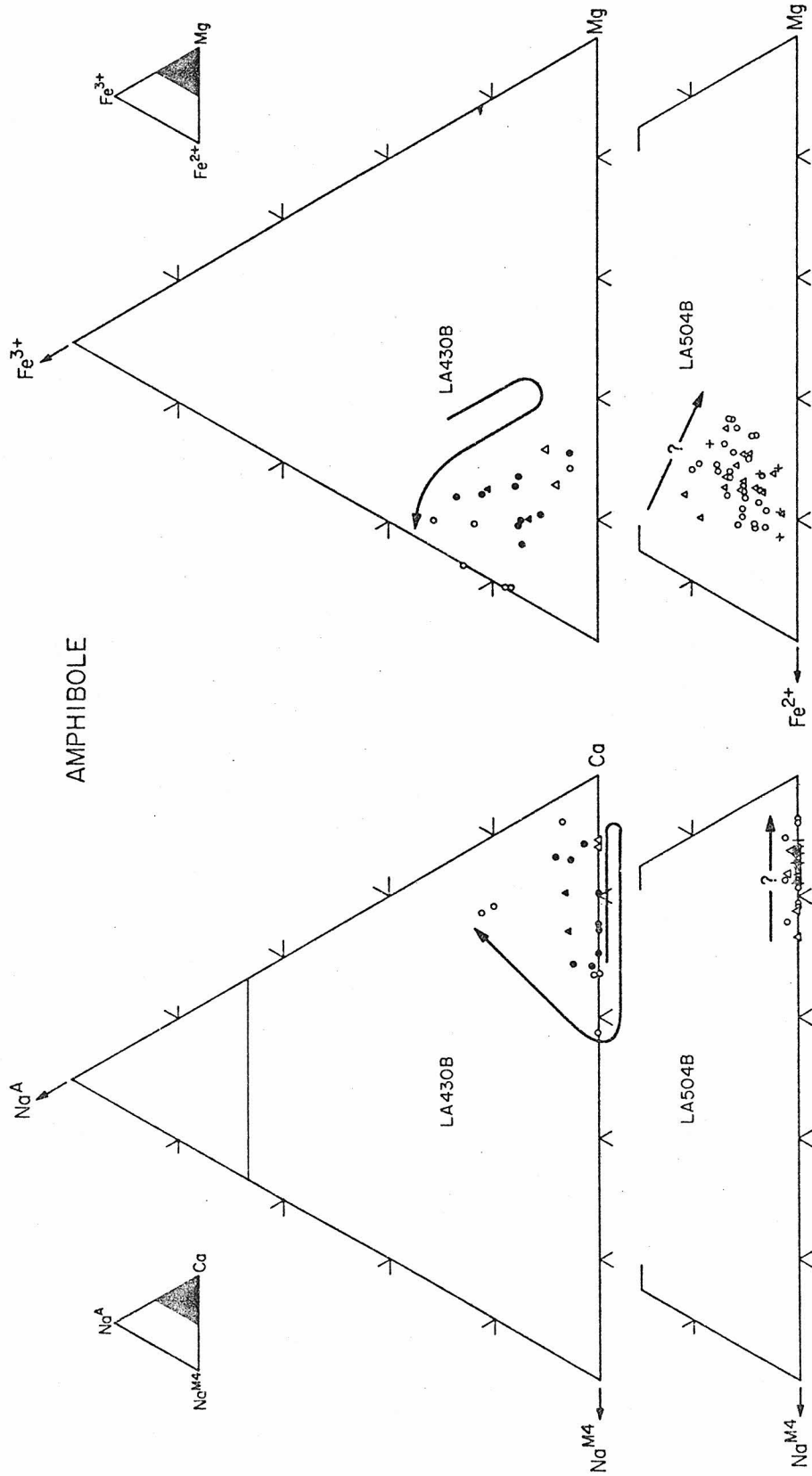
Figure IV-7c
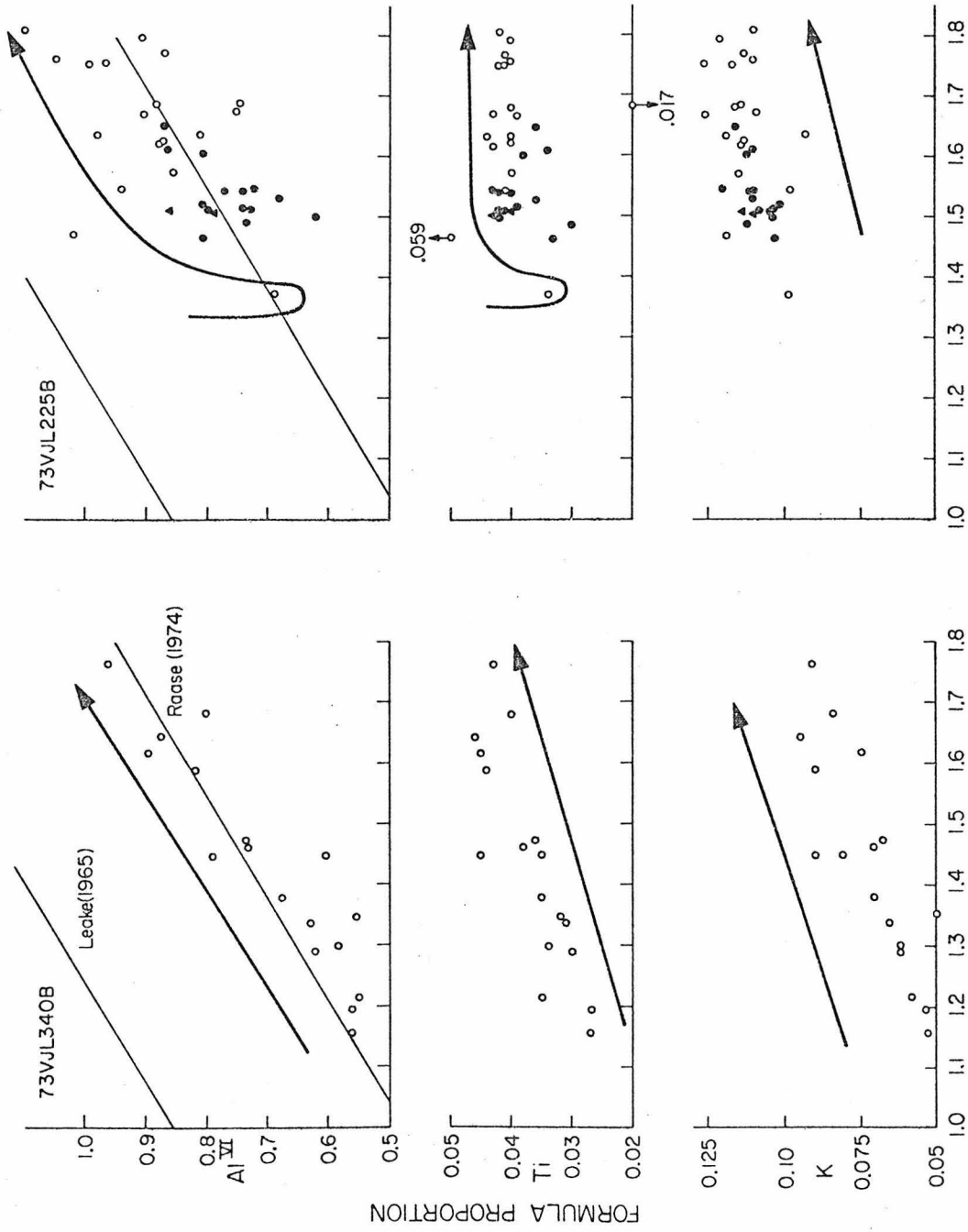
AMPHIBOLE

FORMULA PROPORTION Al^{IV}

Figure IV-8a

AMPHIBOLE
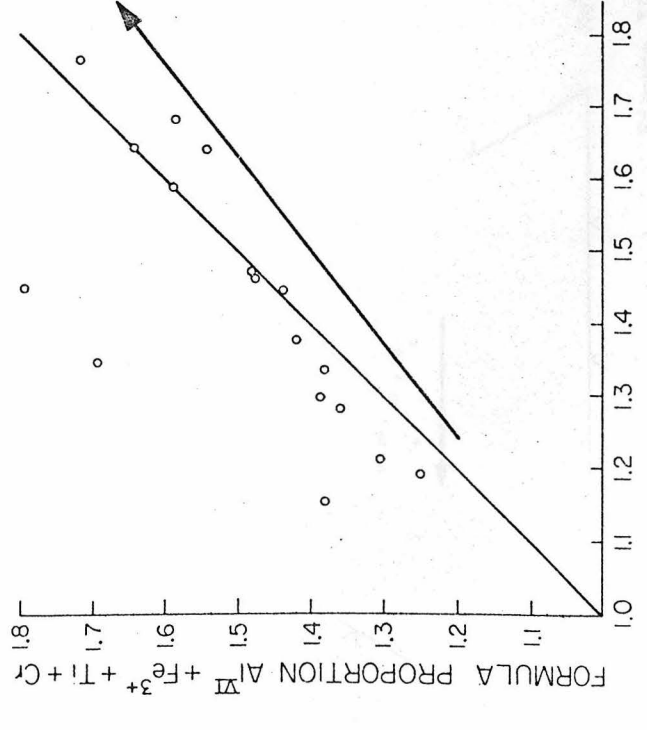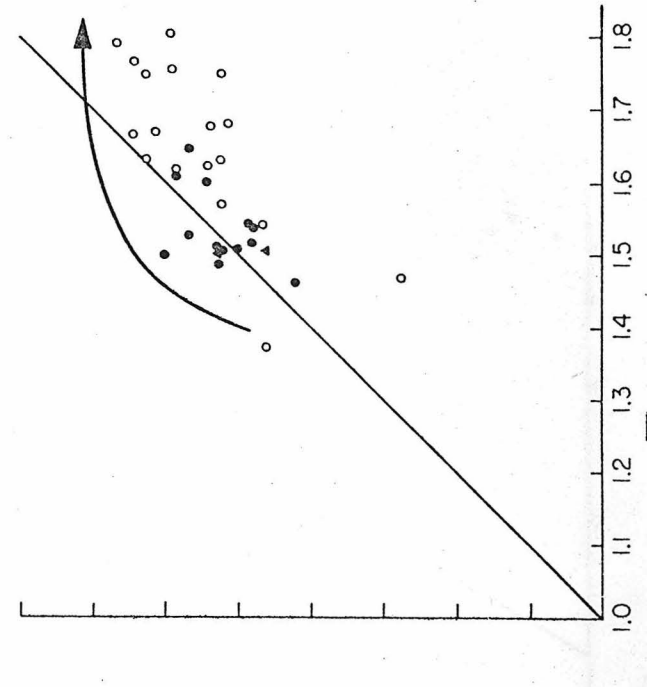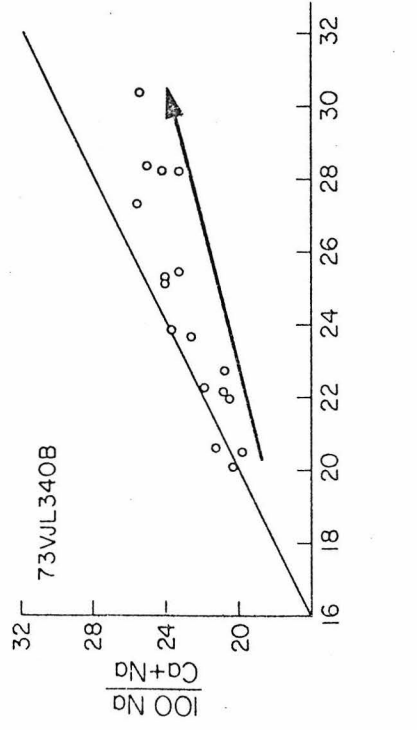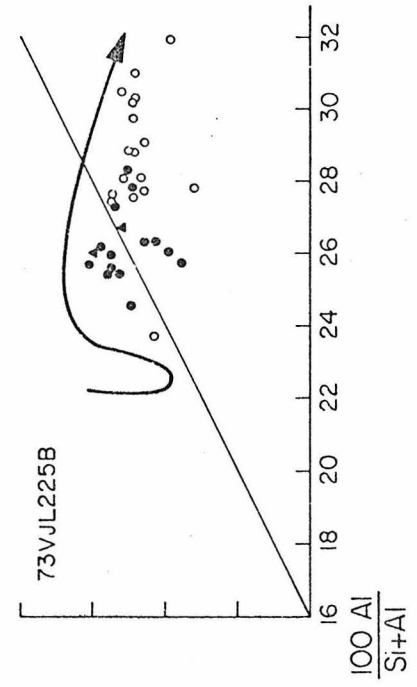
Figure IV-8b
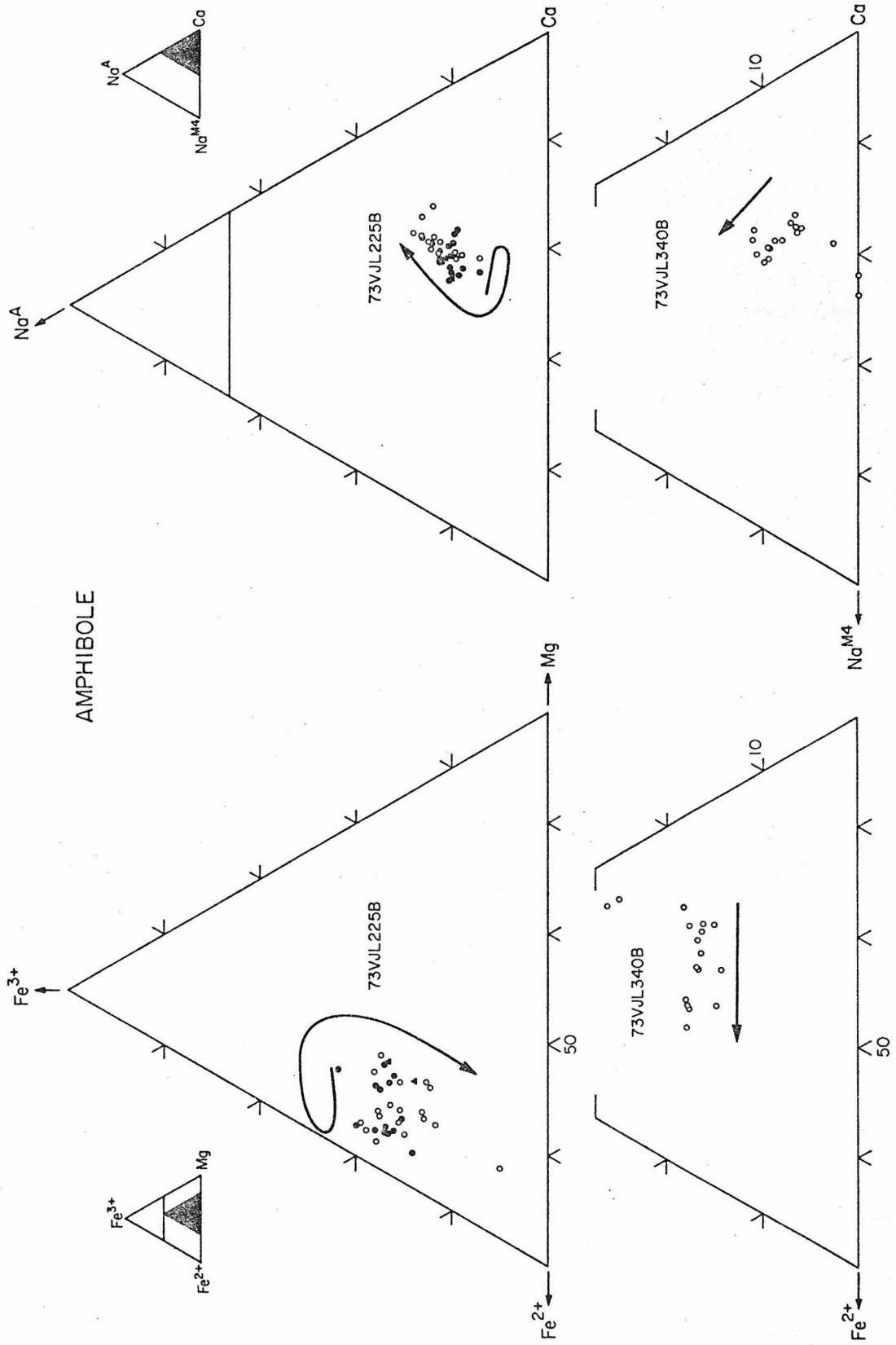
AMPHIBOLE
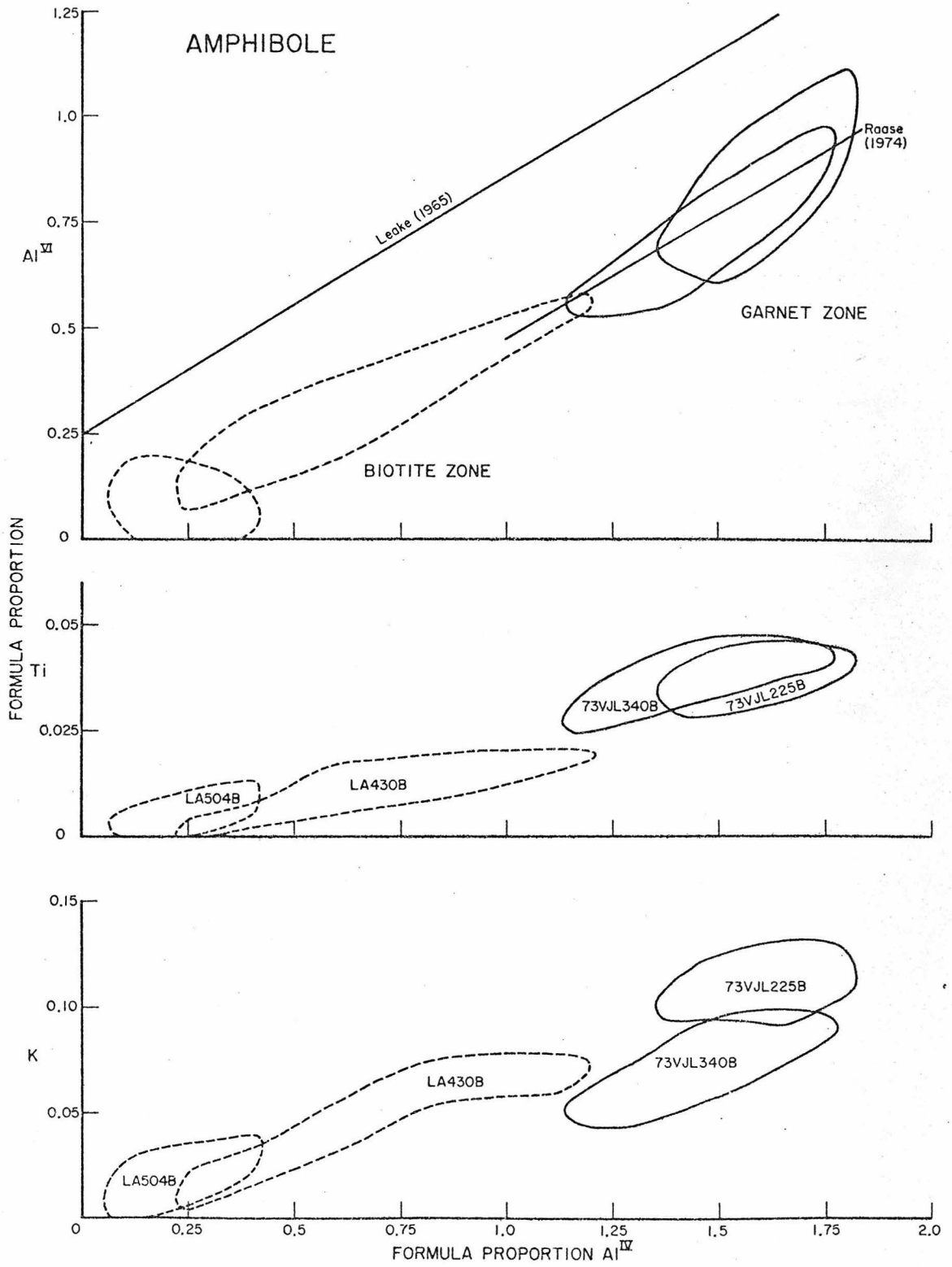
Figure IV-8c

Figure IV-9a

AMPHIBOLE
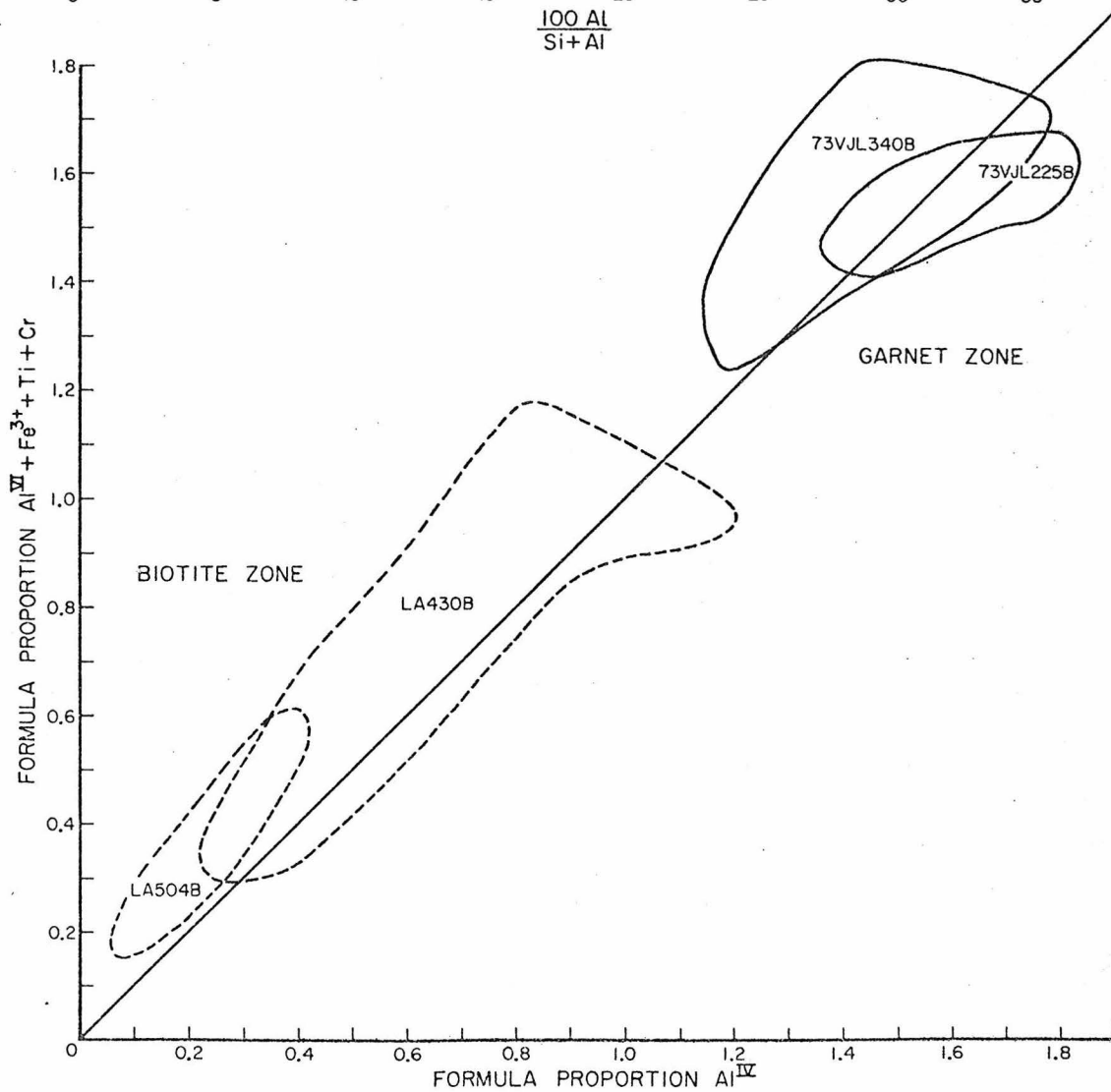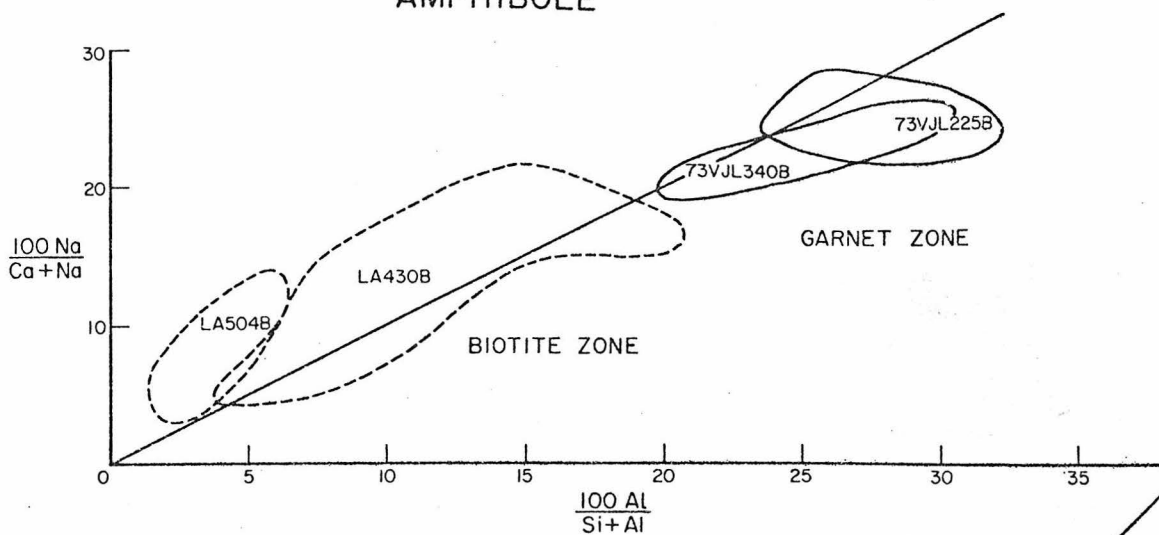
Figure IV-9b
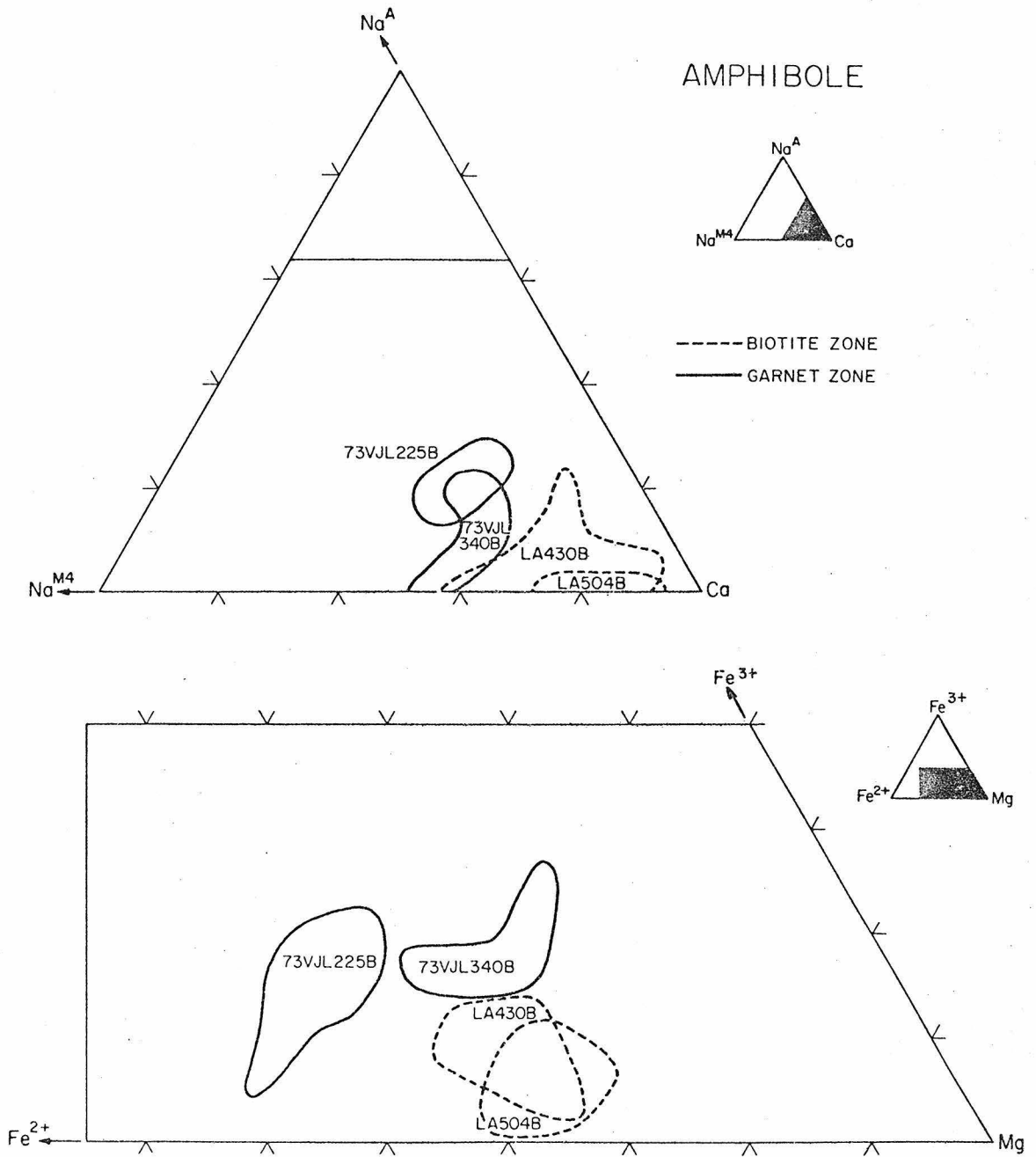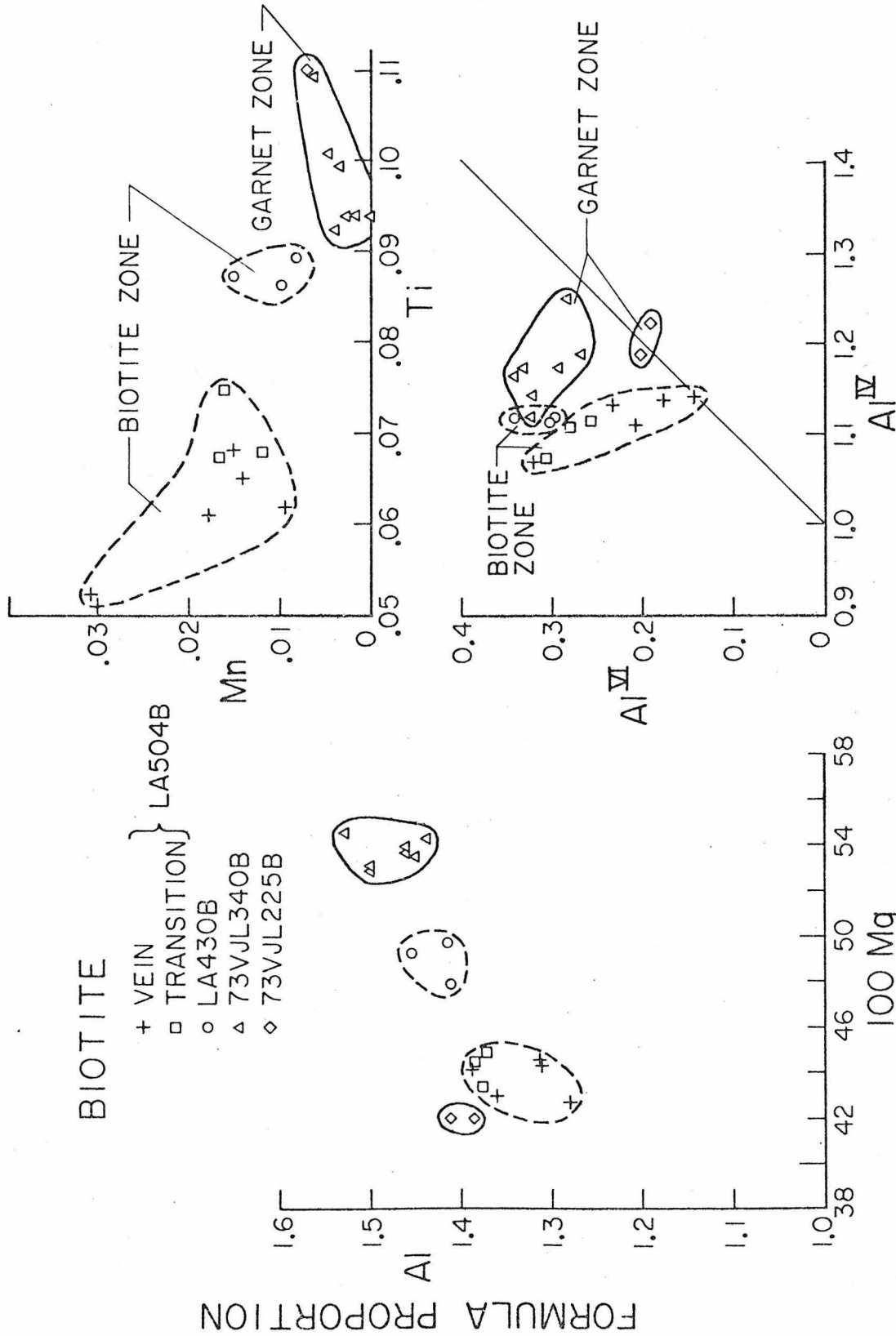
AMPHIBOLE

Figure IV-9c

Figure IV-10

CHLORITE

Figure IV-11

STILPNOMELANE LA504B
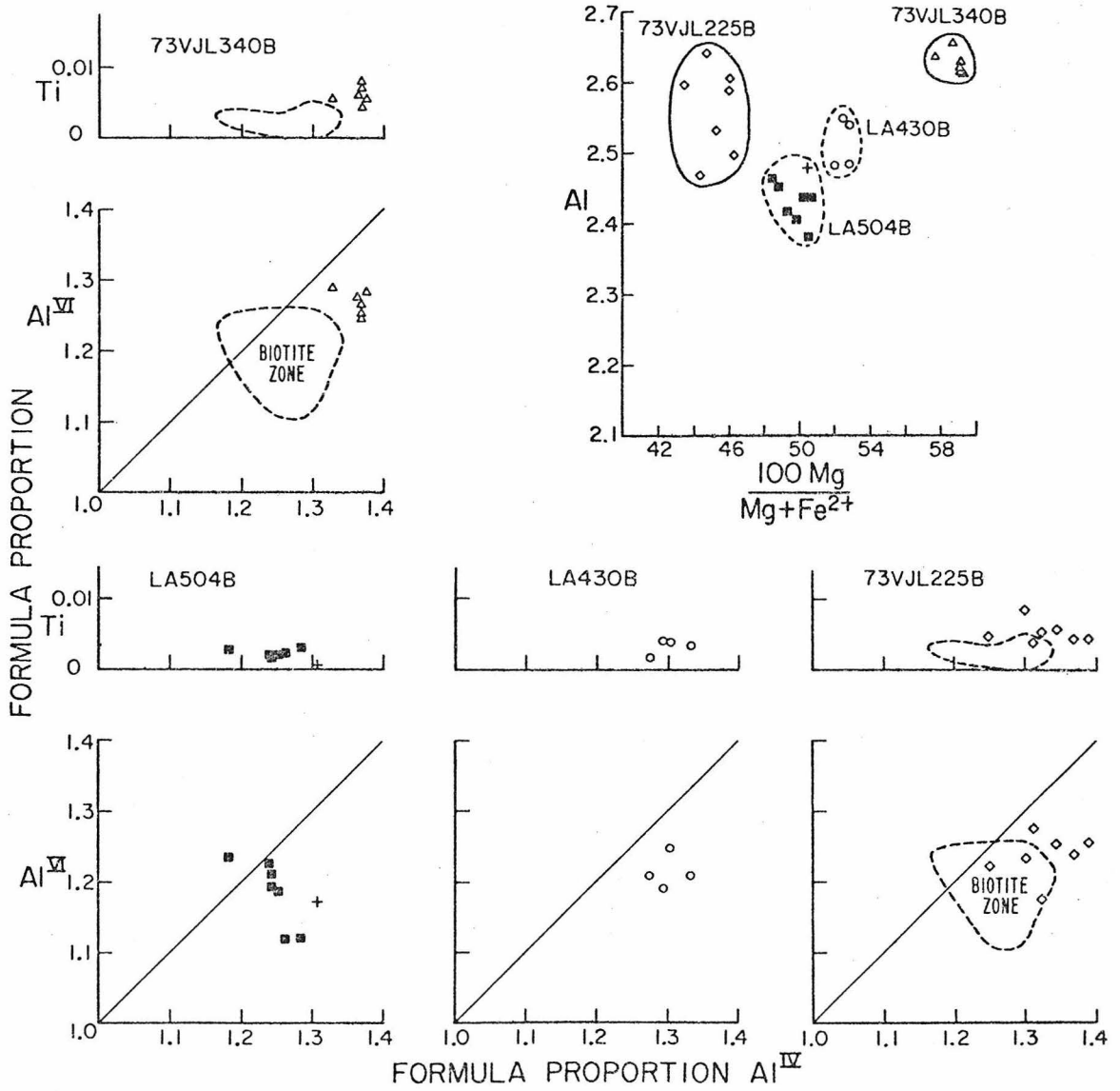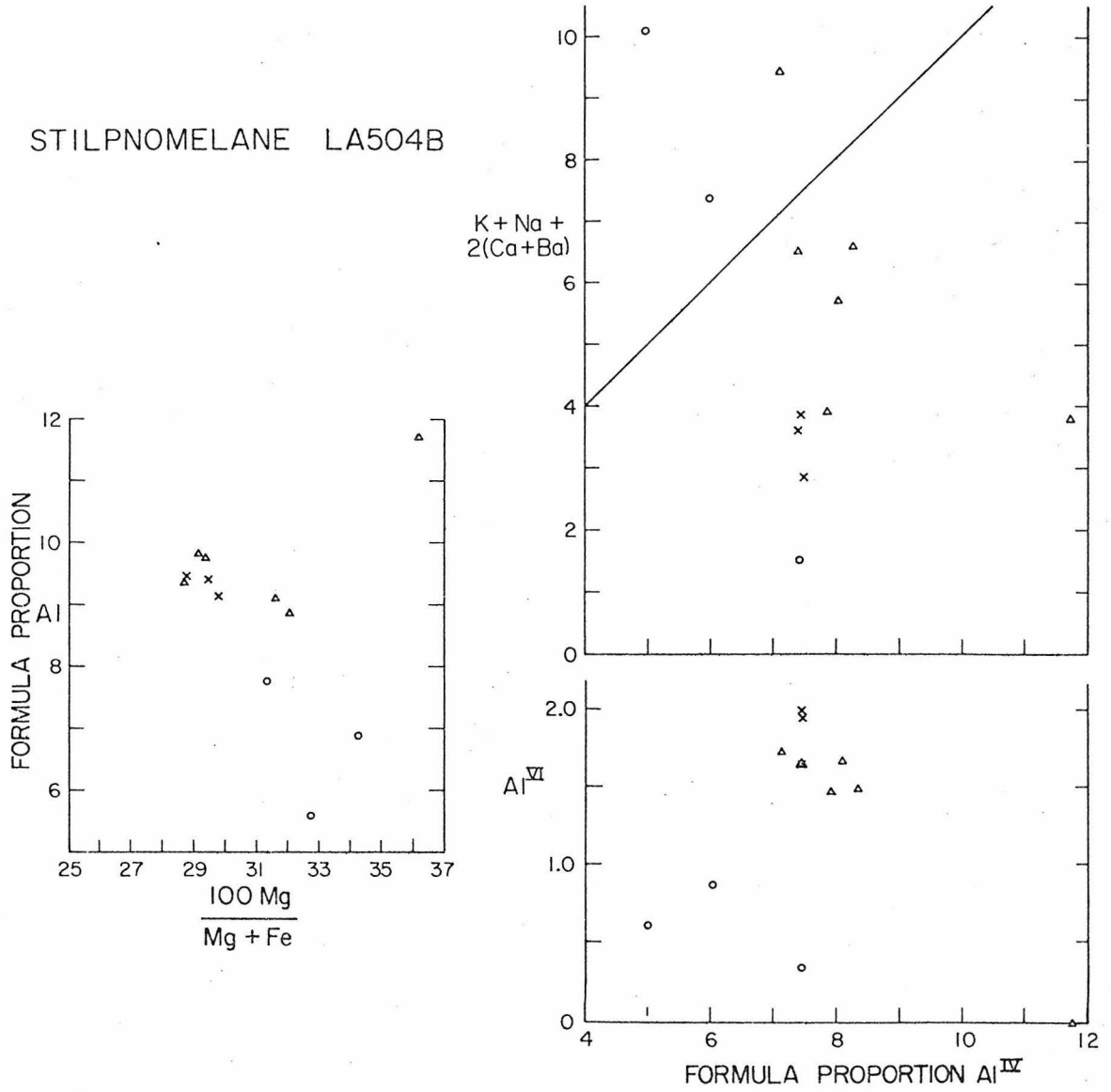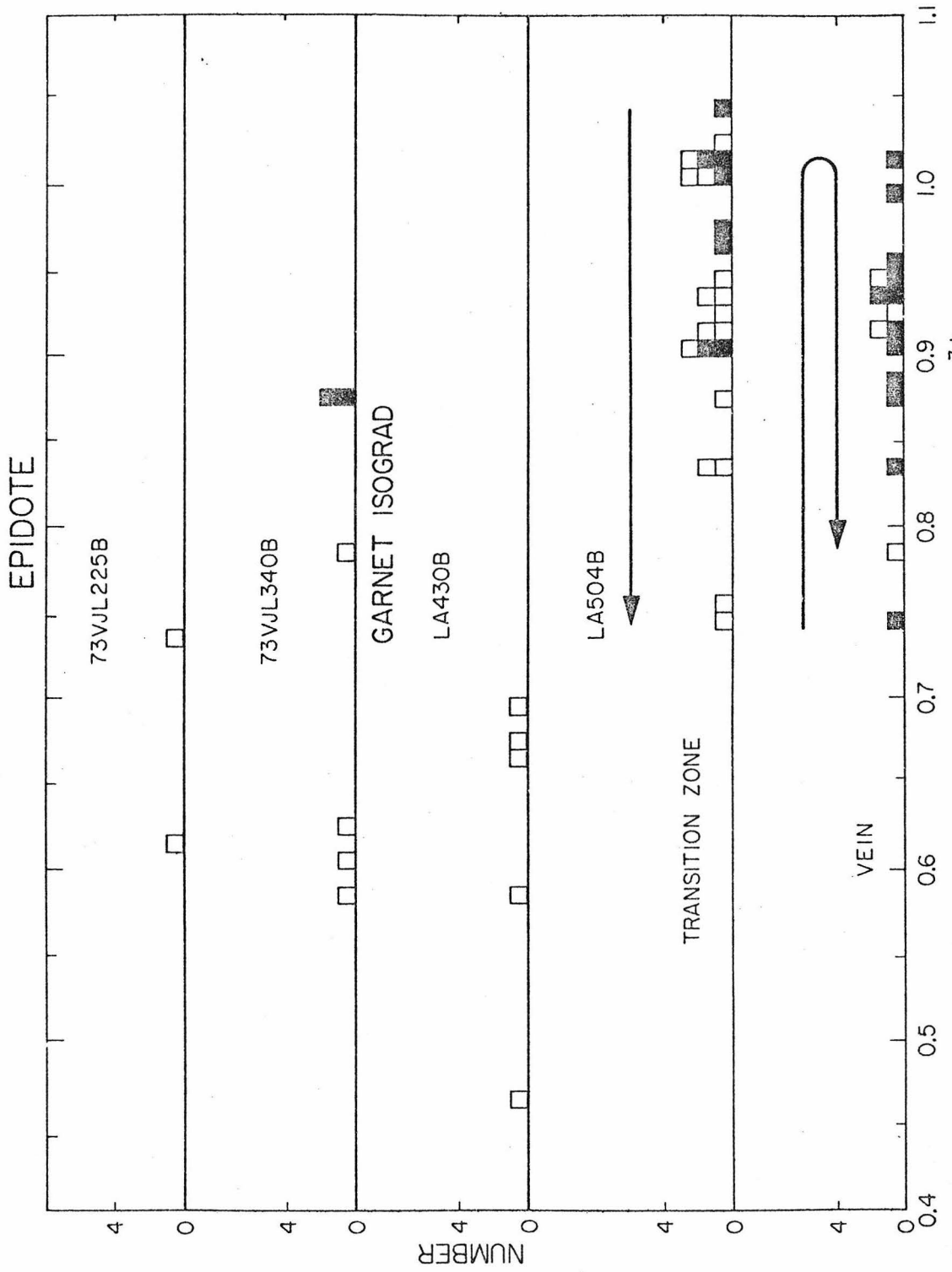
Figure IV-12

FORMULA PROPORTION Fe^{3+}

Figure IV-13

Figure IV-14

CARBONATE

Ca

LA504B

Ca

Fe ⟶ Mg

△ 1% Mn

Ca

LA430B

GARNET ISOGRAD

73VJL225B

Ca

73VJL340B

CaFe

CaMg
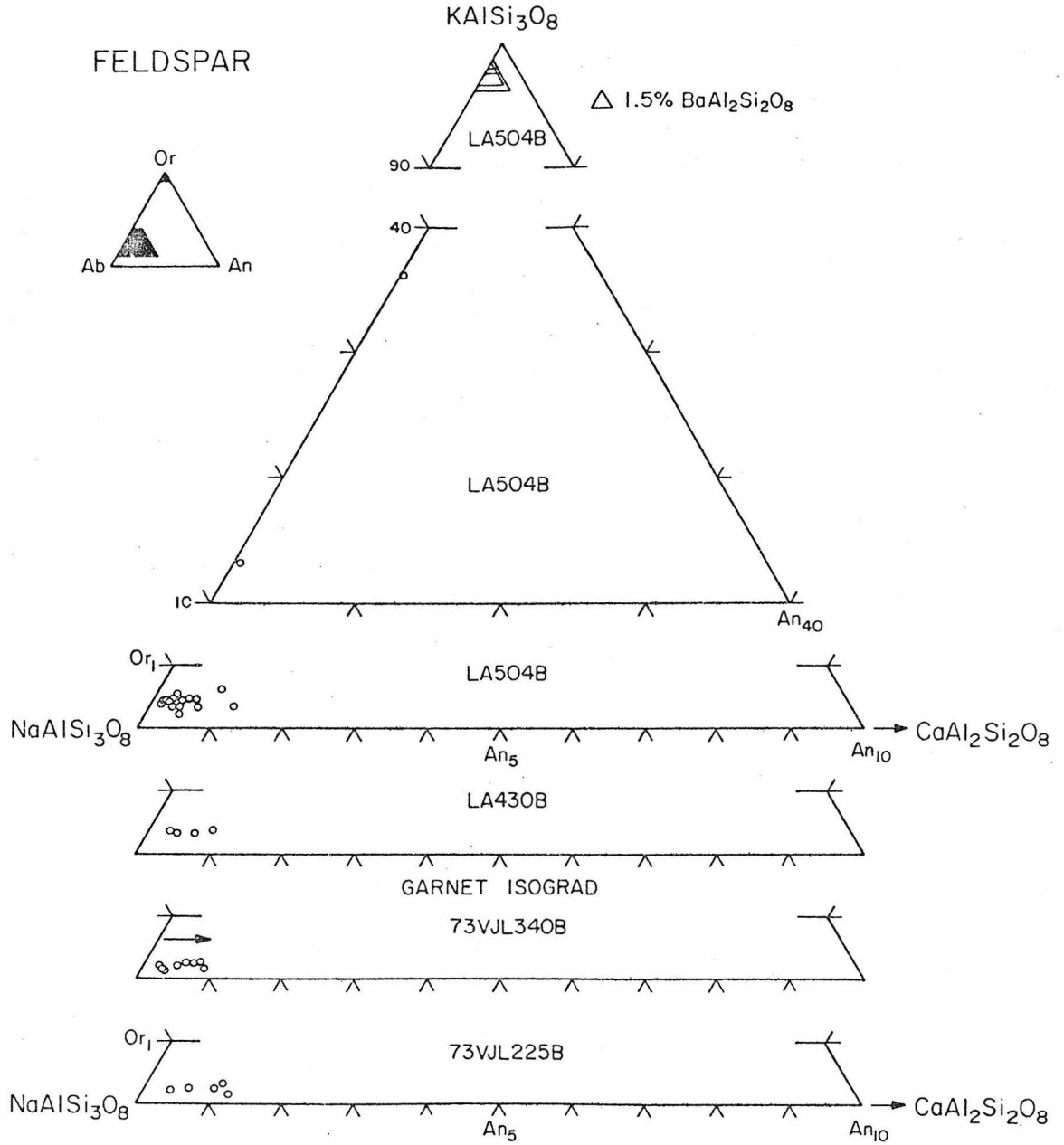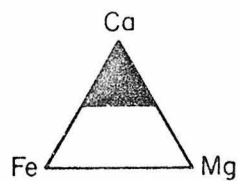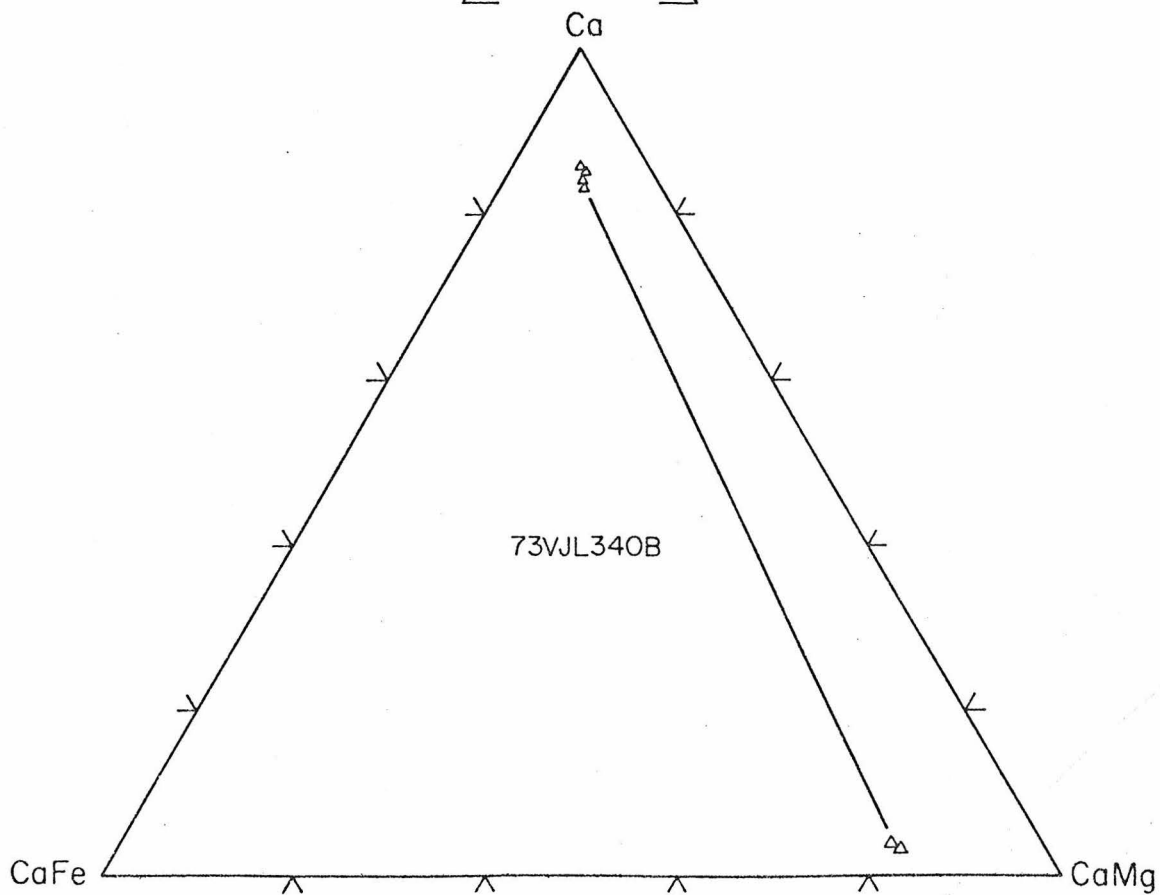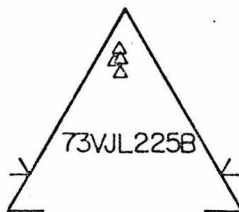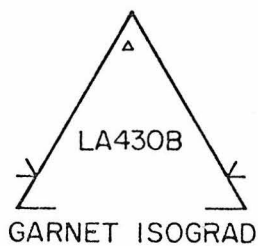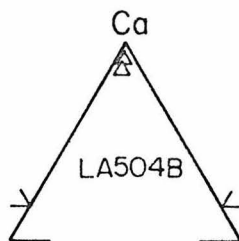
Figure IV-15

Figure IV-16a

SPHENE
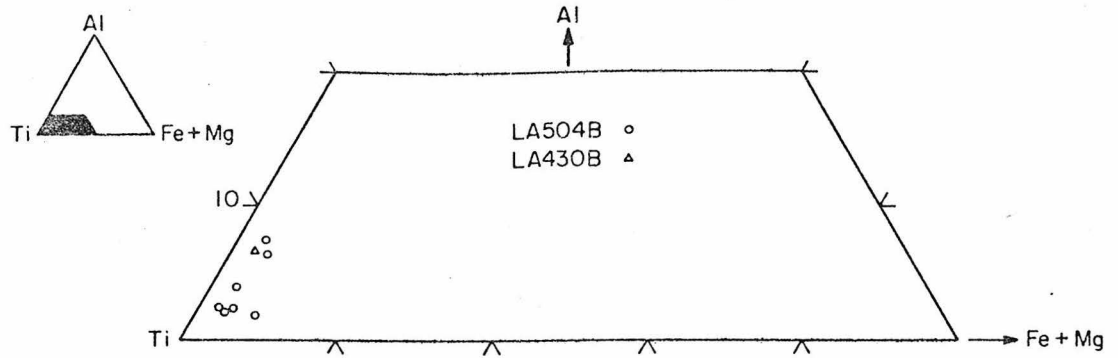
Figure IV-16b

ILMENITE

TILLOTSON PEAK AREA, VERMONT
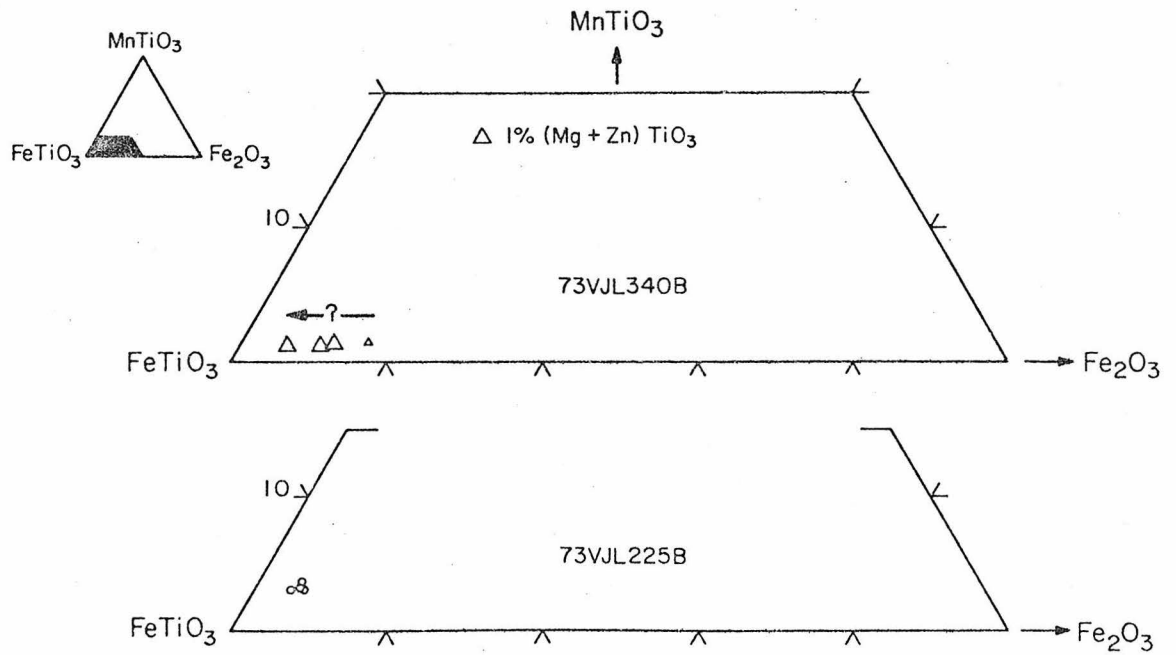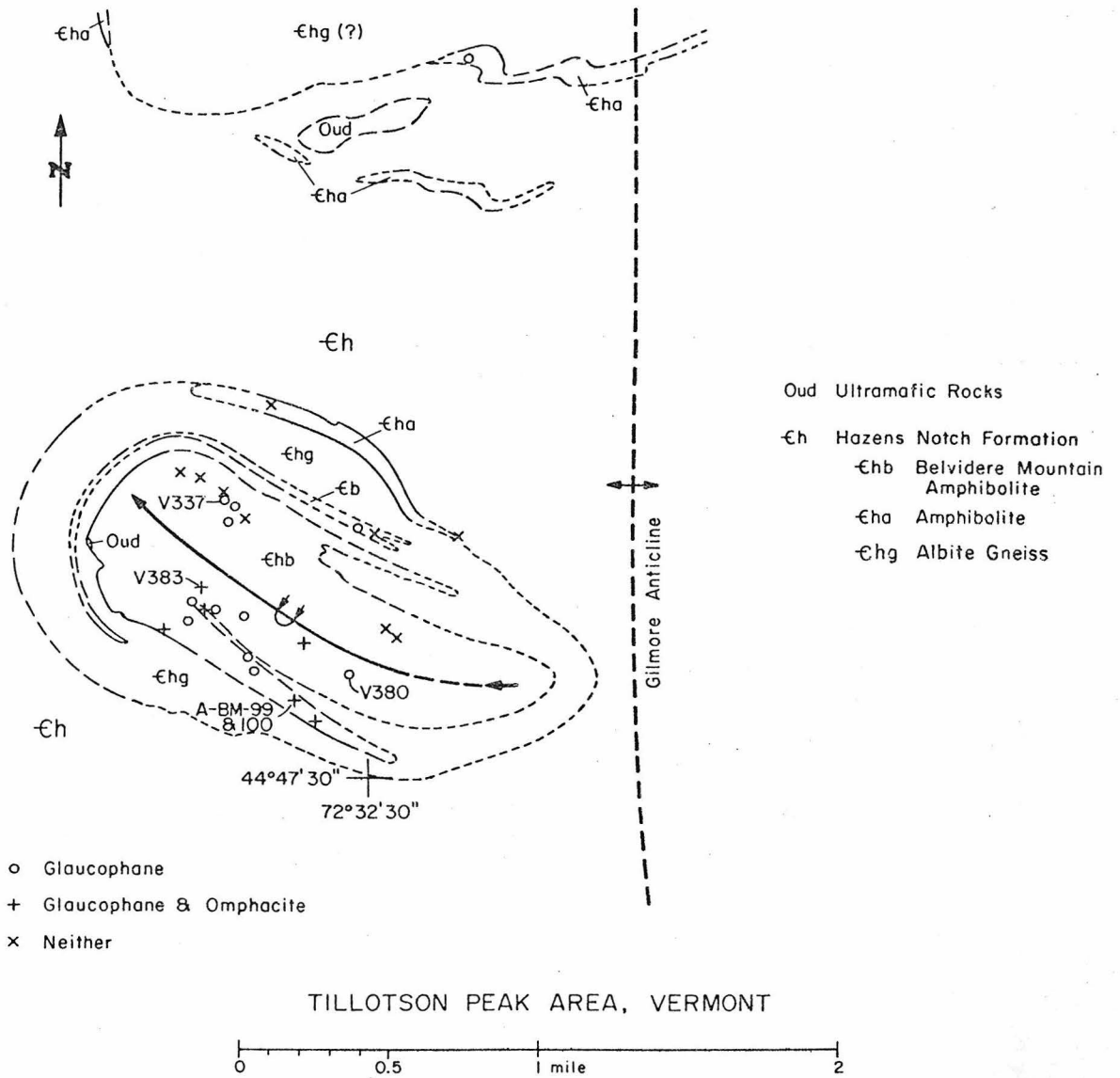
Figure IV-17

SODIC AMPHIBOLE

73VJL337B   75VJL380C   75VJL383B   A-BM-99

FORMULA PROPORTION Al^{IV}
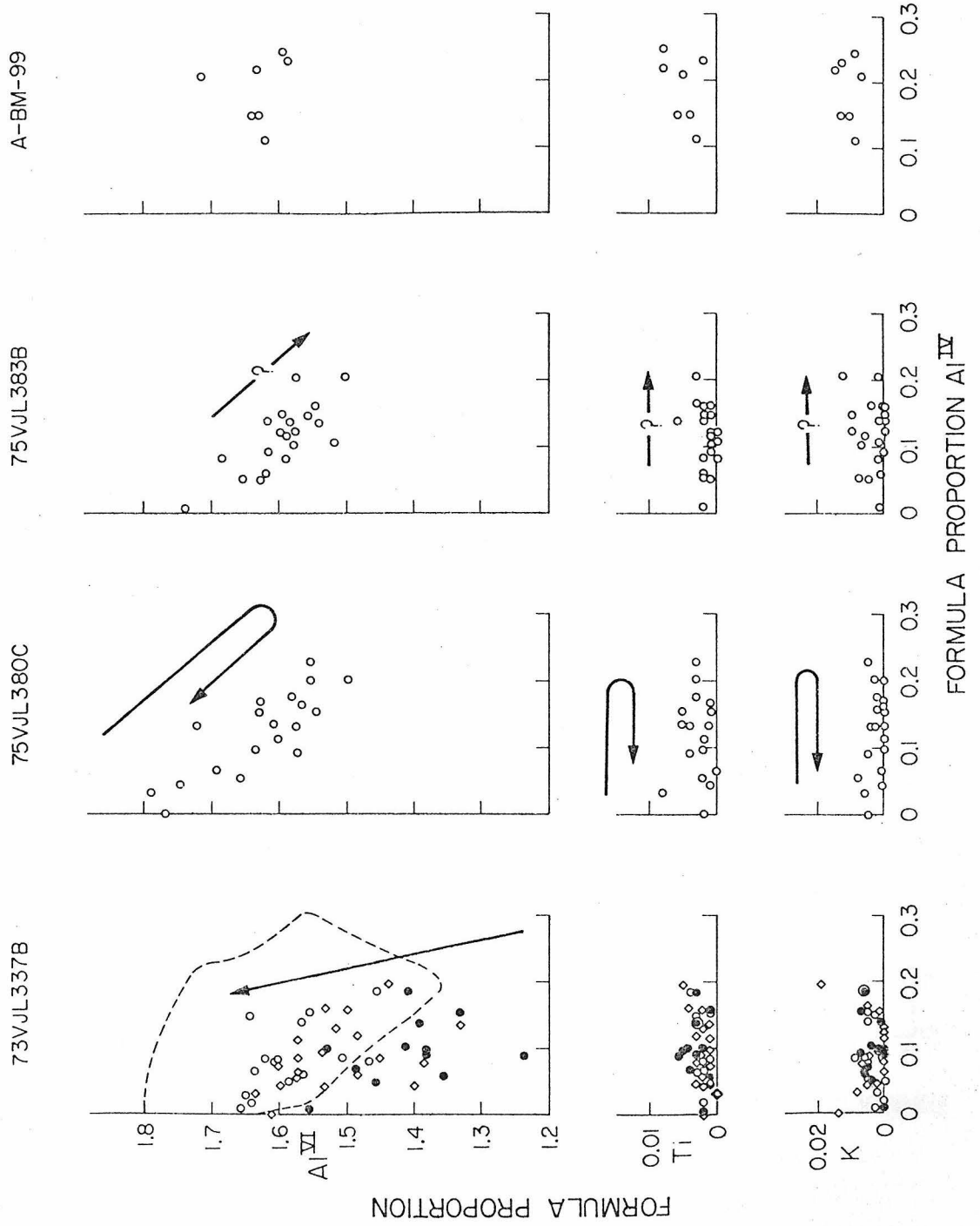
Figure IV-18a

SODIC AMPHIBOLE
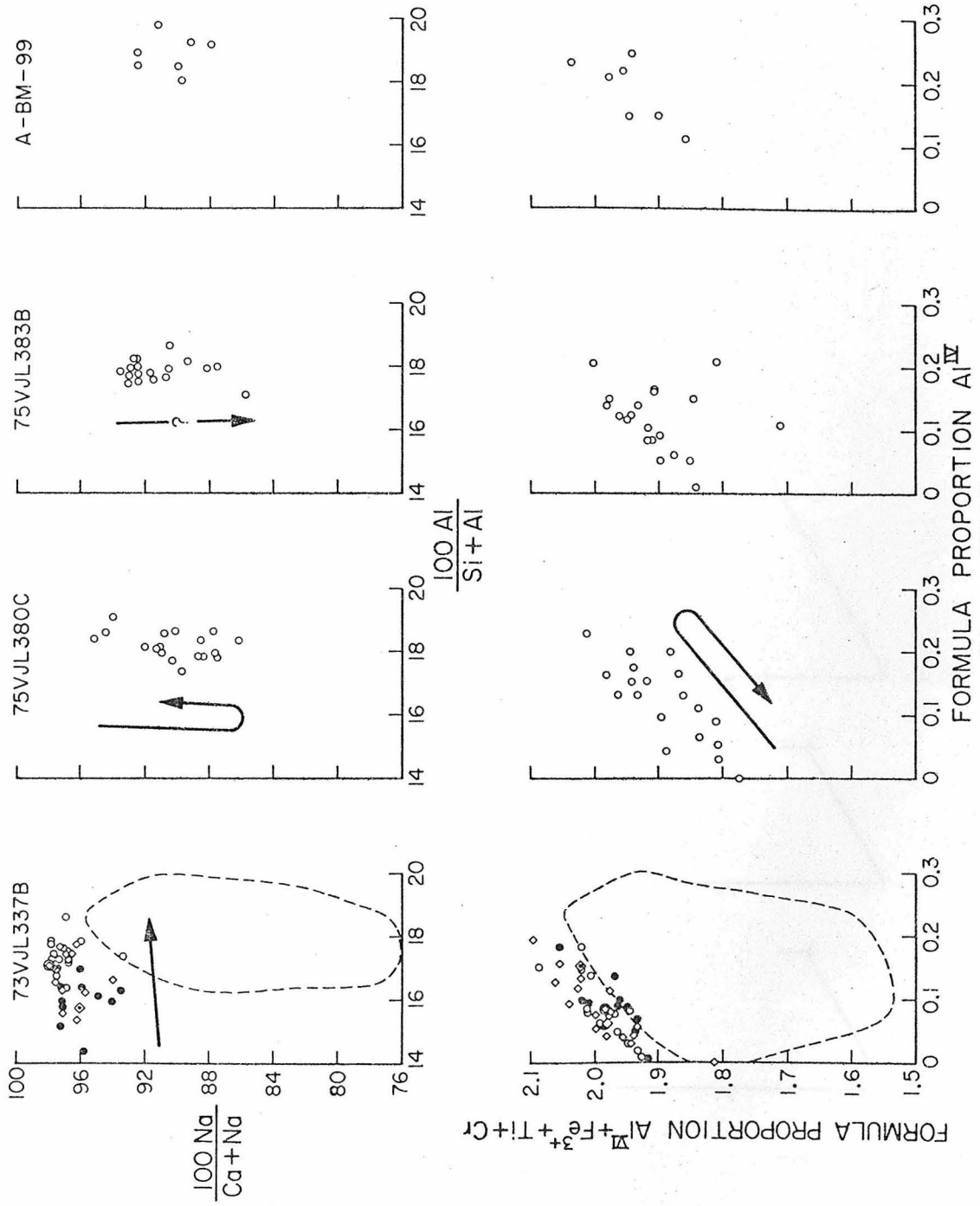
Figure IV-18b

SODIC AMPHIBOLE
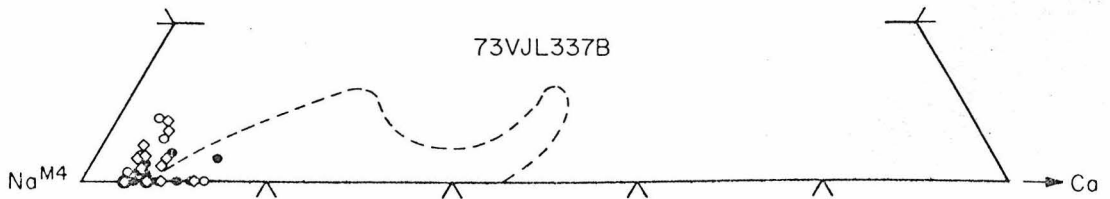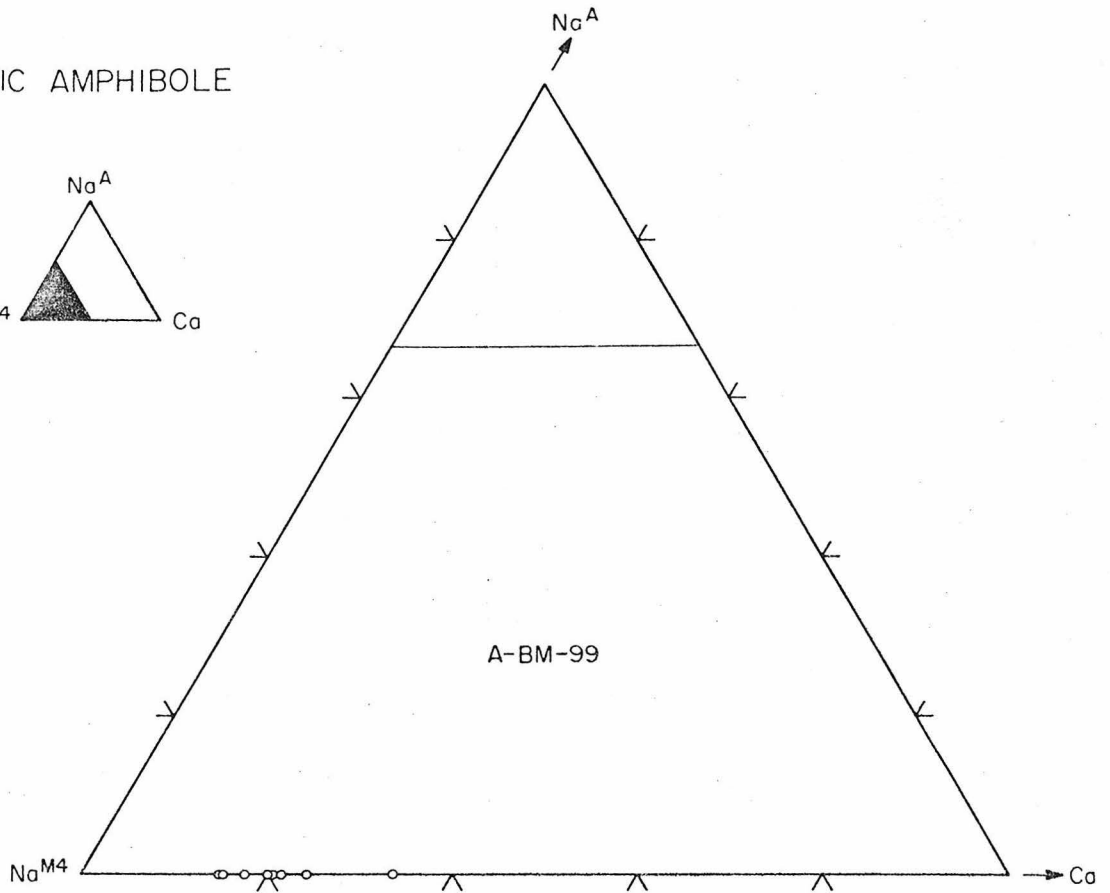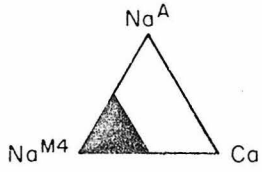
Figure IV-18c
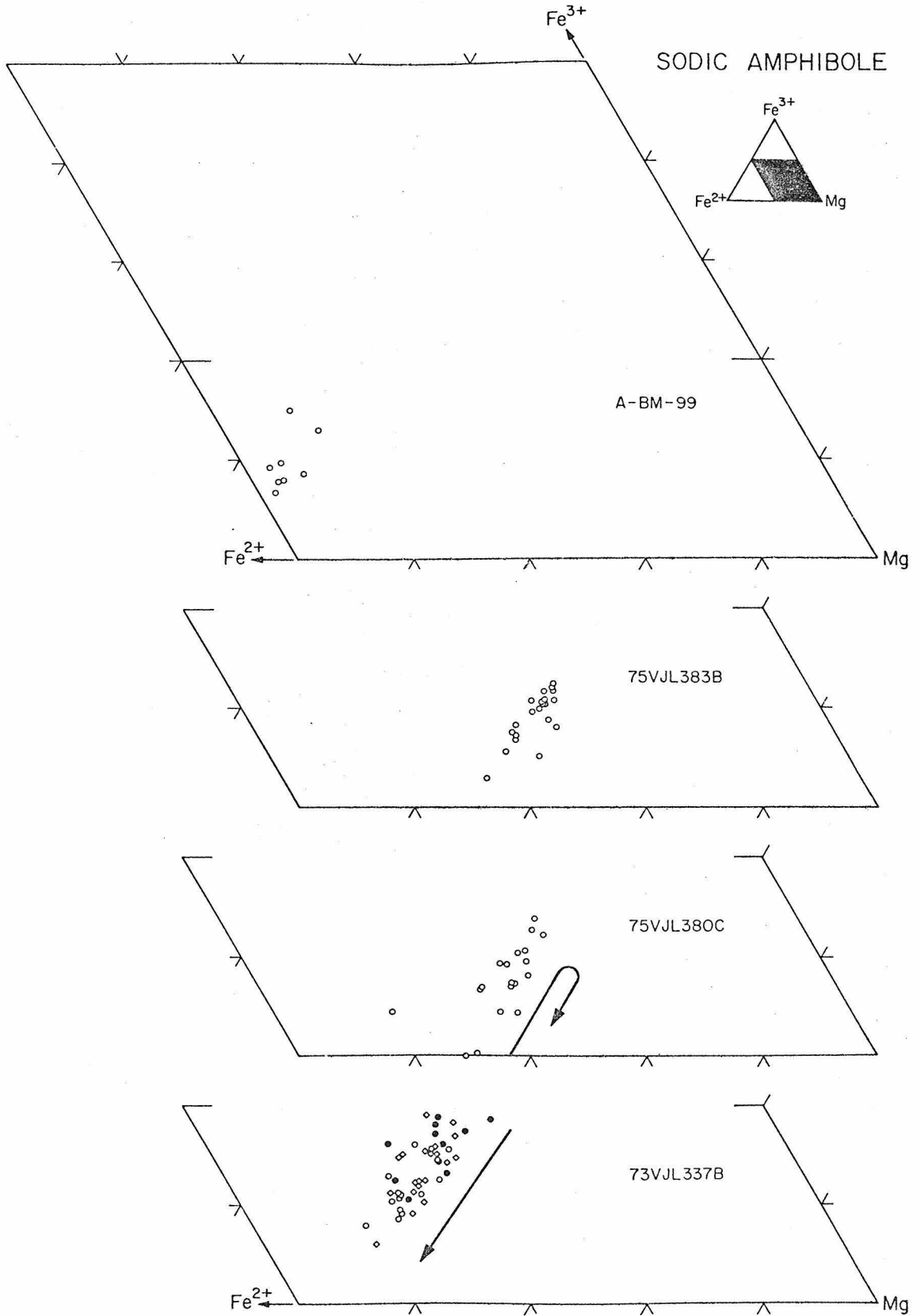
Figure IV-18d

AMPHIBOLE
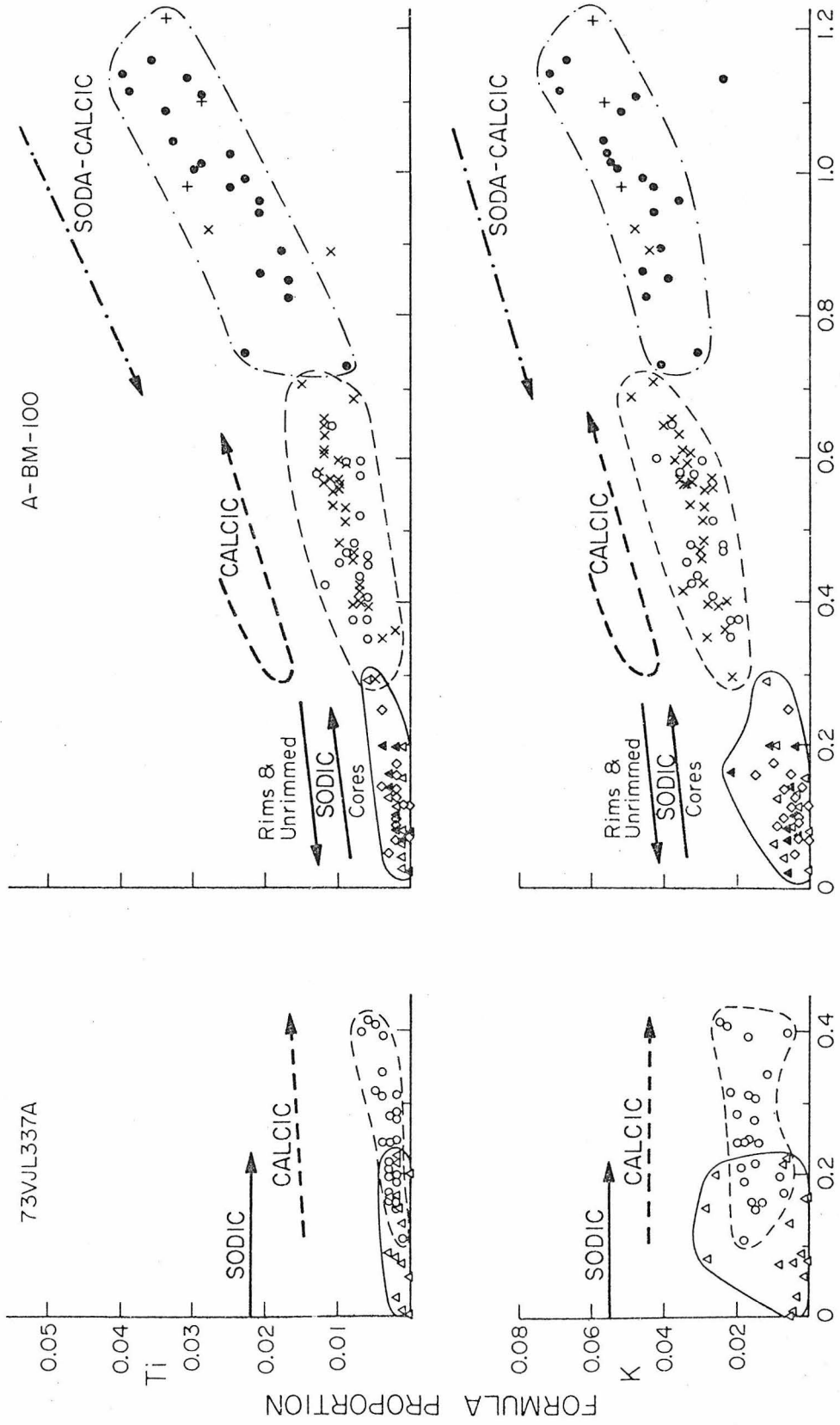
Figure IV-19a
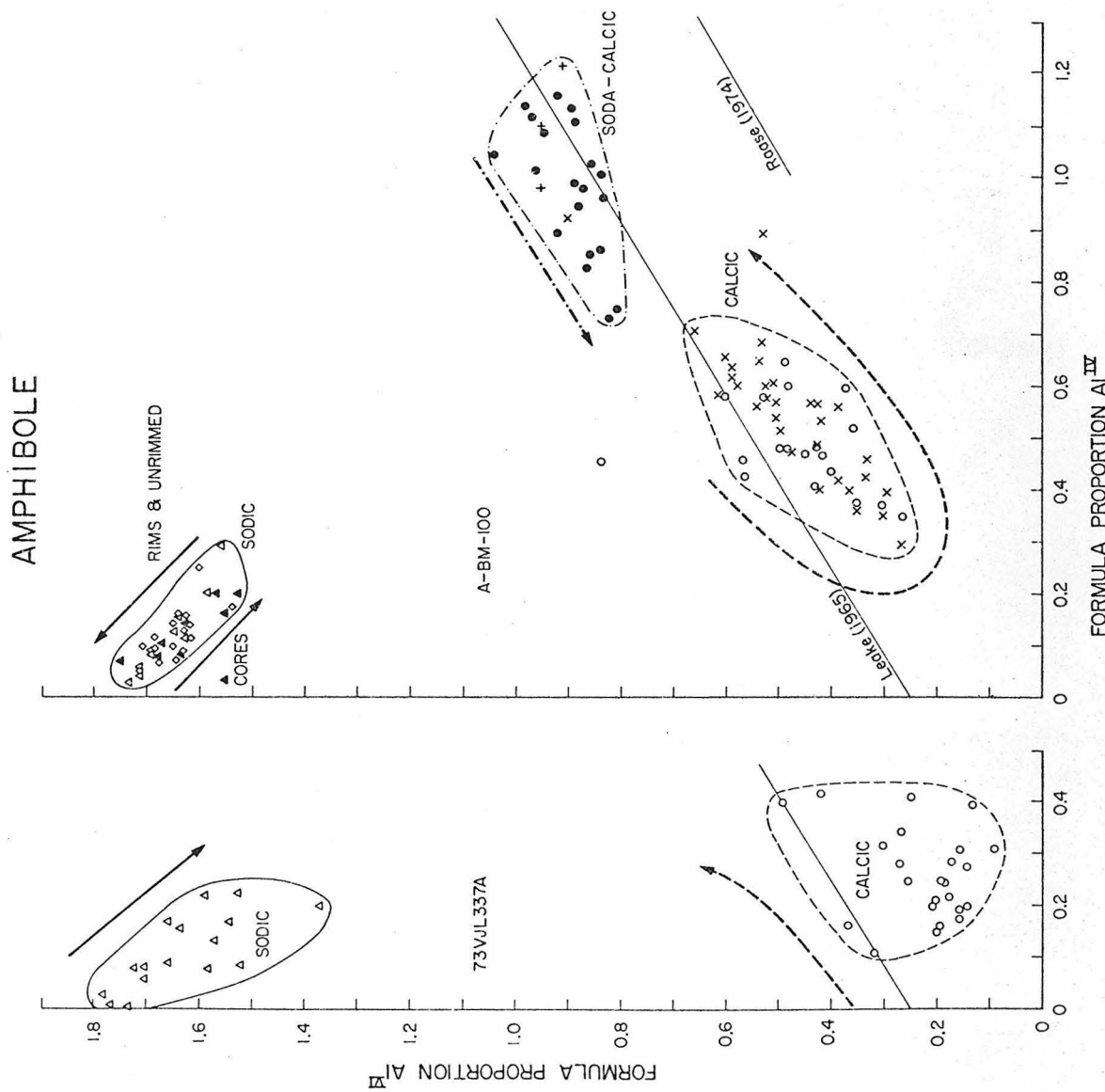
Figure IV-19b

AMPHIBOLE
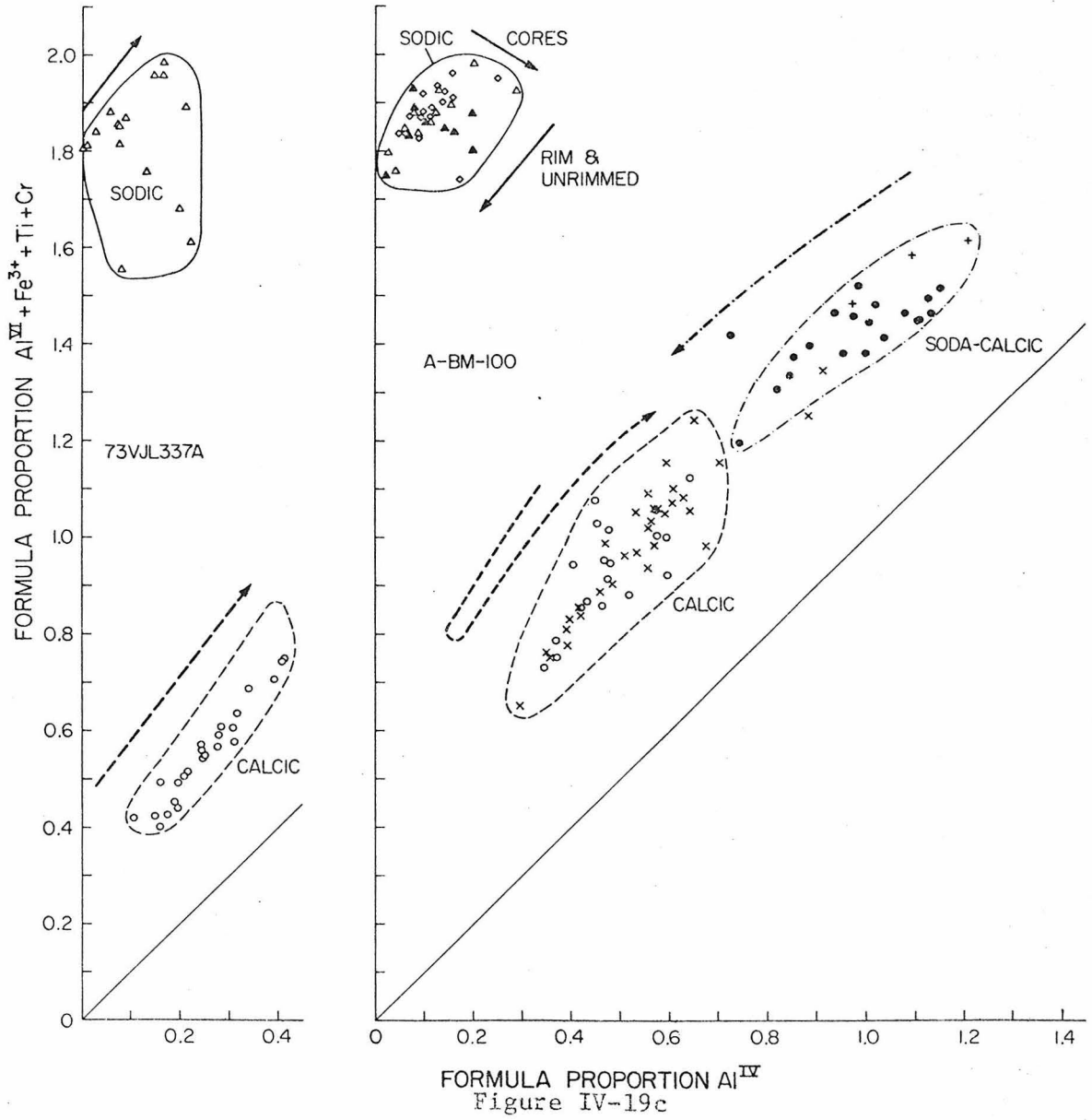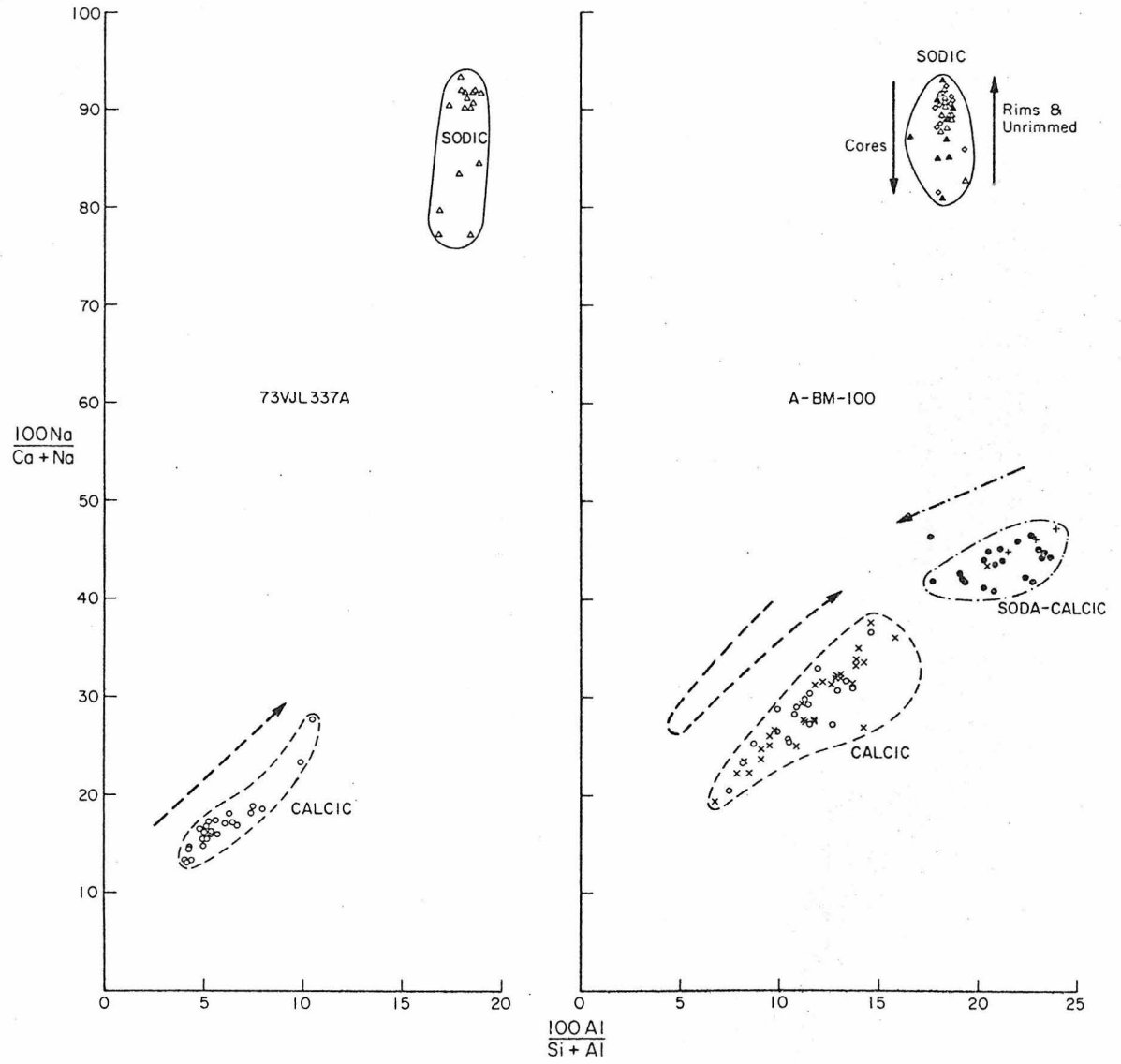
Figure IV-19c

Figure IV-19d

Figure IV-19e
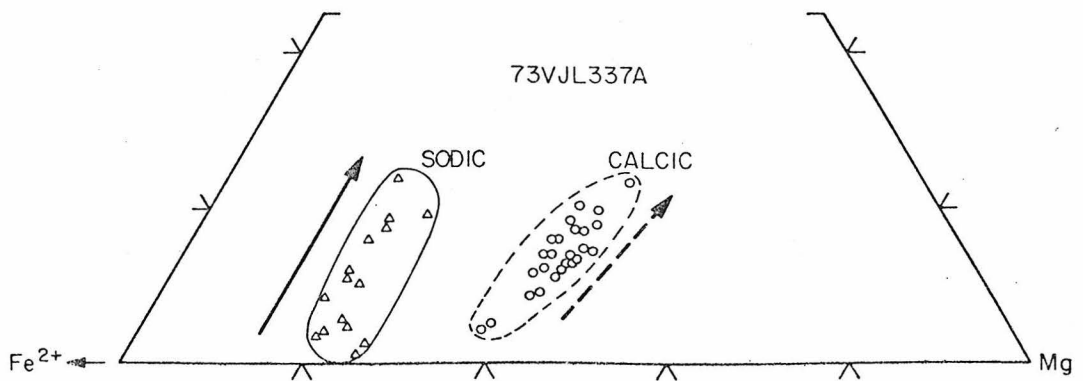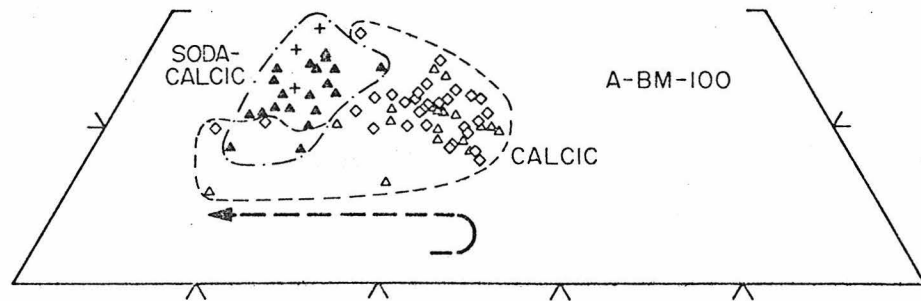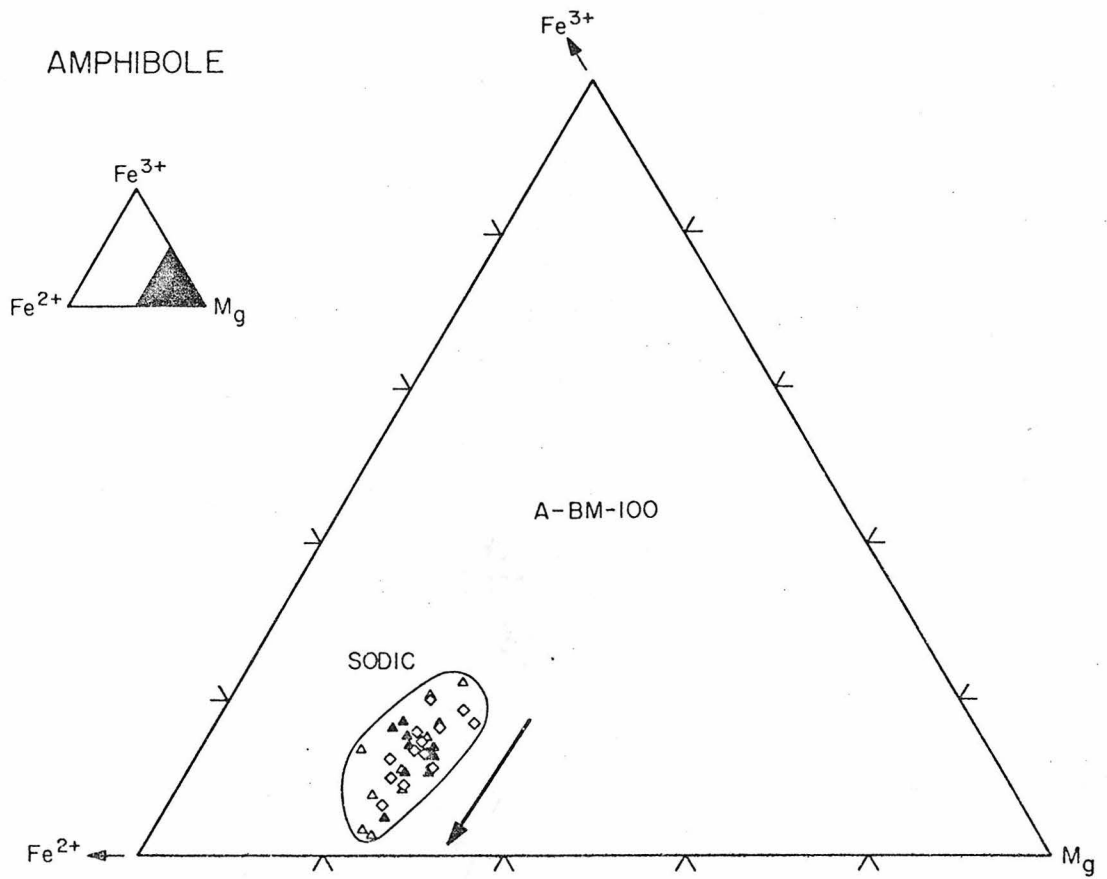
AMPHIBOLE

Figure IV-19f

AMPHIBOLE GRAIN I, A-BM-100 AREA A
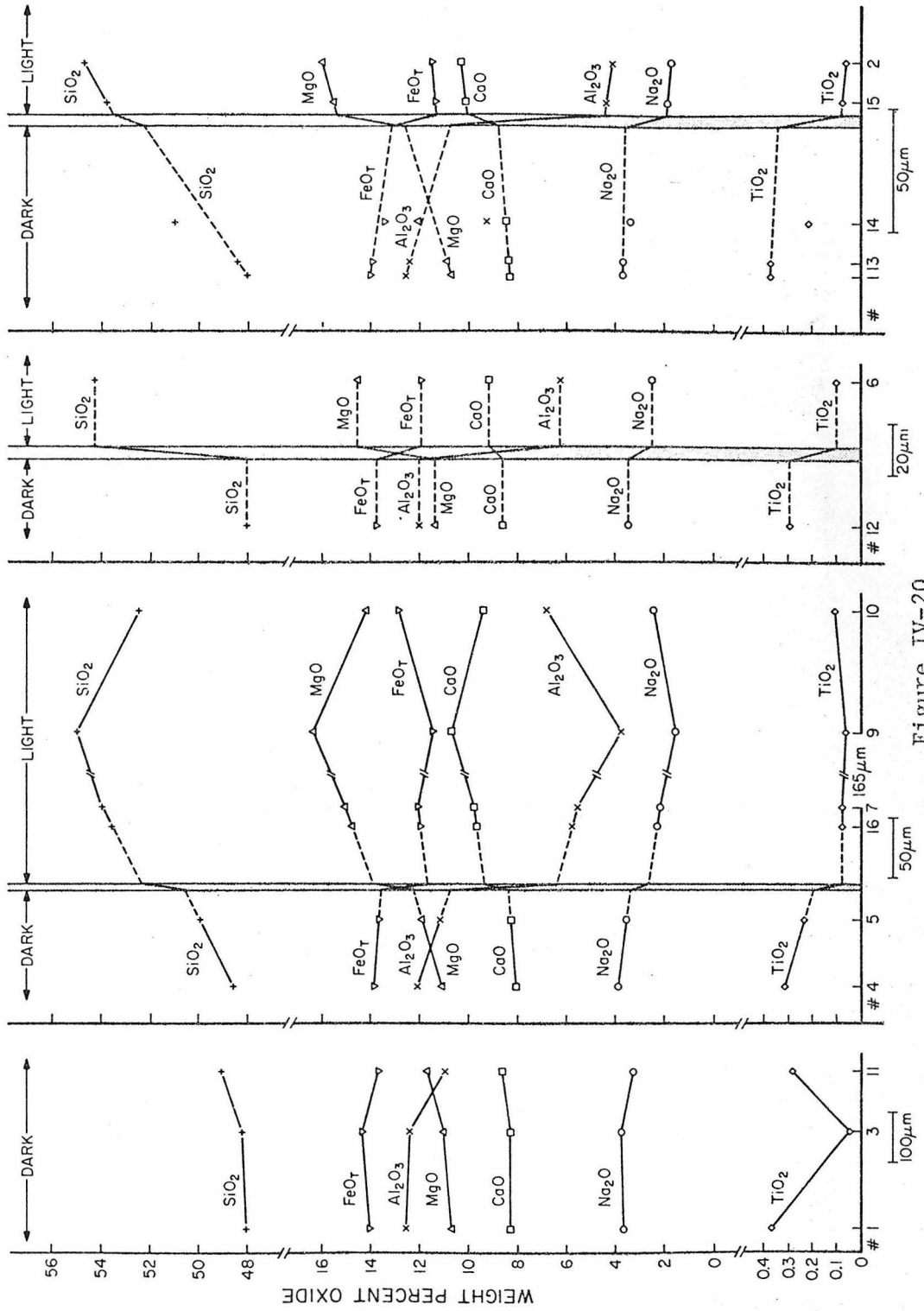
Figure IV-20

AMPHIBOLE GRAIN I, A-BM-IOO AREA C
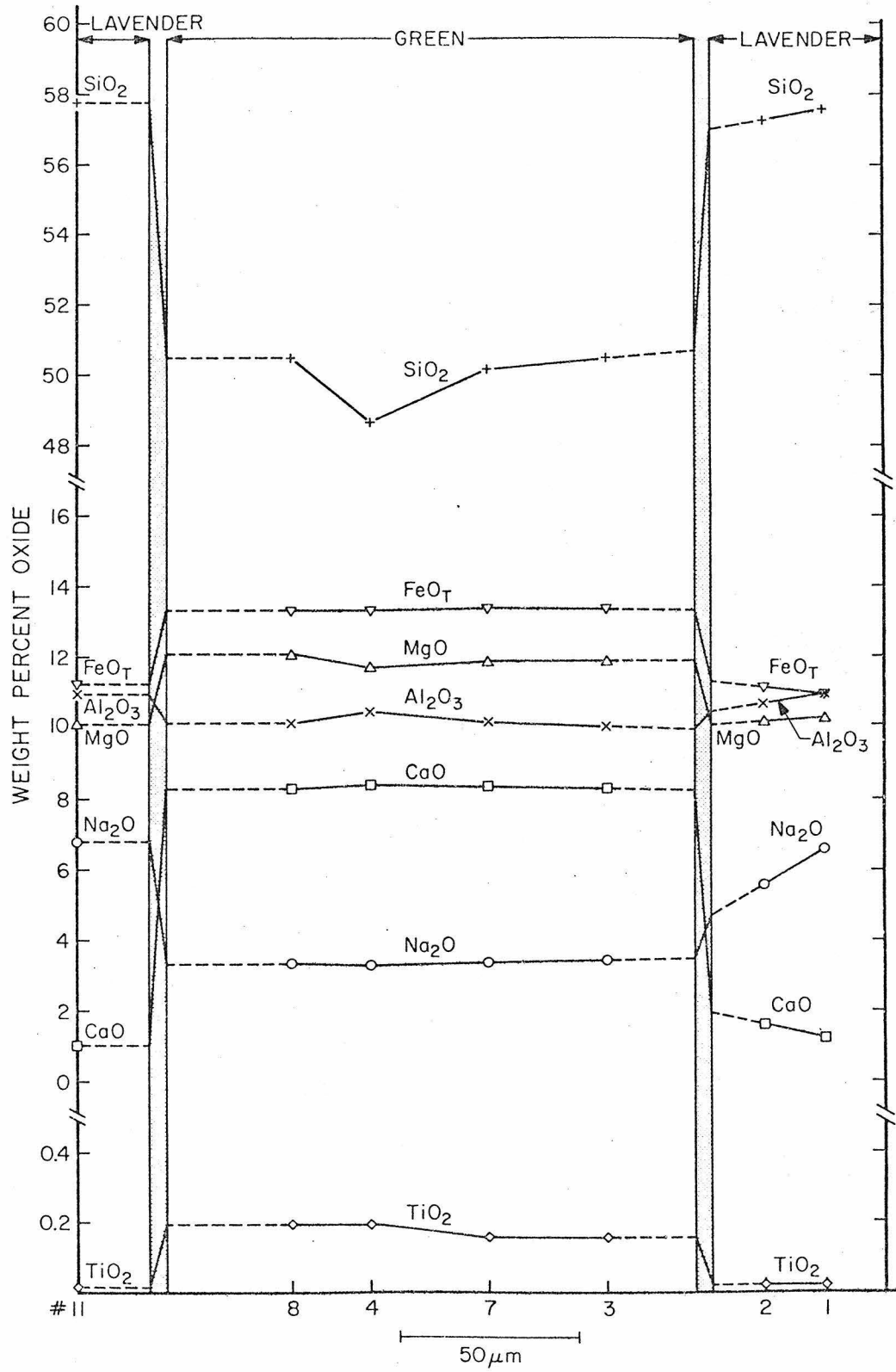
Figure IV-21
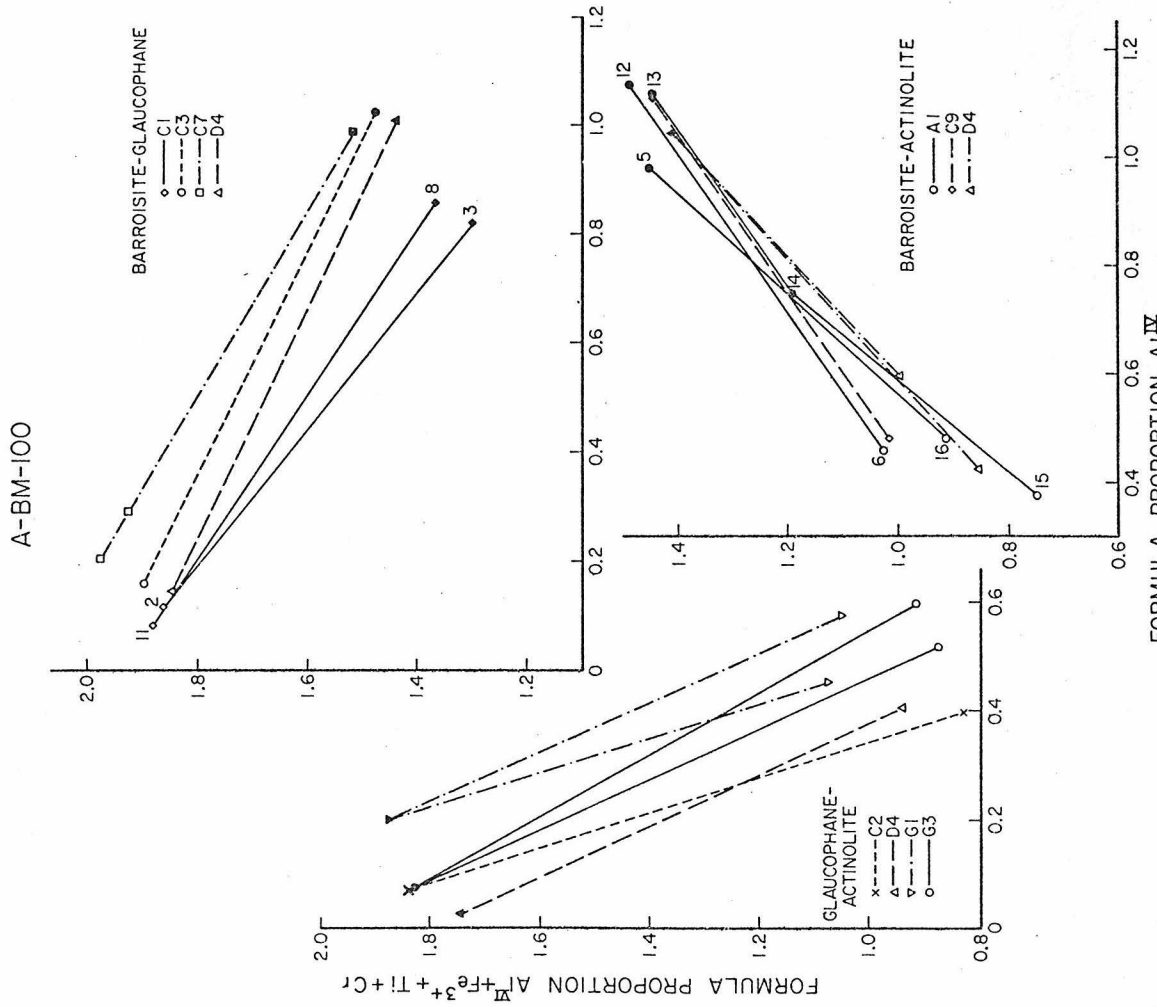
Figure IV-22

AMPHIBOLE 73VJL360B
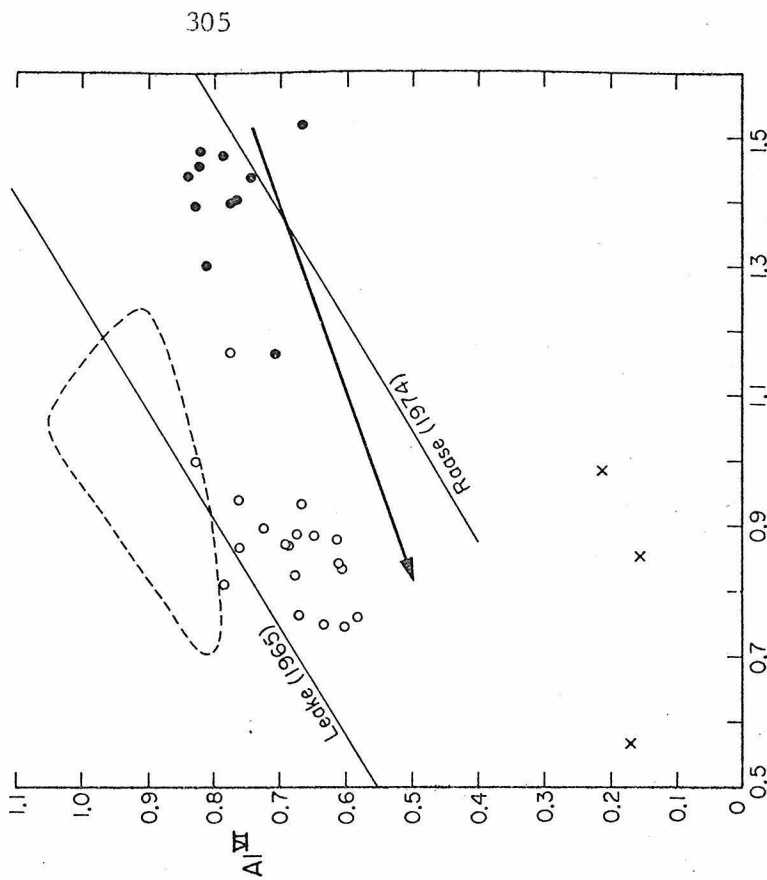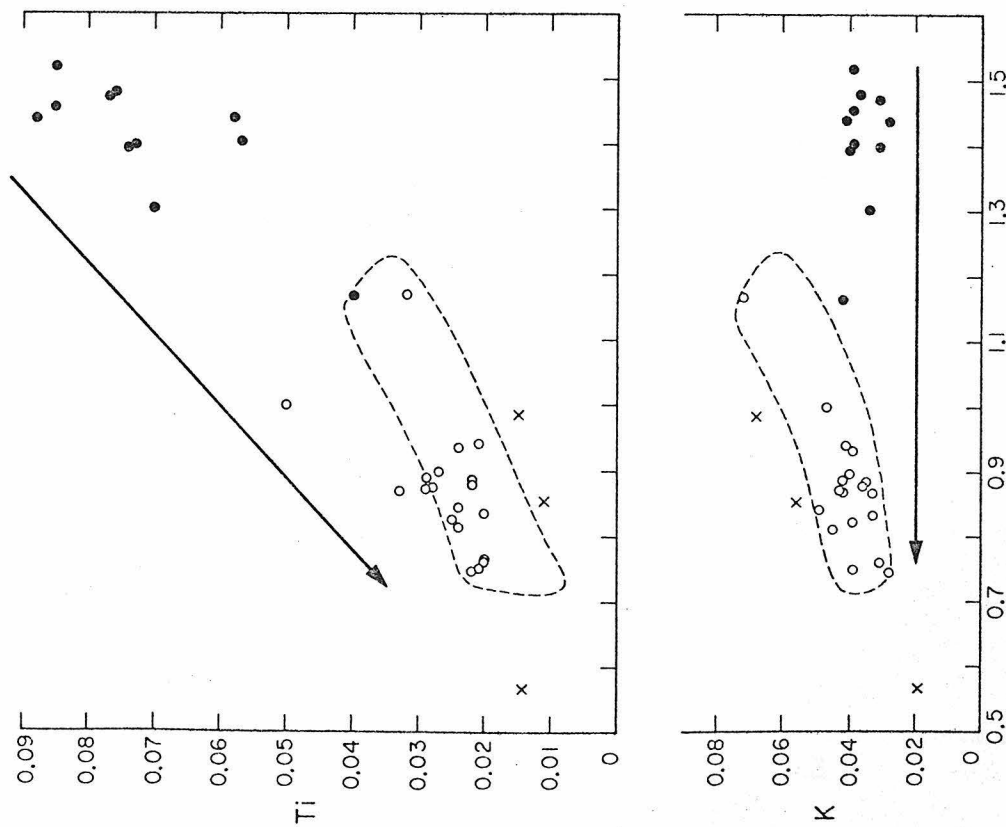
FORMULA PROPORTION Al^{IV}
Figure IV-23a

AMPHIBOLE 73VJL360B
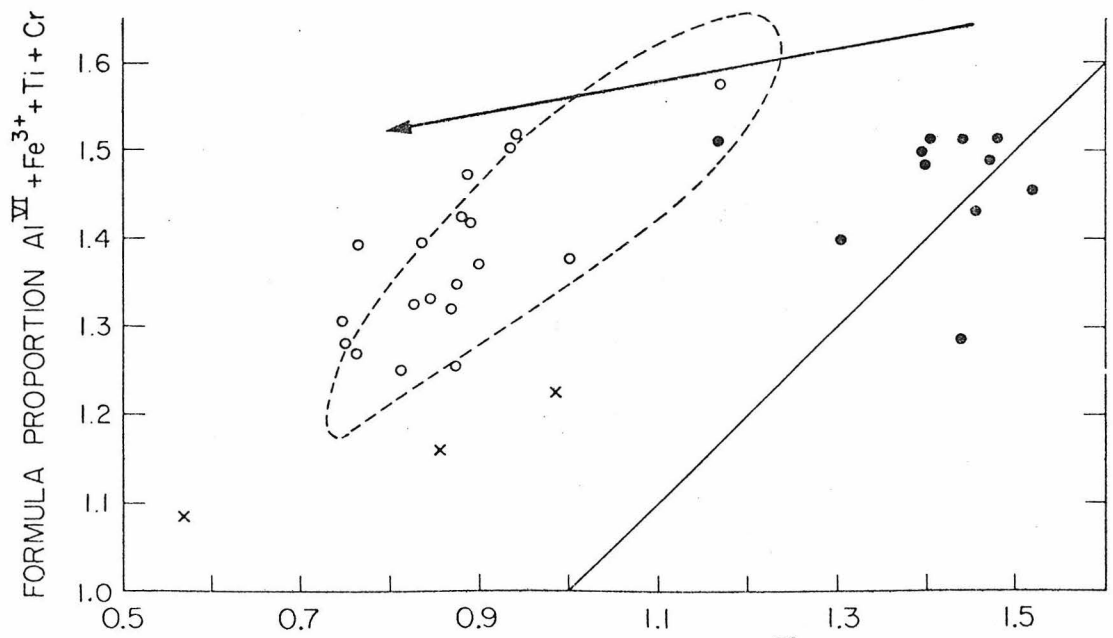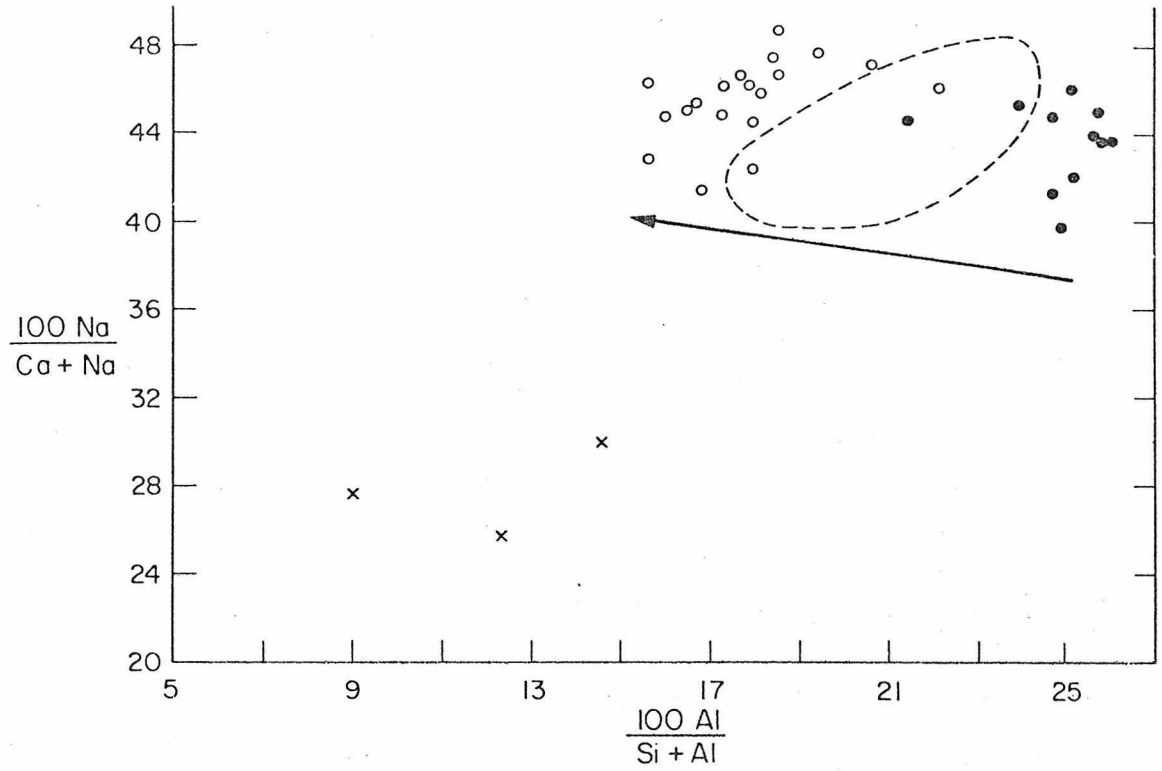
Figure IV-23b

73VJL360B AMPHIBOLE
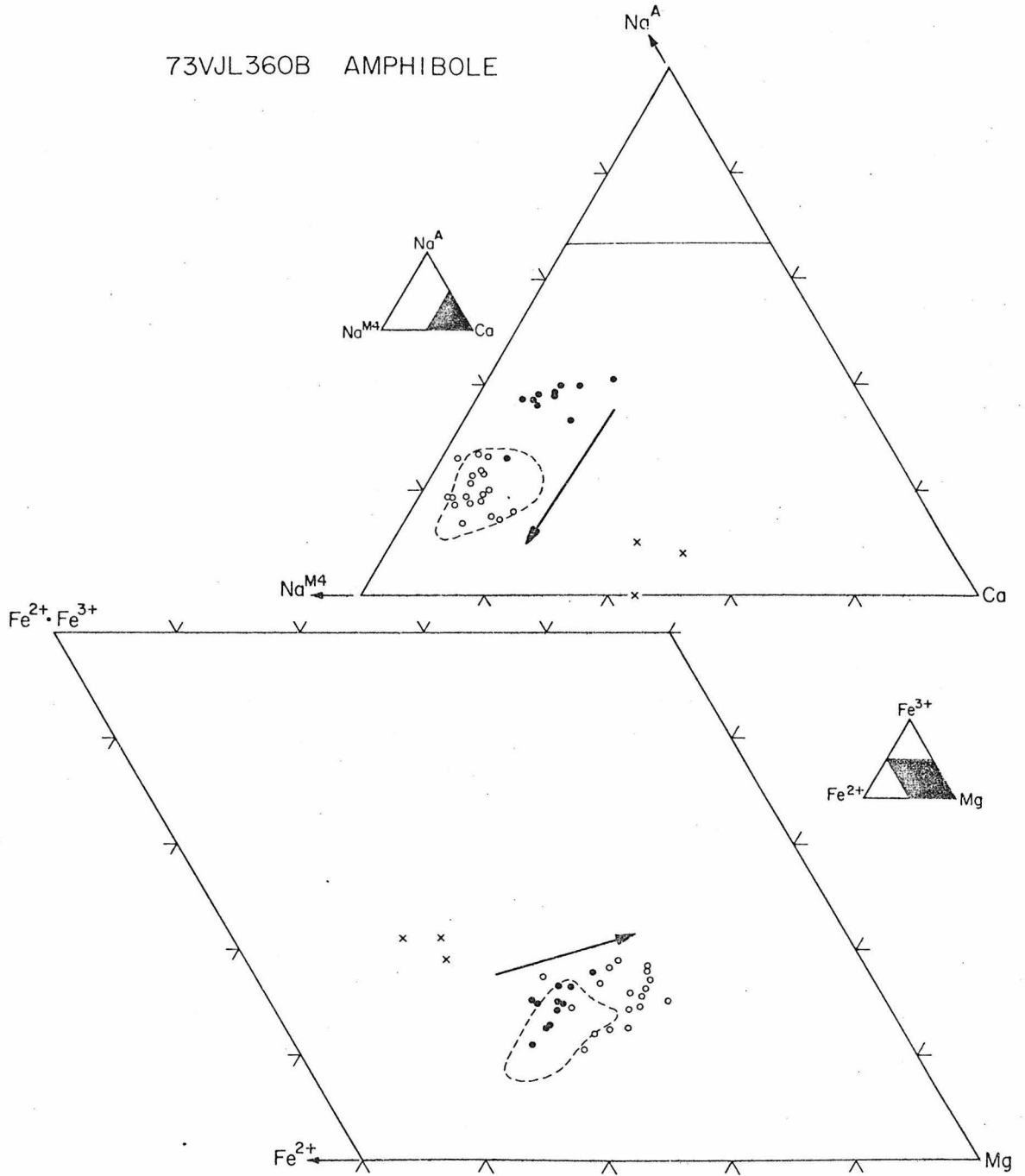
Figure IV-23c

Figure IV-24a

OMPHACITE

Fe^{3+}

Fe^{3+}

A-BM-100

75VJL383B

Fe^{2+}

Mg

Figure IV-24b

$Na\,Al\,Si_2O_6$

$Na\,Al\,Si_2O_6$

$3\%\ (Ca\,Al\,Al\,Si\,O_6 + Na\,Cr\,Si_2O_6$
$+ Ca\,Ti\,Al_2O_6)$

A-BM-100

75VJL383B

$Na\,Fe^{3+}Si_2O_6$

$Ca_2Si_2O_6$
$+FM_2Si_2O_6$
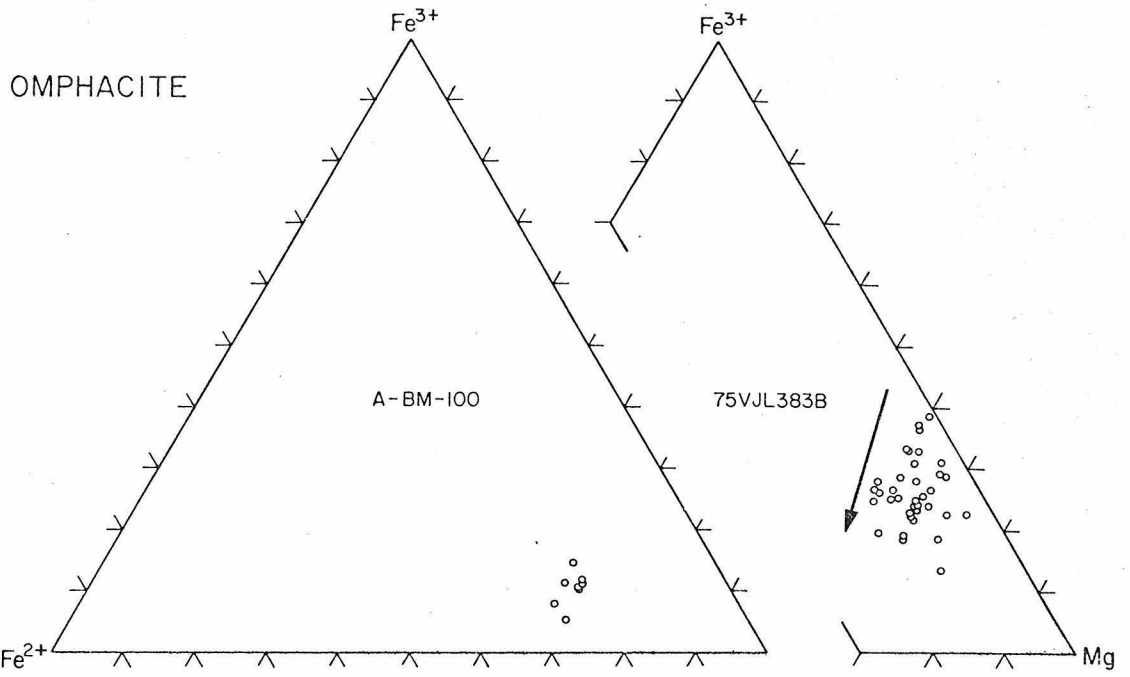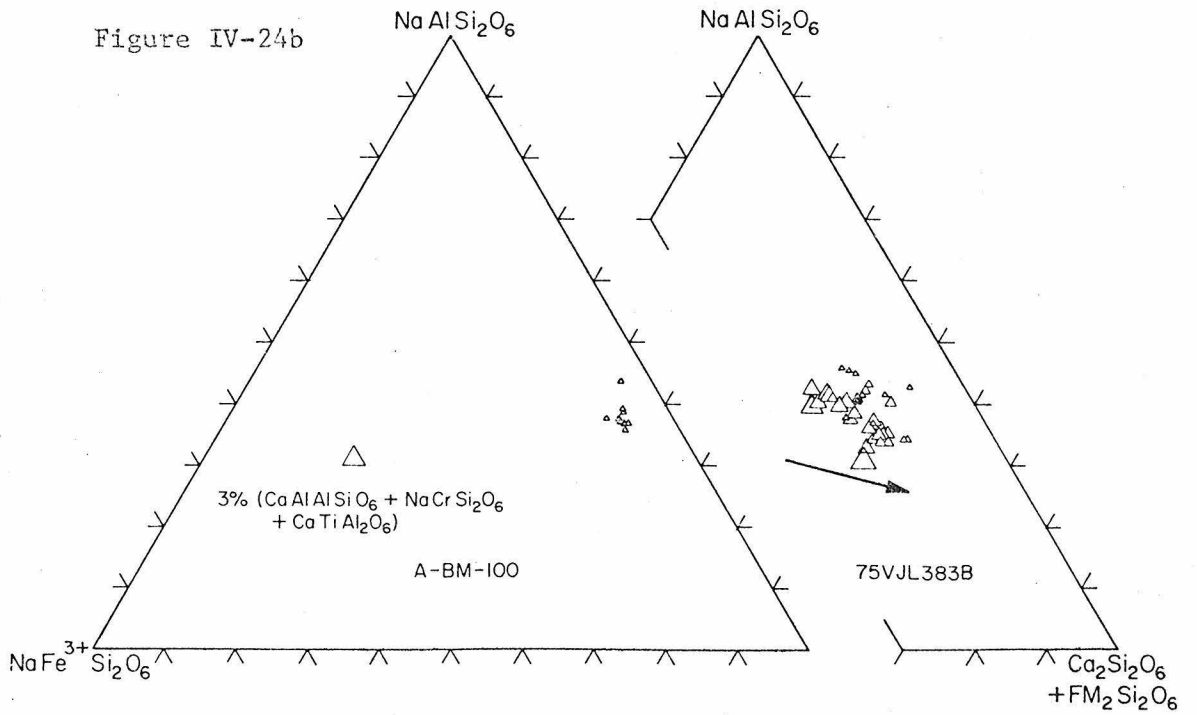
CHLORITE

Figure IV-25a

$$\frac{100\ Mg}{Mg + Fe^{2+}}$$

FORMULA PROPORTION Al

A-BM-99 A-BM-100 73VJL337A 73VJL337B 75VJL380C
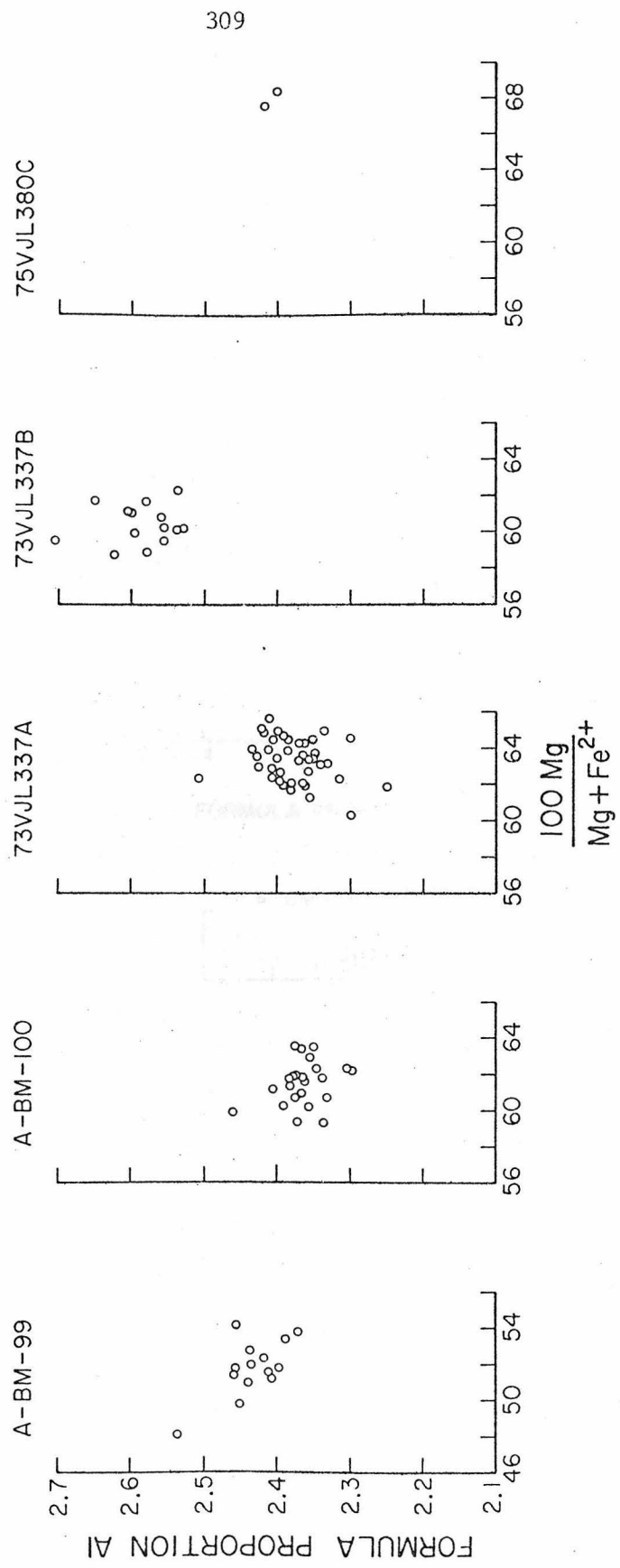
CHLORITE
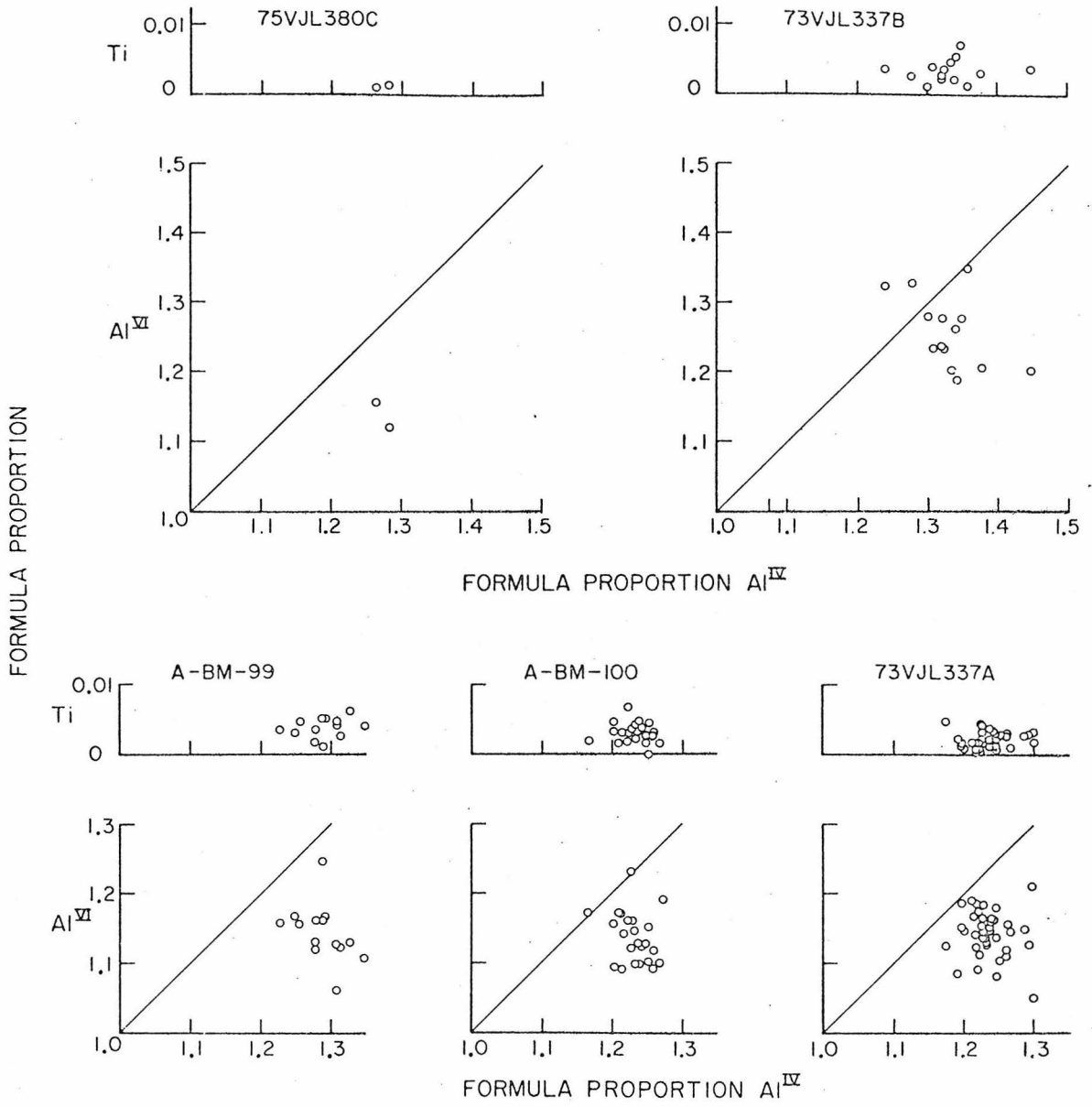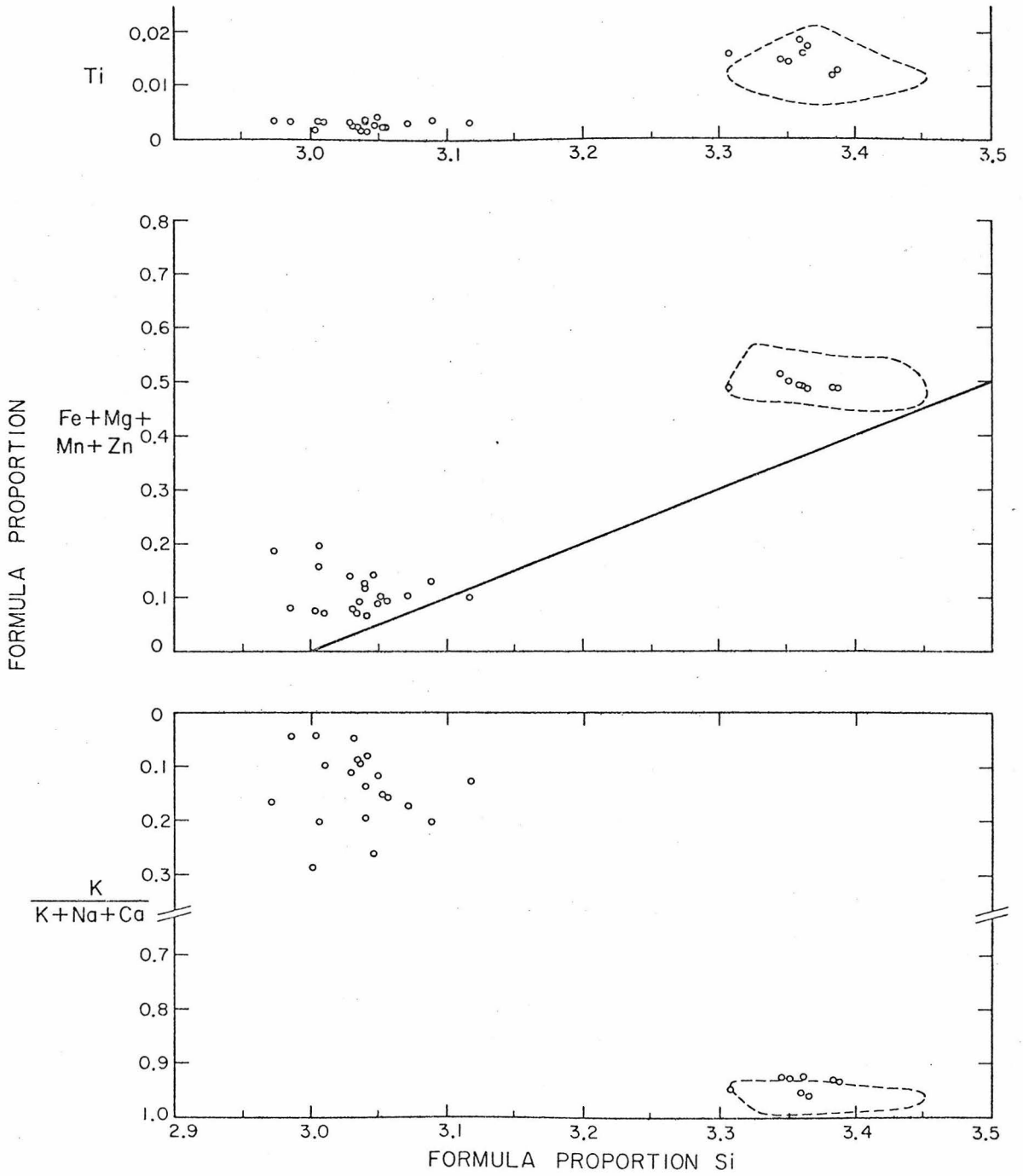
Figure IV-25b

Figure IV-26a

WHITE MICA
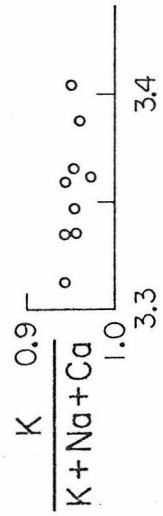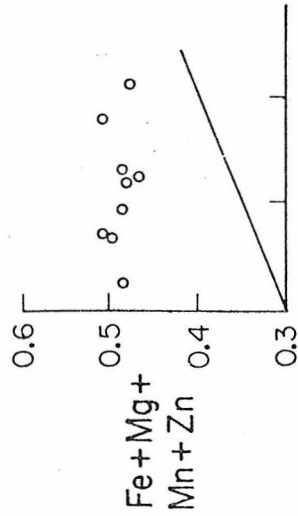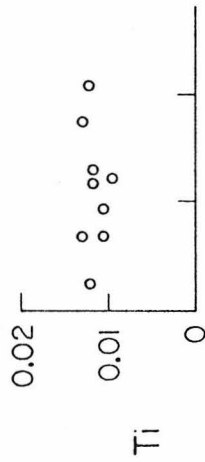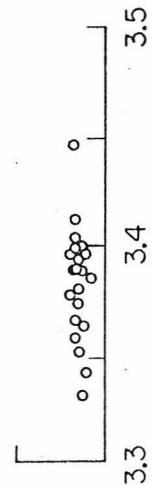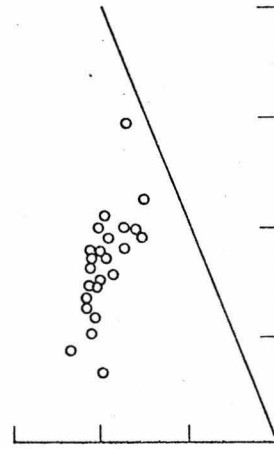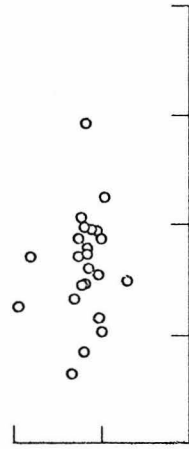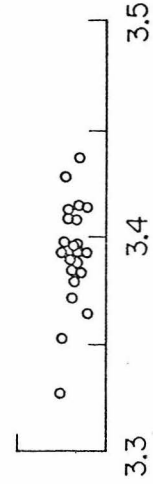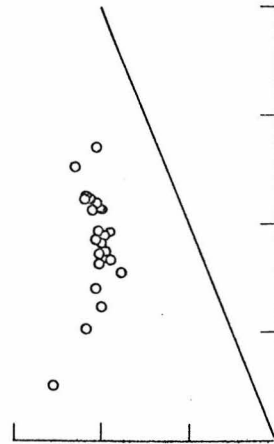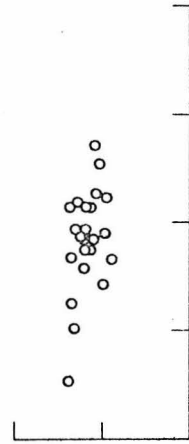
FORMULA PROPORTION Si

Figure IV-26b

WHITE MICA

Fe^{3+}

Fe^{2+}

Mg

73VJL337B

75VJL380C

A-BM-99

A-BM-100

Fe^{2+}

Mg
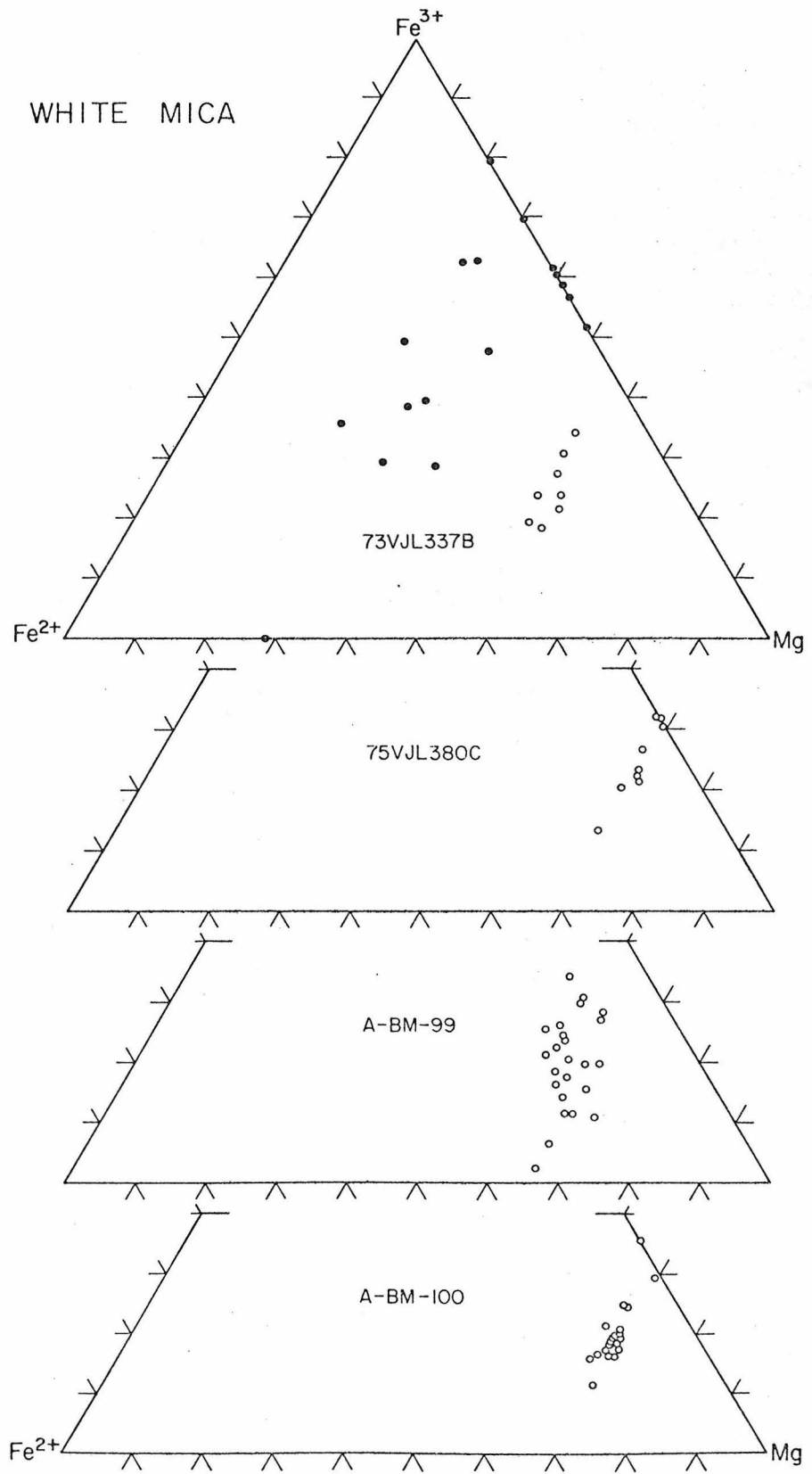
Figure IV-26c

EPIDOTE
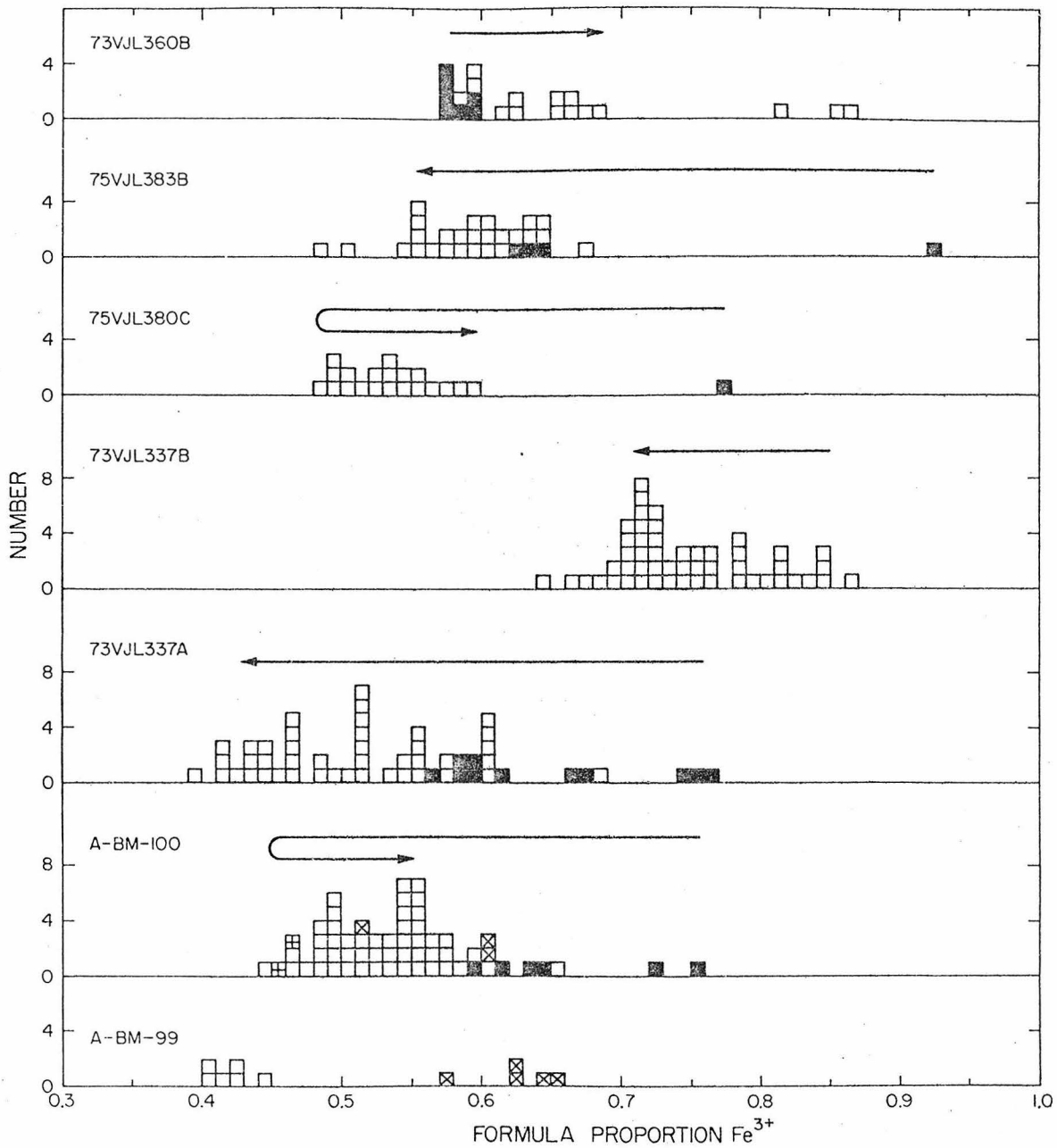
Figure IV-27
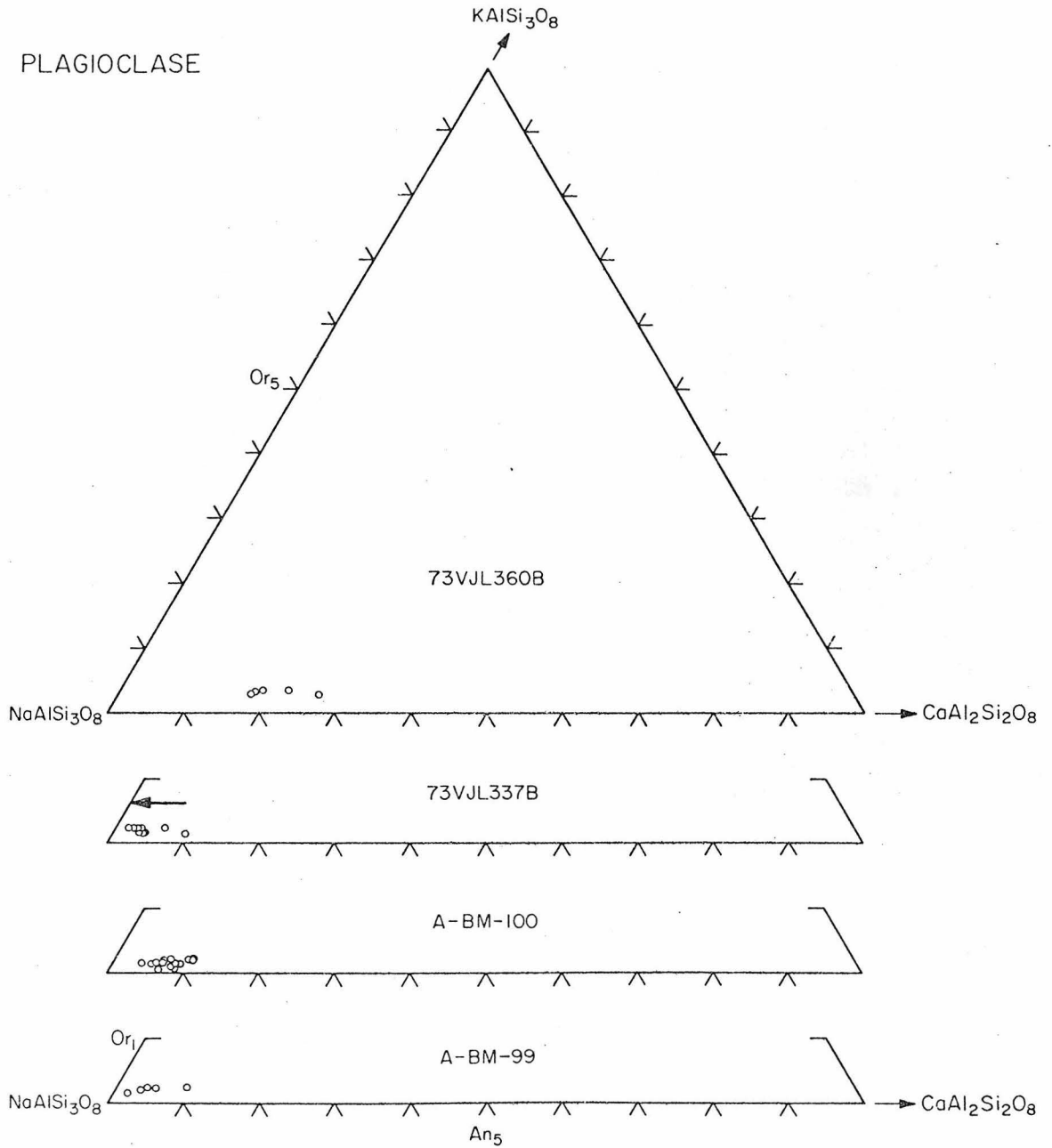
Figure IV-28

Figure IV-29a

GARNET

Mg

Mn

Ca

75VJL380C

73VJL337A

A-BM-IOO

A-BM-99

73VJL360B

Mn

Ca

Fe²⁺
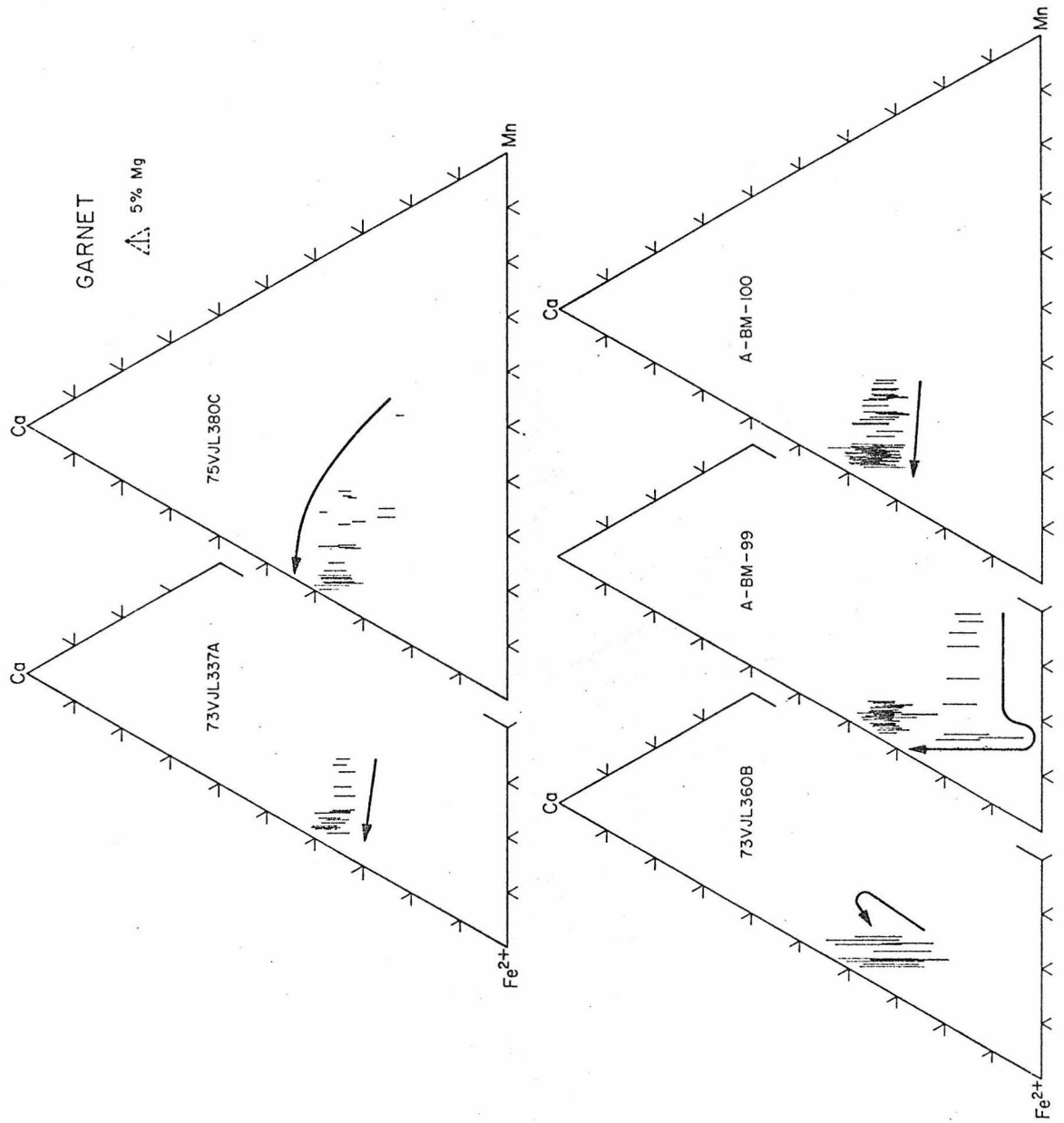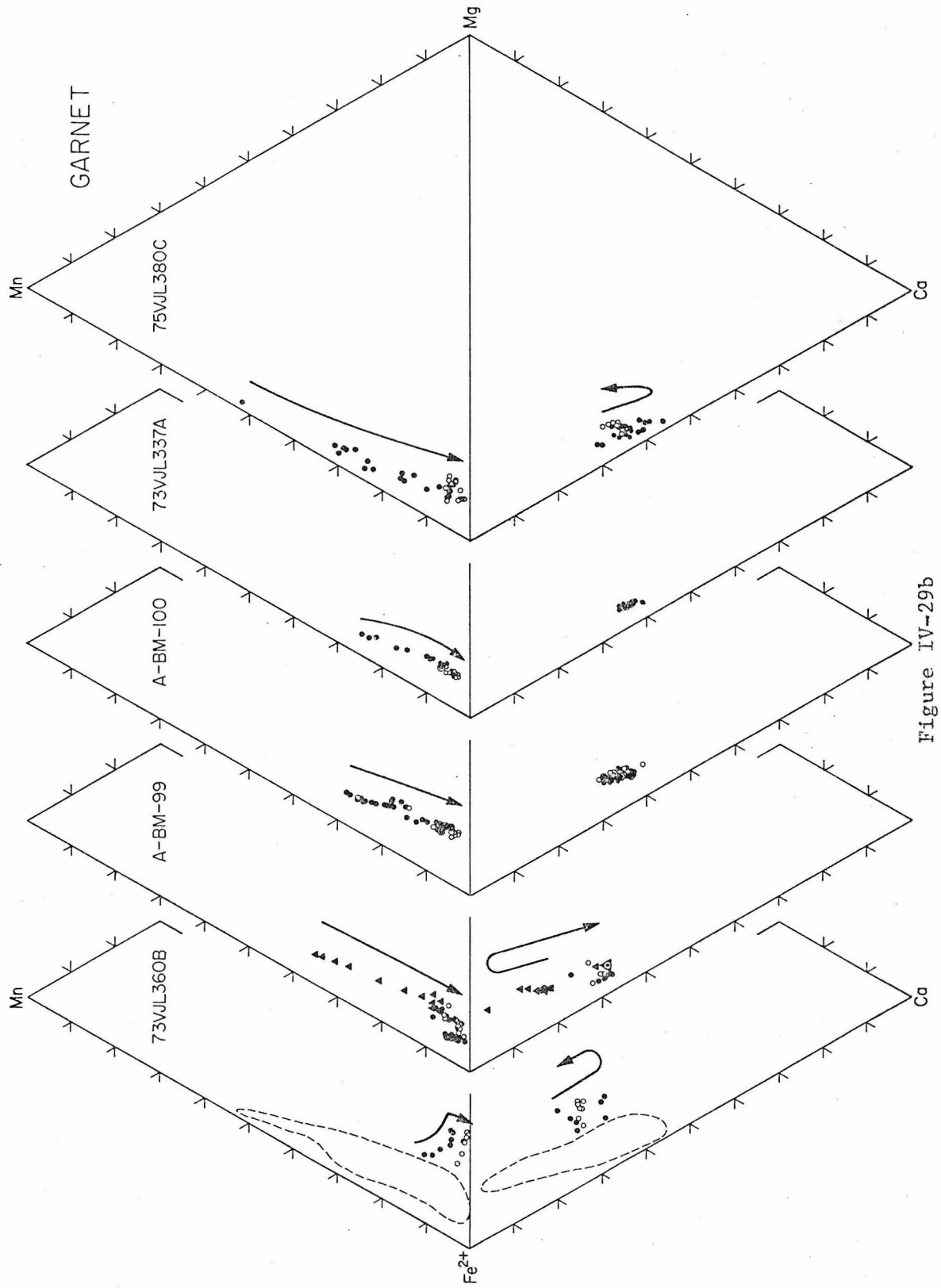
Figure IV-29b

GARNET
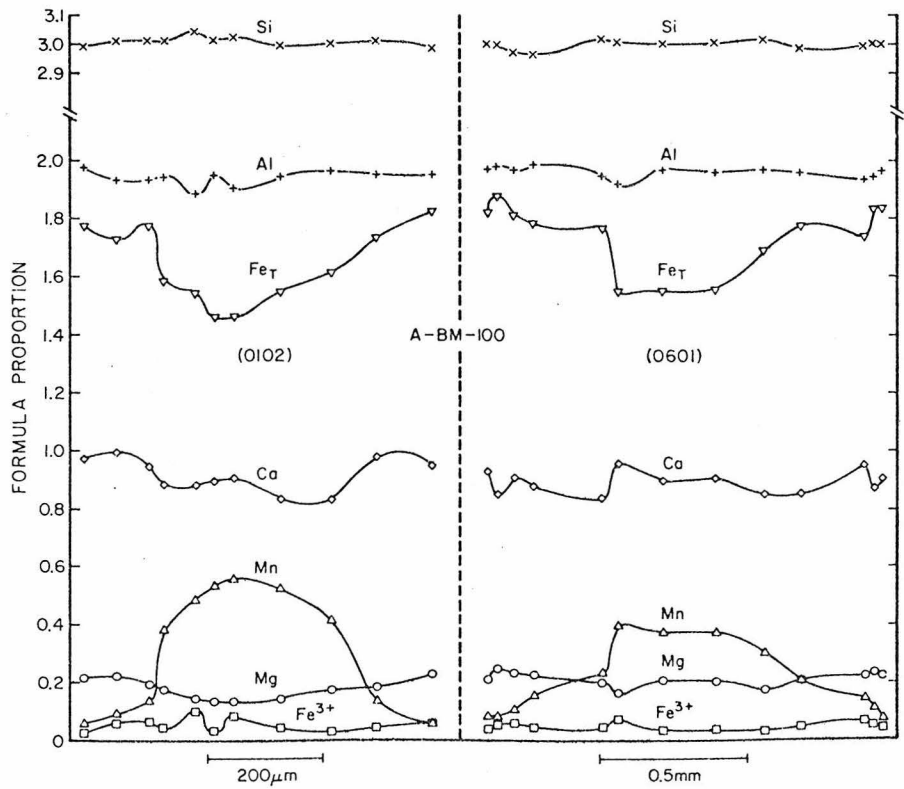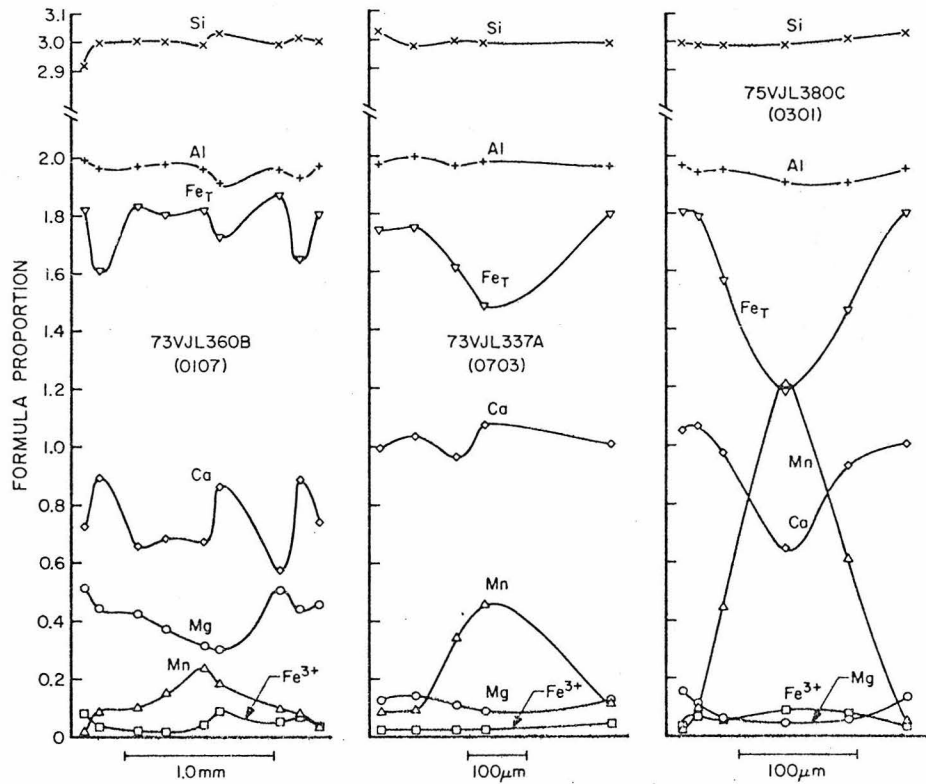
Figure IV-30a

GARNET A-BM-99

Figure IV-30b

CARBONATE

Figure IV-31

SPHENE
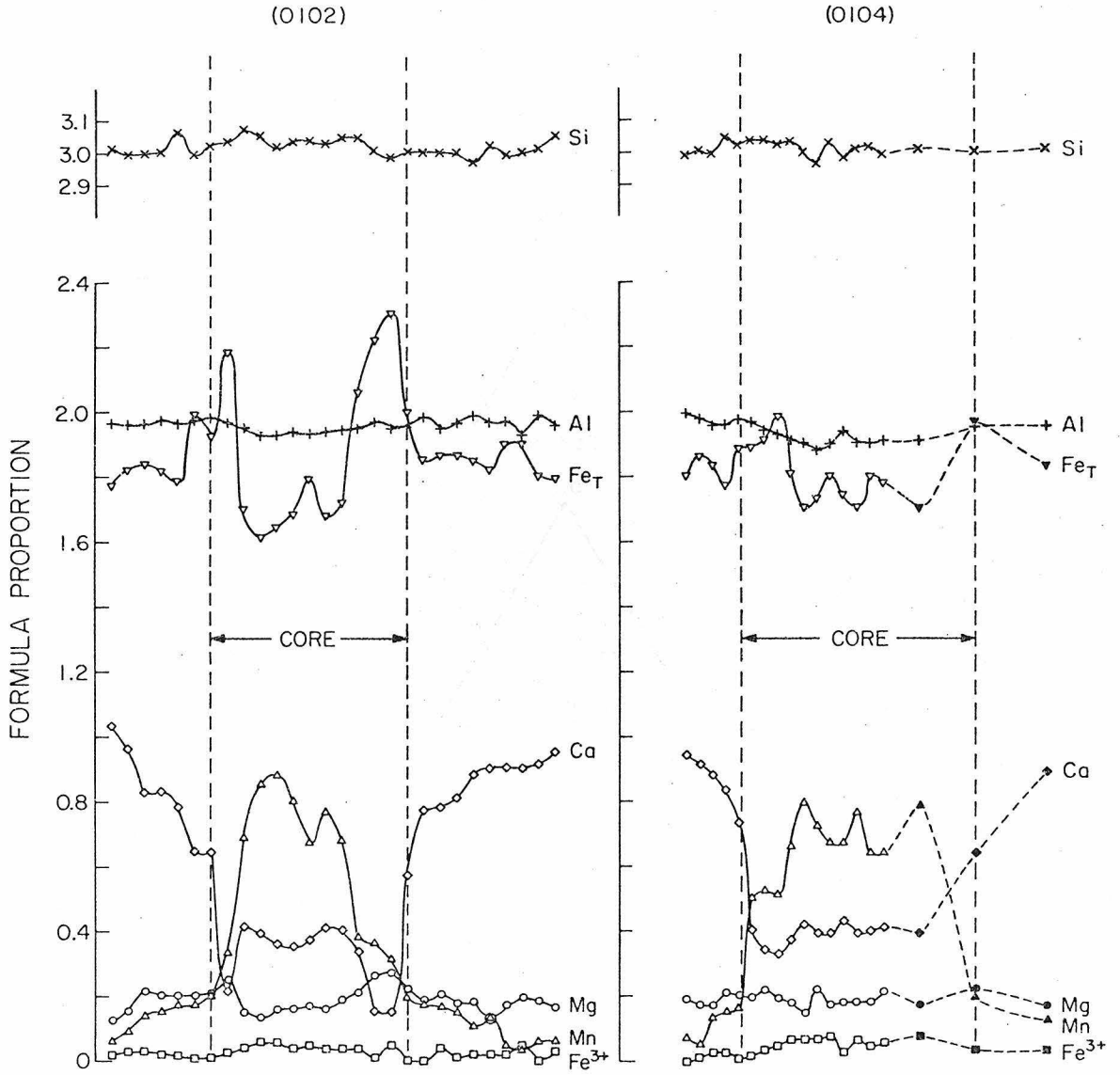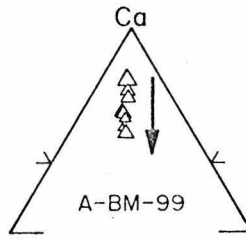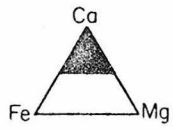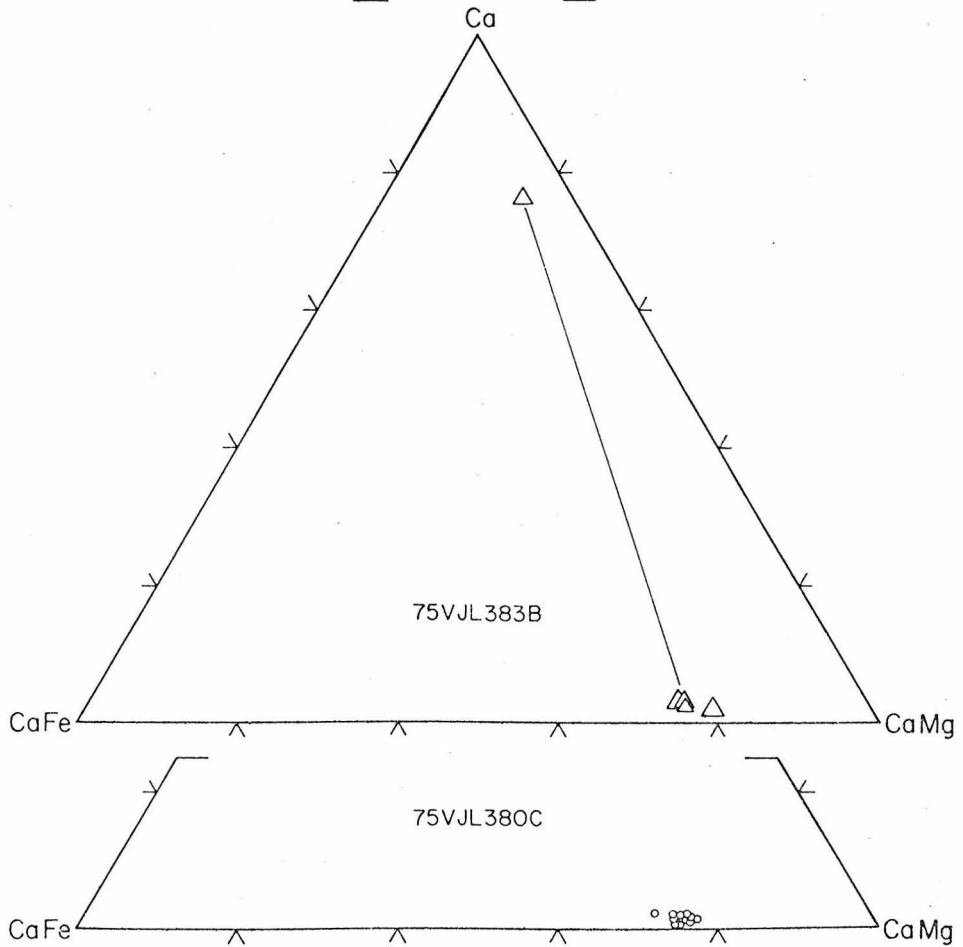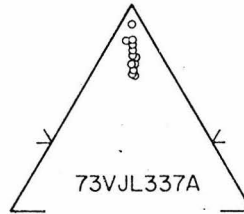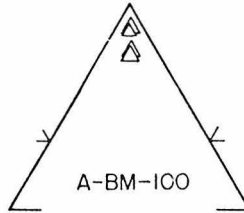
Figure IV-32
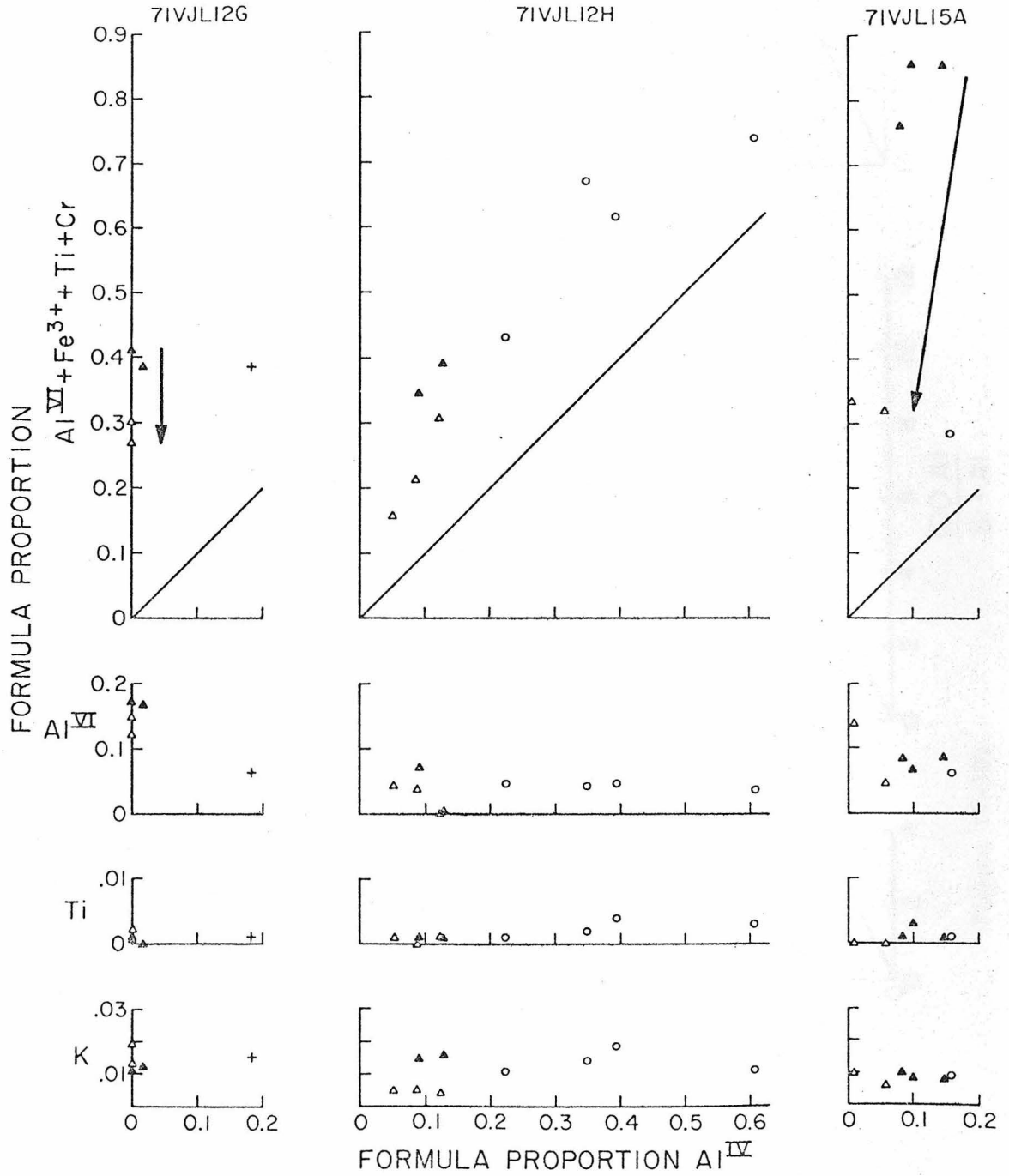
AMPHIBOLE

Figure IV-33a

AMPHIBOLE
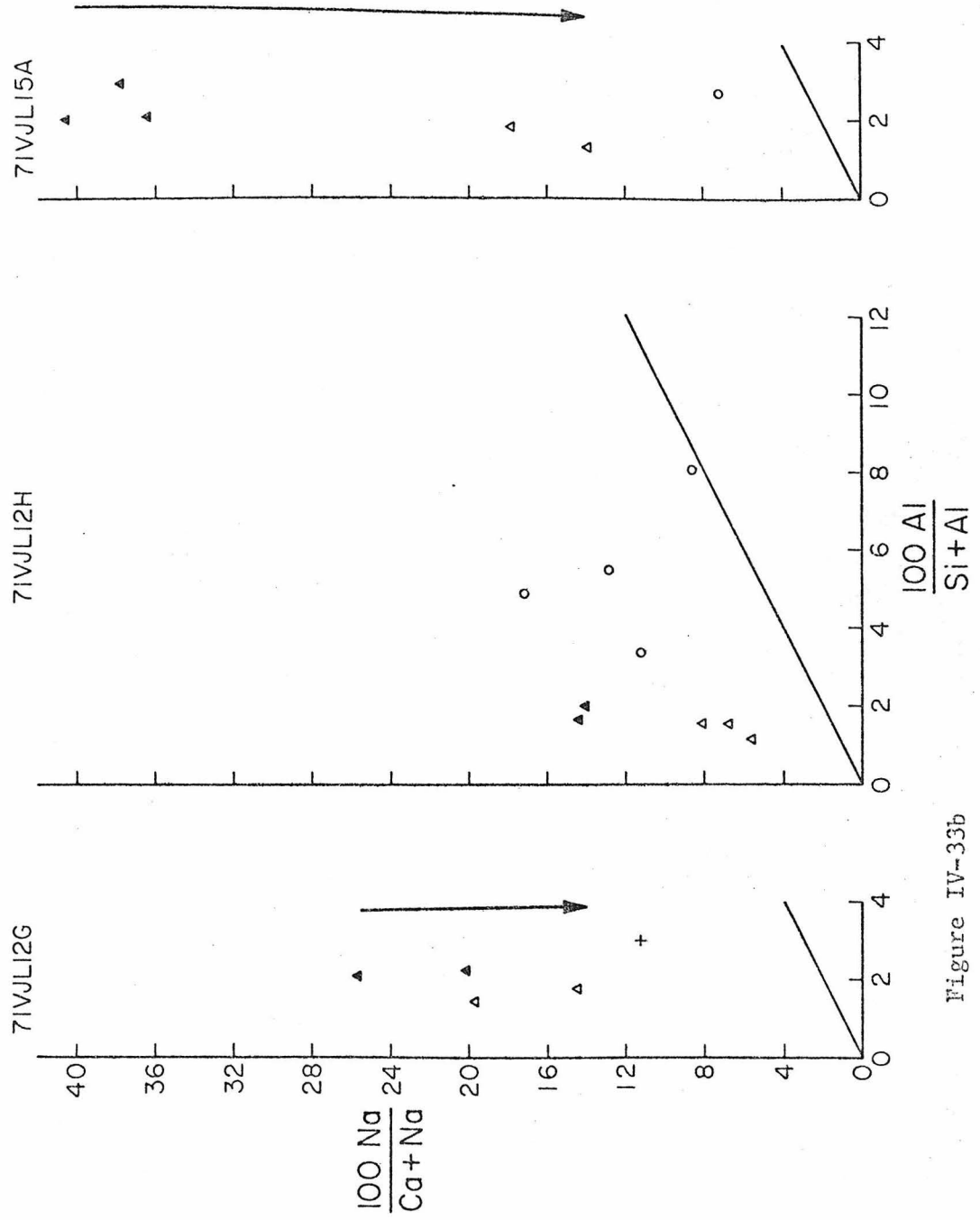
Figure IV-33b

AMPHIBOLE

Figure IV-34a

AMPHIBOLE
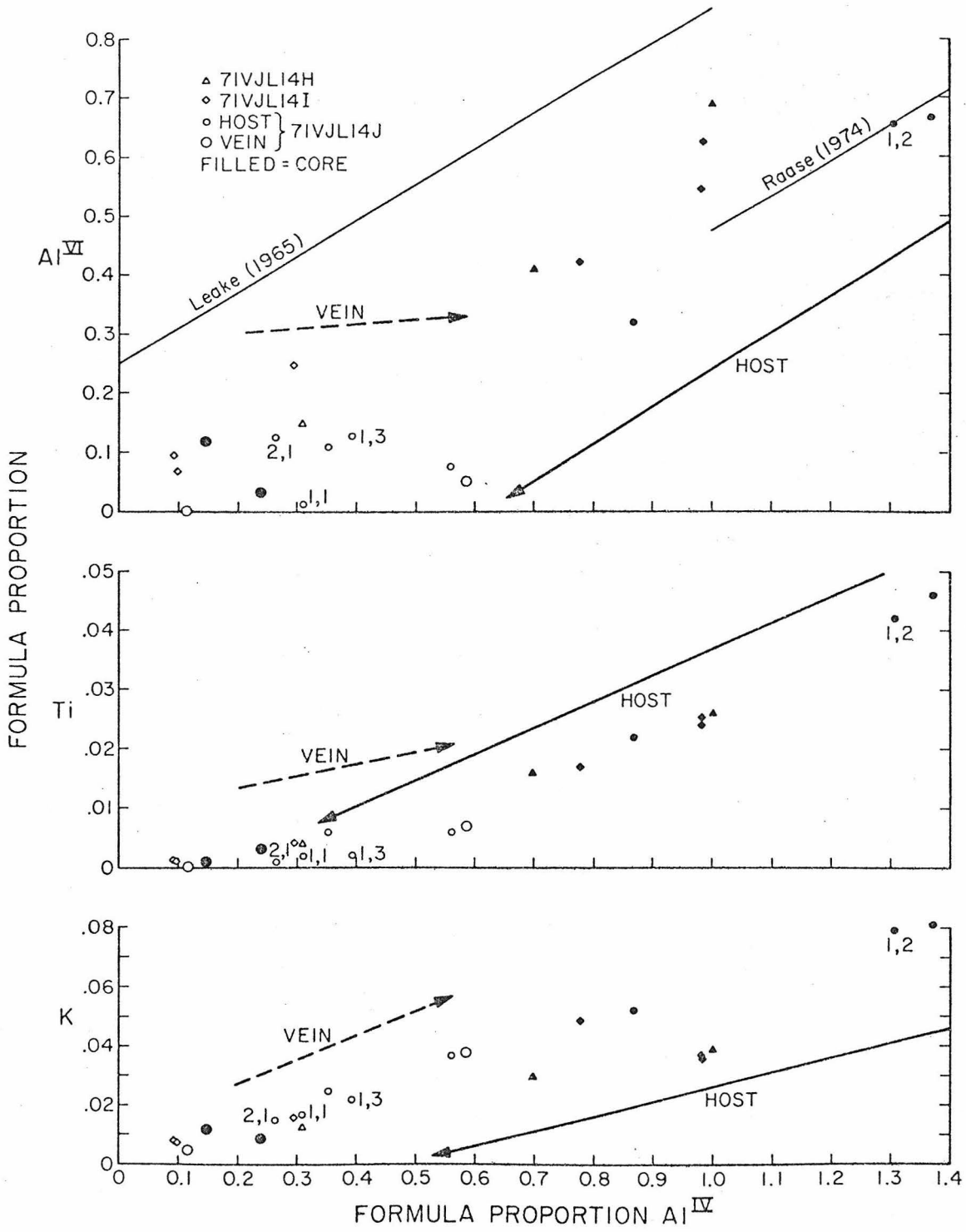
FORMULA PROPORTION Al^{IV}
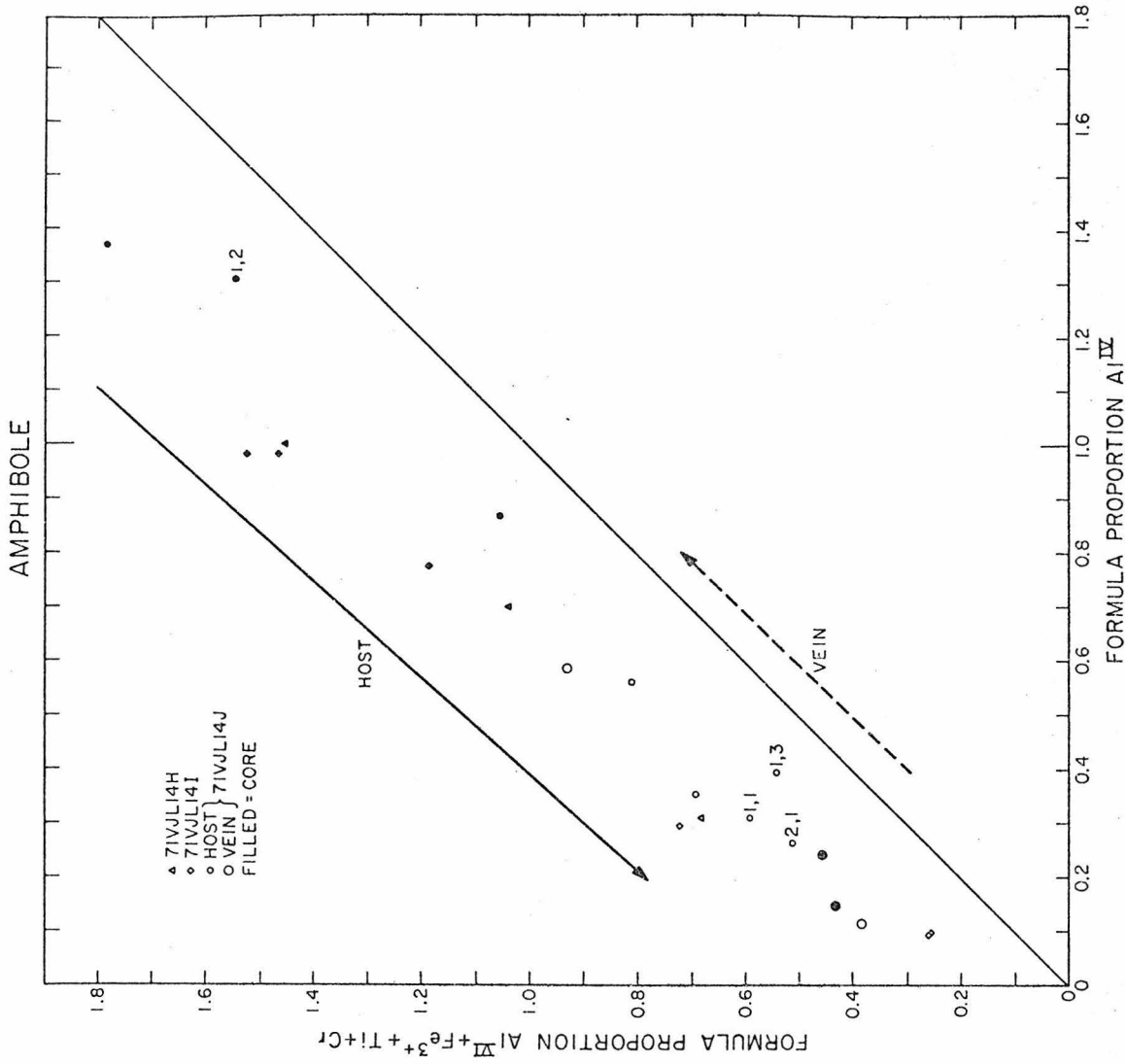
Figure IV-34b

Figure IV-34c

327

Figure IV-35

328
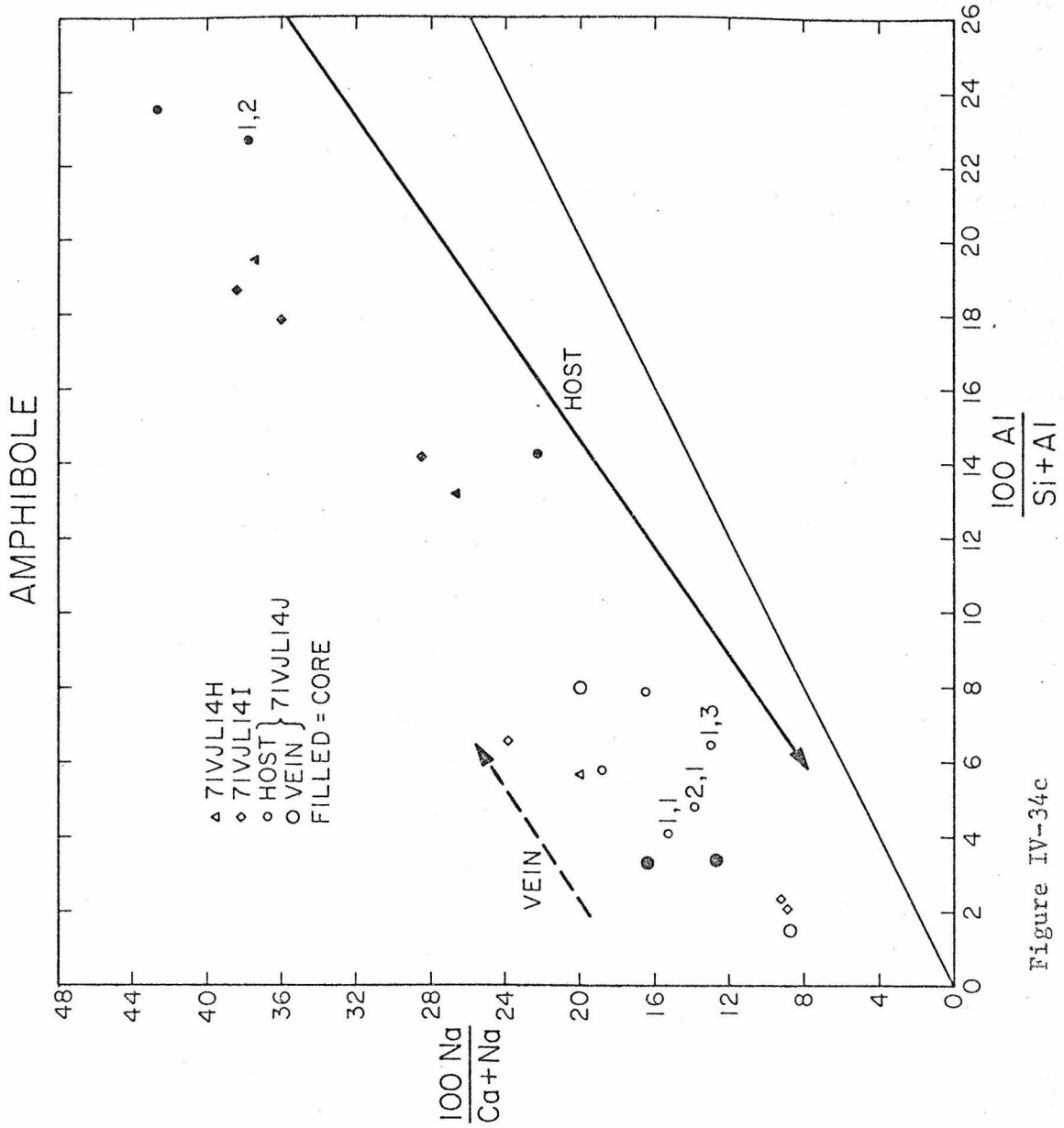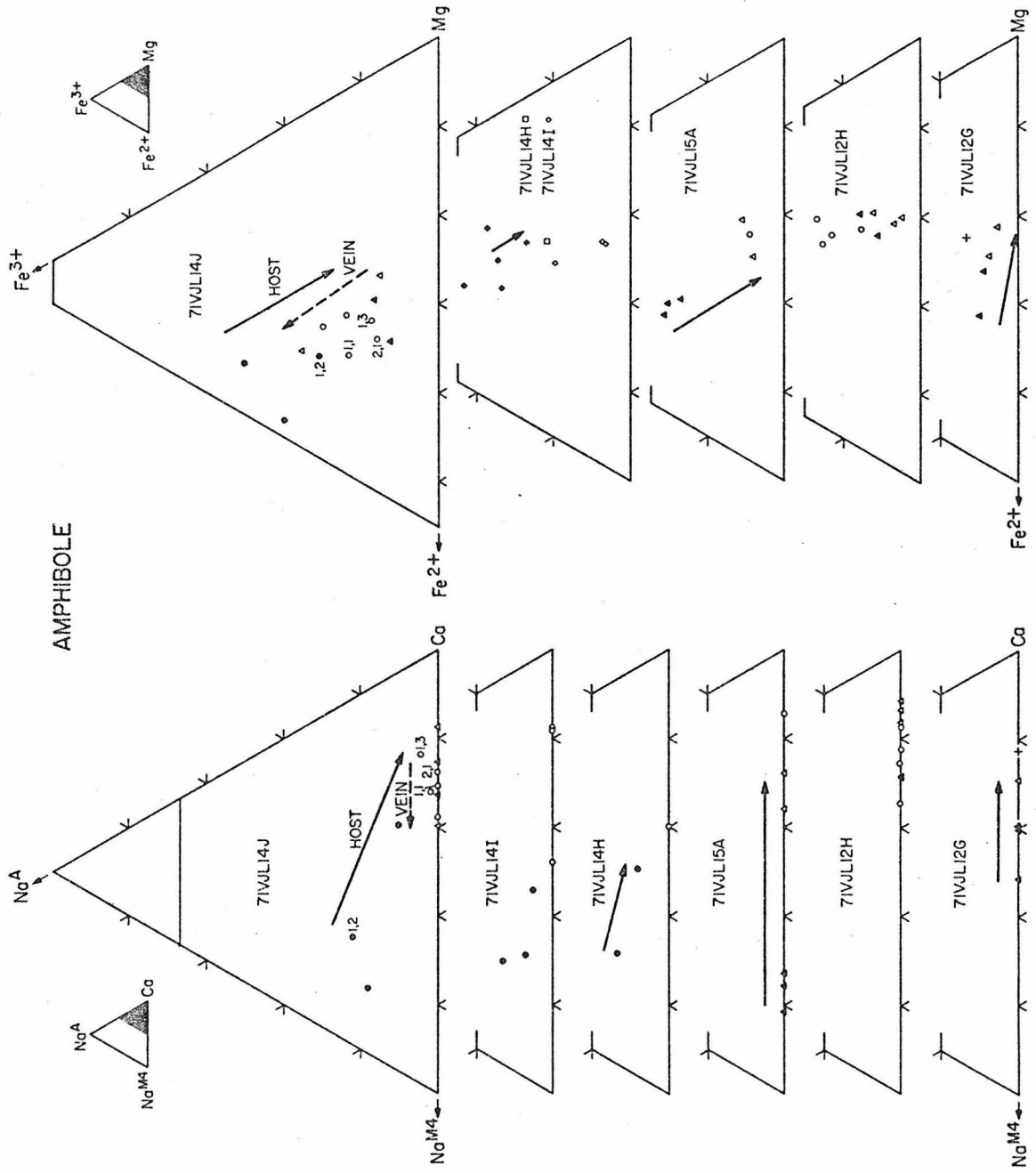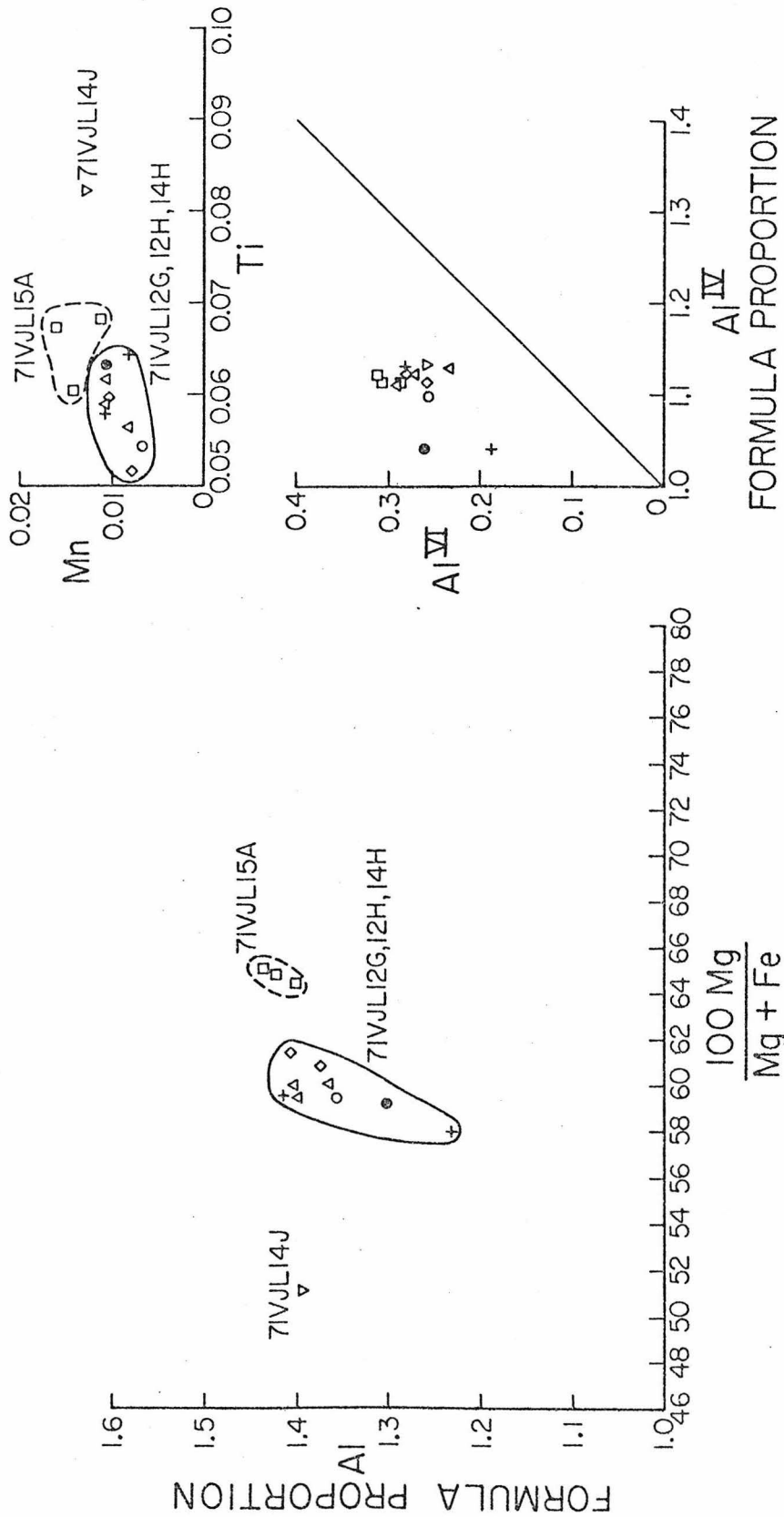
Figure IV-35
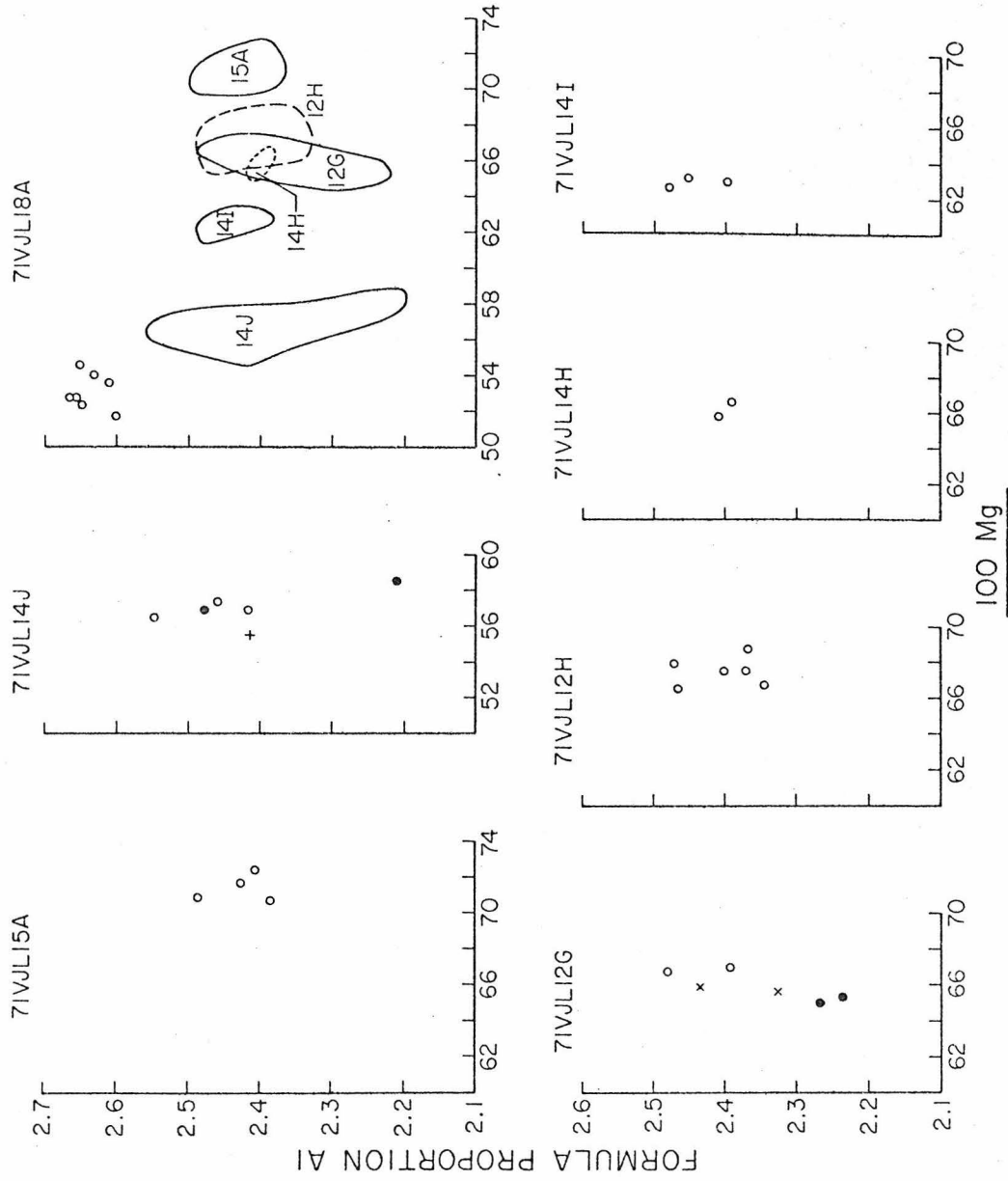
CHLORITE

Figure IV-37a

CHLORITE

FORMULA PROPORTION Al IV

Figure IV-37b

EPIDOTE

FORMULA PROPORTION Fe^{3+}

Figure IV-38

NUMBER

7IVJLI8A

7IVJLI5A

7IVJLI4J

7IVJLI4I

7IVJLI4H

7IVJLI2H

7IVJLI2G

332
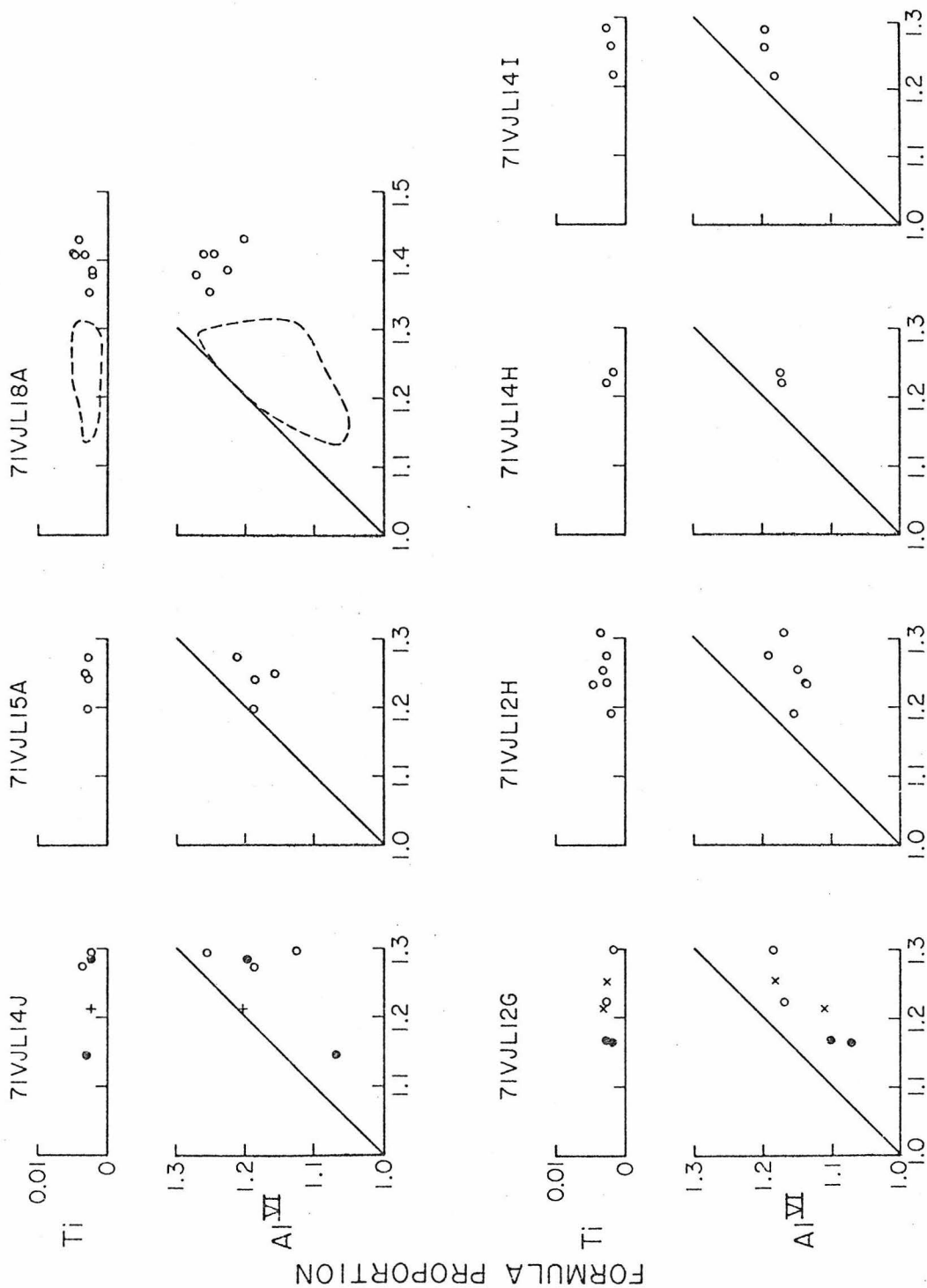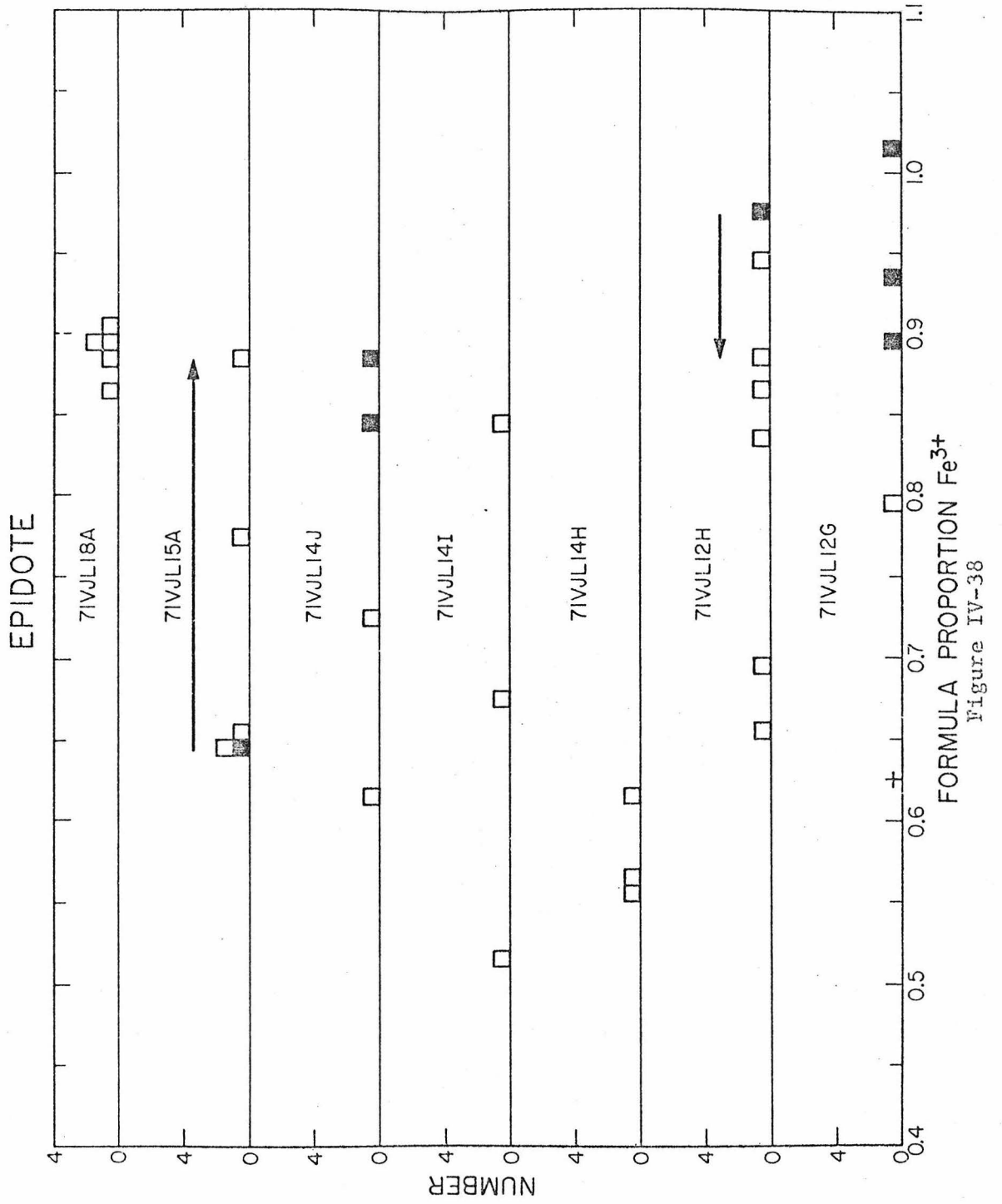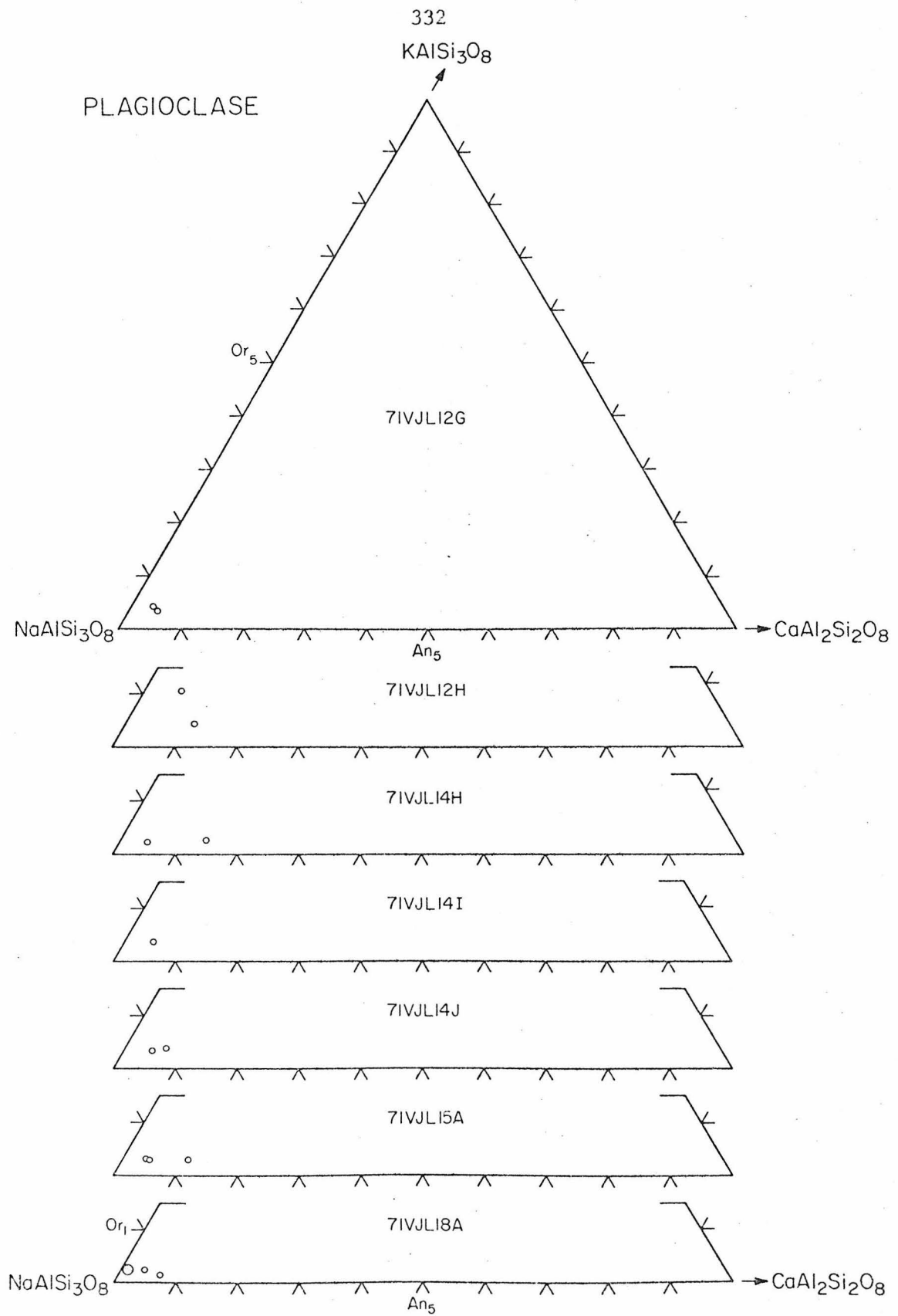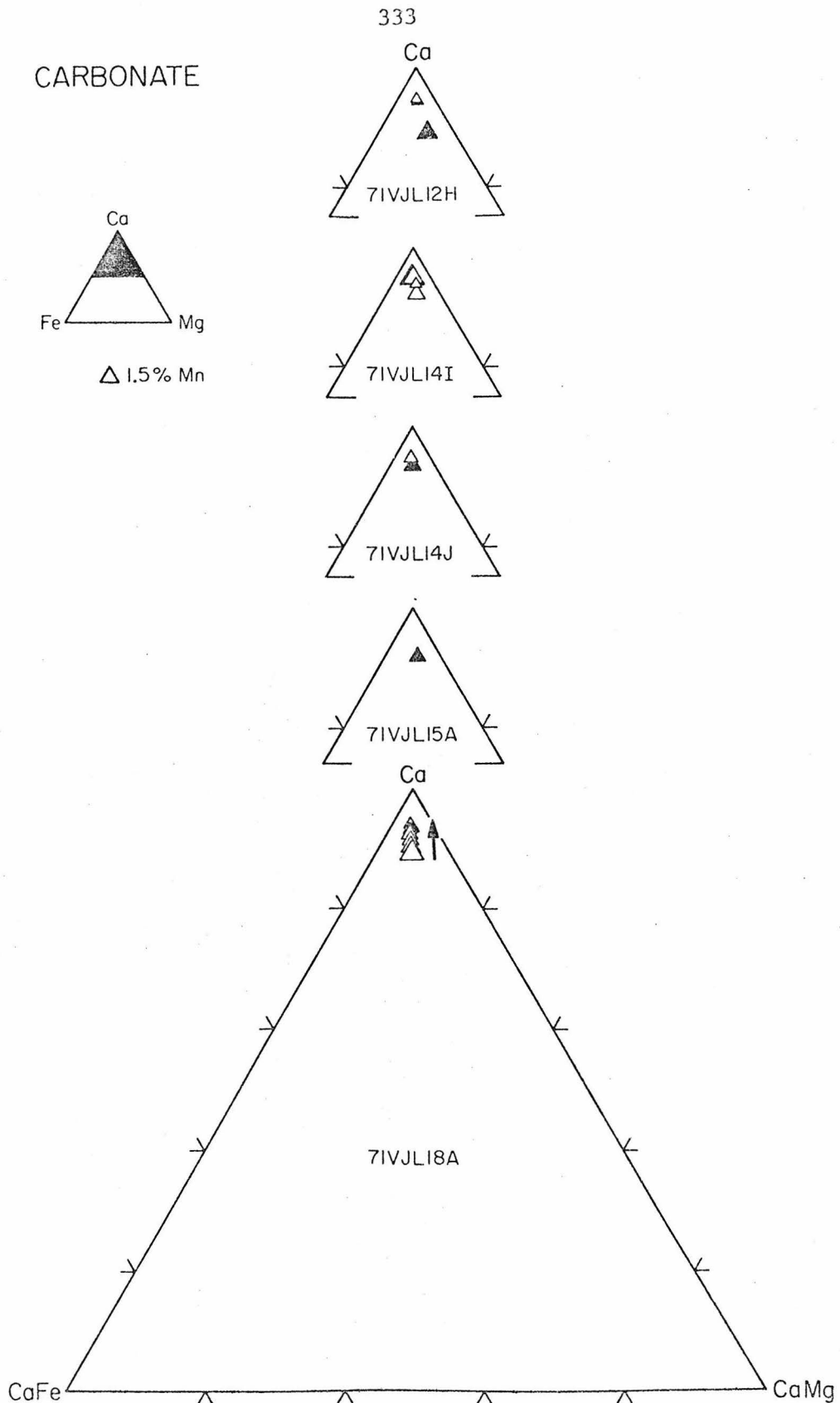
Figure IV-39

Figure IV-40

AMPHIBOLE

Figure IV-41a

335

Figure IV-41b

AMPHIBOLE

Figure IV-41c

Figure IV-42a

AMPHIBOLE

Figure IV-42b

AMPHIBOLE

Mg

Fe^{3+}

Fe^{2+}

71VJL44

Fe^{3+}

Fe^{2+}

71VJL50B

Na^A

Ca

Na^A

$NaM4$

71VJL44

$NaM4$
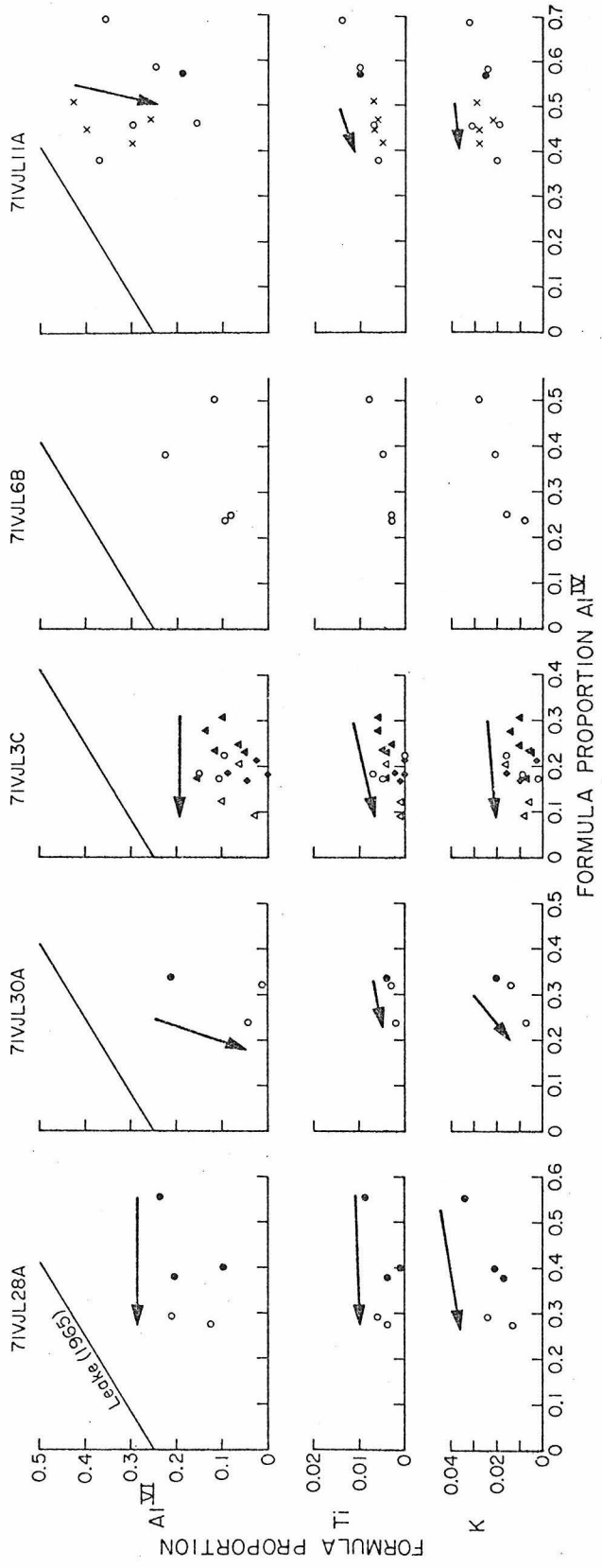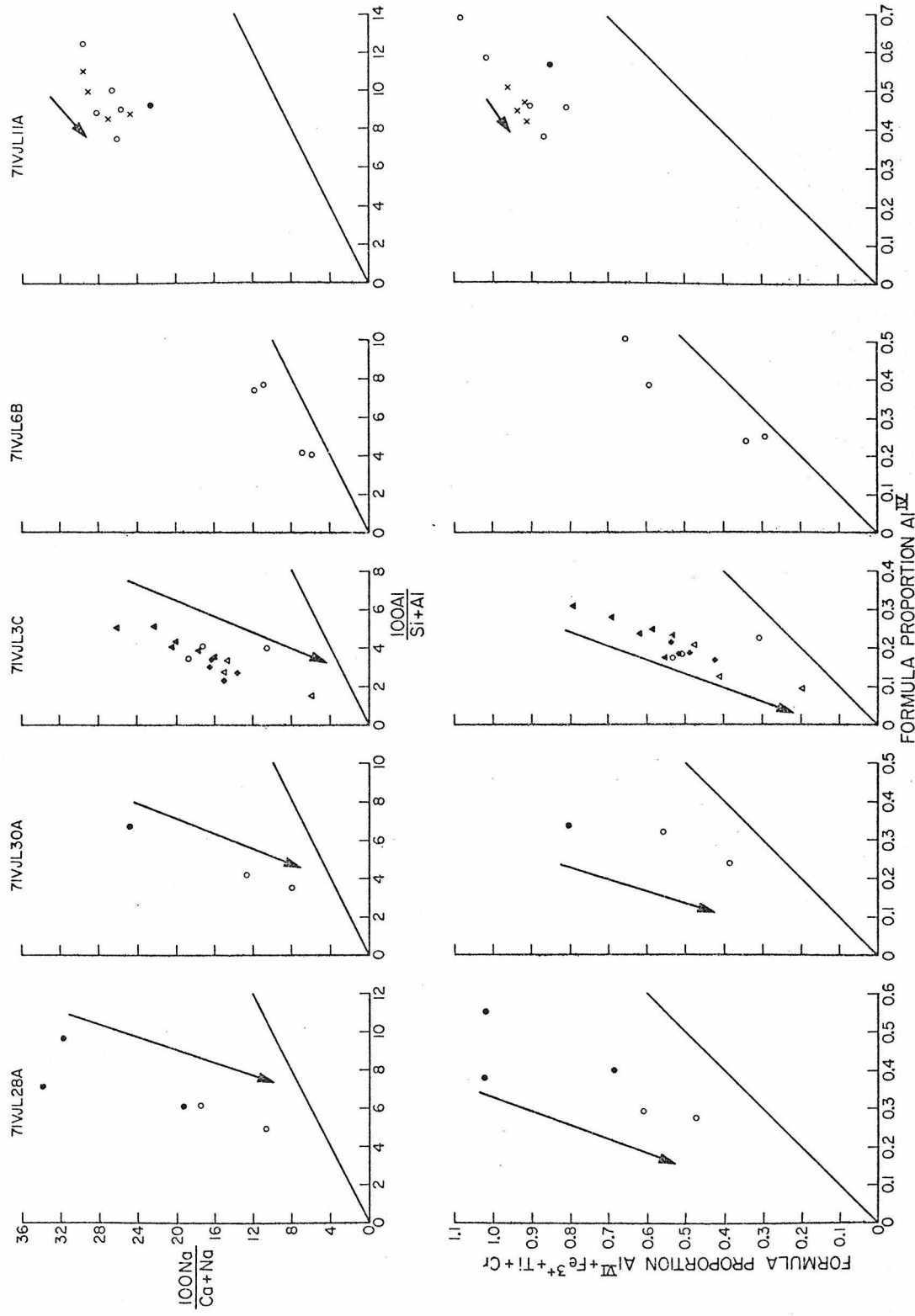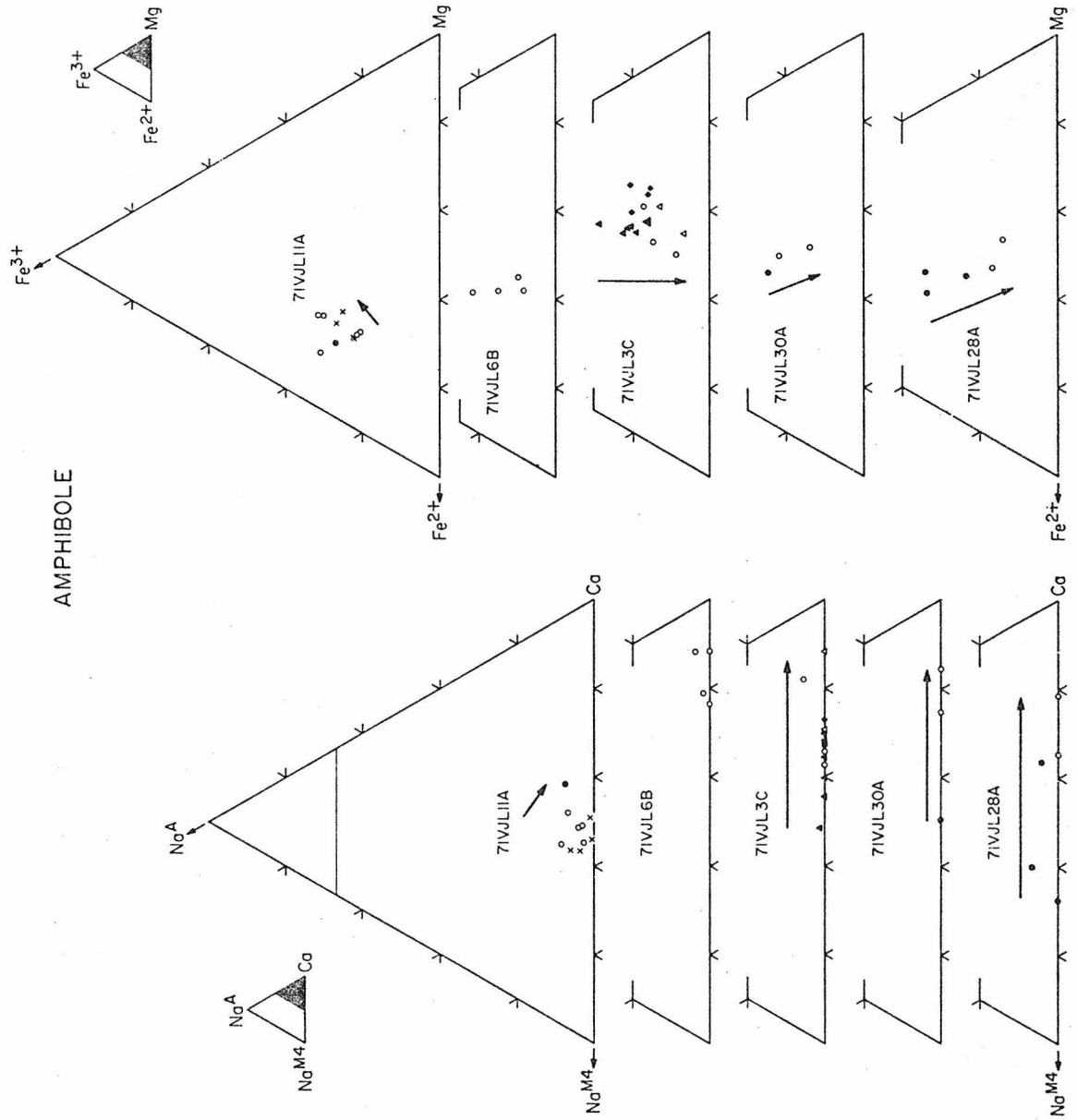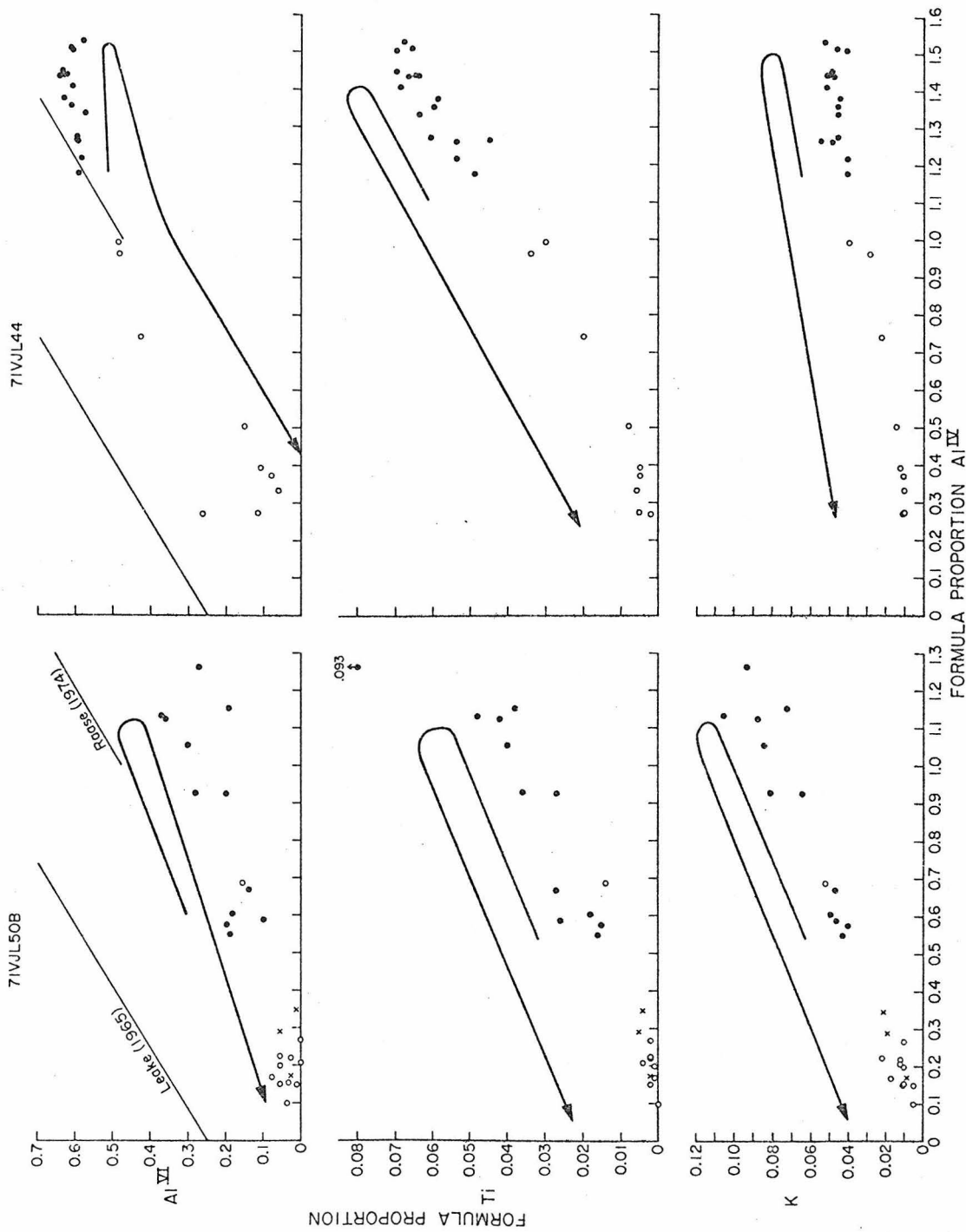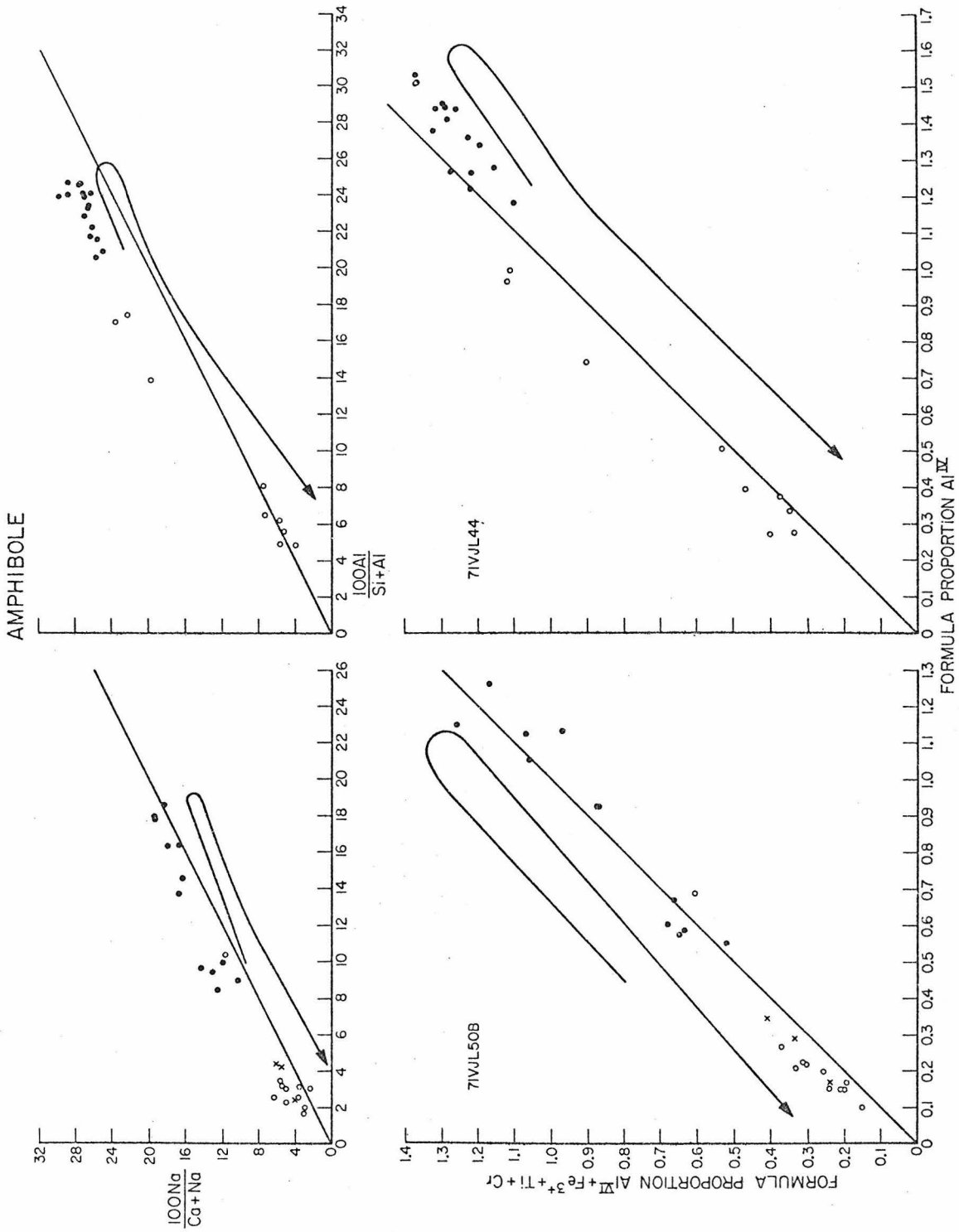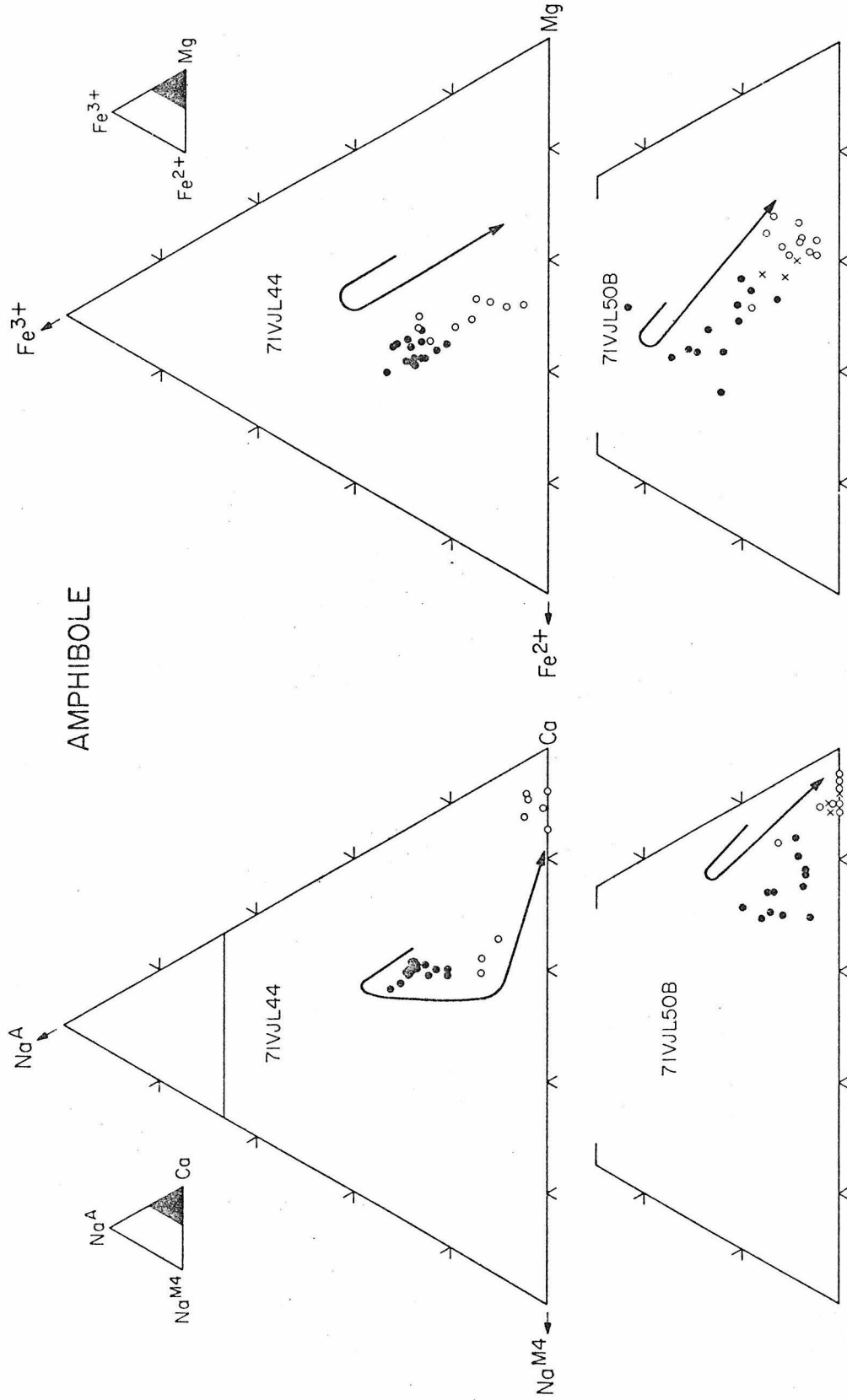
71VJL50B

Figure IV-42c

AMPHIBOLE 7IVJL5B
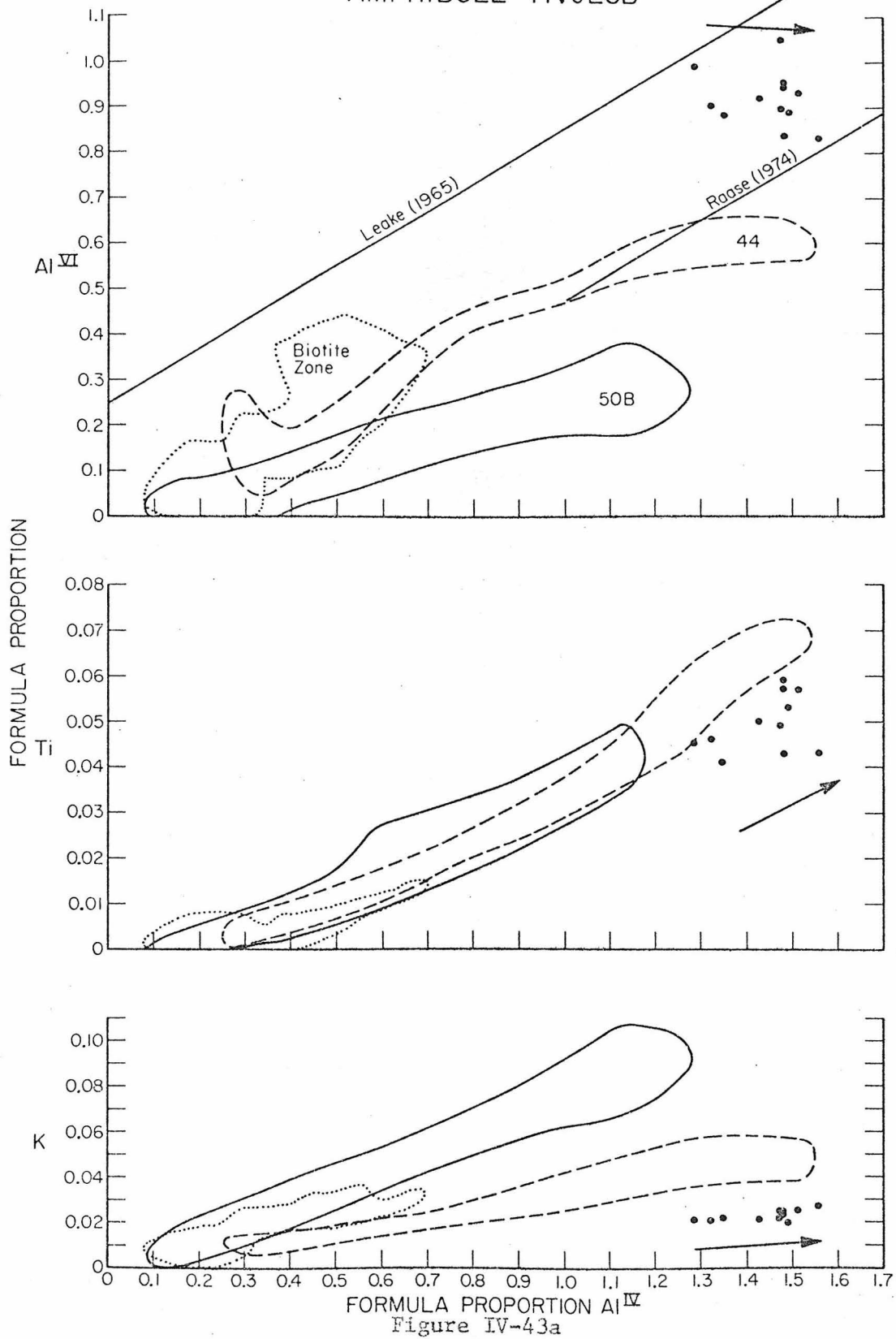
Figure IV-43a

AMPHIBOLE 7IVJL5B

Figure IV-43b

AMPHIBOLE
7IVJL5B
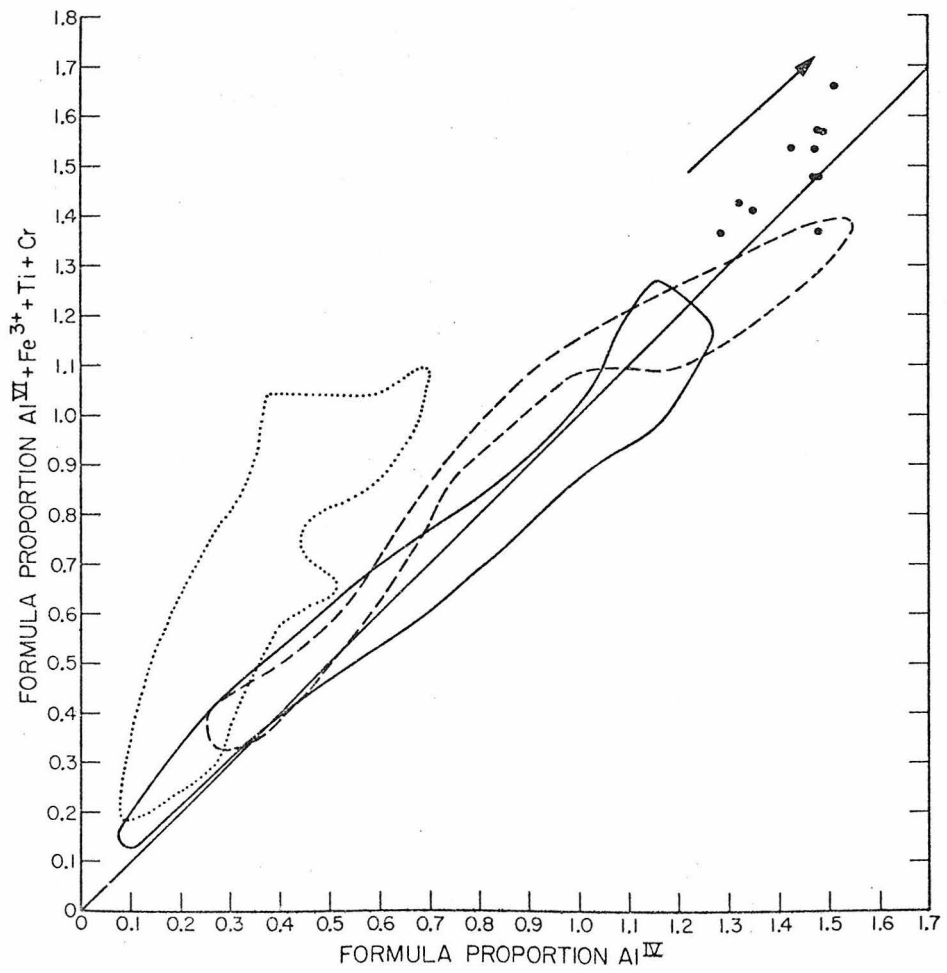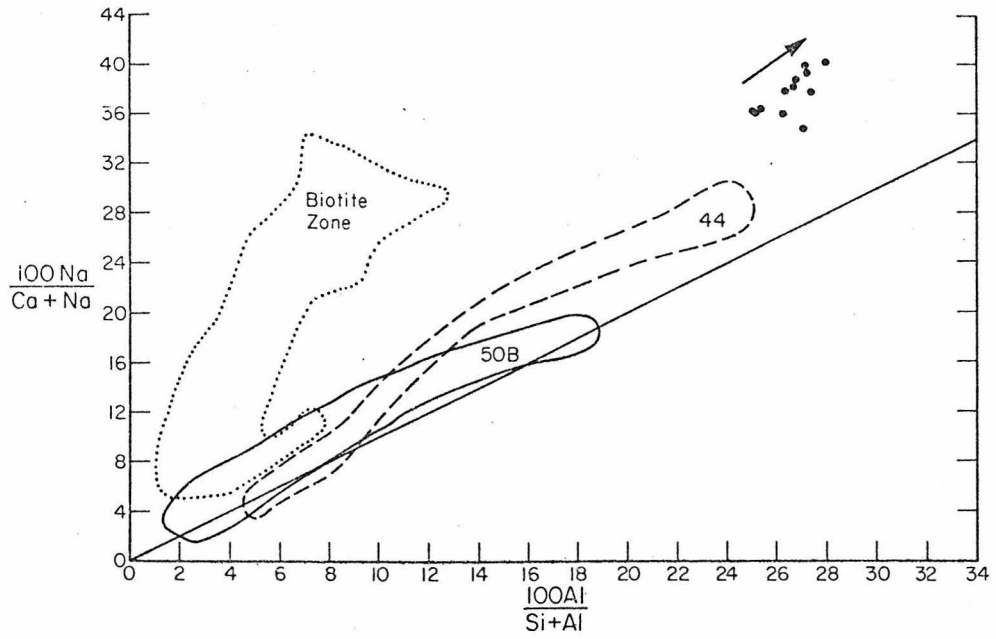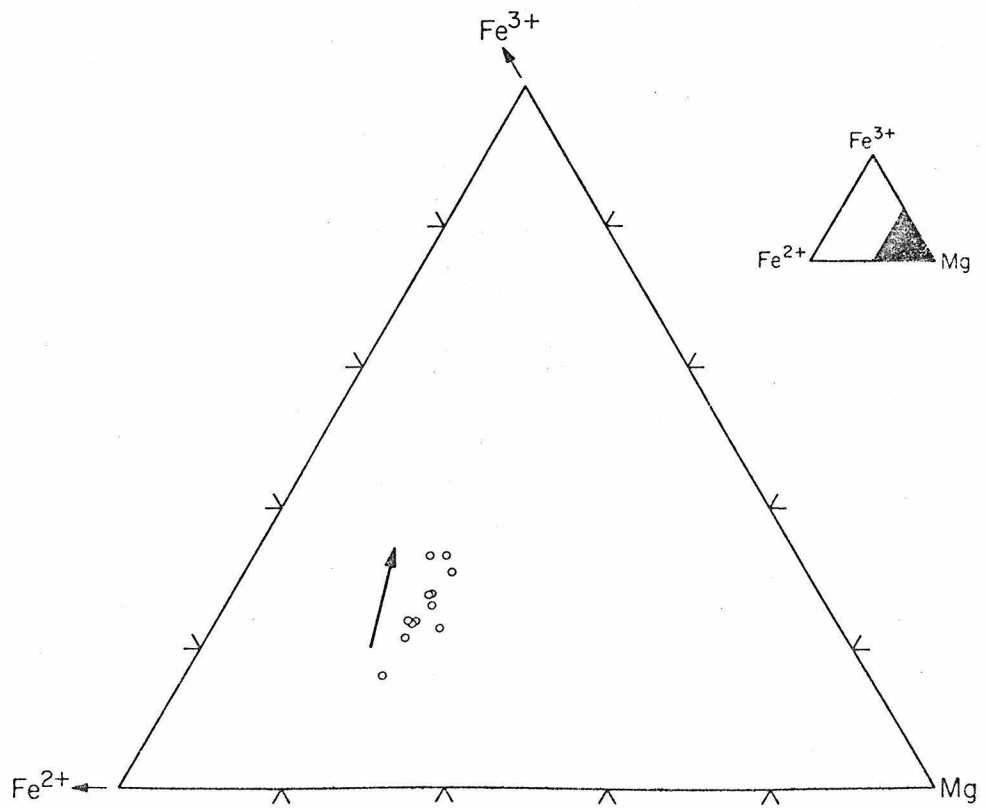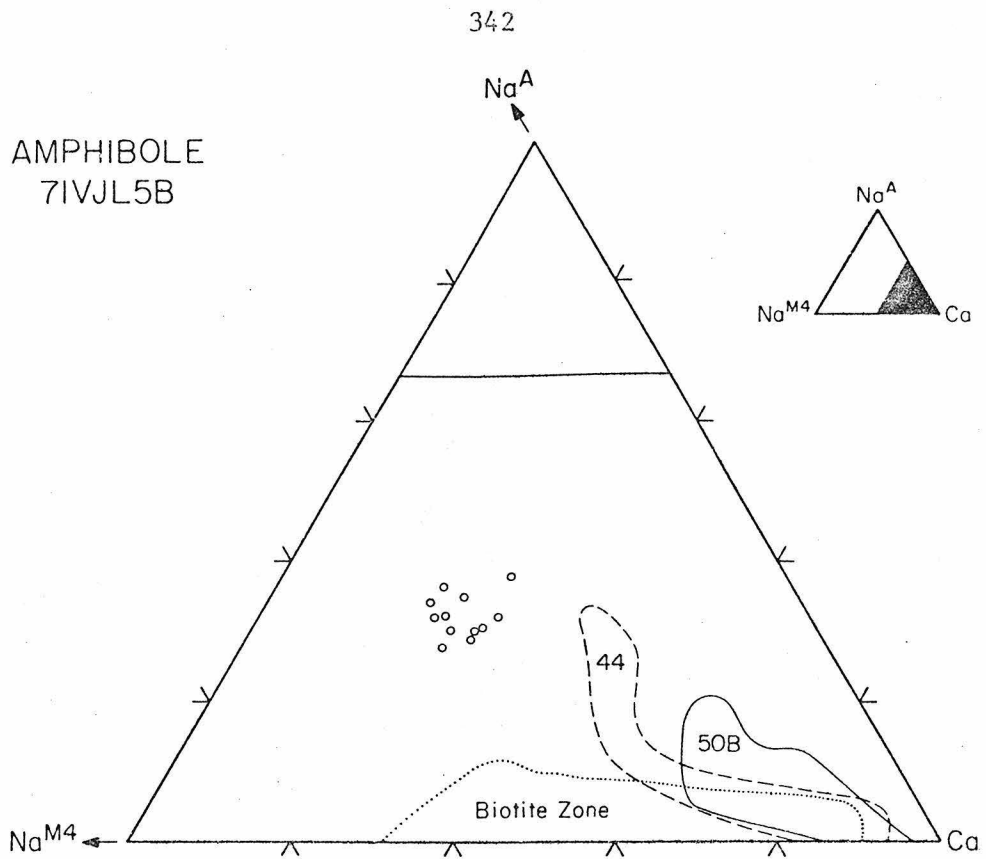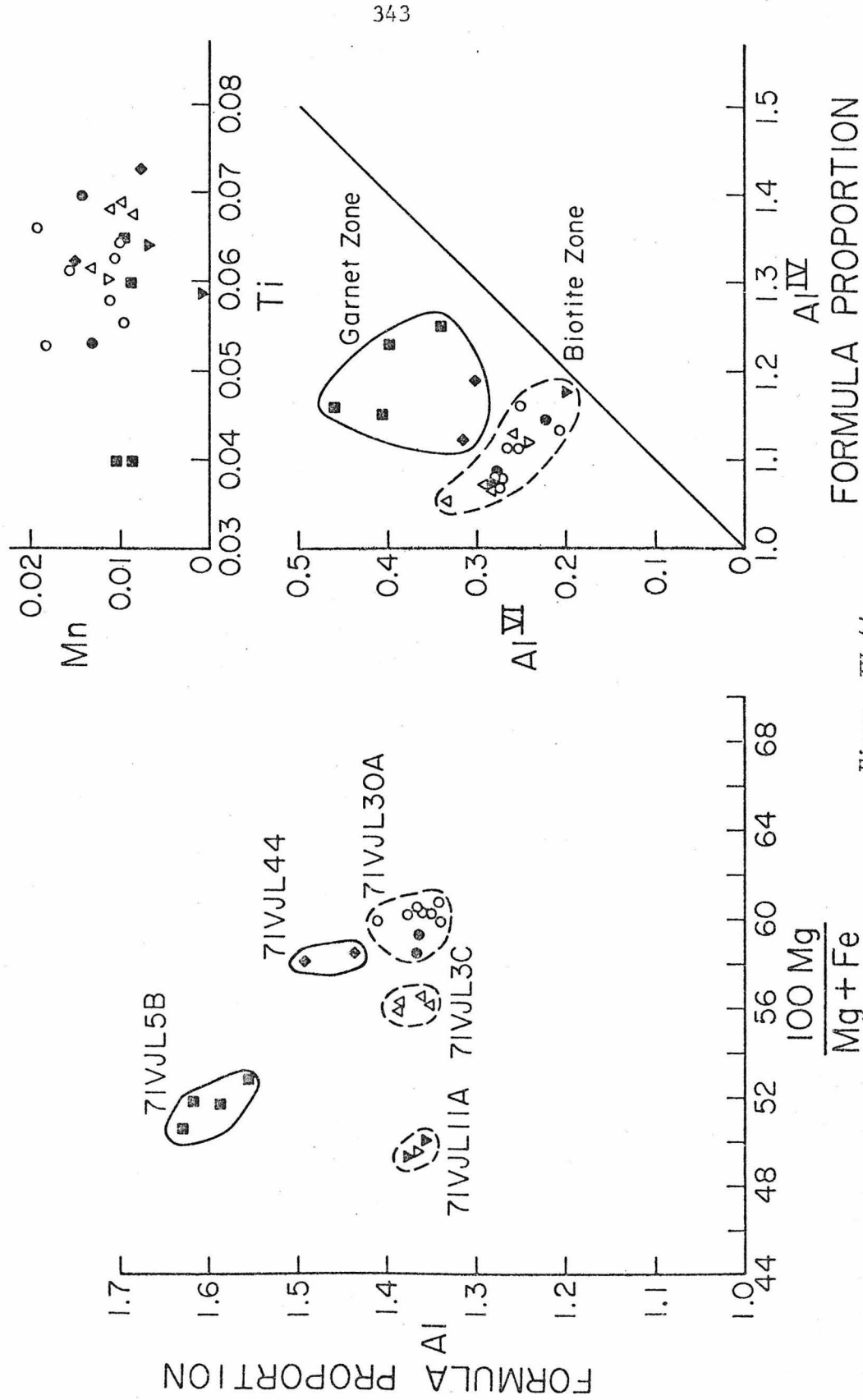
Figure IV-43c

Figure IV-44

WHITE MICA
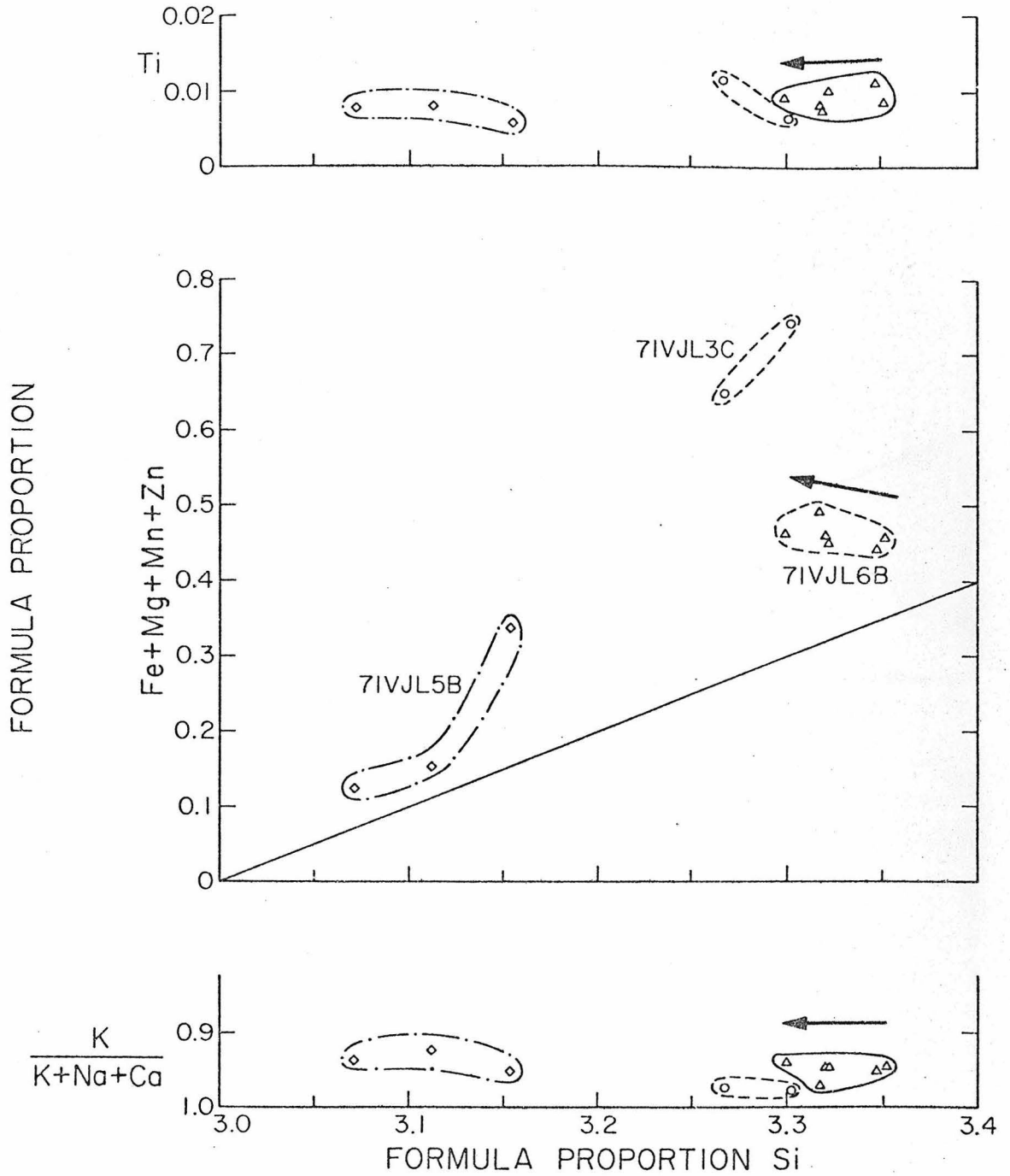
Figure IV-45a

WHITE MICA 7IVJL3H

Figure IV-45b

WHITE MICA

PARAGONITE

MUSCOVITE

7IVJL3H

7IVJL3C

7IVJL5B

7IVJL6B

Fe^{3+}

Fe^{3+}

Mg

Mg

Fe^{2+}
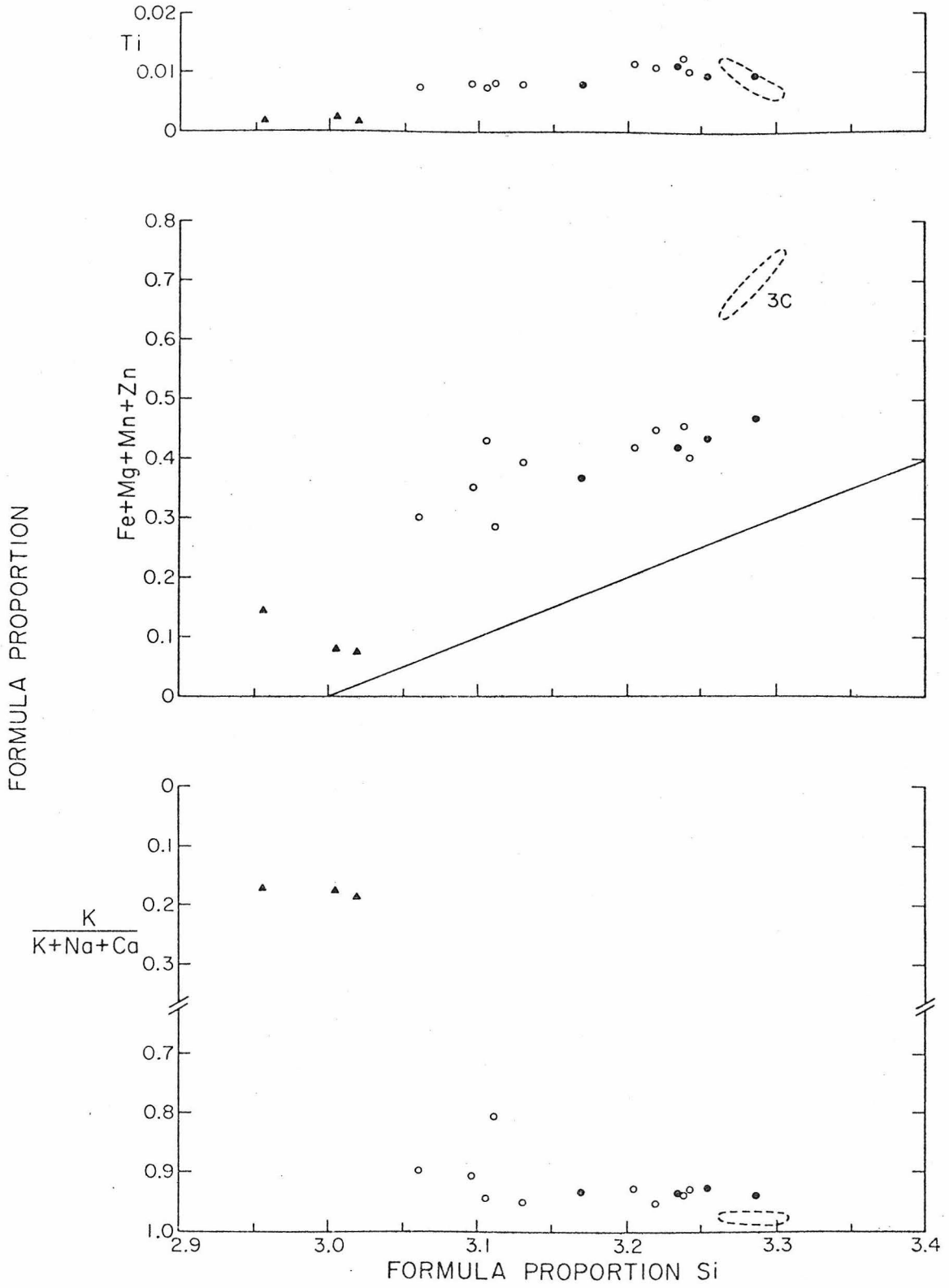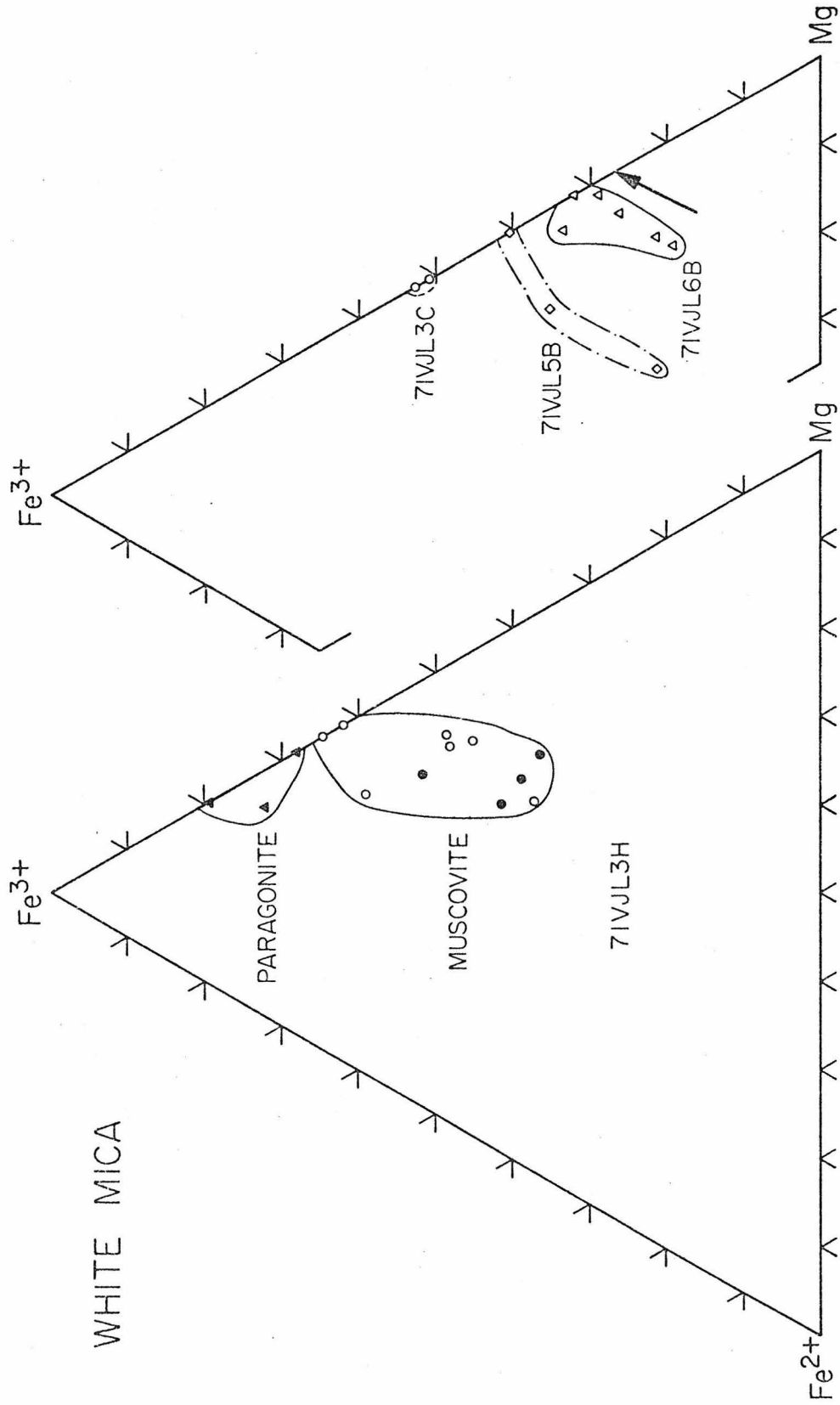
Figure IV-45c

CHLORITE

Figure IV-46

Figure IV-47

PLAGIOCLASE

KAlSi$_3$O$_8$

7IVJL5B

Or$_5$

NaAlSi$_3$O$_8$

An$_5$

CaAl$_2$Si$_2$O$_8$

Or$_1$

7IVJL44

Or$_1$

GARNET ISOGRAD

7IVJL11A

7IVJL6B

7IVJL3H

7IVJL3C

7IVJL30A

Or$_1$

7IVJL28A

NaAlSi$_3$O$_8$

An$_5$

CaAl$_2$Si$_2$O$_8$
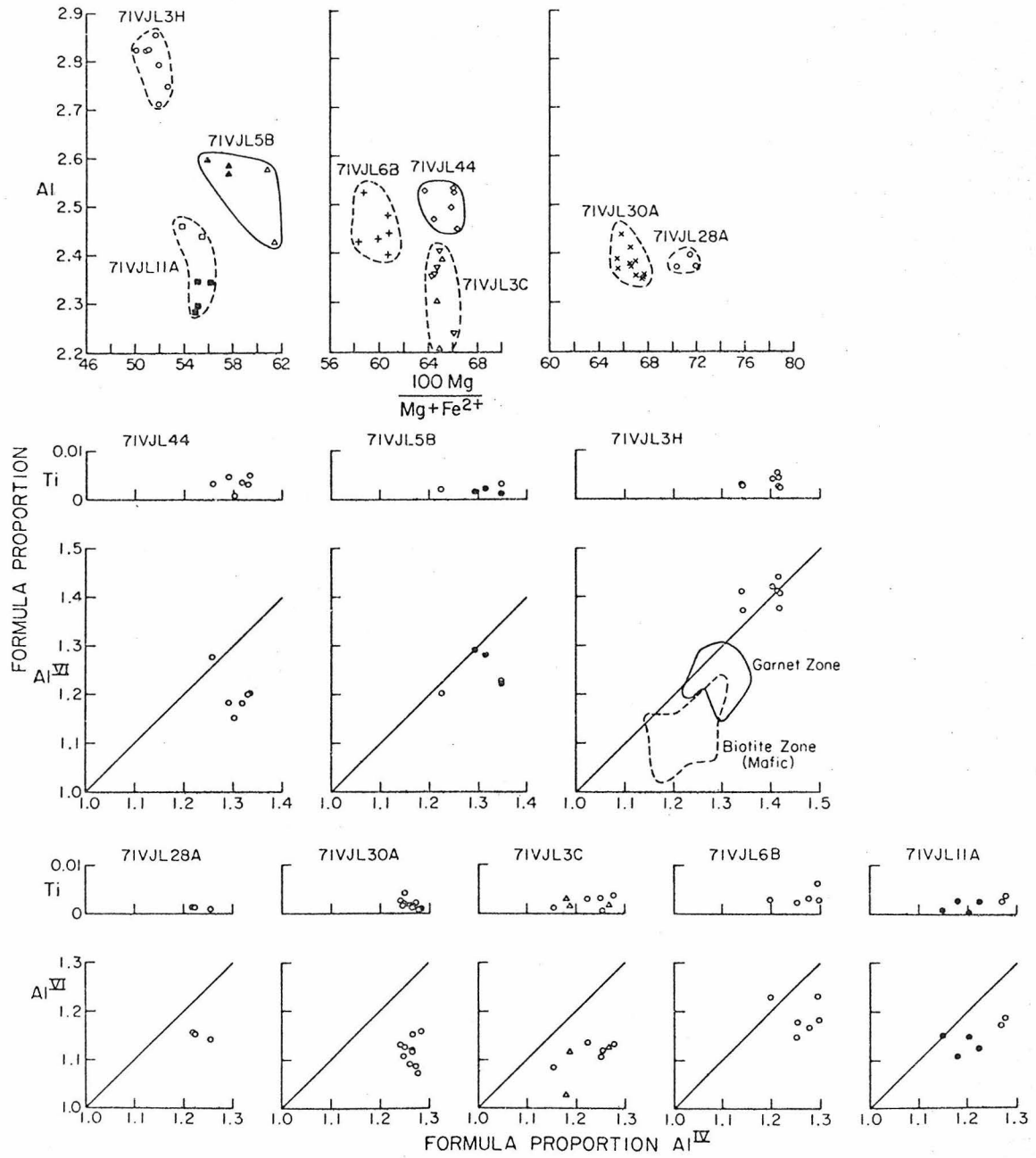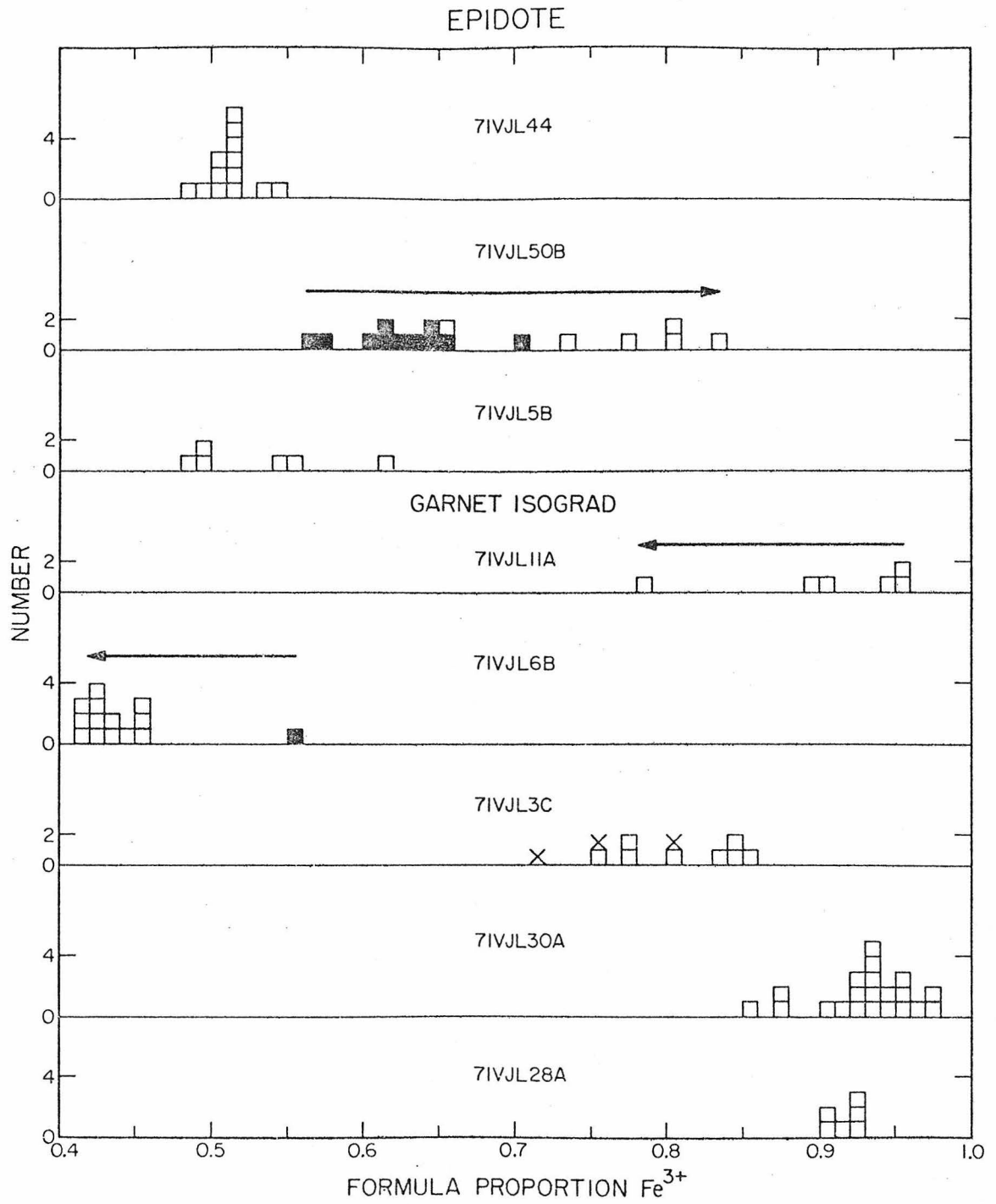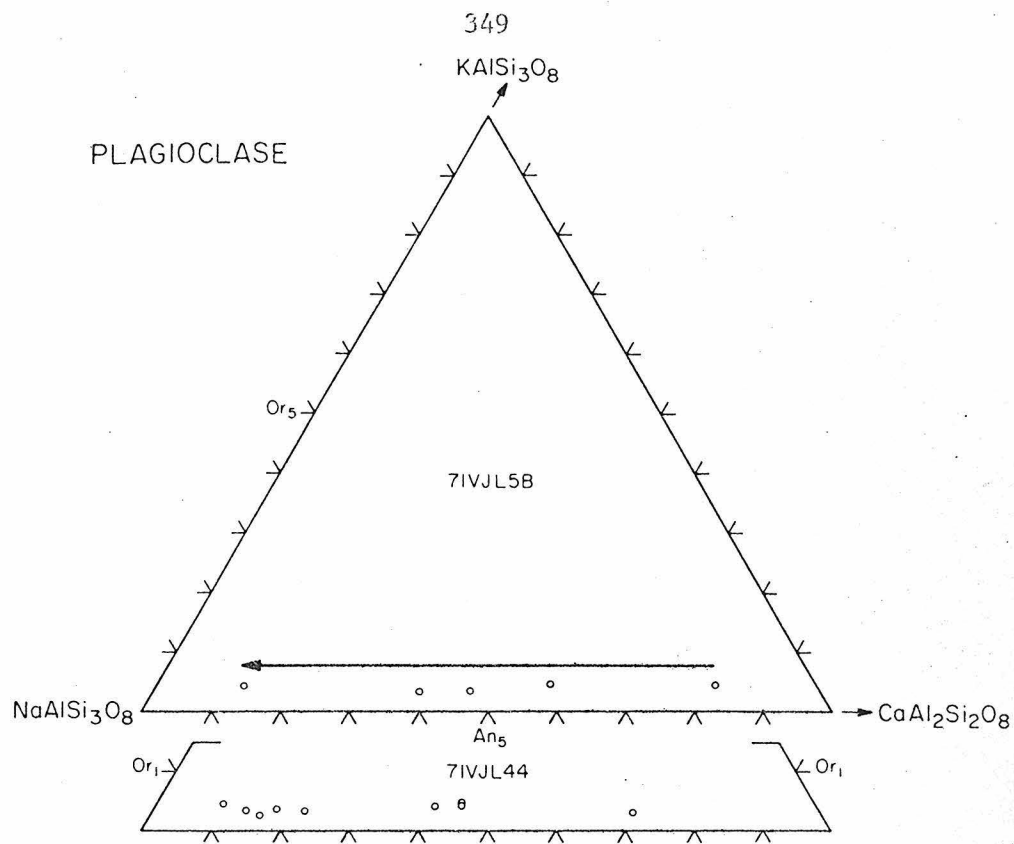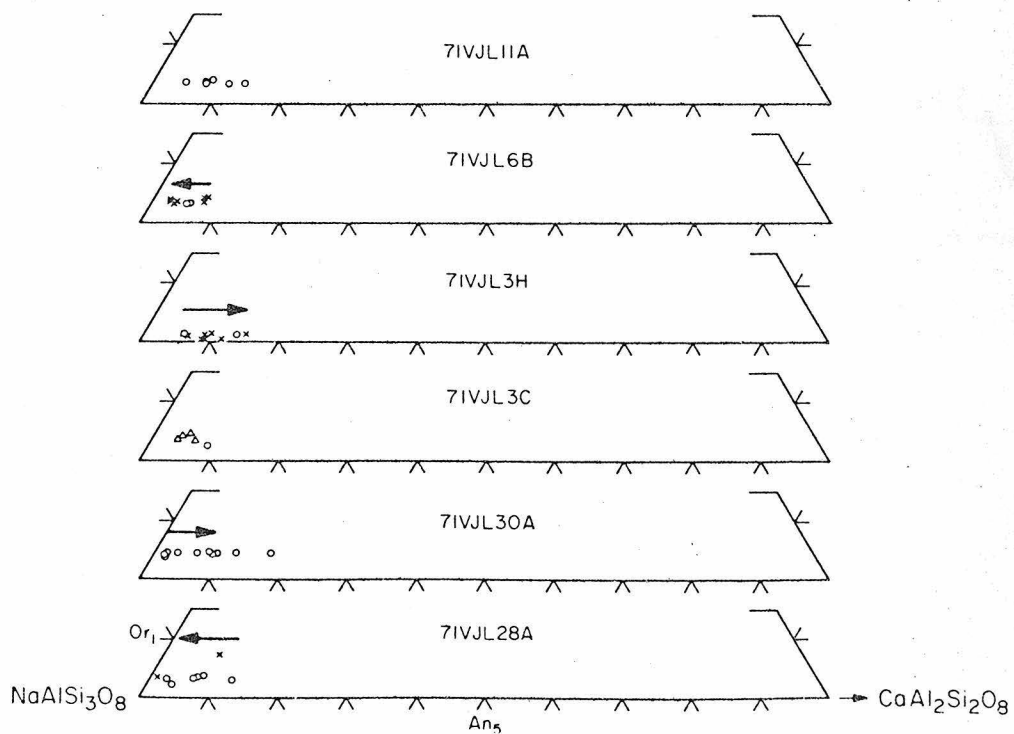
Figure IV-48

PLAGIOCLASE 7IVJL5B

Figure IV-49

GARNET

7IVJL3H

7IVJL5B

} 5% Mg

Ca

Ca

Fe²⁺

Fe²⁺

Mn

Mn

Mn

7IVJL3H

7IVJL5B

Fe²⁺

Mg

Ca

Ca

Figure IV-50

CARBONATE

Ca

Fe — Mg

△ 2% Mn

Ca

7IVJL44

7IVJL28A

7IVJL3OA

7IVJLIIA

Ca

7IVJL3C

7IVJL3H

CaFe

CaMg

Figure IV-51

SPHENE
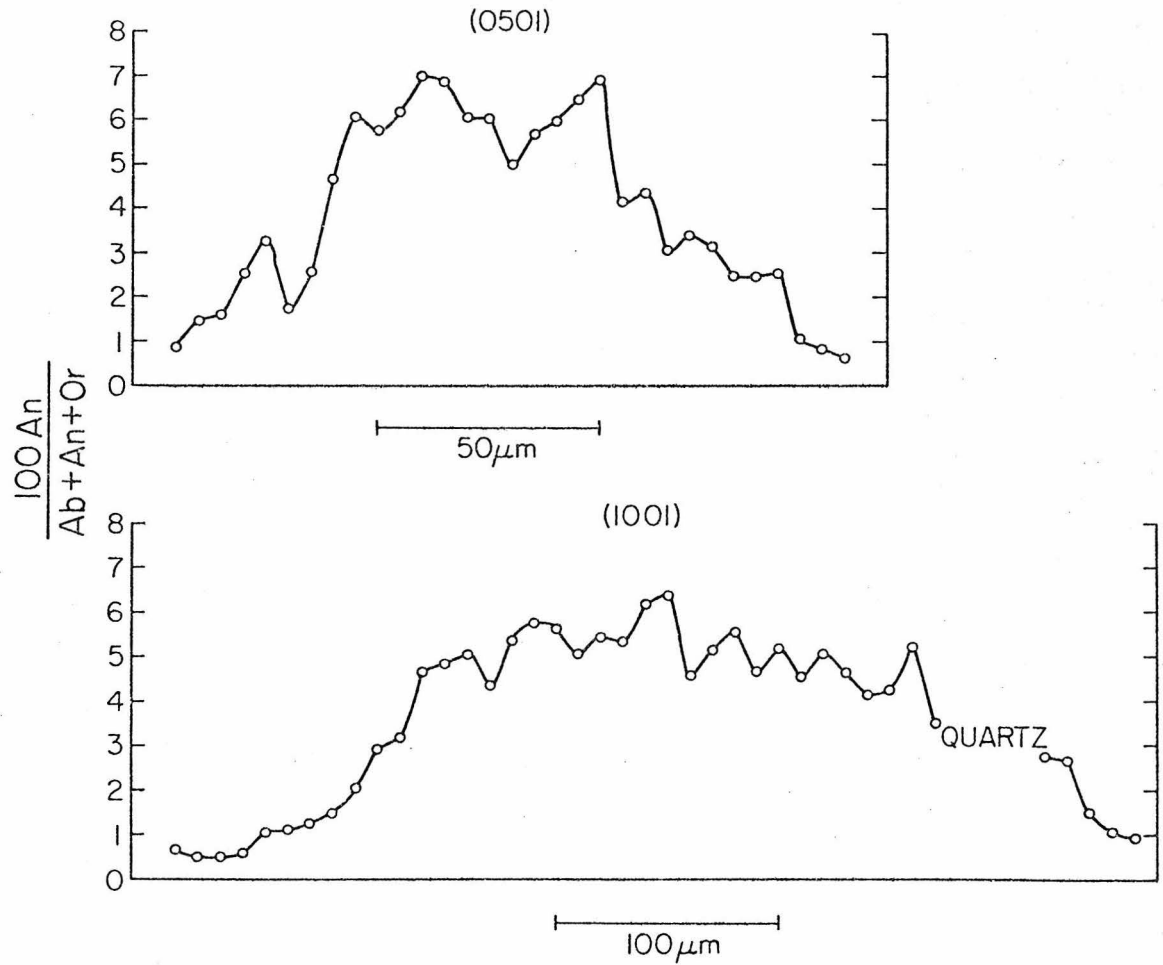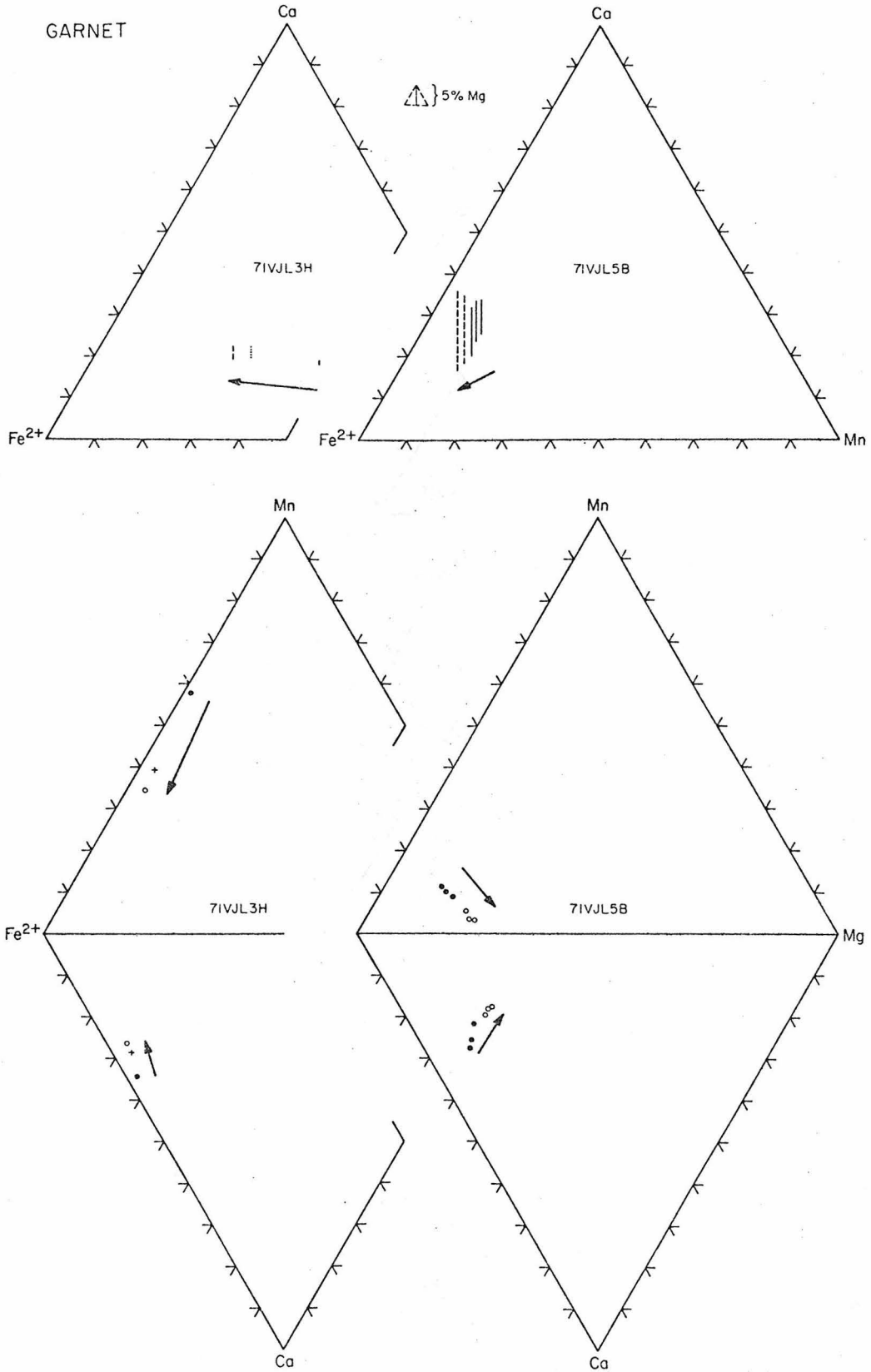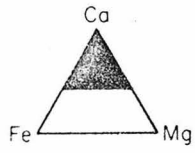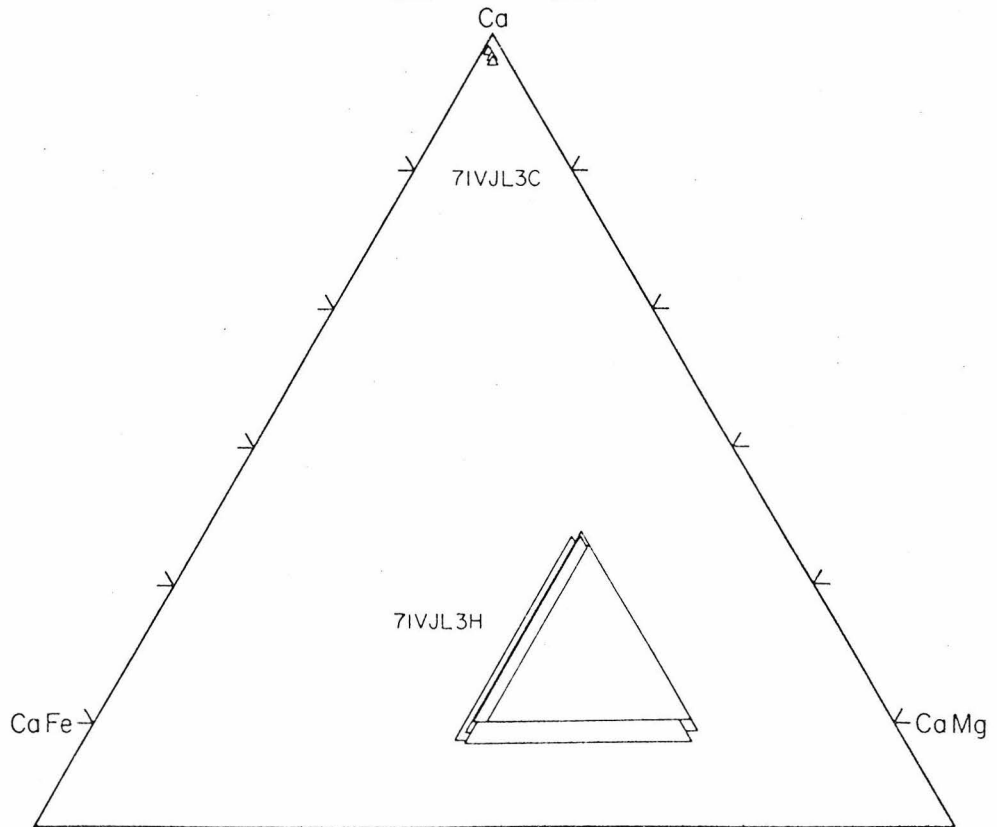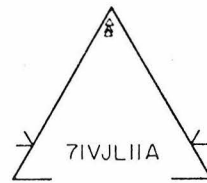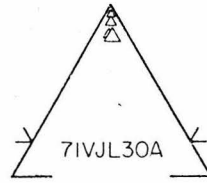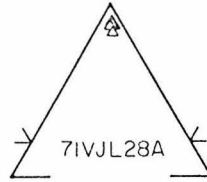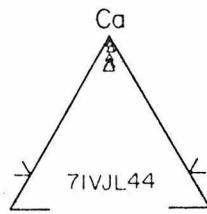
Figure IV-52

AMPHIBOLE 7IVJL38A

Figure IV-53

AMPHIBOLE

7IVJL53

36A

38A
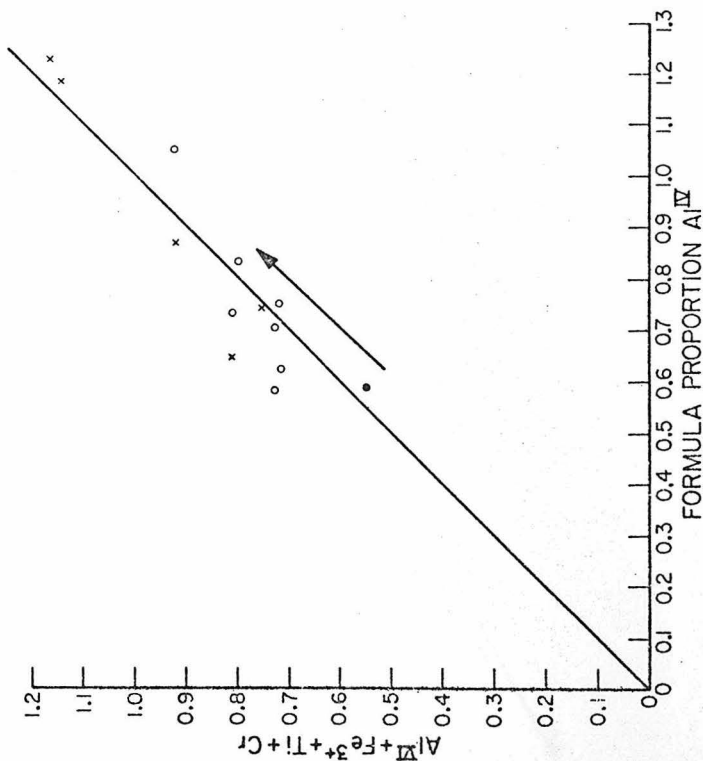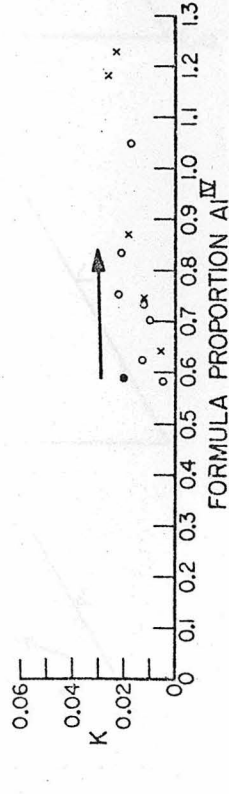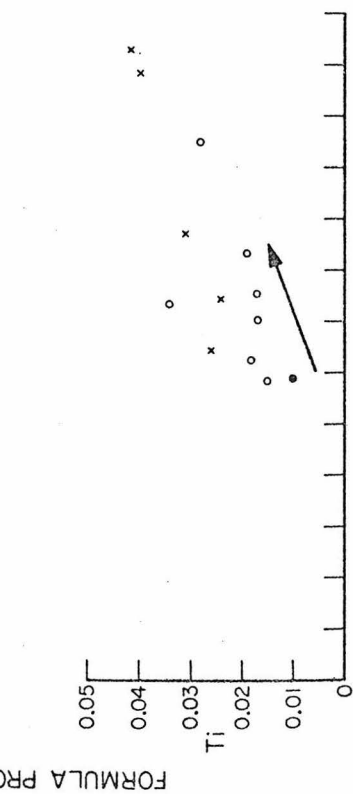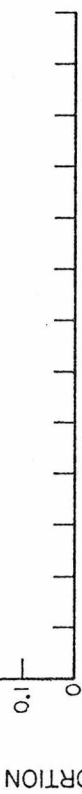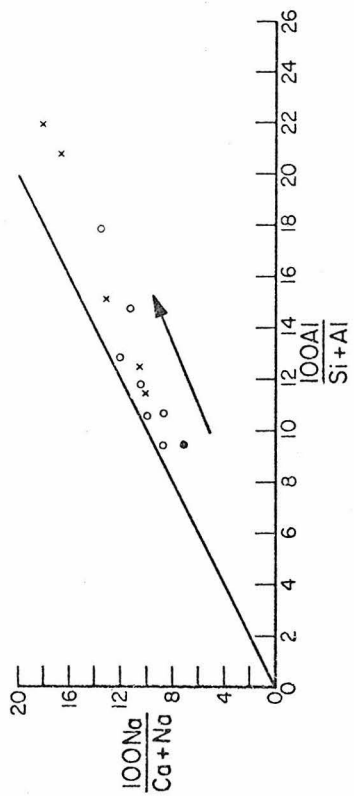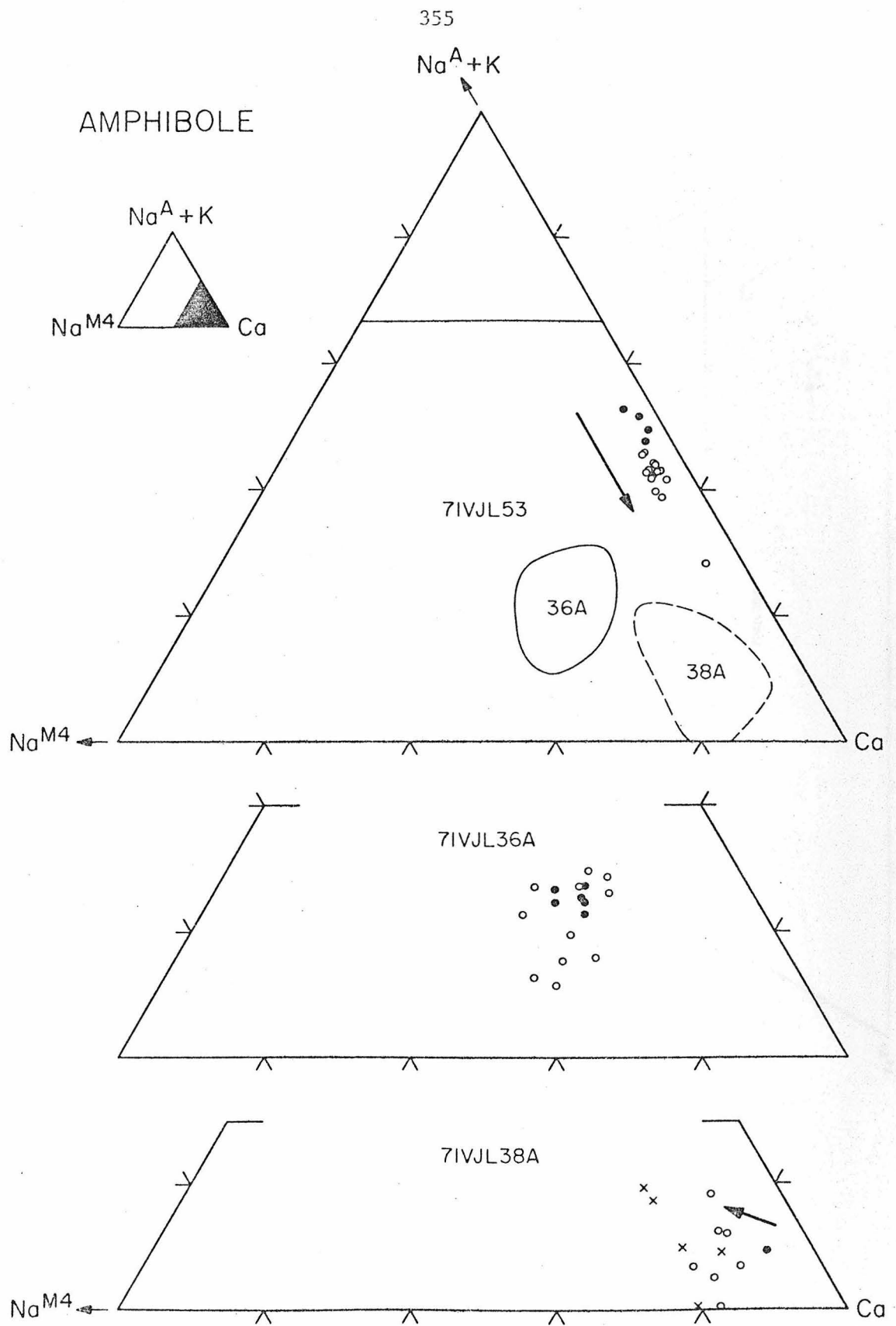
7IVJL36A

7IVJL38A
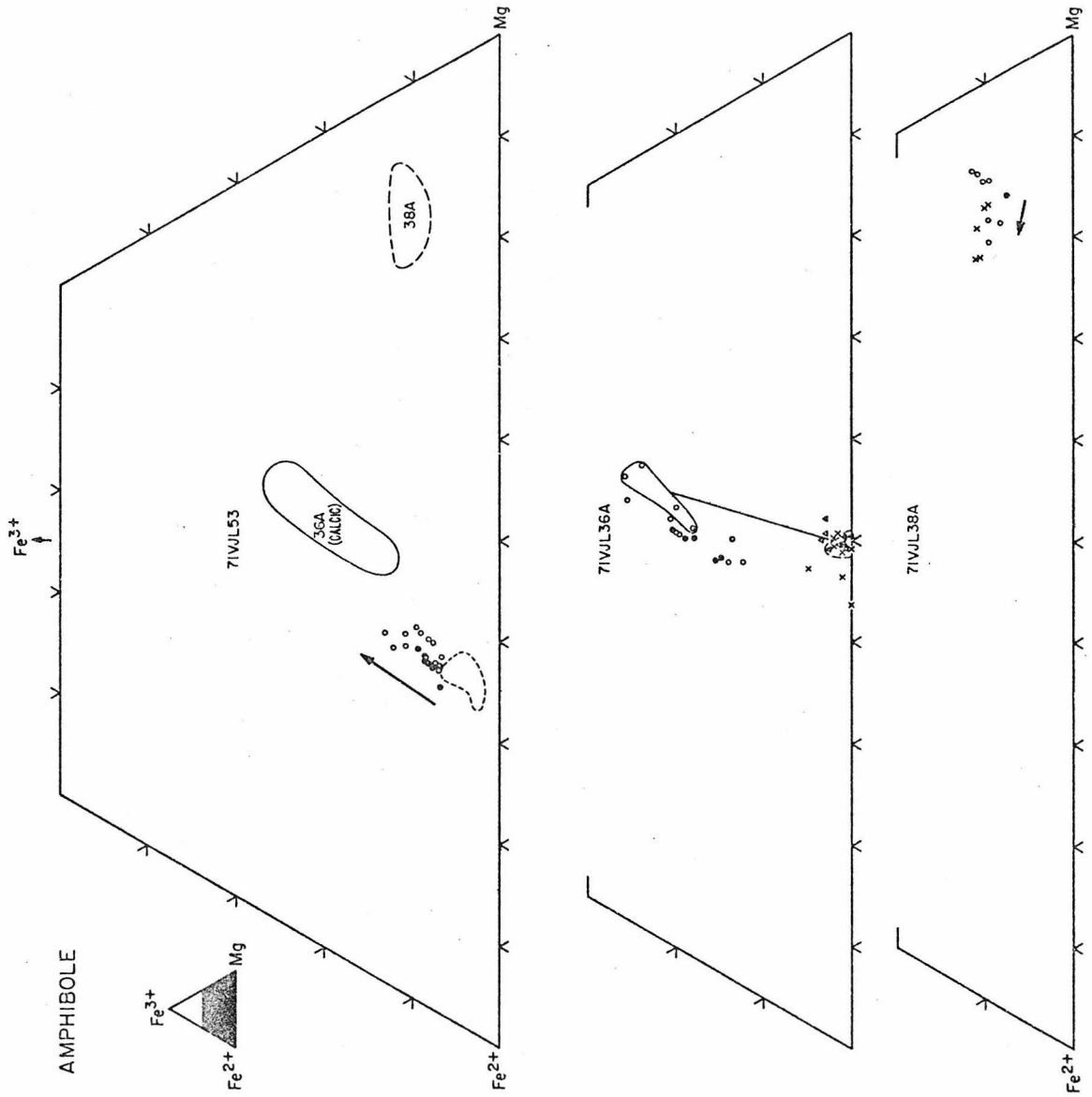
Figure IV-54

Figure IV-55

AMPHIBOLE 71VJL36A
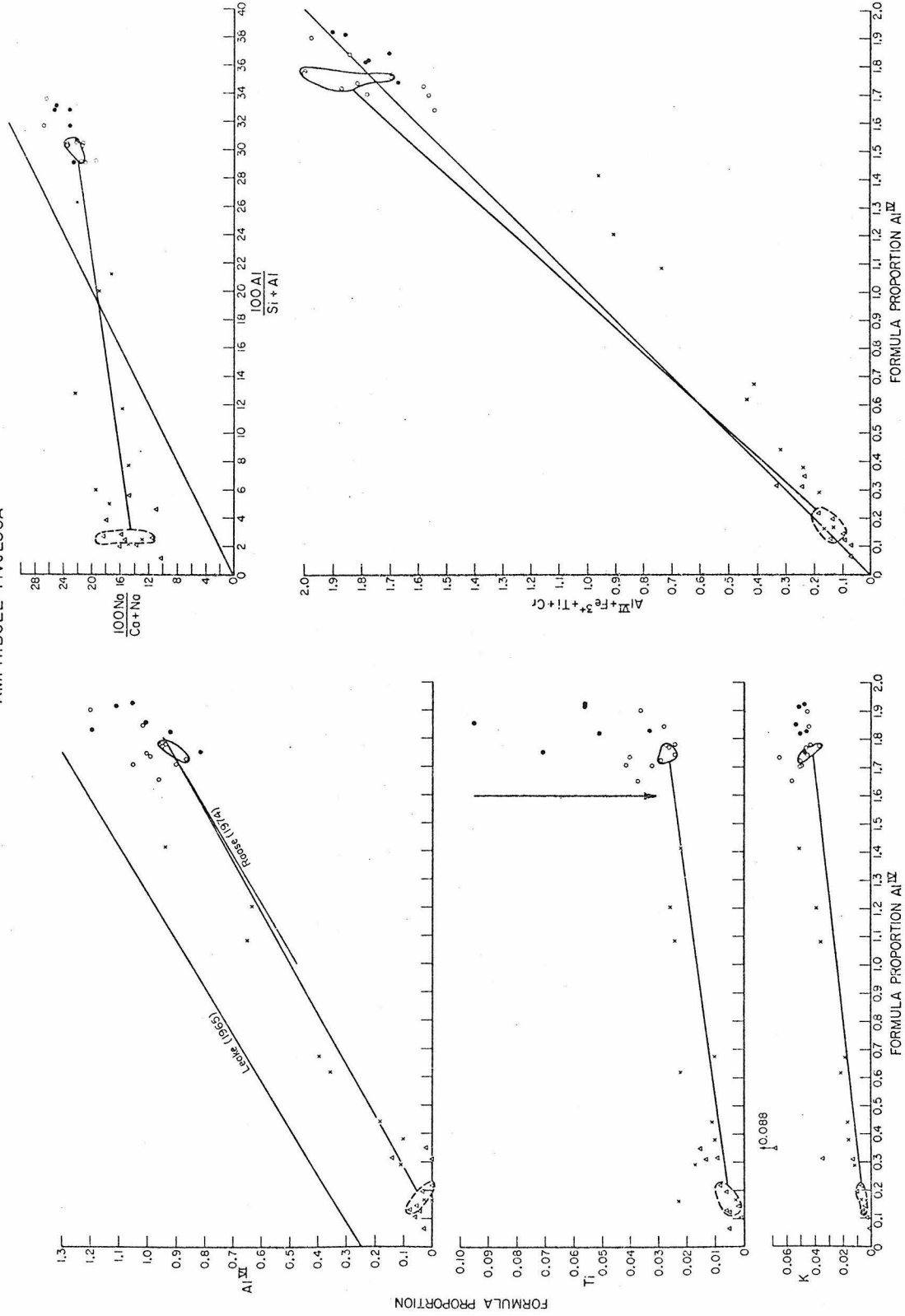
Figure IV-56

AMPHIBOLE 7IVJL53
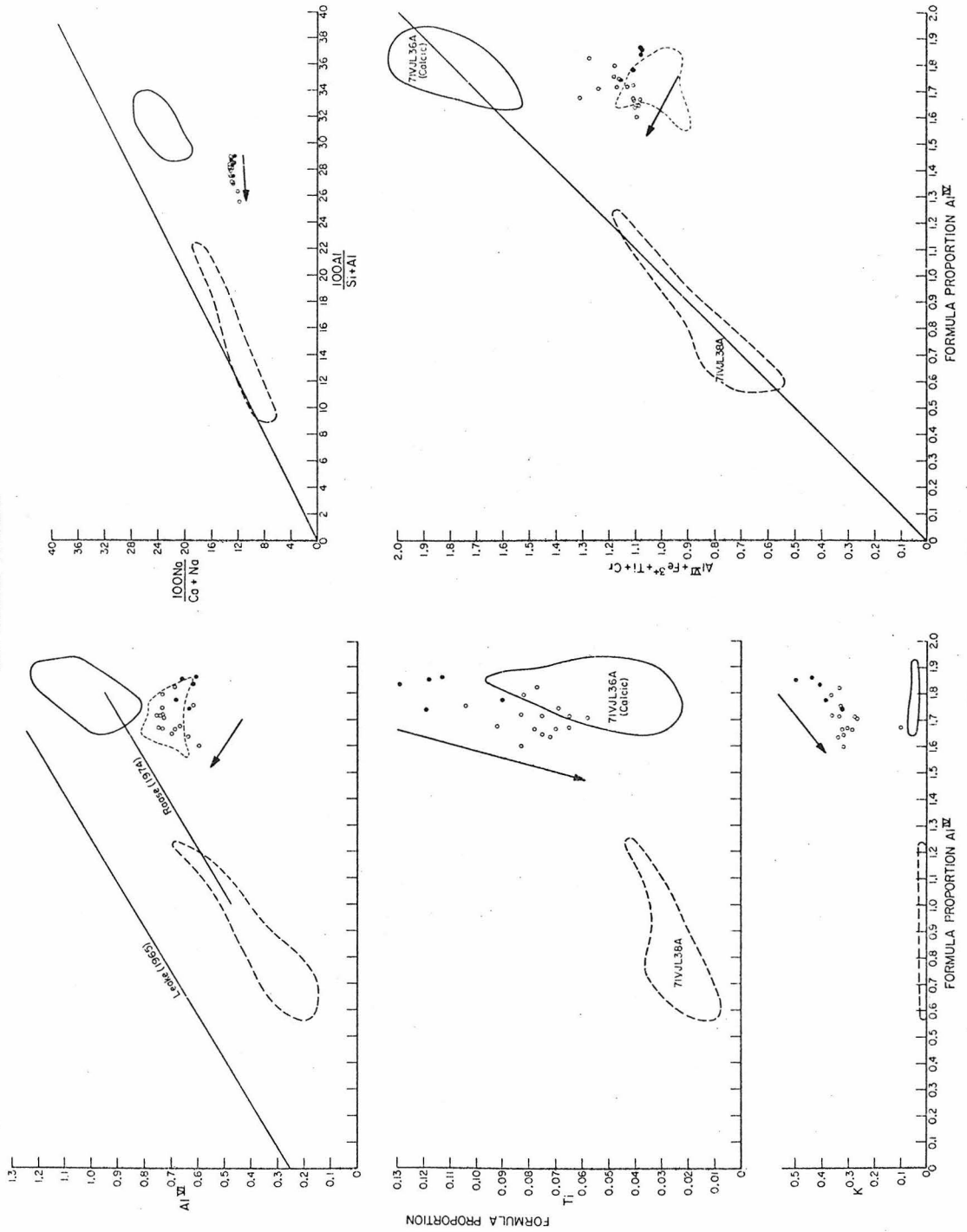
Figure IV-57

Figure IV-58

Figure IV—59a

FELDSPAR

o 7IVJL53
▲ 7IVJL36A
□ 7IVJL38A

KAISi₃O₈

NaAlSi₃O₈

CaAl₂Si₂O₈

SILLIMANITE ZONE

BIOTITE & GARNET ZONES
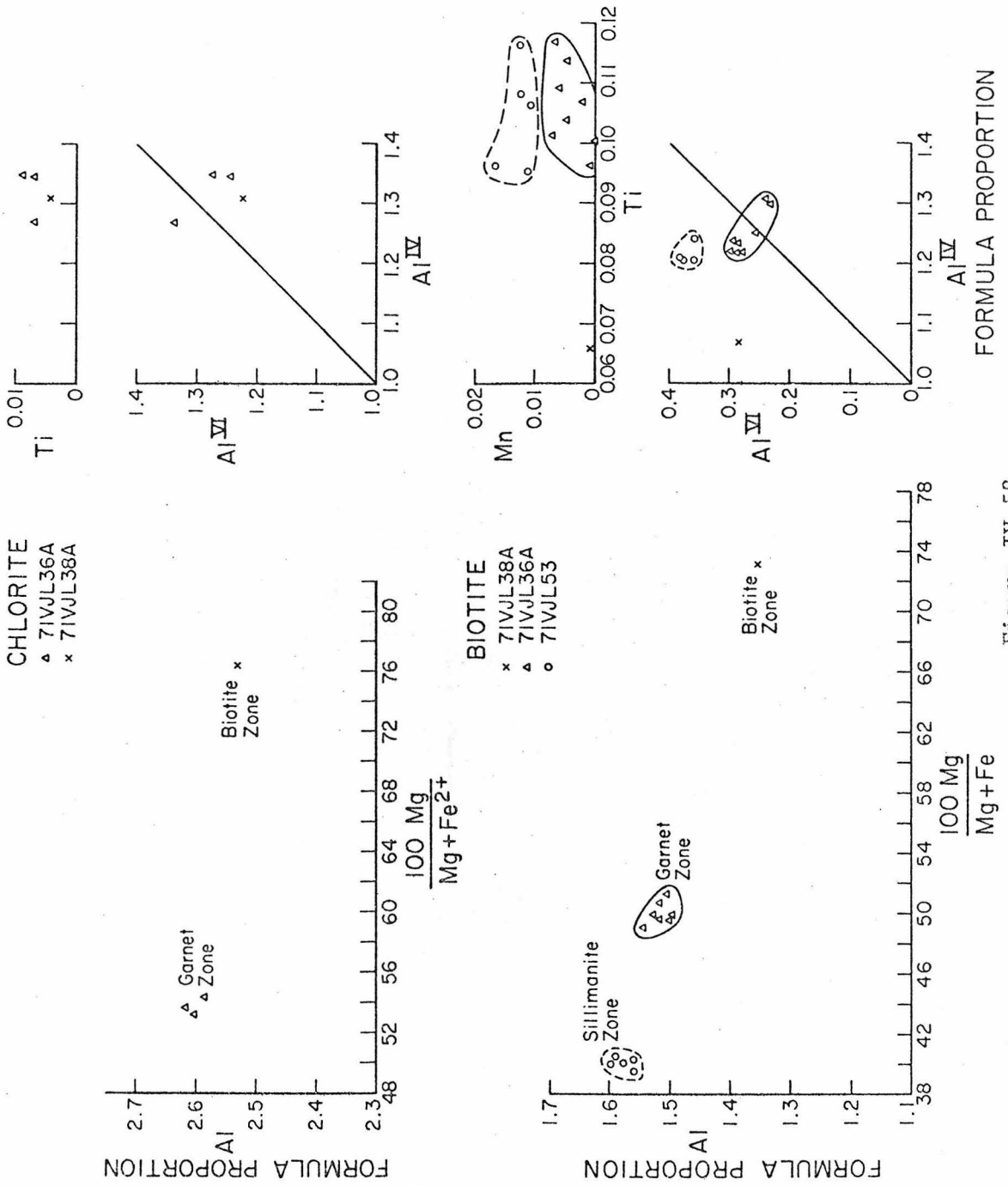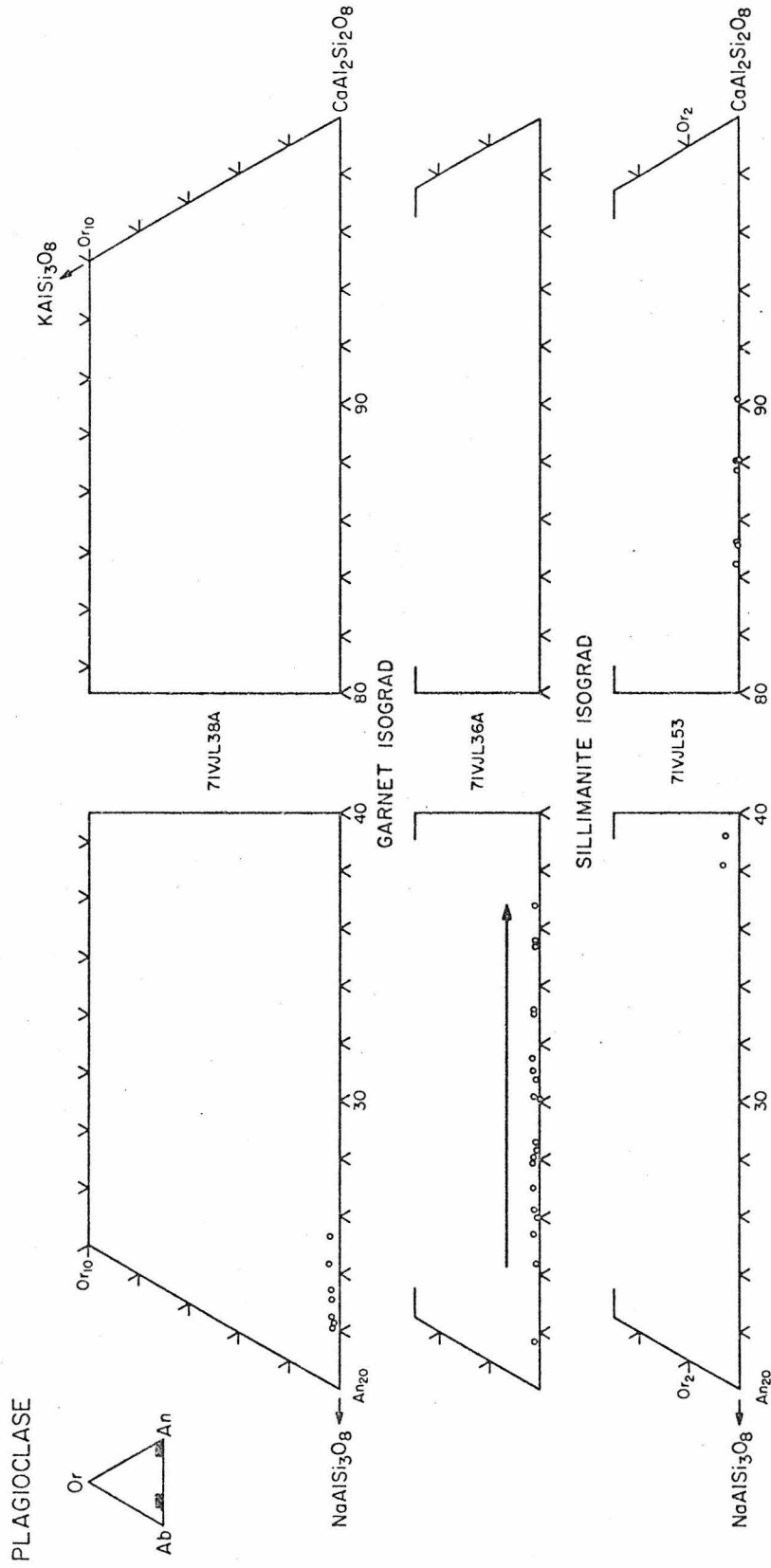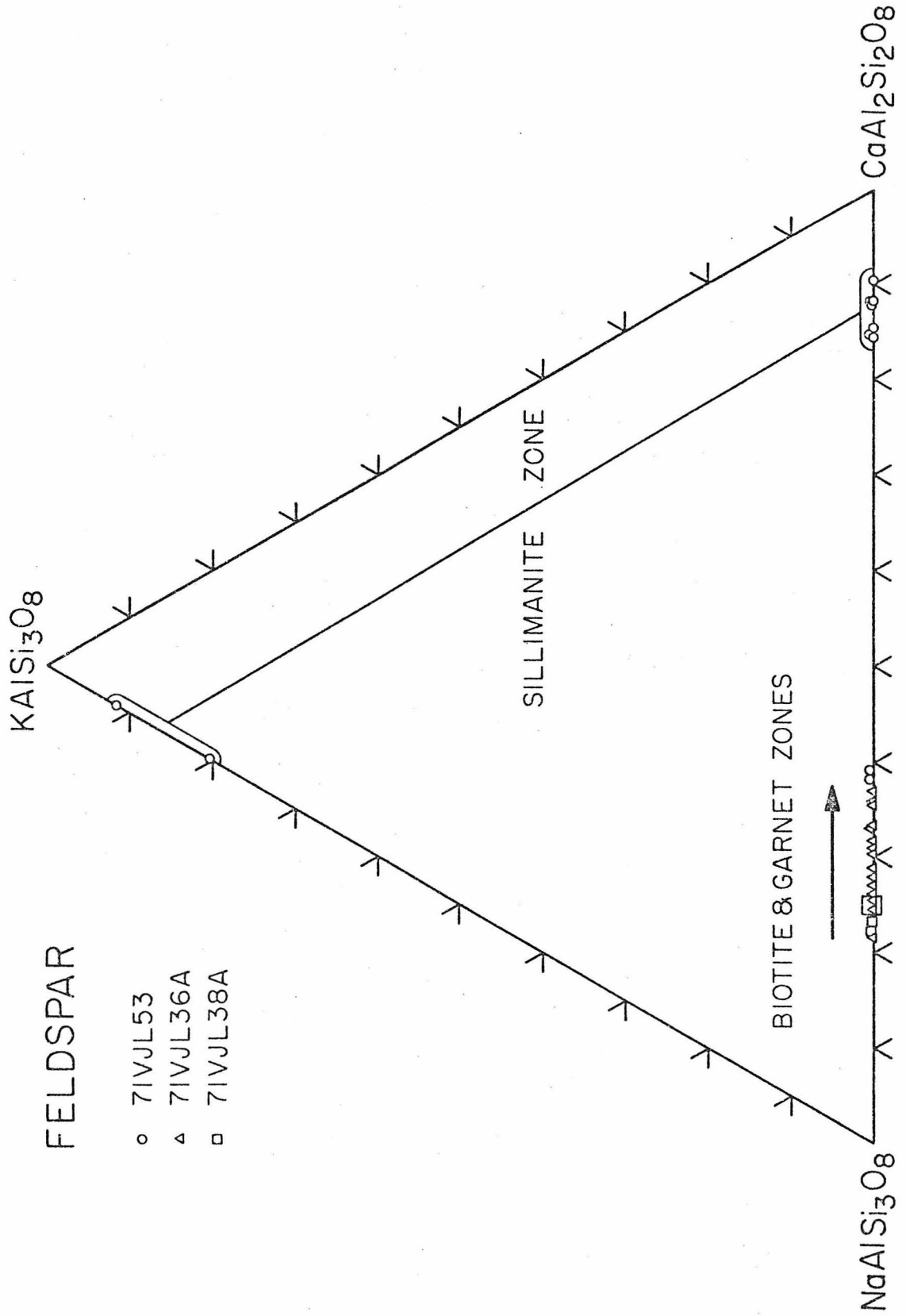
Figure IV-59b

7IVJLI27A AREA B
AMPHIBOLE GRAIN I, EDA TRAVERSE I
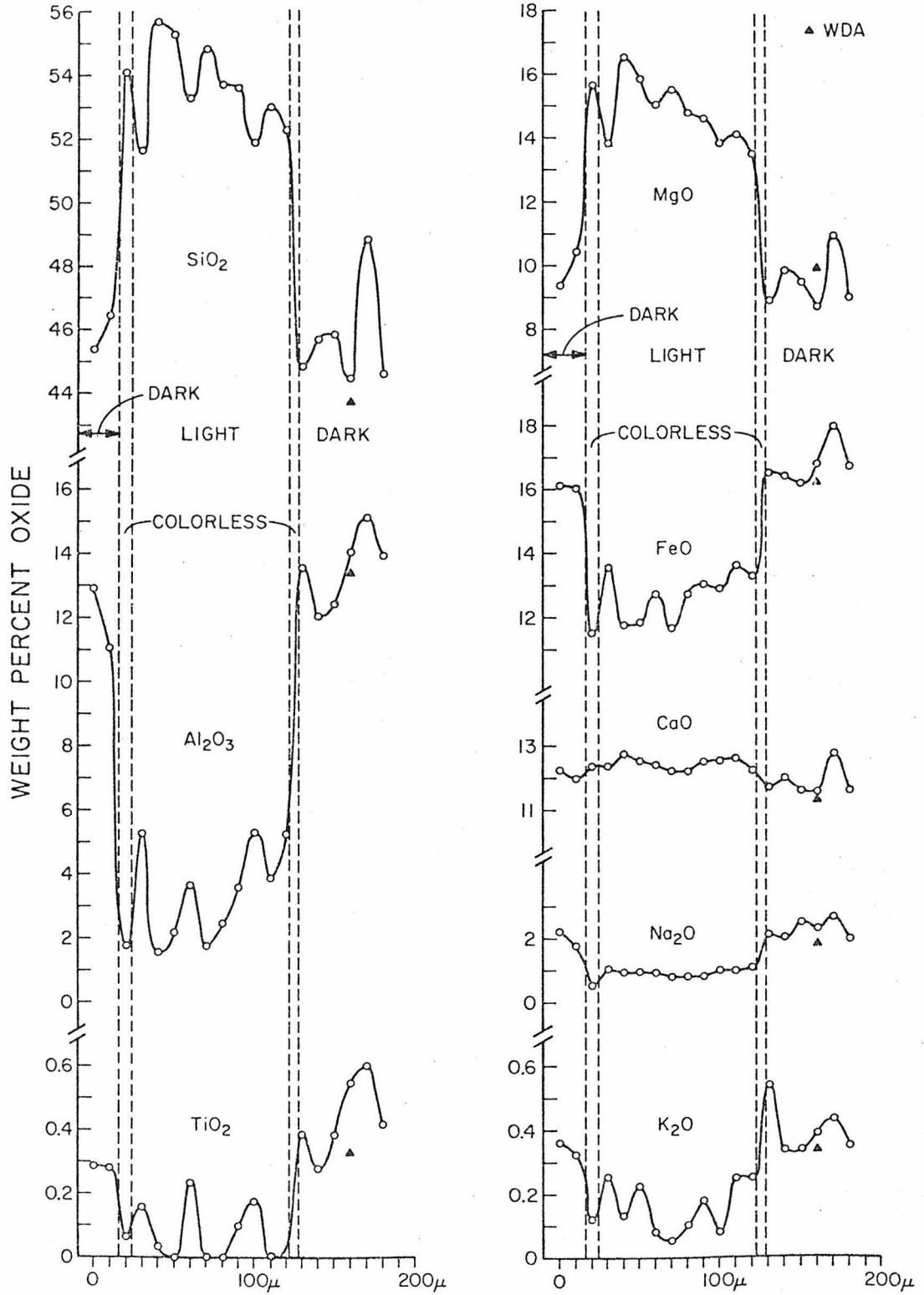
Figure IV-60a

7IVJLI27A AREA B
AMPHIBOLE GRAIN I – EDA TRAVERSE I,I
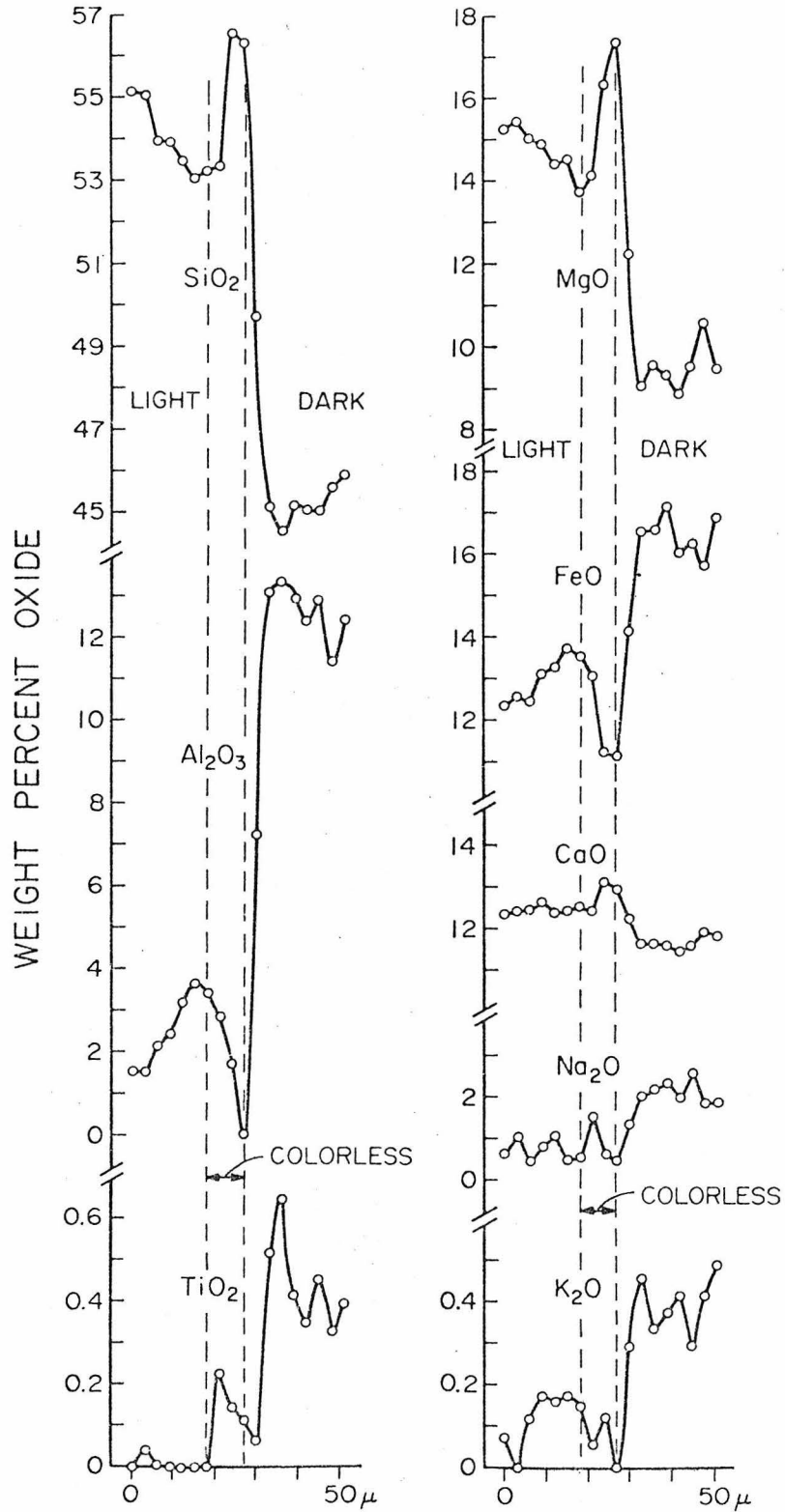
Figure IV-60b

71VJLI27A AREA B
AMPHIBOLE, GRAIN I-TRAVERSE 2
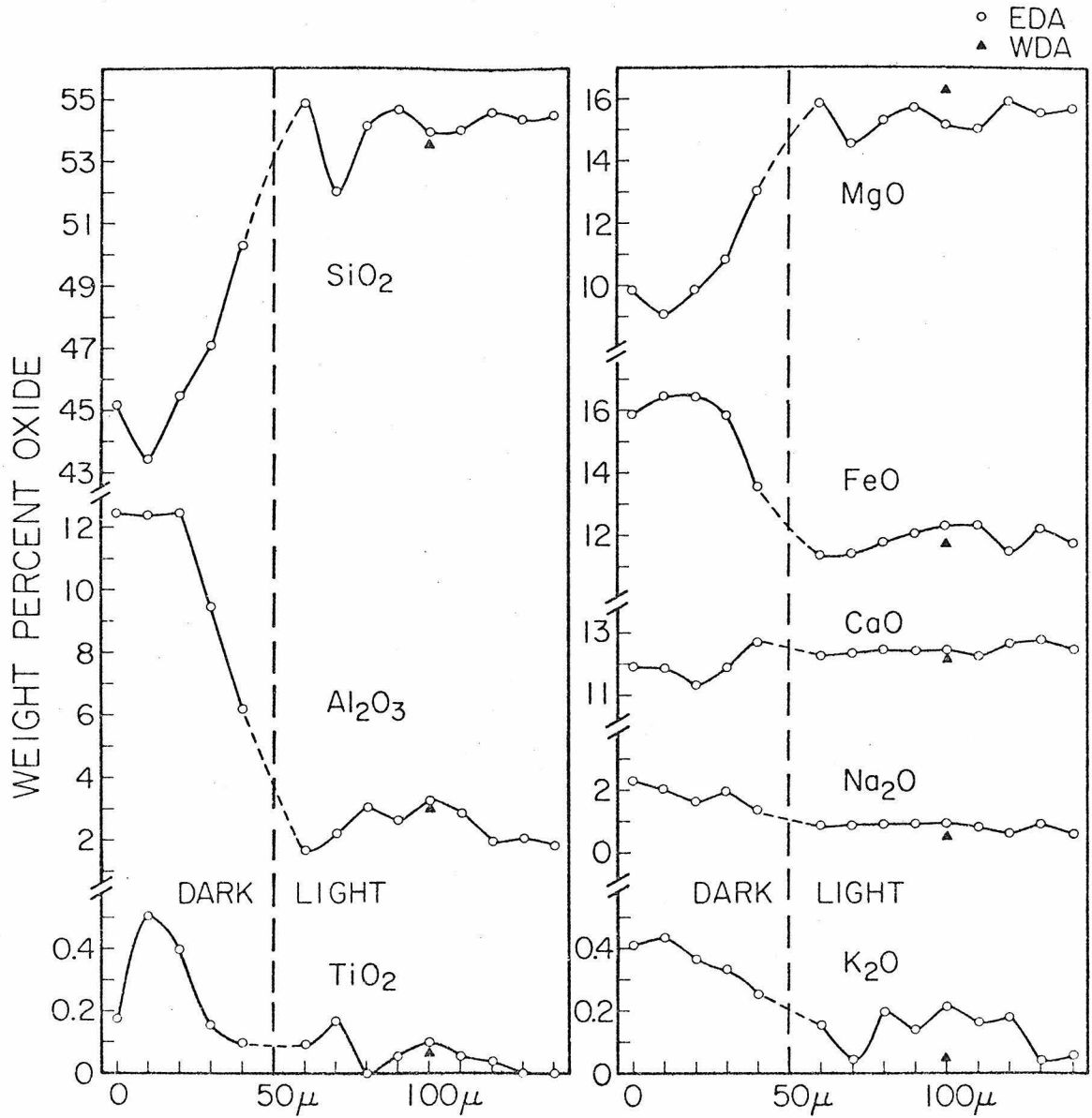
Figure IV-60c

7IVJLI27A AREA B
AMPHIBOLE GRAIN I—EDA TRAVERSE 3
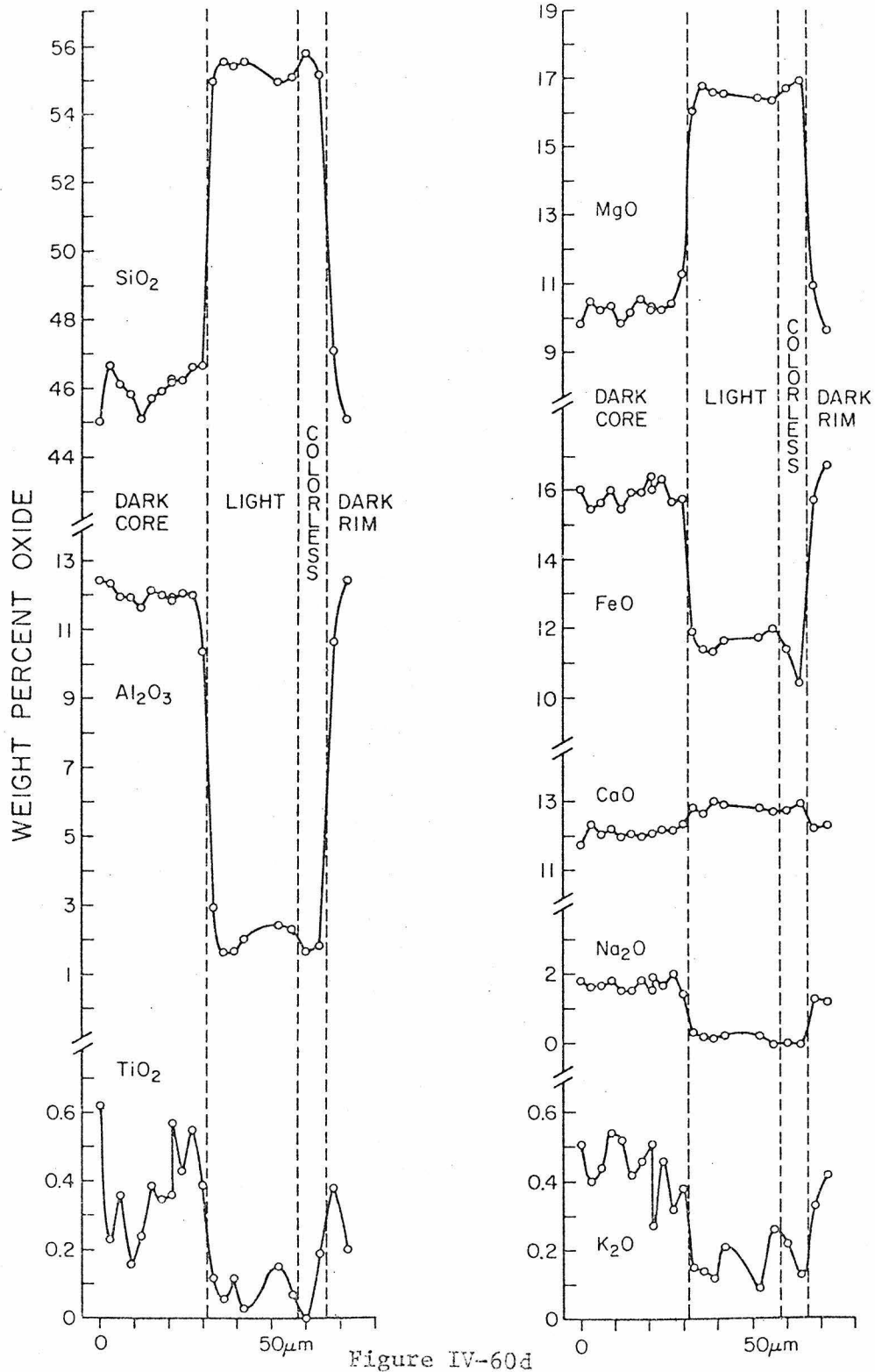
Figure IV-60d

AMPHIBOLE
7IVJLI27A
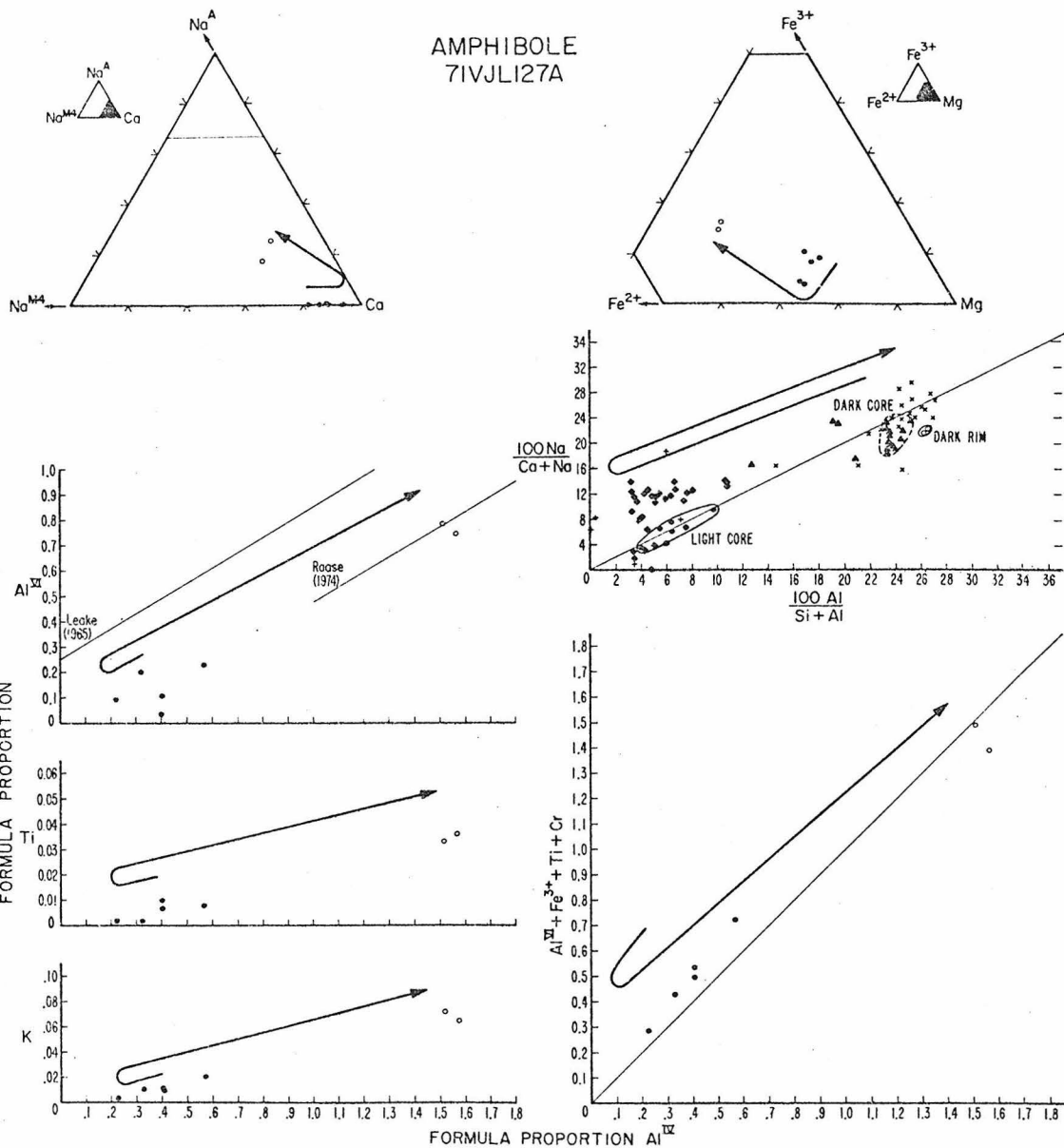
Figure IV-61
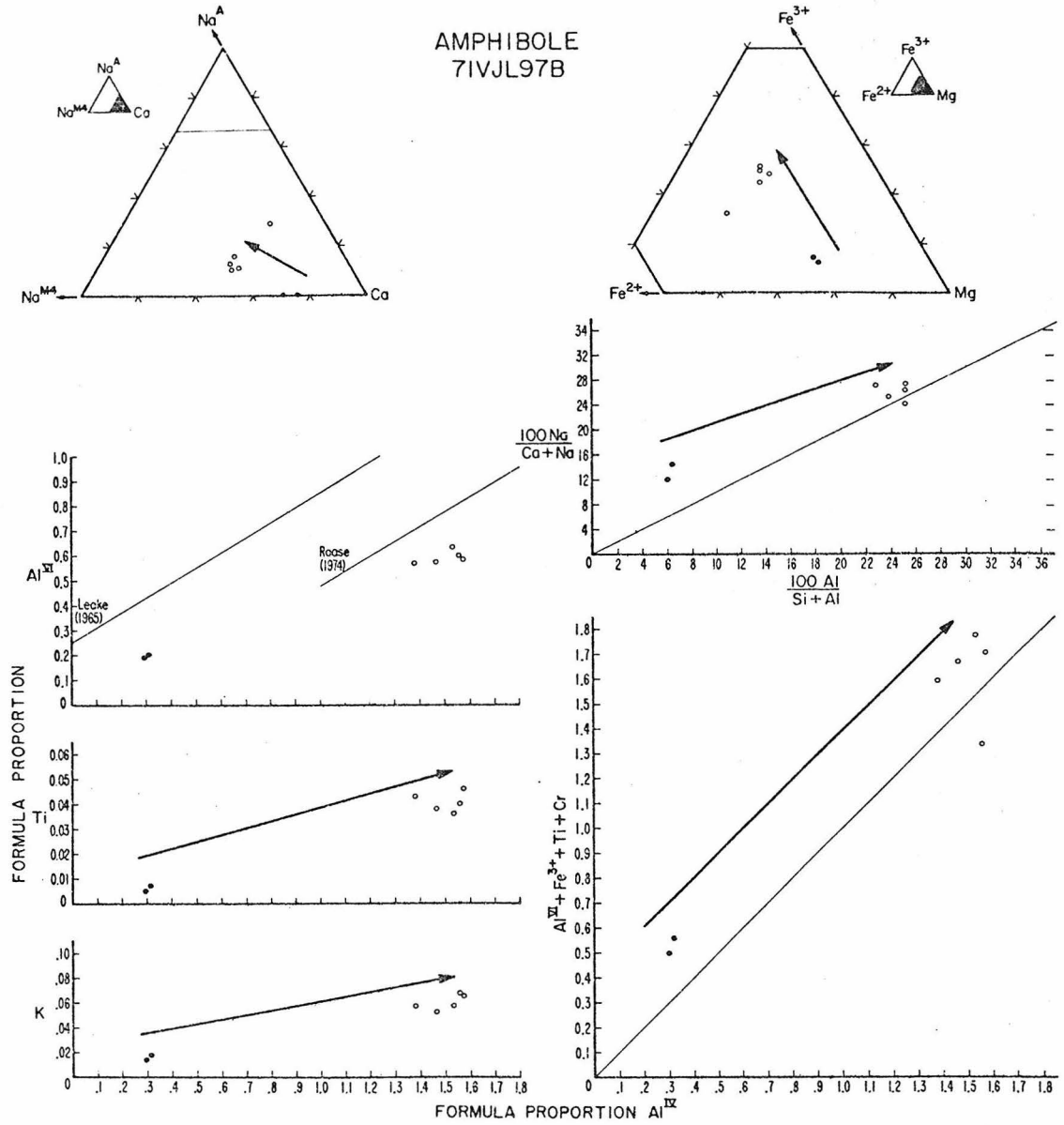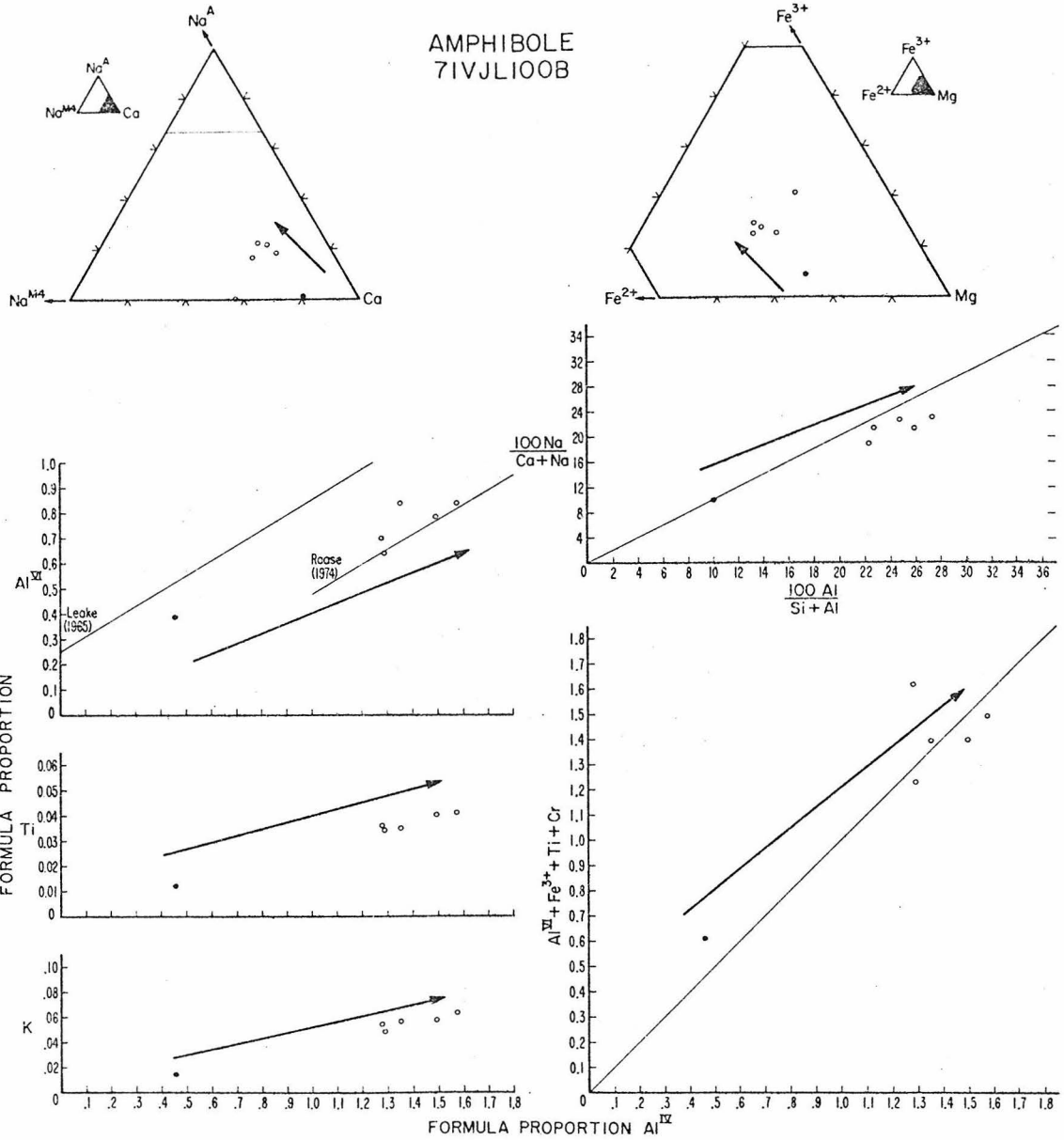
Figure IV-62
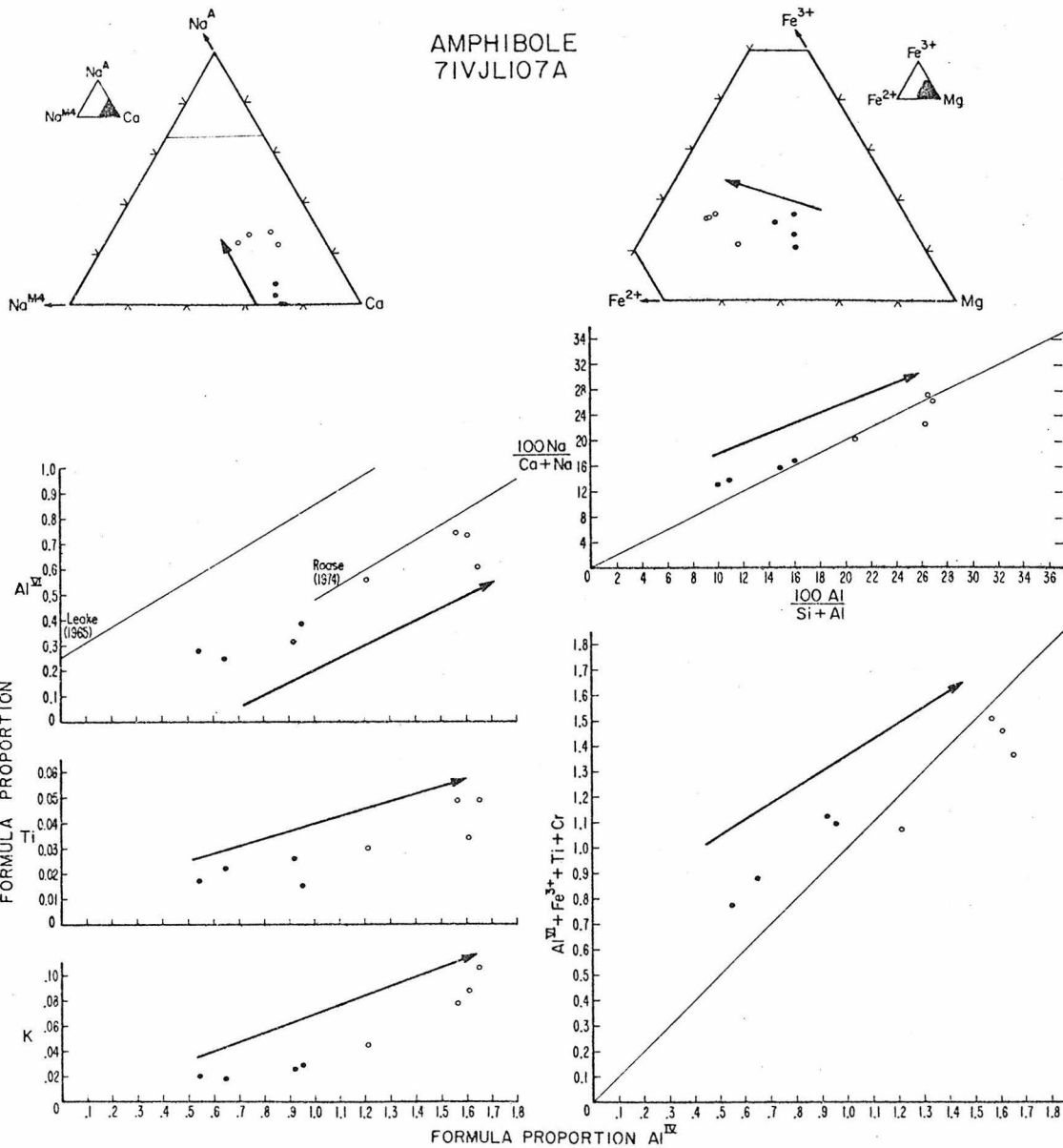
Figure IV-63

Figure IV-64

AMPHIBOLE
71VJLIO8
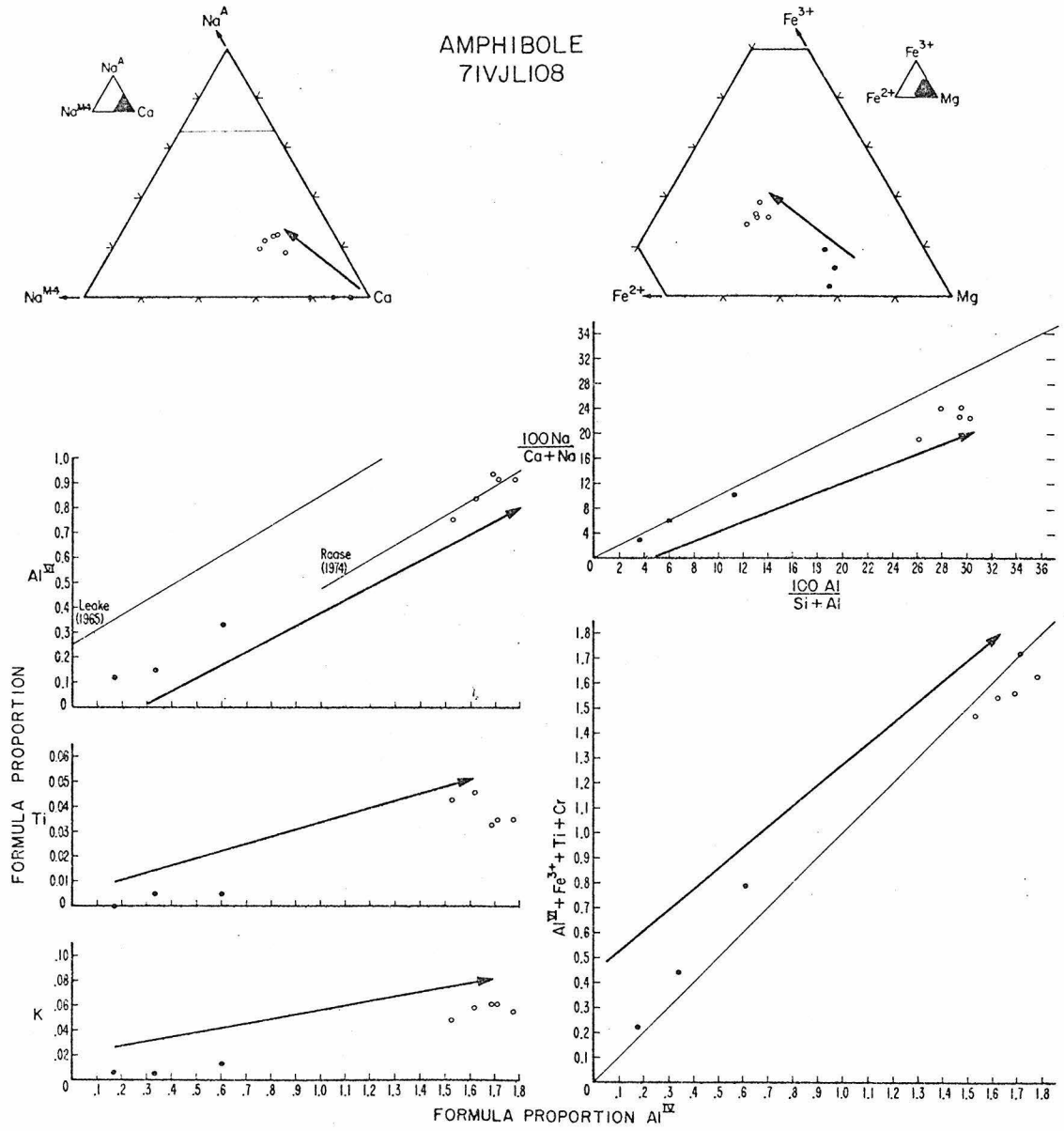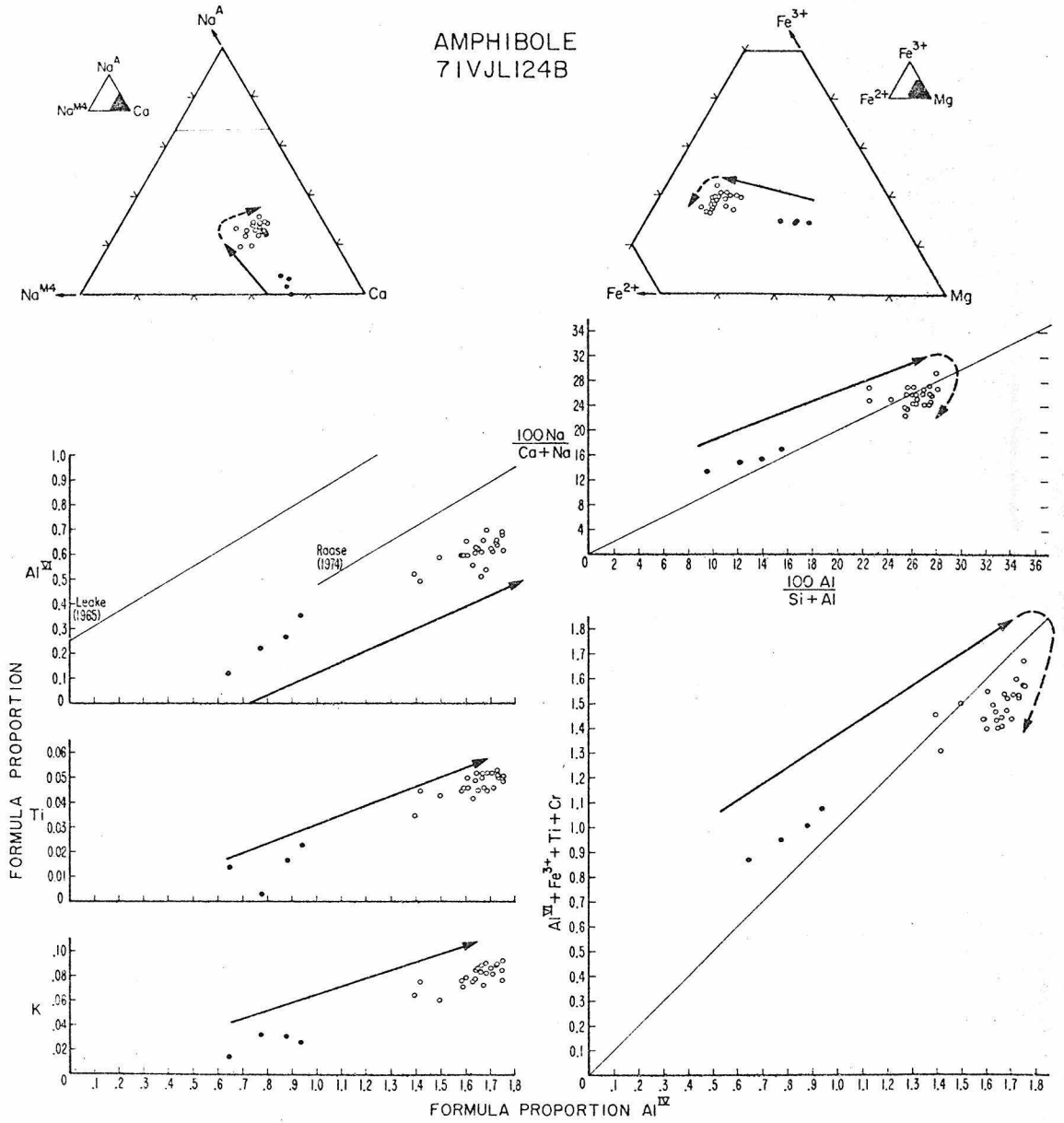
Figure IV-65
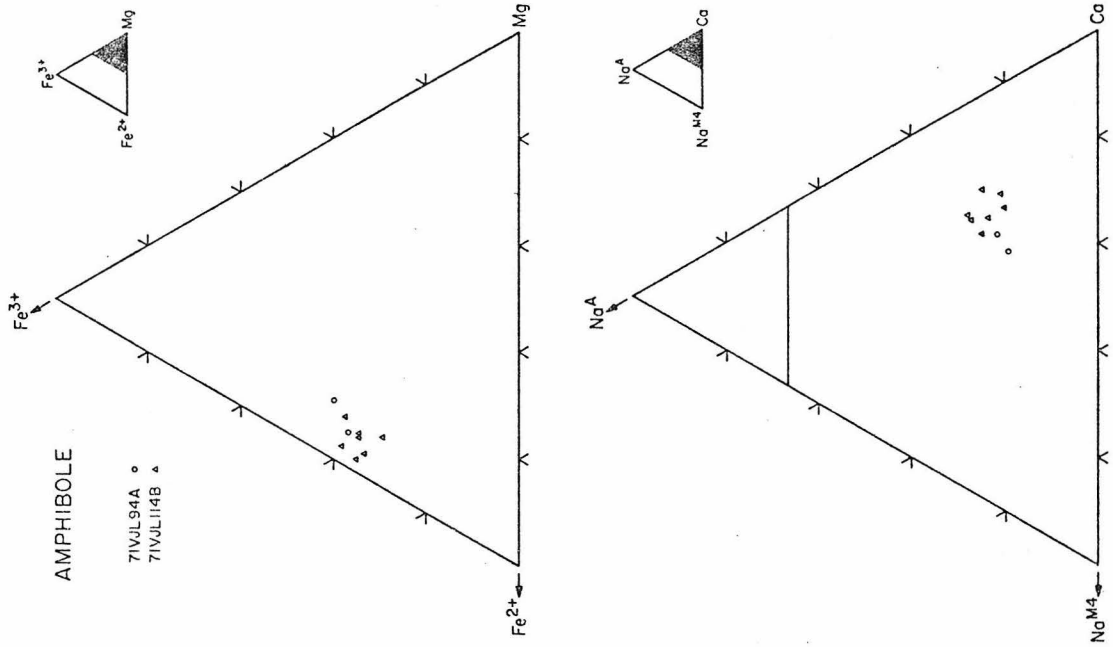
Figure IV-66

Figure IV-67
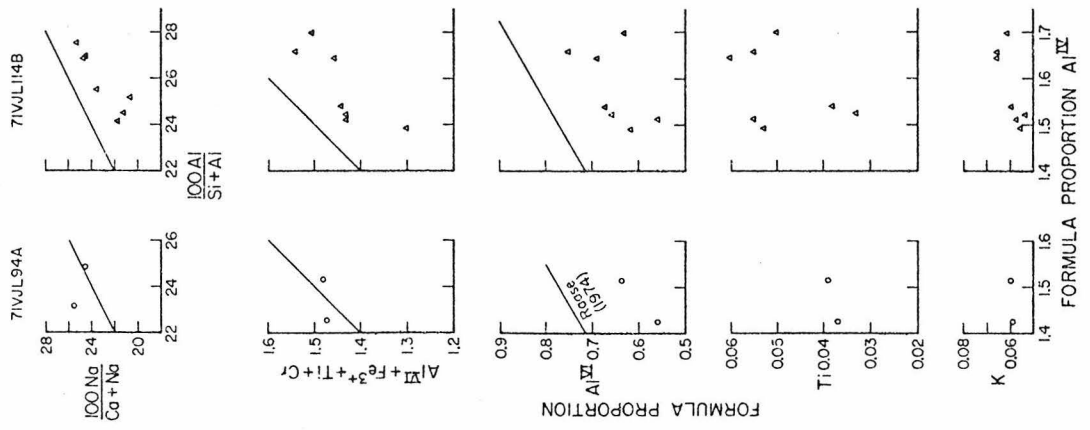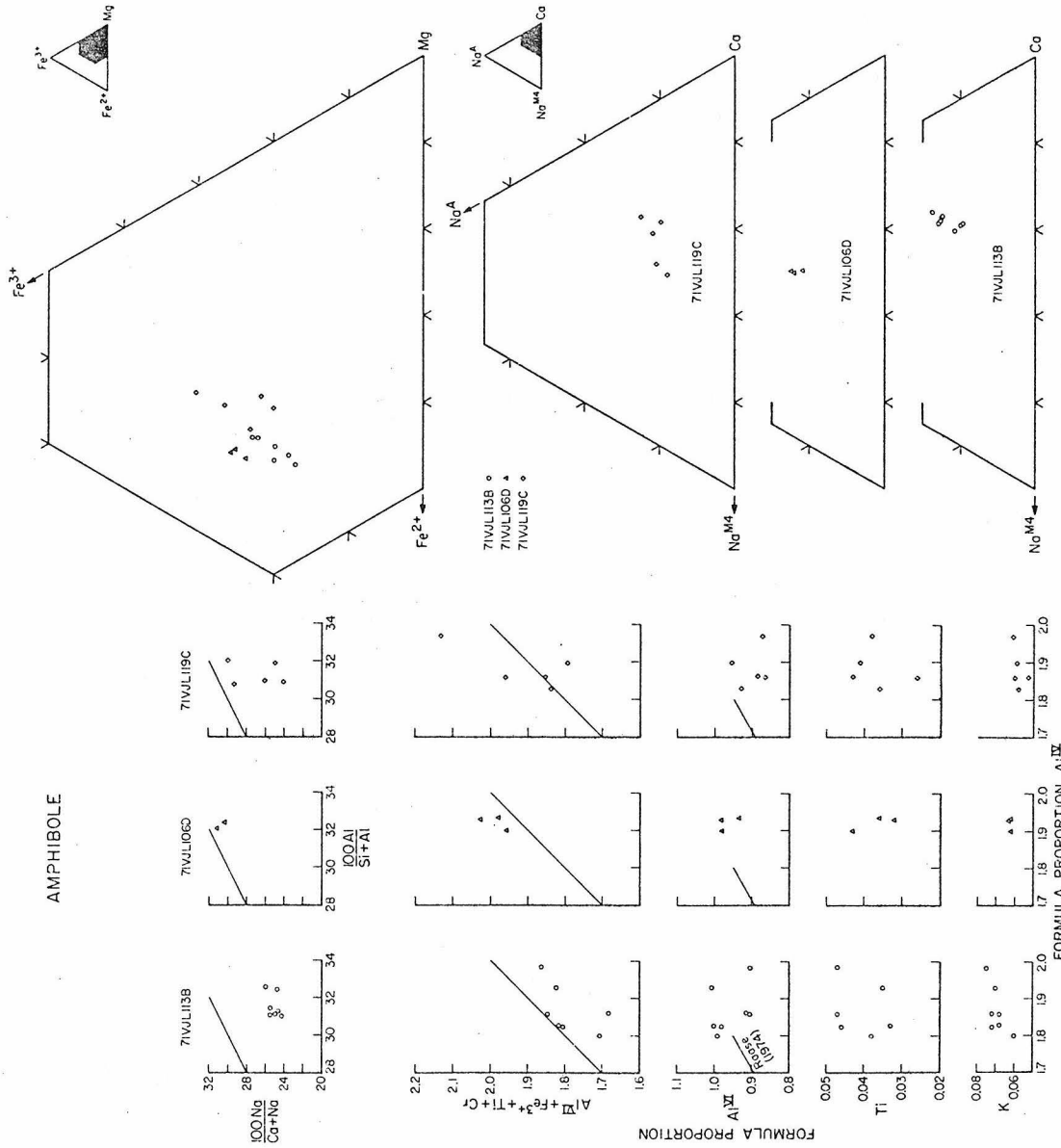
Figure IV-68
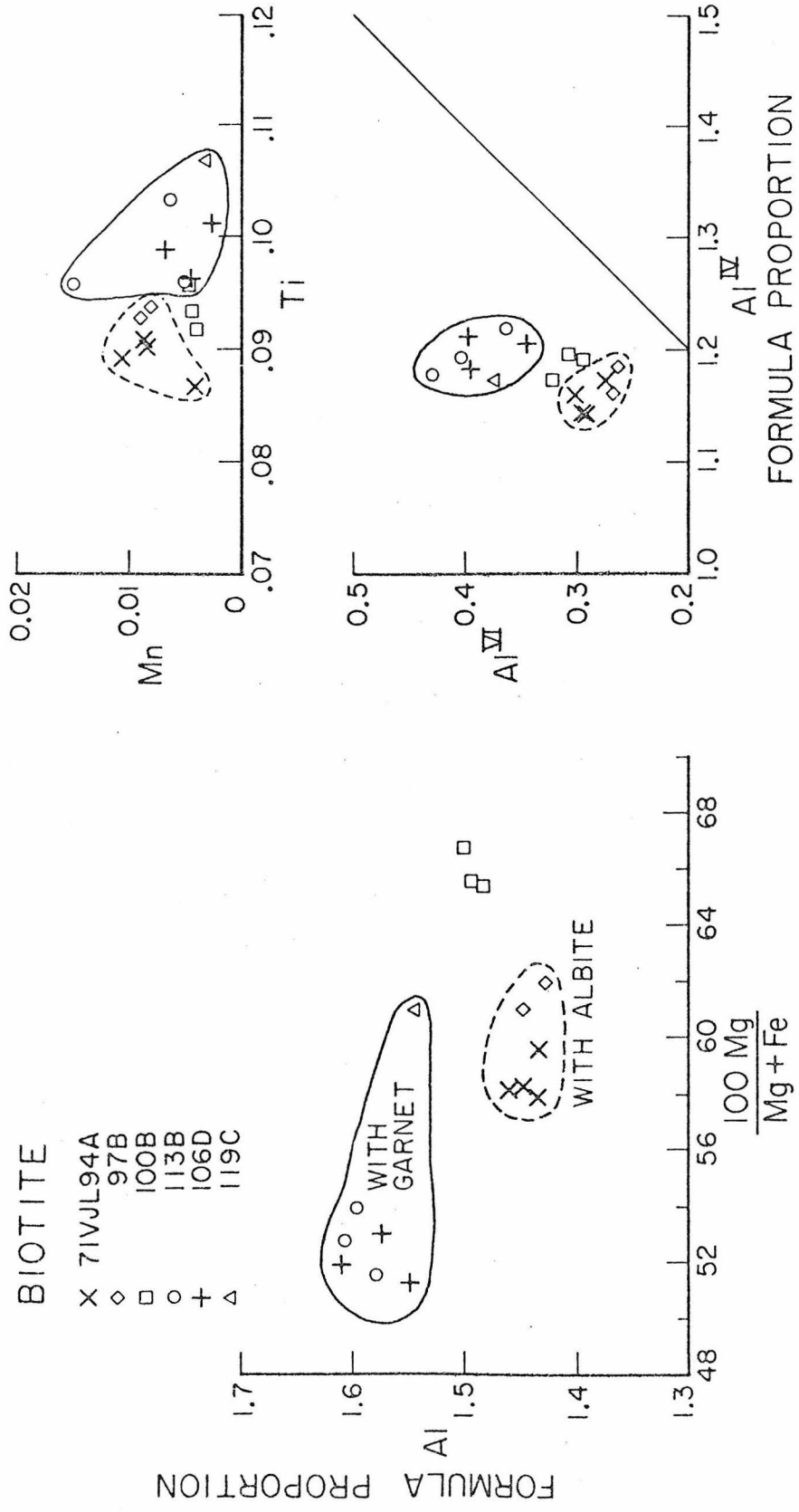
Figure IV-69

Figure IV-70

CHLORITE
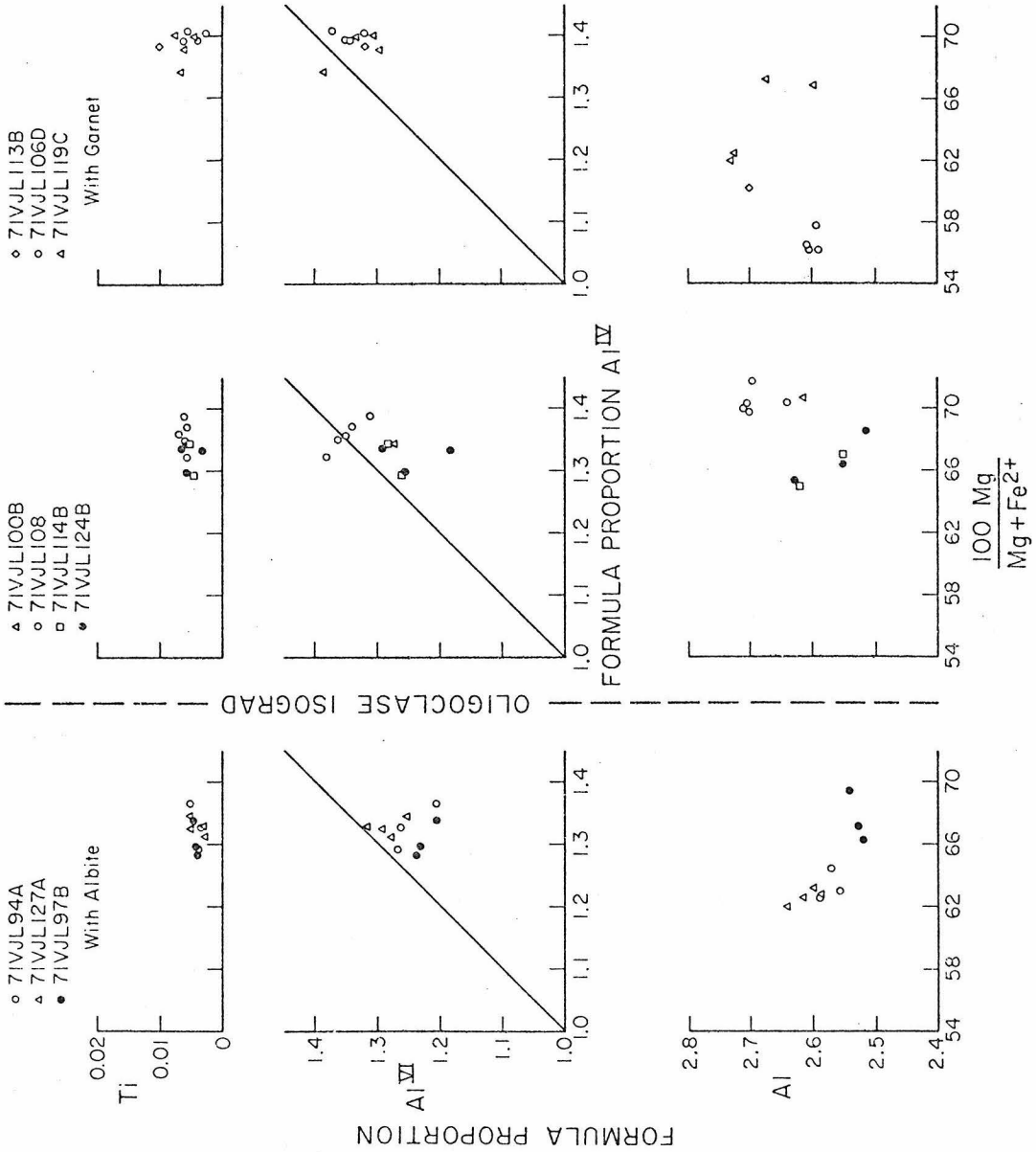
EPIDOTE
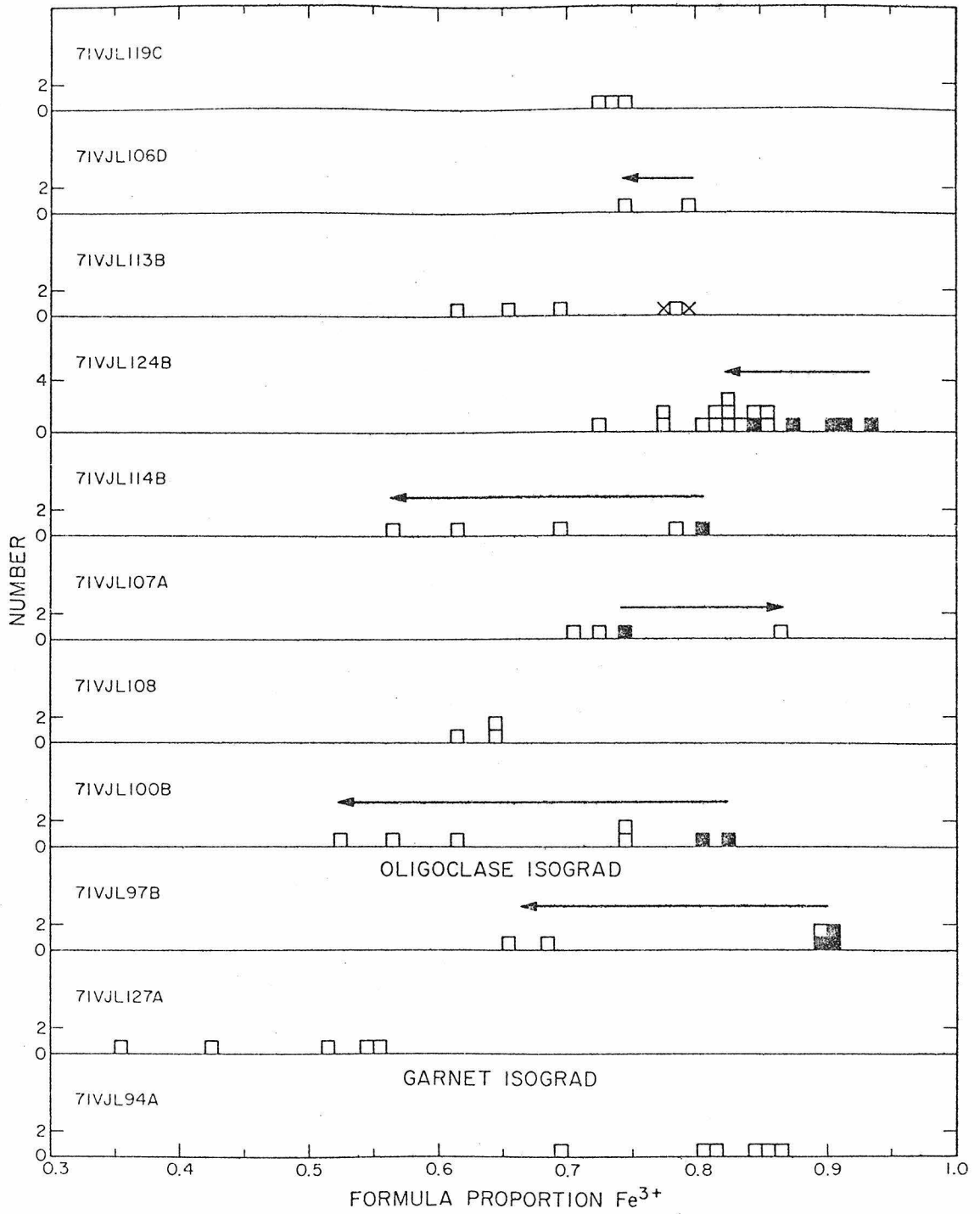
Figure IV-71
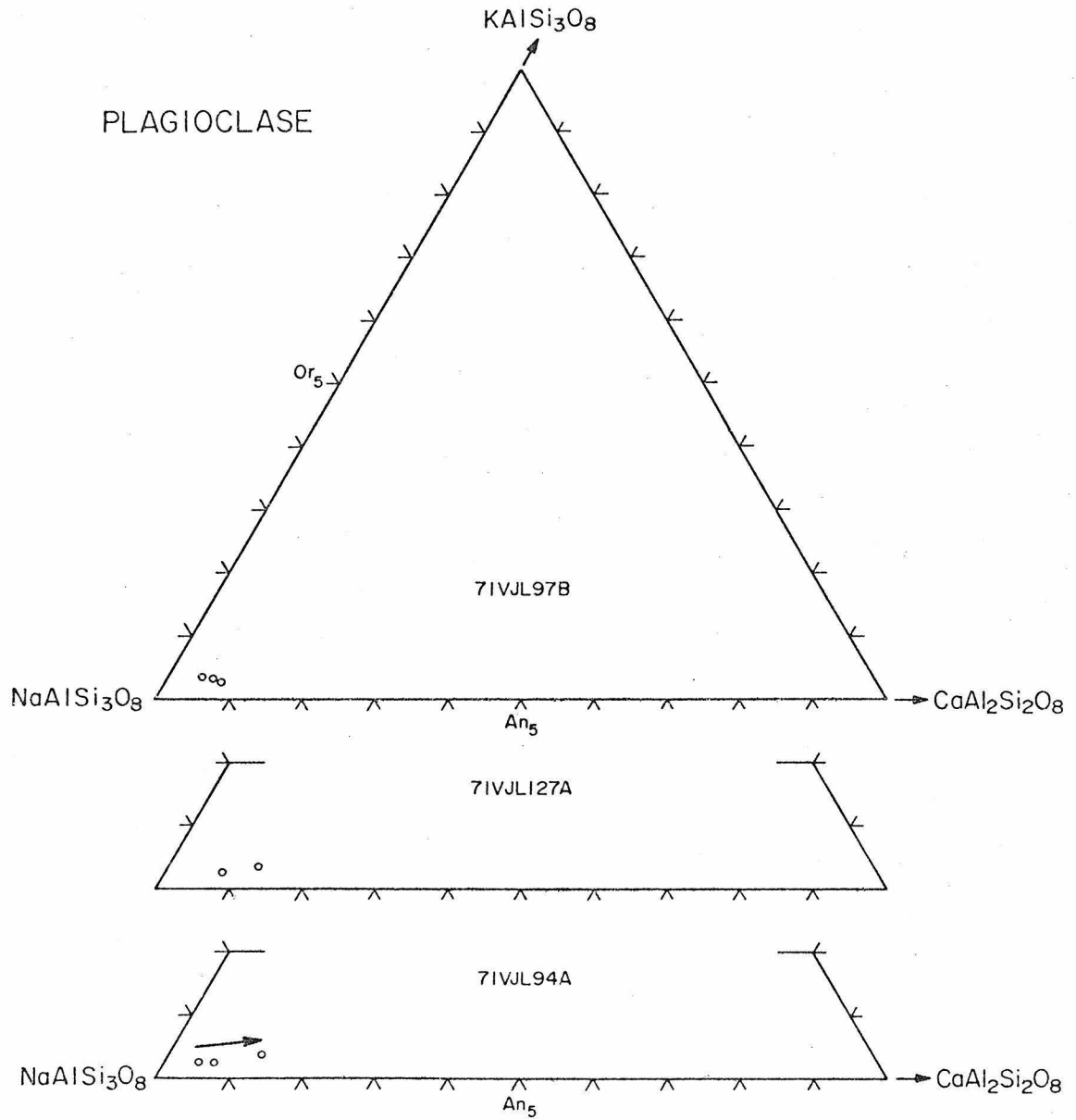
Figure IV-72

PLAGIOCLASE

Figure IV-73

GARNET

△ 5% Mg

71VJL119C

71VJL106D

71VJL113B

Ca

Ca

Fe²⁺

Fe²⁺

Mn

Figure IV-74

CARBONATE

Ca
Fe — Mg

⚠ 1.5% Mn

Ca
7IVJL94A

GARNET ISOGRAD

7IVJL97B

OLIGOCLASE ISOGRAD

7IVJLI14B

7IVJLI24B

Ca

7IVJLI00B

CaFe — CaMg

7IVJLI08

CaFe — CaMg
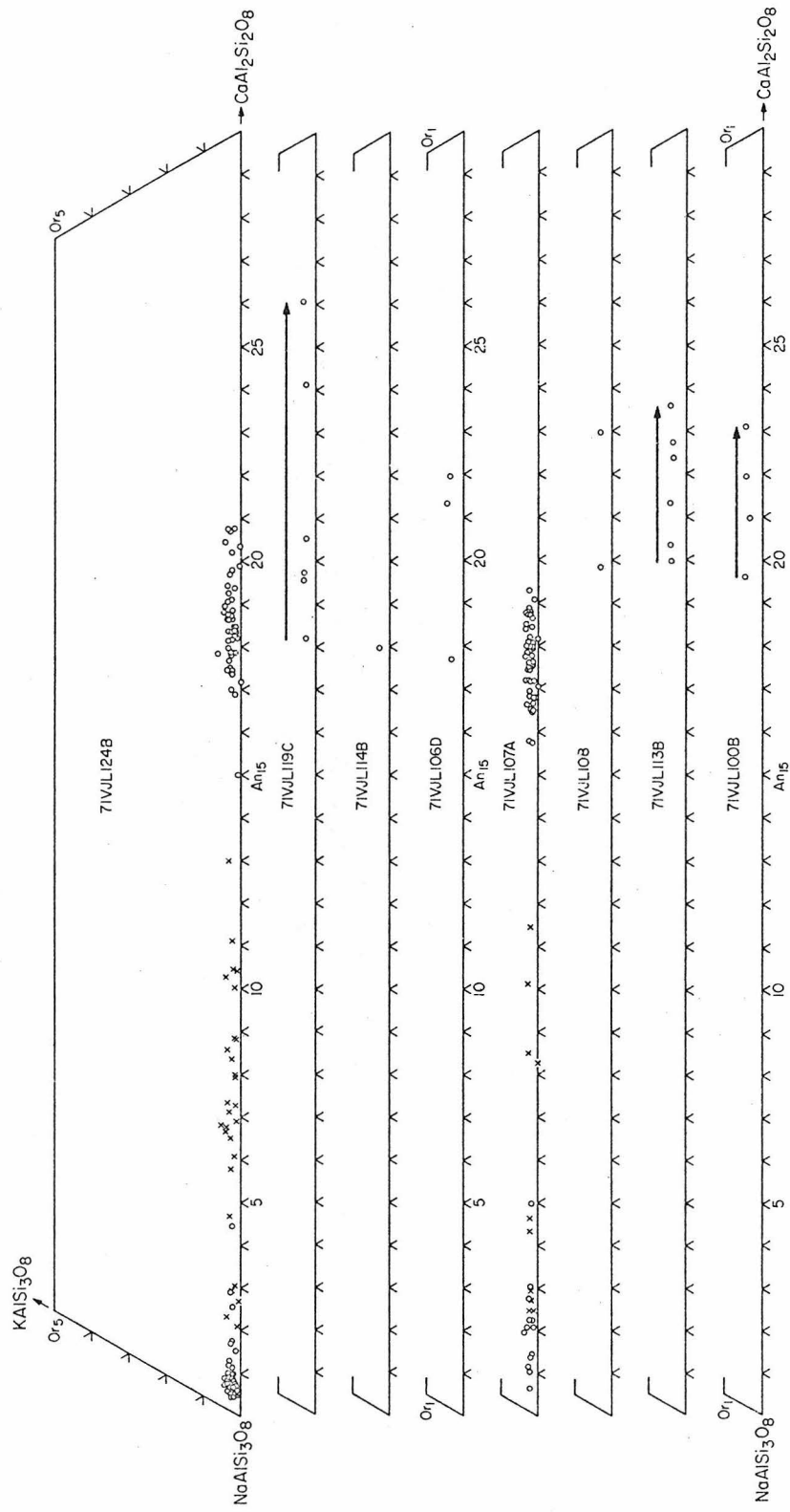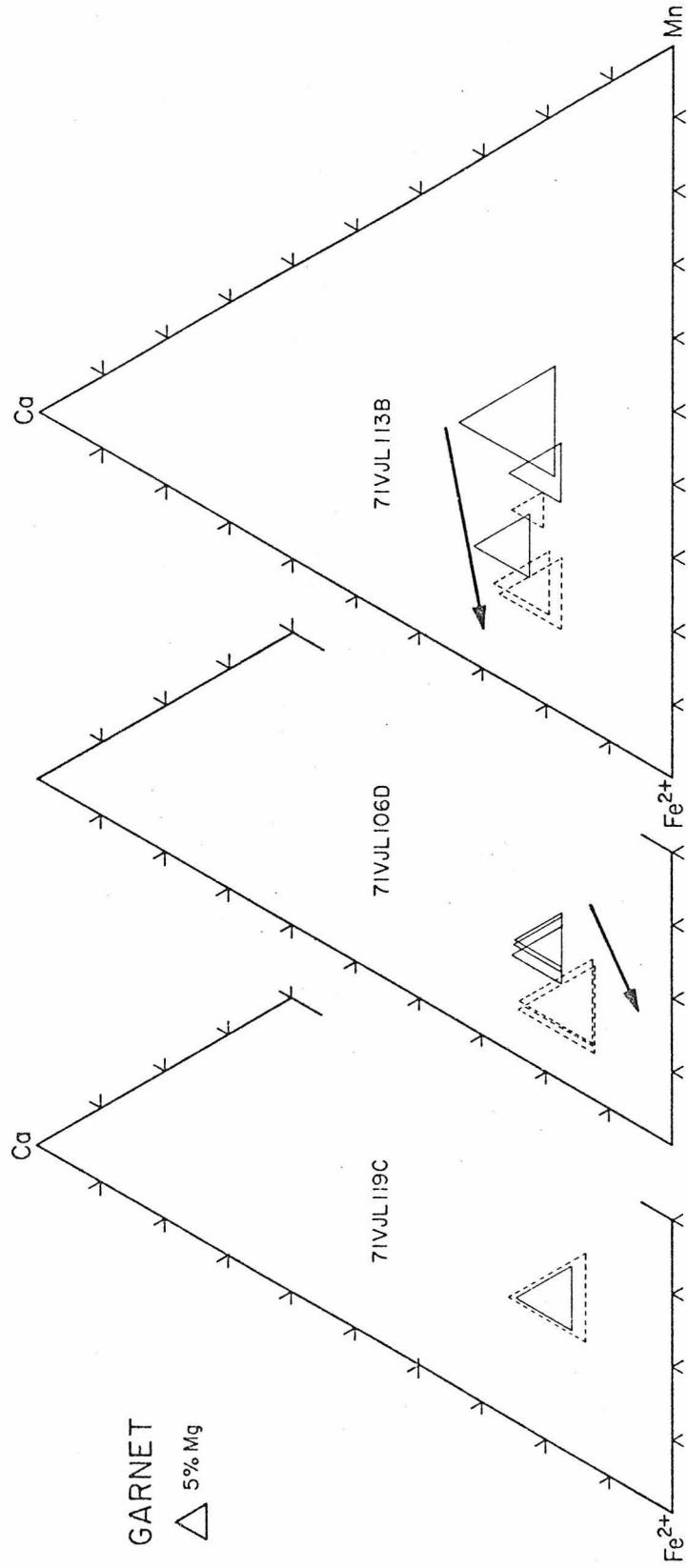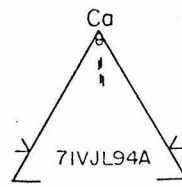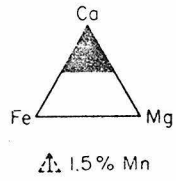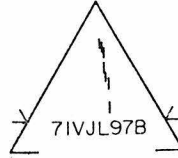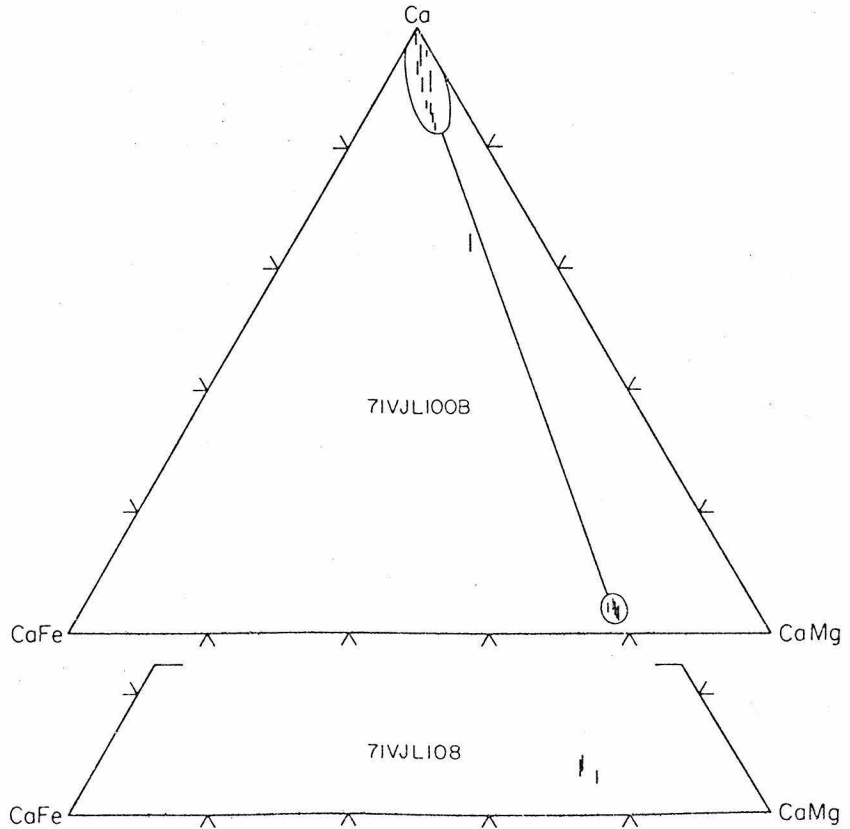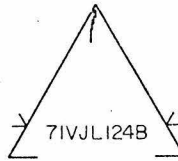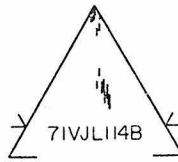
Figure IV-75

Figure IV-76a

SPHENE

71VJL94A ○
71VJL97B △

Figure IV-76b

ILMENITE

71VJL114B

71VJL106D

△ 1.0% (Mg+Zn)TiO₃

71VJL107A

71VJL113B
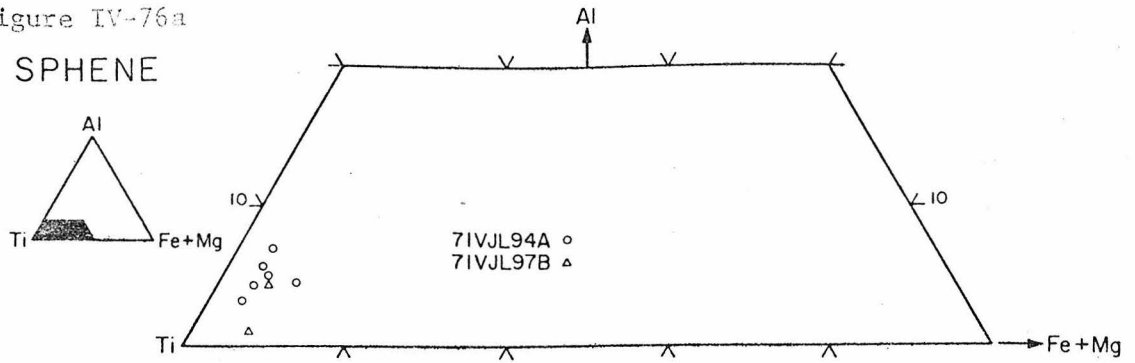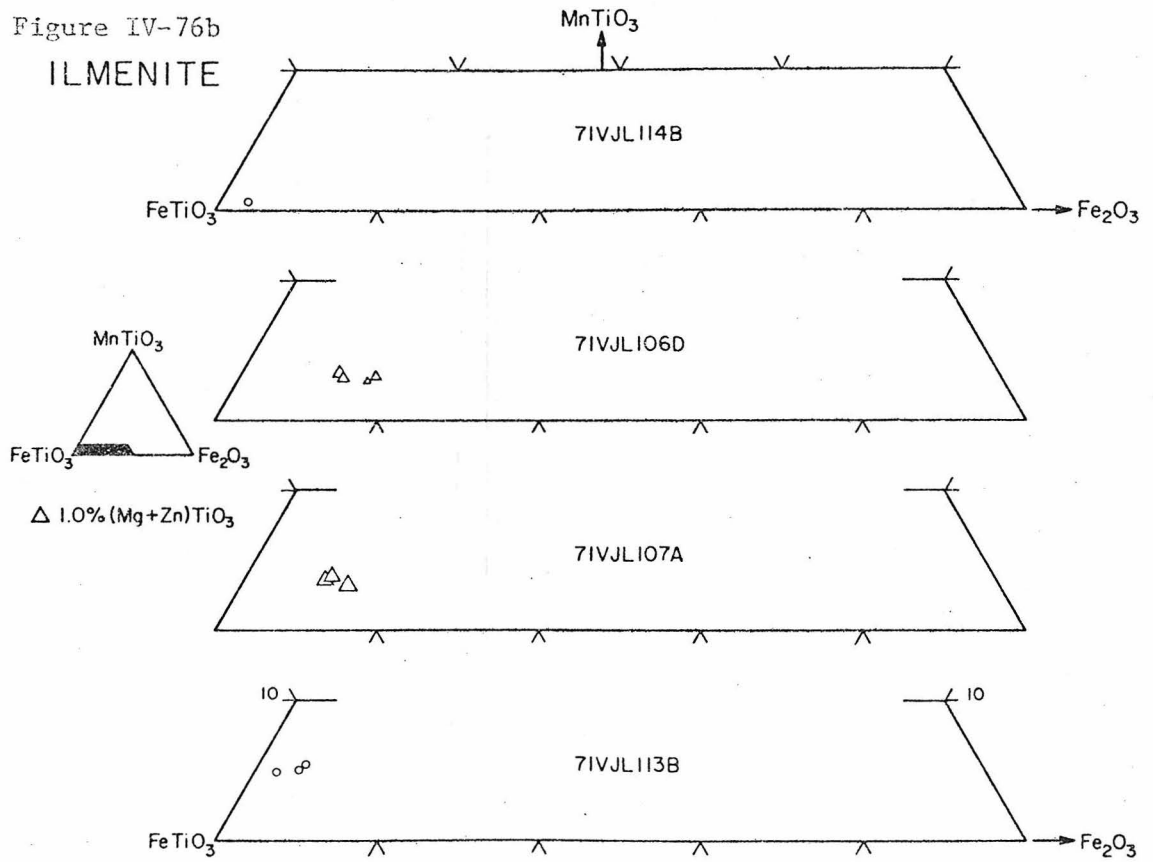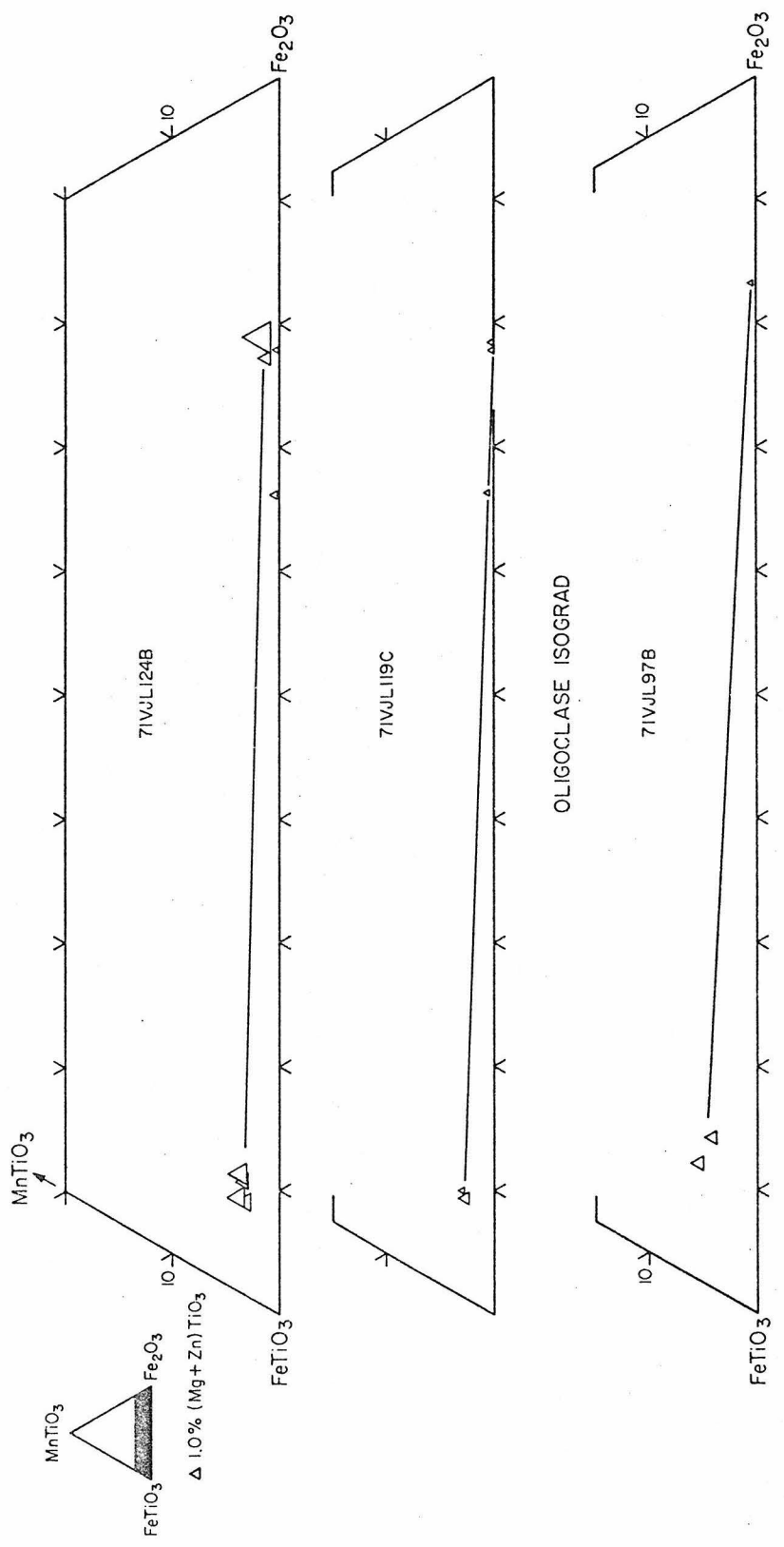
ILMENITE - HEMATITE

Figure IV-76c

AMPHIBOLE
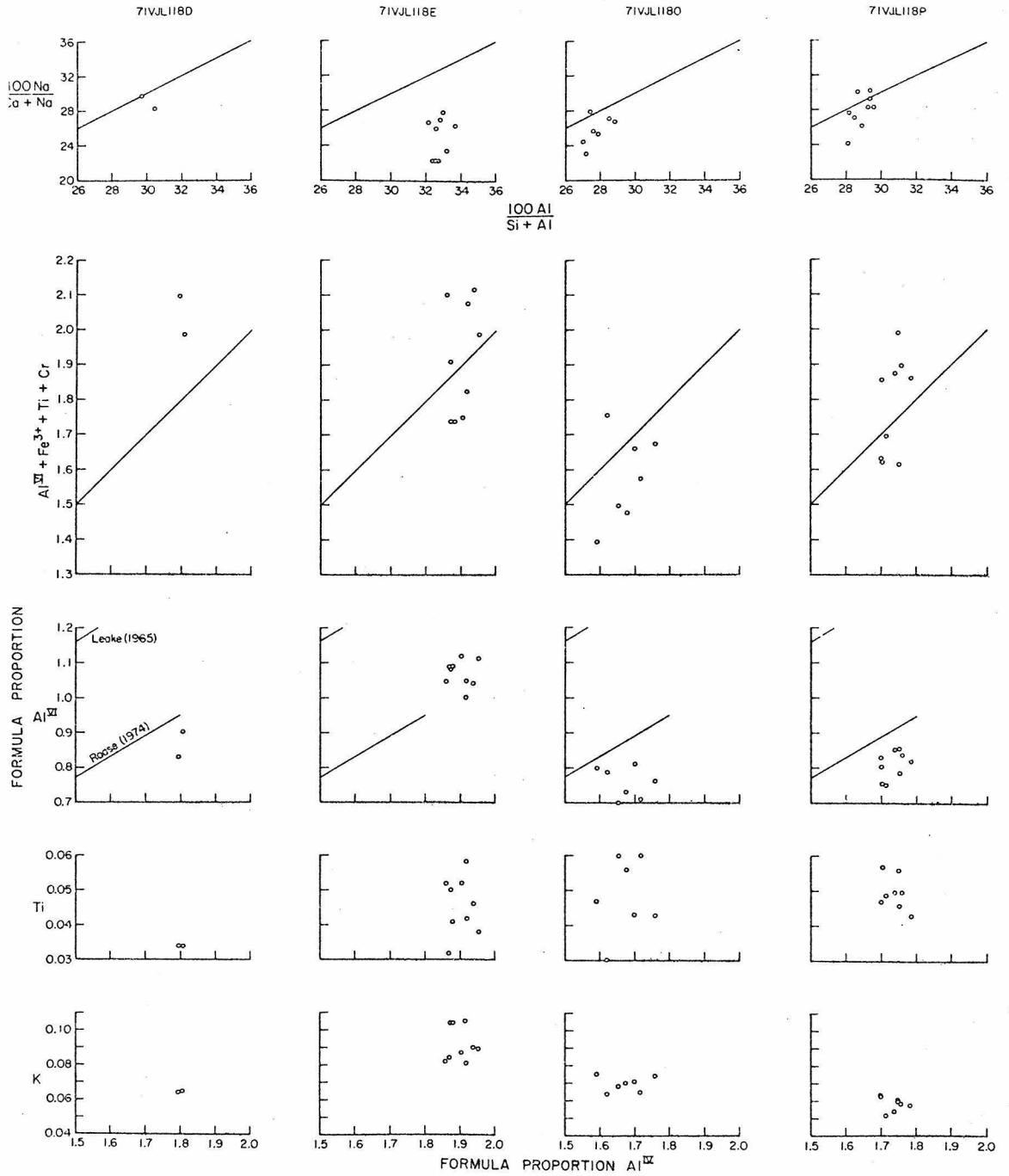
Figure IV-77a
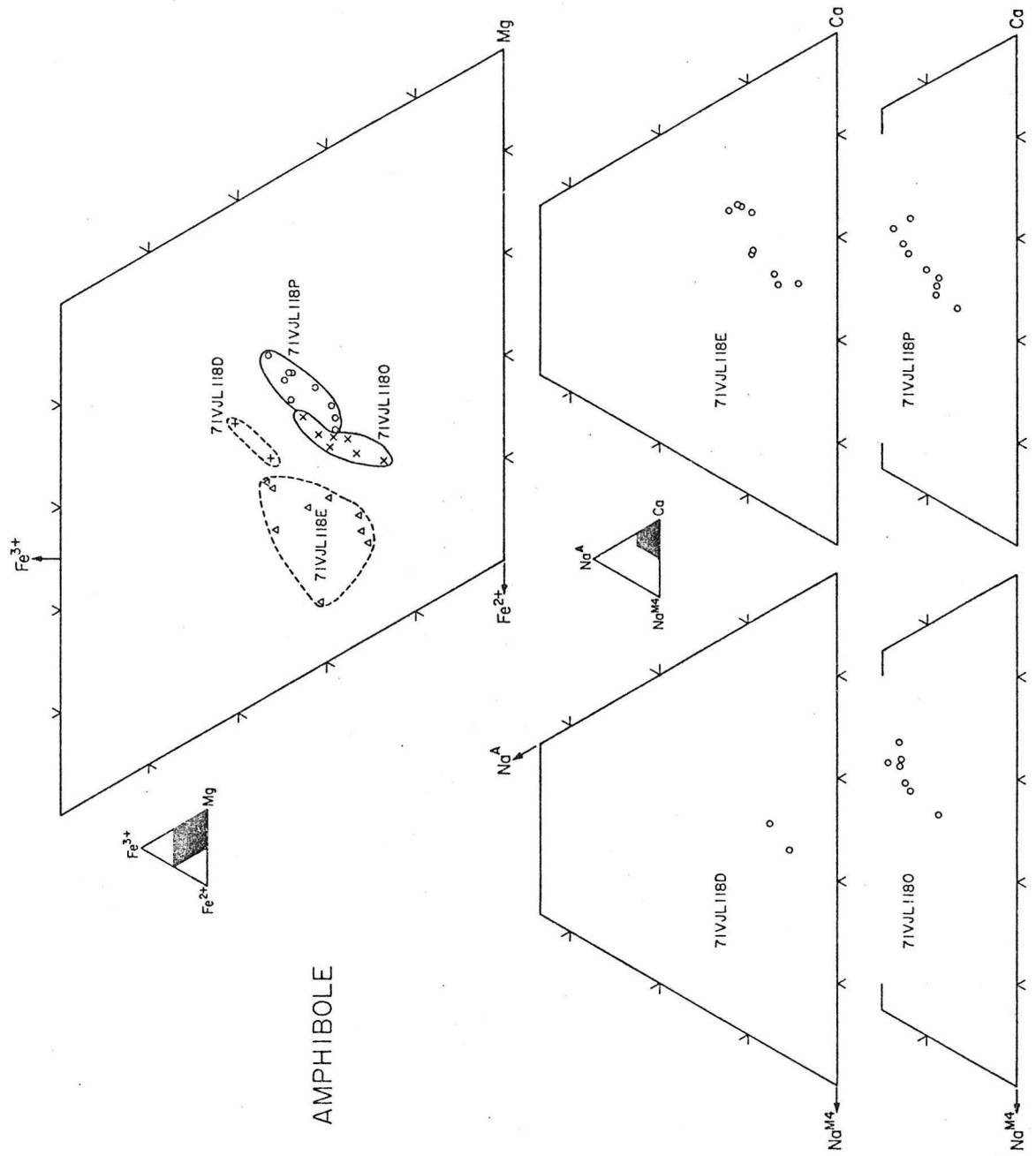
Figure IV-77b

Figure IV-78a

BIOTITE

Figure IV-78b   EPIDOTE
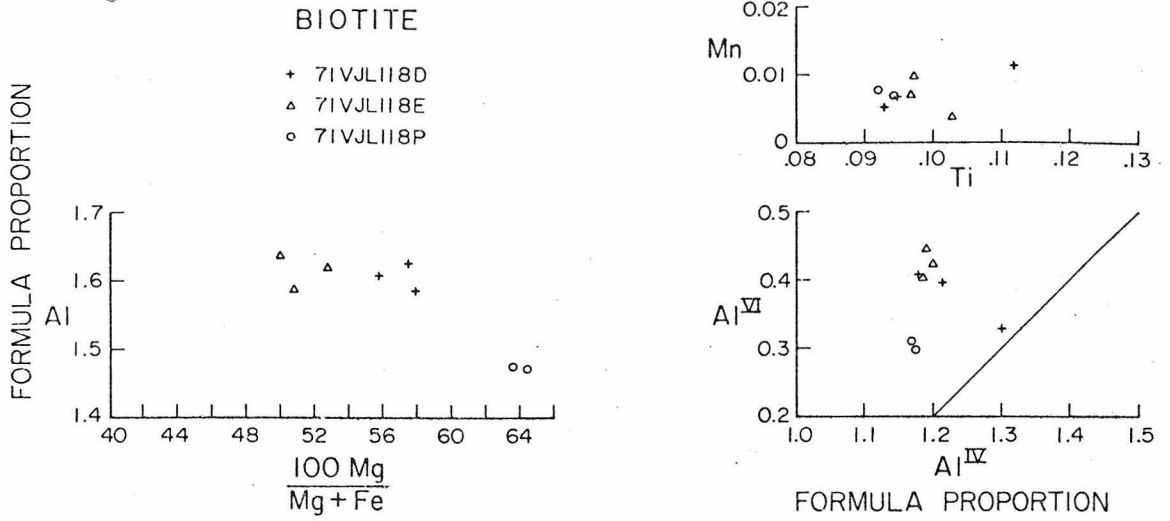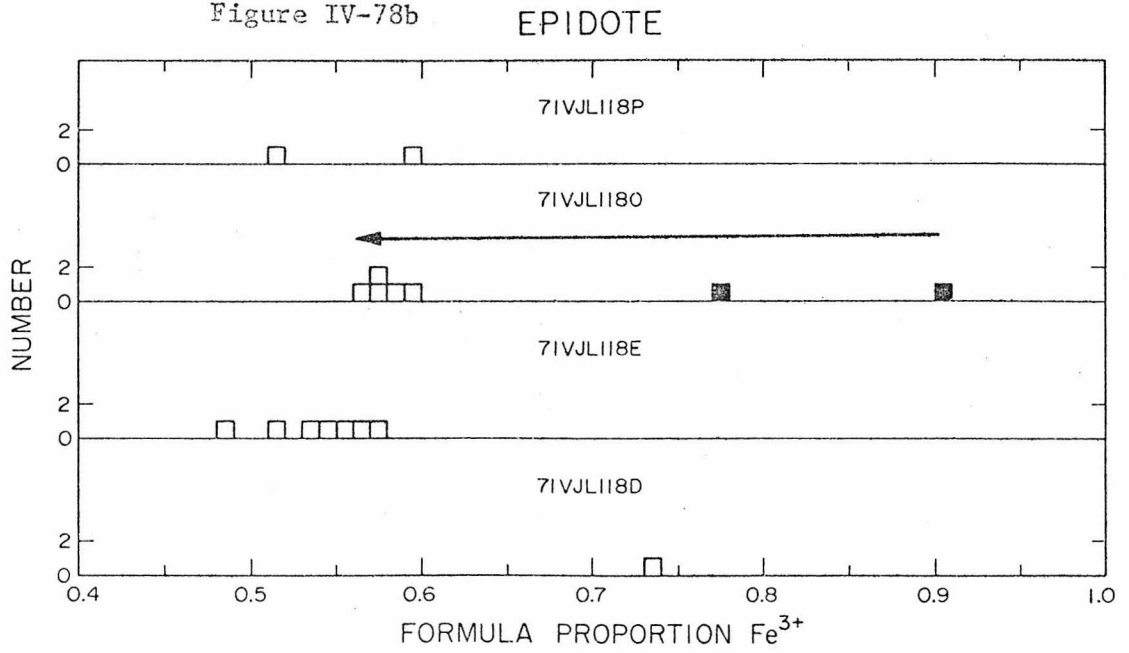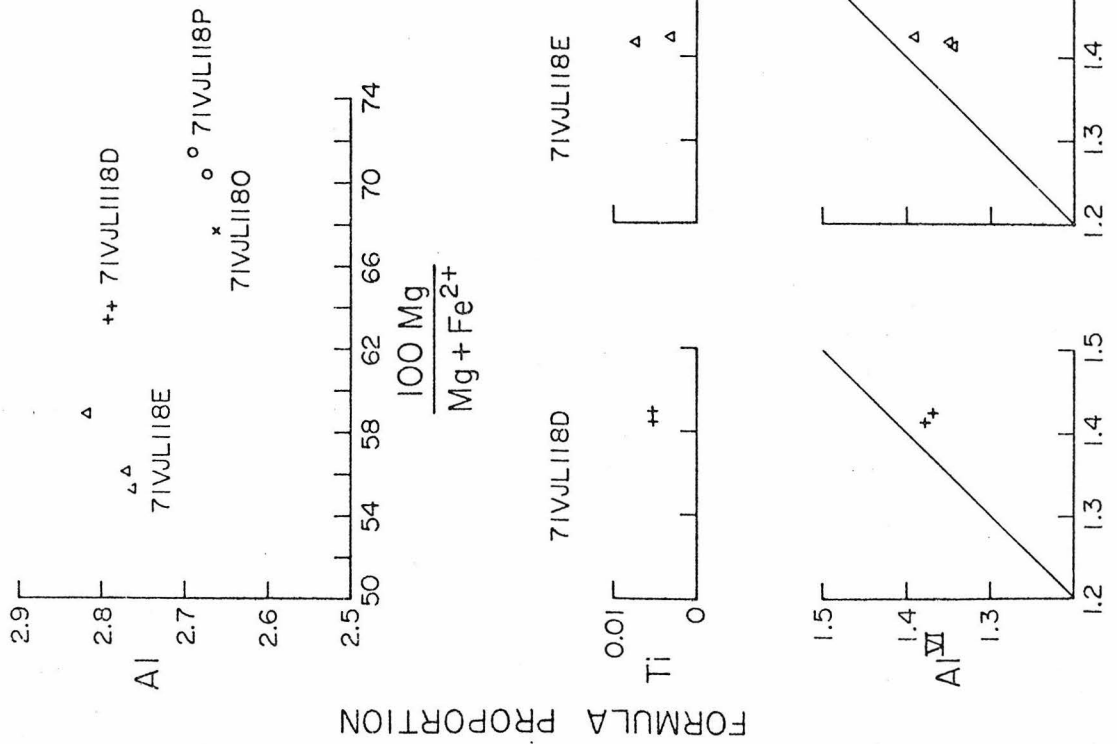
CHLORITE

FORMULA PROPORTION Al^{IV}

Figure IV-79
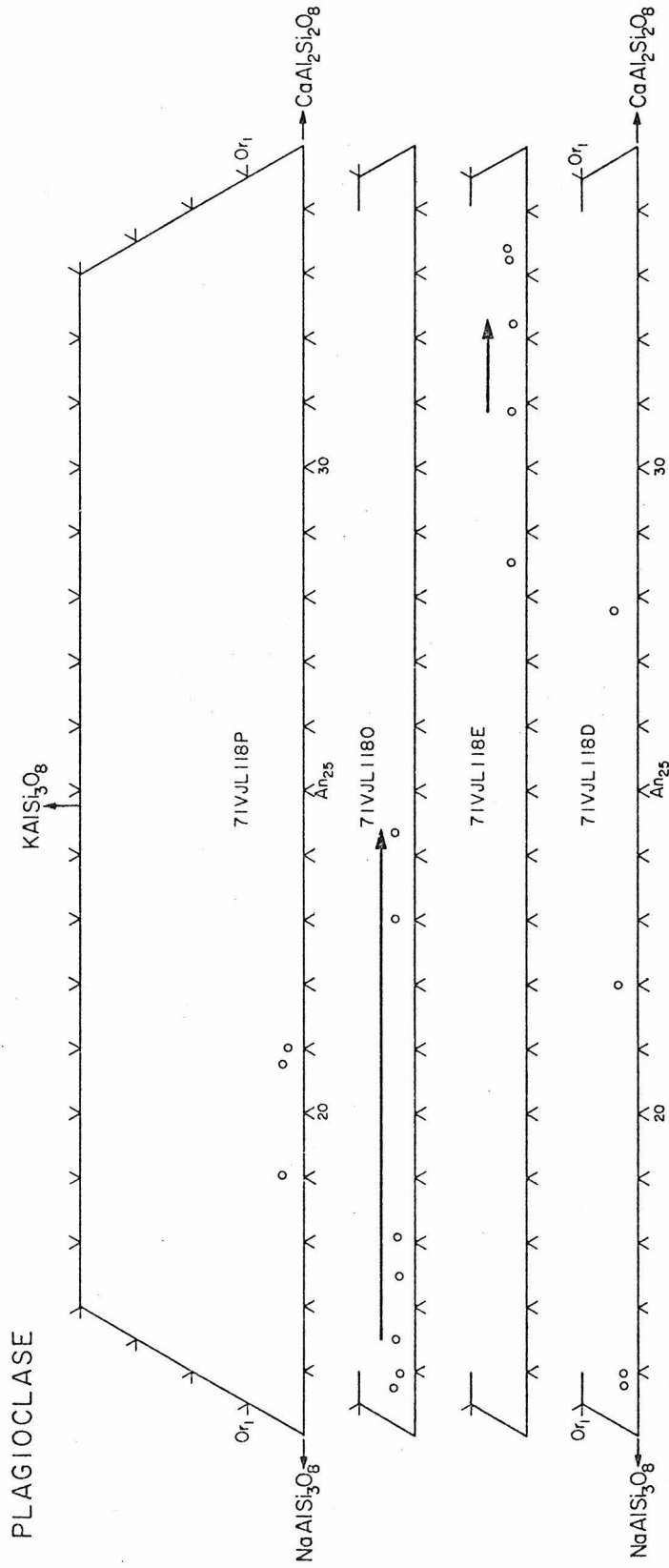
Figure IV-80

Figure IV-81a
CARBONATE

Ca

Fe — Mg

⚠ 1.5% Mn

Ca

71VJLII80

Fe

Mg

Figure IV-81b
GARNET

△ 5% Mg

Ca

50

71VJLII8E

Fe²⁺

Mn

71VJLII8D

Fe²⁺

Mn
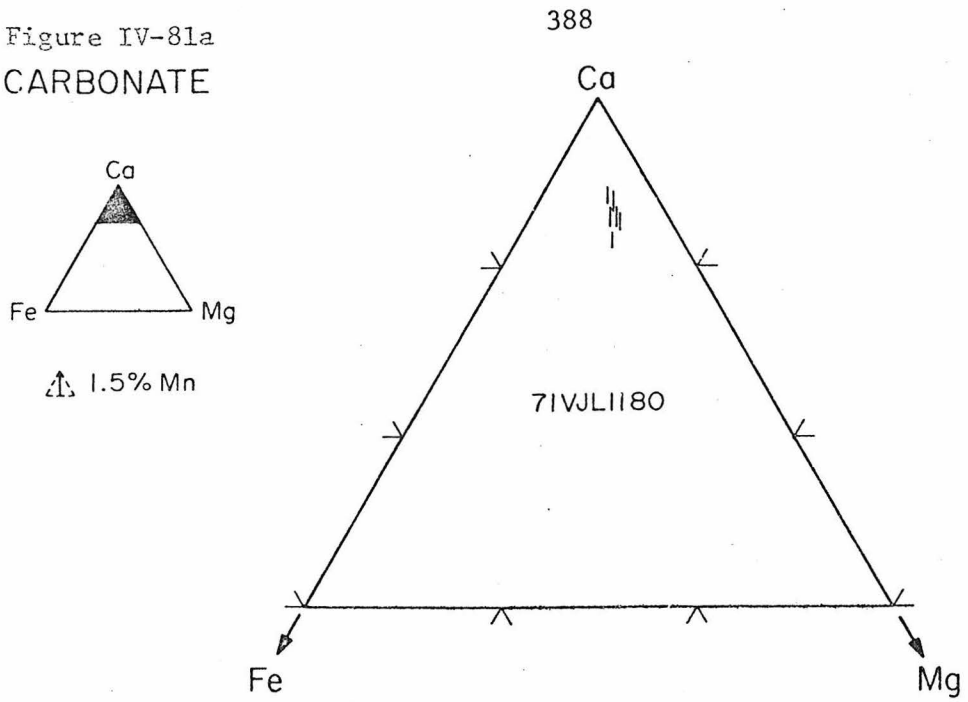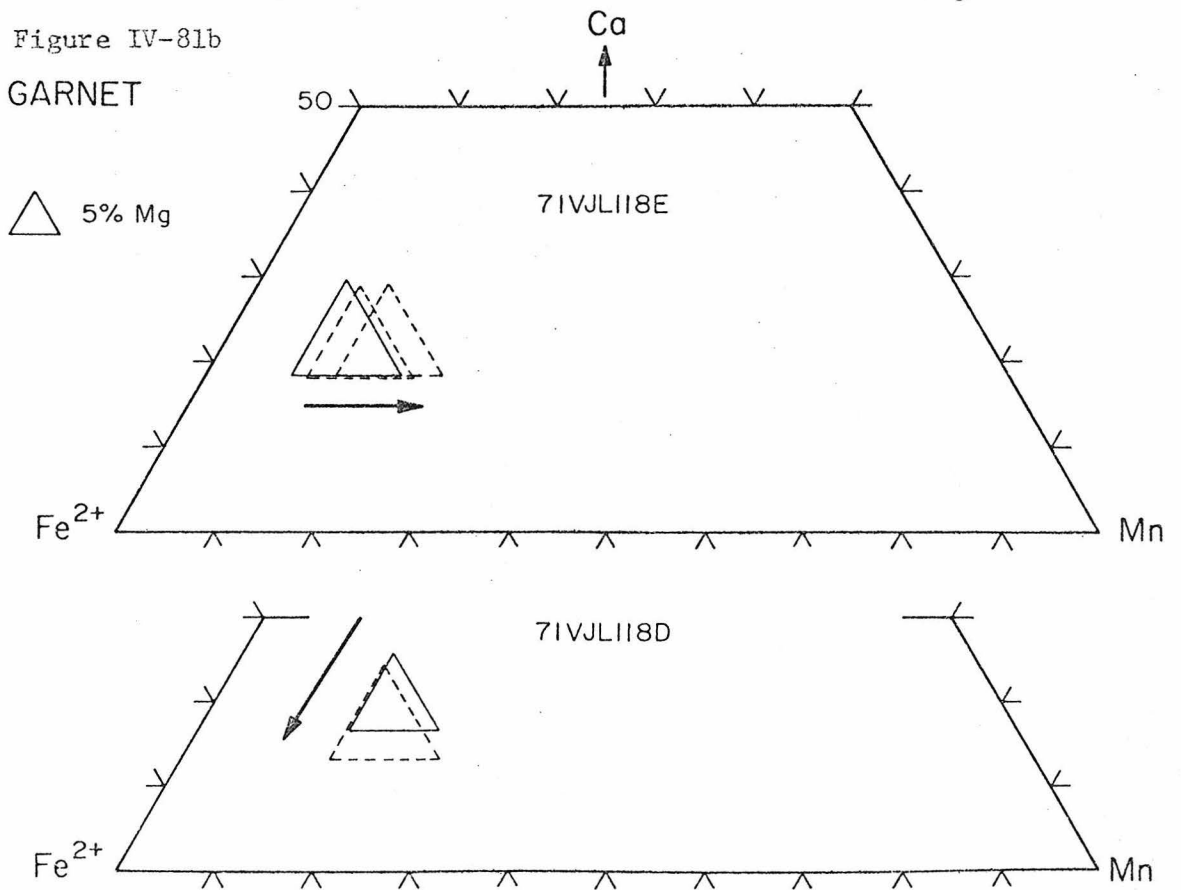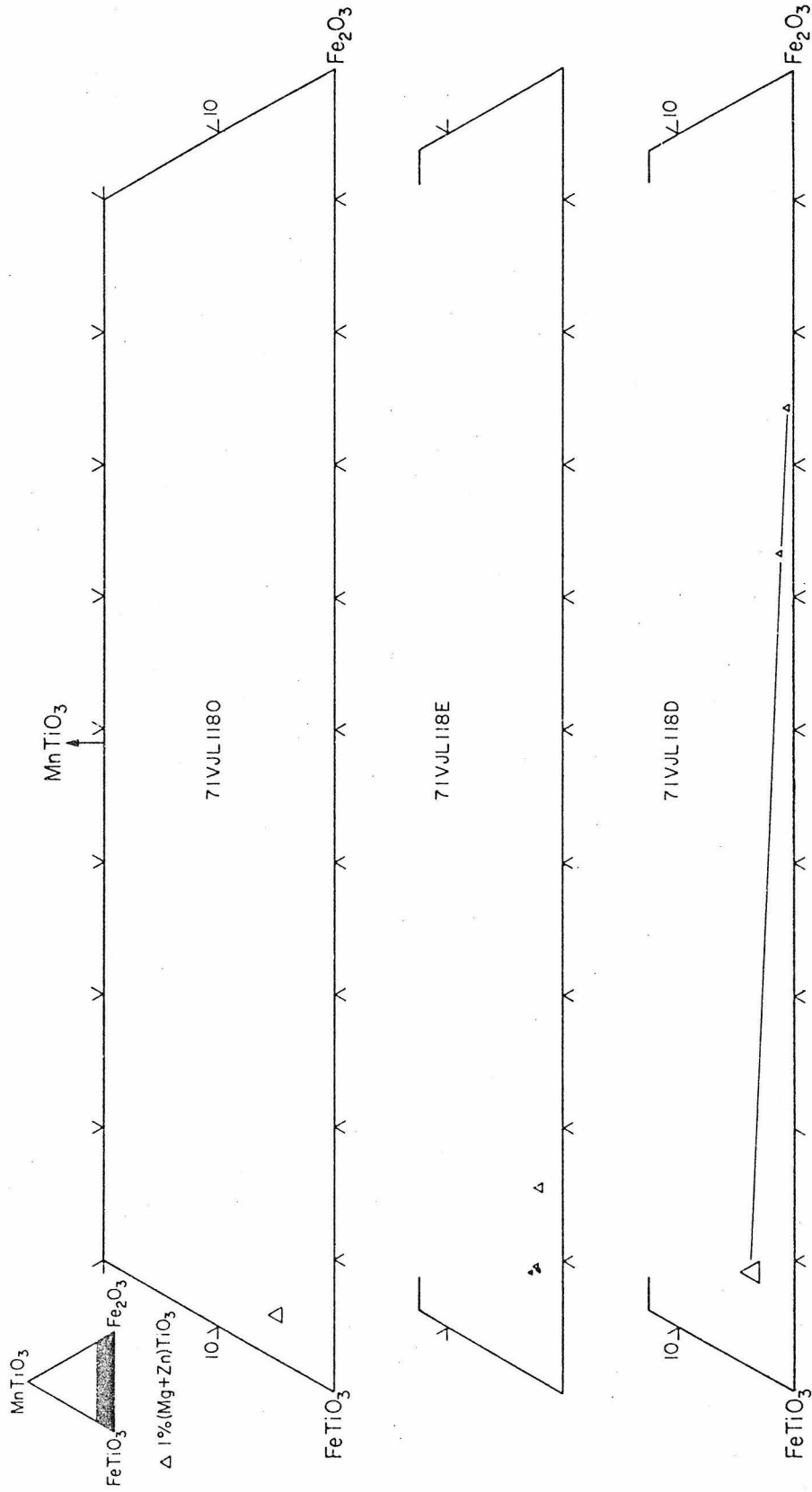
ILMENITE-HEMATITE

Figure IV-82

AMPHIBOLE
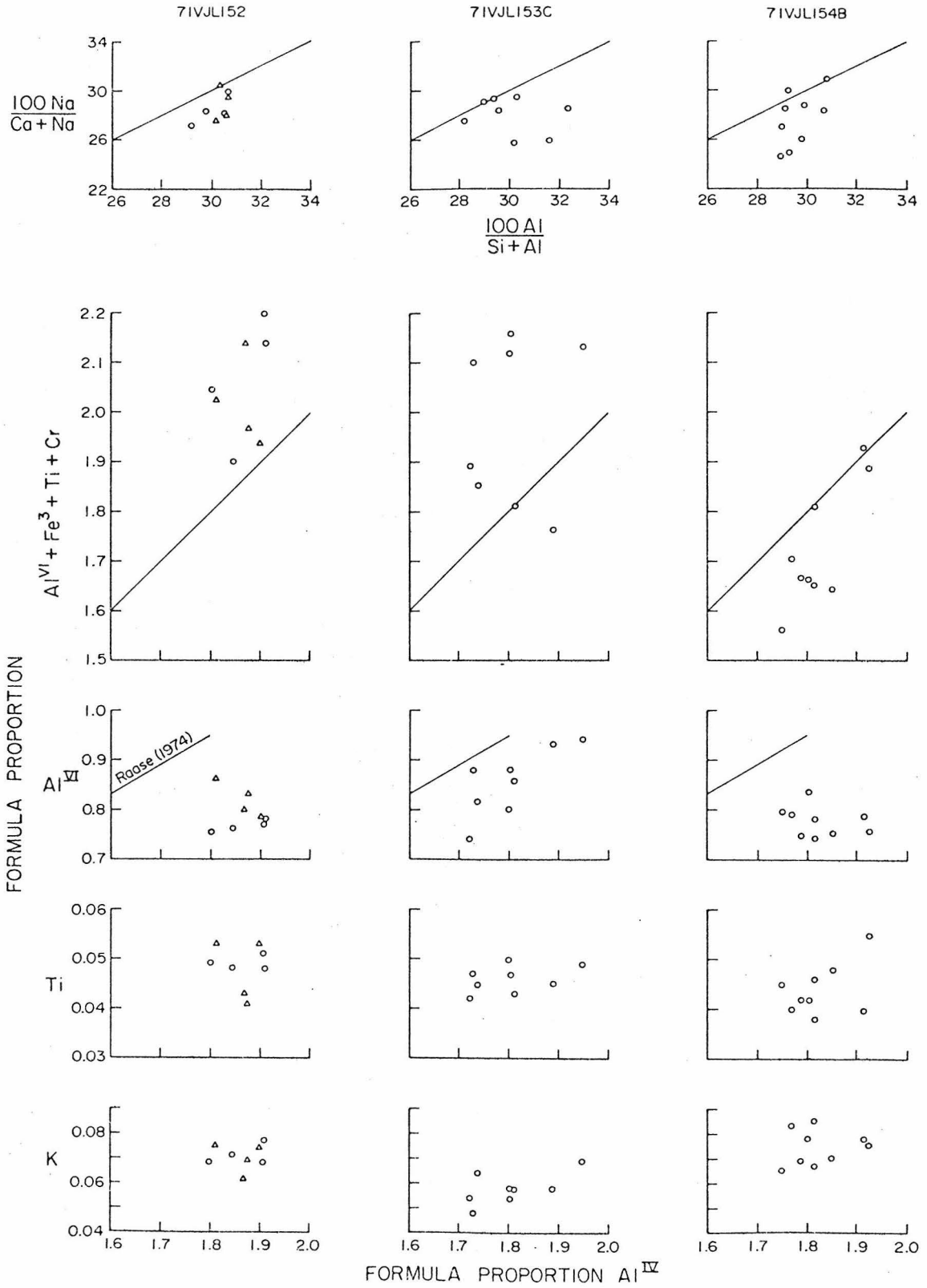
Figure IV-83a
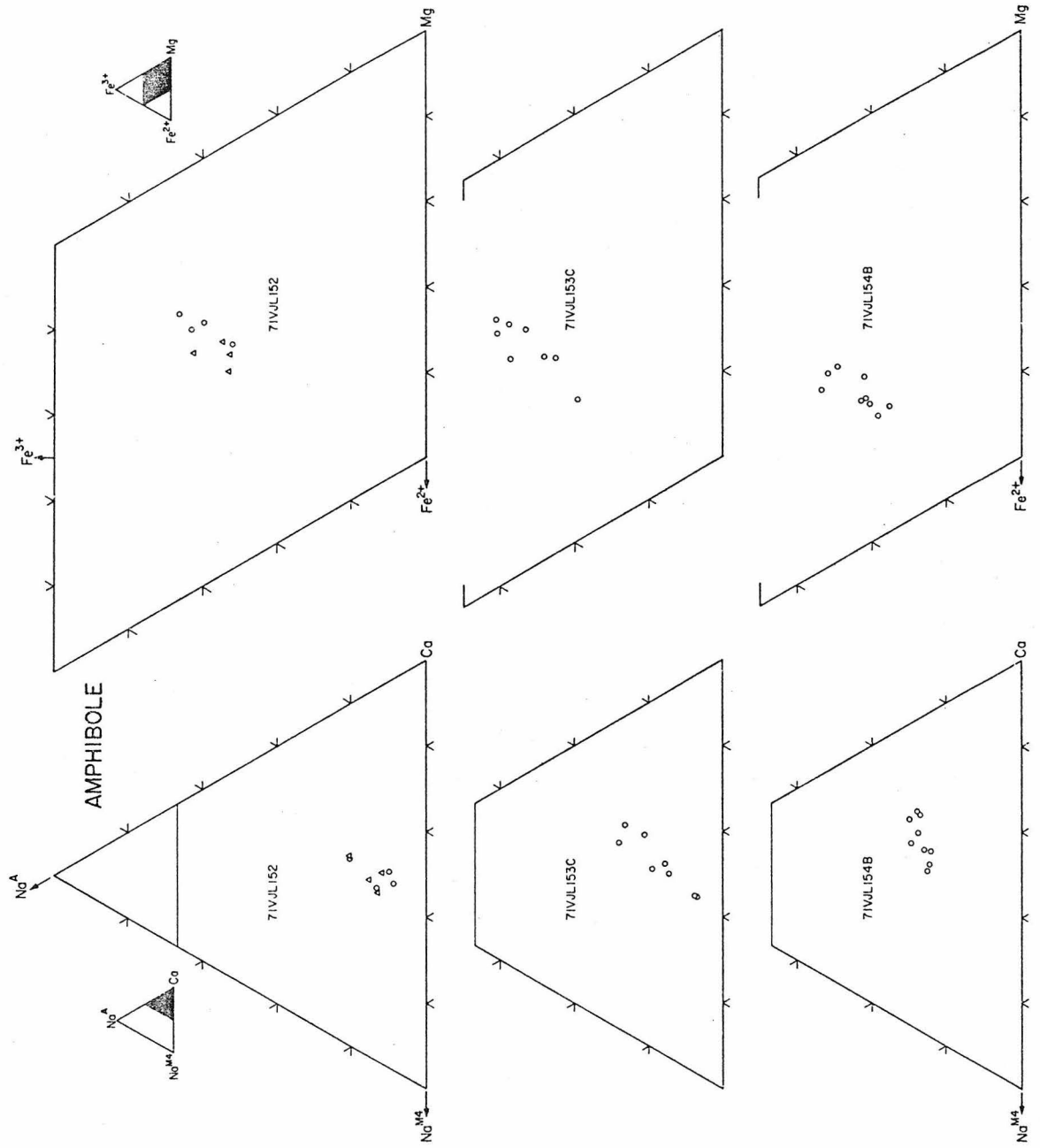
Figure IV-83b

Figure IV-84a

EPIDOTE

Figure IV-84b

BIOTITE
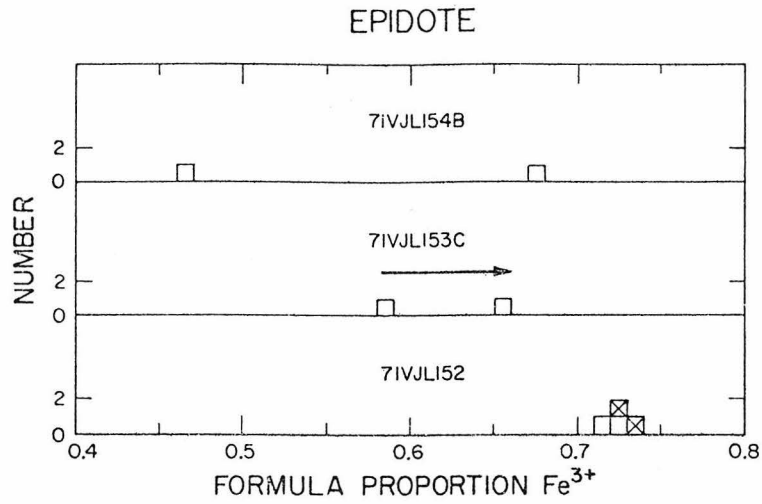
- • SILICIC
- ○ MAFIC } 7IVJLI52
- △ 7IVJLI53C
- ◇ 7IVJLI54B
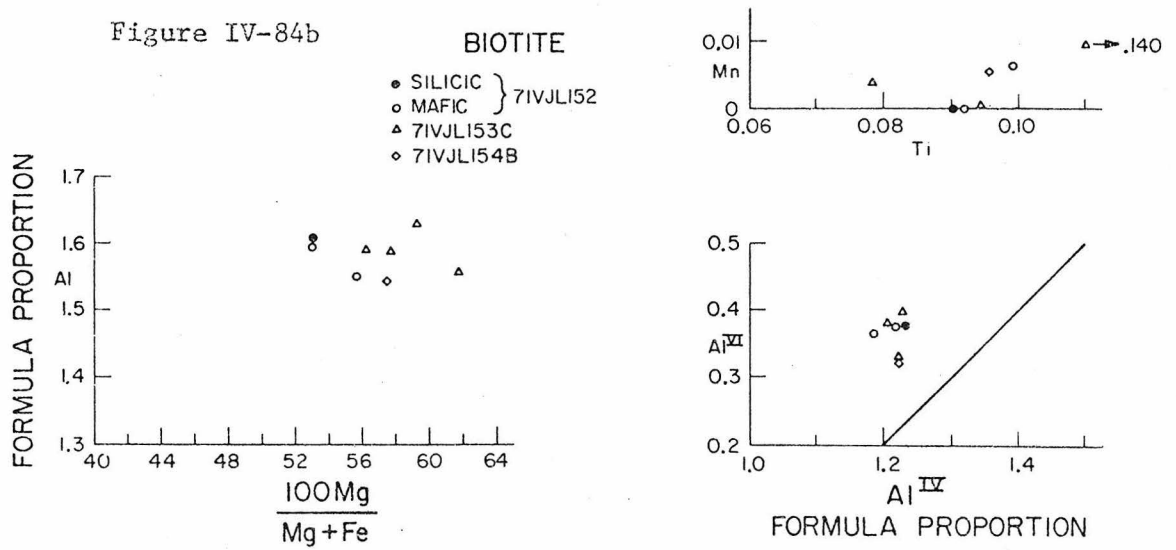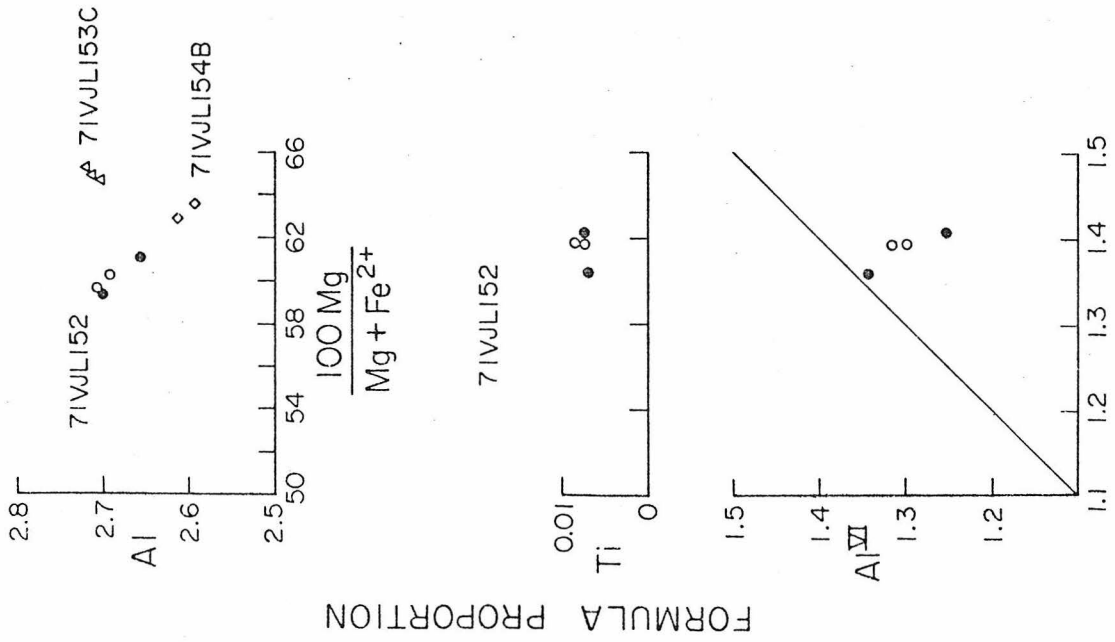
CHLORITE

FORMULA PROPORTION Al^{IV}
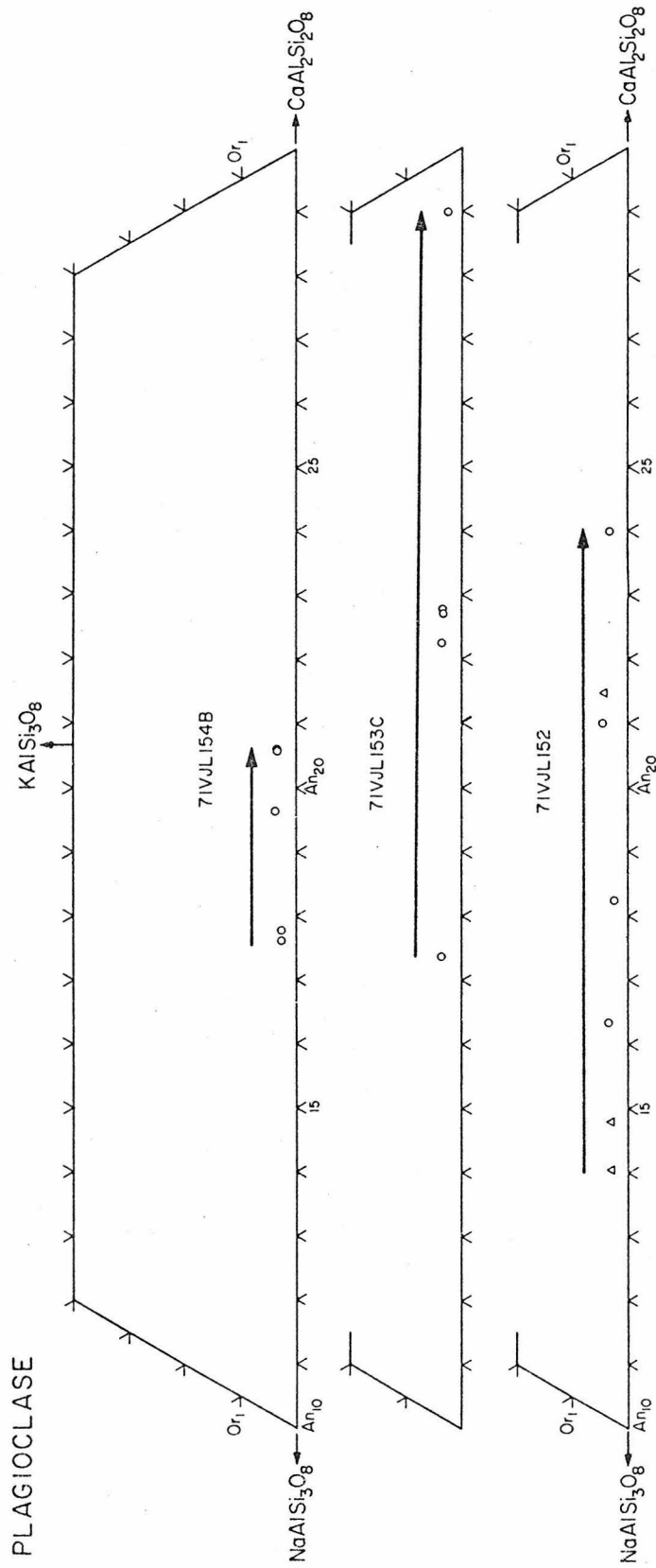
Figure IV-85

Figure IV-86

Figure IV-87

ILMENITE - HEMATITE

Figure IV-88

Figure IV-89

CHLORITE 71VJLI26H

BIOTITE 71VJLI26H

Figure IV-90

WHITE MICA
7IVJLI26H
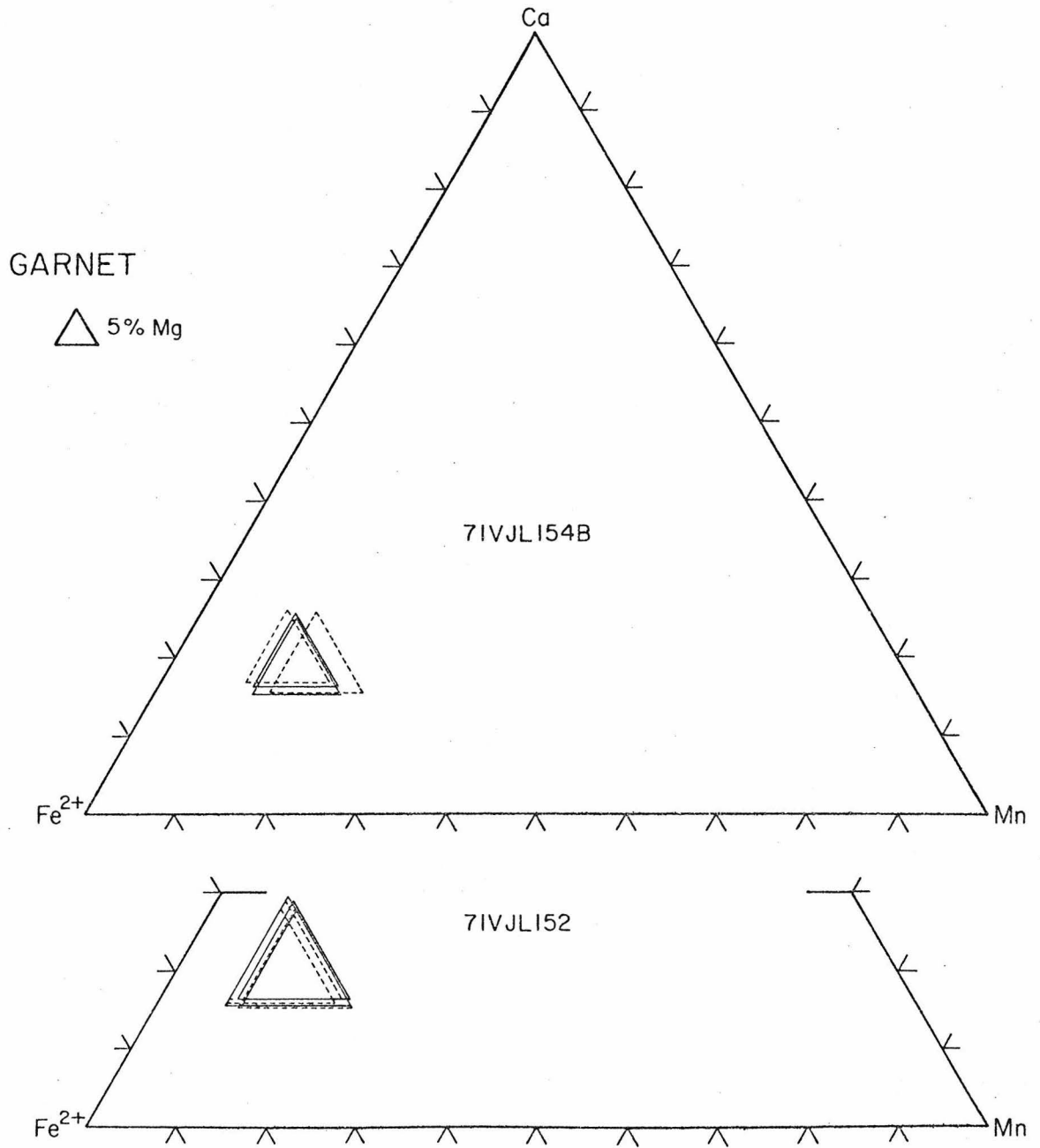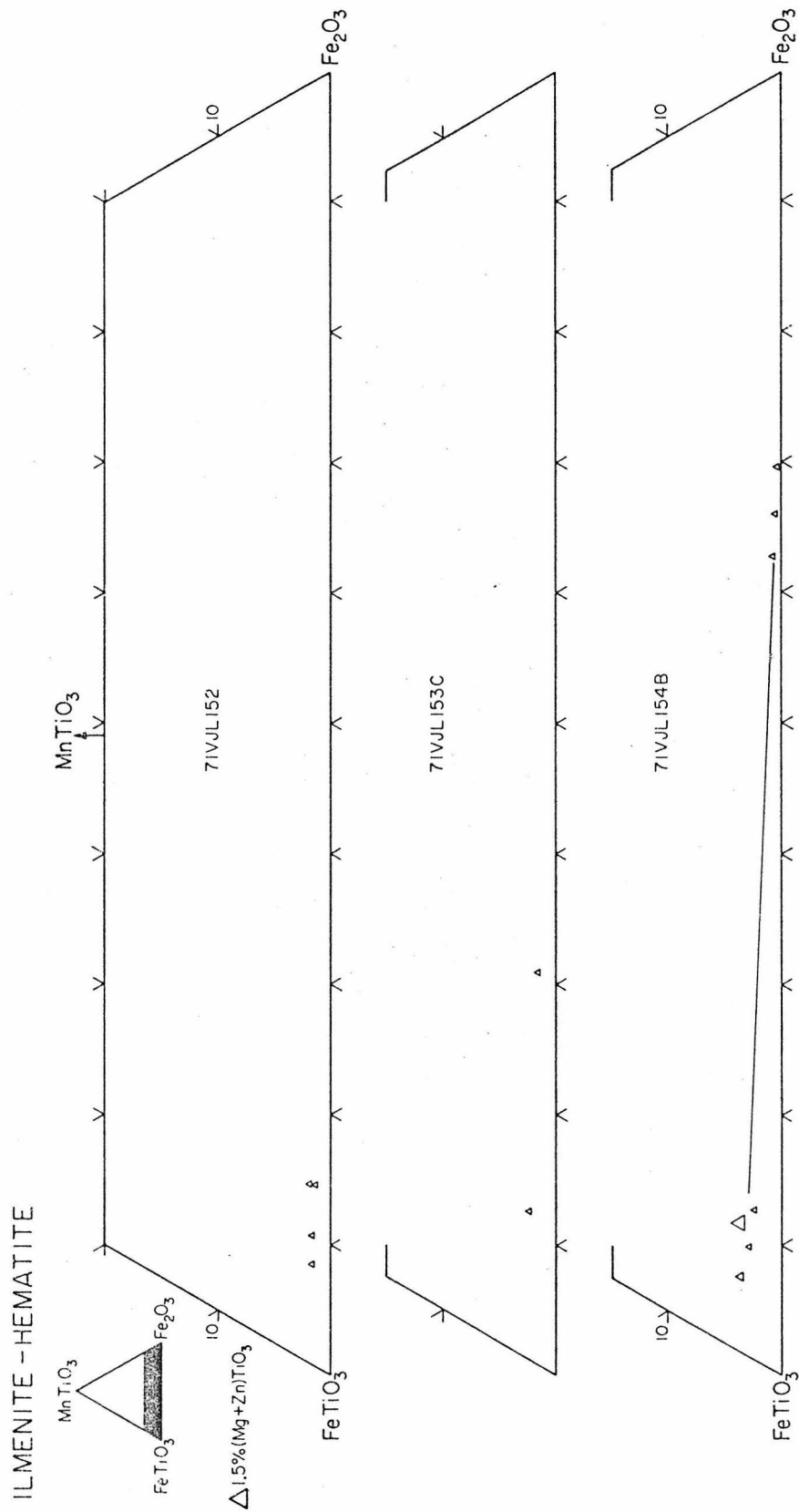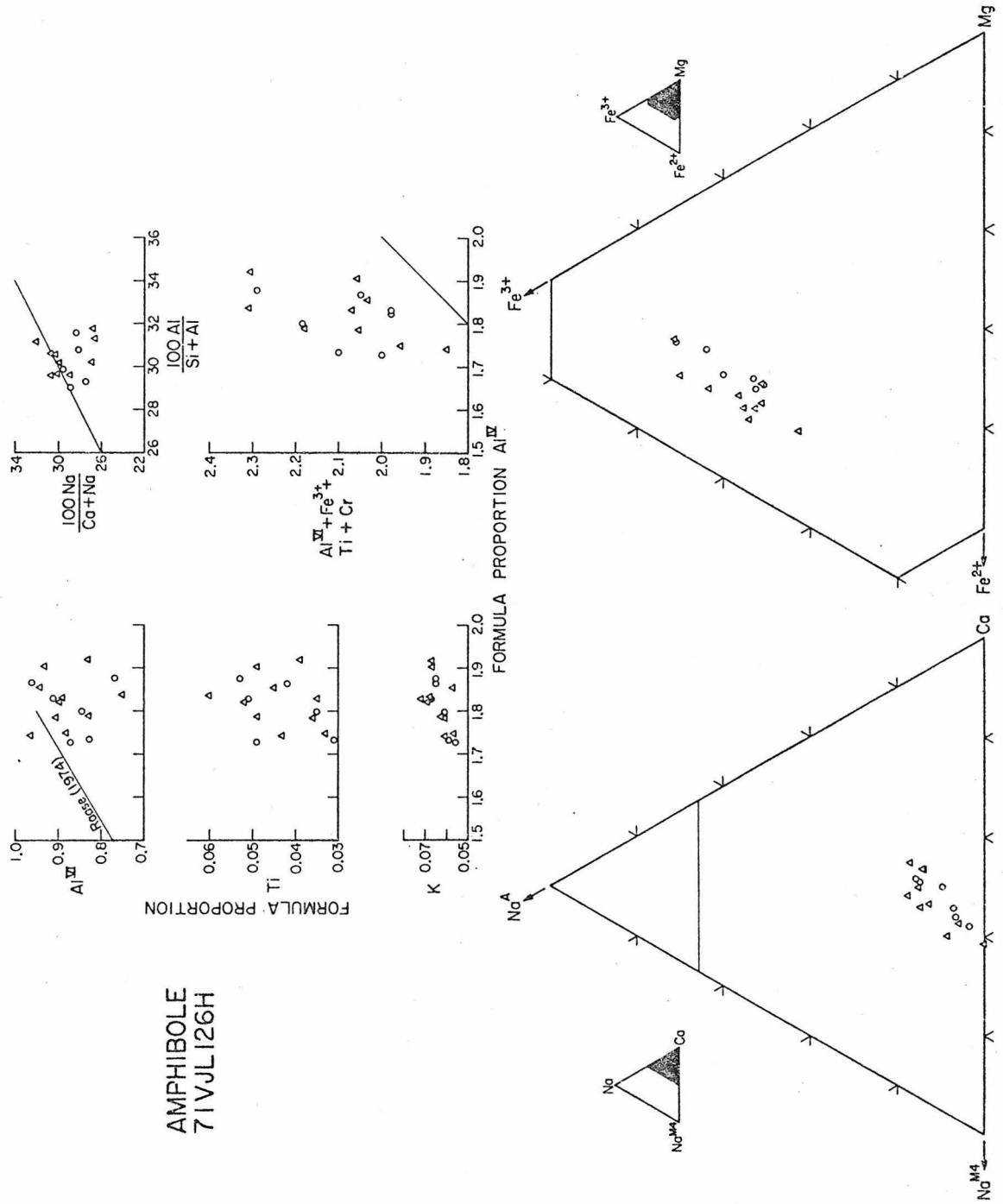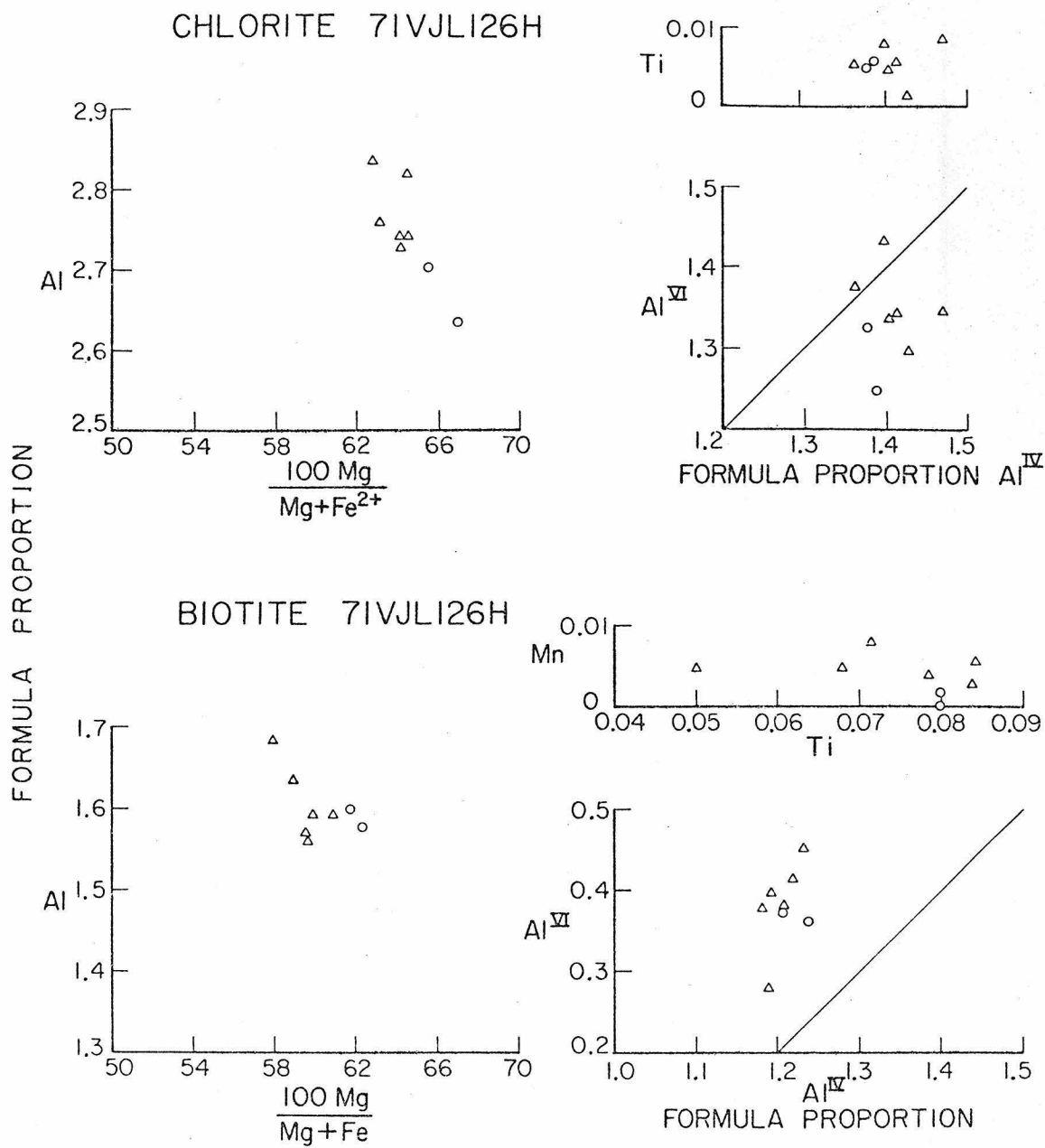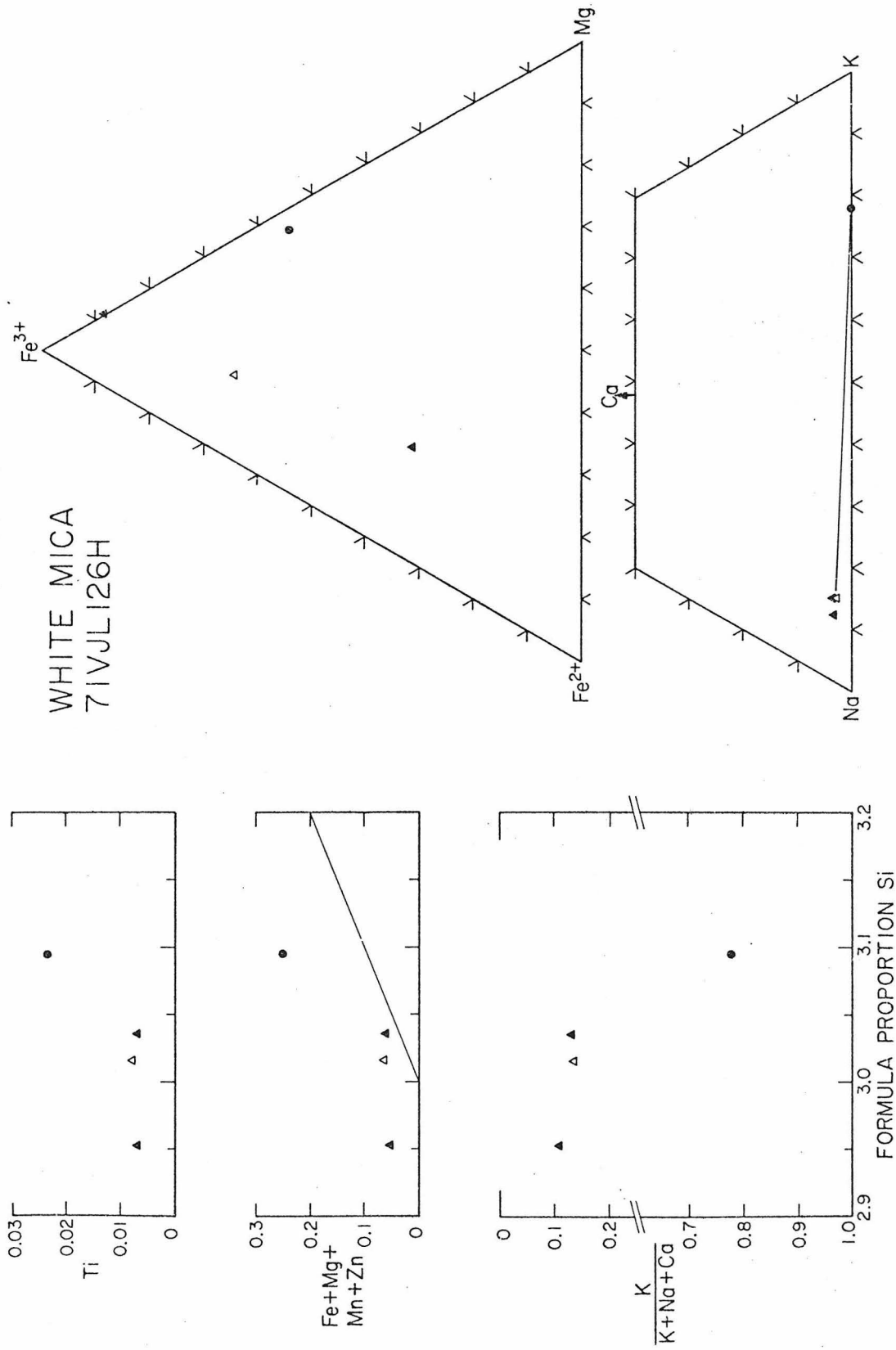
Figure IV-91

Figure IV-92a

PLAGIOCLASE 71VJLI26H
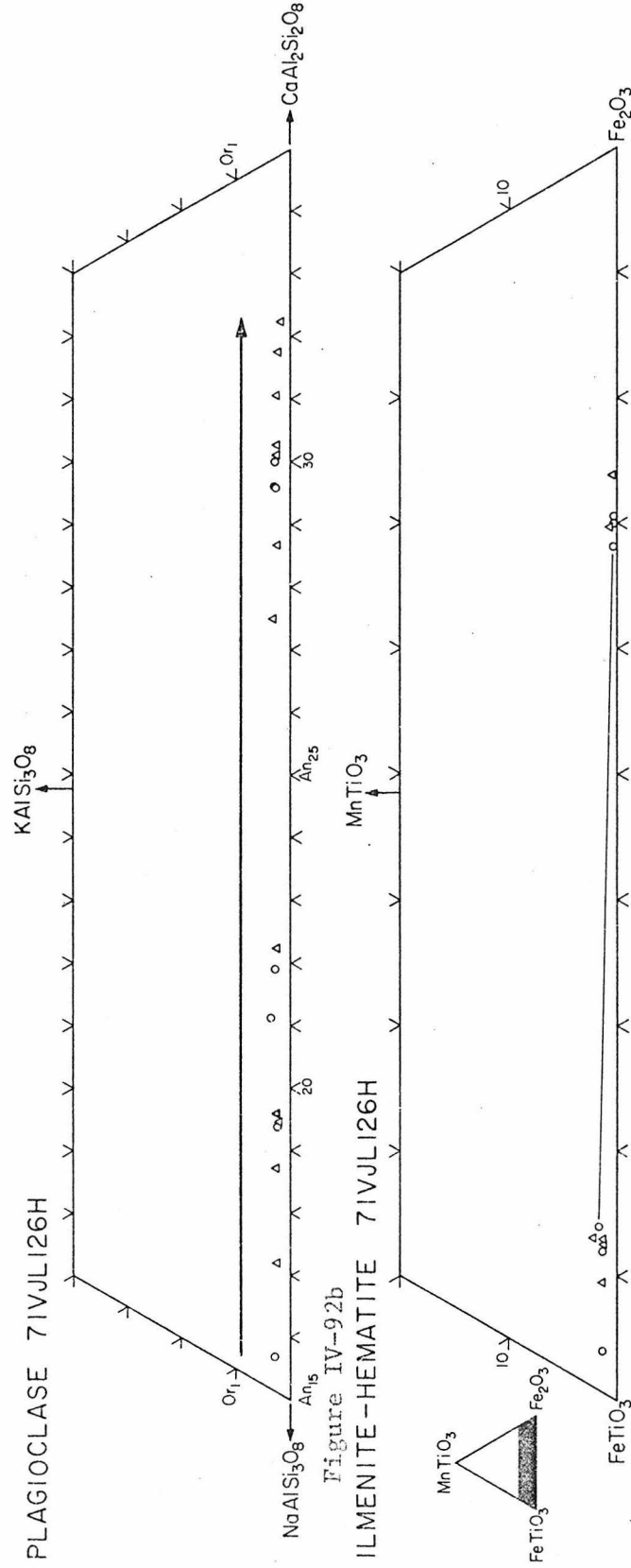
Figure IV-92b

ILMENITE-HEMATITE 71VJLI26H

GARNET
71VJL126H

5% Mg

Ca

Mn

Fe²⁺
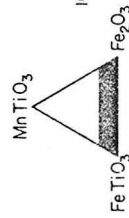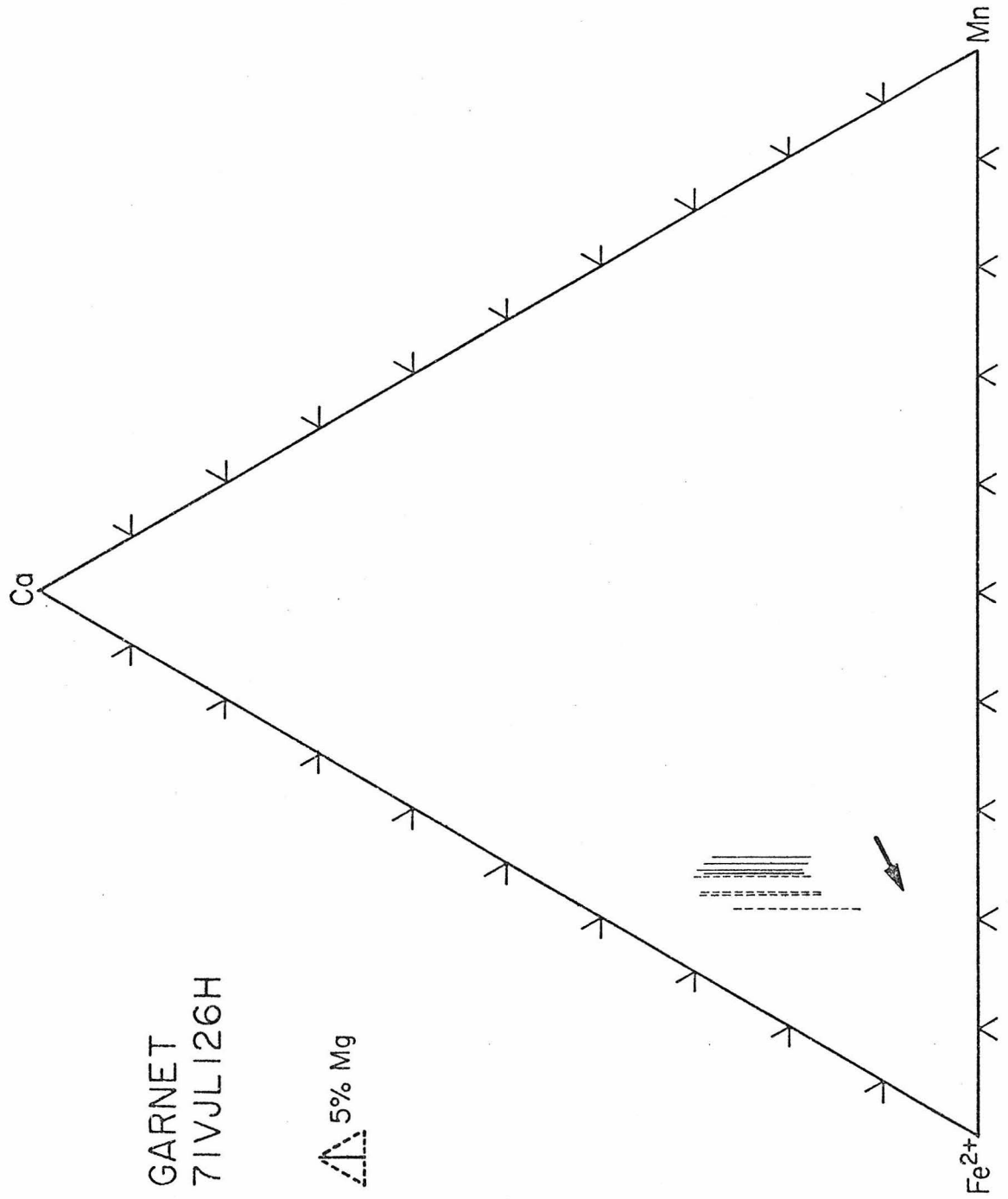
Figure IV-93

Figure IV-94

BIOTITE

CHLORITE
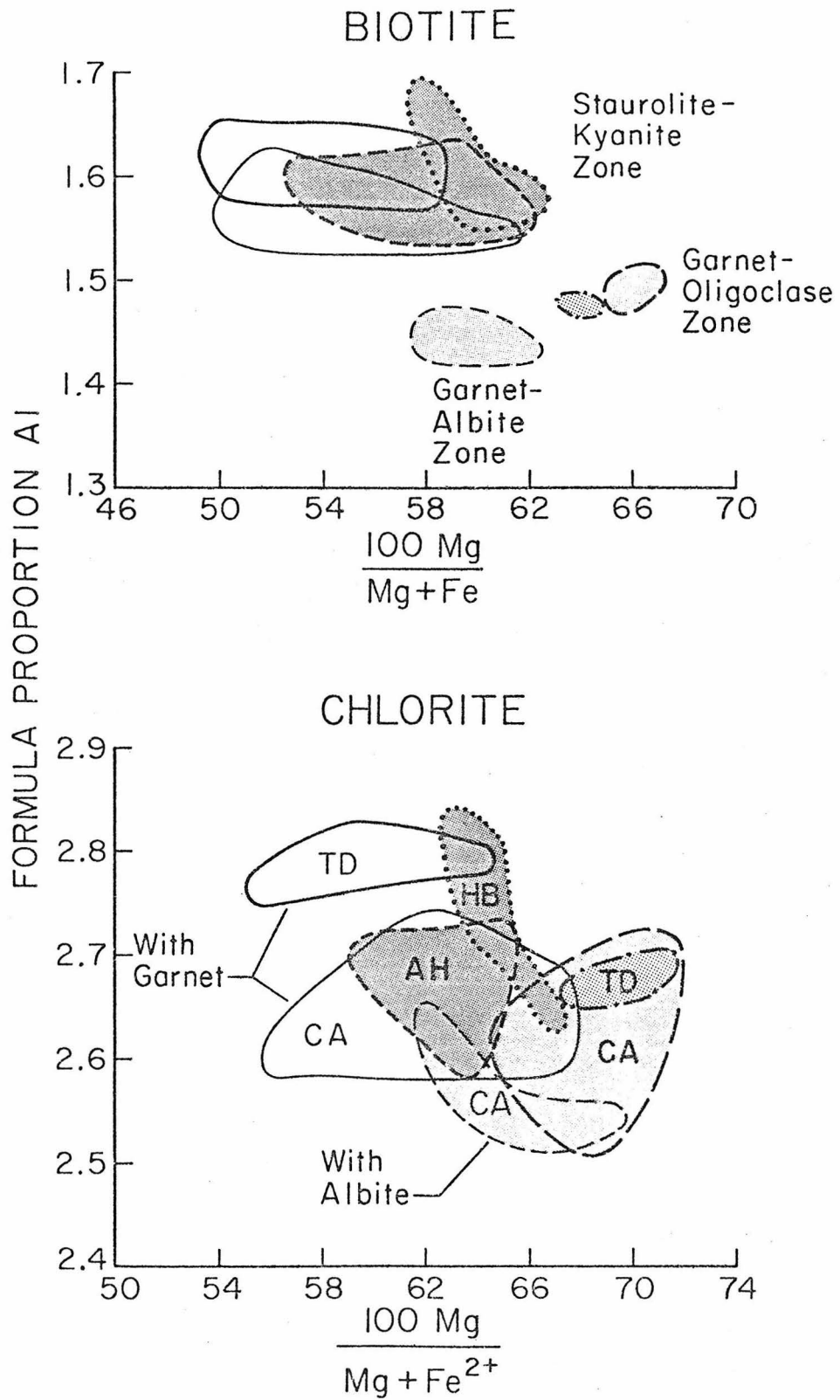
Figure IV-95
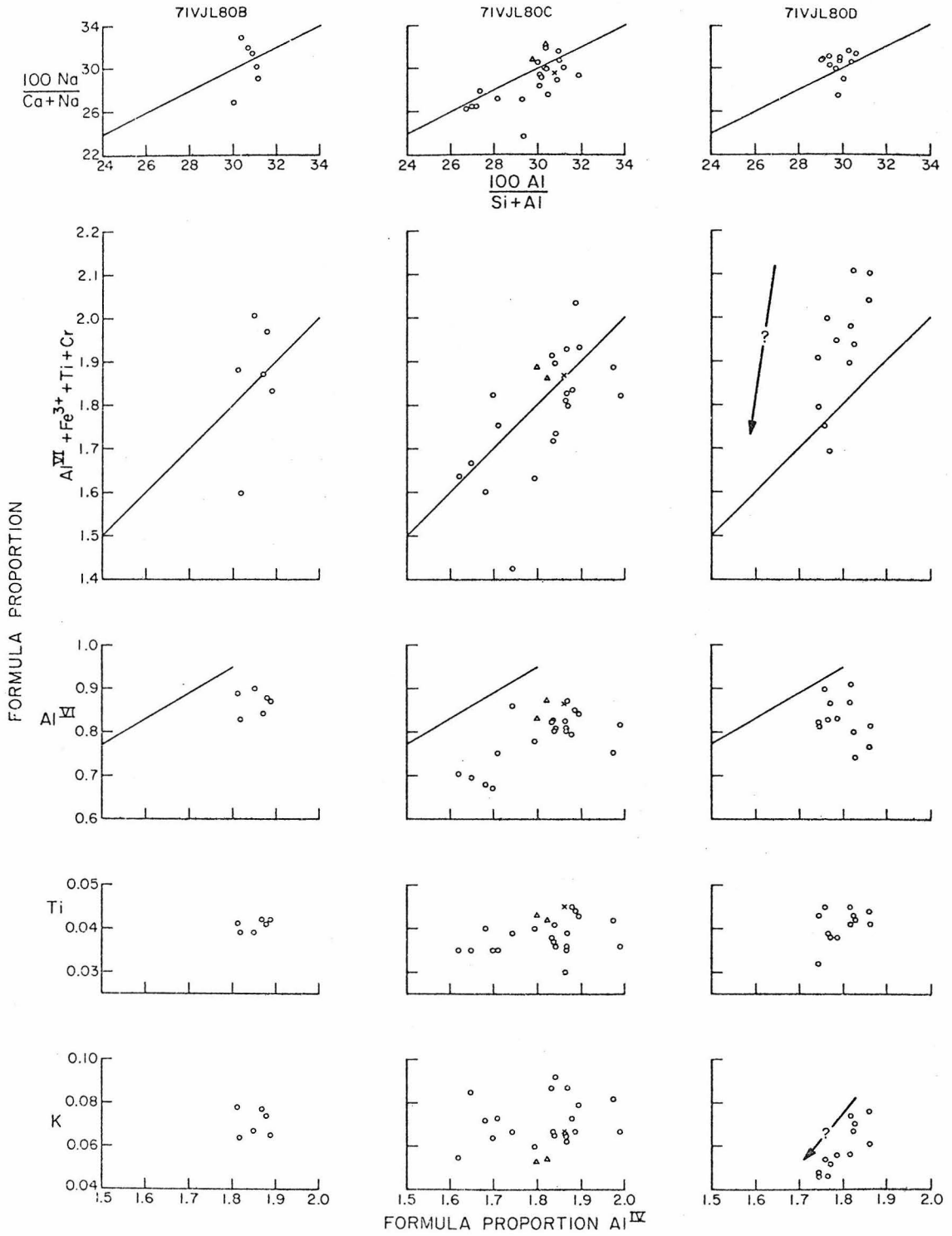
Figure IV-96a
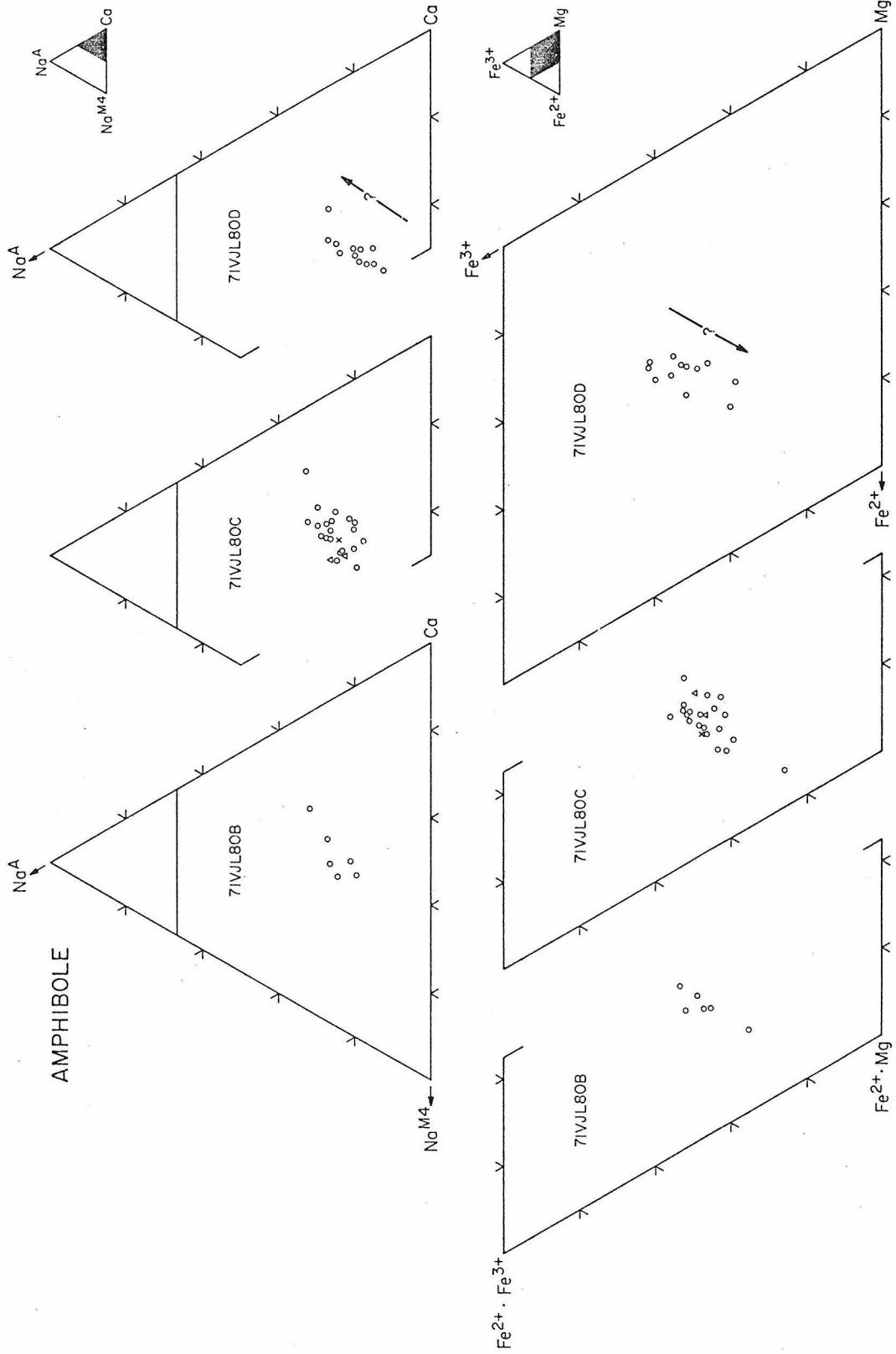
AMPHIBOLE

Figure IV-96b
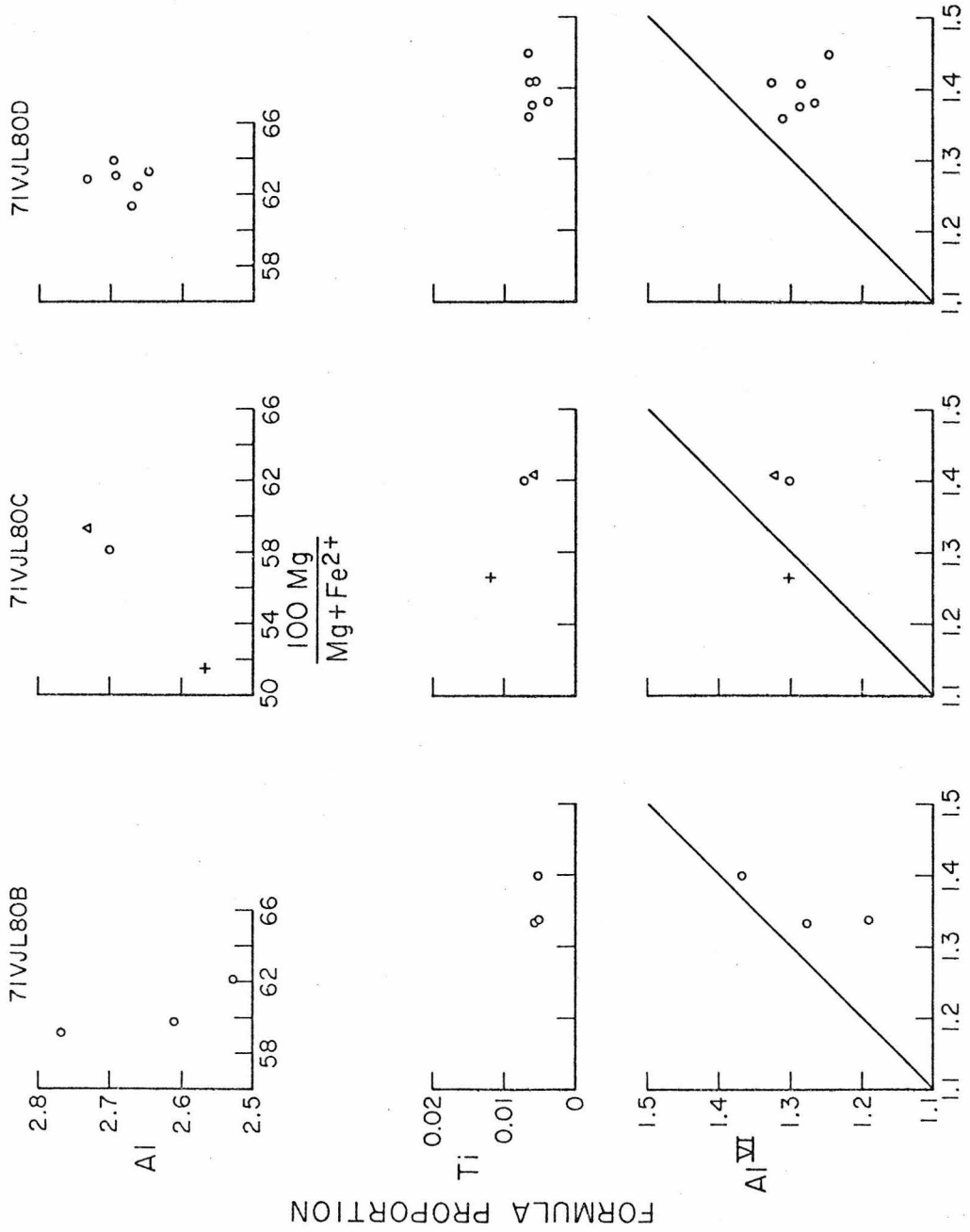
CHLORITE

Figure IV-97

Figure IV-98a   EPIDOTE
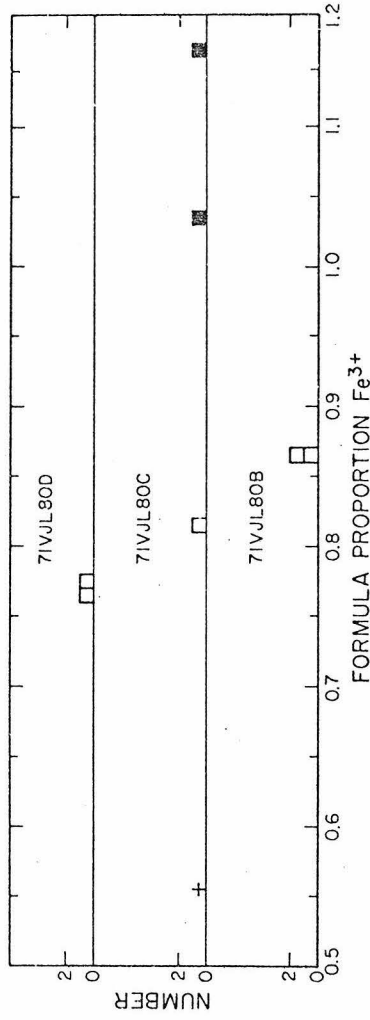
Figure IV-98b   PLAGIOCLASE
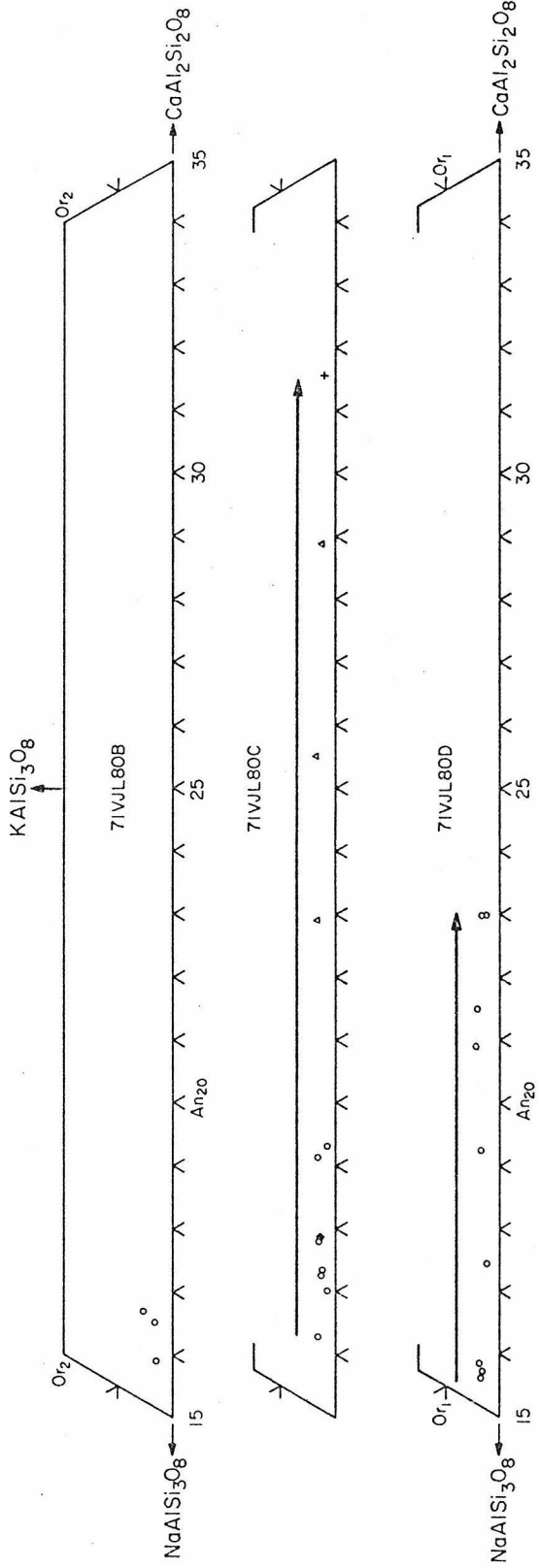
Figure IV-99a
HEMATITE

7IVJL80C
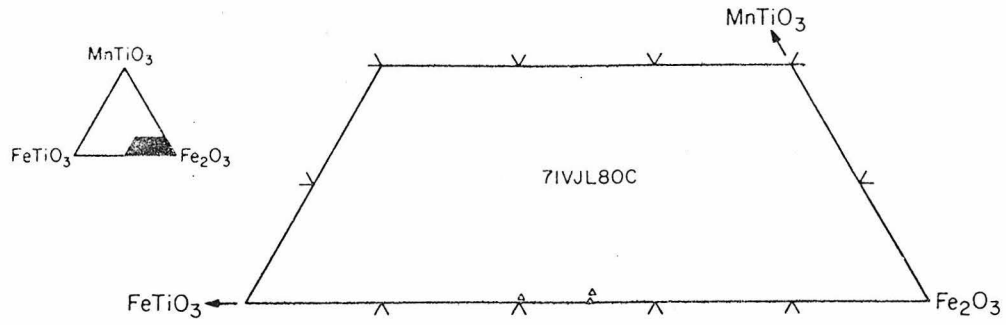
Figure IV-99b

GARNET

△ 5% Mg

7IVJL80C

7IVJL80D
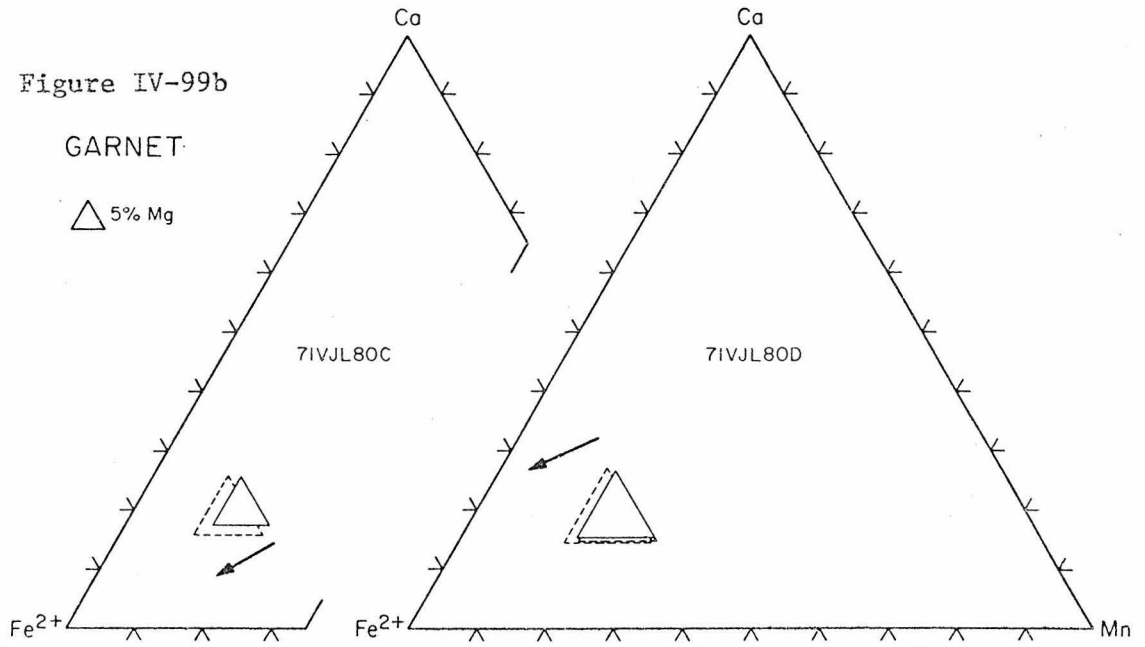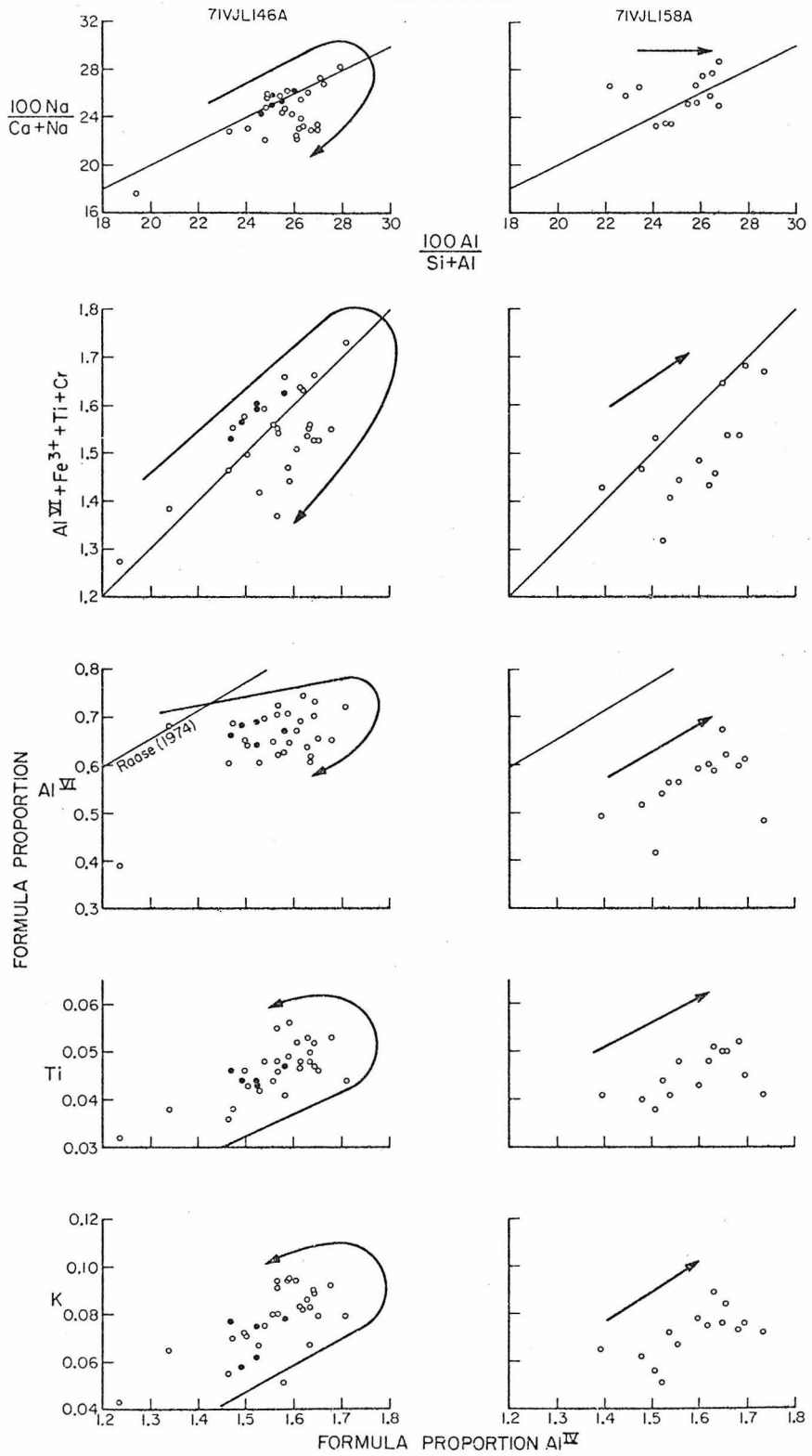
AMPHIBOLE

Figure IV-100a
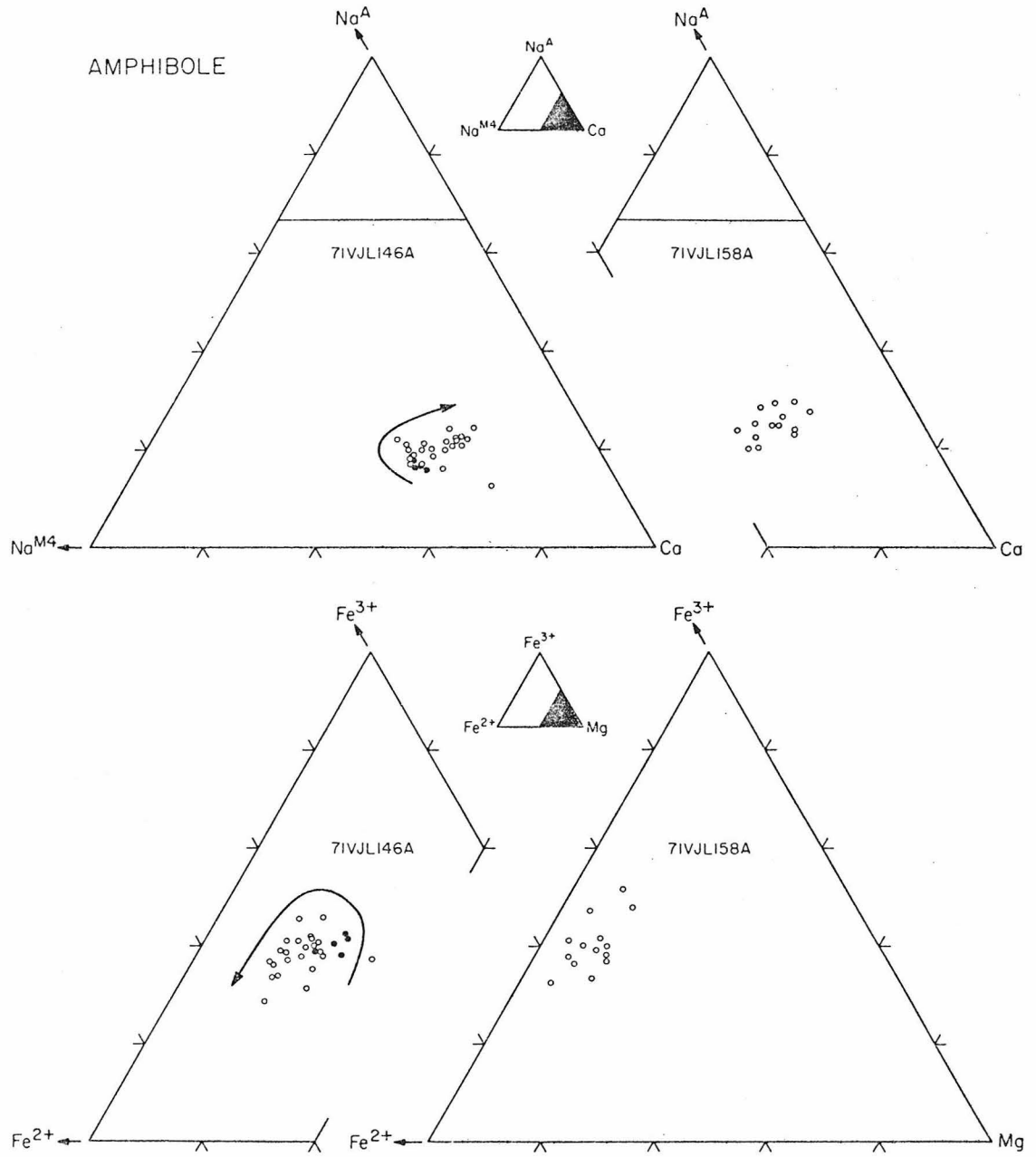
Figure IV-100b

Figure IV-101a

CARBONATE

Ca

Fe △————— Mg

△ 1% Mn

Ca

7IVJLI58A

△

7IVJLI46A

△

Ca Fe   Ca Mg

BIOTITE   CHLORITE

Figure IV-101b   Figure IV-101c

● 7IVJLI46A
○ 7IVJLI58A

$\frac{100\ Mg}{Mg+Fe}$

$\frac{100\ Mg}{Mg+Fe^{2+}}$

Al

Mn

Ti

Ti

Al$^{\text{IV}}$

Al$^{\text{VI}}$

Al$^{\text{IV}}$

Al$^{\text{IV}}$

FORMULA PROPORTION

FORMULA PROPORTION
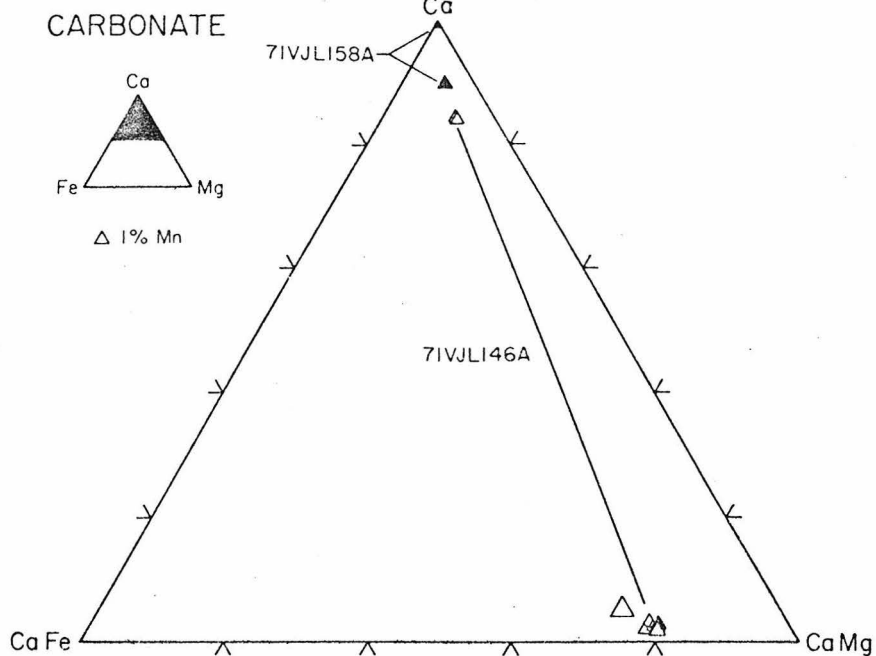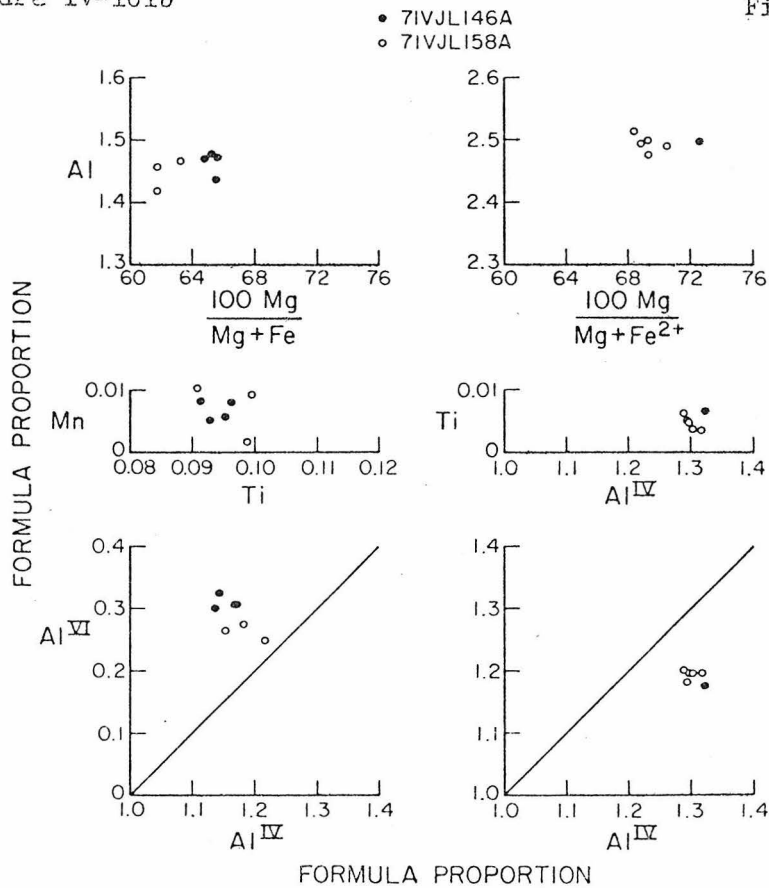
Figure IV-102a   EPIDOTE
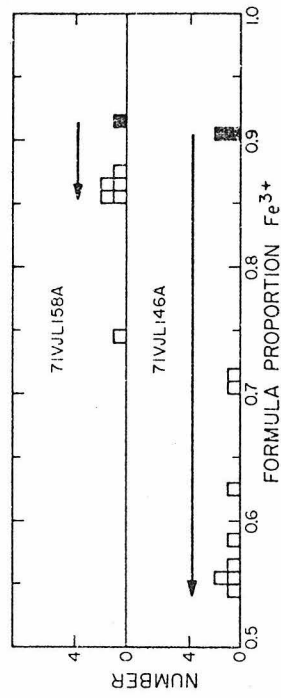
Figure IV-102b   ILMENITE-HEMATITE

Figure IV-102c   PLAGIOCLASE

Ca & Na-Ca AMPHIBOLE

Vermont & Southern Quebec

I — Pinnacle, Hazens Notch, Pinney Hollow, & Stowe (Eden Notch & Worcester Mtns) Fms

II — Underhill Fm Stowe Fm (Elmore Mtn) Saxtons River, Woodstock, & Wilmington Quads

III — Northeastern Vermont

Leake (1965)

Raase (1974)

FORMULA PROPORTION Al^{IV}

FORMULA PROPORTION Al^{VI}
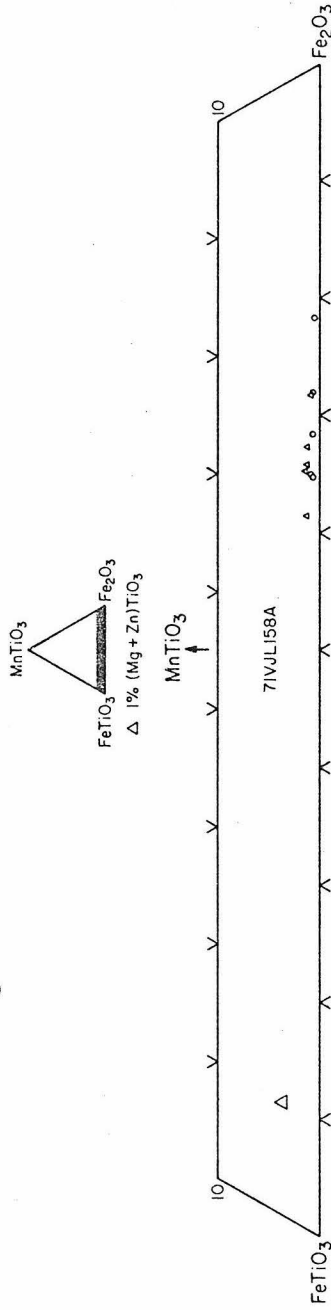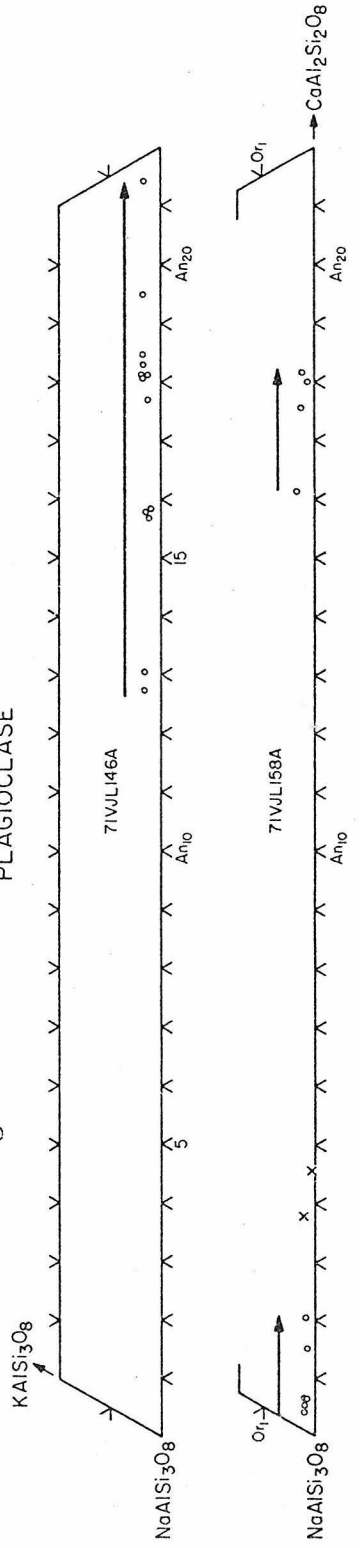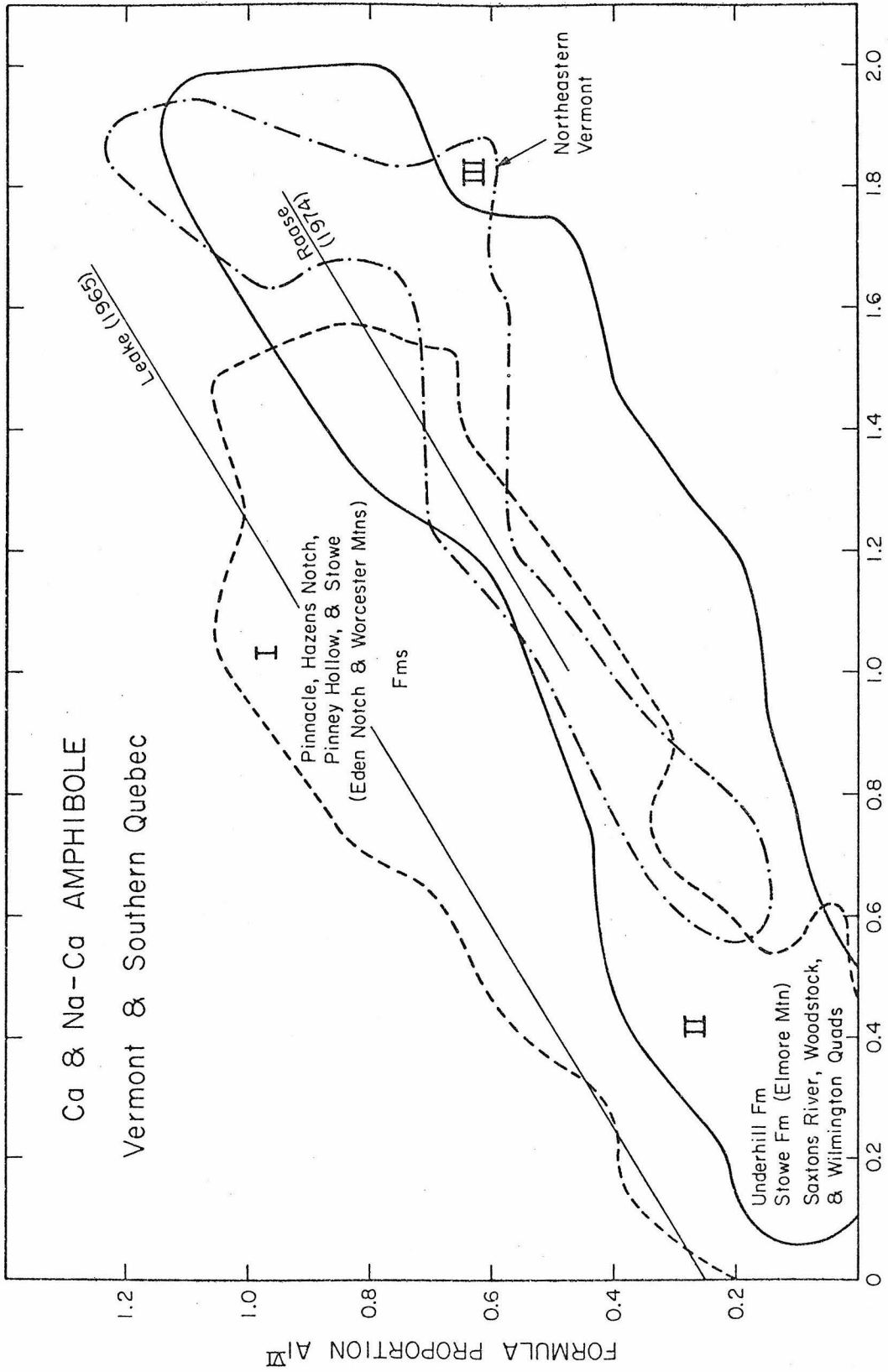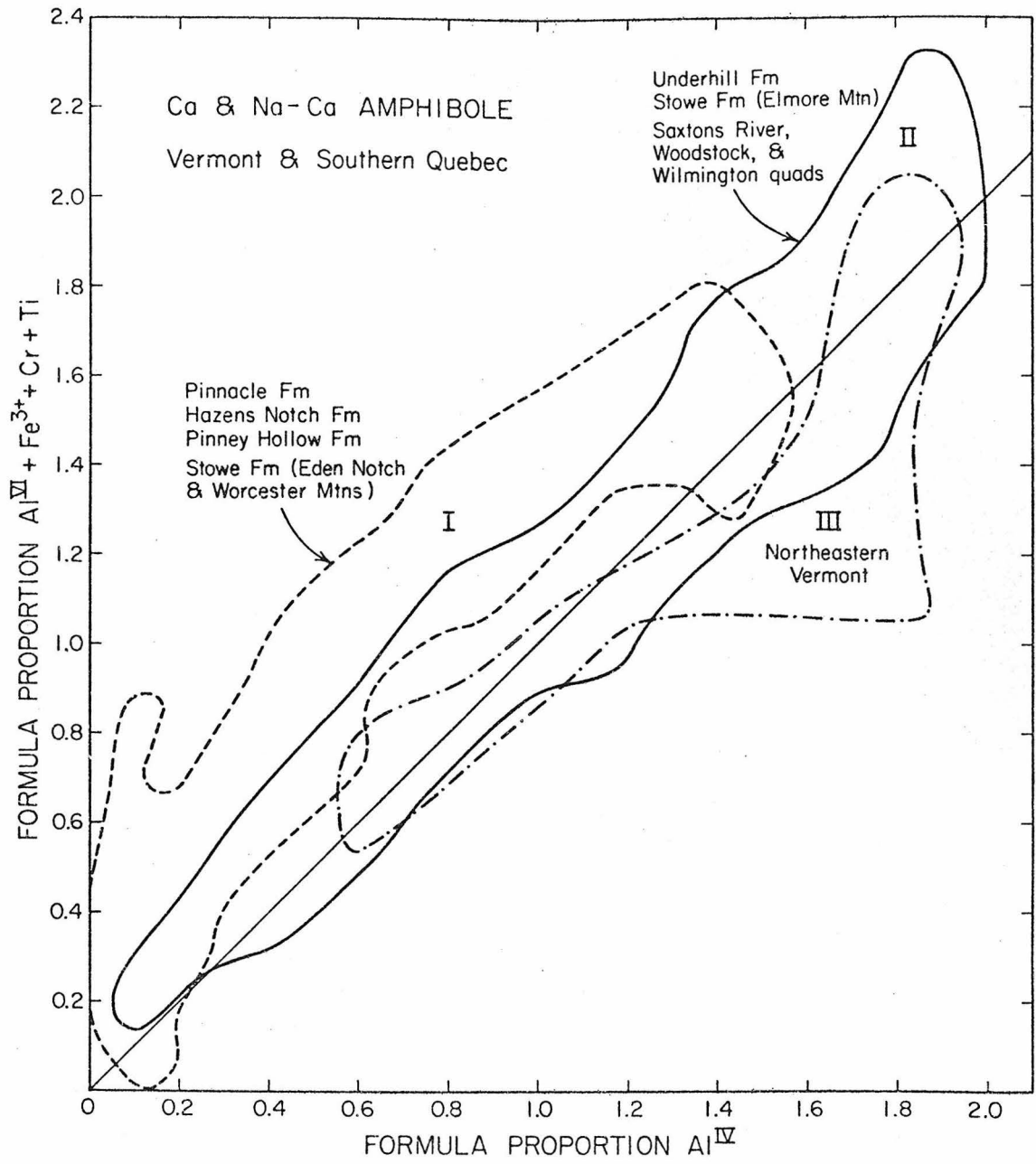
Figure V-1

Figure V-2

Ca & Na–Ca AMPHIBOLE
Vermont & Southern Quebec

Underhill Fm
Stowe Fm (Elmore Mtn)
Saxtons River,
Woodstock, &
Wilmington
quads

Pinnacle, Hazens Notch,
Pinney Hollow, &
Stowe (Eden Notch &
Worcester Mtns)
Fms

Northeastern
Vermont

Figure V–3

Ca & Na–Ca AMPHIBOLE
Vermont & Southern Quebec

I

Pinnacle, Hazens Notch,
Pinney Hollow, &
Stowe (Eden Notch & Worcester Mtns)
Fms

II

Saxtons River, Woodstock, &
Wilmington quads

III

Northeastern Vermont

Underhill Fm
Stowe Fm
(Elmore Mtn)

$\dfrac{100\ Na}{Ca+Na}$

$\dfrac{100\ Al}{Si+Al}$

Figure V-4

Figure V-5

AMPHIBOLE, Underhill Formation

Figure V-6

Figure V-7

Figure V-8

AMPHIBOLE, Pinney Hollow Formation (Granville Notch)

Figure V-9

AMPHIBOLE, Stowe Formation

Figure V-10

AMPHIBOLE, Northeastern Vermont

Figure V-11

AMPHIBOLE, Saxtons River Quadrangle

———— 71VJL94A, 97B, 127A ⎫
                          ⎬ (Chester Amphibolite)
·········· 71VJL127A   ⎭

———— 71VJL100B, 107A, 108, 114B, 124B

——— 71VJL118 O & P (Townshend Dam)

⎧ 71VJL126H (Hinkley Brook)
⎨
⎩ 71VJL152, 153C, 154B (Acton Hill)

$\dfrac{100\ Na}{Ca + Na}$

$\dfrac{100\ Al}{Si + Al}$

Figure V-12

AMPHIBOLE, Woodstock Quadrangle

$\dfrac{100\,Na}{Ca + Na}$

$\dfrac{100\,Al}{Si + Al}$

7IVJL80 B,C,D

Saxtons River Quadrangle:
Hinkley Brook & Acton Hill
Townshend Dam
Chester Amphibolite

STAUROLITE-KYANITE ZONE

HIGH GARNET ZONE

GARNET ZONE

DI

NO GAR

Figure V-13

AMPHIBOLE, Wilmington Quadrangle

$\dfrac{100\,Al}{Si + Al}$

$\dfrac{100\,Na}{Ca + Na}$

D2

D1

GARNET
ZONE

——— 71VJLI46A, 158A

- - - - Saxtons River quadrangle
(Chester Amphibolite)
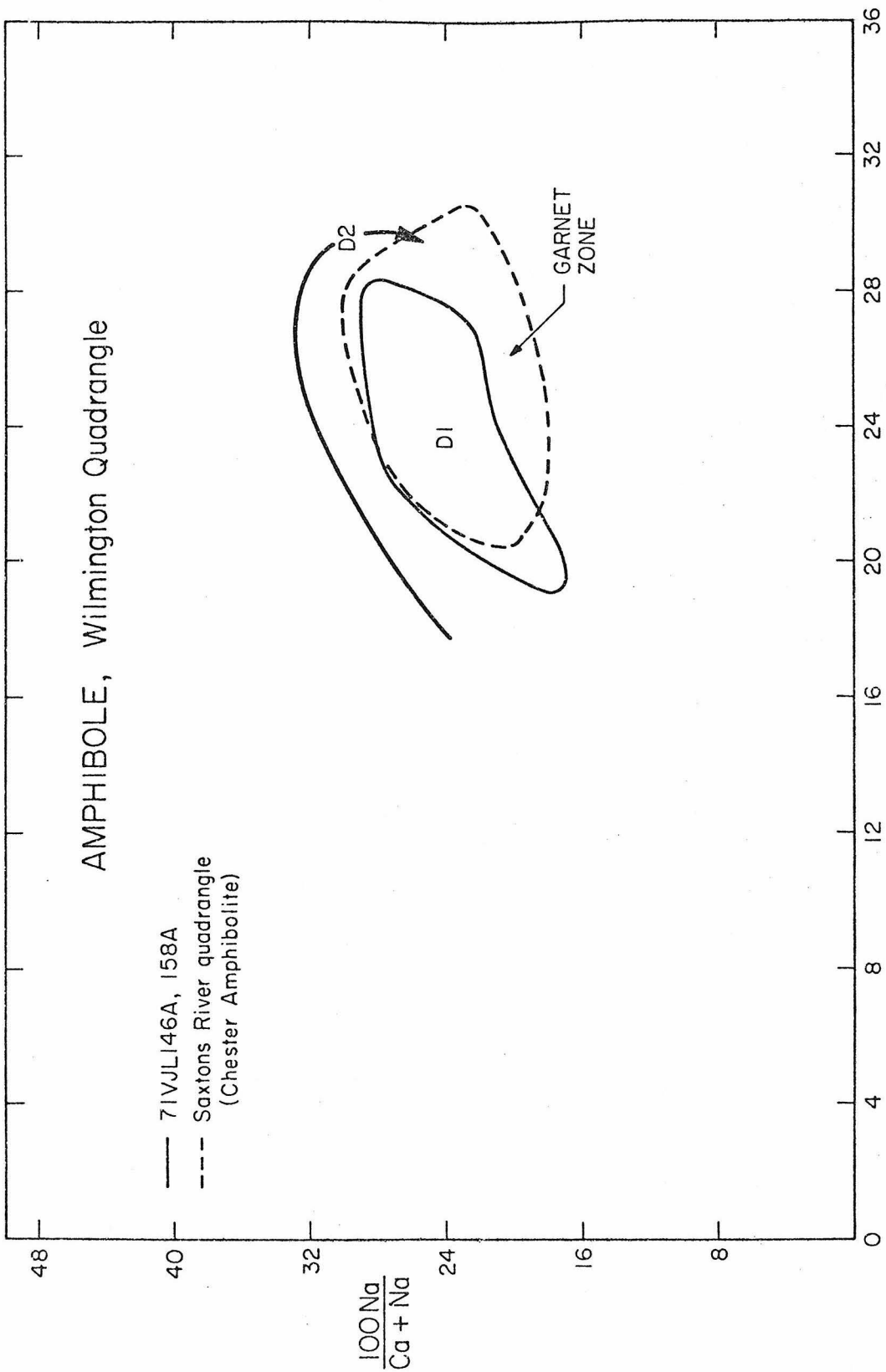
Figure V-14

Figure VI-1c

Figure VI-1b

Figure VI-1a

+ QUARTZ, K PHASE,
Ti PHASE
H₂O & CO₂ MOBILE
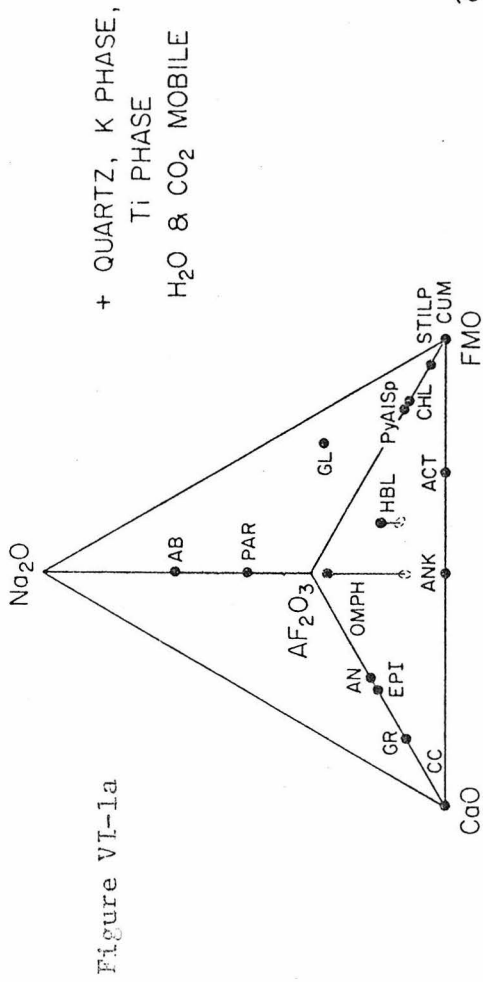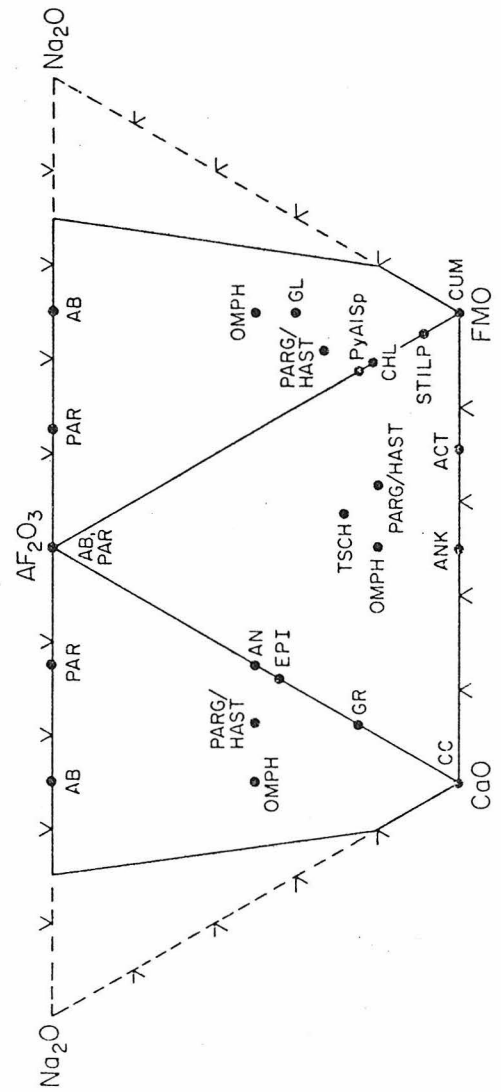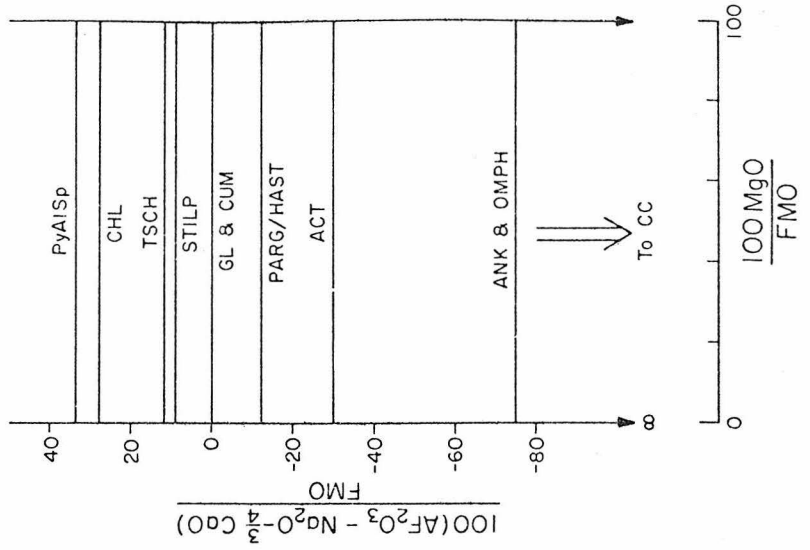
BIOTITE-ALBITE ZONE
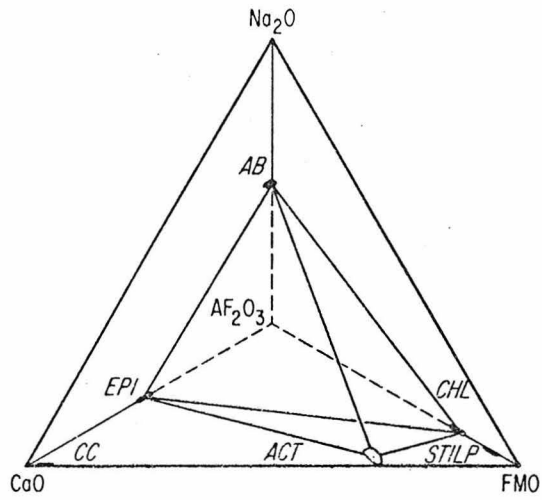
GARNET-ALBITE ZONE
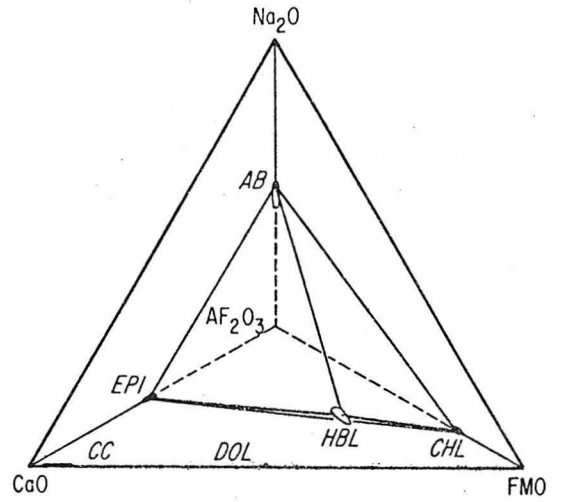
Figure VI-2a

Figure VI-2b

GARNET-OLIGOCLASE ZONE
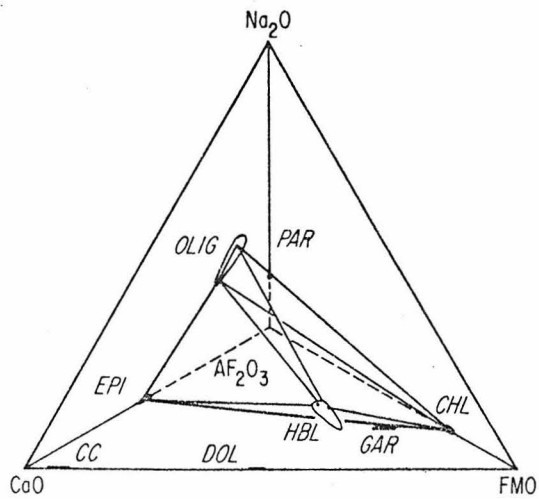
STAUROLITE-KYANITE-OLIGOCLASE ZONE

Figure VI-2c

Figure VI-2d

Figure VI-3a

1 = LA426, 435A, & 504B
2 = 7lVJL68
3 = 7lVJL14J

○ WITH } ACT
● WITHOUT } or STILP

+ A
□ B,C
× D
◇ E
△ F

BIOTITE-ALBITE ZONE

AF_2O_3

Na_2O ← ... → Na_2O

AB

AB

AB

EPI

CHL

ACT

ACT

ACT

CaO CC

STILP

FMO

Figure VI-3b

GARNET-ALBITE ZONE

AF_2O_3

Na_2O ← ... → Na_2O

AB

AB

AB

HBL

EPI

HBL

CHL

HBL

CaO CC

DOL

FMO

Figure VI-3c

1 = 7IVJLII3B
2 = 7IVJLII8E
3 = 7IVJLI08 & II80

GARNET-OLIGOCLASE ZONE

● WITH ·
○ WITHOUT } GAR

+ A
□ B,C
◇ E
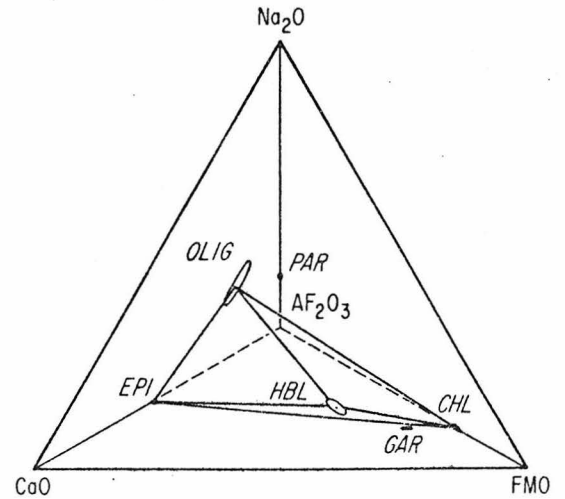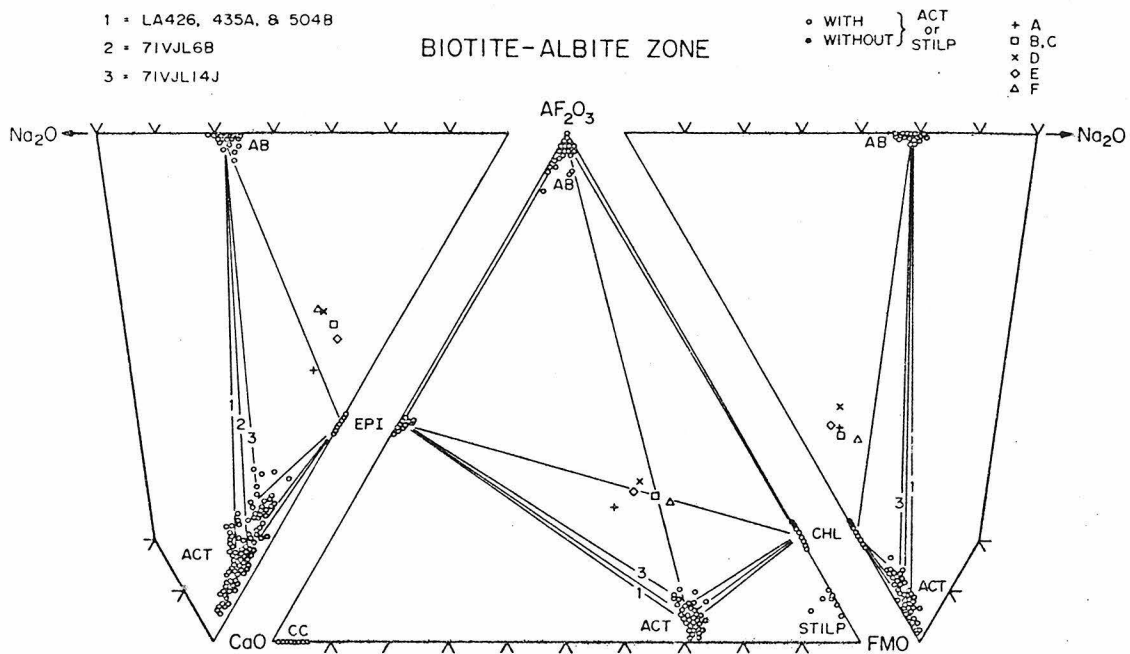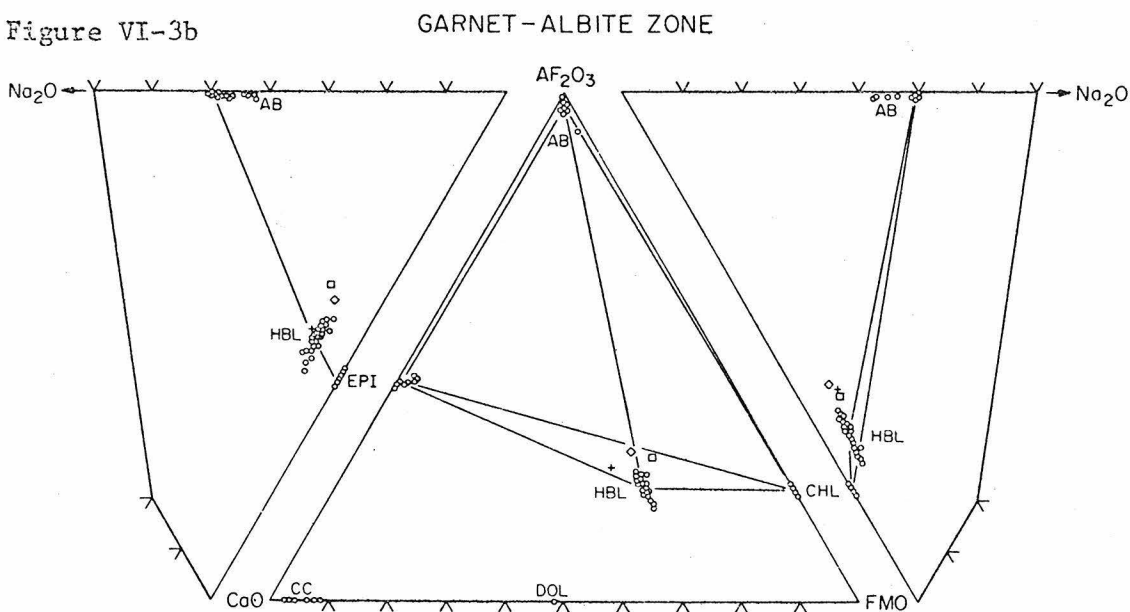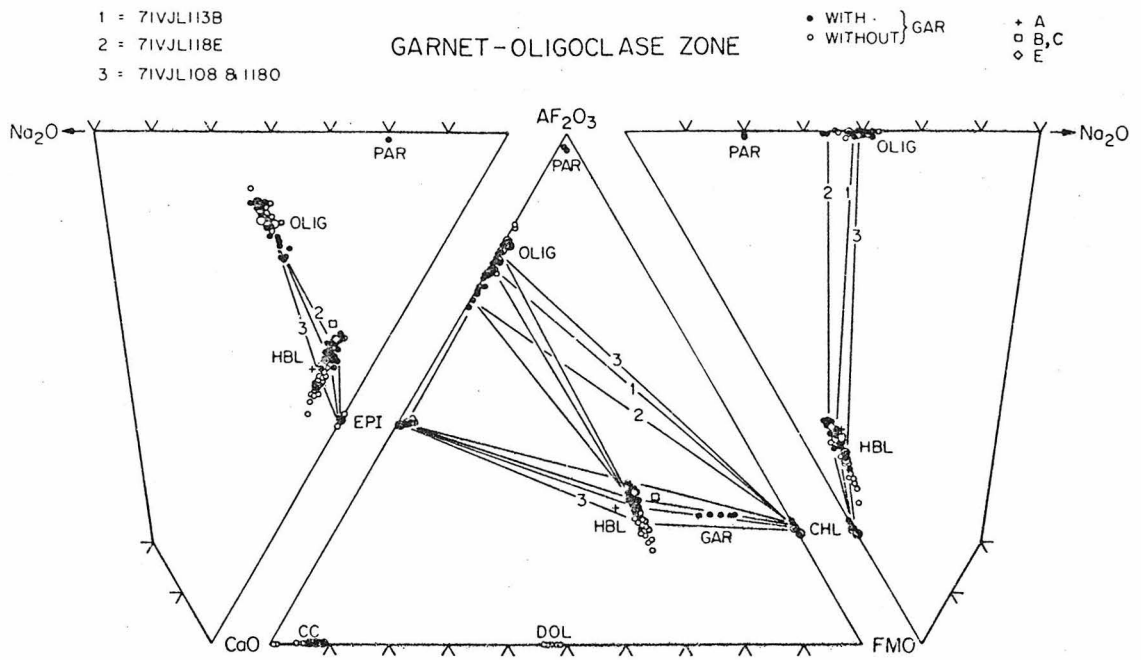
Figure VI-3d   STAUROLITE-KYANITE-OLIGOCLASE ZONE
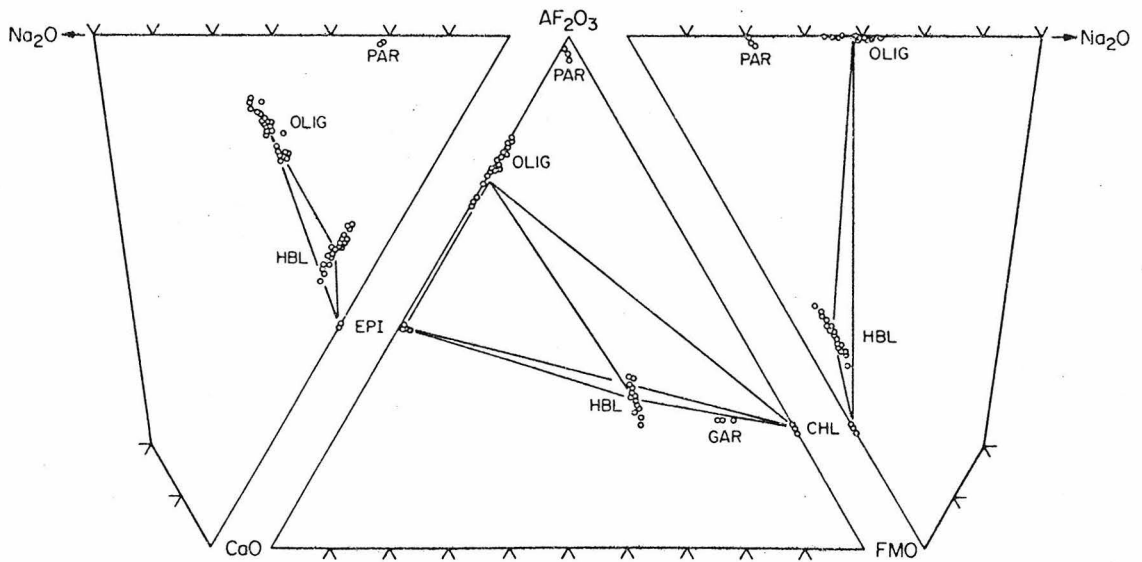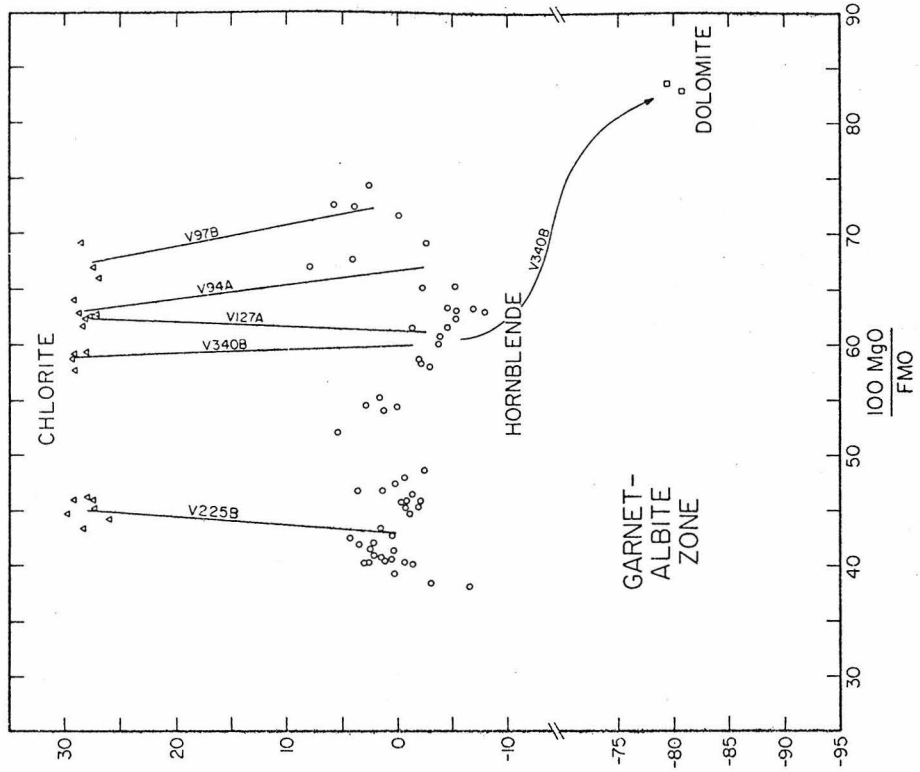
Figure VI-4b
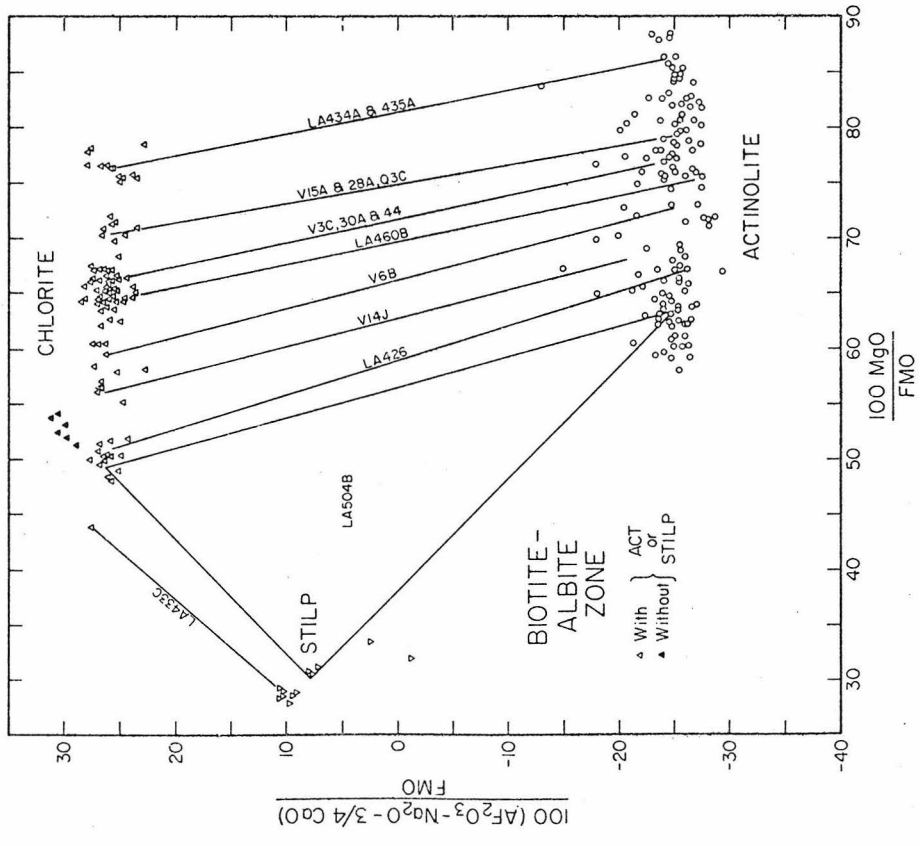
Figure VI-4a

Figure VI-4c

Figure VI-4d

BIOTITE-OLIGOCLASE ZONE
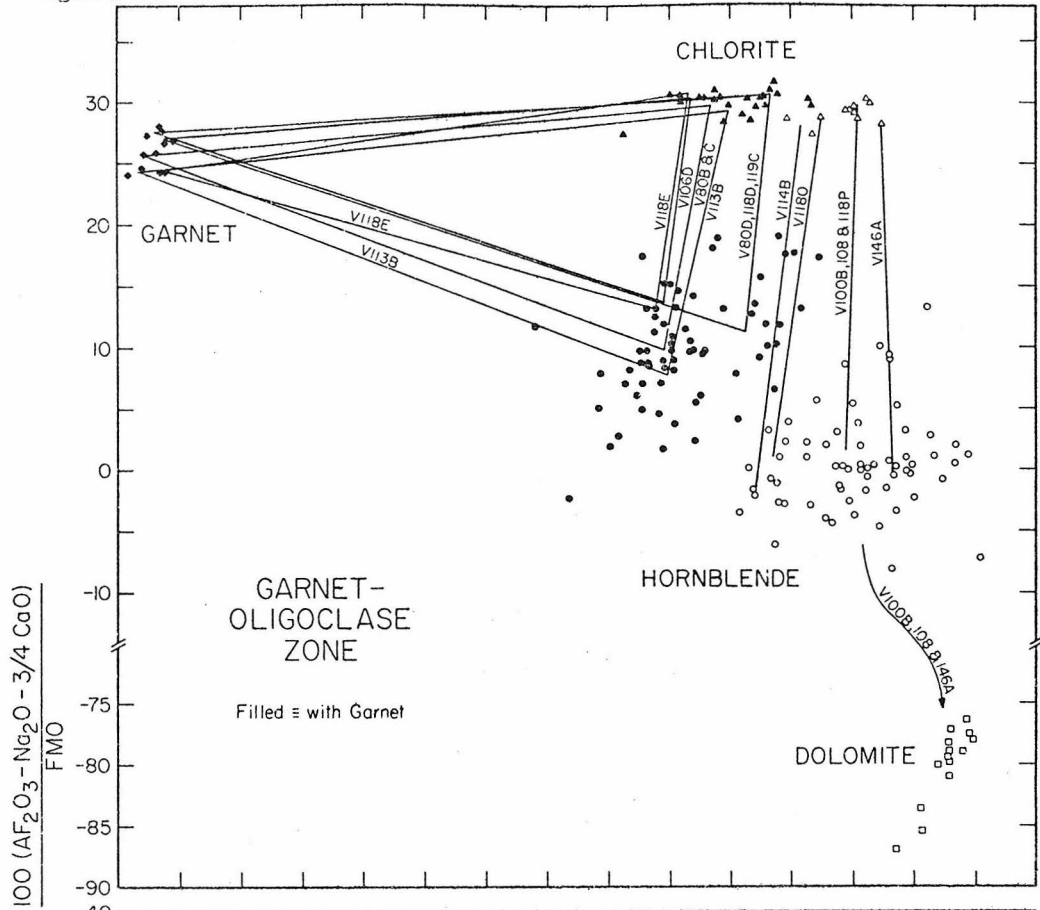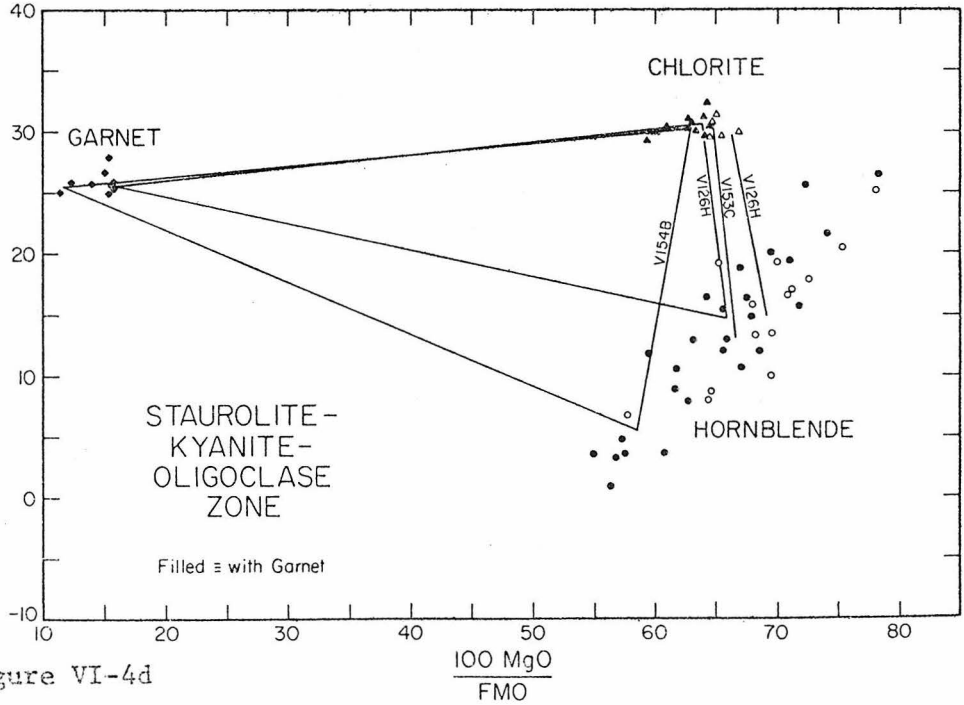
Figure VI-5a

GARNET-OLIGOCLASE/ANDESINE ZONE
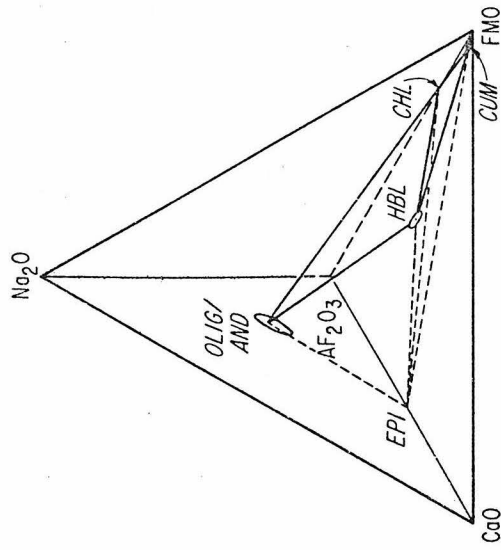
Figure VI-5b
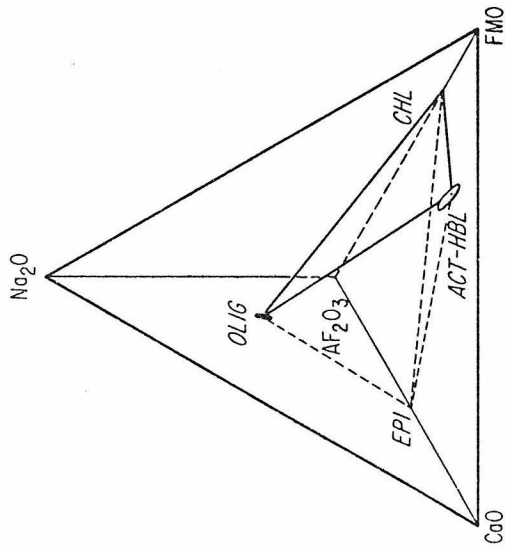
SILLIMANITE-BYTOWNITE ZONE
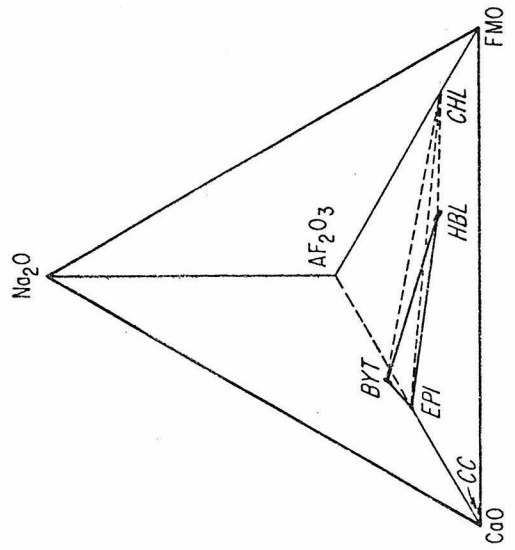
Figure VI-5c

Figure VI-6a   BIO-OLIG ZONE 7IVJL38A   △ MODEL F
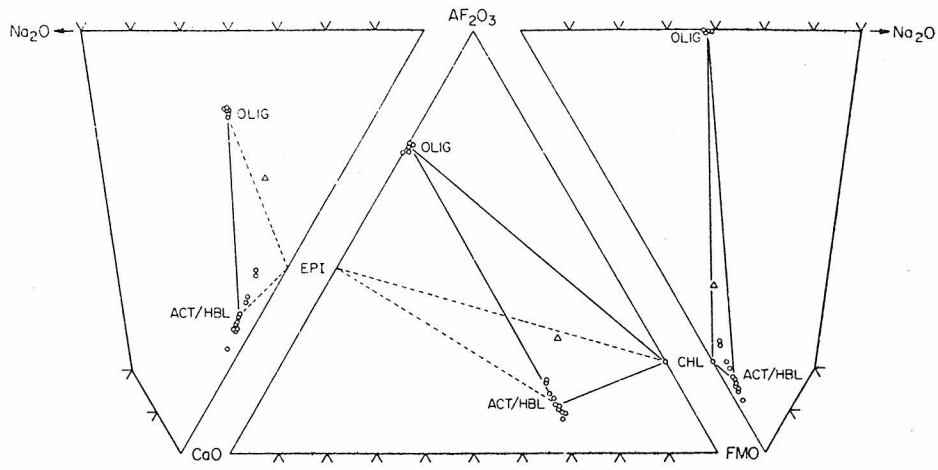
Figure VI-6b   GAR-OLIG/AND ZONE 7IVJL36A   □ MODEL C
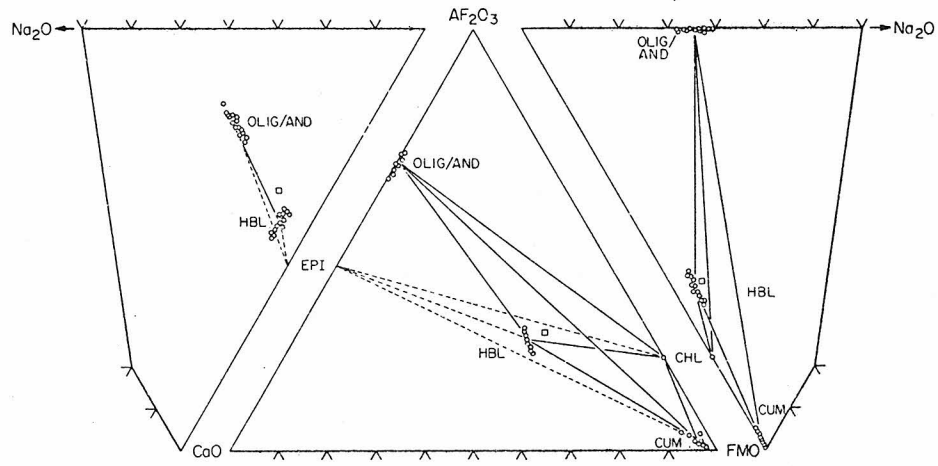
Figure VI-6c   SILL-BYT ZONE 7IVJL53
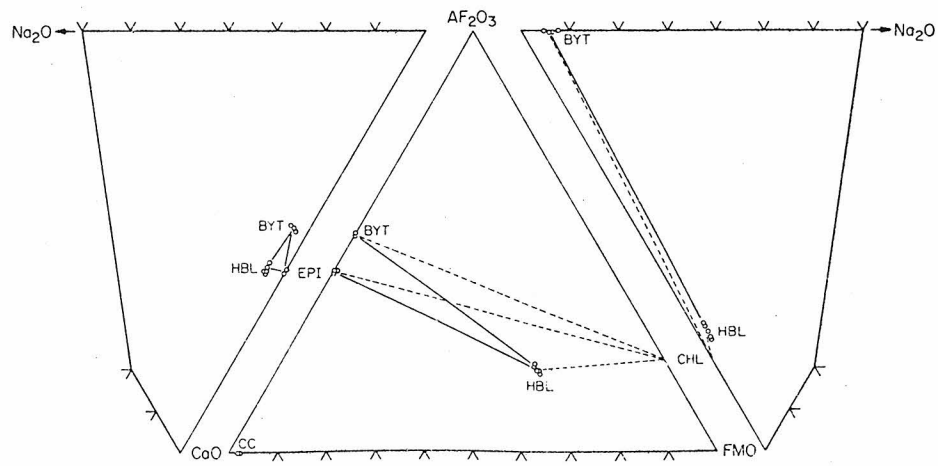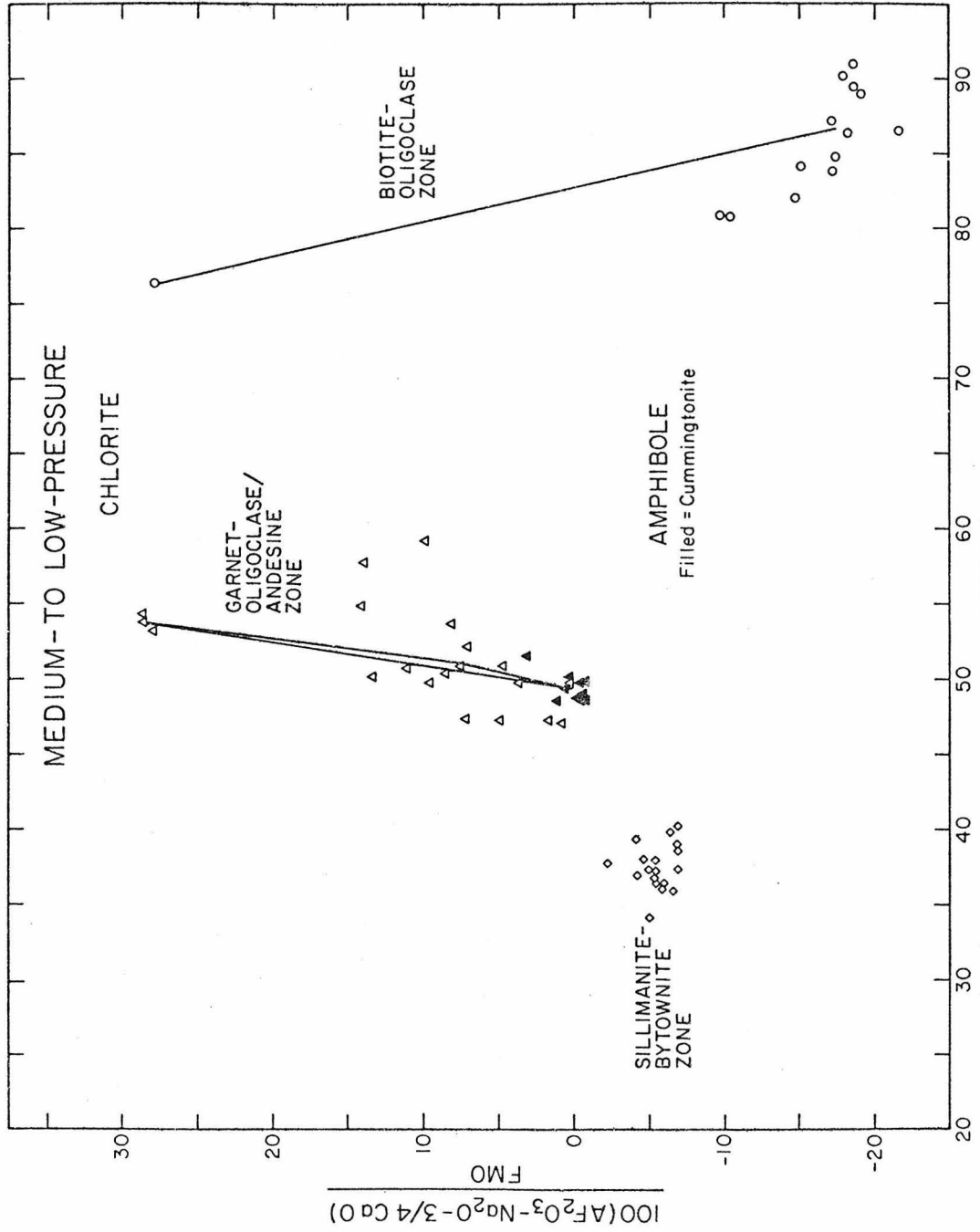
Figure VI-7

TILLOTSON PEAK
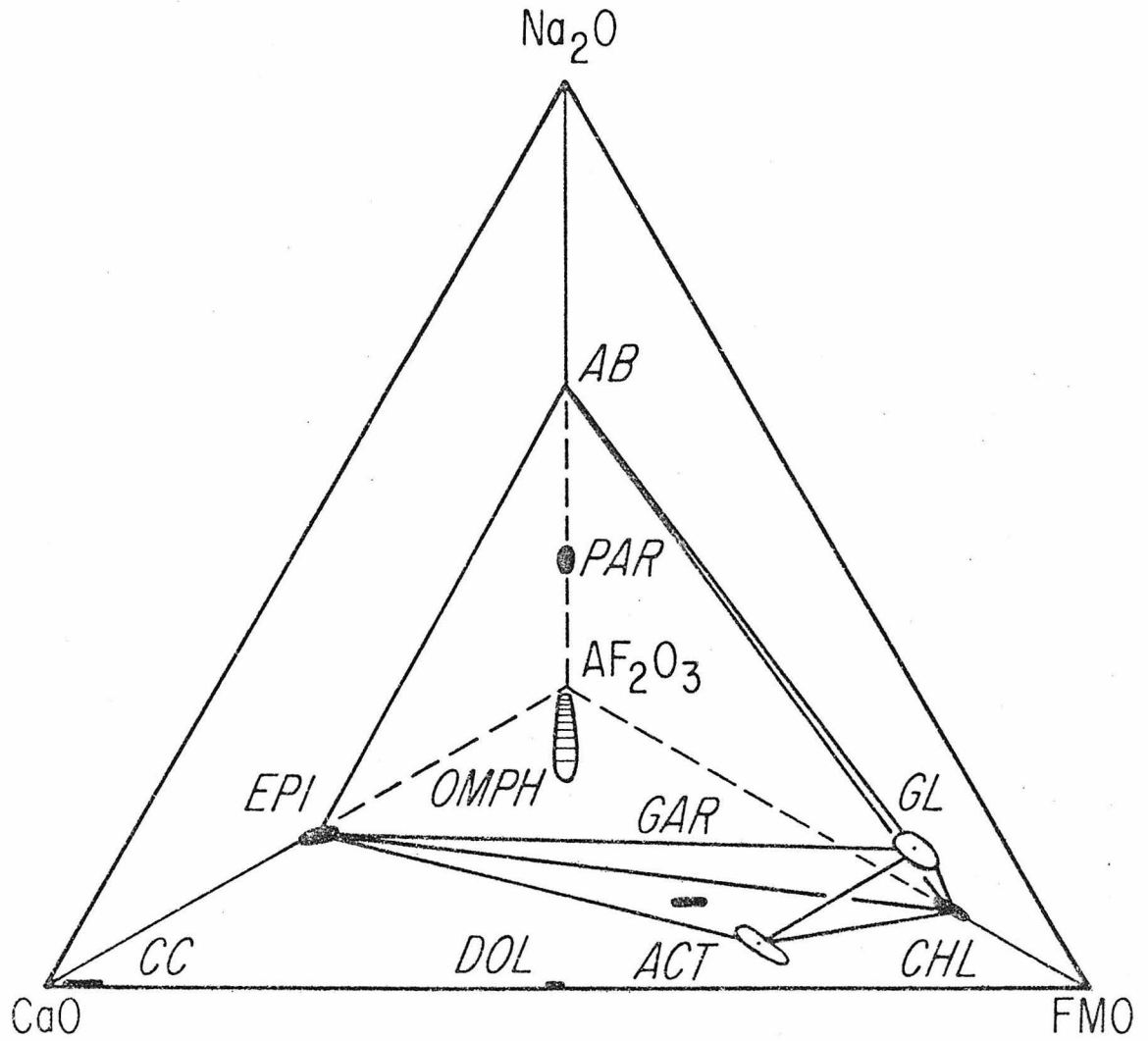
Figure VI-8a
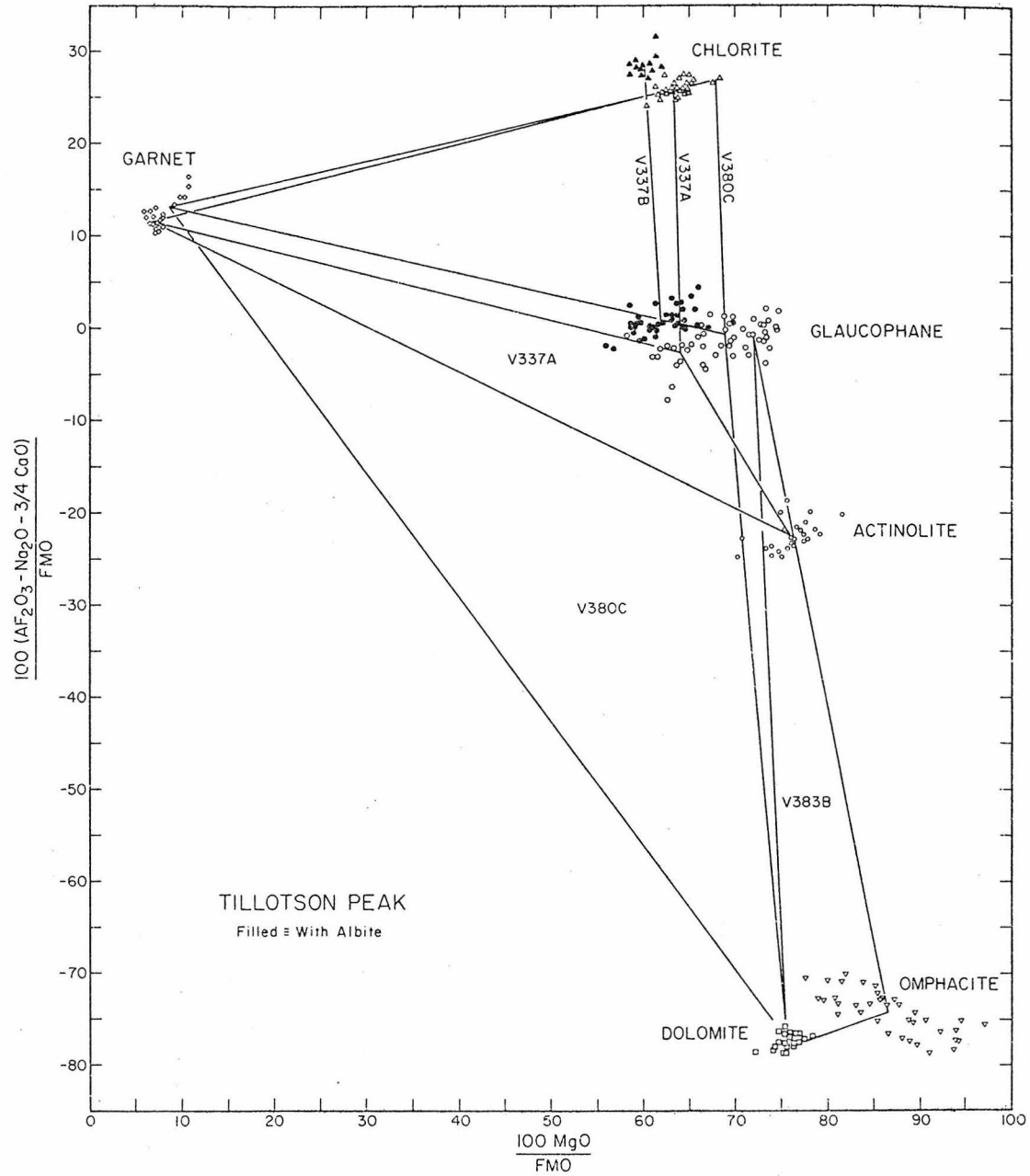
Figure VI-8b

Figure VI-9

MODEL A COEFFICIENTS
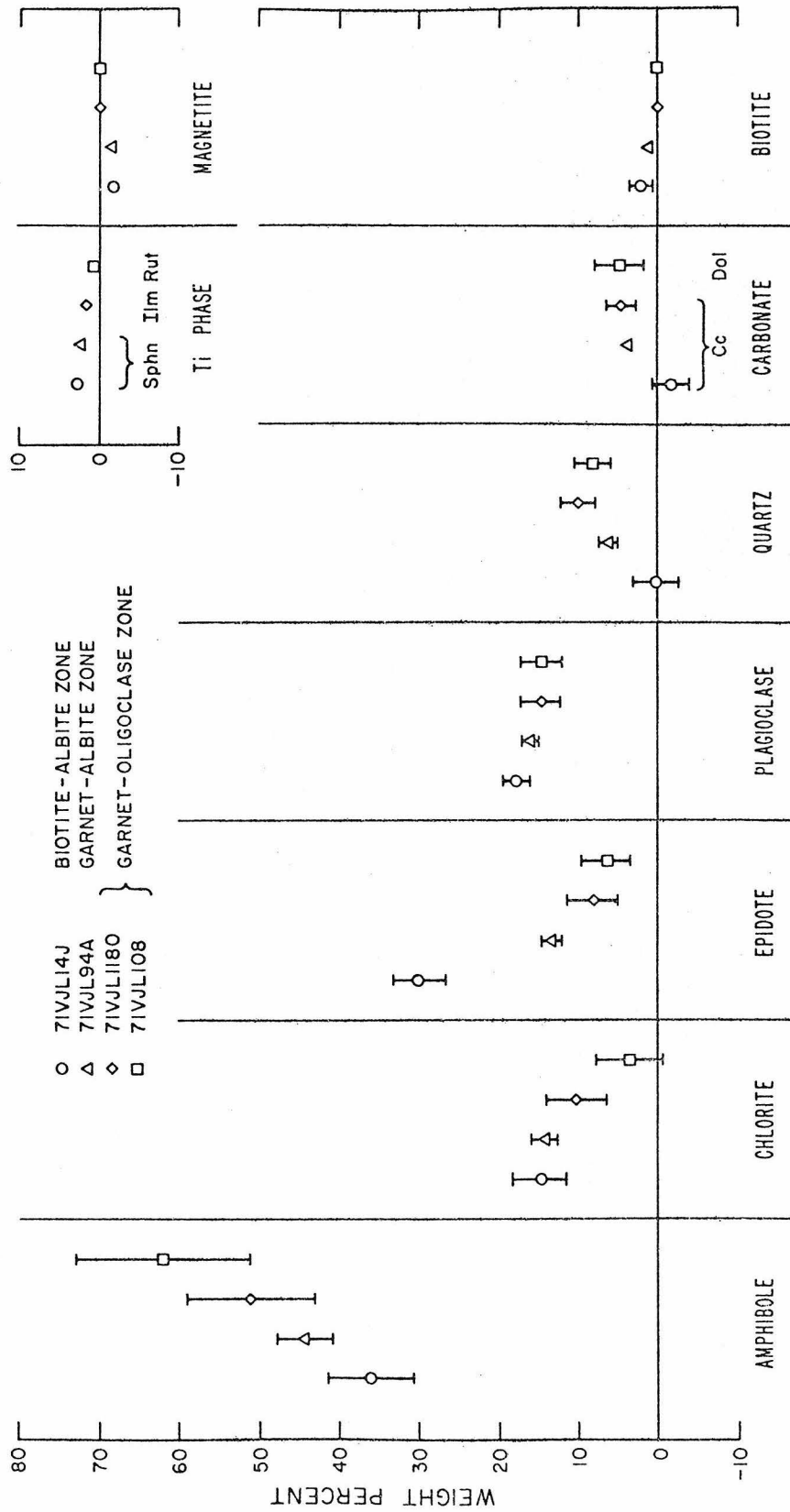
Figure VI-10

MEDIUM – HIGH P, BIOTITE – ALBITE ZONE

□ MODEL B
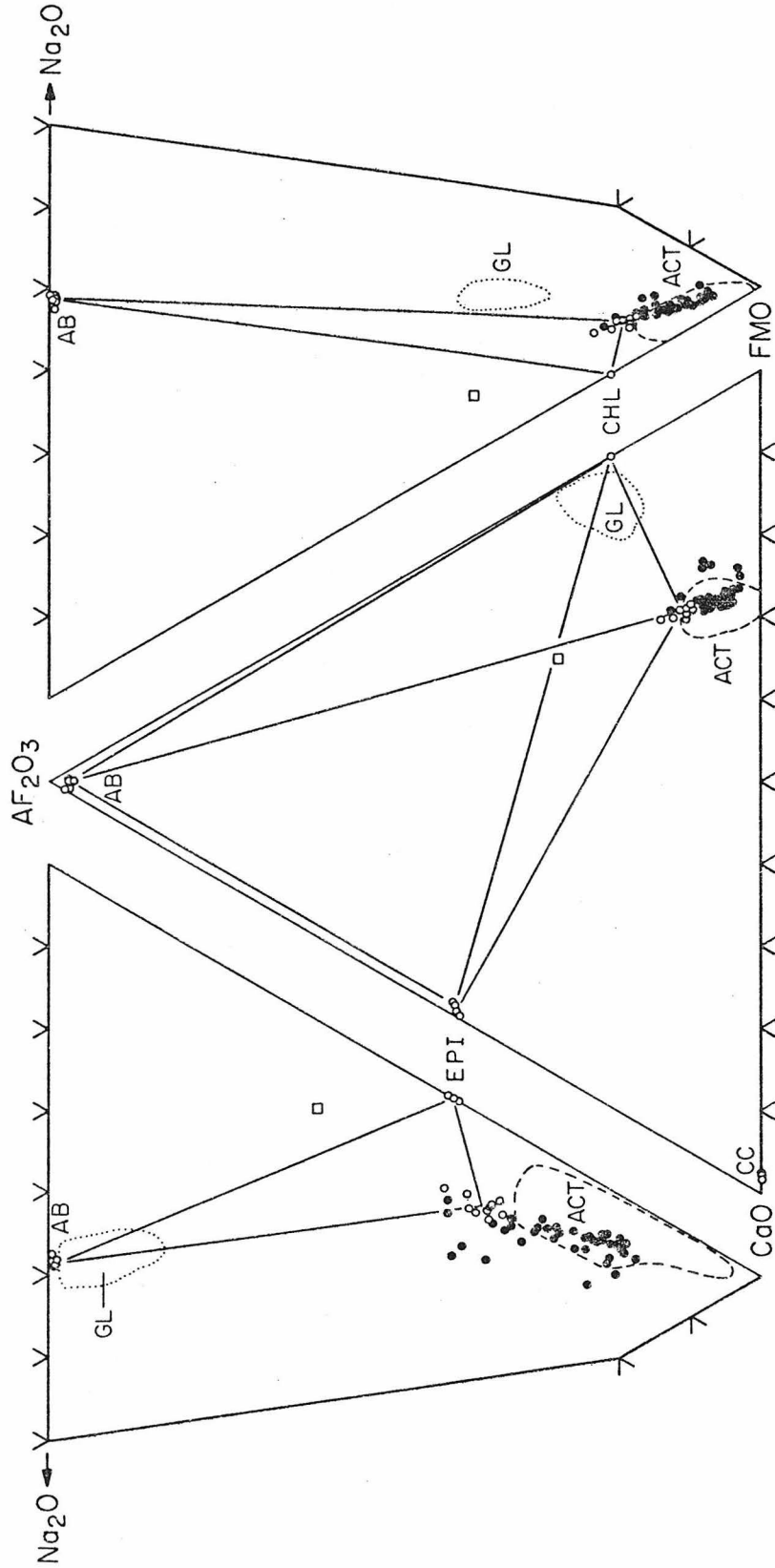
Figure VI-11
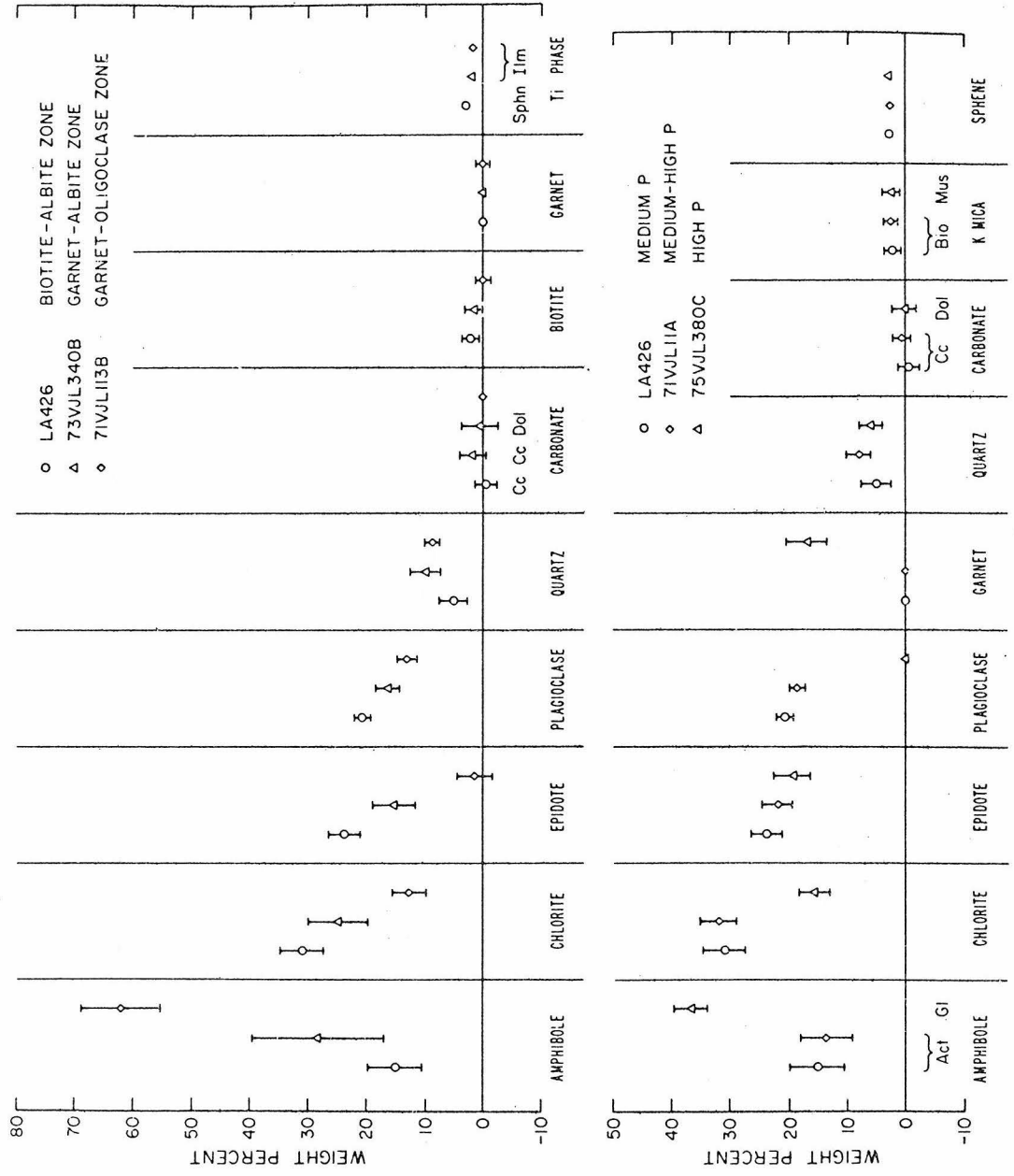
Figure VI-12

MODEL C COEFFICIENTS

MEDIUM-P

MEDIUM- TO LOW-P

71VJLI13B

71VJL36A

O

△

ILMENITE

BIOTITE

GARNET

EPIDOTE

CUMMINGTONITE

QUARTZ

CHLORITE

PLAGIOCLASE

HORNBLENDE

WEIGHT PERCENT

80 70 60 50 40 30 20 10 0 -10
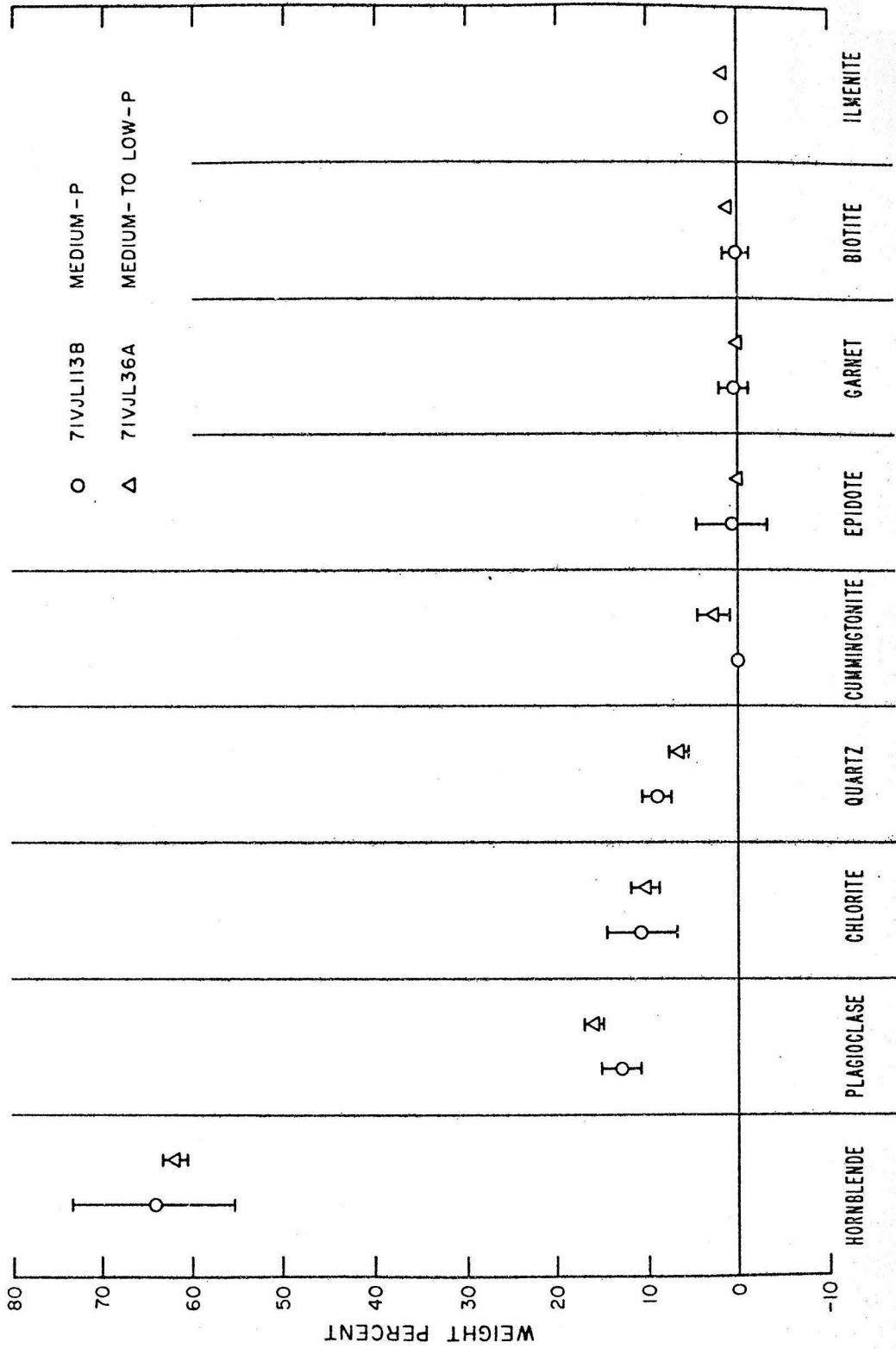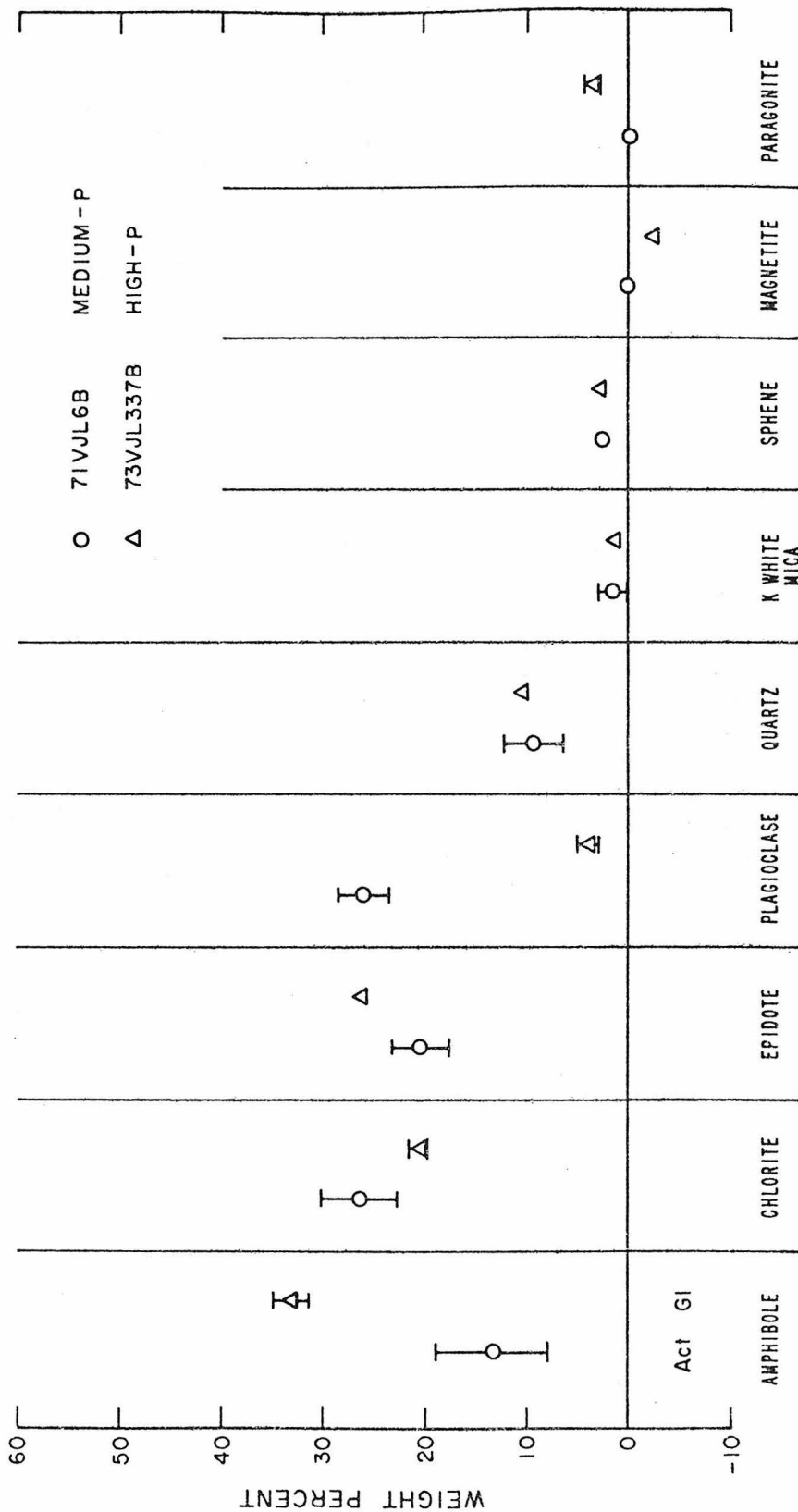
Figure VI-13

Figure VI-14

MODEL E COEFFICIENTS

Figure VI-15

Figure VI-16

MODEL F COEFFICIENTS